78-FM-51
Vol. V, Rev. 1

~~T 79-12405~~

JSC-14483

C.1

STS-1
Operational Flight Profile

Volume V
Descent - Cycle 3

Appendix C
Monte Carlo Dispersion Analysis

Supersedes T 79-12405

Mission Planning and Analysis Division

June 1980

National Aeronautics and
Space Administration

Lyndon B. Johnson Space Center
Houston, Texas

78-FM-51
Vol. V, Rev. 1

JSC-14483

SHUTTLE PROGRAM

STS-1
OPERATIONAL FLIGHT PROFILE

VOLUME V
DESCENT - CYCLE 3

APPENDIX C
MONTE CARLO DISPERSION ANALYSIS

By Moises N. Montez
Flight Analysis Branch

Approved: _____
Claude A. Graves, Jr., Assistant Chief
Flight Analysis Branch

Approved: _____
Ronald L. Berry, Chief
Mission Planning and Analysis Division

Mission Planning and Analysis Division

National Aeronautics and Space Administration

Lyndon B. Johnson Space Center

Houston, Texas

June 1980

CONTENTS

TABLES

FIGURES

Figure

1.0 SUMMARY

This appendix presents the results of three nonlinear Monte Carlo dispersion analyses for the STS-1 Orbiter Descent Operational Flight Profile, Cycle 3 (ref. 1). Fifty randomly selected simulations for the end-of-mission (EOM) descent, the abort-once-around (AOA) descent targeted to the steep target line (ref. 2), and the AOA descent targeted to the shallow target line (ref. 3) were analyzed. These analyses compare the flight environment with systems and operational constraints on the flight environment and, in some cases, use simplified system models as an aid in assessing the Space Transportation System (STS-1) descent flight profile. In addition, descent flight envelopes are provided as a data base for use by system specialists to determine the flight readiness for STS-1. The results of these dispersion analyses supersede the results of the dispersion analysis documented in reference 4.

The three-degree-of-freedom (3-DOF) option and the six-degree-of-freedom (6-DOF) option of the LAND program were used to generate the 150 random trajectories that were analyzed. The 50 EOM simulations are initialized prior to deorbit, and the deorbit burn thrust termination has been modified to include the effects of thrust tail-off dispersions. The initial covariance matrix reflects navigation errors in position and velocity. These errors are due to uncertainties in ground spaceflight tracking and data network (GSTDN) groundstation hardware and location coordinates, atmospheric drag and Earth gravity modeling, and vent and attitude control thrusting (ref. 5). No initial state dispersions were considered. Thus, the actual position and velocity are always on the nominal orbit. Dispersions of the same magnitude as the navigation errors are not expected to significantly change these results. Deorbit maneuvers from orbits that are significantly dispersed from the nominal would affect the dispersions at entry interface (EI). The AOA simulation are initialized 4 minutes prior to EI, which is at 400 000 feet altitude. The initial covariance matrix (refs. 2 and 3) is a 20 by 20 matrix and includes navigation errors and dispersions in position and velocity, accelerometer bias, and inertial platform misalinements.

The results of the approach and landing (A&L) analysis presented in this document were generated using the 6-DOF Monte Carlo option in the LAND program, which was initialized at an altitude of 9950 feet. However, the data developed using the 3-DOF simulation are accurate until preflare conditions are reached during A&L. From preflare to landing, the rotational dynamics are not accurately simulated with the 3-DOF simulation. Results from only one of the two AOA cases are included in this document, since in both cases the A&L phase is the same.

April atmospheres (ref. 6), which are the best atmospheres to use for a March 30 launch, were used in this study. The baselined tactical air navigation (Tacan) selection logic, which selects 1 out of 10 Tacan stations (based on the best Tacan geometry), was also used. A mobil Tacan station was placed 15 miles from the runway and as close as possible to the nominal groundtrack. Data from the air data system (ADS) were used below an Earth-relative velocity of 2500 fps. Baro-altitude was not processed by the flight navigation system between velocities of 1600 fps and 900 fps. Runway redesignations or ground state vector updates were not included in this analysis.

For the EOM, the surface temperatures are acceptable. Structure temperatures are also acceptable because of preentry thermal conditioning. For the steep AOA, the surface temperatures are acceptable, but the structure temperatures are marginal since there is no preentry thermal conditioning. For the shallow AOA, the surface temperatures are high, and the structures temperatures are marginal. These results are based on the simplified TPS model (ref. 7) included in the simulation. Detailed analysis of the envelope of flight conditions and control surface deflections should be made as a part of certifying the TPS for the first flight. Speedbrake, elevon, and body flap hinge moments are acceptable. Range dispersions at entry/TAEM interface are within the accuracy requirement of 5 miles. All landing simulations make the transition to autoland before an altitude of 7000 feet, and there are no minimum entry points (MEP), S-turns, or tailscrapes. Navigation-derived dynamic pressure accuracies exceed the flight control system constraints between Mach 8 and Mach 2.5, and several cases violated the change of yawing moment coefficient due to beta (Cn_β) dynamic and lateral trim constraint line assuming equilibrium flight. In addition, normal load factor transients occur at microwave scanning beam landing system (MSBLS) acquisition and at terminal area energy management (TAEM)/autoland interface. The tire specification limit speed of 222 knots was exceeded in 5 out of 50 EOM landings and 5 out of 50 AOA landings using the autoland mode. The tire certification limit of 218 knots was exceeded five times at EAFB and seven times at Northrup. Crosswind magnitudes at landing were all less than 10 knots at Northrup, but in two cases (10 knots and 11 knots) at EAFB were greater than or equal to crosswind constraint of 10 knots.

Navigation-derived dynamic pressure accuracies exceed the flight control system (FCS) constraints between Mach 8 and Mach 2.5. Violation of these constraints will affect the FCS moding and gains because dynamic pressure is used to perform these two functions. Several cases violated the Cn_β dynamic and lateral trim constraint line. This constraint line was generated by using the April 1979 aerodynamic data, Xc.g. = 66.7 percent, trim flight, 1-inch Yc.g. offset, worst-case elliptical aerodynamic variations, two yaw jets used for trim, maximum sideslip of 1.5 degrees, and bent airframe effects. Integrated guidance, navigation, and control (GN&C) analysis are required to determine the effect of violating the navigation-derived dynamic pressure error constraint and the effect of violating the Cn_β dynamic and lateral trim constraint.

Several metering methods were used to reduce the normal load transients at MSBLS acquisition but were slightly unsuccessful. Therefore, the pilot should expect these transients. MSBLS variances have been increased and should reduce the magnitude of these transients. The landing statistics indicate that 5 out of 50 EOM landings and 5 of 50 AOA landings exceeded the tire specification limit speed of 222 knots. The certification tire limit of 218 knots was exceeded 5 times at EAFB and 7 times at Northrup. Because the landing is expected to be performed manually rather than using the autoland guidance for STS-1, the pilot landing techniques are expected to increase the landing point dispersion to reduce the landing speed to within landing gear and tire limits.

2.0 INTRODUCTION

This appendix presents the results of three nonlinear Monte Carlo analyses for an STS-1 Orbiter Descent Operational Flight Profile Cycle 3. The flight environment is compared with systems and operational constraints on the flight environment, and in some cases, simplified systems models are used as an aid in assessing the STS-1 descent flight profile. In addition, descent flight envelopes are provided as a data base for use by system specialists in determining the flight readiness for STS-1.

The 3-DOF and the 6-DOF Monte Carlo options of the LAND program were used to generate the 150 random trajectories that were analyzed. The end-of-mission (EOM) simulations are initialized prior to deorbit, and the deorbit thrust termination has been modified to include the effects of thrust tail-off dispersions. The initial covariance matrix reflects navigation errors in position and velocity due to uncertainties in GSTDN groundstation hardware and location coordinates, atmospheric drag and Earth gravity modeling, and vent and attitude control thrusting (ref. 5). No initial state dispersions were considered. Thus, the actual position and velocity are always on the nominal orbit. Dispersions of the same order of magnitude as the navigation errors are not expected to significantly change these results. Deorbit maneuvers from orbits that are significantly dispersed from the nominal would affect the dispersions at EI. The AOA simulations are initialized at 4 minutes prior to EI, which is at 400 000 feet altitude. The initial covariance matrix (refs. 2 and 3) is a 20 by 20 matrix and includes navigation errors and dispersions in position and velocity, accelerometer bias, and inertial platform misalinements.

The results of the A&L analysis given in this document were generated using the 6-DOF Monte Carlo option in the LAND program that was initialized at an altitude of 9950 feet.

April atmospheres (ref. 6), which are the best atmospheres to use for a March 30 launch, were considered. The baselined Tacan selection logic, which selects 1 out of 10 Tacan geometry, was used in this study. A mobil Tacan station was included and was located approximately 15 miles from the runway and as close as possible to the nominal groundtrack. Also, data from the air data system were used below an Earth-relative velocity of 2500 fps. Baro-altitude was not processed by the navigation between velocities of 1600 and 900 fps. Runway redesignations or ground state vector updates were not included in this analysis.

Statistical summaries for selected parameters and scatter traces for selected parameters are presented in this appendix. The scatter traces include the expected three-sigma dispersions for the parameters that are normally distributed.

3.0 ACRONYMS

A&L	approach and landing
ADS	air data system
AOA	abort once around

BETA	sideslip angle
C_d	drag coefficient
c.g.	center of gravity
C_L	lift coefficient
C_m	pitching moment coefficient
$Cn\beta$	change of yawing moment coefficient due to beta
CR	change request
DOF	degrees of freedom
EAFB	Edwards Air Force Base
EOM	end of mission
EI	entry interface (400 000 feet altitude)
GAMMA	flightpath angle
GN&C	guidance, navigation, and control
GSTDN	ground spaceflight tracking data network
H	altitude
HAC	heading alinement cylinder
HDOT	altitude rate
HRSI	high-temperature reusable surface insulation
IMU	inertial measurement unit
I_{sp}	specific impulse
LRU	line replacement unit
L/D	lift to drag
MSBLS	microwave scanning beam landing system
MECO	main engine cut-off
MEP	minimum entry point
OMS	orbital maneuvering system

psf	pounds per square foot
RCC	reinforced carbon carbon
RCS	reaction control system
RF	radio frequency
RM	redundancy management
STS	Space Transportation System
Tacan	tactical air navigation system
TPS	thermal protection system

4.0 SUCCESS CRITERIA

The following criteria are used in determining successful results:

a. The TPS surface and structure temperature limits; defined in table I (ref. 8)

b. Control surface hinge moment constraints; defined in table II (ref. 9)

c. Normal load factor less than 2 g's

d. Dynamic pressure less than the 300 psf for Mach numbers greater than 5 and less than 342 psf for Mach numbers less than 5. Dynamic pressure less than 300 psf in the transonic region to conform to compartment venting constraints

e. Maximum descent rate of 400 fps in the transonic region to conform to compartment venting constraints

f. Entry/TAEM interface range within 5 miles of the nominal range-energy profile

g. No trajectory transients at entry/TAEM interface

h. No MEP's

i. No S-turns

j. TAEM/autoland interface box; satisfied before an altitude of 5000 feet; defined in table III (ref. 10)

k. Pitch attitude with respect to the horizontal less than 15.0° at landing (ref. 11)

l. Descent rates at landing less than 9.5 fps (ref. 11)

m. Landing speeds less than the tire limit speed of 222 knots (ref. 12)

n. Lateral position within 60 feet of the runway centerline (ref. 12)

o. Lateral velocity less than 50 fps (ref. 12)

This appendix first defines a set of criteria that is used to determine the acceptability of the flight profile. Model changes that have occurred since the dispersion analysis documented in reference 4 are listed, and then the flight profile major events are outlined from deorbit targeting to landing. A discussion of the atmosphere dispersions, navigation performance, TPS performance, control surface hinge moments, guidance performance, and landing performance follows in that order. The results, in the form of scatter traces, are then compared to system and operational constraints. These flight envelopes and results from simplified system models can be used by system specialists to determine areas that need more detailed analysis prior to STS-1 flight readiness review.

5.0 MODEL CHANGES

Because the dispersion analysis results have already been documented in reference 3, this section will present only model changes. Thrust tail-off dispersions (0.2 fps) have been added to the deorbit burn termination. Also, dispersions in Xc.g., Yc.g. (6-DOF only), and Zc.g. of 1 inch, 0.5 inch and 0.5 inch, respectively, have been included. The distribution for the thrust tail-off dispersions and the c.g. dispersion is assumed to be uniformly distributed.

The aerodynamic data were updated to the April 1979 aerodynamic data (ref. 13) and asymmetric airframe effects have been included in the dispersion model for the 6-DOF simulations. Normal load factor effects on the elevon hinge moments have been added to the simulation. For the guidance simulations, the entry guidance azimuth error dead band of $\pm$12.5 degrees in magnitude (until the first roll reversal is terminated) has been changed to 10.5 degrees. After this, the dead band is expanded to $\pm$17.5 degrees. This increases the ranging capability for very low lift-to-drag (L/D) cases. The TAEM guidance was modified to include a left turn onto the final approach, and a TAEM/autoland transition lockout was added. The autoland guidance was modified such that the A&L profile approximates a manually flown flightpath as specified in the STS-1 groundrules and constraints document (ref. 14). Also, the outer glideslope was changed from 22 degrees to 20 degrees.

For the 6-DOF analysis, the FCS was updated to the model documented in reference 15, and the supporting data were obtained from reference 16. Other modifications included the incorporation of change requests (CR's) 19570A, 19564, 19054, 19182, 19394C, 19415A, 19442, and 19564.

The ADS simulation includes April nonstandard atmosphere corrections to pressure, temperature, and pressure altitude above 12 000 feet mean-sea-level altitude for Edwards Air Force Base (EAFB). Below 12 000 feet, a baro-set is used,

which calibrates the barometric altimeter to sea level based on measured pressure data at the landing site.

6.0 MAJOR EVENTS

For the nominal EOM, a simulation of the ground targeting software generates the desired entry targets for the deorbit burn. The deorbit targeting, which is mission-dependent, provides the capability to achieve the desired EI state vector with either 2-OMS, 1-OMS, or an RCS deorbit maneuver. A 2-OMS deorbit burn is executed for every simulation in the Monte Carlo process. After the deorbit burn, an attitude maneuver is executed to a given inertial attitude. This will result in the proper entry attitude at EI minus 5 minutes. This attitude places the Z-body axis in the orbit plane. Because largest vents are along the Z-body axis, the effects of venting and translational delta-V from the RCS thrusters (which are required to offset the moments introduced by the vents) will degrade the state vector. During this portion of the flight, the navigation system propagates three state vectors using delta-V from three IMU's if the sensed delta-V is greater than a threshold of 1000 micro g's. No external measurements are processed during this period. For the AOA, the simulations are initialized at 4 minutes prior to EI.

During the first phase in the entry portion of flight, the entry attitude of 40° angle of attack, zero bank, and zero yaw is maintained until a drag acceleration level of 4 fps is reached. At this point, entry ranging is activated, and the entry guidance (ref. 10) executes the temperature control phase logic, which is designed to control the trajectory to a optimal profile based on aerodynamic heating considerations and the ranging required to reach the runway. This phase is followed by the equilibrium glide, constant drag, and transition phases. Control is transferred to the TAEM guidance at an Earth-relative velocity of 2500 fps. For the shallow AOA, the entry attitude is a 40° angle of attack, a 90-degree bank angle, and zero yaw. For the steep AOA, the entry attitude is a 40° angle of attack, a zero degree bank angle, and zero yaw.

At the entry/TAEM interface, the TAEM guidance (ref. 10) assumes control of the Orbiter and guides it to a tangent point on the heading alinement circle during the acquisition phase. Control is transferred to the heading alinement phase when the Orbiter is within a specified distance from the alinement circle. This phase is designed to aline the Orbiter to the runway. When the Orbiter is within a specified range of the runway threshold, the prefinal phase is initiated to guide the Orbiter to satisfy the autoland transition criteria. Nominally, the transition to the A&L phase occurs at an altitude of approximately 10 000 feet. During the TAEM phase, the navigation system maintains three state vectors until MSBLS acquisition or landing, whichever occurs first. After MSBLS acquisition, only the last midselected state vector is updated.

The autoland guidance goes first into a trajectory capture mode. Then it tracks the steep glideslope to an altitude of 2000 feet, at which point a pullup maneuver is expected to achieve the desired shallow glideslope. A final flare is performed just before landing.

7.0 DISCUSSION

This section presents a discussion of the simulation results for the EOM steep AOA and shallow AOA atmospheric descents. Figures 1 through 12 contain data for the EOM descent, figures 13 through 22 contain data for the steep AOA descent, and figures 23 through 28 contain data for the shallow AOA descent.

7.1 ATMOSPHERIC DISPERSIONS

Figures 1 and 13 present the atmospheric dispersions for the month of April with respect to the 1962 Standard Atmosphere (ref. 17) and the wind magnitudes and headings for altitudes greater than 800 feet. Figures 2 and 14 present the lower altitude winds for EAFB and Northrup, respectively. The lower altitude winds, which include turbulence (ref. 18), are generated by sampling peak wind statistics at the surface, which describe the wind magnitude distributions between 8:00 and 11:00 a.m. at EAFB or Northrup during April. Wind heading statistics at the surface are sampled, and a wind-turning function is used to relate the 2-kilometer rawinsonde data point to the surface wind heading. Upon landing all wind magnitudes are less than 10 knots at Northrup, but two cases (10 knots and 11 knots) at EAFB were greater than or equal to the crosswind constraint of 10 knots. The statistical atmospheres and winds aloft were generated by using a nominal STS-1 trajectory tape as input to the 4-D global reference atmosphere program (ref. 6). The atmospheres are a function of altitude, longitude, latitude, and month, and they are consistent with the Space Shuttle Orbiter environment specifications (ref. 19).

Density gradients are shown on the density dispersions plot in figures 1(a) and 13(a). These gradients cause the actual drag acceleration, which makes it more difficult to fly the descent profile. Note that the density deviation from the 1962 Standard Atmosphere can be as high as 60 percent at an altitude of 330 000 feet. In the altitude interval between 80 000 feet and 200 000 feet, the mean deviation for April is within 5 percent of the 1962 Standard Atmosphere. This results in a small mean deviation in the altitude error when the drag altitude is incorporated in the navigation data processing.

Pressure dispersions of the atmosphere (figs. 1(c) and 13(c)) affect the baro-altitude measurements. Dispersed static pressures are input to the ADS simulation. This, in turn, derives a pressure altitude. The ADS uses a curve fit based on a 1962 Standard Atmosphere to derive pressure altitude. This pressure altitude is corrected based on a nonstandard monthly mean model and a baro-set, which calibrates the barometer to measured pressure at the landing site before landing to minimize the effects of the nonstandard atmospheres. Because only seasonal nonstandard corrections are available, this analysis used the April corrections above an altitude of 12 000 feet mean-sea-level altitude. Below 12 000 feet, the baro-set was used.

Note that the wind magnitudes (fig. 1(d)) are not constant like the design wind (ref. 11), but instead, exhibit significant wind shears. At approximately 36 000 feet (jet stream), wind magnitudes approach the design values. The average wind heading (fig. 1(e)) is approximately 90 degrees. The discontinuities in the plot of wind heading reflect the crossing of the 180° wind heading rather

than wind heading change. For the AOA case (figs. 13(d) and 13(e)), the wind magnitude and direction were held constant above an altitude of 240 000 feet because the winds generated by the atmosphere program (ref. 6) are not valid when crossing the equator.

7.2 NAVIGATION PERFORMANCE

The navigation measurement incorporation schedule for the EOM steep AOA and shallow AOA is presented in table IV. First, drag altitude is initially processed when the drag acceleration is greater than 11 fps (240 000 feet altitude) and is terminated at an altitude of 85 200 feet or when the barometric altitude is valid, whichever occurs first. Tacan data are initially processed at an altitude of approximately 130 000 feet and are terminated when the MSBLS data are valid or at landing, whichever occurs first. Delaying the incorporation of the Tacan data until reaching 130 000 feet altitude is considered conservative. The decision to incorporate data at 130 000 feet altitude was made as a result of Tacan redundancy management (RM) analysis. This analysis shows that in the two line replacement unit (LRU) cases where a dilemma has occurred, ground and crew assessment of the data would be required. Solution of the dilemma may result in delaying Tacan data incorporation until an altitude of 130 000 feet is reached. Table V presents the Tacan stations used in this analysis. These stations were selected along the groundtrack to improve the altitude channel by using Tacan data.

Figures 3, 15 and 25 present the navigation-derived and/or ADS-derived parameter performance. Figure 3(a) shows that in the three-sigma case, the FCS accuracy requirements (ref. 20) for dynamic pressure will be violated for Mach numbers of less than 8. The divergence in the errors that occurr in the lower Mach number region (Mach 2.5 to Mach 7) is primarily caused by winds and C_d variations. The formula for deriving dynamic pressures uses Earth-relative velocity, which does not contain the effects of wind and is therefore sensitive to wind. Below Mach 2.5, when the ADS dynamic pressure is used, the errors in the three-sigma case slightly exceed the requirements (ref. 21) during the Mach jump region (Mach 0.9 to Mach 1.6). In this region, dynamic pressure is sensitive to navigation error because the navigation altitude is used to derive the free-stream static pressure, which in turn is used in deriving dynamic pressure. Dynamic pressure is used in moding the FCS and in computing FCS gains. Studies on integrated GN&C simulations are required to determine the effects of the dynamic pressure accuracies on the FCS performance.

Figures 3(b) and 15(b) present angle-of-attack accuracy. The angle-of-attack error (above Mach 2.5) is the difference between the navigation-derived angle of attack and the actual angle of attack. Below Mach 2.5, the angle-of-attack error is the difference between the ADS angle of attack and the actual angle of attack. The biggest contributor to errors in the navigation-derived angle of attack is wind because the navigation routine derives angle of attack from the navigation Earth-relative velocity, which does not include the effects of winds. Angle-of-attack errors are cleaned up by the ADS below Mach 2.50. Figures 3(c) and 15(c) present the Mach number errors. The baro-altitude performance is shown in figures 3(d) and 15(d). These figures show that the ADS altitude accuracy requirements are satisfied everywhere except the Mach jump region. Since

the navigation system does not use the baro-altitude in this region, the degraded baro-altitude data did not cause any problems.

The navigation state vector performance is shown in figures 4, 16, and 26. Figures 4(g) and 16(g) show the Tacan station locations relative to the ground-track. Altitude errors and altitude rate errors are the navigation data minus actual data for these two parameters, respectively. All other state vector errors are equal to the actual quantity minus navigation quantity. The errors are computed in a radial, downrange, crossrange (UVW) coordinate system determined by the actual state. Altitude and attitude rate errors are plotted in these figures in place of the radial position error and the radial rate error. The accuracy requirements (ref. 22) used in these figures are used by open loop navigation analysts as an indicator of performance. While the meeting of these constraints ensures satisfactory performance, the violation of them does not necessarily mean unacceptable performance. Integrated guidance and navigation performance analyses such as this Monte Carlo analysis provide a more direct method of assessing the navigation performance.

Note the small mean altitude error on the altitude error plots an an altitude of 150 000 feet. This mean bias is introduced into the state vector by the drag altitude measurement and by tne mismatch between the atmosphere model (1962 Standard Atmosphere) used in the drag-altitude algorithm and the mean of the atmosphere used in the environment (April). This error would be larger for some other time of the year. The downrange error data illustrate how the drag altitude measurement bounds the downrange error through the correlation in the covariance matrix during the drag altitude updating region. Table VI presents a statistical summary of the state vector navigation errors, and table VII presents the state vector dispersion. All the samples were taken at a constant altitude except the entry/TAEM interface and the TAEM/autoland interface samples. These were sampled on the first pass of each particular phase. The errors are expressed in a UVW coordinate system defined at each sample, where U is a radial, V is downrange, and W is crossrange.

7.3 TPS PERFORMANCE

The TPS surface temperatures were evaluated at five control points as well as the backface temperature on panel 2, using the simplified TPS model presented in reference 7. Reference point heat load and heating rate were also evaluated. Table I contains the temperature limits that were used as part of the success criteria. The TPS material temperature limit for the high-temperature reusable surface insulation (HRSI) material is the limit for one-mission capability and greater than the one-mission capability for the reinforced carbon carbon (RCC) reusable material. Because the TPS surface temperatures are computed by using a simplified TPS model that assumes equilibrium radiation, these limiting temperatures have been adjusted to account for inaccuracies in surface temperature prediction by the simplified model.

The method for computing the temperature dispersion has been changed. Previously, statistics were computed on the maximum temperatures on each control point, and the point where the maximum temperatures occurred was variable. This method biases the mean to the high side and reduces scatter in the data. A more realis-

tic approach is to observe the scatter traces and select the velocity where the maximum dispersed temperatures occur on each control point. Statistics are then computed at these selected velocities. In general, this gives a lower mean and a larger scatter in the data. Also, another change made was to treat the body flap and elevon temperature dispersions as uniformly distributed. To arrive at the maximum dispersion used for the body flap and elevon, a cumulative distribution of the data is plotted on probability paper, and an estimate of the maximum is made using the plotted data. The assumption of a uniform distribution results in a reduction of approximately 100° in the maximum body flap temperature. The distribution was checked for all five control points, and control points 1, 3, and 6 were found to be normally distributed.

Tables VIII, IX and X summarize the TPS performance as a function of velocity at the five control points. For all cases, the wing indicated negative margins after three-sigma dispersions and aero heating uncertainties are considered. The AOA cases also show negative margins on the forward chine and on backface temperatures. The negative margins on the wing leading edge, forward chine, and panel 2 can be absorbed by the aerodynamic heating uncertainty. Even though the aerodynamic heating uncertainty on the backface temperature on panel 2 is not as large as the uncertainties on the surface temperatures, it is still the main cause for the negative margin. Detailed analysis of the TPS performance is required by systems specialists. Figures 5, 17, and 27 are scatter plots of heat rate and heat load. Figures 6, 18, and 28 summarize the TPS performance. Also plotted on these figures are the three-sigma wing leading edge and nose and forward chine temperature variations caused by trajectory dispersions. These three-sigma lines are not included for the body flap and elevon because they are not normally distributed. The lines labeled "includes deflection allowances and aerodynamic heating uncertainties" are generated by root-sum squaring the tra-ectory dispersions, random deflection allowances, and aeroheating uncertainties and by adding to the bias deflection allowances and the mean surface temperatures. Deflection allowances are made Yc.g. offset, manufacturing tolerances, maneuver capability, bending under load, and mechanical sensor position error (ref. 23). The effects of pitching moment uncertainty on the elevon and effects of body flap dead band (ref. 23) are already included in the trajectory dispersions from the Monte Carlo simulations. The data do not include the effects of errors in sideslip angle or any lags that may exist in the FCS. The point where transition from laminar flow to turbulent flow occurs is sensitive to the transition criteria. Using the simplified TPS model, this occurs (in most cases) after the body flap is no longer saturated. Detailed thermal analysis is required to verify the control surface temperatures using the flight environment and surface deflections defined in the analysis.

7.4 CONTROL SURFACE DEFLECTIONS AND HINGE MOMENTS

Table II contains the elevon, body flap, and speedbrake hinge moment capability (ref. 9). The values in the table were used as part of the success criteria. These values are the stall limits and, for the elevon only, a soft limit at a deflection of 4° from the schedule and a required rate of 10 deg/sec. The 4° elevon deflection accounts for transient surface deflections required for attitude maneuvers and deflections required for Yc.g. trim that are not included in a 3-DOF simulation. Figures 7, 19, and 29 present the control surface deflec-

tions and hinge moments. Also shown on the elevon hinge moments plots are the stall limits and the soft limit presented in table II. Normal load factor effects were included in the simulation. The activity in the elevon deflection traces at Mach 14 occurs where the switch is made from viscous to nonviscous aerodynamics. Speedbrake, elevon, and body flap moments are satisfactory. Figure 7(b) indicates that the body flap is being saturated (in the up direction) in some cases during TAEM, which will drive the elevon slightly off schedule. The body flap is also observed to be pegged up or down at high altitudes because of large pitching moment uncertainties.

7.5 GUIDANCE PERFORMANCE

Figures 8 through 10, 20 through 22, and 30 through 31 present the guidance performance parameters. Actual data, instead of navigation data, are plotted unless otherwise stated. These figures are divided into the entry guidance performance parameters (figs. 8, 20, and 30), the TAEM guidance performance parameters (figs. 9, 21, and 31), and the autoland guidance performance parameters (figs. 10 and 22).

7.5.1 Entry

For the EOM trajectory, figure 8(a) presents the angle-of-attack envelope expected from EI to landing. The entry guidance uses the navigated angle of attack to fly a preprogramed angle-of-attack profile. The dispersions in the actual angle of attack are due mainly to angle-of-attack modulation to control short-period response to the reference drag profile, IMU misalinements, winds, and L/D dispersions. The vertical traces seen around a velocity of 24 000 fps represent the angle-of-attack history during the coast after the deorbit burn. At 24 000 fps, one of the traces droops below the rest of the traces. This is typical of a low L/D case. A couple of cases stand out above the rest around a velocity of 23 000 fps. For these cases, the drag acceleration is less than the drag reference so that the alpha modulation is delayed until a velocity of 23 000 fps is reached. At this point, the alpha modulation is initiated resulting in a small transient in the angle of attack. The effects of bank reversals on angle of attack are shown at velocities of 9000 and 18 000 fps. The location of the first bank reversal depends on the initial crossrange and can occur at any speed. The change in angle of attack that occurs at TAEM interface (velocity = 2500 fps) is the result of the bank reversal in TAEM required to guide the Orbiter to the heading alinement cylinder (HAC) circle tangent point, altitude errors, latitude rate errors, and energy errors from the reference values. When the Orbiter rolls over the top during TAEM, the coordinated turn compensation logic in the FCS reduces angle of attack in order to maintain 1 g in the vertical direction. Also, because the TAEM guidance flies to a reference altitude and altitude rate, deviations from the reference result in changes in angle of attack.

The bank angle and navigation heading error histories for the EOM (figs. 8(d) and 8(e) show that all of the cases are headed toward the HAC circle tangent point and do not require a bank reversal at TAEM initiation. The maximum heading error (navigated heading to the HAC) at TAEM initiation, is approximately

+16°. The minimum reference bank angle (fig. 8(b)) at the end of entry is approximately 30°. This indicates that entry guidance has delivered the vehicle to TAEM with more than adequate ranging margins in all cases. Figure 8(f) presents the drag reference profiles computed by the entry guidance. Entry does not fly a preselected drag reference, but instead, recomputes the reference every 1.92 seconds on each simulated entry based on the existing conditions. The effects of the state vector updates on the drag reference when Tacan measurements are incorporated can be seen on these figures at a velocity of approximately 6000 fps. Transients in the drag reference, at this point, are caused by the guidance response to the state vector updates. These transients are insignificant. The drag reference dispersions at TAEM interface also indicate that the ranging maneuver margin is adequate. Other indicators of maneuver margin at TAEM interface are normal load factor, angle of attack, bank angle, and range error. Figure 8(g) presents the actual drag acceleration histories. Several limit lines and OFT-1 guidelines converted to the drag velocity plane are shown on these plots. Figure 8(h) presents the normal load factors expected for STS-1 and shows that the margins during the entry phase are adequate. Figures 8(i) through 8(u) present the dispersions in several aerodynamic parameters that will be useful for postflight analysis.

For the AOA trajectories, the discussion of most of the figures is similar to the discussion of the corresponding figures for the EOM and will not be repeated. Because the AOA trajectory to Northrup required less crossrange maneuverability than an AOA to Edwards, the trajectory performance is very similar to the EOM.

7.5.2 TAEM

The discussion of the figures during the TAEM phase is very similar for the EOM and AOA; therefore both sets of figures will be discussed simultaneously.

Figures 9, 21, and 31 present the TAEM guidance performance parameters. Actual energy as a function of predicted navigated range during the TAEM phase are illustrated in figures 9(a), 21(a), and 31(a). The S-turn boundary, minimum entry point boundary, and the entry/TAEM accuracy requirements are also included. The results on figures 9(a), 21(b), and 31(b) show that there are no MEP's and no S-turns and that the entry guidance delivered the Orbiter well within the entry TAEM accuracy requirements. Figures 9(b), 21(b), and 31(b) present actual altitude as a function of predicted navigated range-to-go to the runway threshold. Note how the dispersions are reduced at an altitude of 18 500 feet when the MSBLS is acquired. Figures 9(c), 21(c), and 31(c) present the dynamic pressure dispersions.

Also plotted in this figure are the structural design limit line, the flight control design constraint line, and the sonic boom 2-psf over-pressure guideline. Most cases cut across the sonic boom 2-psf over-pressure line. The sonic boom boundary is a function of angle of attack and dynamic pressure. Analysis with similar dynamic pressure dispersions has shown maximum over-pressure of approximately 2.2 psf for the nominal entry. Figures 9(d), 21(d), and 31(d) present the angle-of-attack dispersions. Several limit lines are also plotted on these figures. These are the FCS design limits rolloff, nose slice, buffet onset

line, Cn^{β} dynamic and lateral trim constraint line, and the venting constraint line. Several cases violated the Cn^{β} dynamic and lateral trim constraint line in the angle-of-attack-velocity plane. This constraint line was generated with the April 1979 aerodynamic data, Xc.g. = 66.7 percent, trim flight, 1-inch Yc.g. offset, worst-case elliptical variations, two yaw jets used for trim, maximum sideslip of 1.5°, and bent airframe effects. This line is based upon the assumption of equilibrium flight. Since equilibrium flight is not maintained, these boundaries are more accurately defined as a function of dynamic pressure so the dispersion data were compared to the constraints in the angle of attack and dynamic pressure plane (figs. 9(e) through 9(k), figs. 21(e) through 21(k), and figs. 31(e) through 31(k)) at several Mach numbers. These data indicate that all the dispersed cases remained inside the constraints during TAEM. Violations of the Cn^{β} dynamic and lateral trim line (figs. 9(d), 21(d), and 31(d)), and the rolloff, nose slice, and buffet onset line require more detailed analysis by system specialists.

Figures 9(l), 21(l), and 31(l) present the bank-angle histories. The bank-angle history data define the effects of the navigation state vector updates on the bank angle when the Tacan is acquired. This occurs at a velocity of approximately 6000 fps. Some activity is seen around this region but none of any significance. The point at which the heading alinement phase begins is clearly seen on these figures at a velocity of approximately 800 fps. Figures 9(m), 21(m), and 31(m) present pitch angle as a function of velocity. These figures show that there were no tailscrapes and that adequate margins exist. Figures 9(n), 21(n), and 31(n) present normal load factors as a function of velocity. Normal load factors, as seen in these figures, are approximately 2.00 g's three-sigma during the heading alinement phase, primarily because of a tailwind. These require large bank angles to stay on the circle and in turn, cause large normal load factors. Also, when MSBLS cleans up the state vector, the guidance drives the Orbiter back to the reference profile, and some of these maneuvers lead to large normal load factors. Figures 9(o), 21(o), and 31(o) present the altitude rate dispersions. These figures show that none of the cases violated the venting constraint line.

7.5.3 Autoland

Fifty randomly selected EOM trajectories and 50 AOA trajectories, initialized at an altitude of 9950 feet, were analyzed using the 6-DOF option of the LAND program. The 6-DOF simulation included all of the error models used in the 3-DOF simulations. In addition, the 6-DOF simulation included the FCS documented in reference 15 and the turbulence model documented in reference 18.

Figures 10 and 22 present the autoland guidance performance parameters. The sampling technique for the initial state errors does not include wind effects so that the dynamic pressure may exceed the autoland capture criteria. As a result, initial performance is conservative. The results are representative shortly after the initialization point. Figures 10(a), 22(a), 10(b), and 22(b) (groundtrack and altitude range) indicate that all simulations were satisfactorily delivered to the vicinity of the runway threshold. Figures 10(c) and 22(c) show that all of the cases landed on the runway. The 0.5° elevation line in the figure represents the elevation angle below which no elevation data will be

available from the MSBLS. Figures 10(d) and 22(d) indicate the transition point to the final flare maneuver. The radial rate error, navigation minus actual, is shown in figures 10(e) and 22(e). The bias that builds up below an altitude of 225 feet is the result of using the MSBLS elevation data between 1.3° and 0.5° elevation angle. In this region, the model used (which is considered realistic) exhibits a mean bias in the elevation measurement. Figures 10(f) and 22(f) present dynamic pressure versus navigated range. Navigated range was selected as the independent parameter because the actual range was unavailable. Because the MSBLS measurements are very accurate, the navigated range is a good approximation of the actual range. Also plotted in figures 10(f) and 22(f) are the flight control system design limit line and certification criteria line. The dynamic pressure dispersions in these figures are acceptable. Figures 10(g) and 22(g) present the angle-of-attack dispersions and show adequate margins with respect to the flight control system design limit. Sideslip angle, bank angle, and pitch angle presented in figures 10(h), 22(h), 10(i), 22(i), 10(j), 22(j), respectively. Figures 10(j) and 22(j) indicate that there are not tailscrape cases. Normal load factors (figs. 10(k) and 22(k)) are less than the STS-1 guideline of 2 g's. Figures 10(e) and 22(e) present the altitude rate and figures 10(m), 10(n), 10(o), 22(m), 22(n), and 22(o) present the body rates.

The elevator deflection (figs. 10(p) and 22(p)) exhibits an increase when the body flap is retracted (figs. 10(r) and 22(r)) to the trial position at autoland guidance initiation. A decrease in the elevator setting occurs when the speedbrake is retracted (figs. 10(s) and 22(s)) prior to the preflare maneuver. This decrease, in four cases (fig. 10(p)), was delayed until a range of approximately 9000 feet because the speedbrake for these cases was not retracted until an altitude of 1000 feet (fig. 10(s)). Figures 10(q) and 22(q) present the aileron histories, and figures 10(t) and 22(t) present the rudder deflections. The maximum allowable surface rates in the LAND program are functions of the hinge moments. The control surface rates are presented in figures 10(u) through 10(y) and figures 22(u) through 22(y). Hinge moments are presented in figures 10(z) through 10(ff) and figures 22(z) through 22(ff). The elevon hinge moments are conservative because the total variation in the hinge moment coefficient is assumed to be the same for the inboard and outboard elevons. The data book specifies that the variation must be divided by the square root of two. Stall limits and soft limits based on a required rate (ref. 9) are also plotted on the hinge moment traces. All of the hinge moments are acceptable.

Table XI presents the landing statistics. The statistics are given in terms of the mean, maximum value, and minimum value (instead of means and sigmas) because the distribution of some of the listed parameters cannot be reasonably approximated by a normal distribution (figs. 11 and 23). Figures 12 and 24 present the cumulative distribution of the surface winds for EAFB and Northrup, respectively. These winds are valid for Runway 23 at EAFB or Runway 17 at Northrup for the month of April between 9 and 11 a.m. local time. For EAFB, 2 out of 50 cases had crosswinds at landing, which were greater than or equal to 10 knots. The landing statistics indicate that 5 out of 50 EOM landings and 5 out of 50 AOA landings exceeded the tire specification limit speed of 222 knots. Because the landing is expected to be manual, rather than using the autoland guidance for STS-1, the pilot landing techniques are expected to increase the landing point dispersion to reduce the landing speed within landing gear constraints and improve energy margin.

8.0 CONCLUSIONS

For the EOM, the surface temperatures are acceptable. Structure temperatures are also acceptable because of the preentry thermal conditioning. For the steep AOA, the surface temperatures are acceptable, but the structure temperatures are marginal because there is no preentry thermal conditioning. For the shallow AOA, the surface temperatures are high, and the structures temperatures are marginal. These results are based on the simplified TPS model (ref. 7) included in the simulation. Detailed analysis of the envelope of flight conditions and control surface deflections should be made as a part of certifying the first flight readiness. Speedbrake, elevon, and body flap hinge moments are acceptable. Range dispersions at entry/TAEM interface are within the accuracy requirement of 5 miles. All the landing simulations transitioned to autoland before reaching an altitude of 7000 feet. Also, there are no MEP's, S-turns, or tailscrapes. Navigation-derived pressure accuracies exceed the flight control system constraints below Mach numbers of less than 8, and several cases violated the C_{n_β} dynamic and lateral trim constraint line assuming equilibrium flight. Normal load factor transients occur at MSBLS acquisition and at TAEM/autoland interface. Out of 50 EOM landings and 50 AOA landings, 5 each exceeded the tire specification limit speed of 222 knots. The tire certification limit speed of 218 knots was exceeded five times at EAFB and seven times at Northrup. Crosswind magnitudes at landing were all less than 10 knots at Northrup, but two cases (10 knots and 11 knots) at EAFB were greater than or equal to the crosswind constraint of 10 knots.

Violation of navigated-derived dynamic pressure between Mach 8 and 2.5 will affect the FCS moding and gains to some degree because dynamic pressure is used to perform the moding and gain scaling. Assuming equilibrium flight, several cases violated the C_{n_β} dynamic and lateral trim constraint line. This constraint line was generated with April 1979 aerodynamic data, $X_{c.g.}$ = 66.7 percent, trim flight, 1-inch $Y_{c.g.}$ offset, worst case elliptical variations, two yaw jets used for trim, maximum sideslip of 1.5 degrees, and bent airframe effects. Integrated GN&C analysis is required to determine the effect of violating the navigation-derived dynamic pressure error constraint and the effect of violating the C_{n_β} dynamic and lateral trim and the rolloff, nose slice, and buffet onset constraint. The ADS altitude accuracy requirement line is violated during the Mach jump region. These violations did not cause any problems because the navigation system does not use the baro-altitude during the Mach jump region. Several metering methods were used to reduce the normal load transients at MSBLS acquisition but were unsuccessful. Therefore, the pilot should expect these transients. The landing statistics indicate that 5 out of 50 EOM landings and 5 out of 50 AOA landings exceeded the tire specification limit speed of 222 knots. Because the landing is expected to be manual rather than using the autoland guidance for STS-1, the pilot landing techniques are expected to increase the landing point dispersion to reduce the landing speed within landing gear constraints.

9.0 REFERENCES

1. Mission Planning and Analysis Division: STS-1 Operations Flight Profile, Descent Cycle 3. May 1980.

2. Venables, G.: MDTSCP AOA Steep Linear Dispersion Analysis for STS-1 Cycle 3 (to be published).

3. Venables, Glen: MDTSCP AOA Shallow Linear Dispersion Analysis for STS-1 Cycle 2 Prime, TM 1.4-TM-D1131-080, July 30, 1979.

4. Mission Planning and Analysis Division: Operational Flight Profile Deorbit to Landing, Appendix C - Monte Carlo Dispersion Analysis. JSC IN 78-FM-51, May 1979.

5. Wollenhaupt, W. R.: Pre-Deorbit Navigation Uncertainties for OFT-1 Nominal Deorbit. JSC Memorandum, FM85 (78-263), June 30, 1978.

6. Justus, C. G.,: Woodrum, A. W.; Roper, R. G.; and Smith, O. E.: Four D Global Reference Atmosphere, NASA TMX-64872, September 1974.

7. Rockwell/Houston Simplified Weight Synthesis Program (Rev. 3). Rockwell International, SEH-ITA-75-192, May 1978.

8. Faget, M. A.: Thermal Data Input for Support of OFP Cycle 3. JSC Memorandum ES32-7/78-87m, August 2, 1978.

9. Barton, Richard L.: Hinge Moment Constraints for Monte Carlo Program. JSC Memorandum EX43/7903-21, March 30, 1979.

10. Space Shuttle Orbital Flight Test Level C Functional Subsystem Software Requirements Document, - Guidance, Navigation, and Control (Part A) Guidance, Entry through Landing, SD-76-SH-0001C, December 15, 1978.

11. Shuttle Operational Data Book, Shuttle Systems Performance and Constraints. Systems Requirements and GFE Branch, Integration Division, Program Office. JSC-08934, Vol. I, Rev. A, Amendment 74, October 1976.

12. Orbiter Vehicle End Item Specification for the Space Shuttle System Part 1, Performance and Design Requirements. Rockwell International MJ070-0001-1B, January 15, 1976.

13. Aerodynamic Design Data Book - Vol. Orbiter Vehicle, Rev. K. Rockwell International, SD72-SH-0600-L, October 1978. (with April 1979 update).

14. Mission Planning and Analysis Division: STS-1 Operational Flight Profile Groundrules and Constraints - Cycle 3. JSC 14483, Vol. I, Rev. 2, September 1979.

15. Space Shuttle Orbital Flight Test Level C Functional Subsystem Software Requirement Document - Guidance, Navigation, and Control (Part C) Flight Control, Entry through Landing, SD-76-SH-0007B, May 1, 1979.

16. Hooks, I. F.,: Data to Support Entry FCS FSSR Usage, Memorandum FR-94-79, July 18, 1979.

17. U. S. Standard Atmosphere. NASA, USAF, USWB, 1962.

18. Fichtl, G. H.: Stochastic Wind and Turbulence Models for Application to Monte Carlo Simulation of Return Trajectories of the Space Shuttle Orbiter for 30 Km to the Surface at JSC. MSFC Memorandum S and E-AEROYA-44-73, July 10, 1973.

19. Smith, O. E.: A Global Reference Atmosphere for Space Shuttle Engineering Analysis. MSFC Memorandum ES42-7-75, March 19, 1976.

20. Orbital Flight Test Program Phase II (Entry) Systems Design Review. Rockwell International. SV75-BB, September 1975.

21. Air Data Substantiation Report. STS Aero Sciences, Rockwell International SD75-SH-0038, Rev. B. December 1978.

22. Entry Navigation Analysis. Presentation made by Neil Hutchinson to Arnie Aldrich, February 3, 1977.

23. Johnson, B. C.: Updated Design to and Evaluation Control Surface Deflections. Rockwell International Internal letter SAS/MR and I-75-164, November 5, 1979.

TABLE I.- SIMPLIFIED TPS MODEL SURFACE AND STRUCTURE TEMPERATURE LIMITS

Control point	Location/material	Temperature, limit °F
1	Nose, RCC	2950
2	Body flap, HRSI	2600
3	Wing-leading edge, RCC	2950
4	Elevon, HRSI	2600
6	Fwd chine, HRSI	2700
	Backface temperature panel 2	350

TABLE II.- CONTROL SURFACE ACTUATOR HINGE MOMENT CONSTRAINTS

Control surface	Stall hinge moment x 10^6, in.-lb, HM_{STALL}	Soft limit[a] hinge moment $\pm$ 10^6, in.-lb	Reference dimension, ft^2-in.(Sc)	Maximum rate, deg/sec	Surface weight, lb, W	Moment arm, in., ℓ	Comments
Inboard elevon	$\pm$0.955	$\pm$0.90	19 047	43	1220	37.3	MOOG actuator at 2900 psi near $\delta_e = 0$
Outboard elevon	$\pm$.460	$\pm$.44	19 047	43	728	26.8	
Body flap	$\pm$1.400		10 935	1.5	1325	24.3	For two hydraulic systems operation
Speedbrake	$\pm$ 2.400		7 331	16.0	Not applicable		For two hydraulic systems operation
Rudder	$\pm$.750		7 331	23.0	Not applicable		For two hydraulic systems operation

[a]This column was added to aid in interpreting hinge moments generated by 3-DOF programs that do not reflect transient elevon deflections required for rapid attitude maneuvers. These hinge moments correspond to a 10-deg/sec rate on the actuator capability curve.

TABLE III.- AUTOLAND CAPTURE ZONE

Altitude, ft	Altitude[a] error, ft	Crossrange error, ft	Flightpath angle error, deg	Dynamic pressure error, psf
>10 000	1000	1000	4	24
10 000	1000	1000	4	24
[b]5 000	50	100	.5	24

[a]All errors are with respect to the reference values.
[b]Linear ramp as a function of altitude between 10 000 and 5000 feet.

TABLE IV.- MEASUREMENT INCORPORATION SCHEDULE

Measurement	Nominal measurement[a]		
	Incorporation altitude, ft		
	EOM	Steep AOA	Shallow AOA
Drag altitude	240 000		240 000
First Tacan station acquisition[b]	157 200 San Luis Obispo (SBP)	155 900 Douglas (DUG)	155 600 Douglas (DUG)
Second Tacan station acquisition	114 900 Avenal (AVE)	111 300 Columbus (CUS)	113 000 Columbus (CUS)
Third Tacan station acquisition	110 100 Fellows (FLW)	103 300 Deming (DMG)	101 800 Deming (DMG)
Fourth Tacan station acquisition	105 300 Bakersfield (BFL)	79 200 Holloman (HMN)	78 800 Holloman (HMN)
Fifth Tacan station acquisition	95 900 Gorman (GMN)		
Sixth Tacan station acquisition	82 300 Mobile (MBL)		
Barometric altimeter	82 900	80 500	81 270
MSBLS	18 500	18 500	18 500
Radar altimeter[c]	100	100	100

[a]Altitude with respect to runway.
[b]Data are not incorporated until an altitude of 130 000 feet.
[c]Radar altimeter data sent directly to the autoland guidance.

TABLE V.- TACAN STATION LOCATIONS STS-1

Location	Channel	ID	Latitude	Longitude	Altitude
		End of mission			
San Luis Obispo	71	SBP	35.252200N	120.759535W	1262
Paso Robles	90	PRB	35.672467N	120.627037W	618
Gaviota	112	GVO	34.531392N	120.090901W	2418
Avenal	118	AVE	35.646917N	119.978411W	506
Fellows	122	FLW	35.093044N	119.865624W	3695
Bakersfield	101	BFL	35.484615N	119.097326W	359
Gorman	108	GMN	34.804171N	118.861431W	4714
Mobile[a]	11	MBL	34.938140N	106.403893W	2364
Mobile[a]	69	PMD	32.940857N	106.403893W	3771
Edwards	111	EDW	34.982385N	117.73254W	2127
		Abort once around			
Tuscon	118	TUS	32.122633N	110.820659W	2687
Cochise	105	CIE	32.033475N	109.758132W	4077
Douglas	25	DUG	31.472660N	109.602013W	3996
Edwards	111	EDW	34.982385N	117.732540W	2127
Silver City	55	SVC	32.637631N	108.161152W	5260
Columbus	49	CUS	31.819047N	107.574465W	3852
Deming	23	DMN	32.275077N	107.605580W	4159
Truch	74	TCS	33.282338N	107.280578W	4764

[a]U.S. Air Force mobile Tacan station.

TABLE V.- Concluded

Location	Channel	ID	Latitude	Longitude	Altitude
Holloman	85	HMN	32.862078N	106.108879W	3936
Mobile	69	MBL	32.940857N	106.403893W	3771

TABLE VI.- STATE NAVIGATION ERRORS (NAV-ACTUAL) (3-SIGMA)

Parameter, unit	Deorbit ignition	Entry interface (H = 400 000 ft)	Postblackout (H = 140 000 ft)	Entry/TAEM interface (V = 2500 fps)	TAEM/autoland interface (H = 10 000 ft)	Landing
			End of mission			
U, ft[a]	4 134	4 370	6 628	1 889	43	11
V, ft[a]	30 048	47 845	36 981	1 151	47	49
W, ft[a]	2 583	2 913	13 405	1 623	56	12
UDOT, fps	33.9	55	36	17	1.7	1.5
VDOT, fps	4.2	5	21	13	1.6	2.1
WDOT, fps	3.3	5	33	17	2.4	1.1
H, ft		4 433	[b]6 641	1 855	43	11
HDOT, fps		3.5	25	17	1.7	1.5
GAMMA, deg		.008	.20	.40	.17	.24
			Shallow abort once around			
U, ft		17 160	6 995	1 856	45	9.
V, ft		388 937	44 839	1 349	55	50
W, ft		29 941	9 223	1 771	61	13
UDOT, fps		90	42	14	1.8	1.4
VDOT, fps		16	24	10	2.2	1.7

[a]U = radial, V = downrange, and W = crossrange.
[b]Mean error 4600 feet.

TABLE VI.- Concluded

Parameter, unit	Deorbit ignition	Entry interface (H = 400 000 ft)	Postblackout (H = 140 000 ft)	Entry/TAEM interface (V = 2500 fps)	TAEM/autoland interface (H = 10 000 ft)	Landing
			Abort once around			
WDOT, fps		6	26	14	3.3	1.2
H, ft		17 234	6 984	1 856	45	9
HDOT, fps		15	27	14	1.8	1.4
GAMMA, deg		.035	.2	.3	.2	.2
			Steep abort once around			
U, ft		17 265	7 657	1 920	43	9
V, ft		82 600	37 484	1 029	50	56
W, ft		27 239	8 109	2 001	52	15
UDOT, fps		81	40	17	2.2	1.3
VDOT, fps		16	23	7	2.0	2.0
WDOT, fps		10	27	16	3.2	1.0
H, ft		16 773	7 645	1 920	43	9
HDOT, fps		21	27	17	2.2	1.3
GAMMA, deg		.049	.2	.4	.2	.2

TABLE VII.- STATE DEVIATIONS (ACTUAL REFERENCE) (THREE-SIGMA)

Parameter, unit	Entry interface (H = 400 000 ft)	Entry/TAEM interface (V = 2500 fps)	TAEM/autoland interface (H = 10 000 ft)
	End of mission		
U, ft	1 327	6 276	2 588
V, ft	313 815	10 707	7 158
W, ft	3 482	26 973	176
UDOT, fps	358	118	38
VDOT, fps	6	54	103
WDOT, fps	17	676	18
H, ft	977	6 315	2 596
HDOT, fps	5	118	38
GAMMA, deg	.012	2.7	.49
	Shallow abort once around		
U, ft	53 222	5 428	737
V, ft	2 622 284	10 682	2 061
W, ft	35 896	16 675	184
UDOT, fps	3 048	141	30
VDOT, fps	65	72	79
WDOT, fps	169	588	18
H, ft	358	5 406	743
HDOT, fps	39	141	30
GAMMA, deg	.09	3.28	.62

TABLE VII.- Concluded

Parameter, unit	Entry interface (H = 400 000 ft)	Entry/TAEM interface (V = 2500 fps)	TAEM/autoland interface (H = 10 000 ft)
	Steep abort once around		
U, ft	11 959	5 292	397
V, ft	1 073 191	10 967	1 106
W, ft	28 799	21 750	155
UDOT, fps	1 250	126	30
VDOT, fps	25	63	79
WDOT, fps	48	561	16
H, ft	1 005	5 266	400
HDOT, fps	13	126	30
GAMMA, deg	.031	3.0	.6

TABLE VIII.- TPS PERFORMANCE EOM

(Maximum TPS Temperature, °F)

Control point	Control point location	Nominal	Mean	Trajectory	Surface deflection		Aero heating	Combined	3-sigma	Simplified model limit, °F	Margin, °F
					Bias	Random					
				Velocity = 24 000 fps							
1	Nose	2505	2495	90	0	0	180	201	2696	2950	254
2	Body flap	1217	1275	265	0	33	247	363	1638	2600	962
3	Wing	2654	2642	99	0	0	272	289	2931	2950	19
4	Elevon	1733	1729	55	4	34	135	154	1883	2600	717
6	Fwd chine	2469	2457	87	0	0	187	206	2664	2700	36
Panel 2		324	325	8			37	38	363	350	-13
				Velocity = 23 400 fps							
1	Nose	2520	2508	73	0	0	180	194	2703	2950	247
2	Body flap	1224	1276	256	0	33	247	357	1633	2600	967
3	Wing	2671	2657	80	0	0	272	284	2940	2950	10
4	Elevon	1744	1737	43	4	34	135	150	1887	2600	713
6	Fwd chine	2483	2471	72	0	0	187	200	2671	2700	29
				Velocity = 22 800 fps							
1	Nose	2524	2515	62	0	0	180	184	2698	2859	241
2	Body flap	1224	1278	221	0	33	247	333	1611	2600	989
3	Wing	2676	2654	124	0	0	272	299	2953	2950	-3

TABLE VIII.- Continued

(Maximum TPS Temperature, ^{o}F)

Control point	Control point location	Nominal	Mean	Trajectory	Surface deflection		Aero heating	Combined	3-sigma	Simplified model limit, ^{o}F	Margin, ^{o}F
					Bias	Random					
Velocity = 22 800 fps (concluded)											
4	Elevon	1747	1746	47	4	34	135	151	1897	2600	703
6	Fwd chine	2485	2478	70	0	0	187	200	2678	2700	22
Velocity = 22 200 fps											
1	Nose	2524	2523	62	0	0	180	190	2714	2950	236
2	Body flap	1667	1656	473	0	33	247	535	2190	2600	410
3	Wing	2676	2668	86	0	0	272	285	2953	2950	-3
4	Elevon	1747	1750	40	4	34	135	149	1899	2600	701
6	Fwd chine	2485	2485	60	0	0	187	196	2681	2700	19
Velocity = 21 600 fps											
1	Nose	2524	2525	61	0	0	180	190	2715	2950	235
2	Body flap	1970	2008	287	0	33	247	380	2388	2600	212
3	Wing	2675	2670	34	0	0	272	285	2955	2950	-5
4	Elevon	1747	1751	49	4	34	135	151	1903	2600	697
6	Fwd chine	2487	2487	58	0	0	187	196	2682	2700	18

TABLE VIII.- Continued

(Maximum TPS Temperature, ^{o}F)

Control point	Control point location	Nominal	Mean	Trajectory	Surface deflection		Aero heating	Combined	3-sigma	Simplified model limit, ^{o}F	Margin, ^{o}F
					Bias	Random					
				Velocity = 21 000 fps							
1	Nose	2521	2523	61	0	0	180	190	2713	2950	237
2	Body flap	1997	2034	251	0	33	247	354	2388	2600	212
3	Wing	2672	2669	90	0	0	272	286	2955	2950	-5
4	Elevon	1745	1750	34	4	34	135	147	1897	2600	703
6	Fwd chine	2483	2485	59	0	0	187	196	2681	2700	19
				Velocity = 20 400 fps							
1	Nose	2517	2520	60	0	0	180	190	2710	2950	240
2	Body flap	2027	2054	202	0	33	247	321	2374	2600	226
3	Wing	2666	2664	86	0	0	272	285	2950	2950	0
4	Elevon	1742	1754	83	4	34	135	166	1920	2600	680
6	Fwd chine	2481	2482	57	0	0	187	196	2678	2700	22
				Velocity = 19 800 fps							
1	Nose	2516	2521	65	0	0	180	191	2712	2950	238
2	Body flap	2062	2082	188	0	33	247	312	2394	2600	206
3	Wing	2666	2662	105	0	0	272	291	2953	2950	-3
4	Elevon	1891	1922	212	4	34	135	258	2180	2600	420

TABLE VIII.- Continued

(Maximum TPS Temperature, ^{o}F)

Control point	Control point location	Nominal	Mean	Trajectory	Surface deflection		Aero heating	Combined	3-sigma	Simplified model limit, ^{o}F	Margin, ^{o}F
					Bias	Random					
Velocity = 19 800 fps (concluded)											
6	Fwd chine	2480	2484	61	0	0	187	197	2680	2700	20
Velocity = 19 200 fps											
1	Nose	2520	2521	71	0	0	180	193	2714	2950	236
2	Body flap	2103	2110	175	0	33	247	304	2414	2600	186
3	Wing	2669	2657	133	0	0	272	303	2960	2950	-10
4	Elevon	2215	2217	132	4	34	135	196	2413	2600	187
6	Fwd chine	2484	2483	66	0	0	187	198	2681	2700	19
Velocity = 18 600 fps											
1	Nose	2513	2498	82	0	0	180	198	2696	2950	254
2	Body flap	2125	2125	161	0	33	247	297	2422	2600	178
3	Wing	2664	2616	190	0	0	272	332	2948	2950	2
4	Elevon	2316	2306	68	4	34	135	159	2465	2600	135
6	Fwd chine	2474	2462	75	0	0	187	201	2663	2700	37

TABLE VIII.- Concluded

(Maximum TPS Temperature, °F)

Control point	Control point location	Nominal	Mean	Trajectory	Surface deflection		Aero heating	Combined	3-sigma	Simplified model limit, °F	Margin, °F
					Bias	Random					
Velocity = 18 000 fps											
1	Nose	2456	2470	63	0	0	180	191	2660	2950	290
2	Body flap	2102	2132	161	0	33	247	297	2429	2600	171
3	Wing	2546	2565	162	0	0	272	317	2881	2950	69
4	Elevon	2302	2323	44	4	34	135	150	2473	2600	127
6	Fwd chine	2422	2435	58	0	0	187	196	2631	2700	69
Velocity = 16 000 fps											
1	Nose	2386	2390	58	0	0	180	189	2579	2950	371
2	Body flap	2102	2120	163	0	33	247	298	2418	2600	182
3	Wing	2523	2521	120	0	0	272	297	2818	2950	132
4	Elevon	2315	2327	54	4	34	135	153	2481	2600	119
6	Fwd chine	2351	2353	53	0	0	187	194	2548	2700	152

TABLE IX.- TPS PERFORMANCE - STEEP AOA

(Maximum TPS Temperature, ^{o}F)

Control point	Control point location	Nominal	Mean	Trajectory	Surface deflection		Aero heating	Combined	3-sigma	Simplified model limit, ^{o}F	Margin, ^{o}F
					Bias	Random					
				Velocity = 24 000 fps							
1	Nose	2515	2523	87	0	0	180	200	2723	2950	227
2	Body flap	1223	1279	249	0	33	247	352	1631	2600	969
3	Wing	2665	2677	98	0	0	272	289	2966	2950	-16
4	Elevon	1741	1748	51	4	34	135	152	1900	2600	700
6	Fwd chine	2479	2481	81	0	0	187	204	2685	2700	15
Panel 2		321	322	10			37	38	360	350	-10
				Velocity = 23 400 fps							
1	Nose	2536	2537	73	0	0	180	194	2731	2950	219
2	Body flap	1235	1283	268	0	33	247	366	1649	2600	951
3	Wing	2687	2694	82	0	0	272	284	2978	2950	-28
4	Elevon	1756	1757	47	4	34	135	151	1908	2600	692
6	Fwd chine	2499	2493	72	0	0	187	200	2693	2700	7
				Velocity = 22 800 fps							
1	Nose	2538	2537	73	0	0	180	194	2731	2950	219
2	Body flap	1246	1397	516	0	33	247	573	1971	2600	629
3	Wing	2692	2693	83	0	0	272	284	2978	2950	-28

TABLE IX.- Continued

(Maximum TPS Temperature, ^{o}F)

Control point	Control point location	Nominal	Mean	Surface deflection			Aero heating	Combined	3-sigma	Simplified model limit, ^{o}F	Margin, ^{o}F
				Trajectory	Bias	Random					
				Velocity = 22 800 fps (concluded)							
4	Elevon	1757	1756	39	4	34	135	148	1905	2600	695
6	Fwd chine	2499	2494	68	0	0	187	199	2693	2700	17
				Velocity = 22 200 fps							
1	Nose	2536	2536	64	0	0	180	191	2727	2950	223
2	Body flap	1793	1830	476	0	33	247	537	2367	2600	233
3	Wing	2687	2689	75	0	0	272	282	2971	2950	-21
4	Elevon	1756	1757	50	4	34	135	152	1909	2600	691
6	Fwd chine	2498	2495	59	0	0	187	196	2691	2700	9
				Velocity = 21 600 fps							
1	Nose	2534	2533	62	0	0	180	190	2724	2950	226
2	Body flap	1986	2017	292	0	33	247	384	2401	2600	199
3	Wing	2684	2685	74	0	0	272	282	2967	2950	-17
4	Elevon	1755	1756	34	4	34	135	147	1903	2600	697
6	Fwd chine	2497	2494	58	0	0	187	196	2690	2700	10

TABLE IX.- Continued

(Maximum TPS Temperature, ^{o}F)

Control point	Control point location	Nominal	Mean	Surface deflection			Aero heating	Combined	3-sigma	Simplified model limit, ^{o}F	Margin, ^{o}F
				Trajectory	Bias	Random					
				Velocity = 21 000 fps							
1	Nose	2530	2528	61	0	0	180	190	2718	2950	232
2	Body flap	2014	2037	272	0	33	247	369	2405	2600	195
3	Wing	2679	2676	77	0	0	272	283	2959	2950	-9
4	Elevon	1753	1752	32	4	34	135	147	1899	2600	701
6	Fwd chine	2494	2490	58	0	0	187	196	2686	2700	14
				Velocity = 20 400 fps							
1	Nose	2522	2522	62	0	0	180	190	2713	2950	237
2	Body flap	2043	2058	232	0	33	247	340	2398	2600	202
3	Wing	2661	2665	86	0	0	272	285	2950	2950	0
4	Elevon	1752	1757	69	4	34	135	159	1917	2600	683
6	Fwd chine	2486	2486	59	0	0	187	196	2682	2700	18
				Velocity = 19 800 fps							
1	Nose	2520	2521	65	0	0	180	191	2712	2950	238
2	Body flap	2079	2085	208	0	33	247	324	2409	2600	191
3	Wing	2655	2658	100	0	0	272	290	2948	2950	2
4	Elevon	1937	1930	198	4	34	135	246	2176	2600	424

TABLE IX.- Continued

(Maximum TPS Temperature, ^{o}F)

Control point	Control point location	Nominal	Mean	Surface deflection			Aero heating	Combined	3-sigma	Simplified model limit, ^{o}F	Margin, ^{o}F
				Trajectory	Bias	Random					
Velocity = 19 800 fps (concluded)											
6	Fwd chine	2484	2484	62	0	0	187	197	2681	2700	19
Velocity = 19 200 fps											
1	Nose	2522	2521	72	0	0	180	134	2715	2950	235
2	Body flap	2115	2113	196	0	33	247	317	2430	2600	170
3	Wing	2658	2655	127	0	0	272	300	2955	2950	-5
4	Elevon	2240	2232	139	4	34	135	201	2433	2600	167
6	Fwd chine	2486	2485	68	0	0	187	199	2684	2700	16
Velocity = 18 600 fps											
1	Nose	2521	2517	72	0	0	180	194	2711	2950	239
2	Body flap	2150	2140	194	0	33	247	316	2456	2600	144
3	Wing	2661	2654	126	0	0	272	300	2954	2950	-4
4	Elevon	2334	2332	78	4	34	135	163	2495	2600	105
6	Fwd chine	2485	2480	64	0	0	187	198	2678	2700	22

TABLE IX.- Concluded

(Maximum TPS Temperature, ^{o}F)

Control point	Control point location	Nominal	Mean	Trajectory	Surface deflection		Aero heating	Combined	3-sigma	Simplified model limit, ^{o}F	Margin, ^{o}F
					Bias	Random					
Velocity = 18 000 fps											
1	Nose	2504	2503	66	0	0	180	192	2695	2950	255
2	Body flap	2160	2156	193	0	33	247	315	2471	2600	129
3	Wing	2651	2643	109	0	0	272	293	2936	2950	14
4	Elevon	2340	2349	76	4	34	135	162	2511	2600	89
6	Fwd chine	2468	2465	60	0	0	187	196	2662	2700	38
Velocity = 16 000 fps											
1	Nose	2336	2368	73	0	0	180	194	2562	2950	388
2	Body flap	2095	2125	122	0	33	247	277	2402	2600	198
3	Wing	2371	2455	193	0	0	272	334	2789	2950	161
4	Elevon	2303	2318	61	4	34	135	156	2474	2600	126
6	Fwd chine	2310	2336	63	0	0	187	197	2533	2700	167

TABLE X.- TPS PERFORMANCE - SHALLOW AOA

(Maximum TPS Temperature, °F)

Control point	Control point location	Nominal	Mean	Trajectory	Surface deflection		Aero heating	Combined	3-sigma	Simplified model limit, °F	Margin, °F
					Bias	Random					
					Velocity = 24 000 fps						
1	Nose	2544	2548	73	0	0	180	194	2742	2950	208
2	Body flap	1241	1251	281	0	33	247	375	1627	2600	973
3	Wing	2695	2702	77	0	0	272	283	2985	2950	-35
4	Elevon	1762	1766	53	4	34	135	153	1919	2600	681
6	Fwd chine	2508	2508	71	0	0	187	200	2708	2700	-8
Panel 2		324	326	15	--	--	37	40	366	350	-16
					Velocity = 23 400 fps						
1	Nose	2573	2574	77	0	0	180	196	2770	2950	180
2	Body flap	1245	1308	413	0	33	247	483	1790	2600	810
3	Wing	2734	2737	83	0	0	272	285	3022	2950	-72
4	Elevon	1782	1783	50	4	34	135	152	1935	2600	665
6	Fwd chine	2527	2526	78	0	0	187	203	2729	2700	-29
					Velocity = 22 800 fps						
1	Nose	2562	2564	84	0	0	180	199	2763	2950	187
2	Body flap	1572	1613	417	0	33	247	486	2099	2600	501
3	Wing	2720	2721	93	0	0	272	287	3009	2950	-59

TABLE X.- Continued

(Maximum TPS Temperature, ^{o}F)

Control point	Control point location	Nominal	Mean	Surface deflection			Aero heating	Combined	3-sigma	Simplified model limit, ^{o}F	Margin, ^{o}F
				Trajectory	Bias	Random					
				Velocity = 22 800 fps (concluded)							
4	Elevon	1775	1777	59	4	34	135	155	1932	2600	668
6	Fwd chine	2519	2521	80	0	0	187	203	2724	2700	-24
				Velocity = 22 200 fps							
1	Nose	2563	2563	77	0	0	180	196	2759	2950	191
2	Body flap	1985	1954	351	0	33	247	431	2385	2600	215
3	Wing	2719	2718	88	0	0	272	286	3004	2950	-54
4	Elevon	1775	1777	56	4	34	135	154	1931	2600	669
6	Fwd chine	2521	2522	74	0	0	187	201	2723	2700	-23
				Velocity = 21 600 fps							
1	Nose	2566	2564	73	0	0	180	194	2758	2950	192
2	Body flap	2024	2019	291	0	33	247	383	2402	2600	198
3	Wing	2721	2717	85	0	0	272	285	3002	2950	-52
4	Elevon	1778	1778	51	4	34	135	152	1930	2600	670
6	Fwd chine	2526	2524	70	0	0	187	200	2724	2700	-24

TABLE X.- Continued

(Maximum TPS Temperature, °F)

Control point	Control point location	Nominal	Mean	Surface deflection			Aero heating	Combined	3-sigma	Simplified model limit, °F	Margin, °F
				Trajectory	Bias	Random					
				Velocity = 21 000 fps							
1	Nose	2564	2560	75	0	0	180	195	2755	2950	195
2	Body flap	2055	2046	253	0	33	247	355	2401	2600	199
3	Wing	2718	2711	91	0	0	272	287	2998	2950	-48
4	Elevon	1776	1777	74	4	34	135	162	1938	2600	662
6	Fwd chine	2525	2521	72	0	0	187	200	2721	2700	-21
				Velocity = 20 400 fps							
1	Nose	2558	2555	74	0	0	180	195	2750	2950	200
2	Body flap	2082	2072	202	0	33	247	321	2393	2600	207
3	Wing	2711	2703	95	0	0	272	288	2991	2950	-41
4	Elevon	1814	1827	244	4	34	135	285	2112	2600	488
6	Fwd chine	2520	2517	71	0	0	187	200	2717	2700	-17
				Velocity = 19 800 fps							
1	Nose	2558	2554	80	0	0	180	197	2751	2950	199
2	Body flap	2122	2107	175	0	33	247	304	2411	2600	189
3	Wing	2707	2698	110	0	0	272	294	2992	2950	-42
4	Elevon	2092	2090	283	4	34	135	319	2409	2600	191

TABLE X.- Continued

(Maximum TPS Temperature, ^{o}F)

Control point	Control point location	Nominal	Mean	Trajectory	Surface deflection		Aero heating	Combined	3-sigma	Simplified model limit, ^{o}F	Margin, ^{o}F
					Bias	Random					
				Velocity = 19 800 fps (continued)							
6	Fwd chine	2521	2517	77	0	0	187	202	2720	2700	-20
				Velocity = 19 200 fps							
1	Nose	2562	2556	86	0	0	180	200	2756	2950	194
2	Body flap	2165	2143	152	0	33	247	292	2435	2600	165
3	Wing	2712	2696	129	0	0	272	[illegible]	2997	2950	-47
4	Elevon	2351	2331	111	4	34	135	182	2513	2600	87
6	Fwd chine	2525	2518	82	0	0	187	204	2723	2700	-23
				Velocity = 18 600 fps							
1	Nose	2259	2552	85	0	0	180	199	2752	2950	198
2	Body flap	2193	2171	151	0	33	247	291	2463	2600	137
3	Wing	2713	2697	126	0	0	272	300	2996	2950	-46
4	Elevon	2385	2381	90	4	34	135	170	2551	2600	49
6	Fwd chine	2520	2514	80	0	0	187	203	2717	2700	-17

TABLE X.- Concluded

(Maximum TPS Temperature, °F)

Control point	Control point location	Nominal	Mean	Trajectory	Surface deflection		Aero heating	Combined	3-sigma	Simplified model limit, °F	Margin, °F
					Bias	Random					
Velocity = 18 000 fps											
1	Nose	2542	2540	81	0	0	180	197	2737	2950	213
2	Body flap	2209	2188	147	0	33	247	289	2477	2600	123
3	Wing	2695	2689	109	0	0	272	293	2982	2950	-32
4	Elevon	2402	2403	92	4	34	135	171	2573	2600	27
6	Fwd chine	2503	2500	74	0	0	187	201	2301	2700	-1
Velocity = 16 000 fps											
1	Nose	2352	2370	121	0	0	180	217	2596	2950	354
2	Body flap	2135	2142	136	0	33	247	284	2426	2600	174
3	Wing	2390	2453	283	0	0	272	393	2846	2950	104
4	Elevon	2323	2346	94	4	34	135	172	2518	2600	82
6	Fwd chine	2325	2348	99	0	0	187	212	2560	2700	140

TABLE XI.- LANDING STATISTICS

Parameter	Nominal	Mean	Maximum	Minimum
End of mission				
Altitude rate, fps	2.25	3.03	8.56	0.43
Pitch angle, deg	8.95	9.72	13.13	7.55
Groundspeed, kn	194	188	235	153
Equivalent airspeed, kn	188	184	217	152
True airspeed, kn	194	191	226	158
Range from threshold, ft	2682	1800	4319	9.2
Lateral position, ft	0	0	5	-23
Lateral rate, fps	0	0	2.0	-1.0
Energy reserve, sec	4.46	--	7.04	-.43
Abort once around				
Altitude rate, fps	2.18	2.54	6.78	0.63
Pitch angle, deg	8.90	9.31	11.14	7.75
Groundspeed, kn	204	198	236	170
Equivalent airspeed, kn	191	188	214	168
True airspeed, kn	204	201	228	179
Range from threshold, ft	2940	2307	4481	462
Lateral position, ft	0	0	13.	-16
Lateral rate, fps	0	0	2.9	-1.7
Energy reserve, sec	4.62	--	6.42	1.61

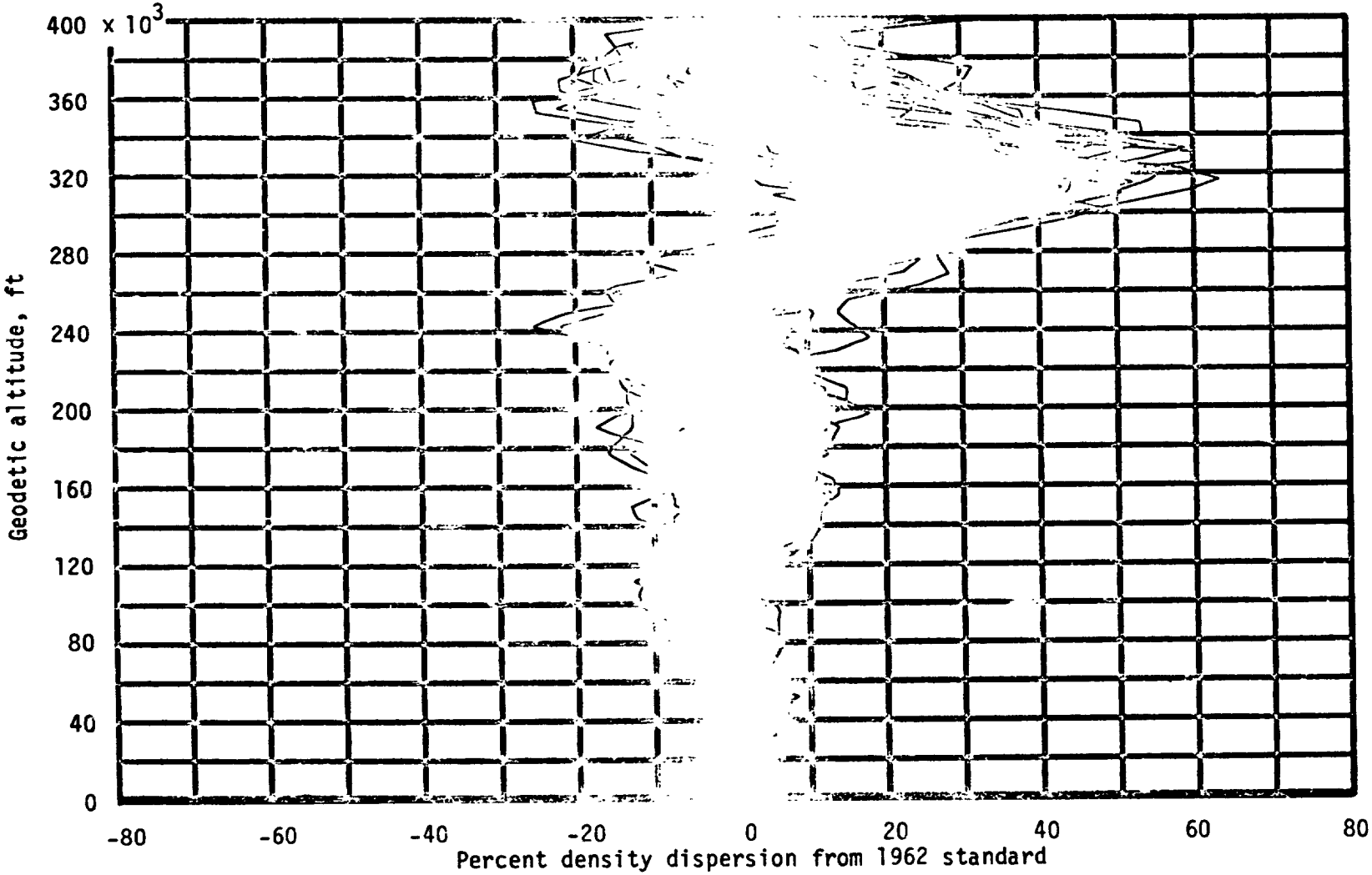

(a) Density.

Figure 1.- Atmospheric dispersions - April - end of mission.

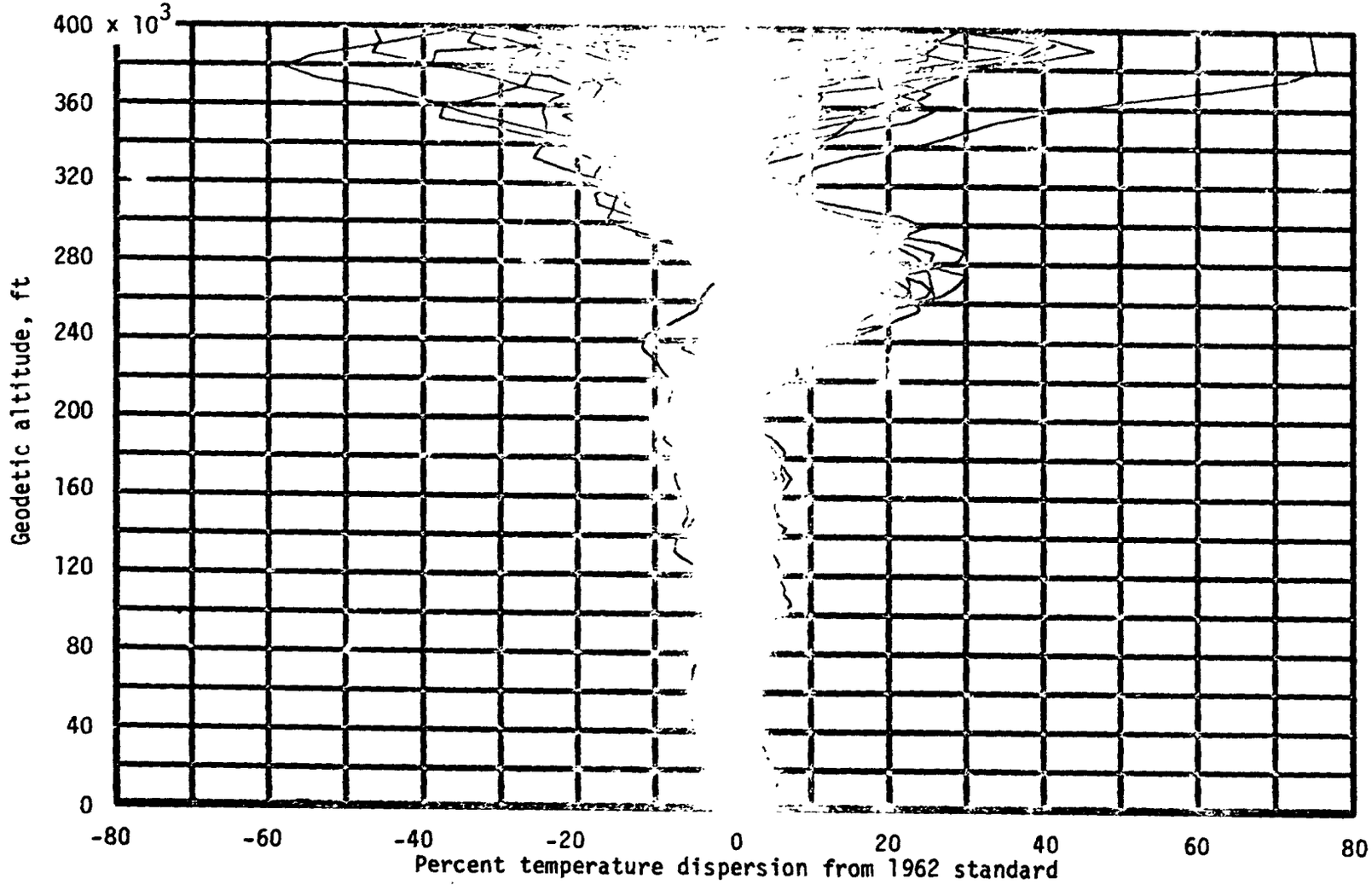

(b) Temperature.

Figure 1.- Continued.

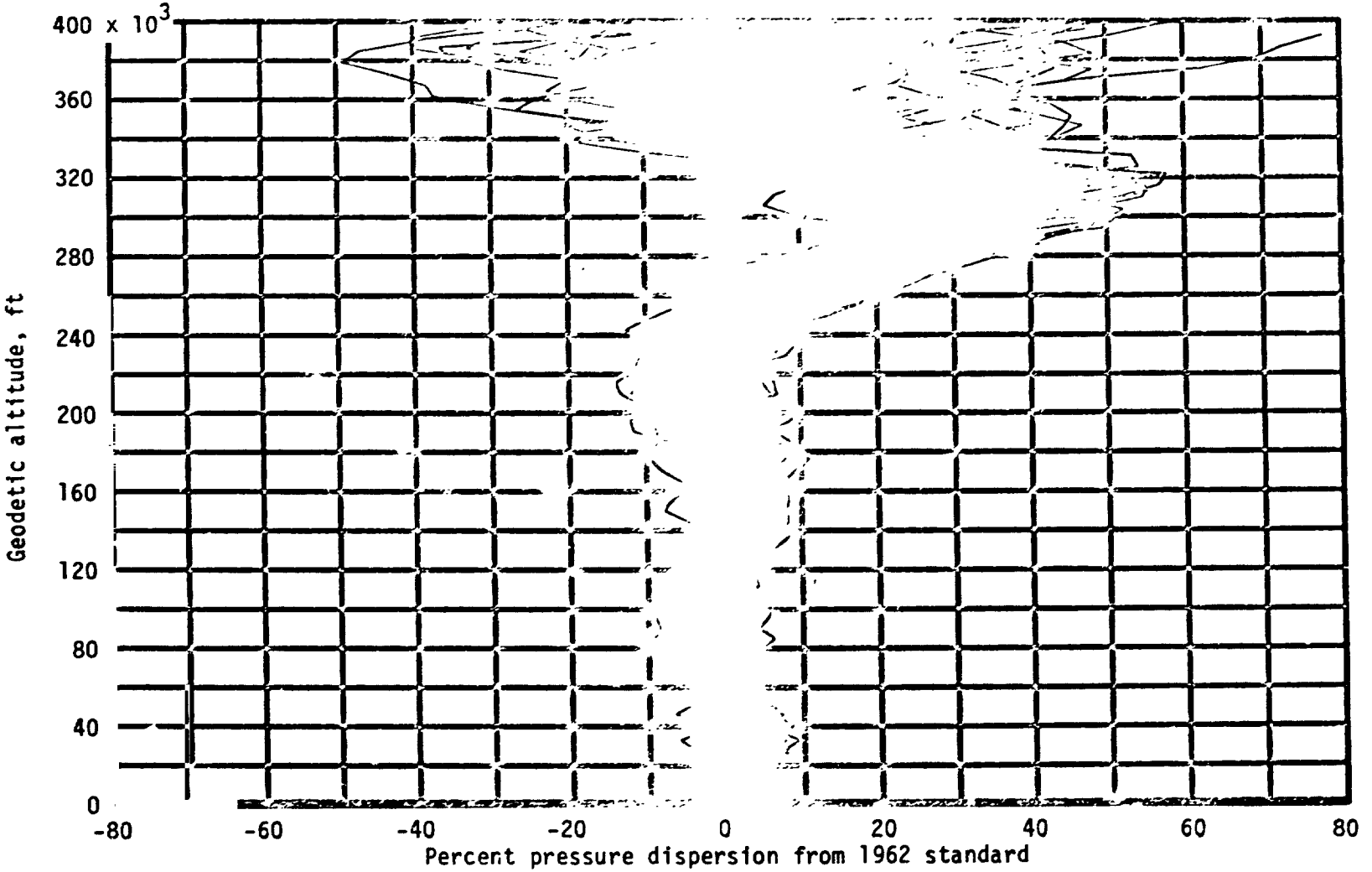

(c) Pressure.

Figure 1.- Continued.

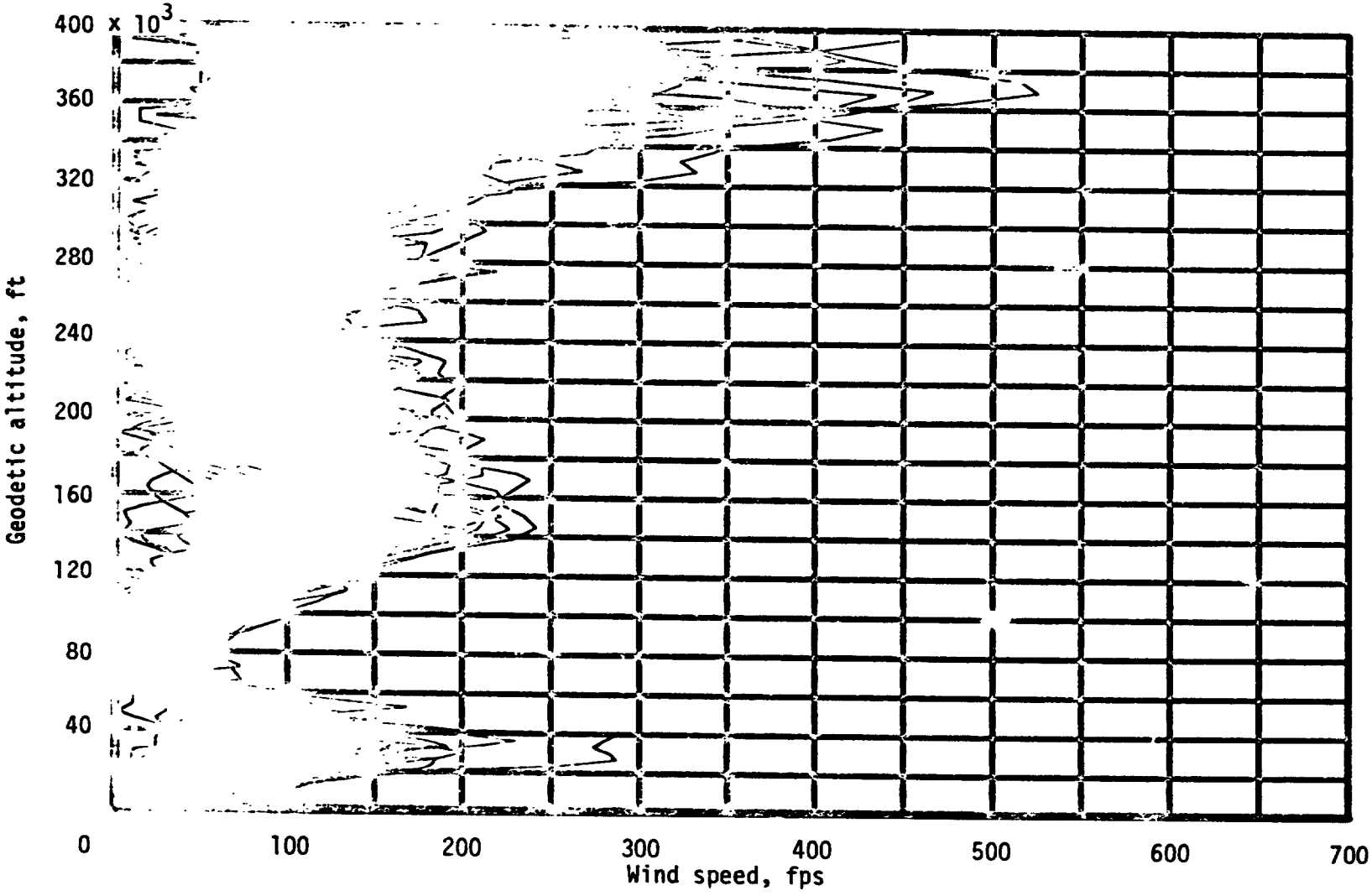

(d) Wind magnitude.

Figure 1.- Continued.

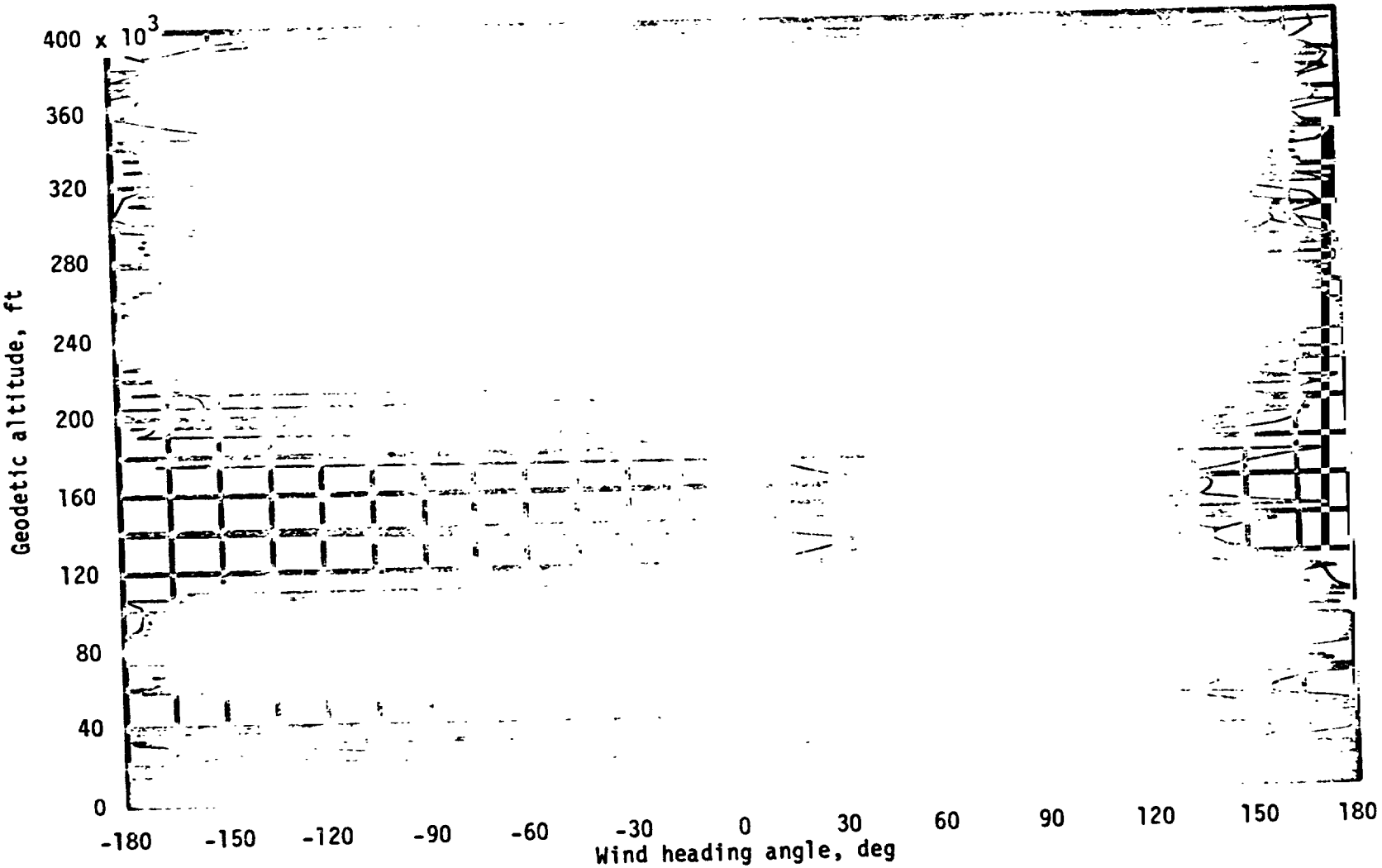

(e) Wind heading angle.

Figure 1.- Concluded.

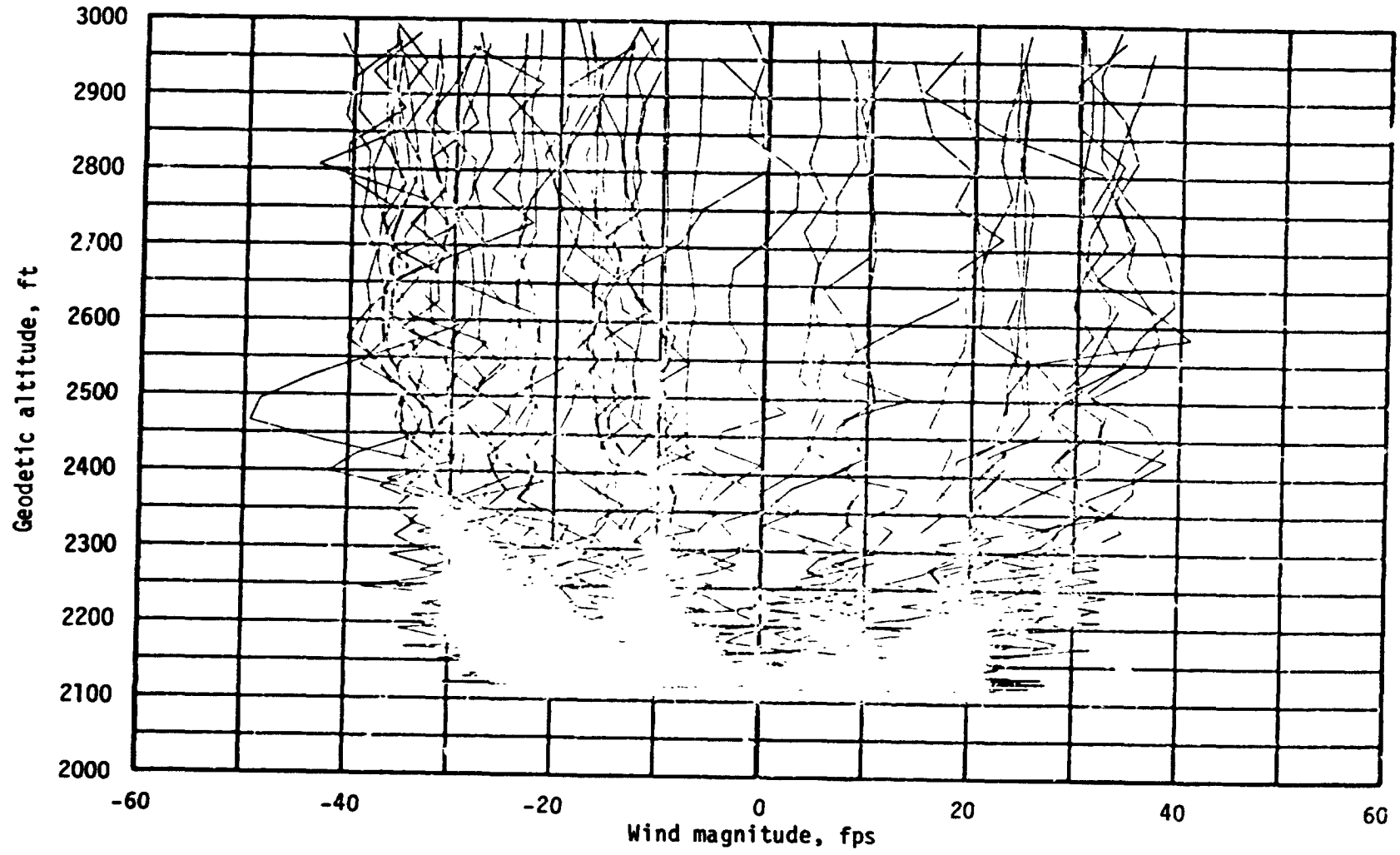

(a) Head or tail wind components.

Figure 2.- Surface winds in runway coordinates - end of mission.

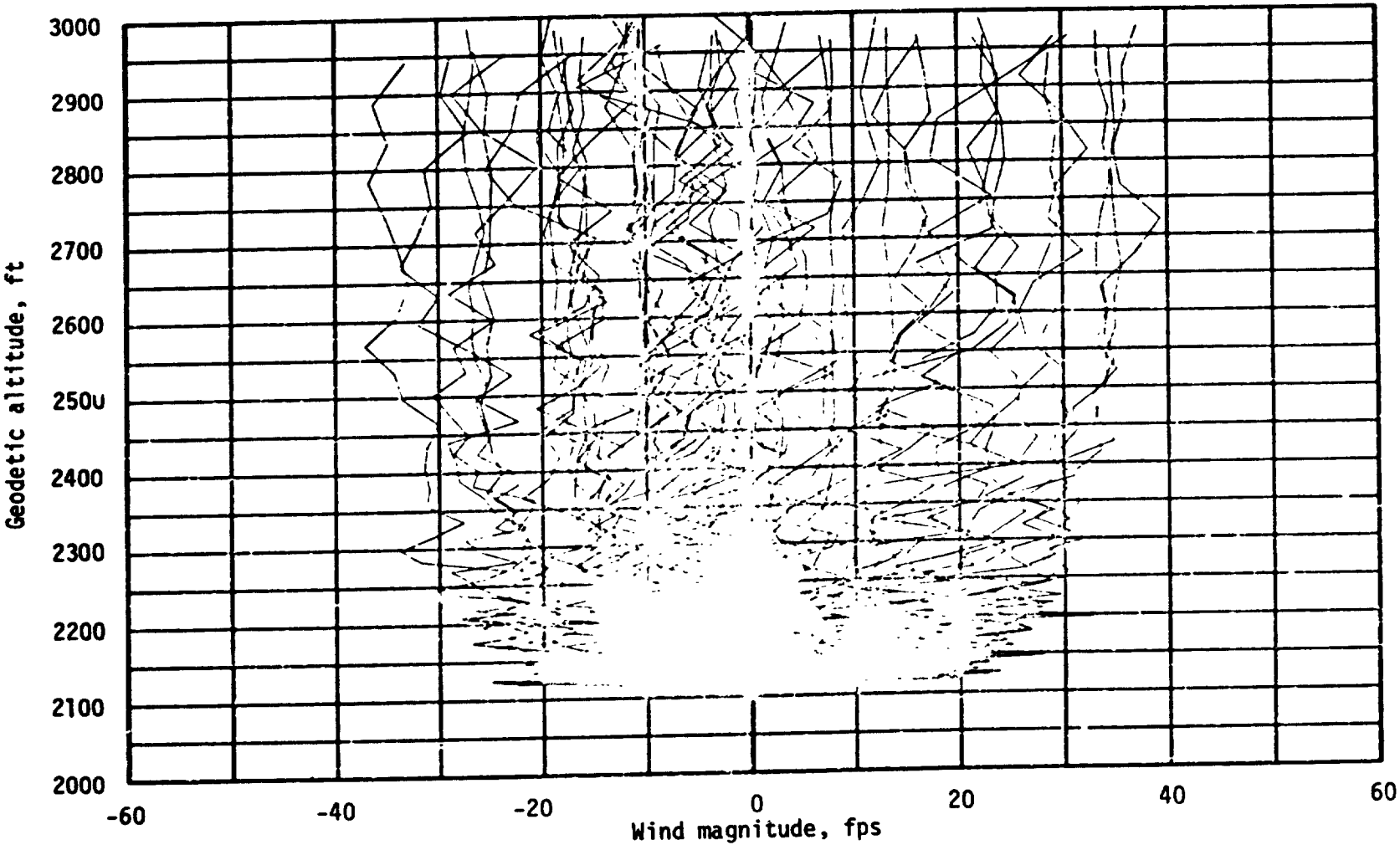

(b) Crosswind components.

Figure 2.- Concluded.

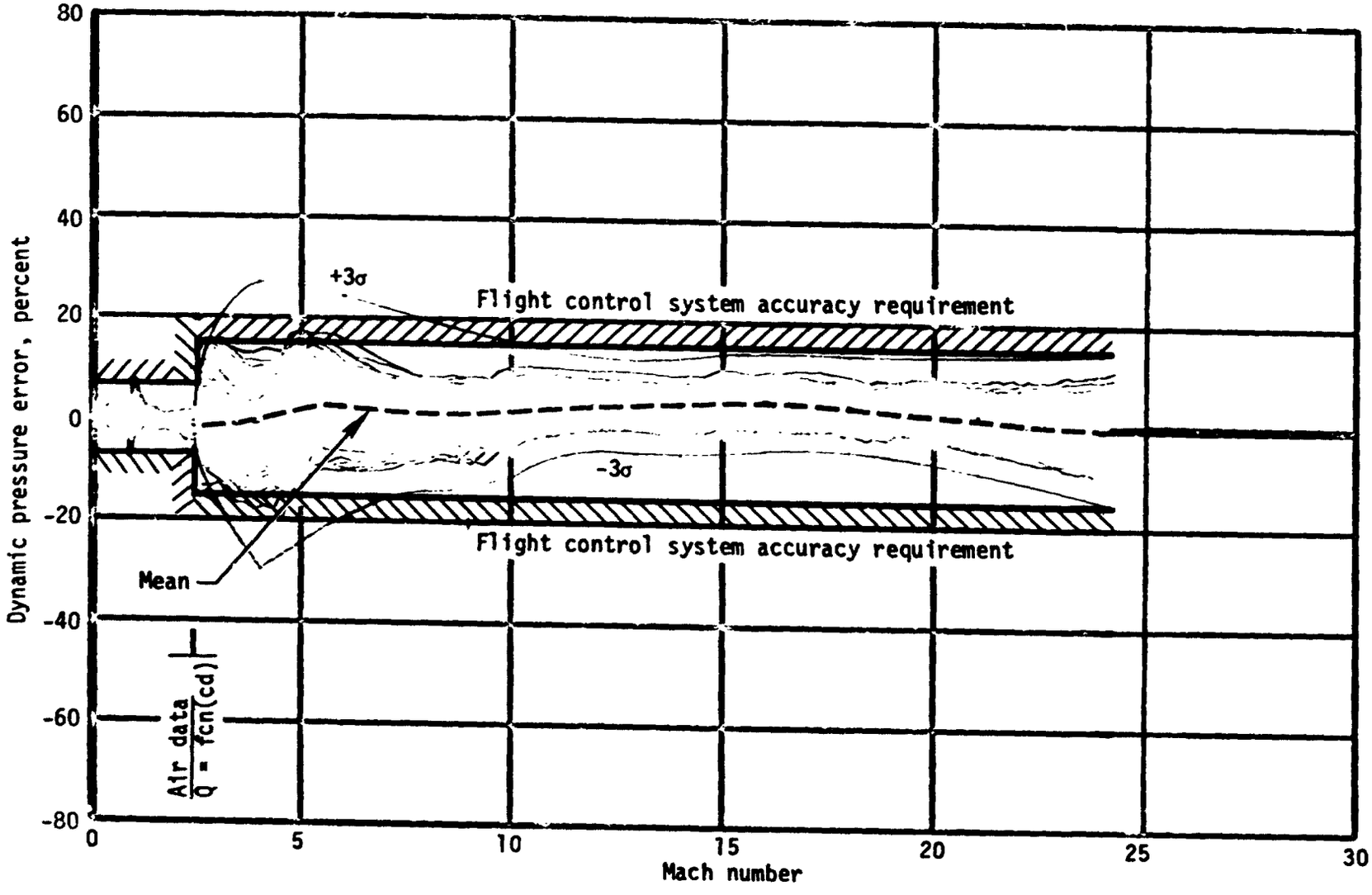

(a) Percent dynamic pressure error.

Figure 3.- Nav derived and/or air data derived parameter performance - end of mission.

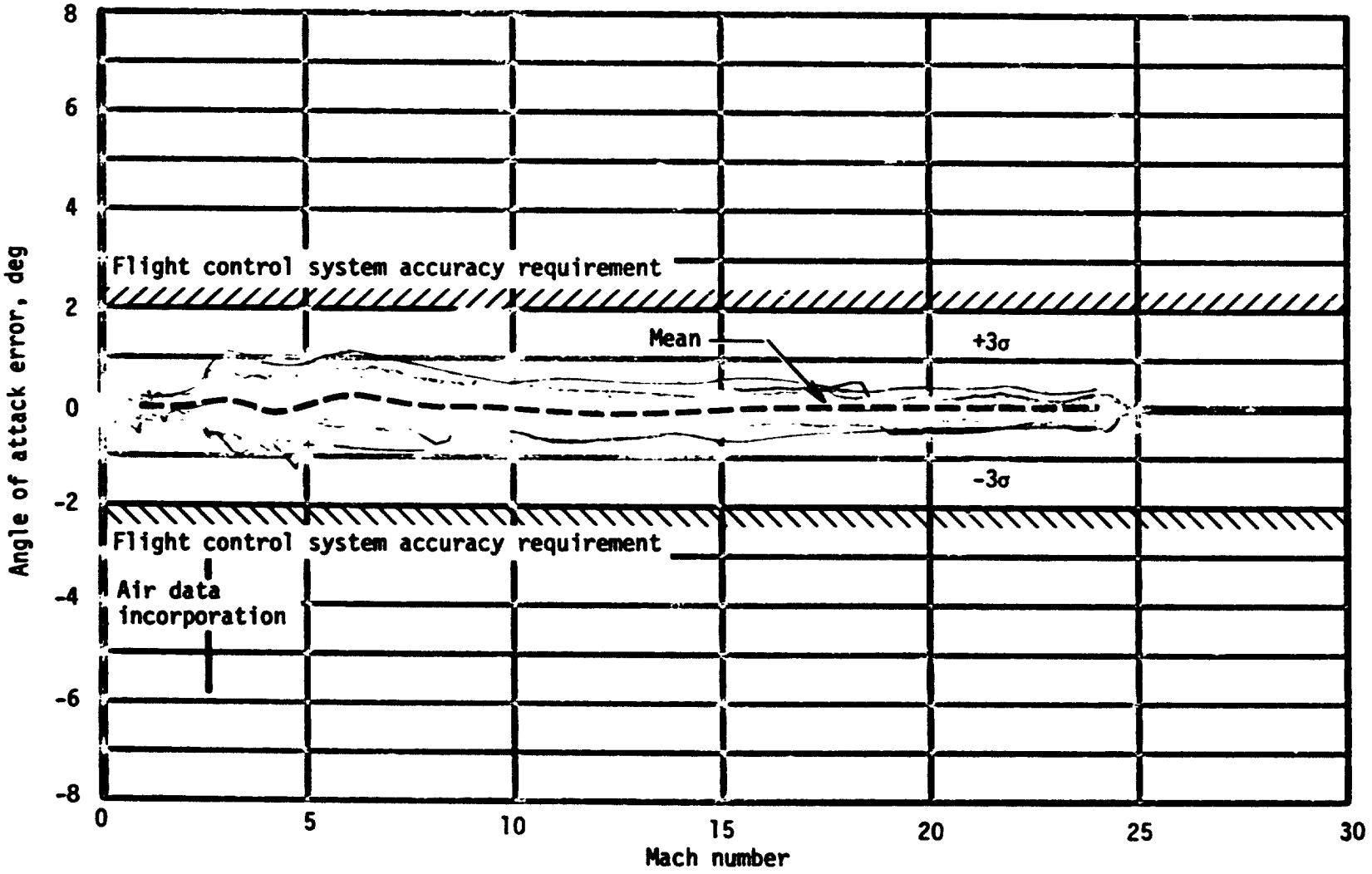

(b) Angle of attack error.

Figure 3.- Continued.

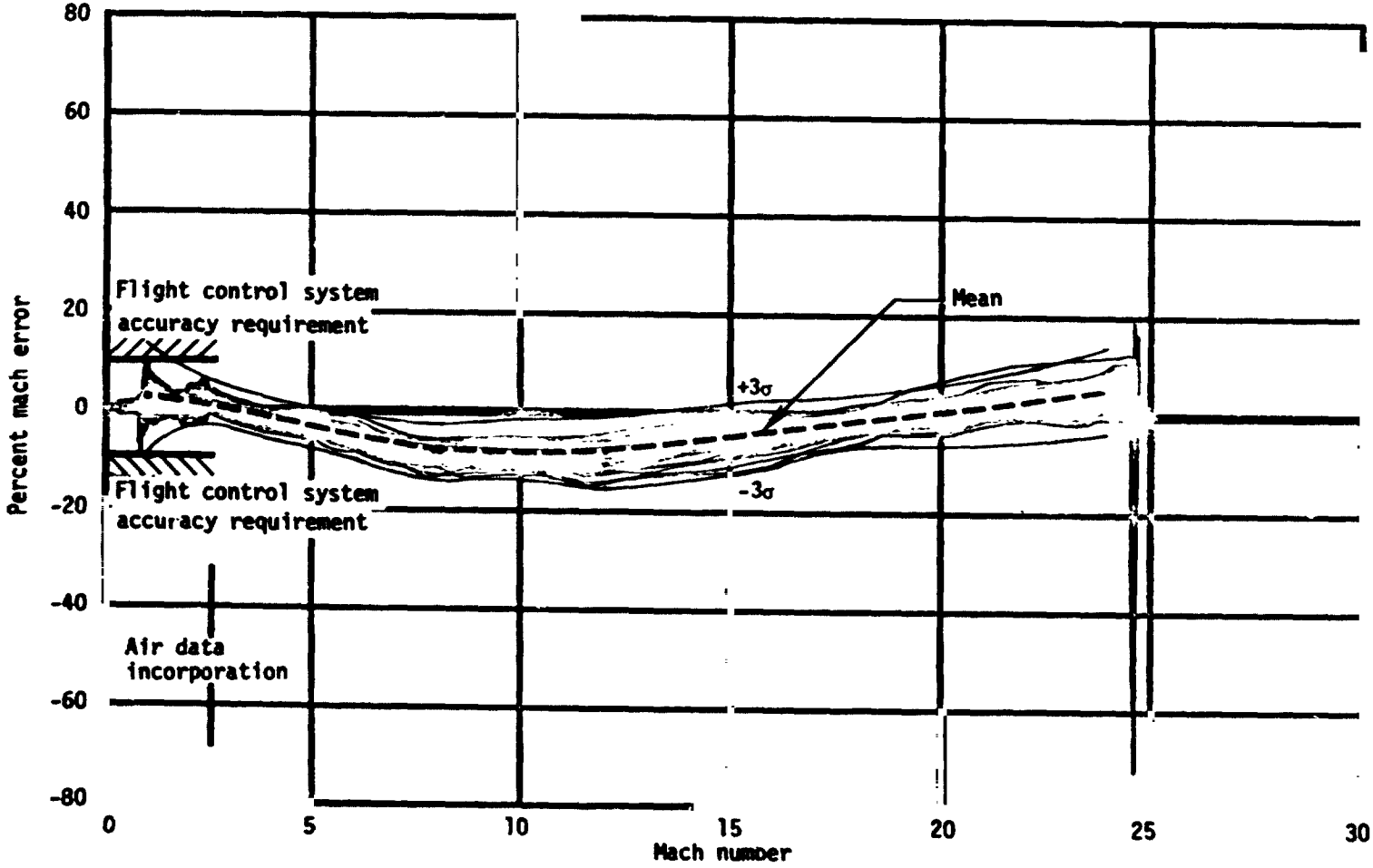

(c) Percent mach number error.

Figure 3.- Continued.

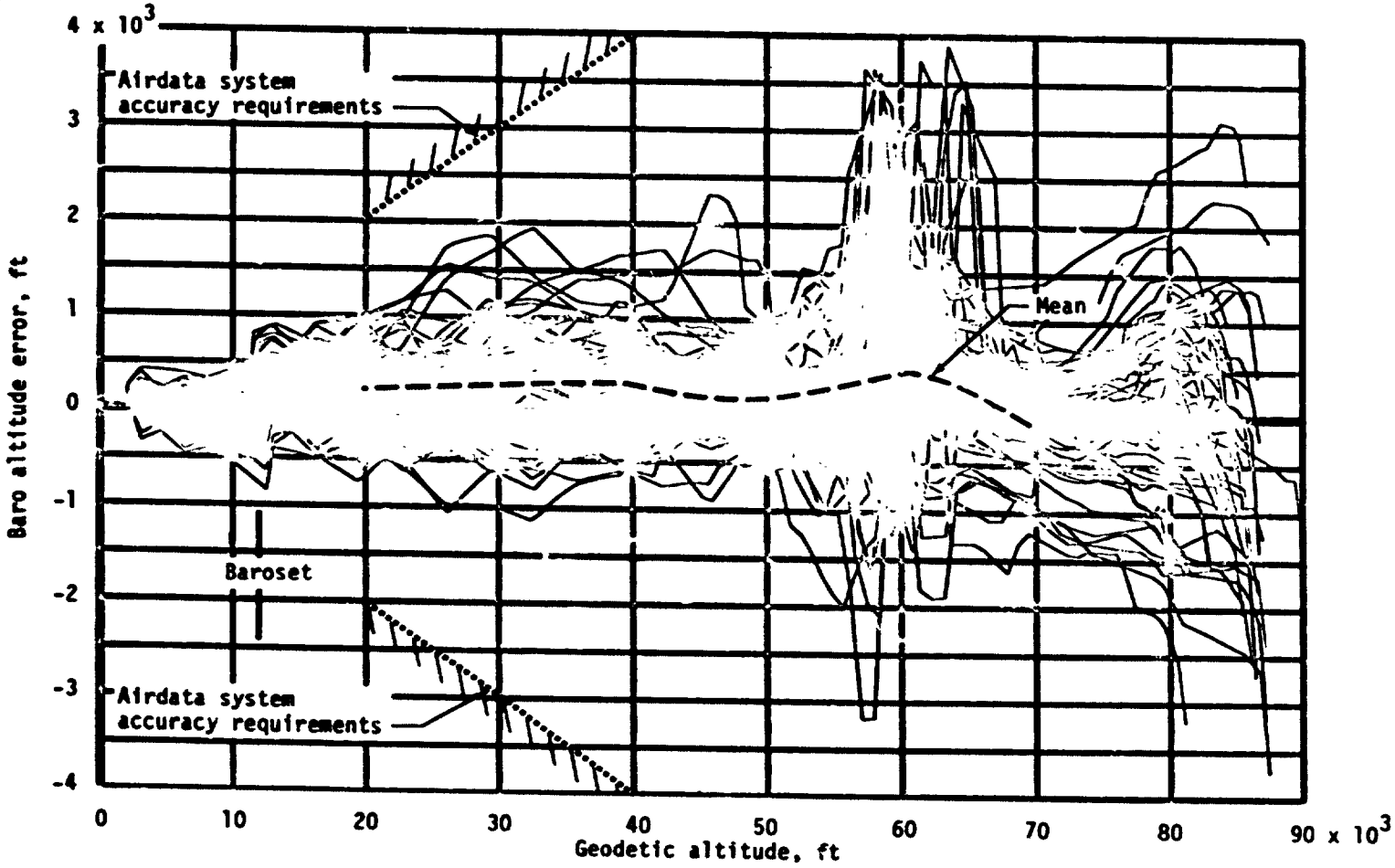

(d) Baro altitude error.

Figure 3.- Concluded.

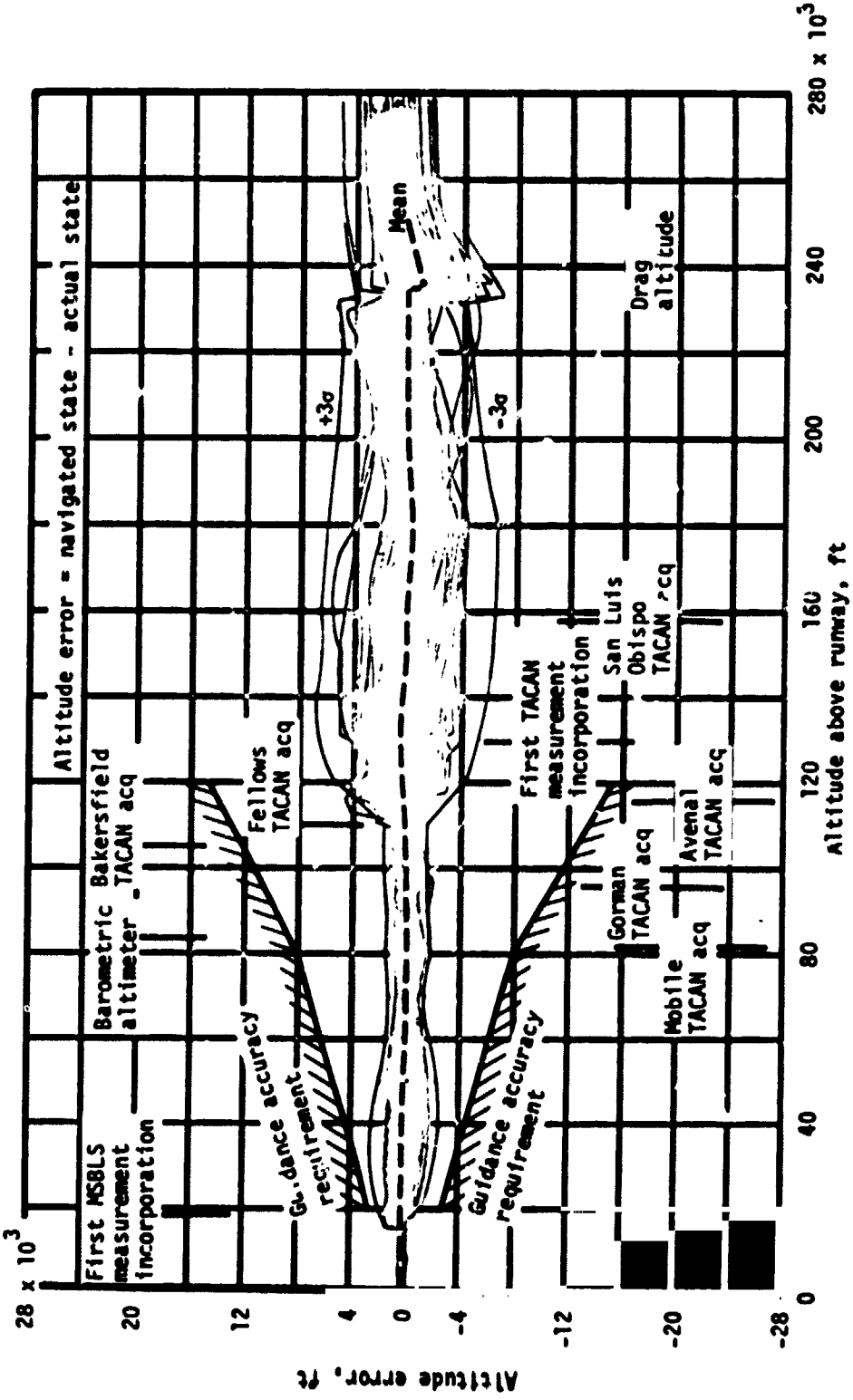

(a) Altitude error.

Figure 4.- Navigated state vector performance - end of mission.

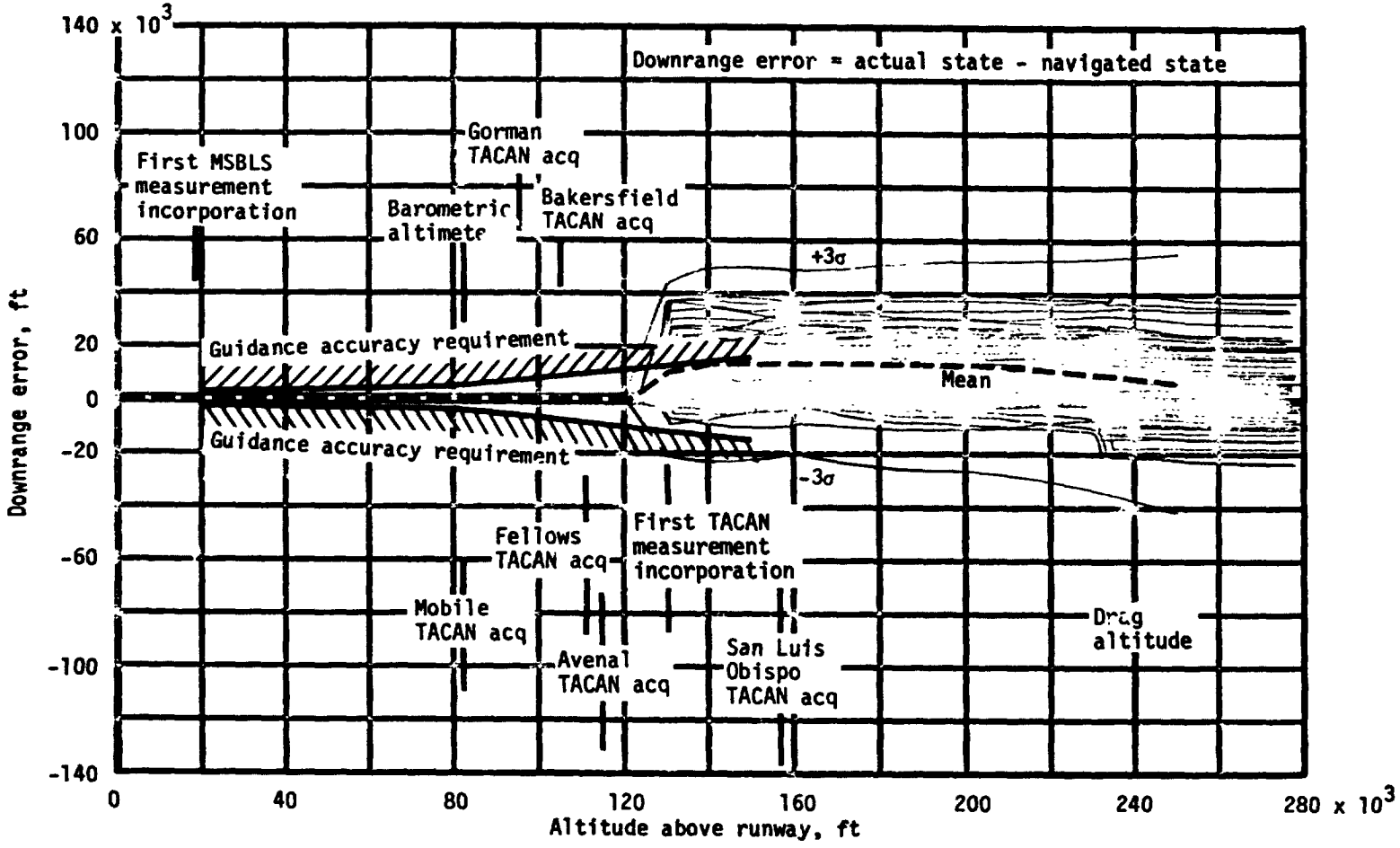

(b) Downrange error.

Figure 4.- Continued.

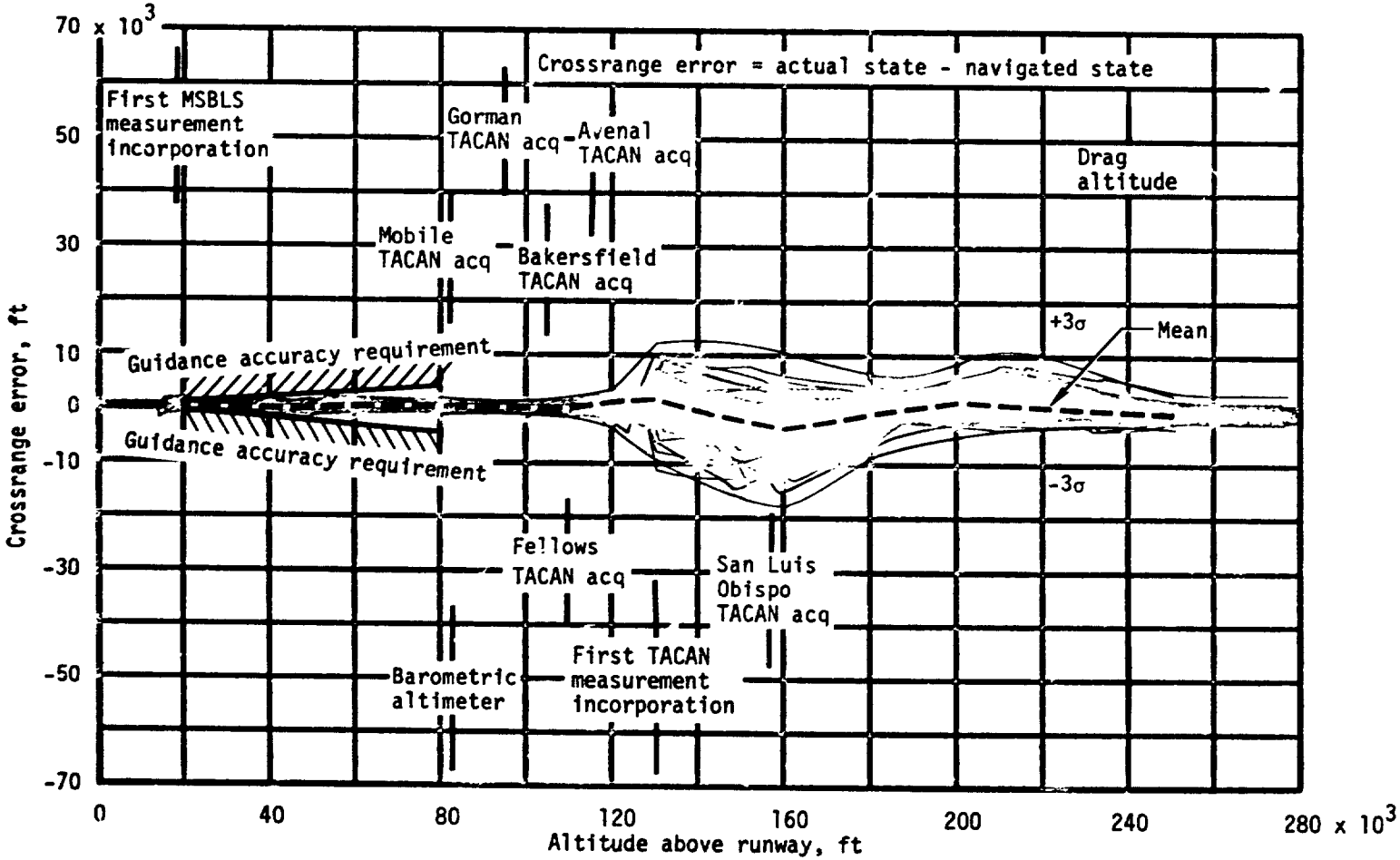

(c) Crossrange error.

Figure 4.- Continued.

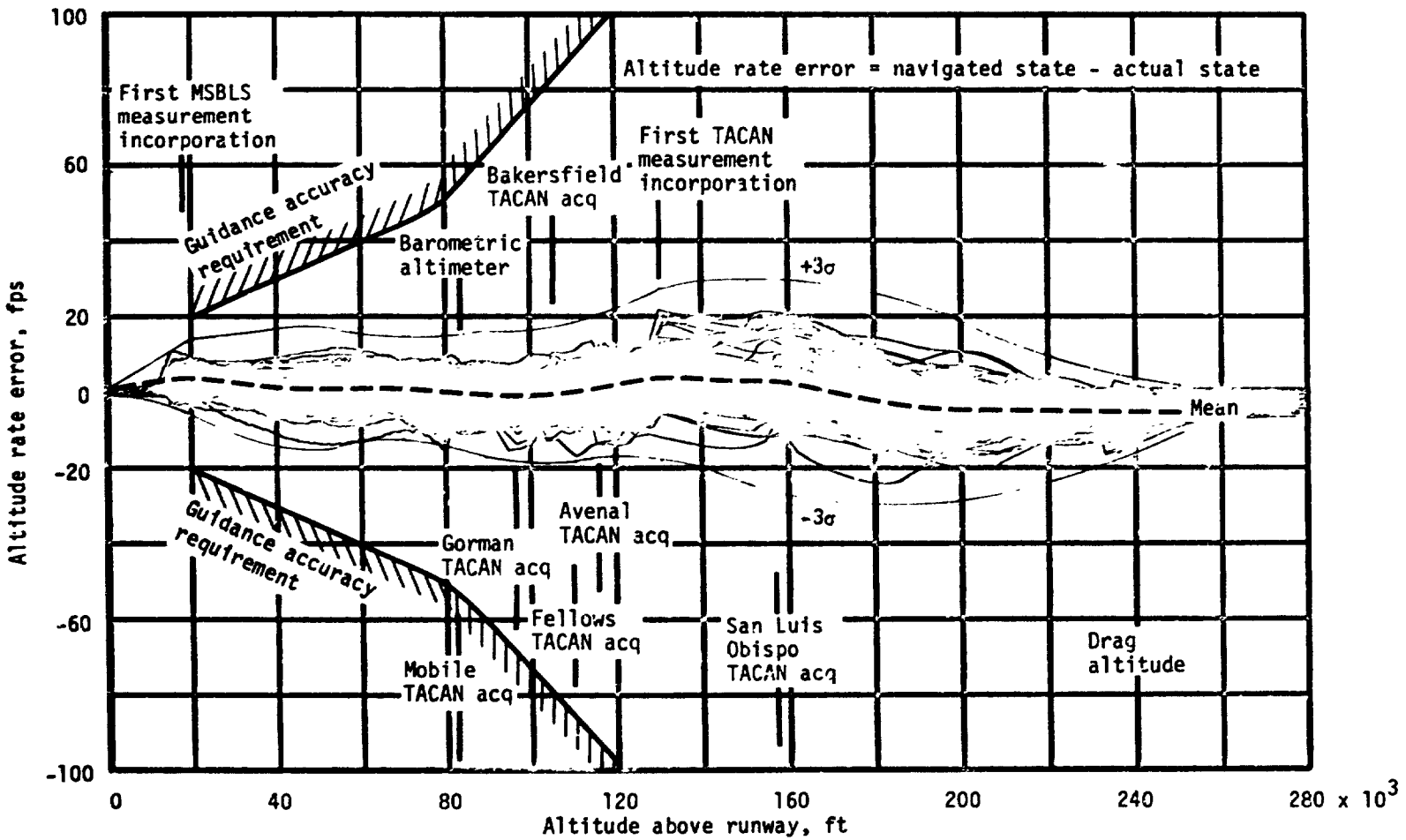

(d) Altitude rate error.

Figure 4.- Continued.

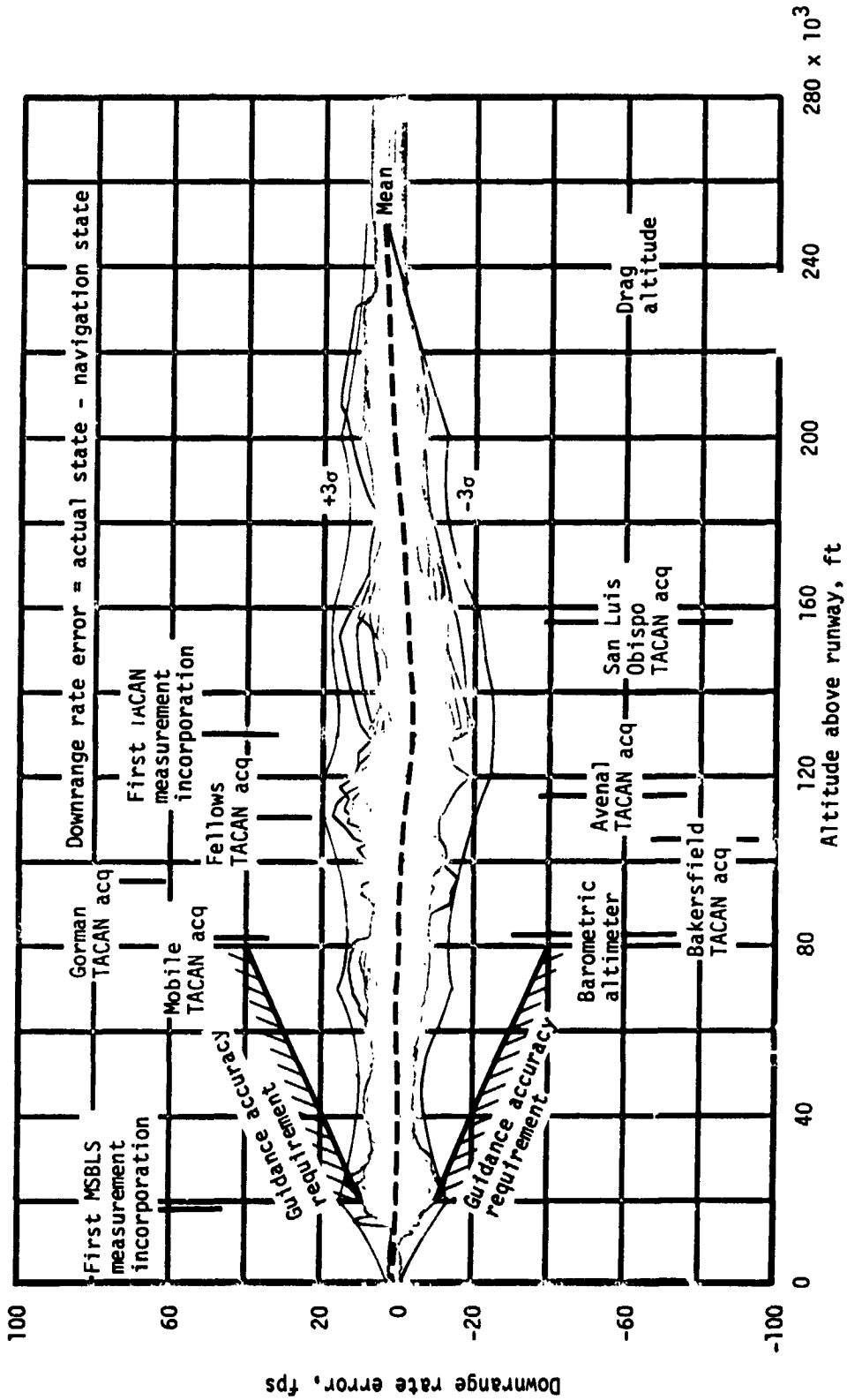

(e) Downrange rate error.

Figure 4.- Continued.

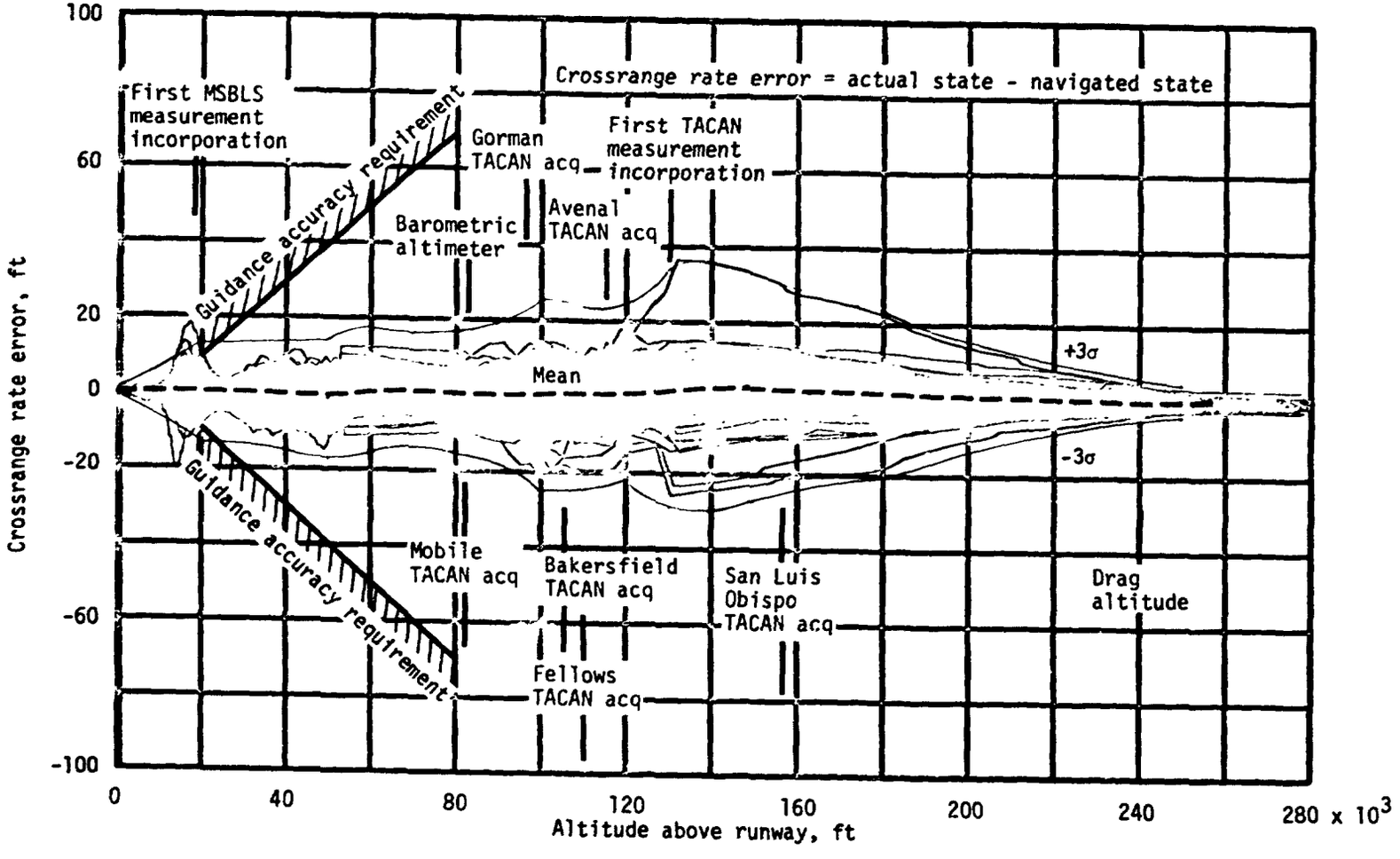

(f) Crossrange rate error.

Figure 4.- Continued.

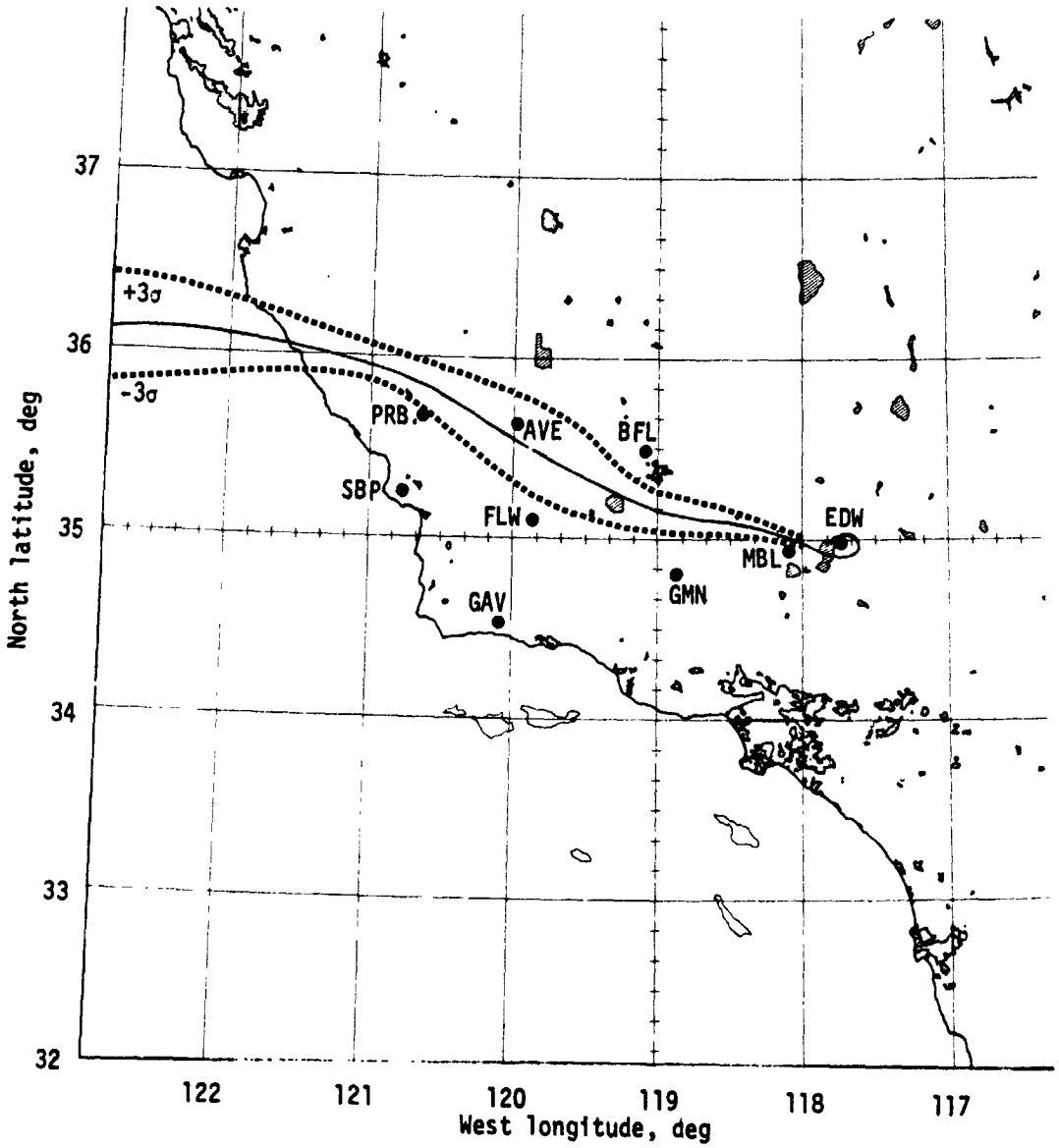

(g) TACAN station locations and groundtrack.

Figure 4.- Concluded.

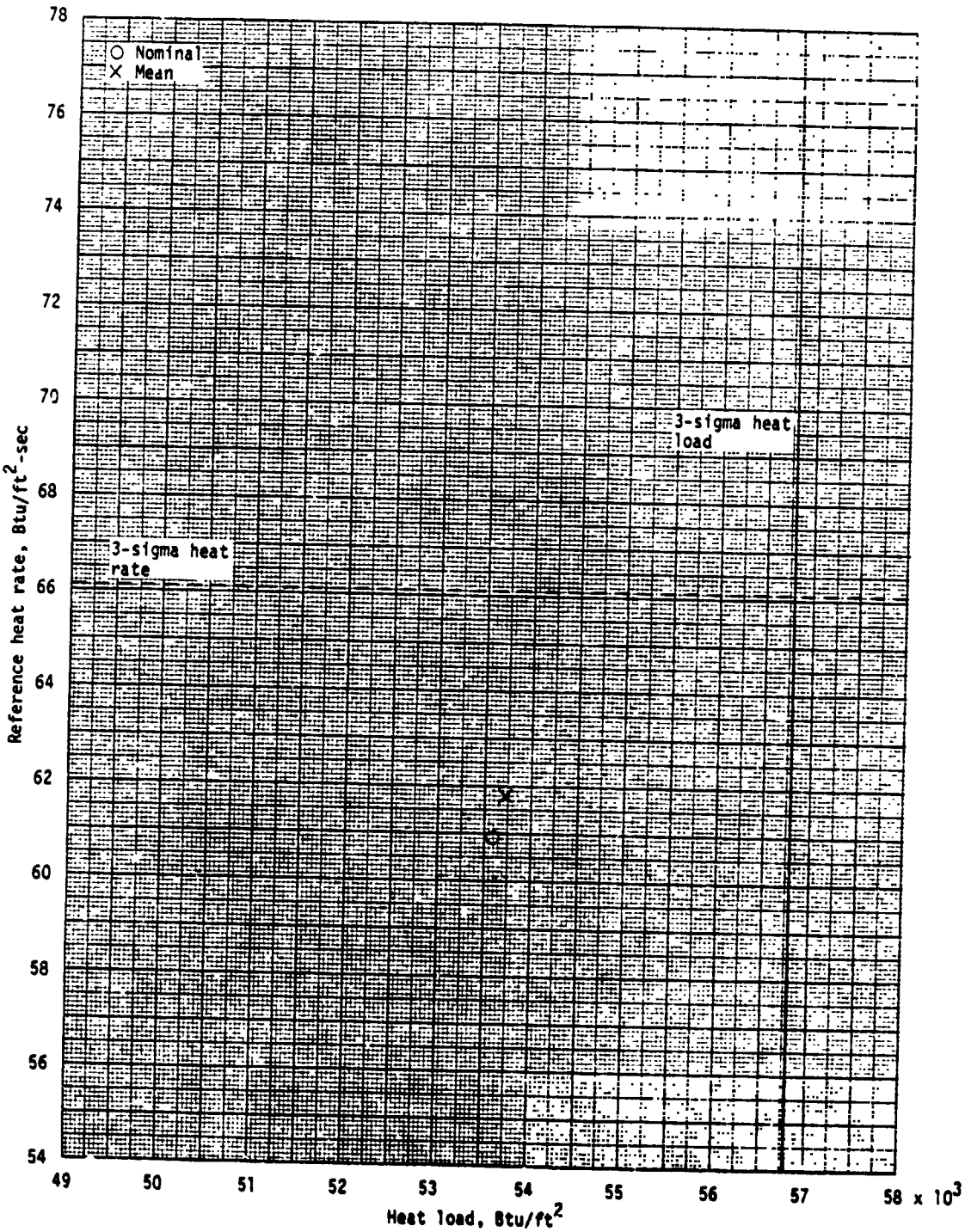

Figure 5.- Heat rate - heat load scatter plot - end of mission.

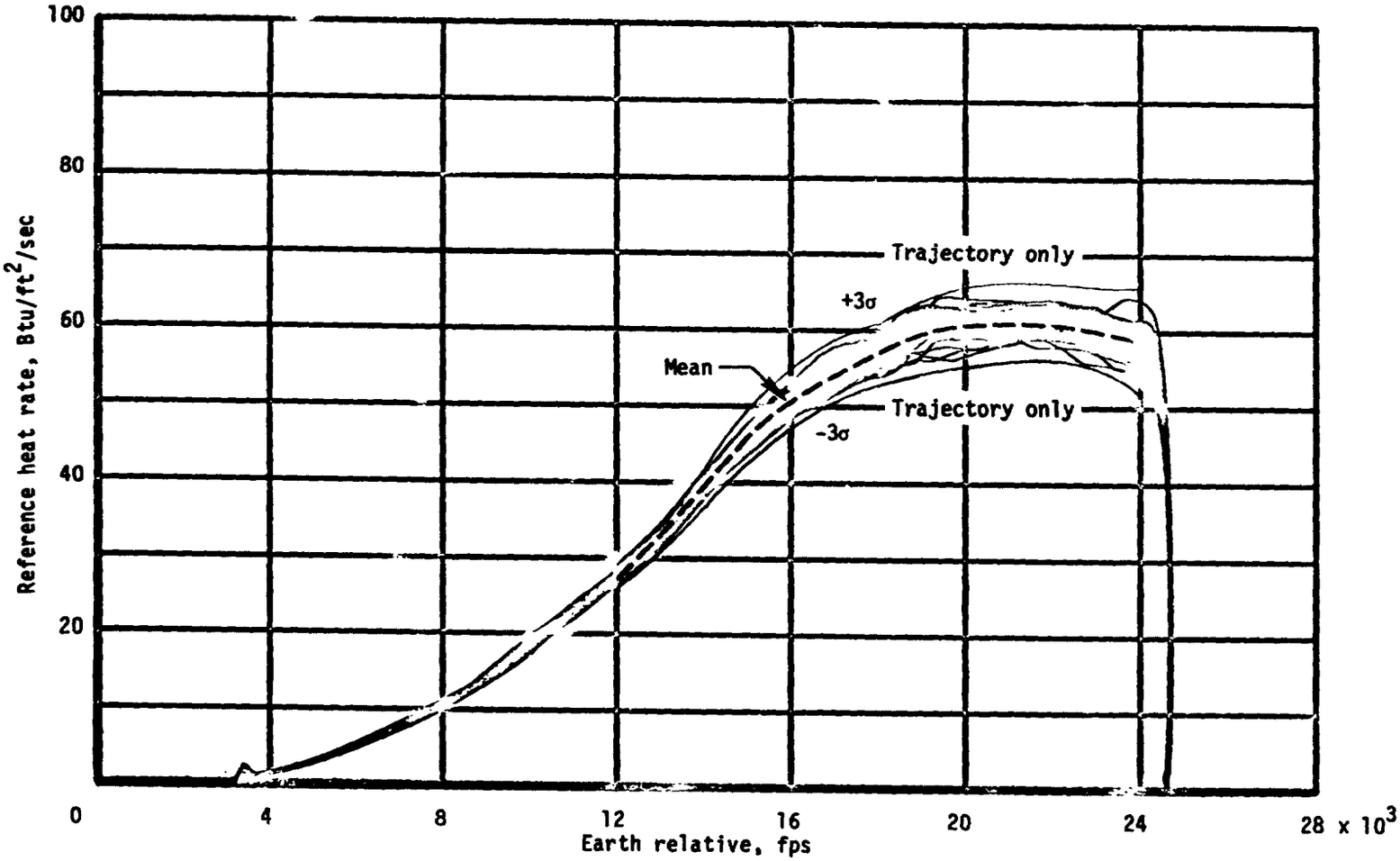

(a) Heat rate.

Figure 6.- TPS performance - end of mission.

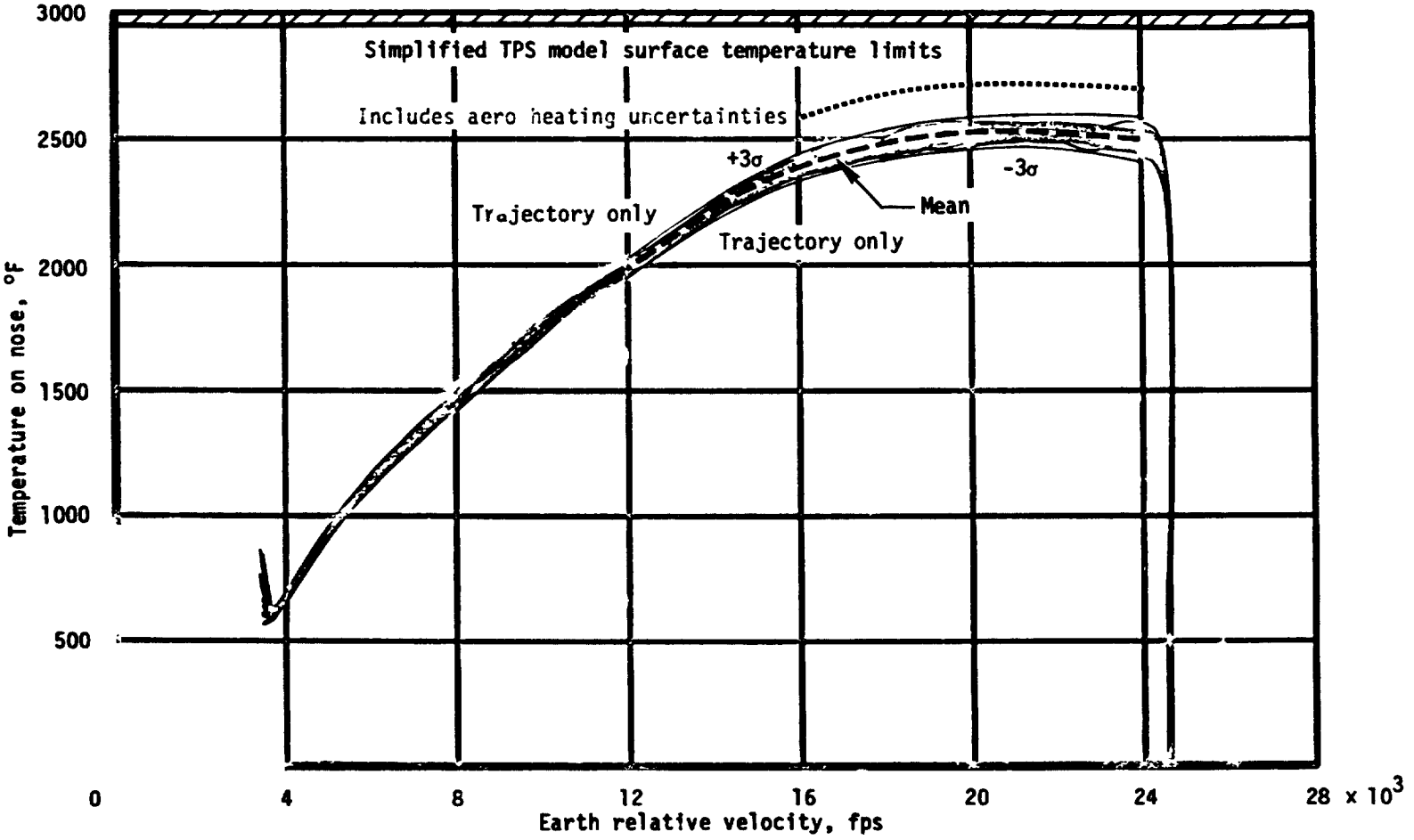

(b) Nose surface temperature.

Figure 6.- Continued.

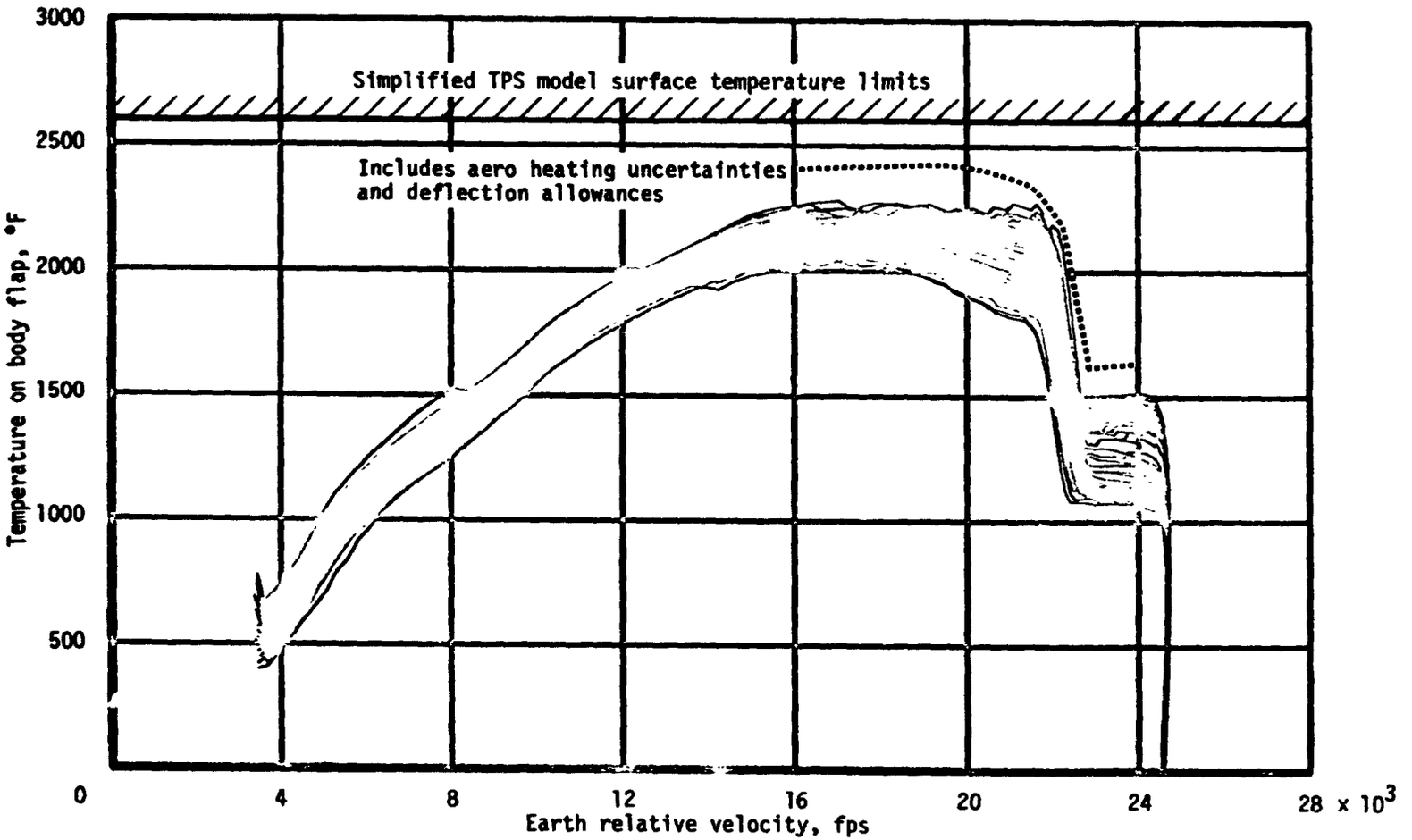

(c) Body-flap surface temperature.

Figure 6.- Continued.

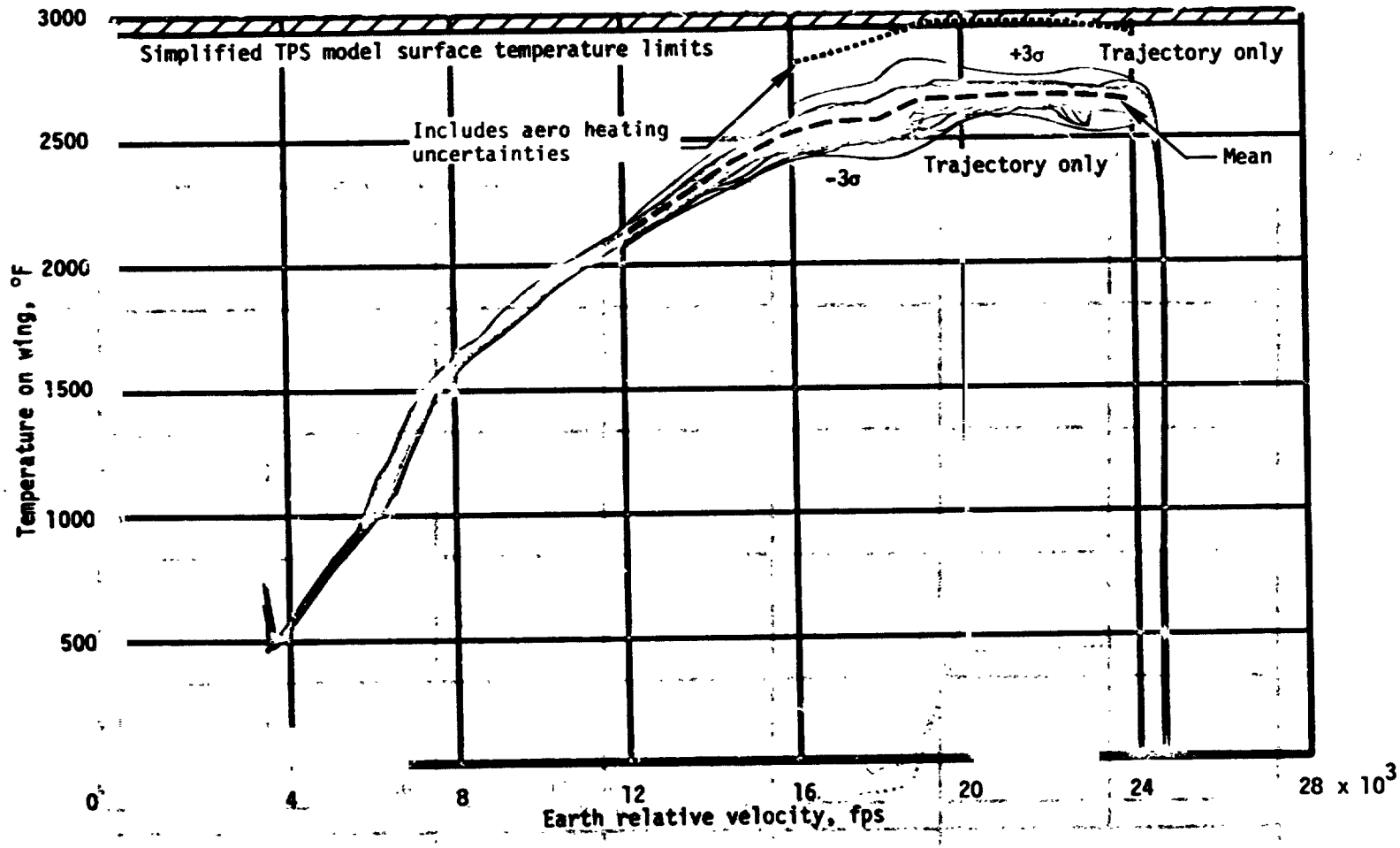

(d) Wing surface temperature.

Figure 6.- Continued.

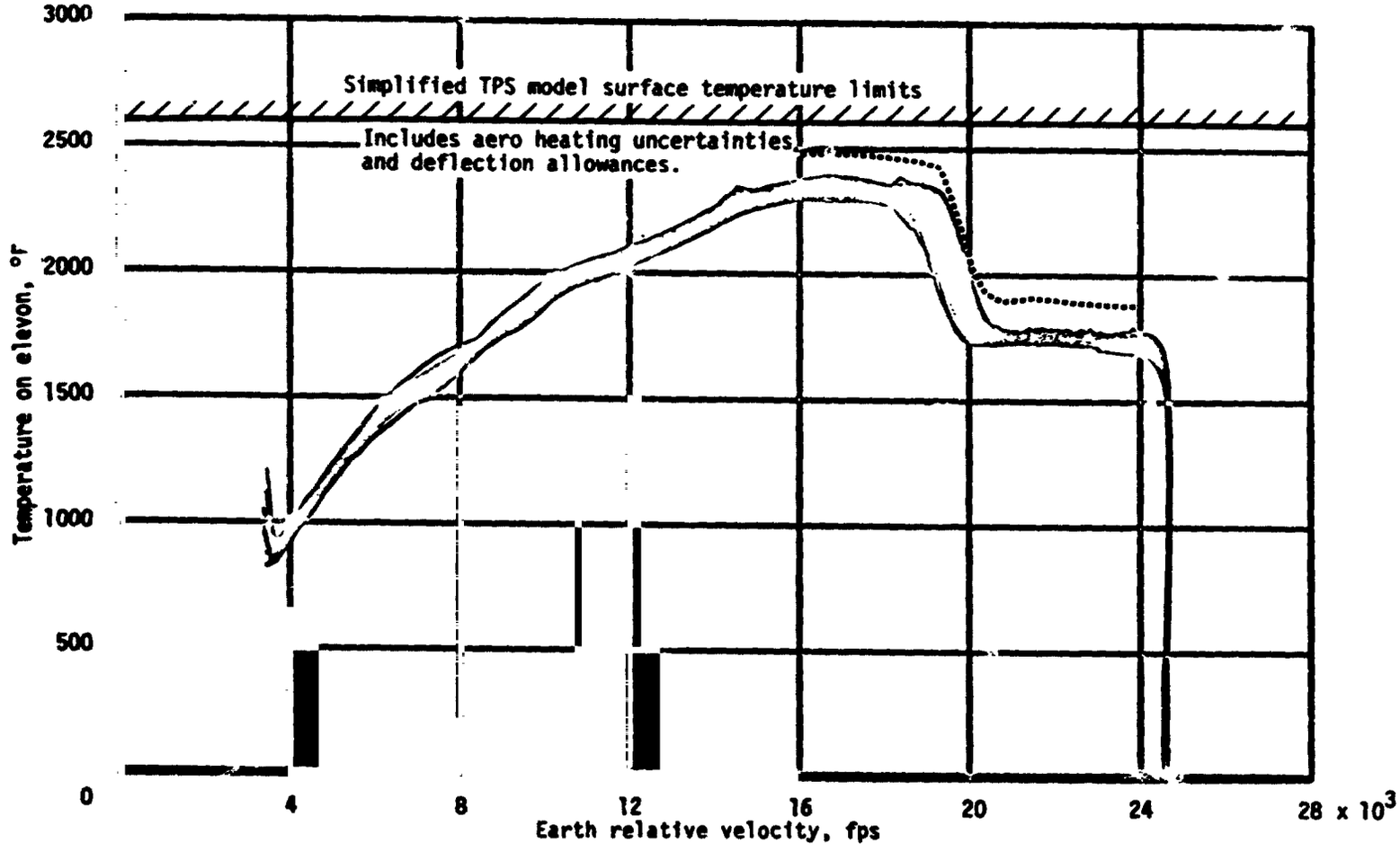

(e) Elevon surface temperature.

Figure 6.- Continued.

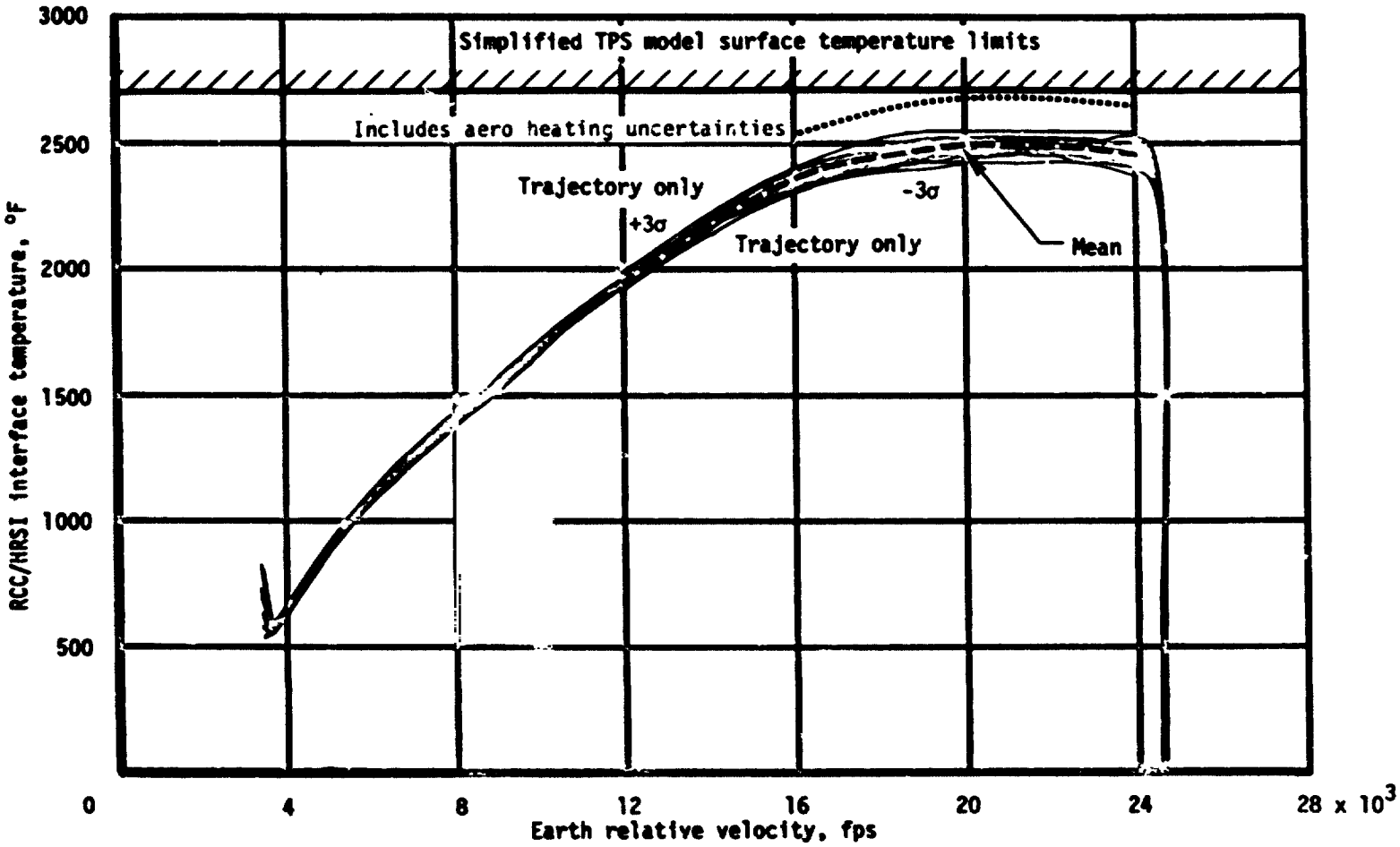

(f) RCC/HRSI interface (CP6) surface temperature.

Figure 6.- Concluded.

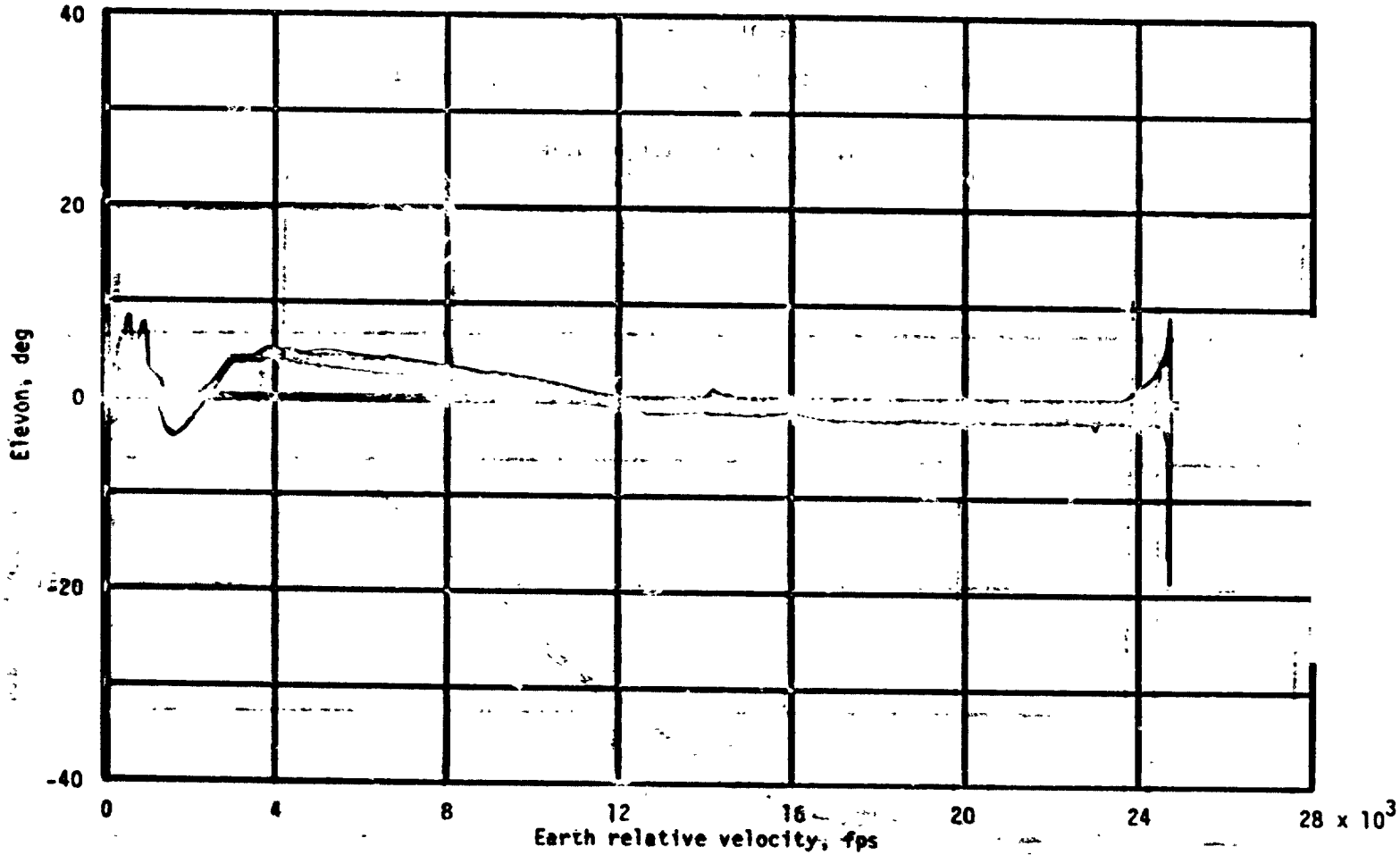

(a) Elevon deflection.

Figure 7.- Control surface deflections and hinge moments - end of mission.

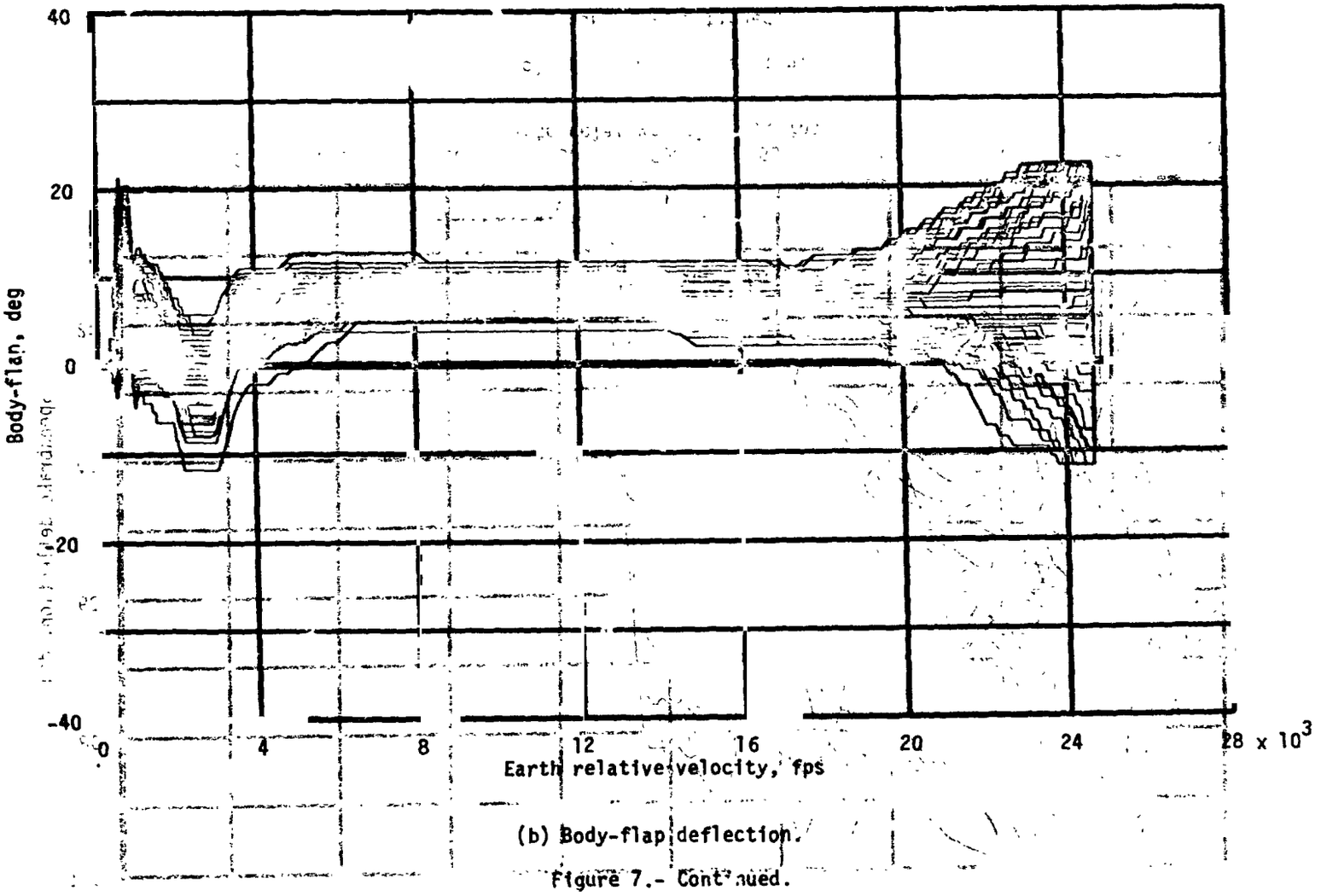

(b) Body-flap deflection.

Figure 7.- Continued.

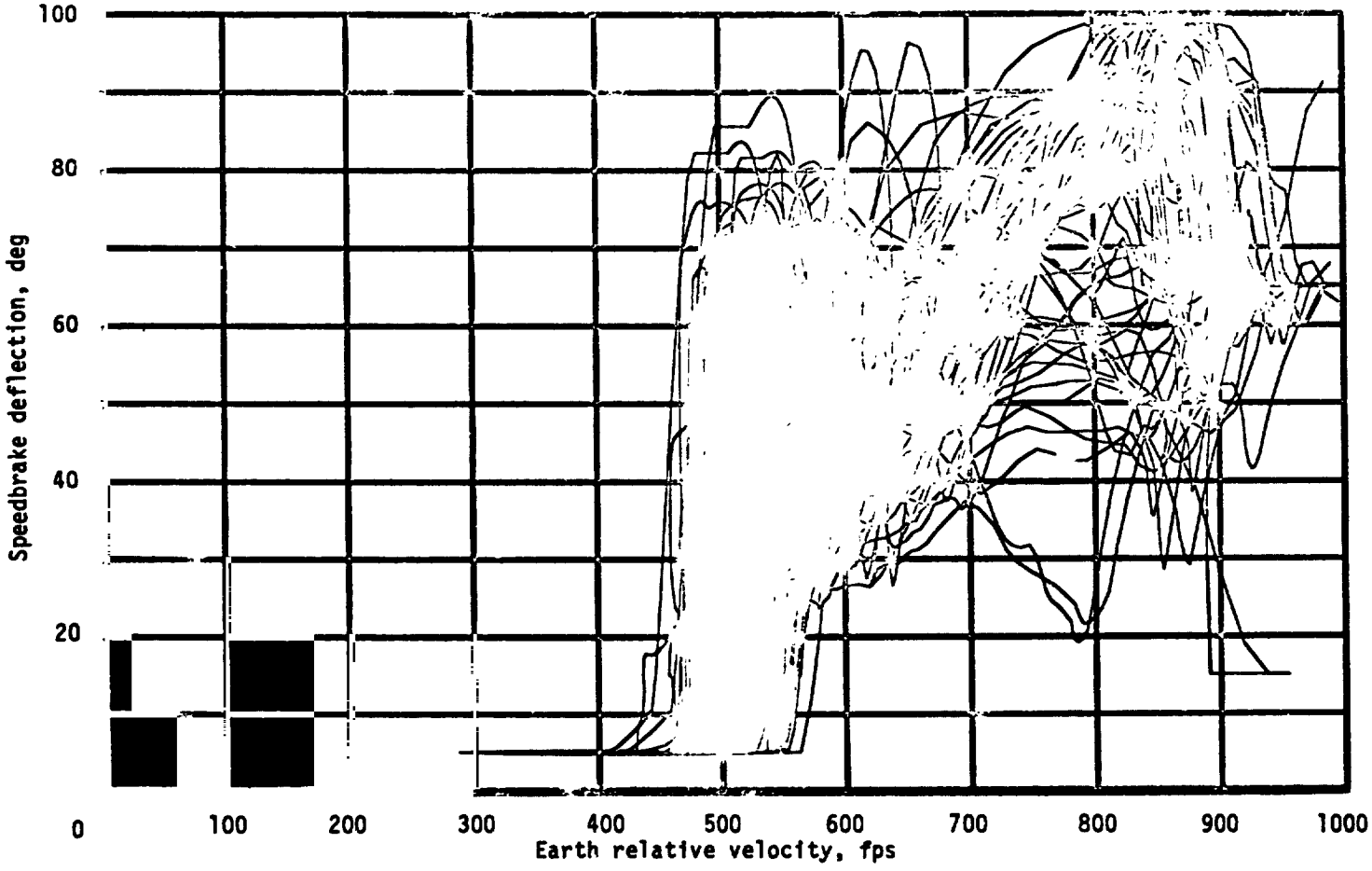

(c) Speedbrake deflection.

Figure 7.- Continued.

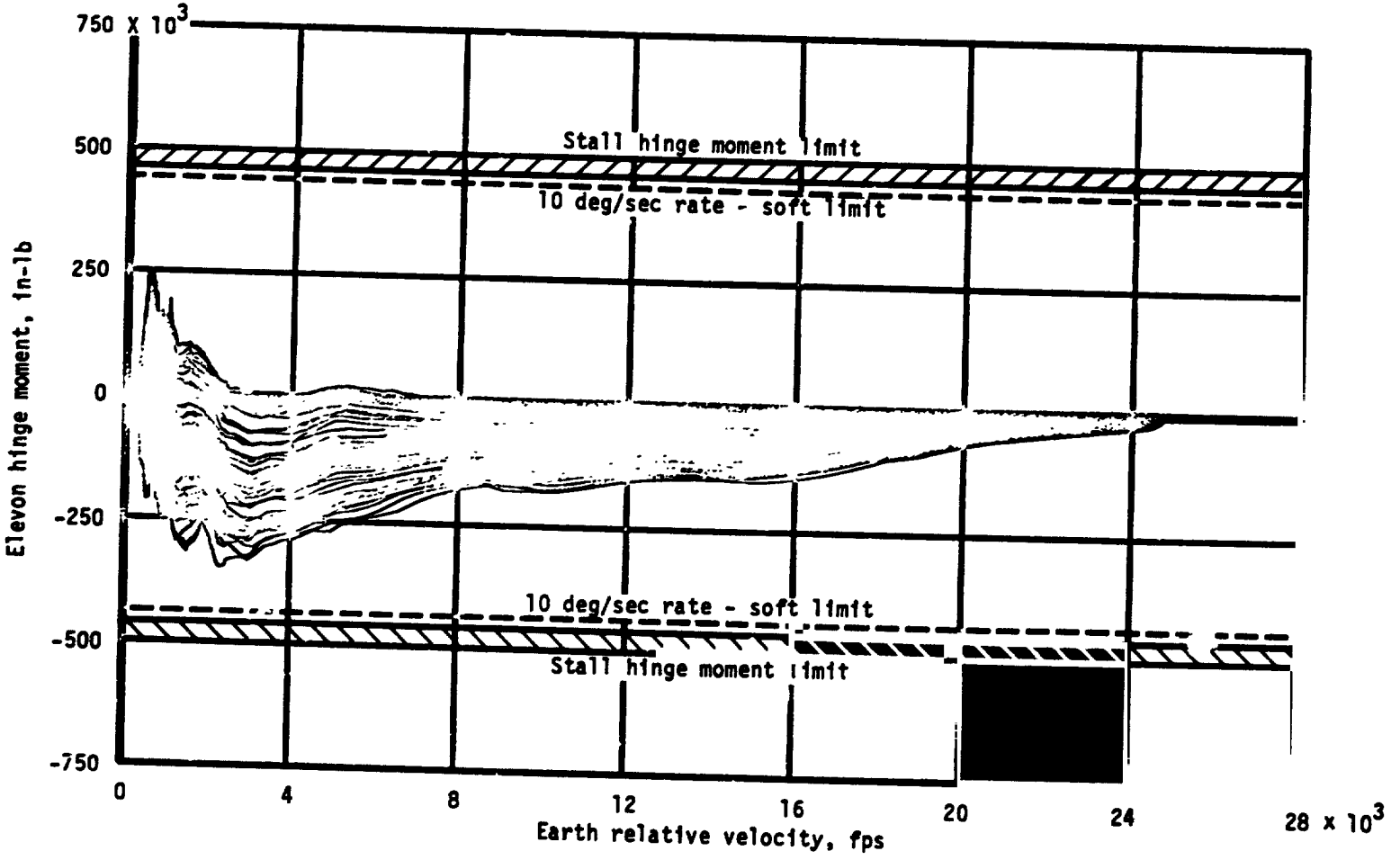

(d) Outboard elevon hinge moment.

Figure 7.- Continued.

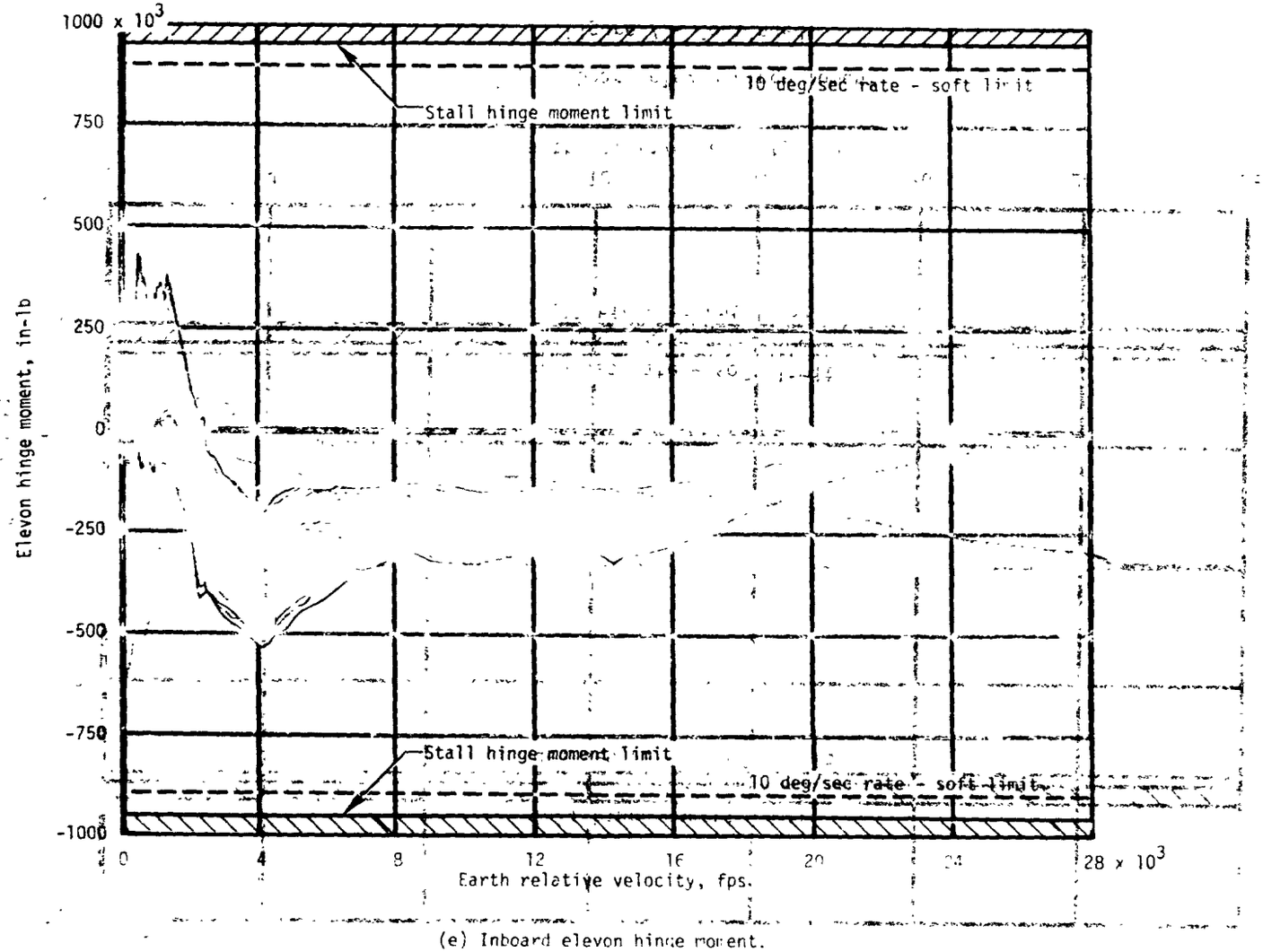

(e) Inboard elevon hinge moment.

Figure 7.- Continued.

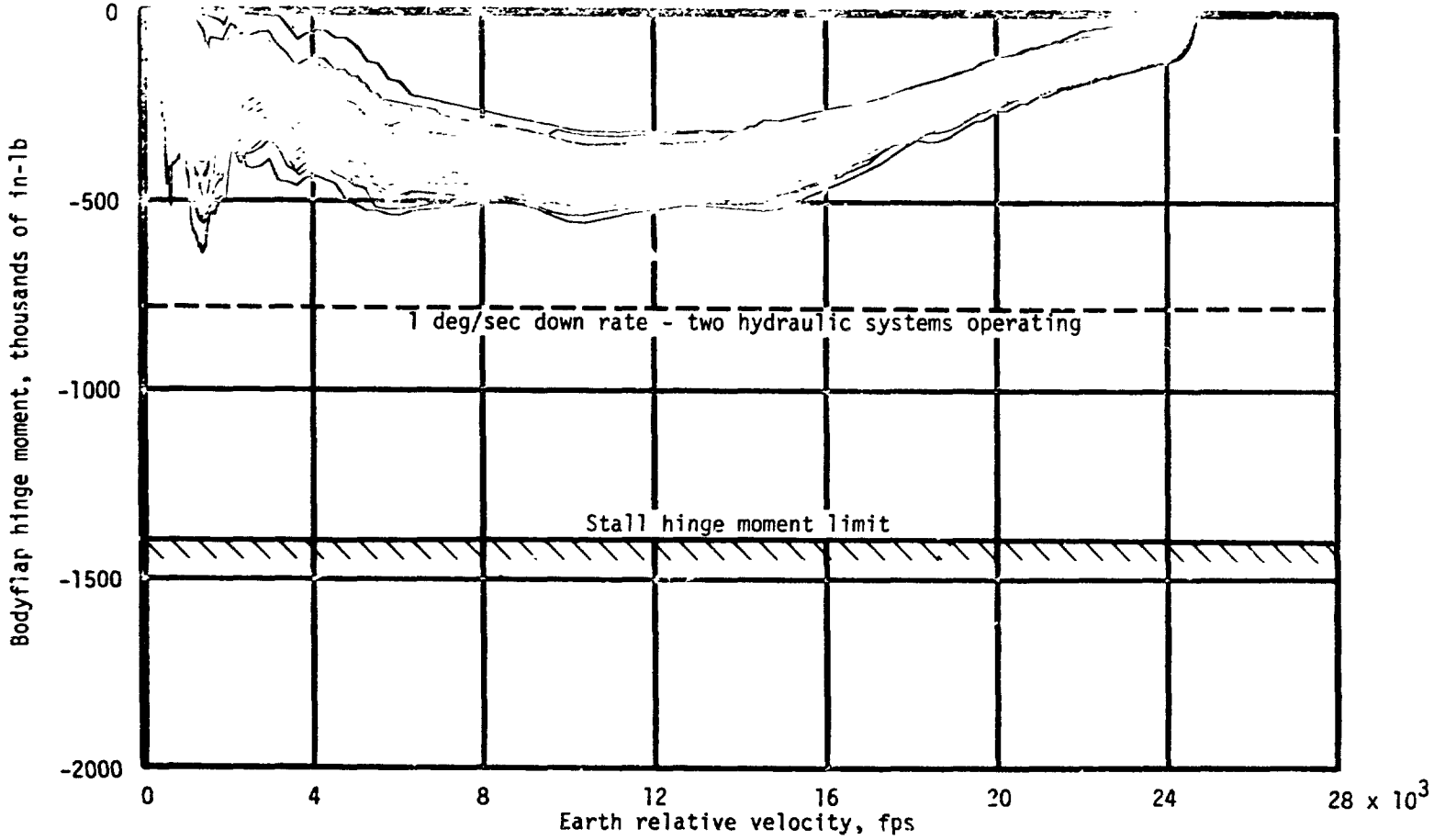

(f) Bodyflap hinge moment.

Figure 7.- Continued.

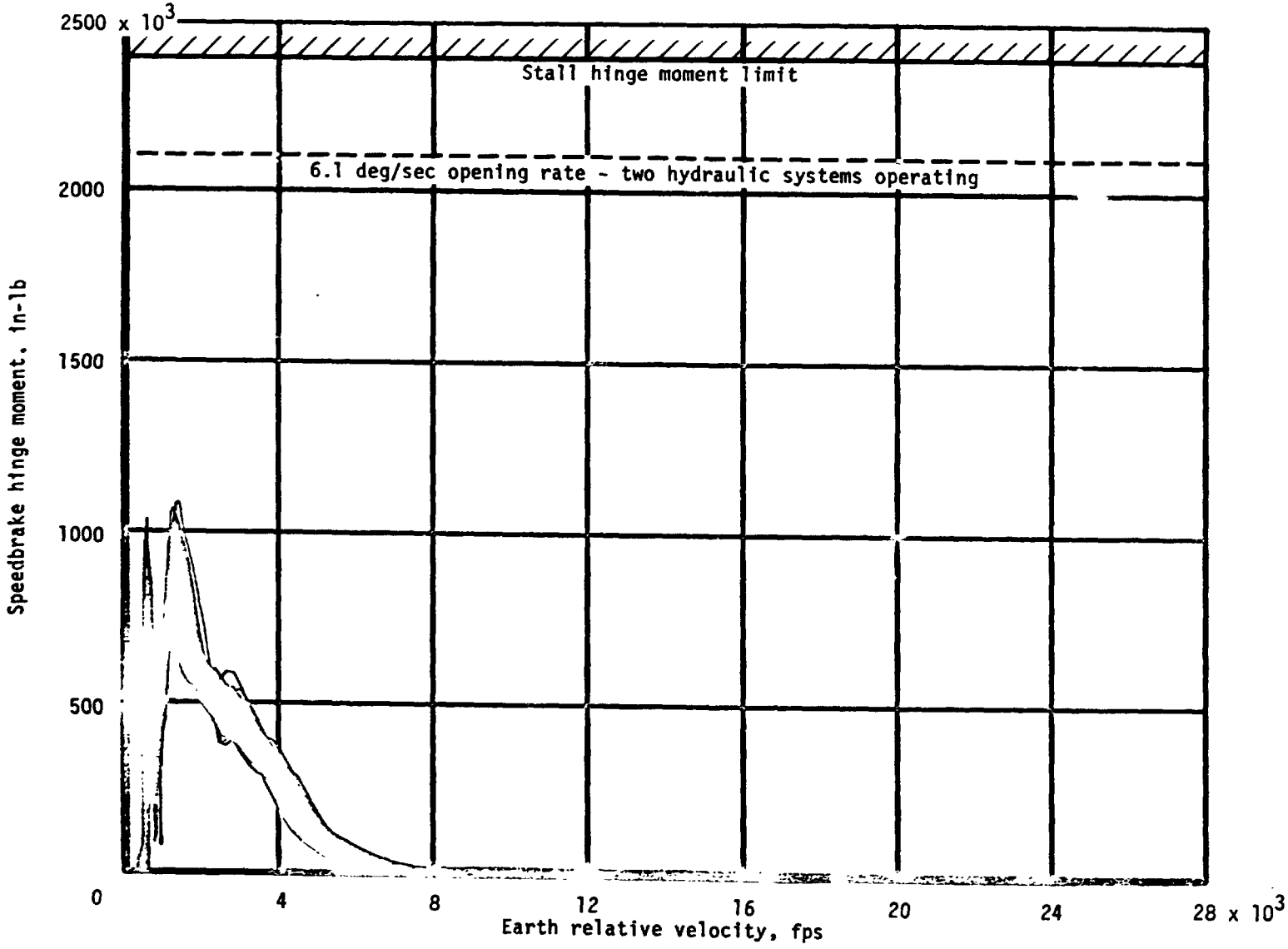

(g) Speedbrake hinge moment.

Figure 7.- Concluded.

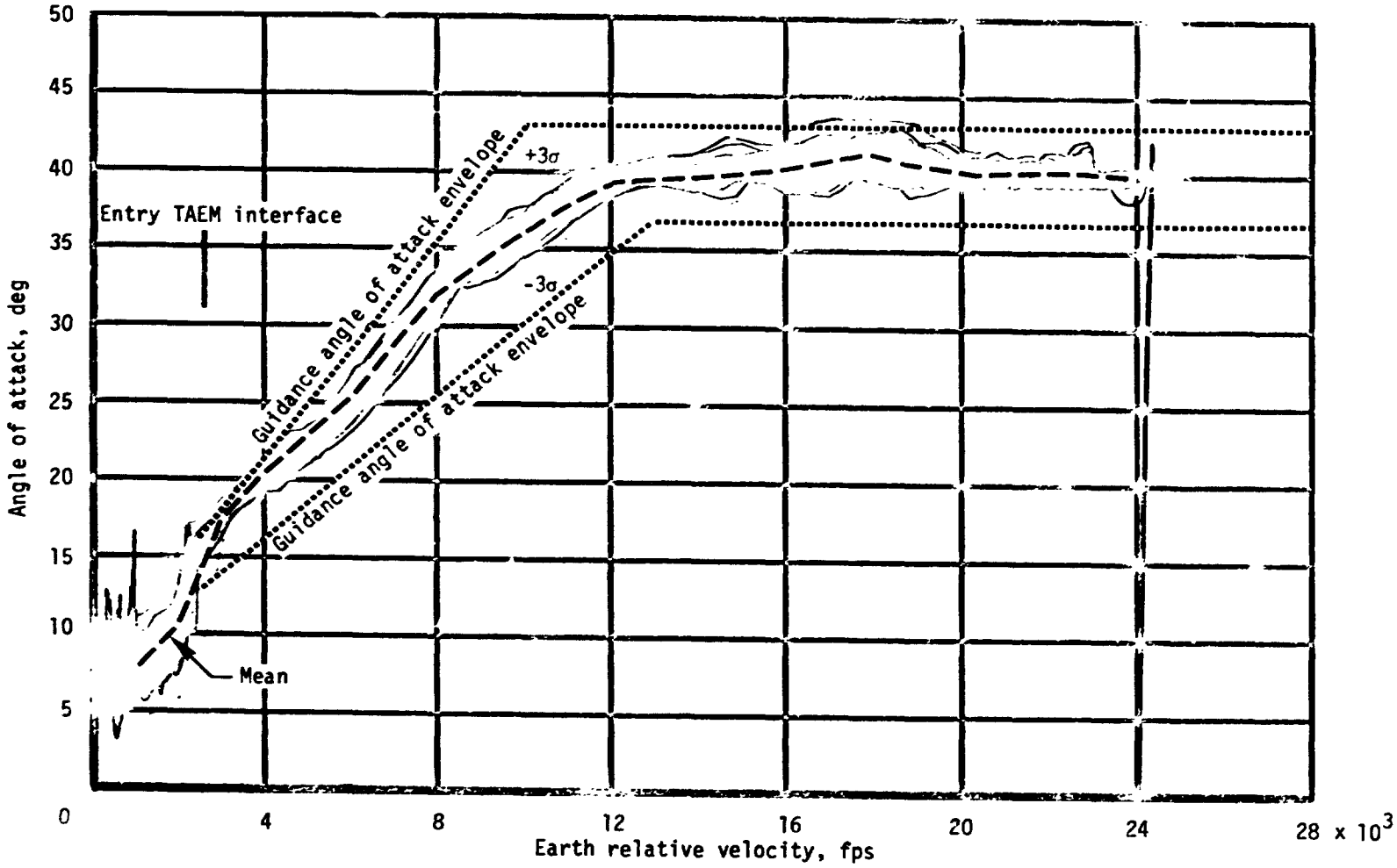

(a) Angle of attack.

Figure 8.- Entry guidance performance parameters - end of mission.

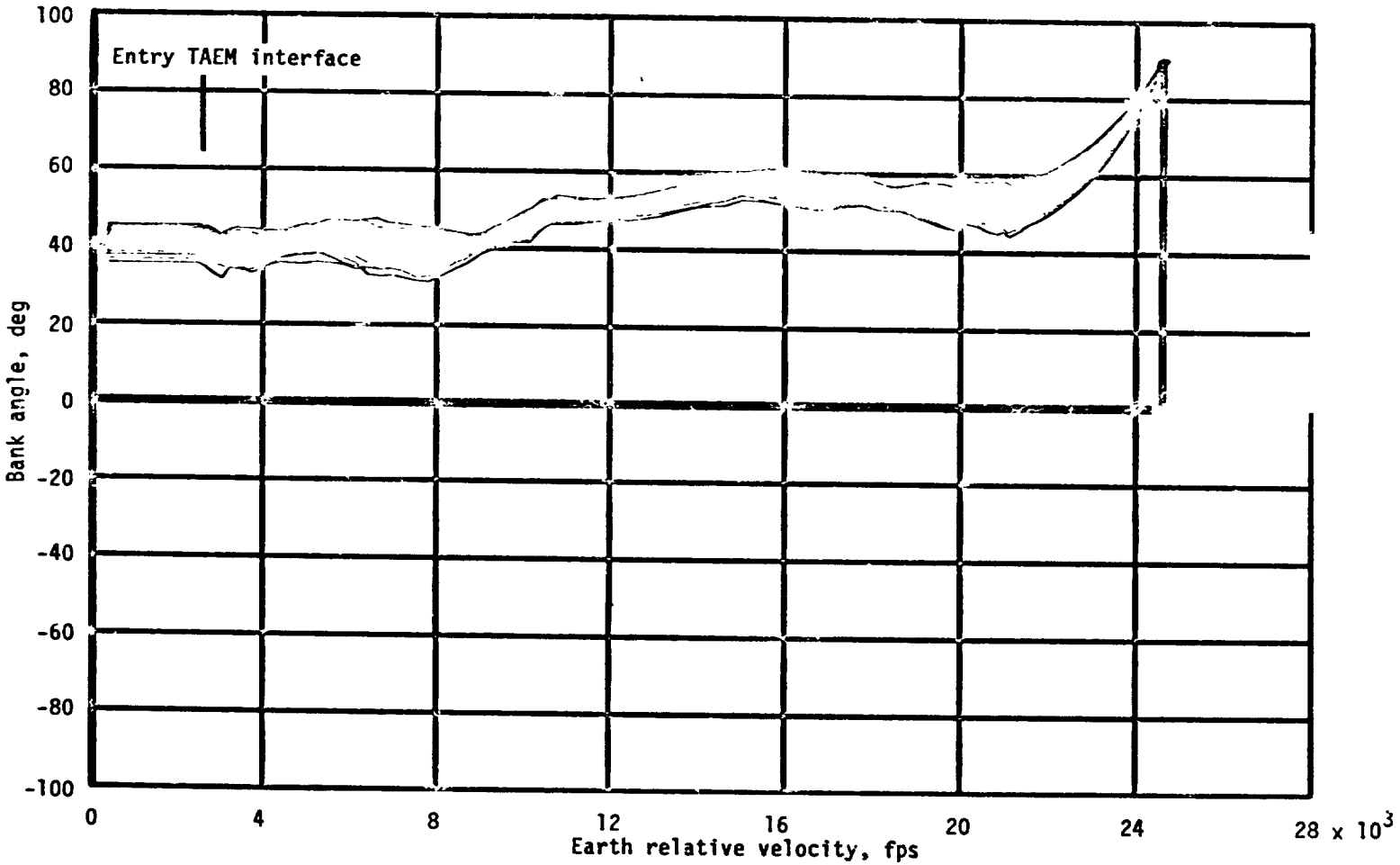

(b) Reference bank angle.

Figure 8.- Continued.

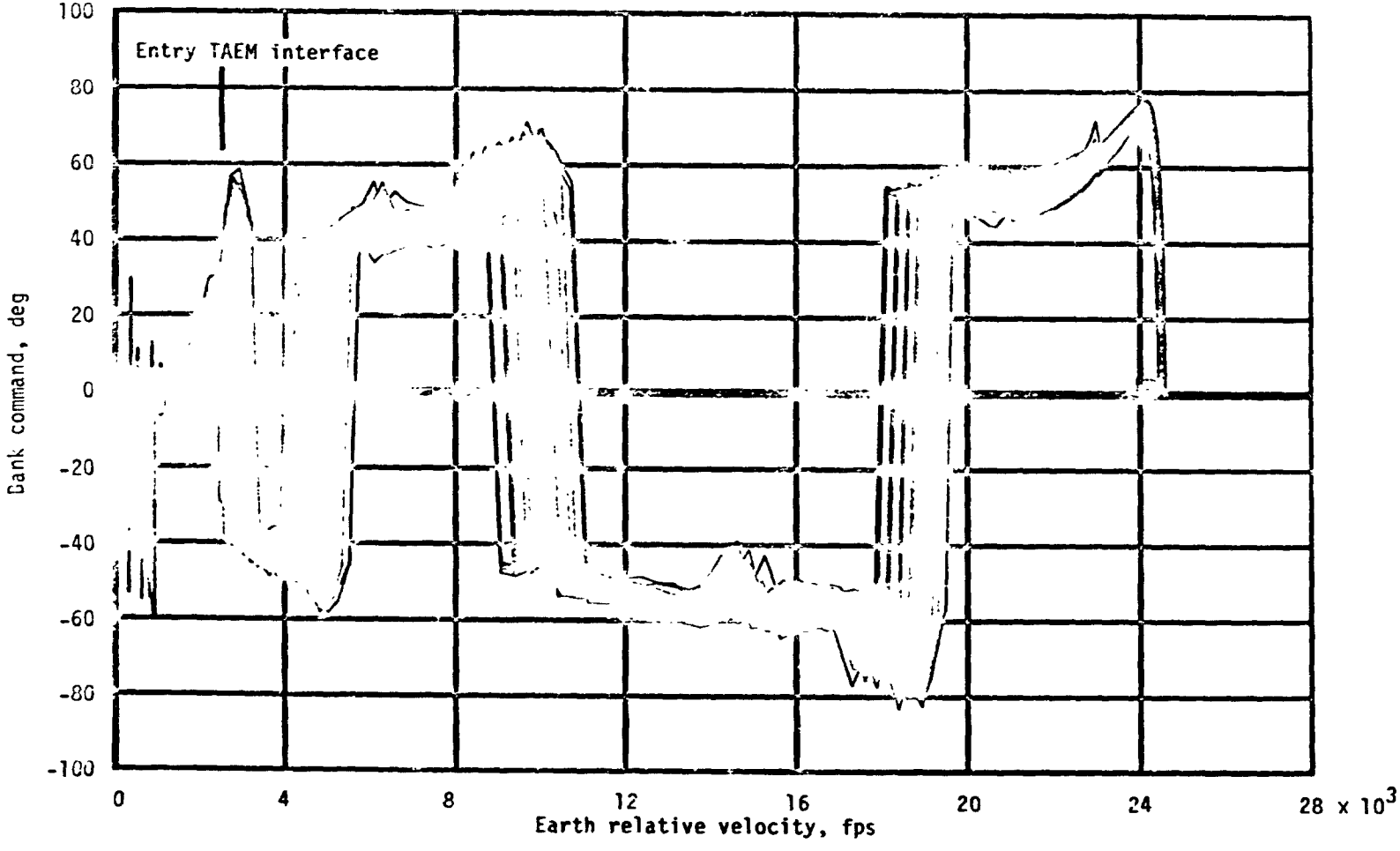

(c) Bank command.

Figure 8.- Continued.

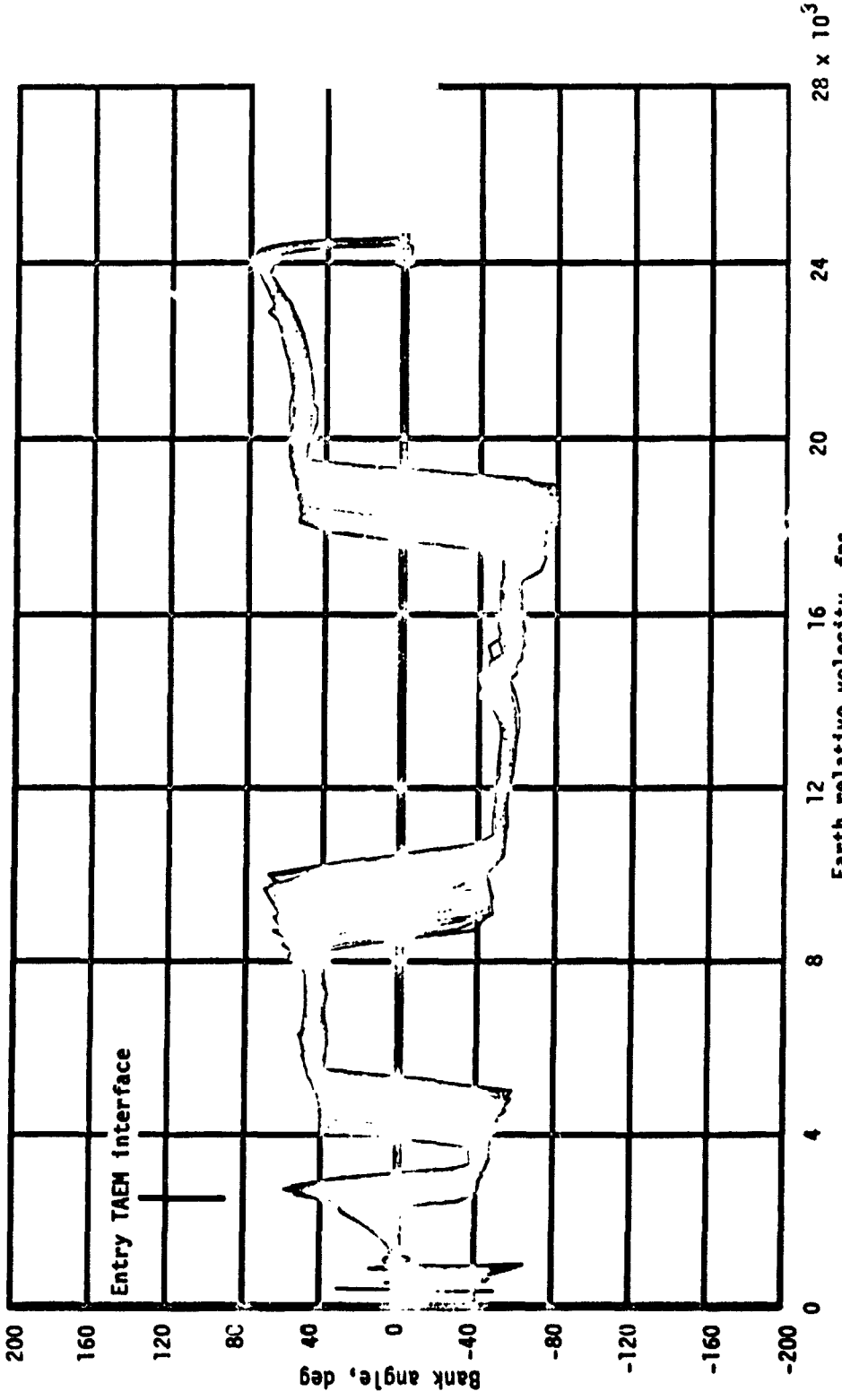

(d) Bank angle.

Figure 8.- Continued.

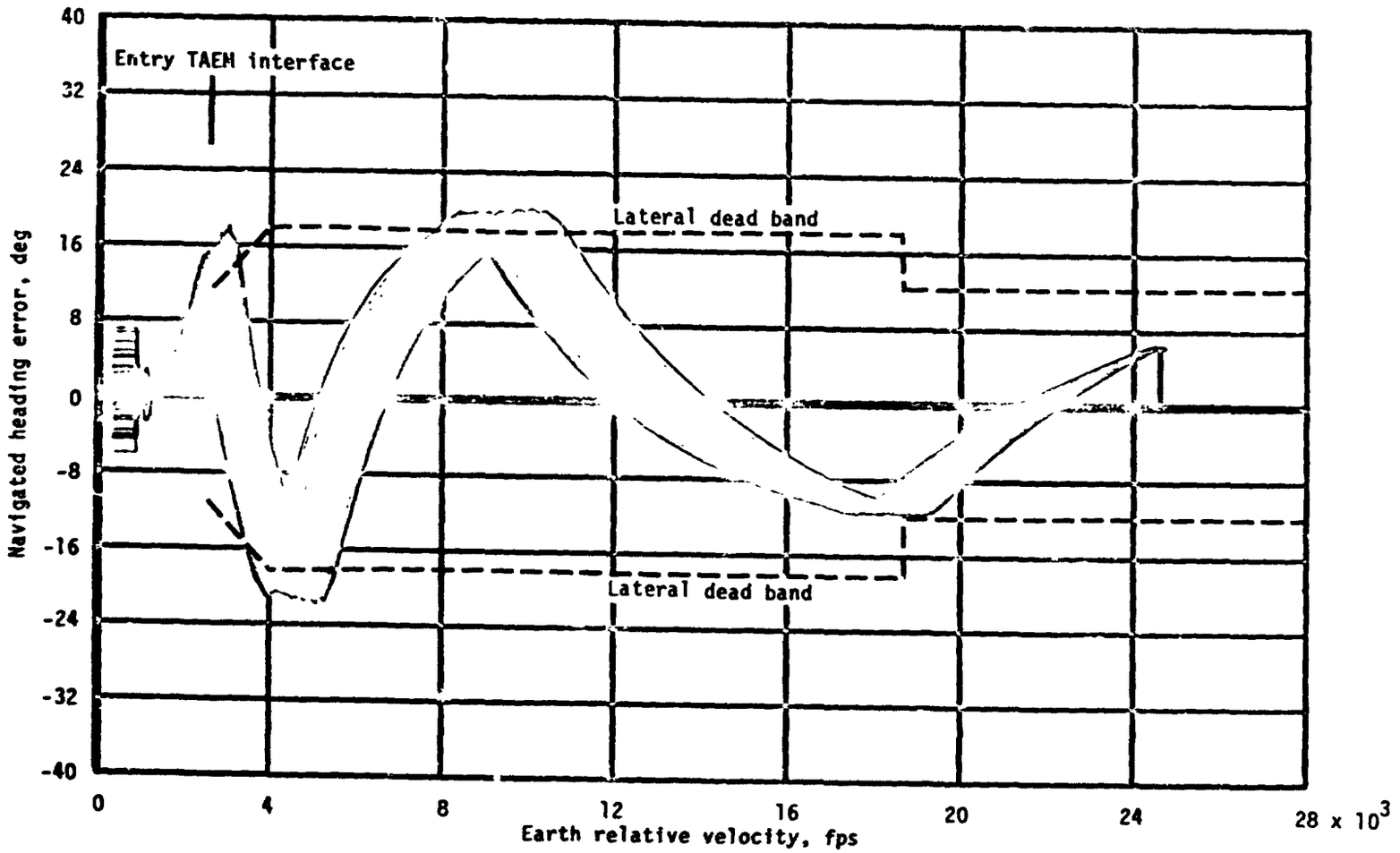

(e) Navigated heading error.

Figure 8.- Continued.

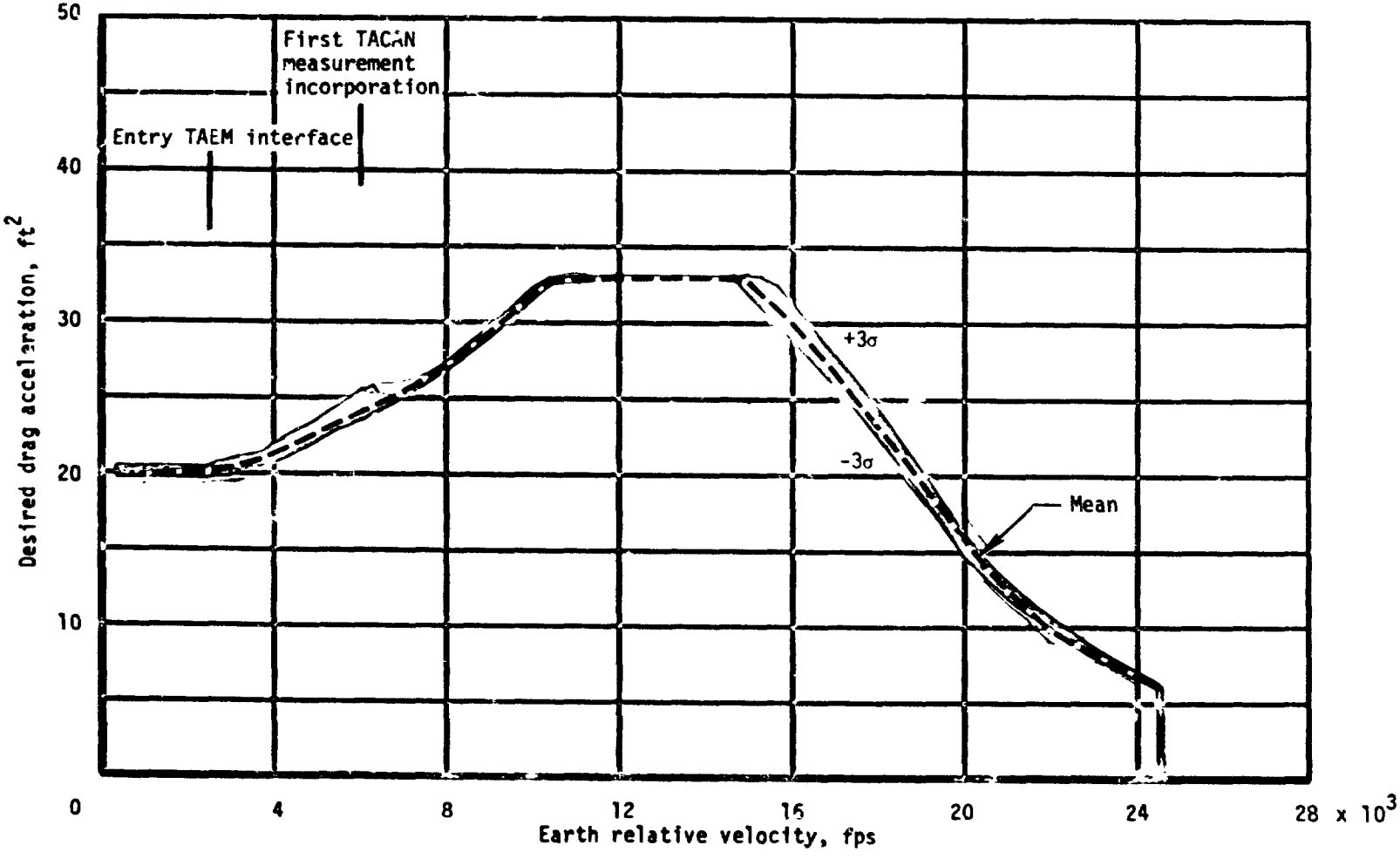

(f) Desired drag acceleration.

Figure 8.- Continued.

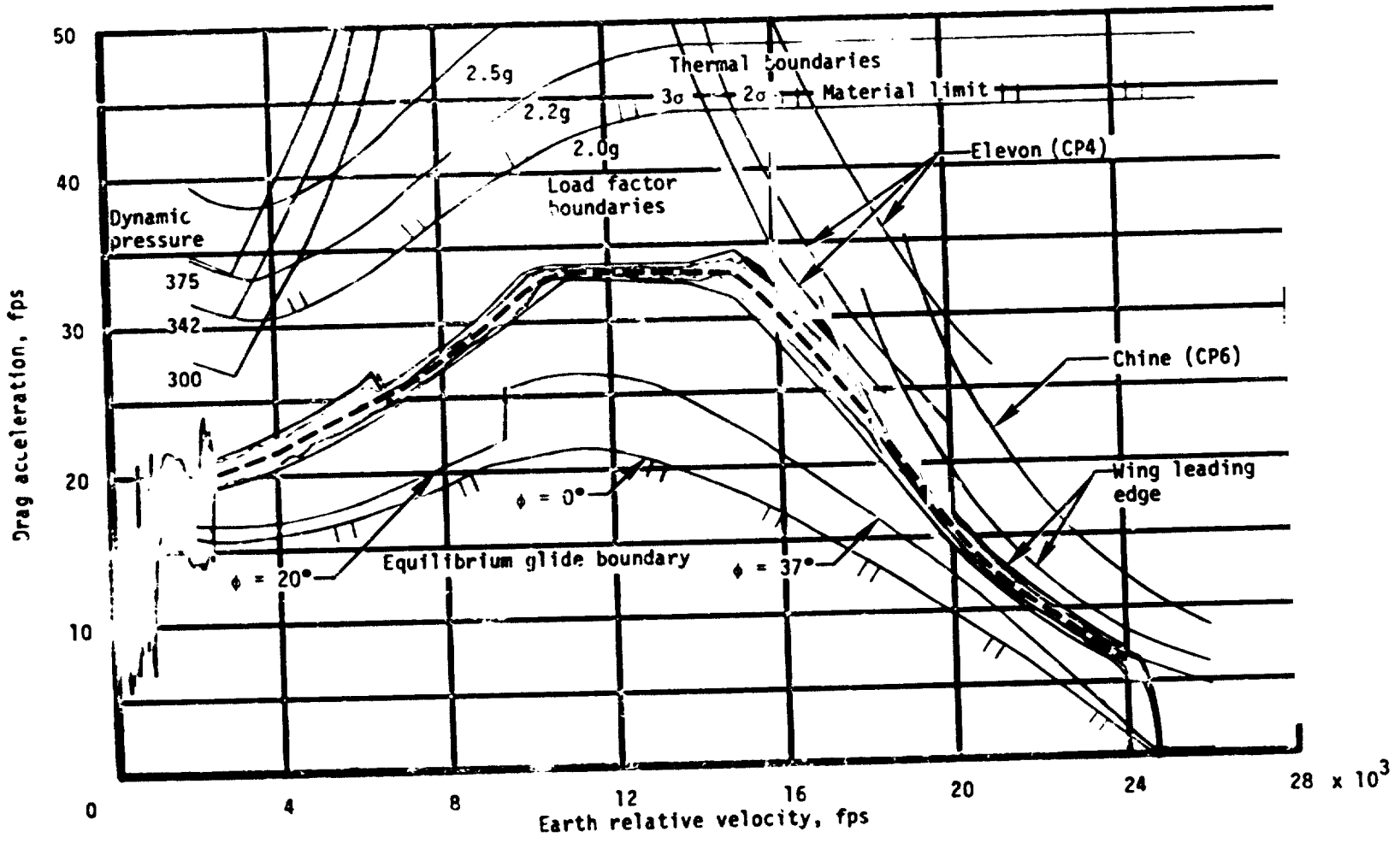

(g) Drag acceleration.

Figure 8.- Continued.

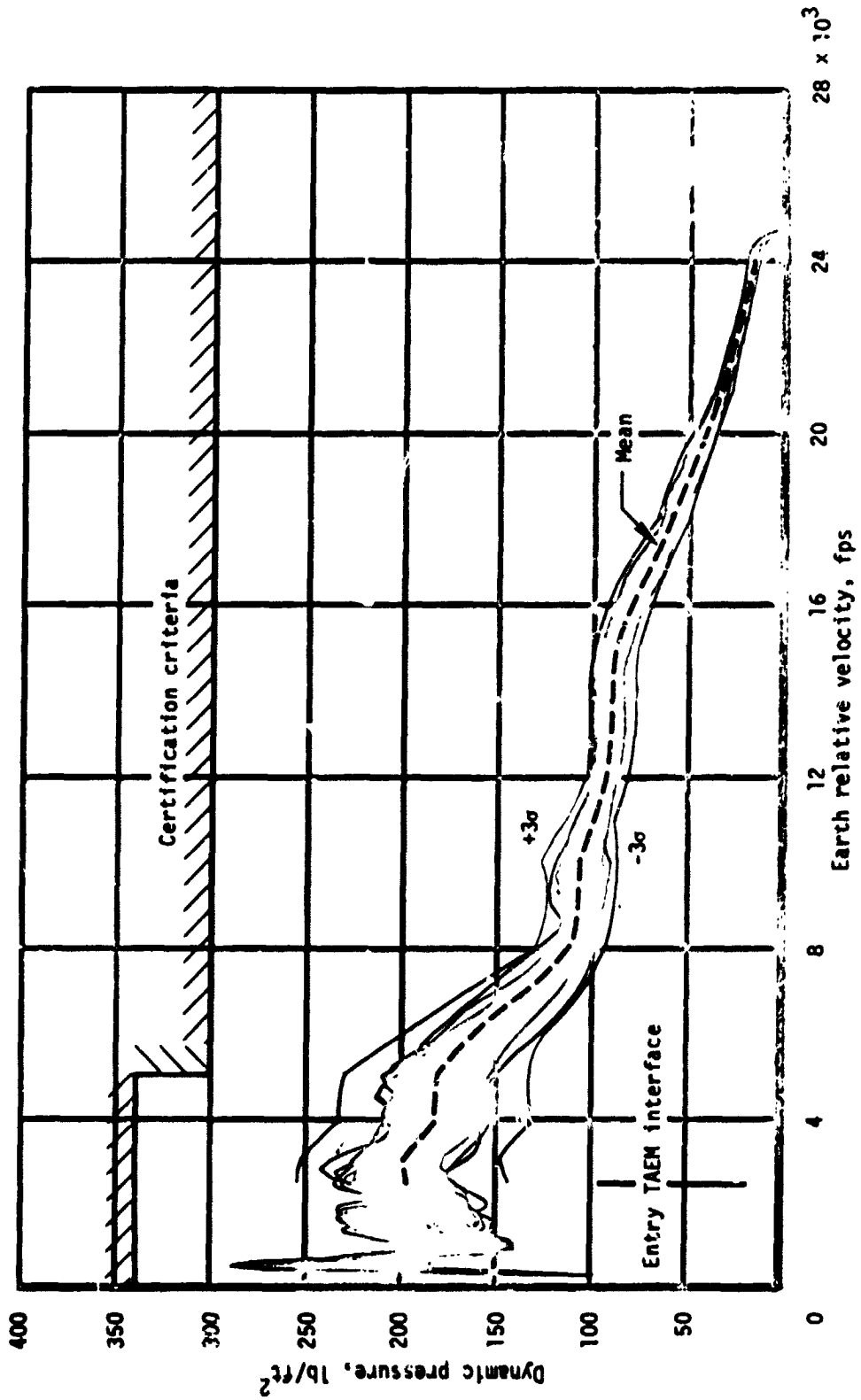

(h) Dynamic pressure.

Figure 8.- Continued.

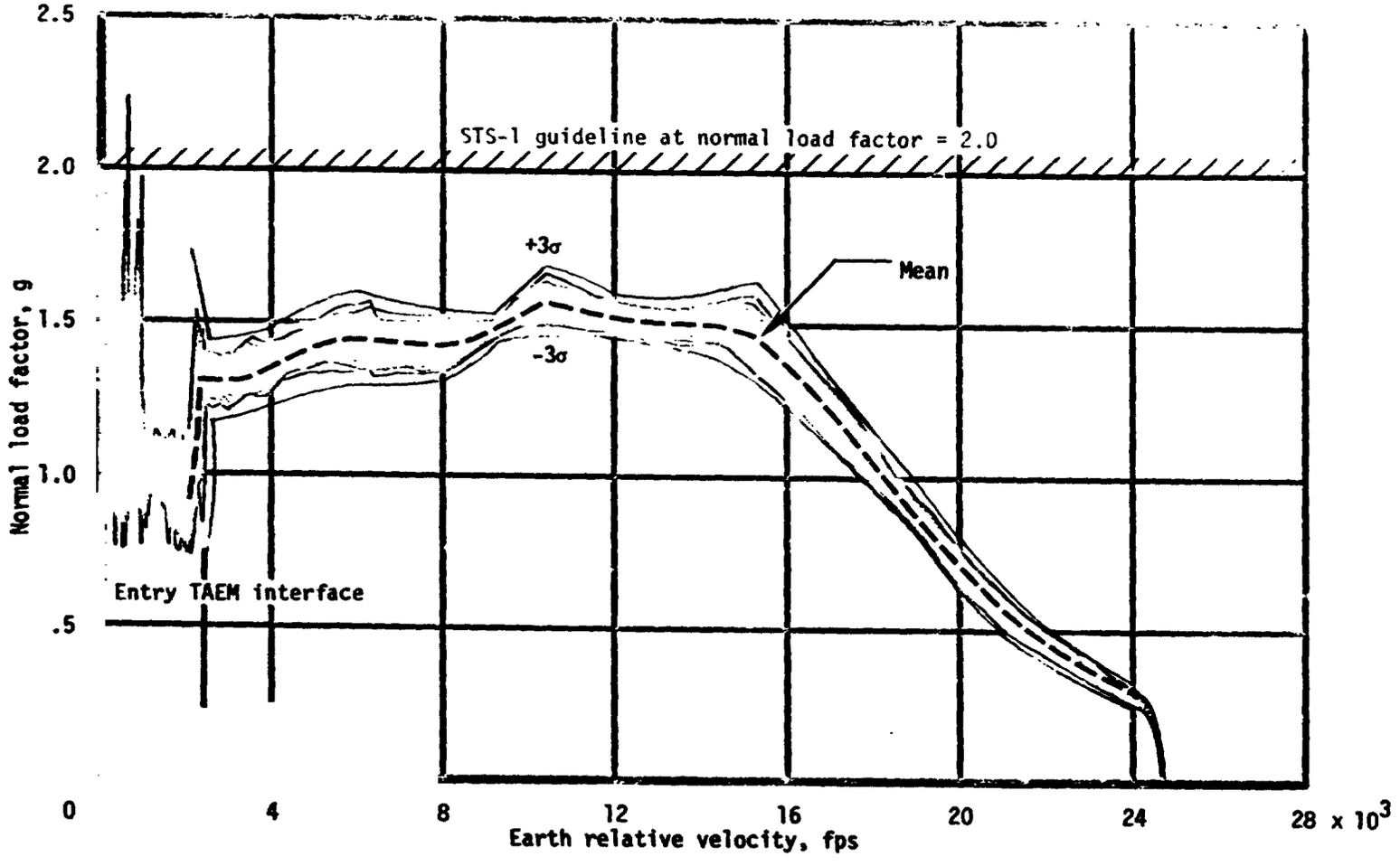

(i) Normal load factor.

Figure 8.- Continued.

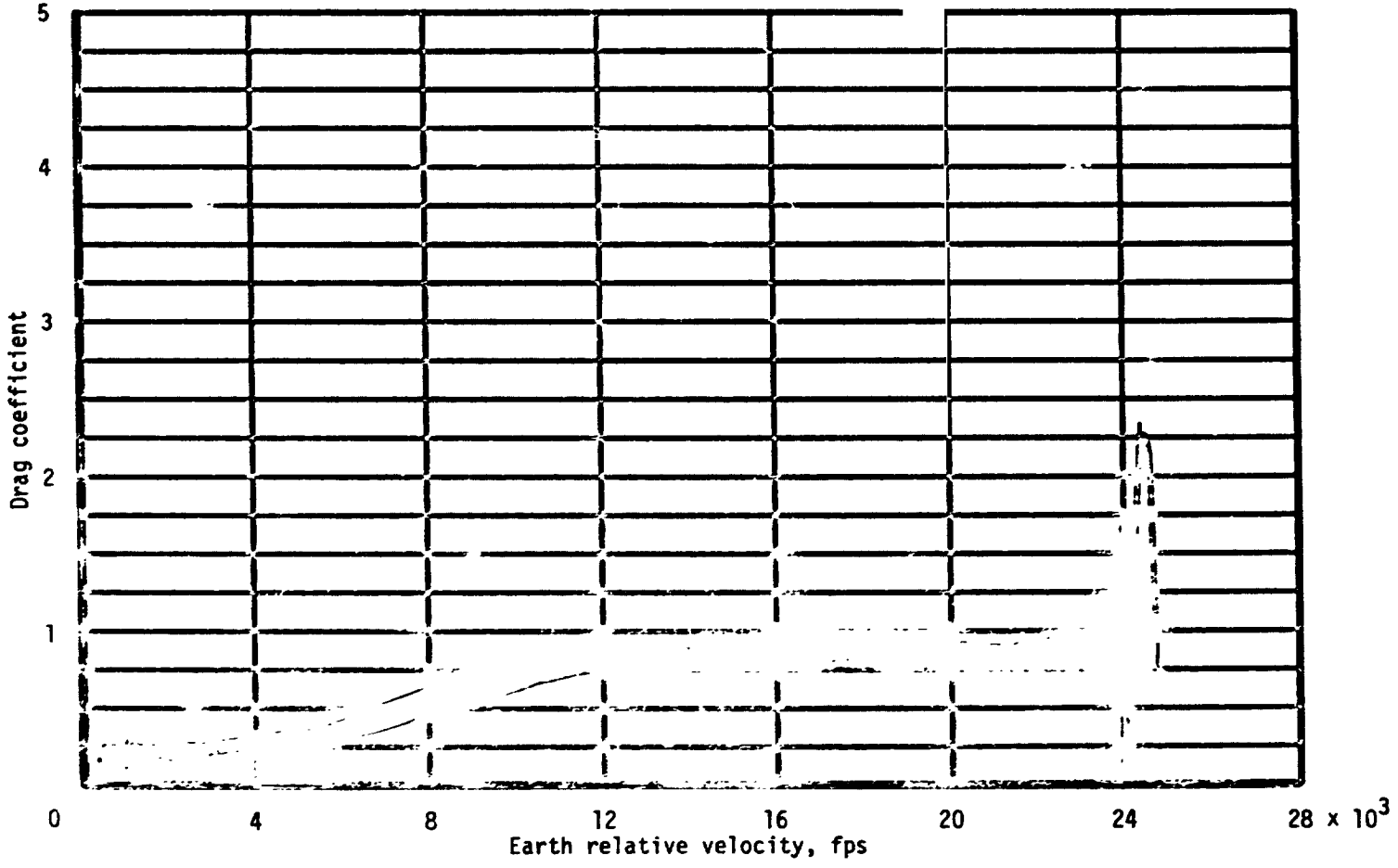

(j) Drag coefficient.

Figure 8.- Continued.

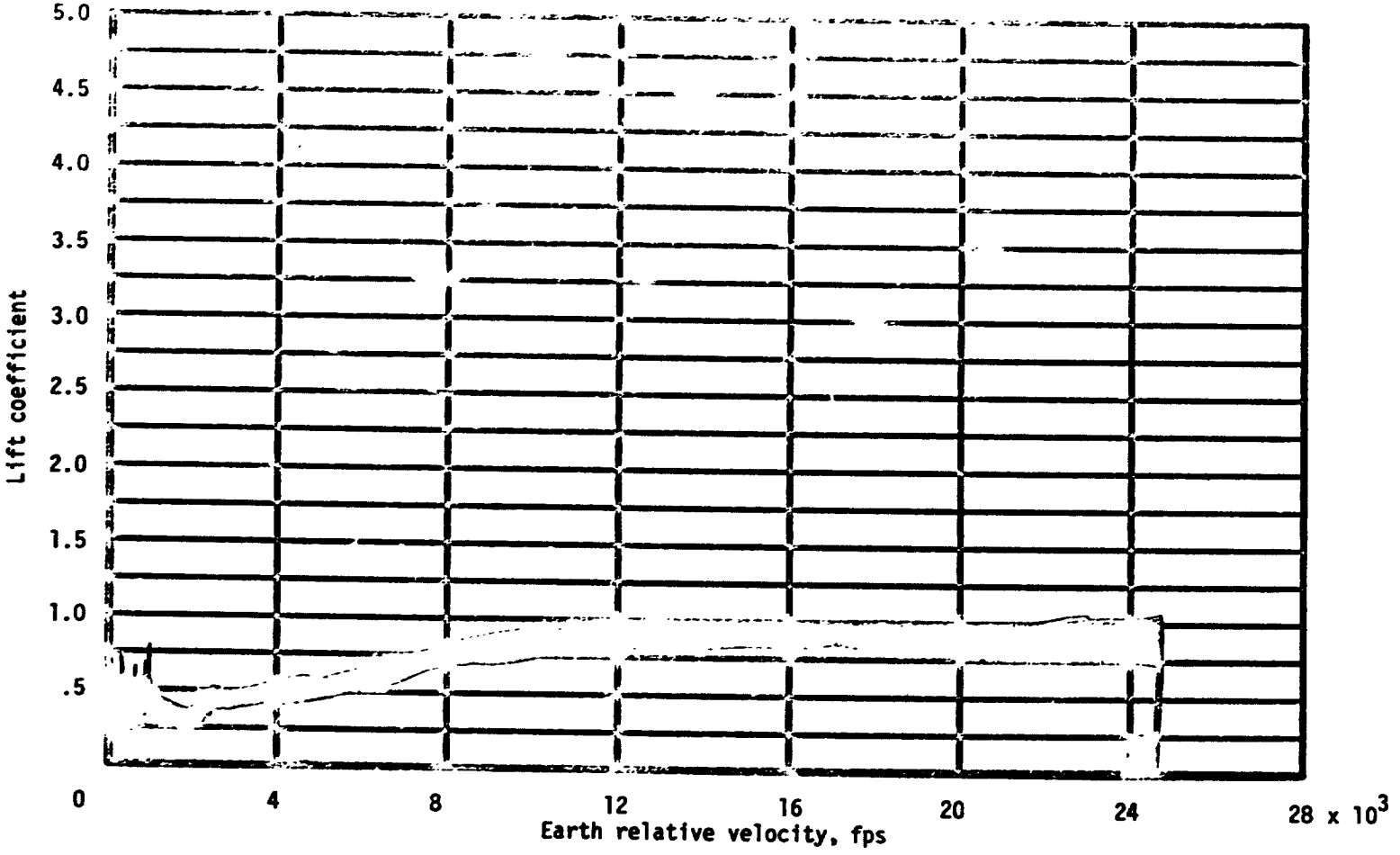

(k) Lift coefficient.

Figure 8.- Continued.

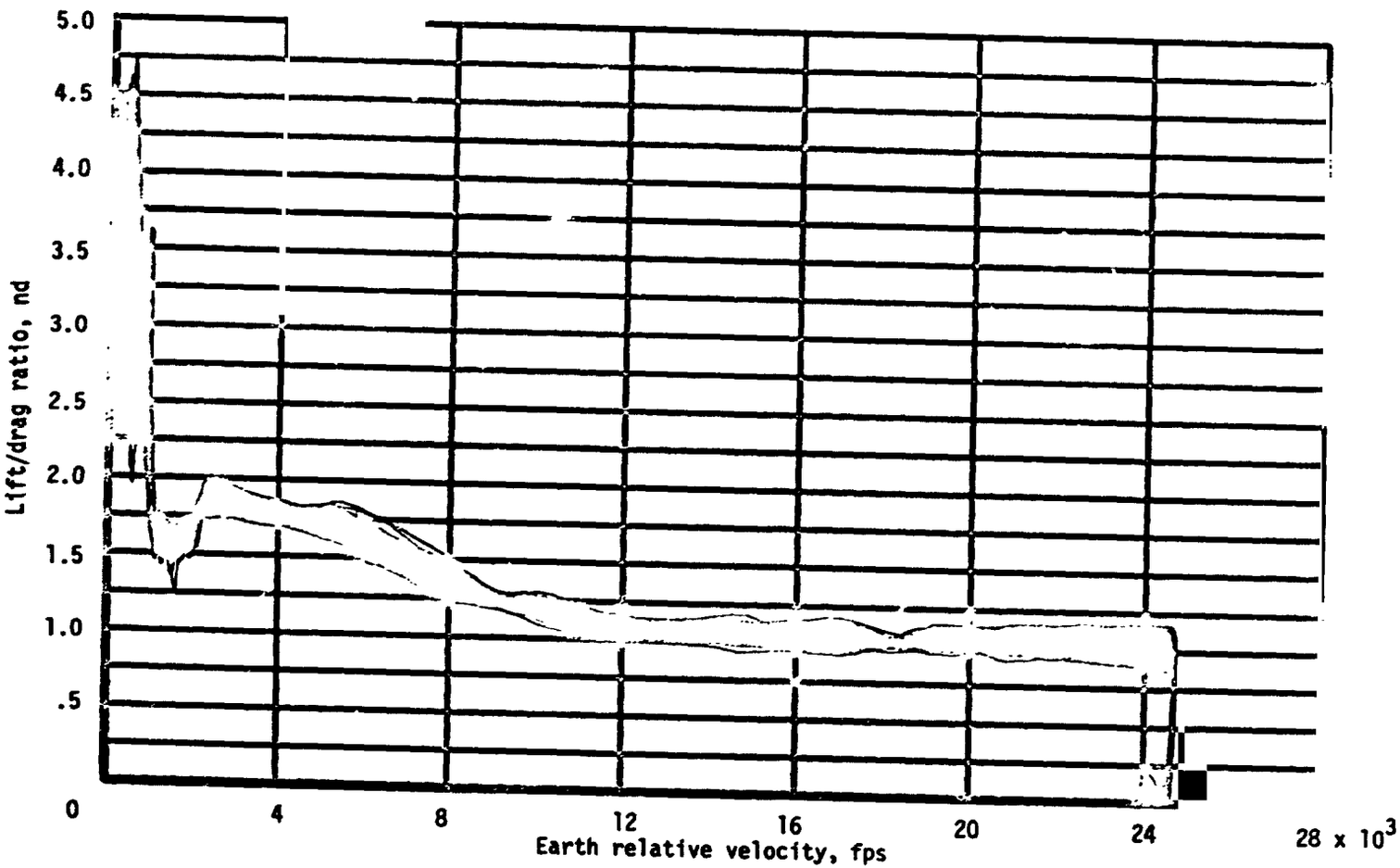

(1) Lift to drag ratio.

Figure 8.- Continued.

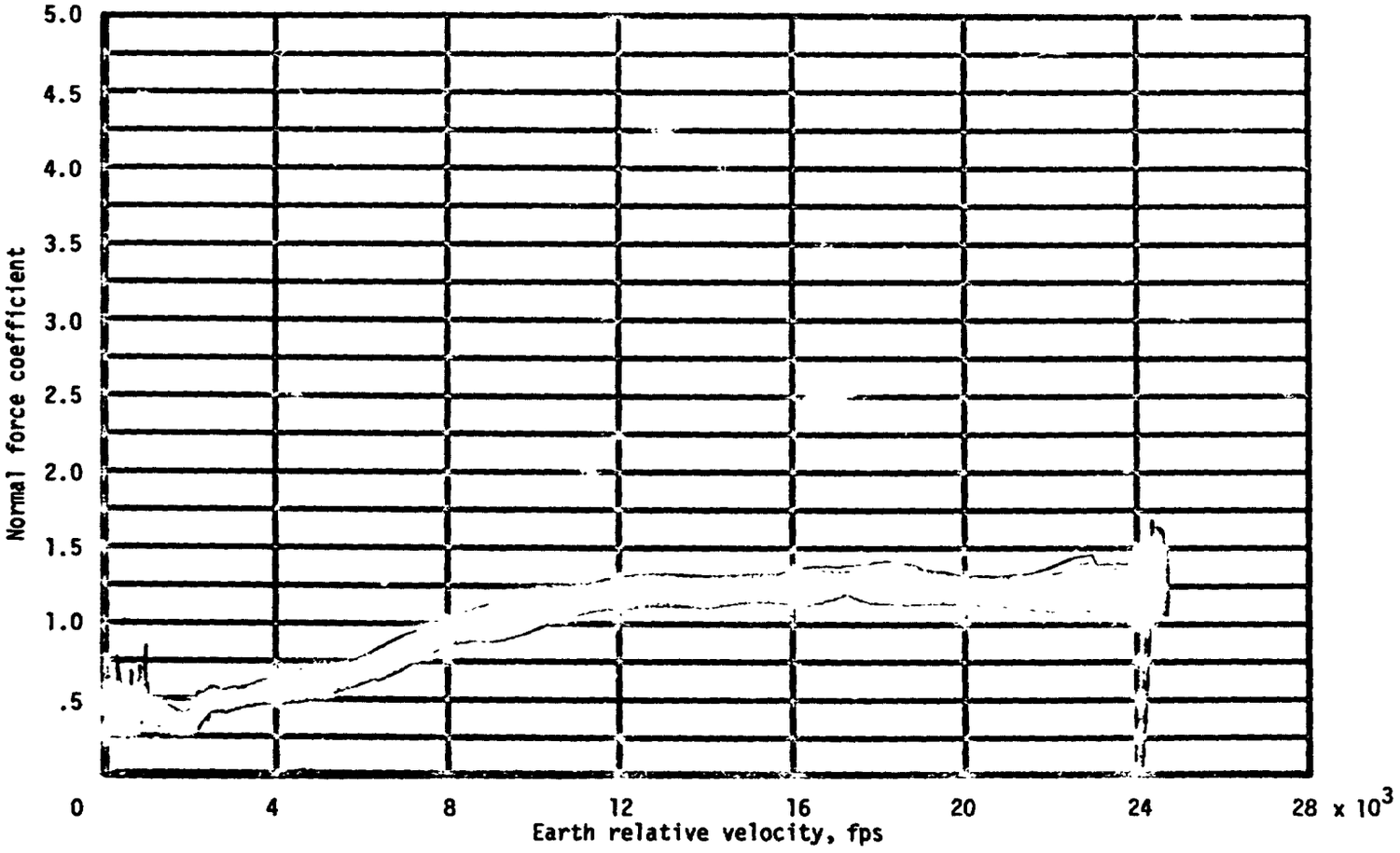

(m) Normal force coefficient.

Figure 8.- Continued.

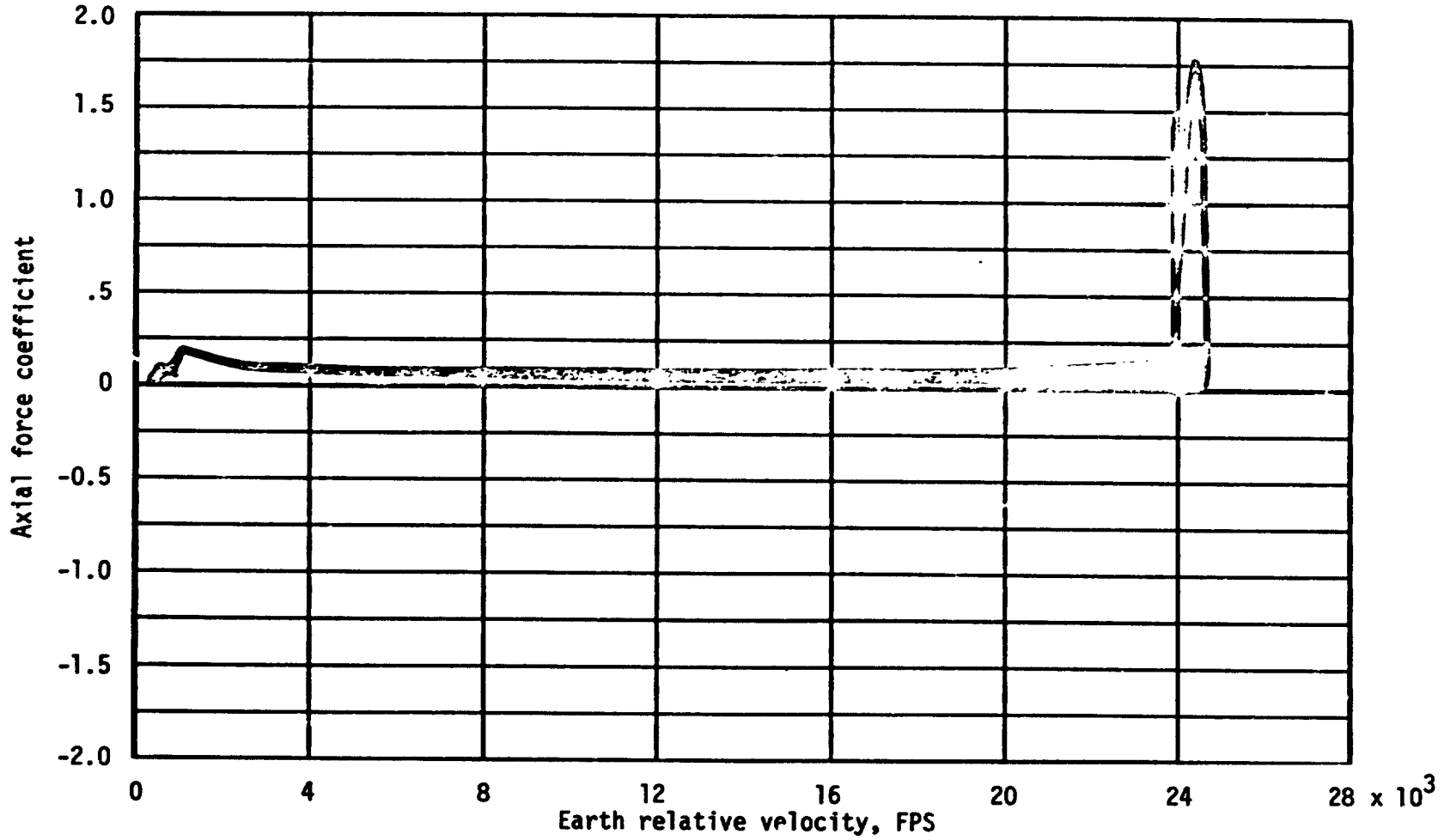

(n) Axial force coefficient.

Figure 8.- Continued.

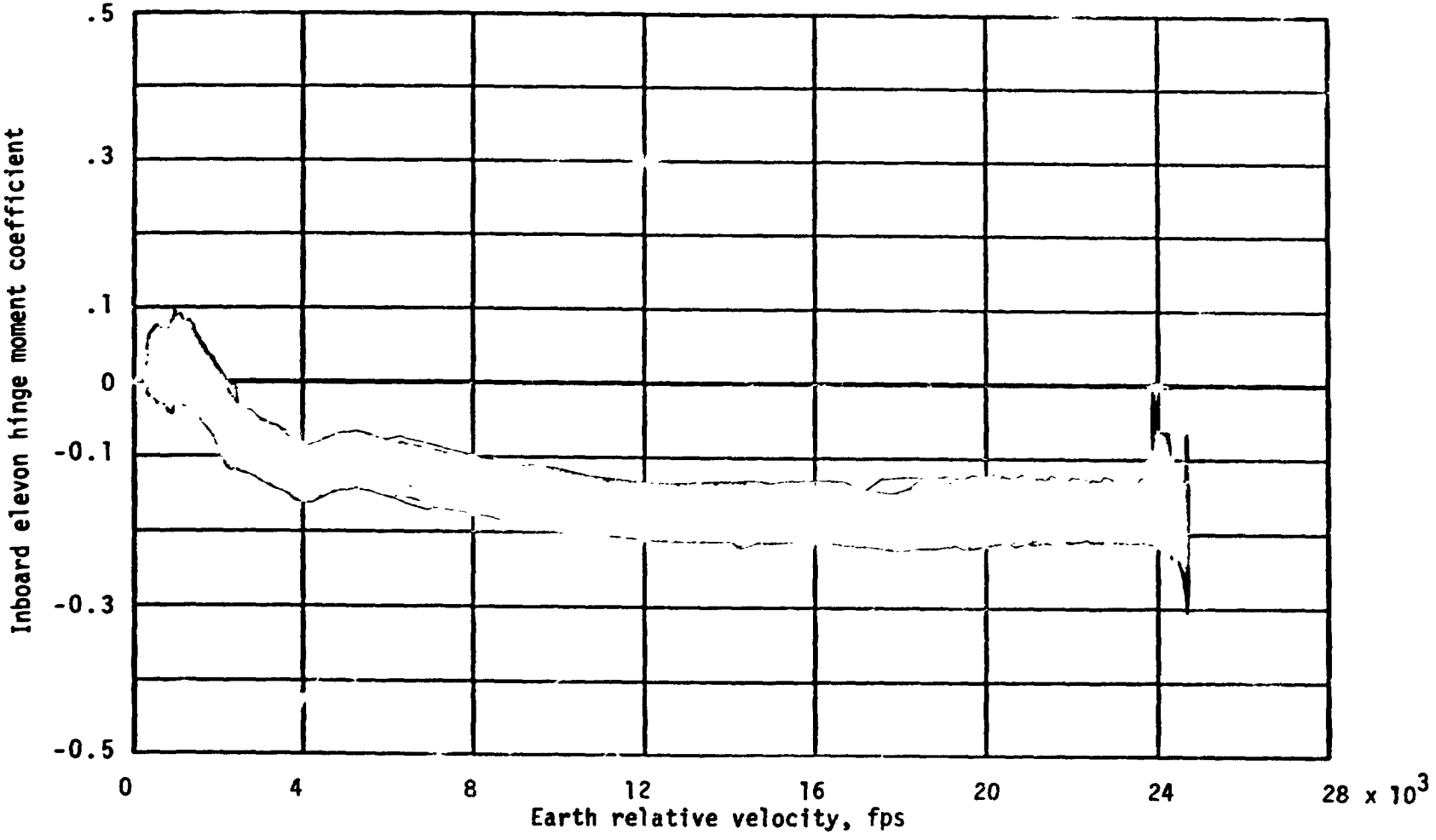

(o) Inboard elevon hinge moment coefficient.

Figure 8.- Continued.

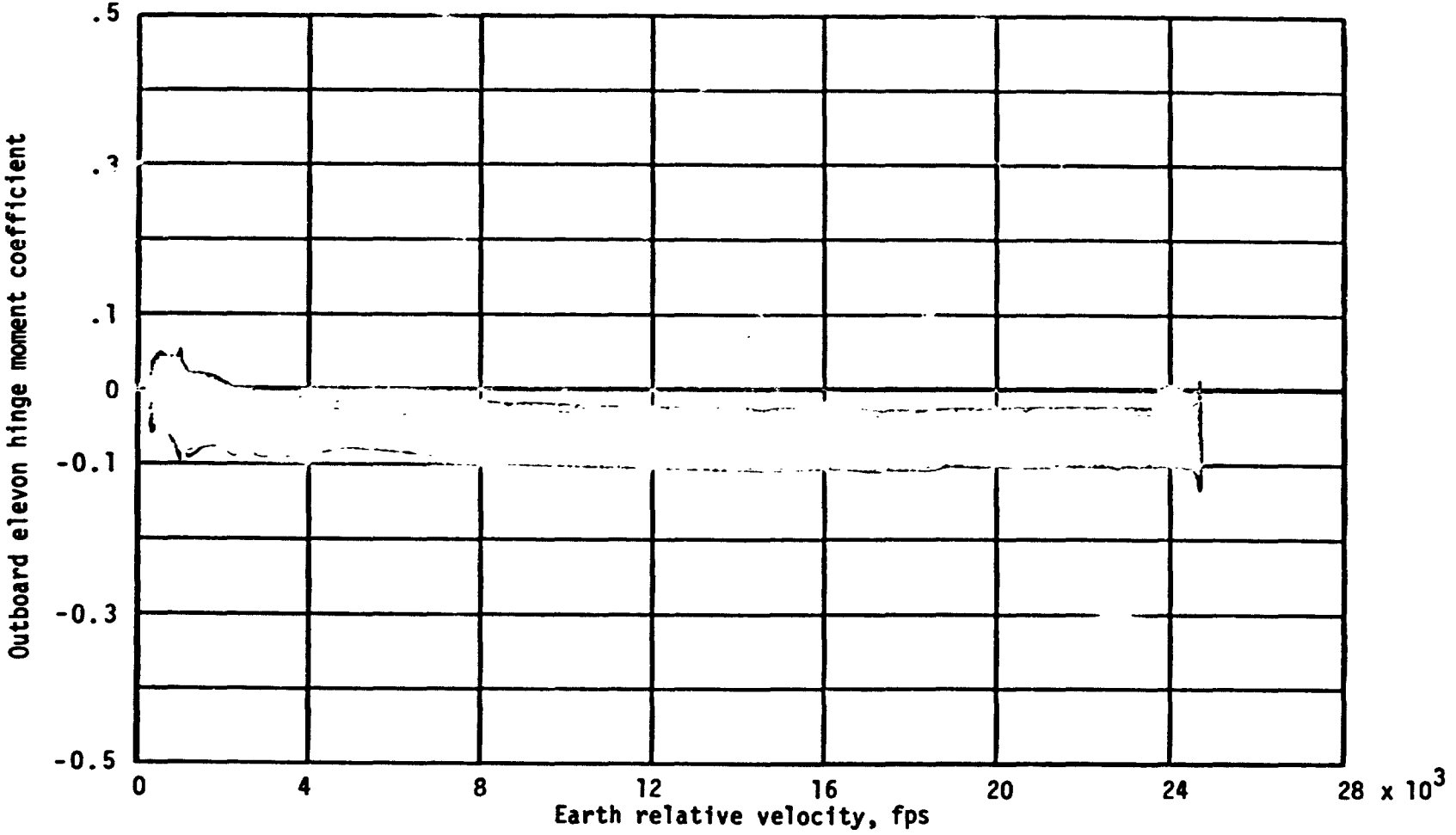

(p) Outboard elevon hinge moment coefficient.

Figure 8.- Continued.

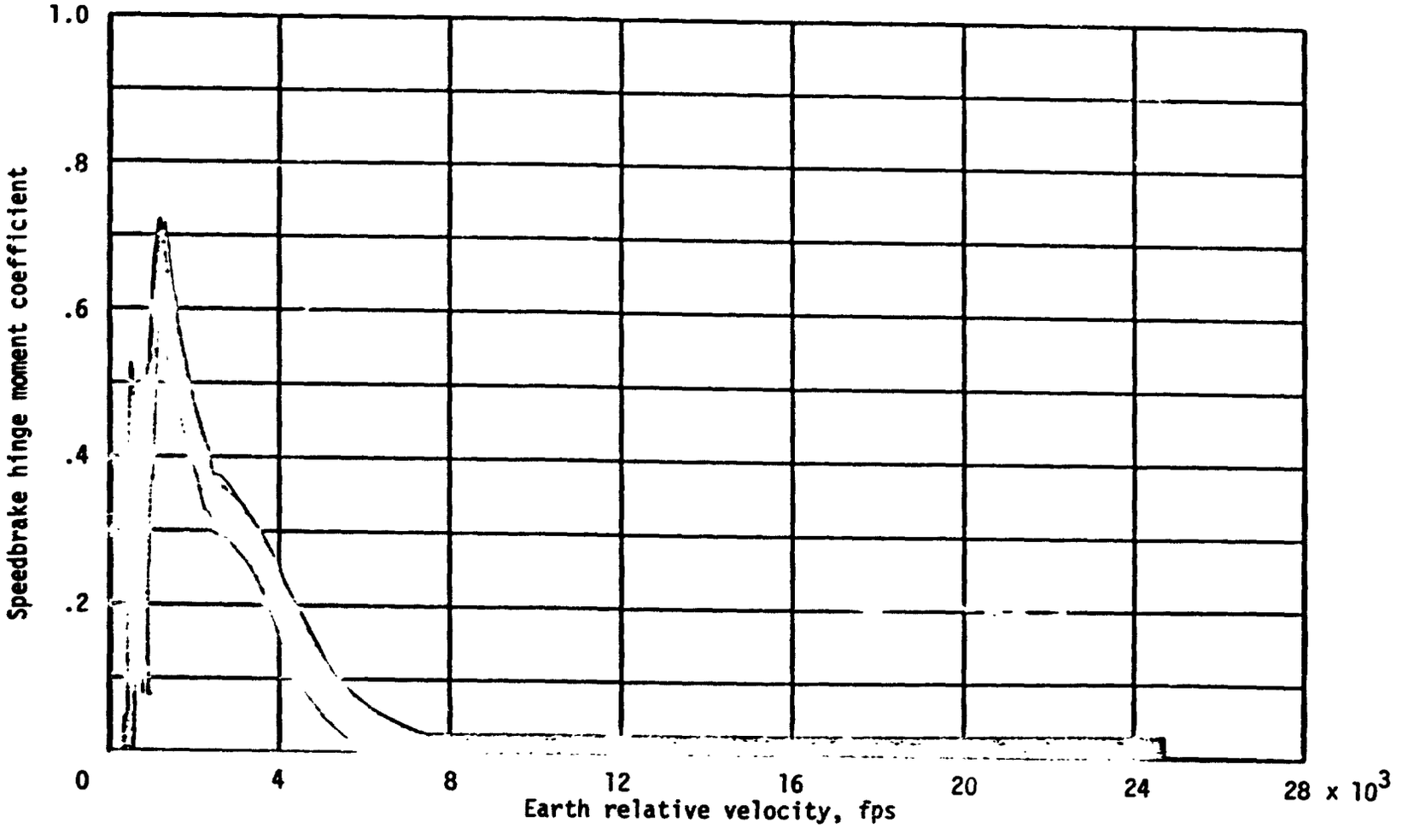

(q) Speedbrake hinge moment coefficient.

Figure 8.- Continued.

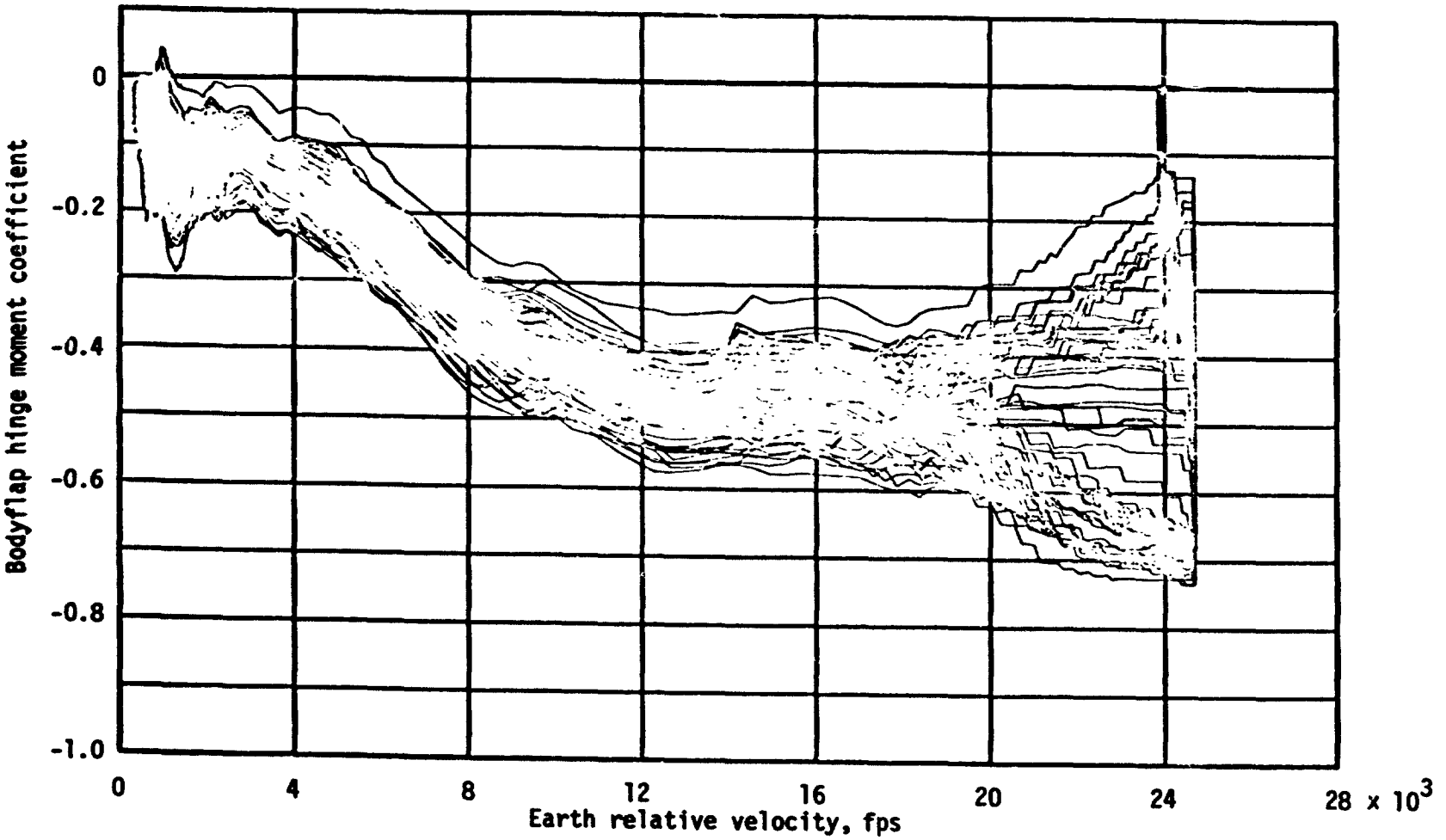

(r) Bodyflap hinge moment coefficient.

Figure 8.- Continued.

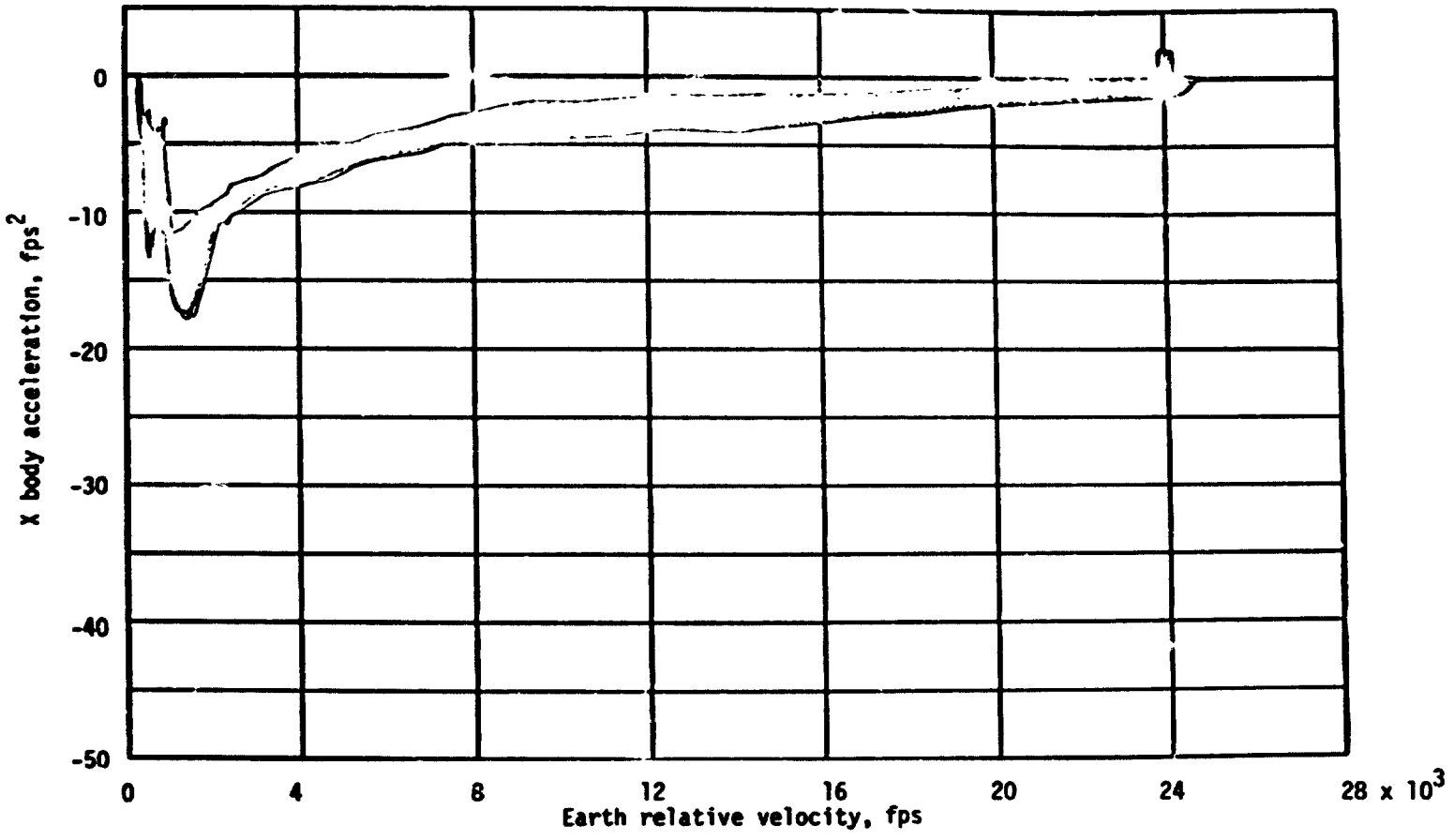

(s) X body acceleration.

Figure 8.- Continued.

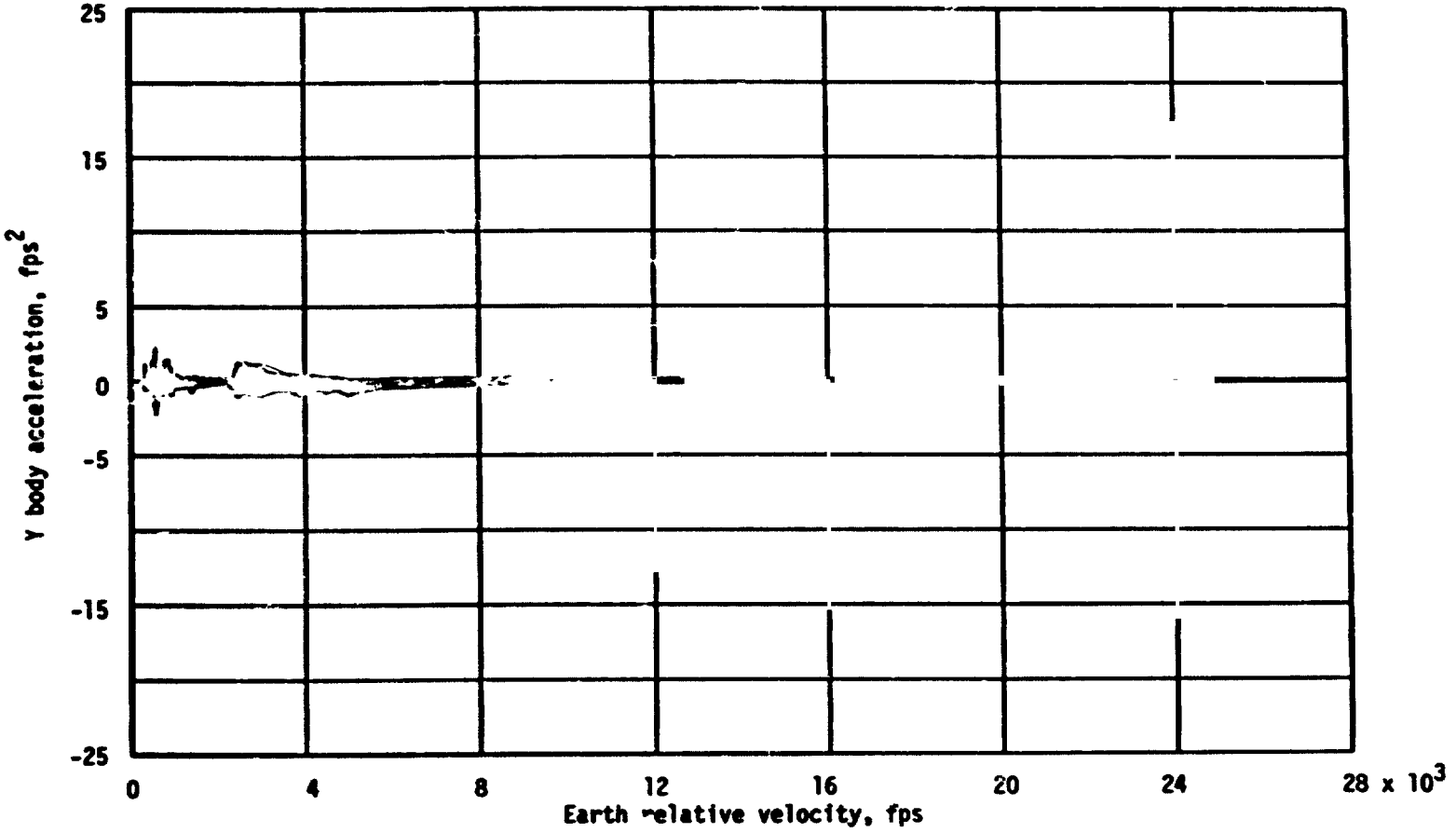

(t) Y body acceleration.

Figure 8.- Continued.

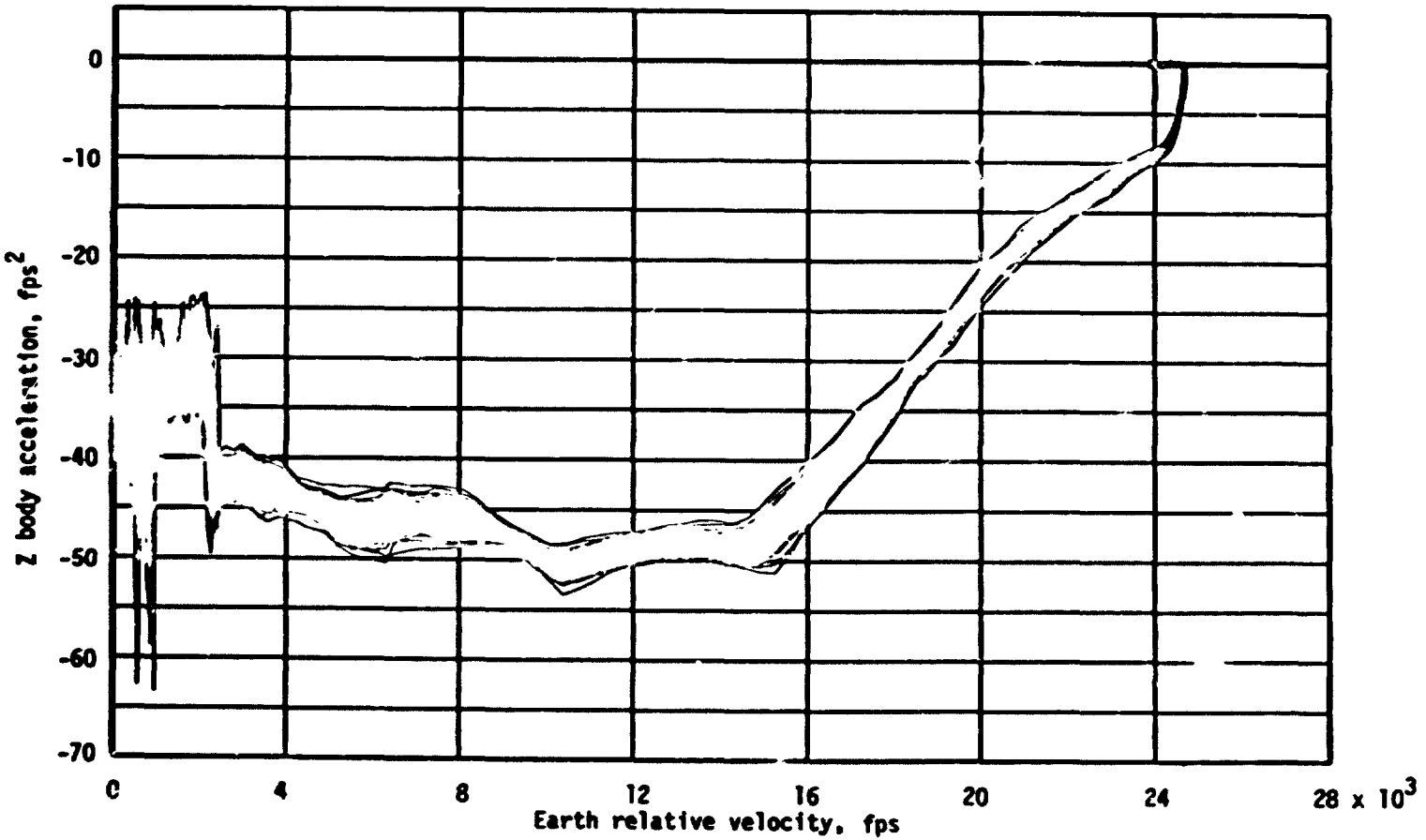

(u) Z body acceleration.

Figure 8.- Concluded.

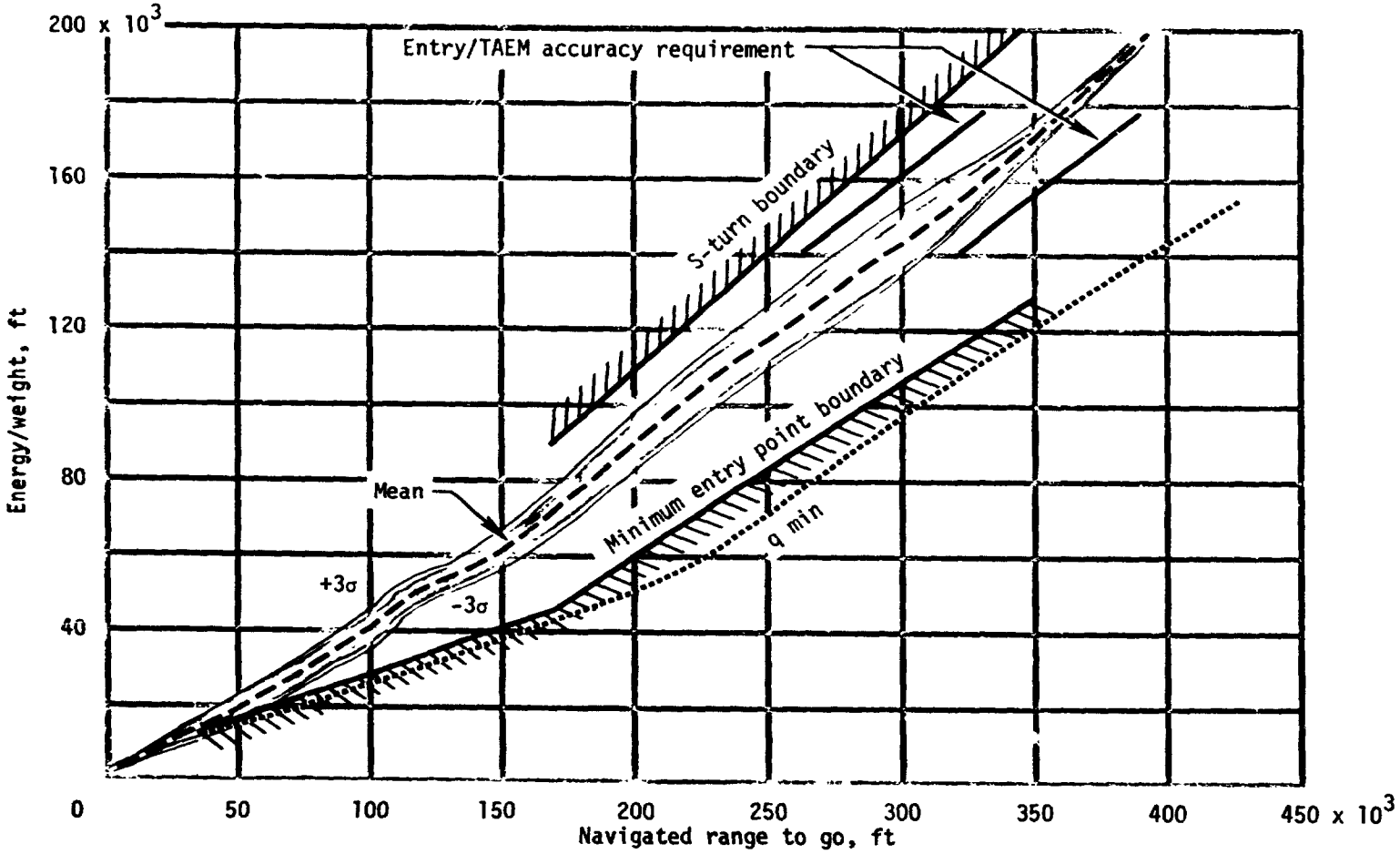

(a) Energy.

Figure 9.- TAEM guidance performance - end of mission.

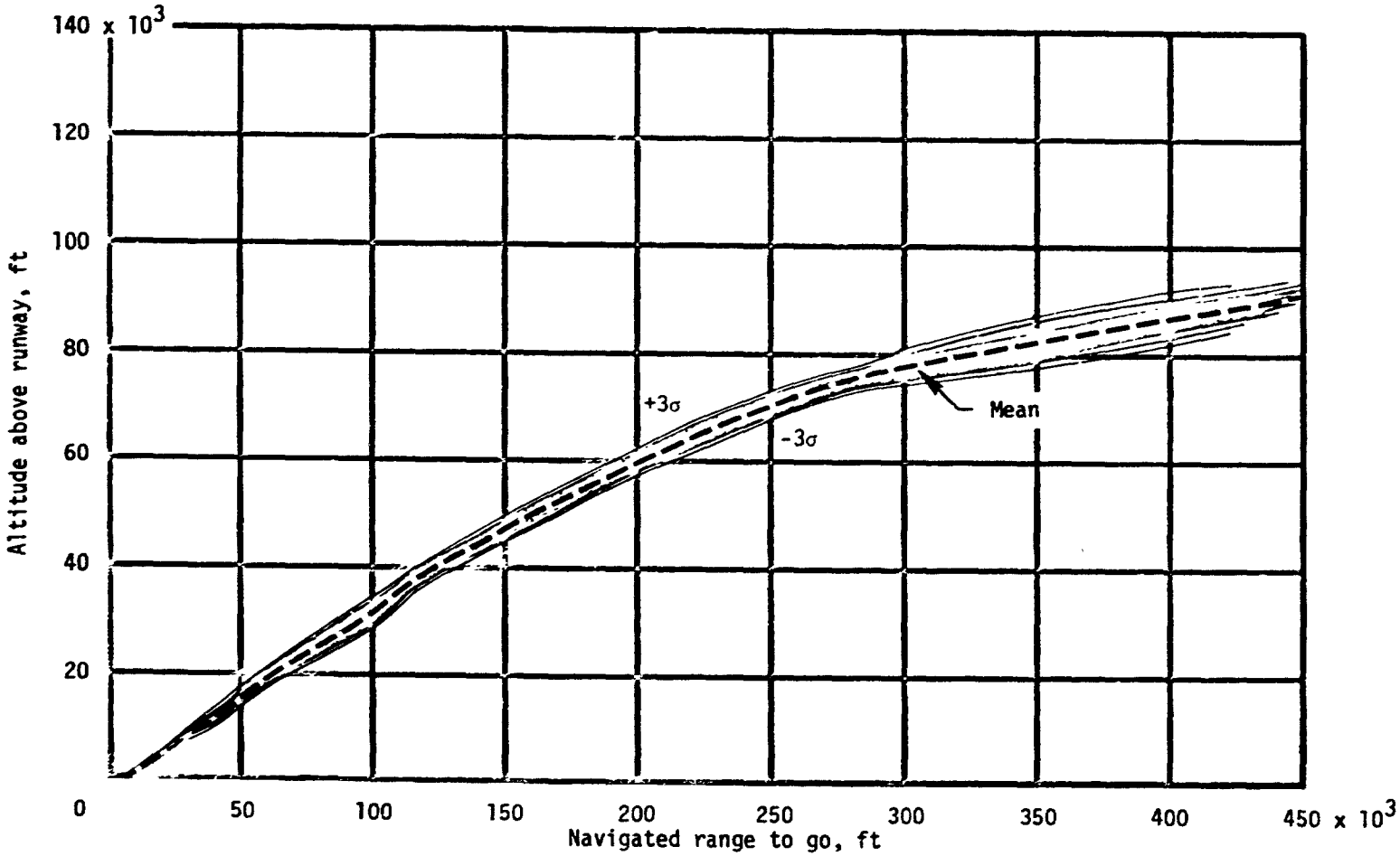

(b) Altitude.

Figure 9.- Continued.

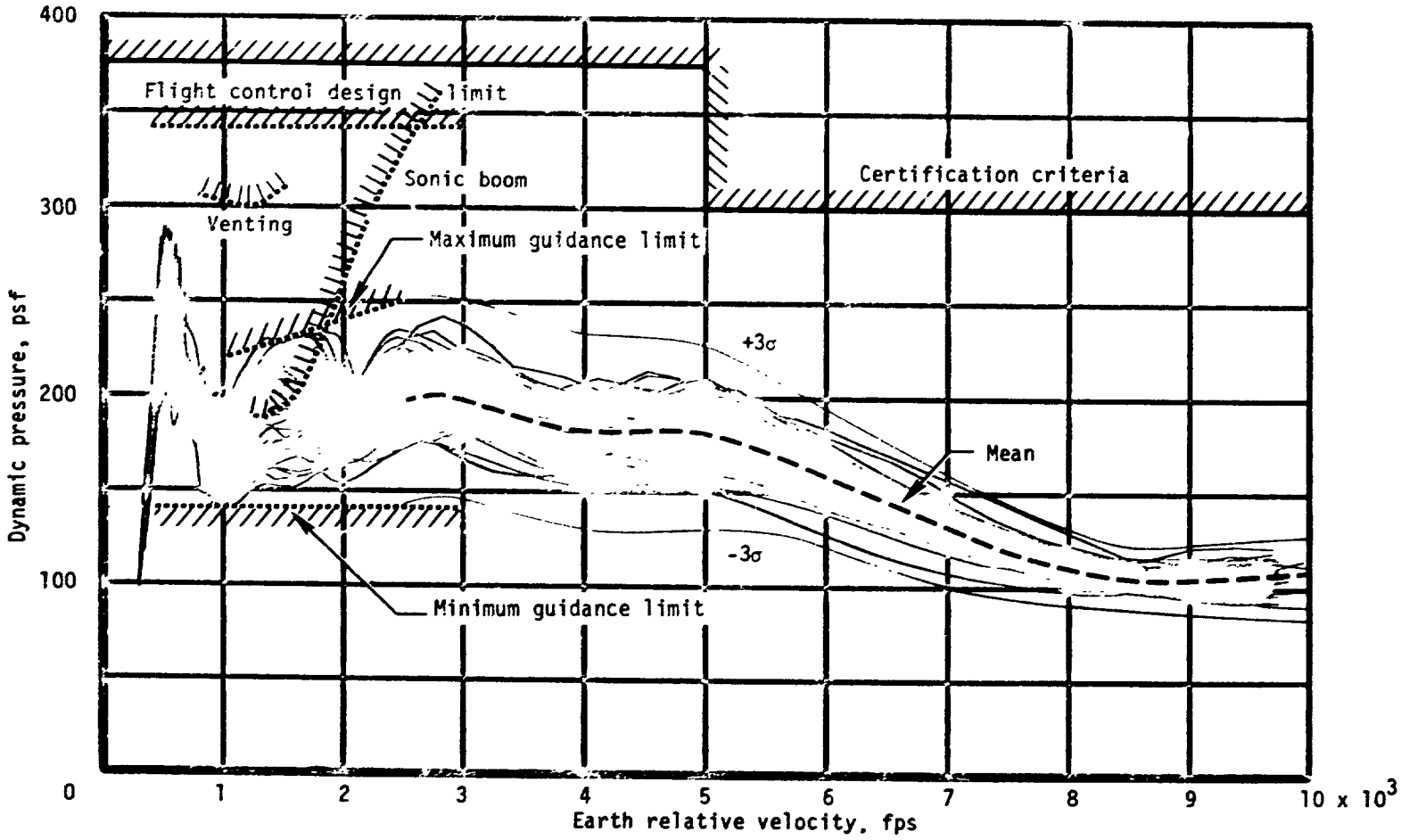

(c) Dynamic pressure.

Figure 9.- Continued.

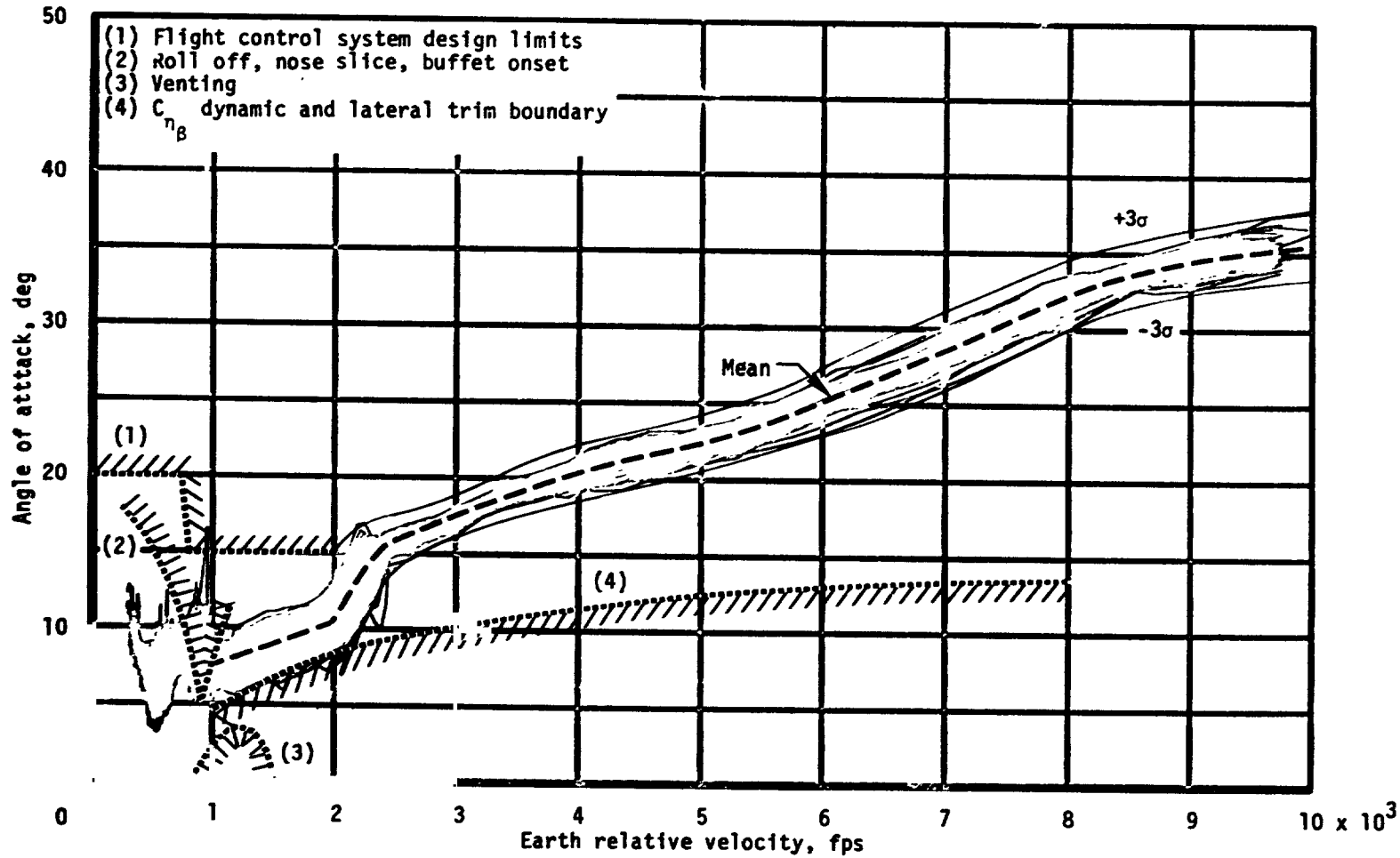

(d) Angle of attack.

Figure 9.- Continued.

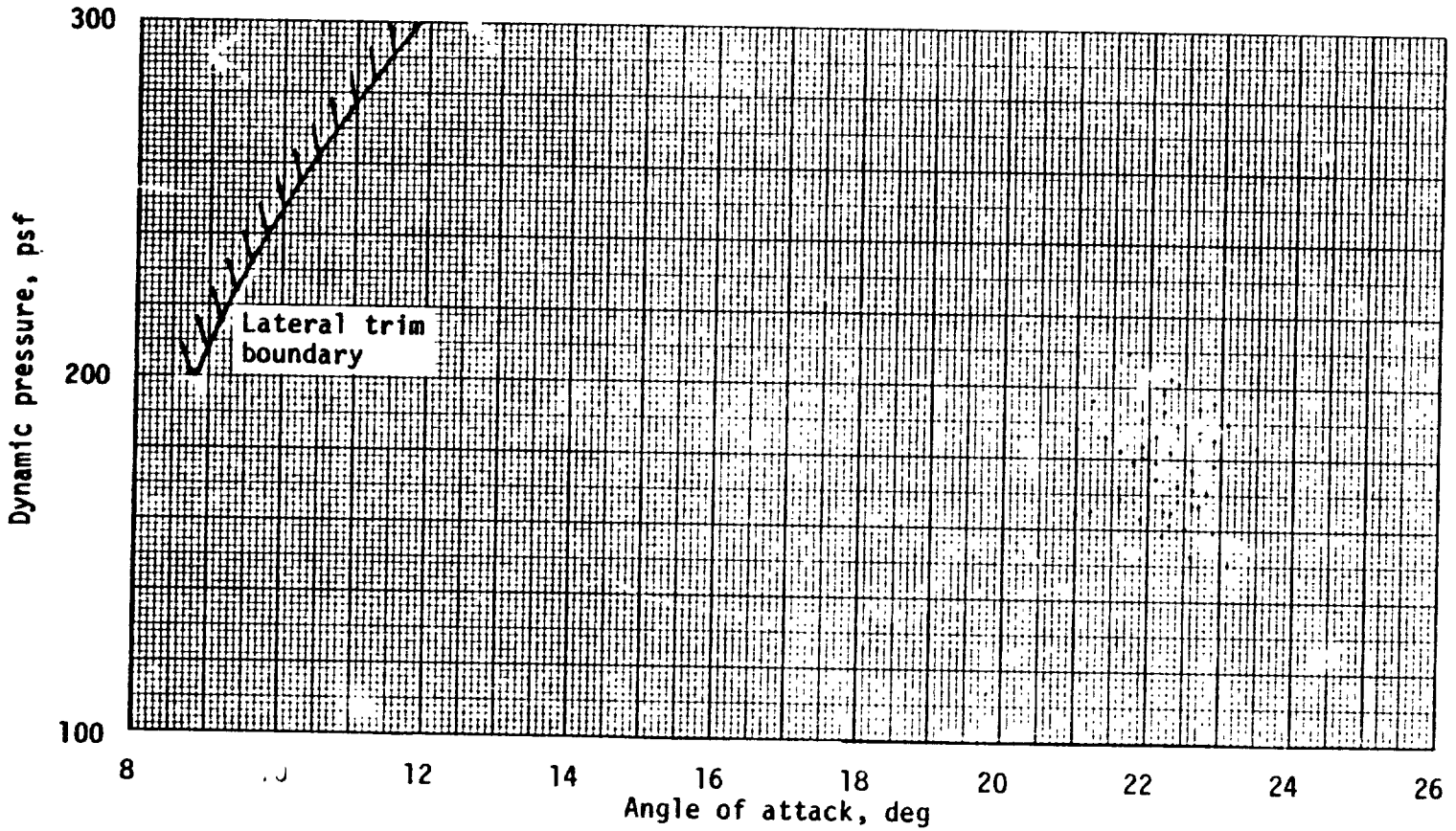

(e) Dynamic pressure - angle of attack scatter plot - Mach = 5.0

Figure 9.- Continued.

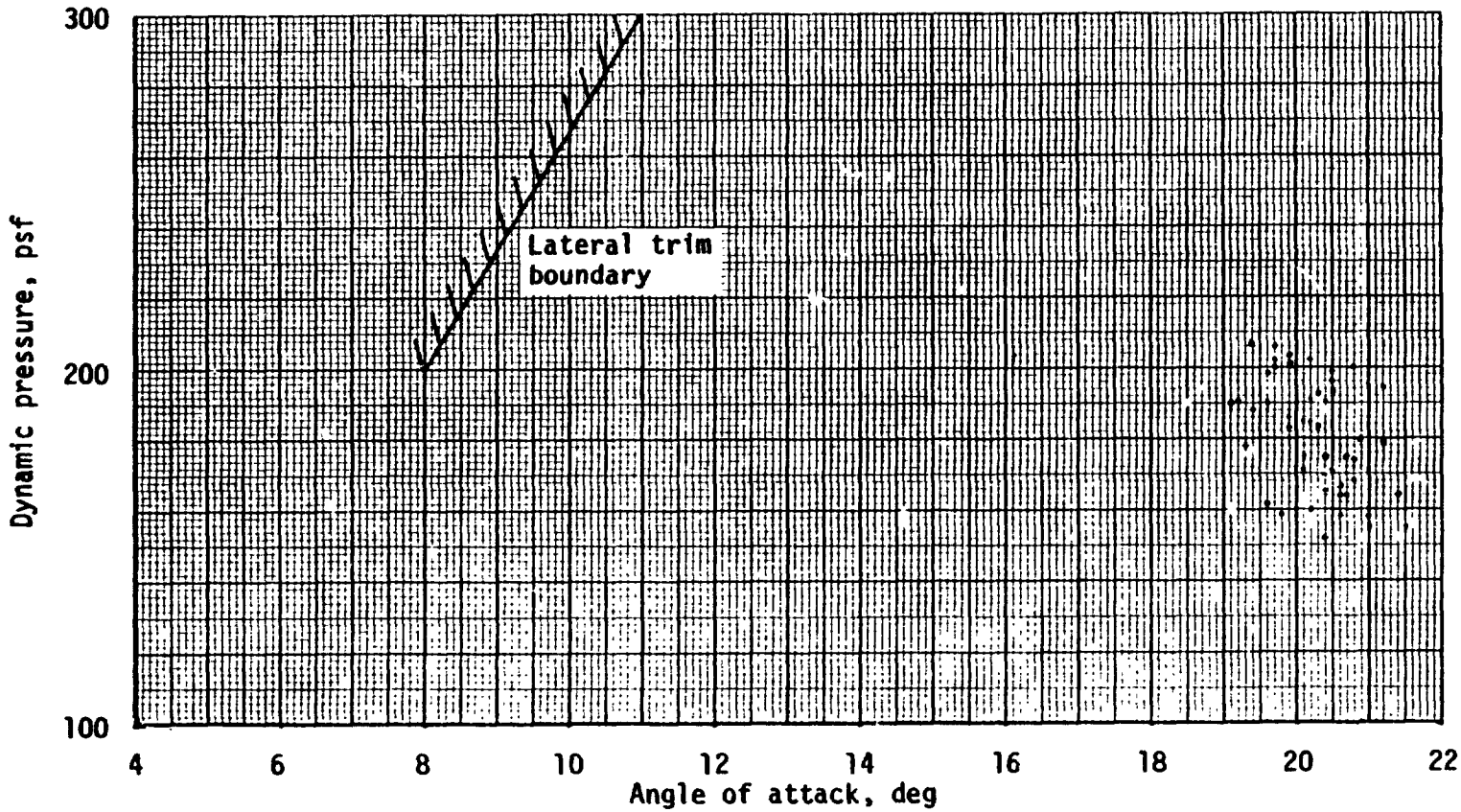

(f) Dynamic pressure - angle of attack - Mach = 4.0

Figure 9.- Continued.

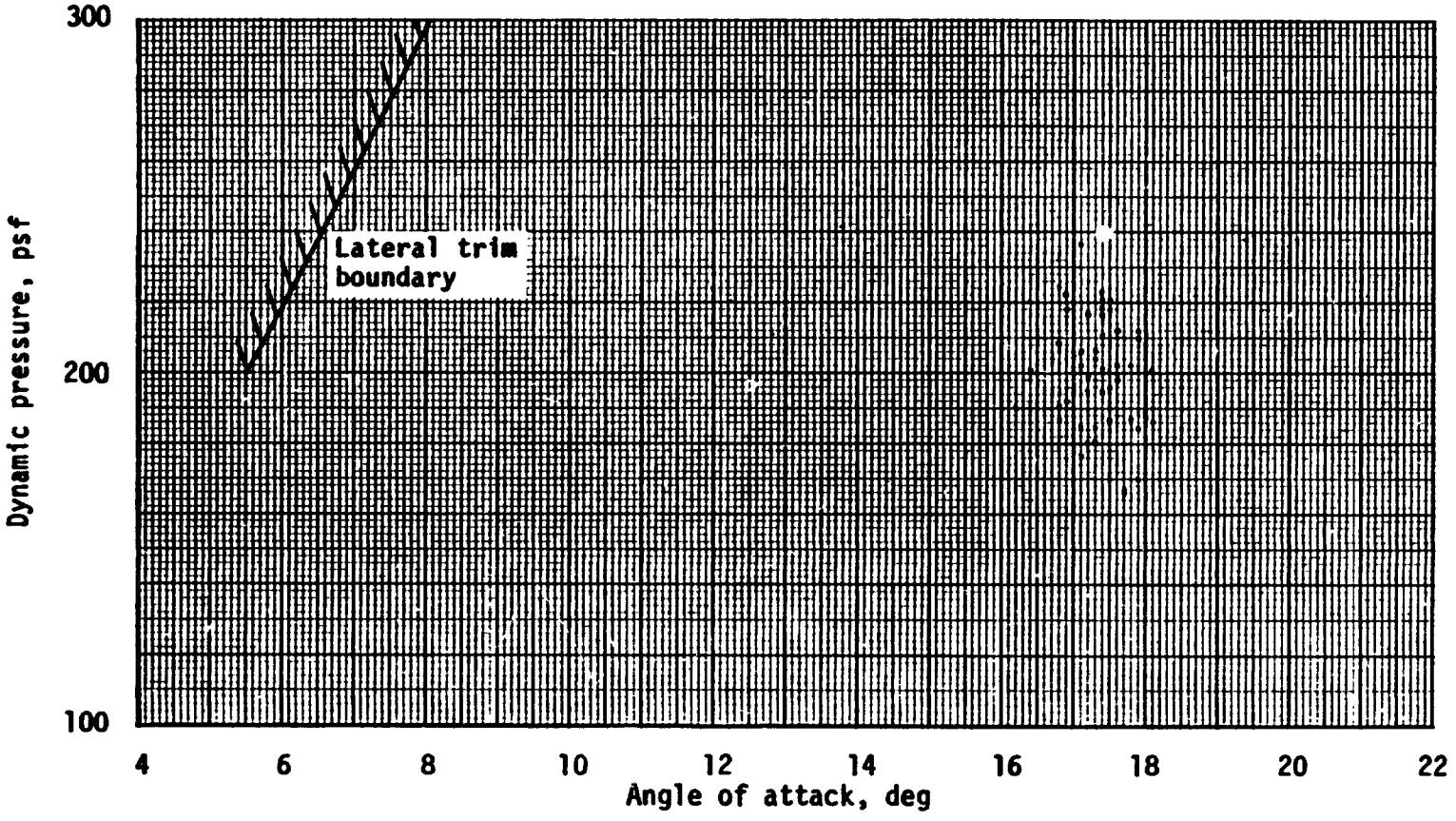

(g) Dynamic pressure - angle of attack - Mach = 3.0

Figure 9.- Continued.

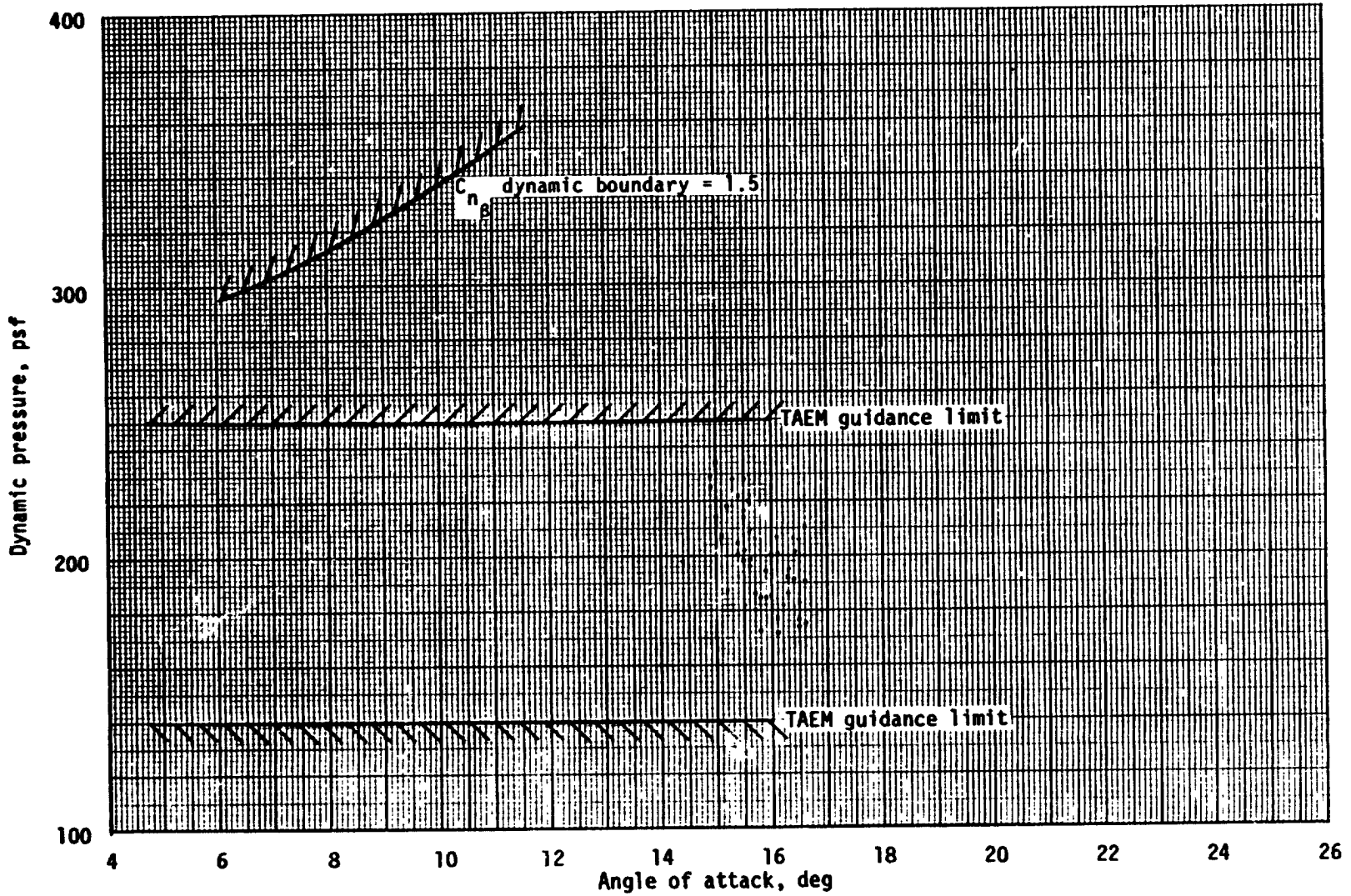

(h) Dynamic pressure - angle of attack - Mach = 2.5

Figure 9.- Continued.

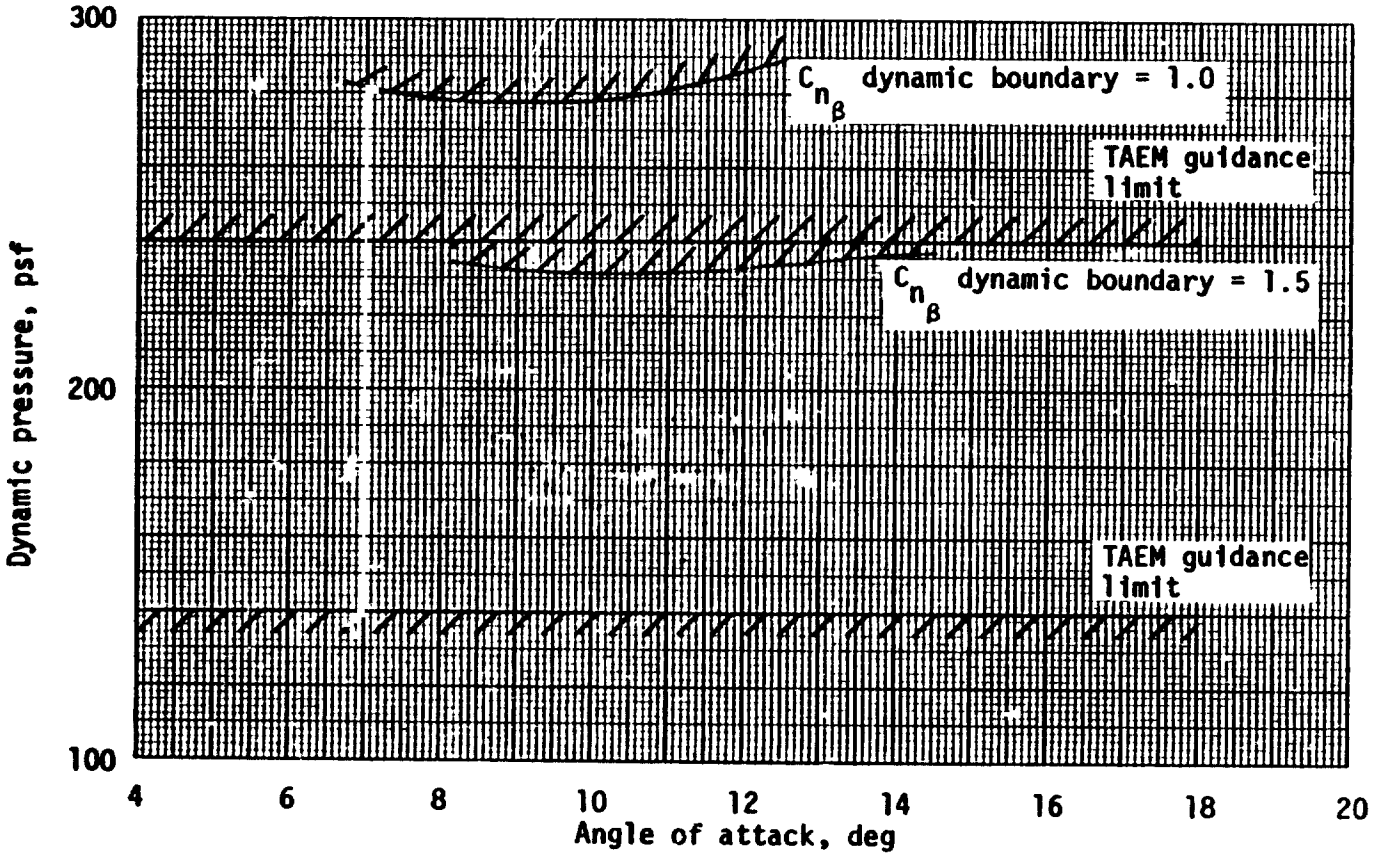

(i) Dynamic pressure - angle of attack scatter plot - Mach = 2.0

Figure 9.- Continued.

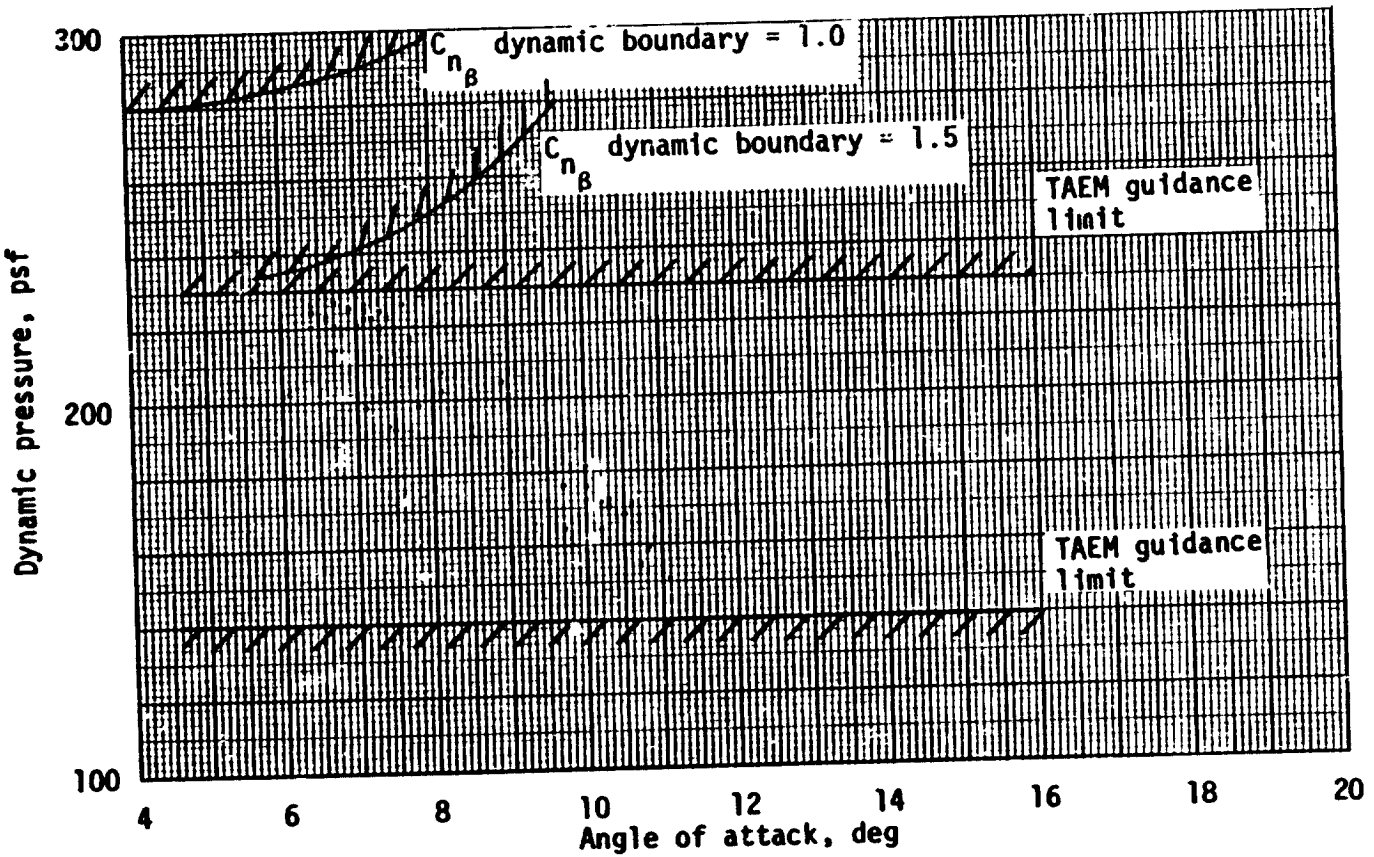

(j) Dynamic pressure - angle of attack scatter plot - Mach = 1.5

Figure 9.- Continued.

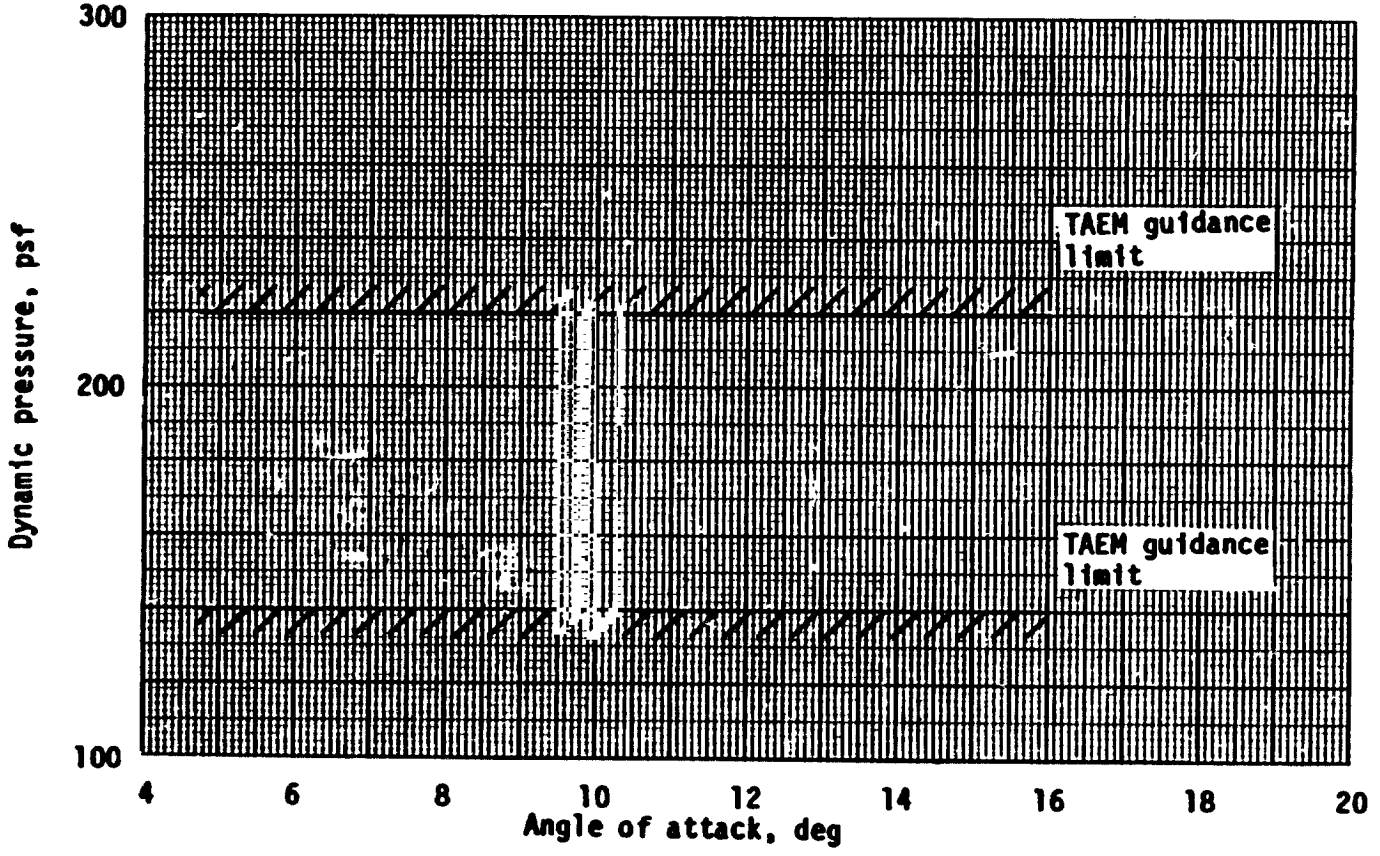

(k) Dynamic pressure - angle of attack scatter plot - Mach = 1.0

Figure 9.- Continued.

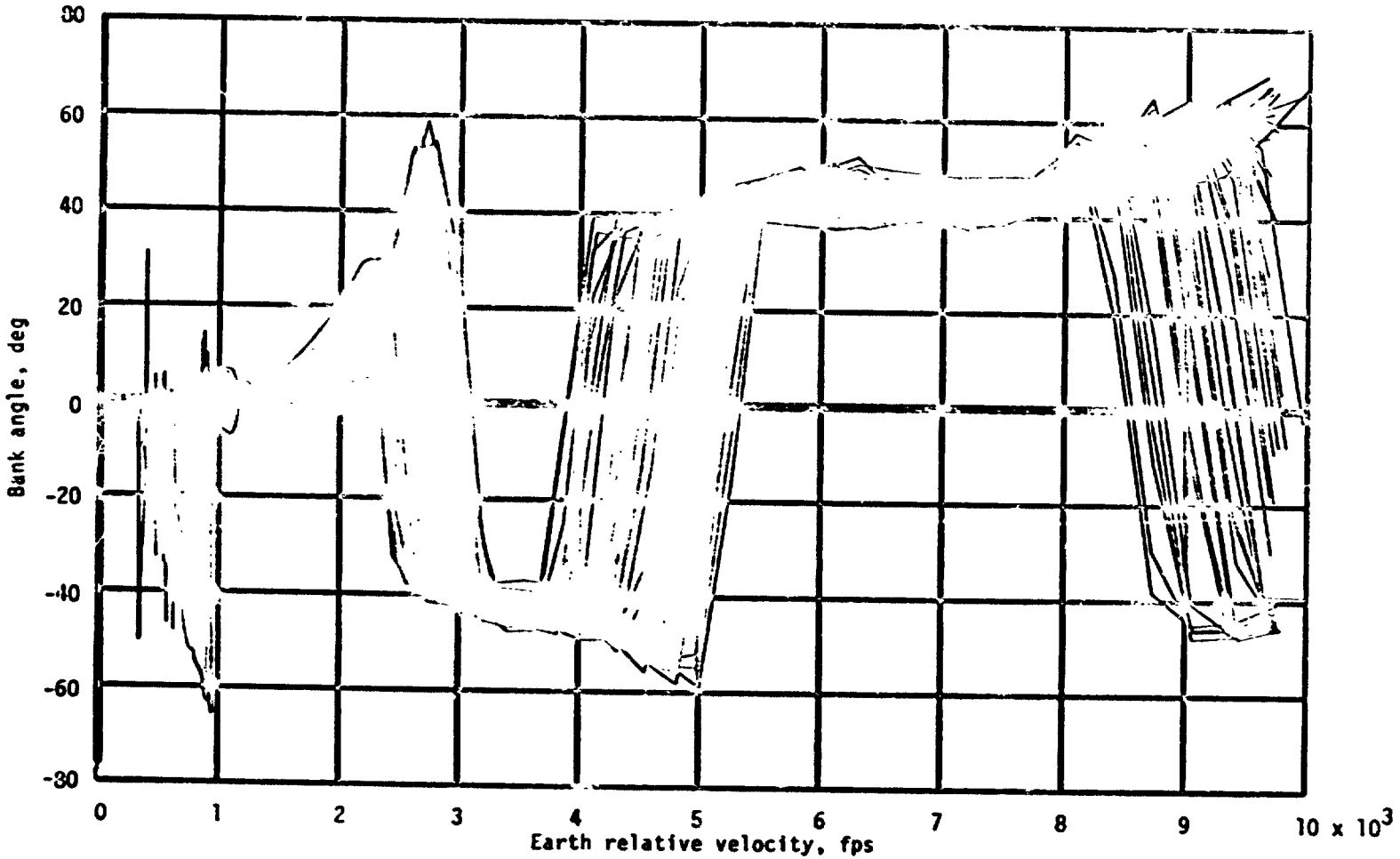

(1) Bank angle.

Figure 9.- Continued.

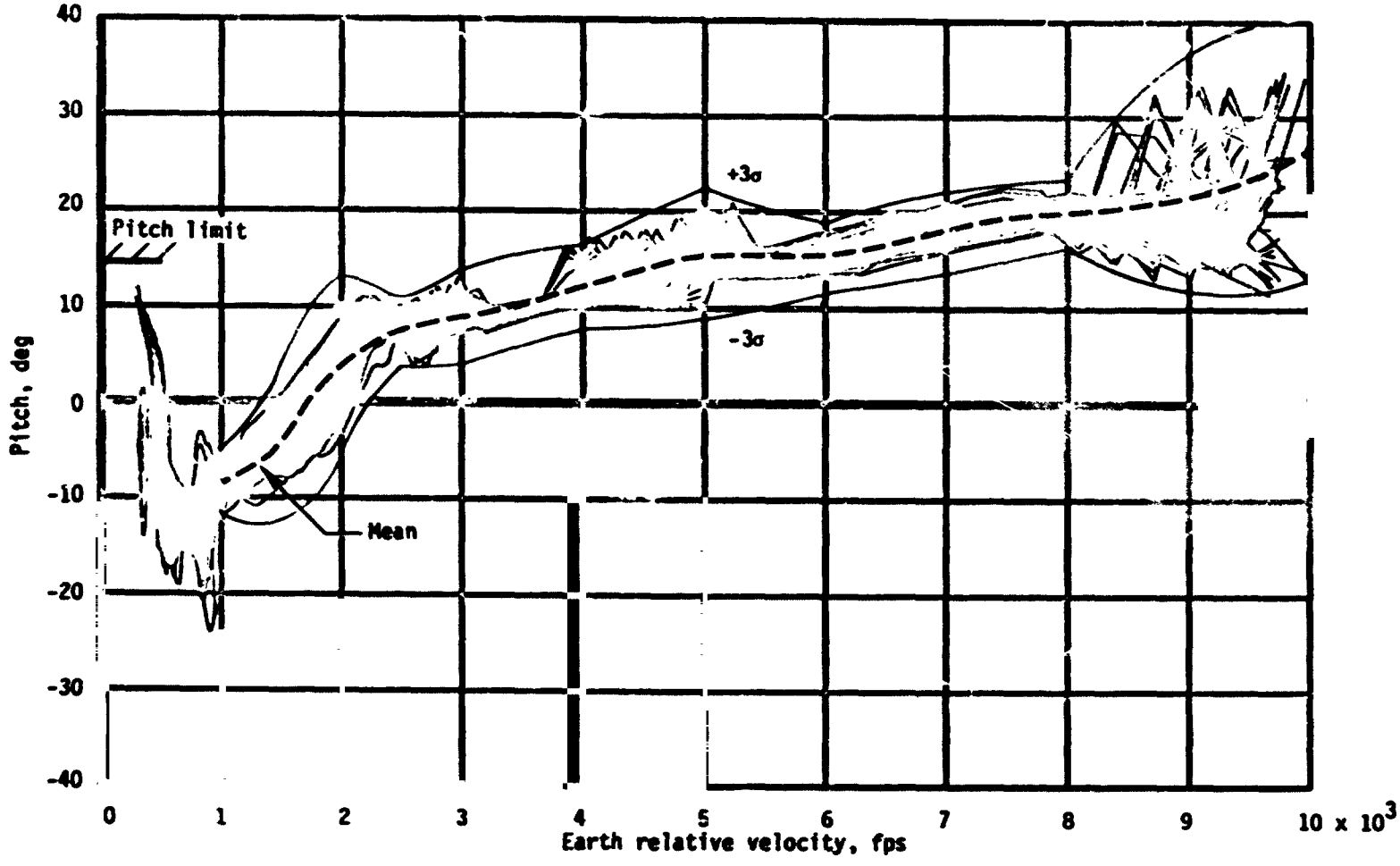

(m) Pitch angle.

Figure 9.- Continued.

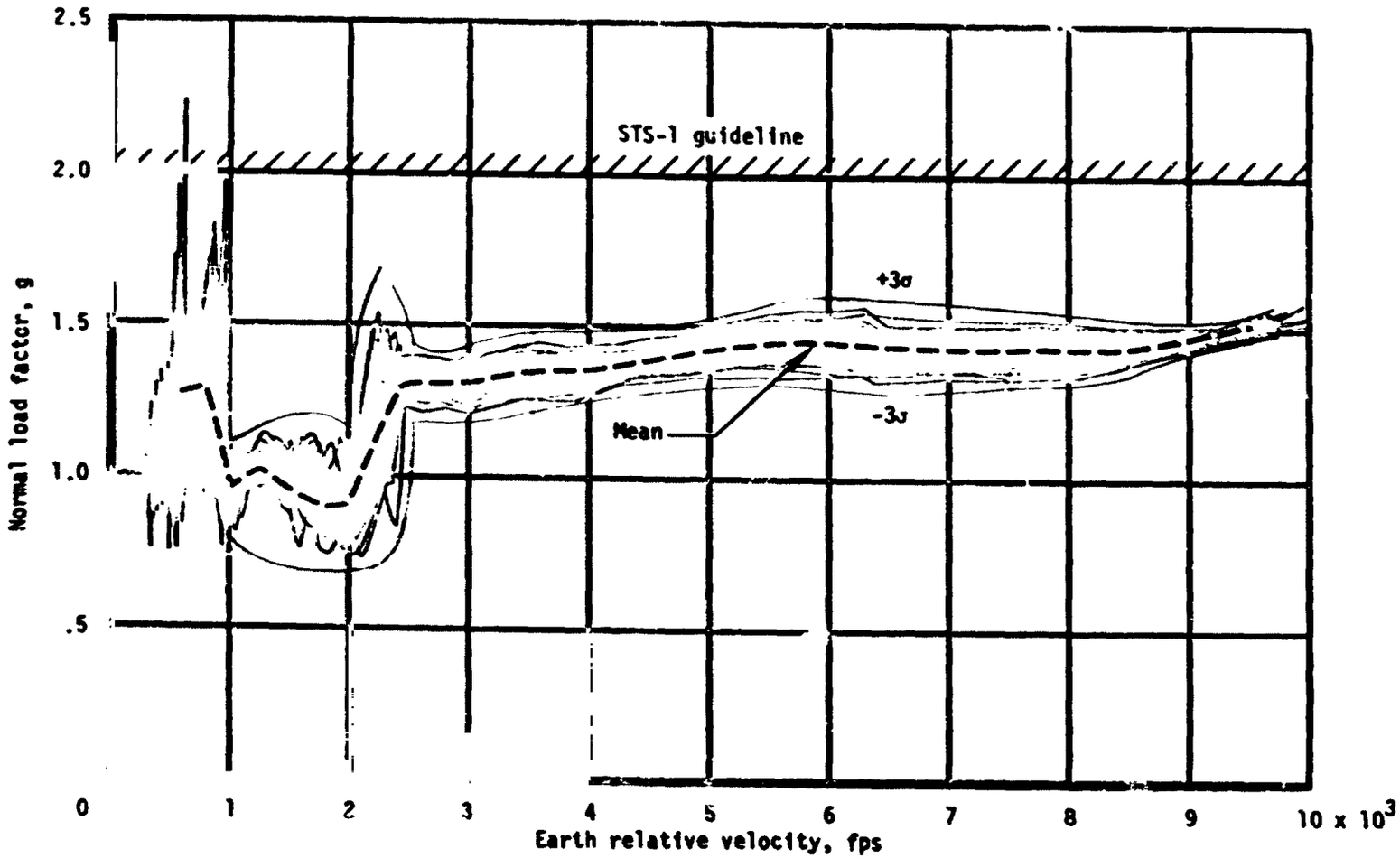

(n) Normal load factor.

Figure 9.- Continued.

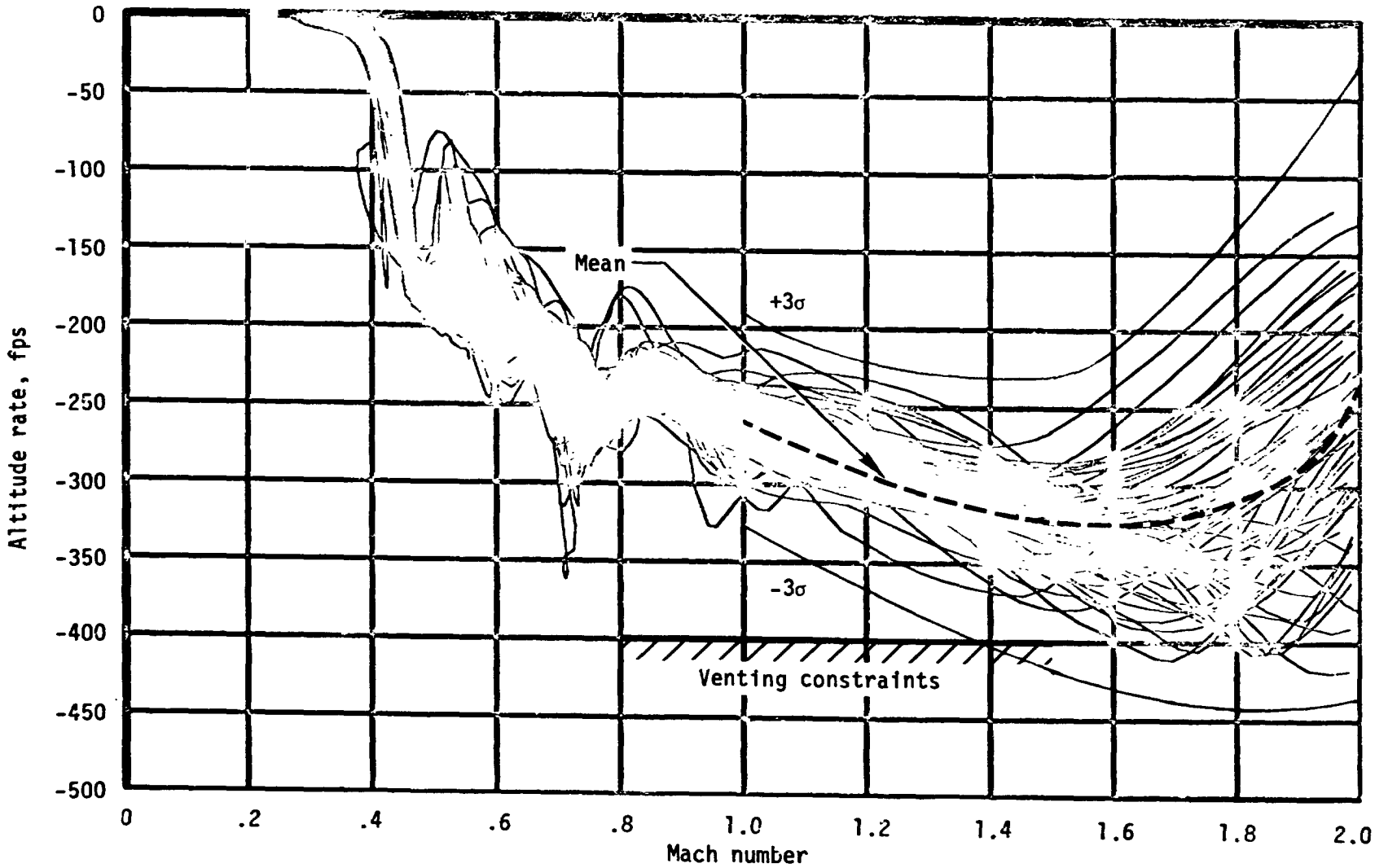

(o) Altitude rate.

Figure 9.- Concluded.

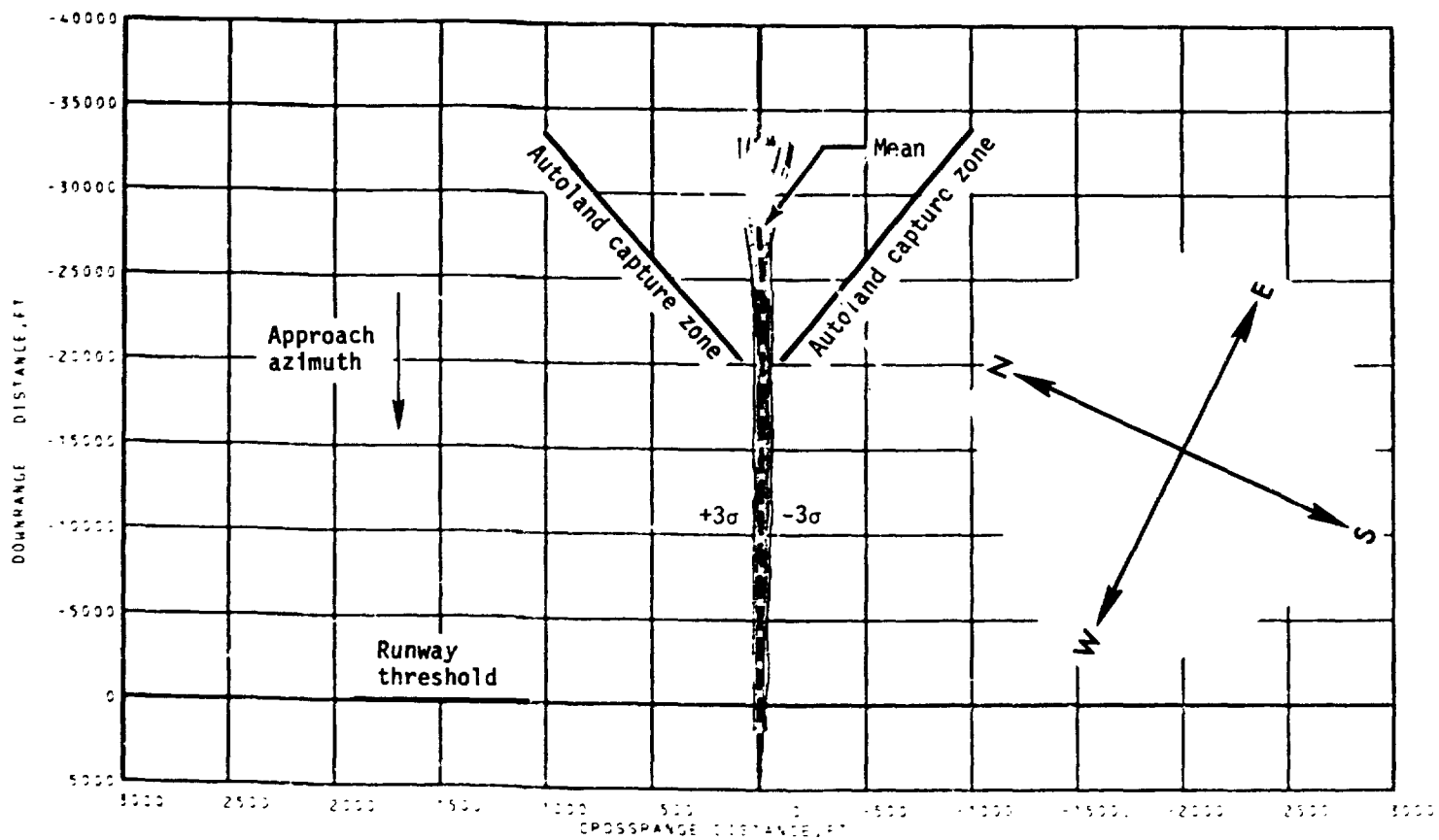

(a) Groundtrack.

Figure 10.- Autoland guidance performance parameters.

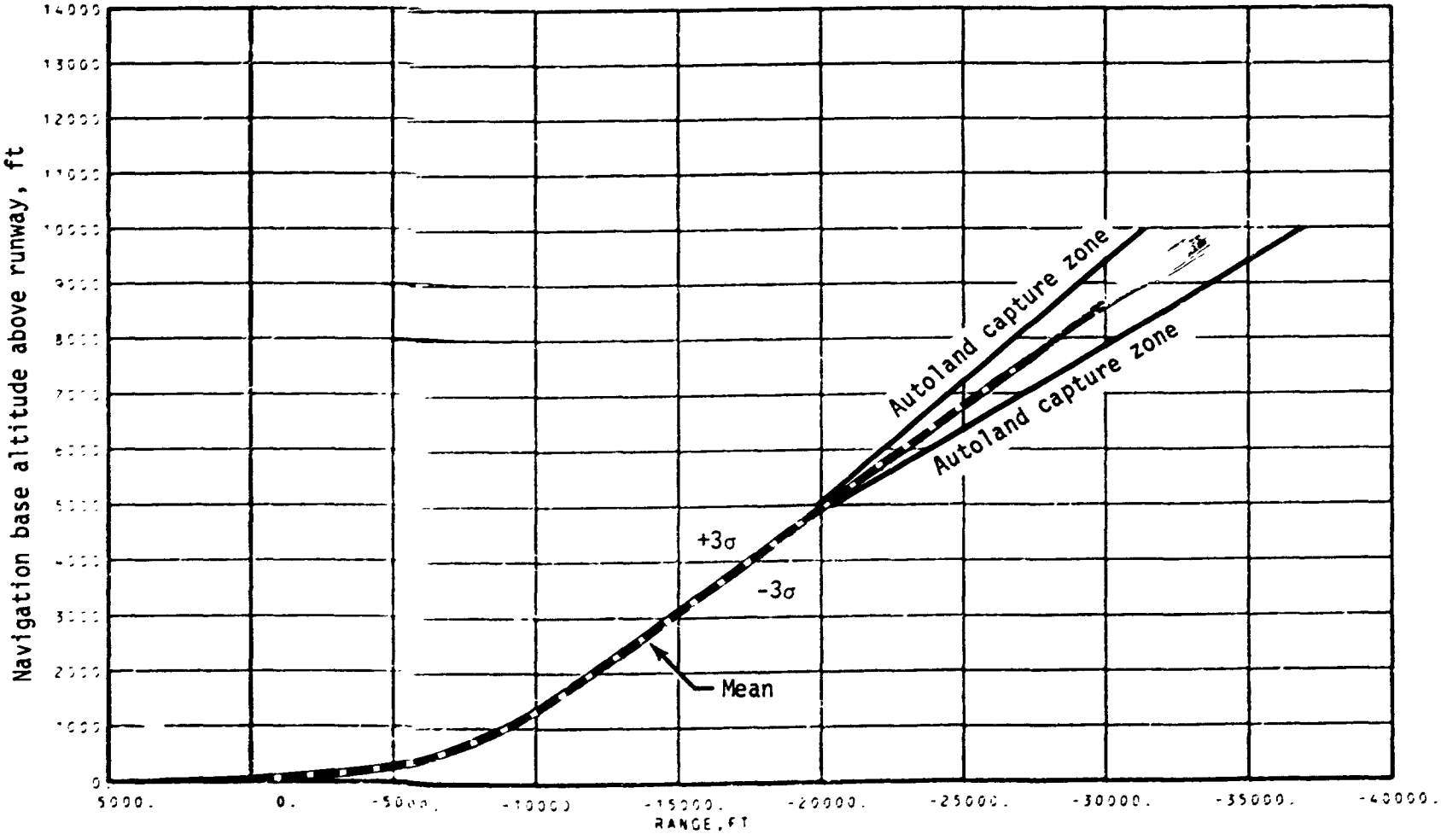

(b) Navigation base altitude (10 000 feet to landing).

Figure 10.- Continued.

(c) Main gear altitude (350 feet to landing).

Figure 10.- Continued.

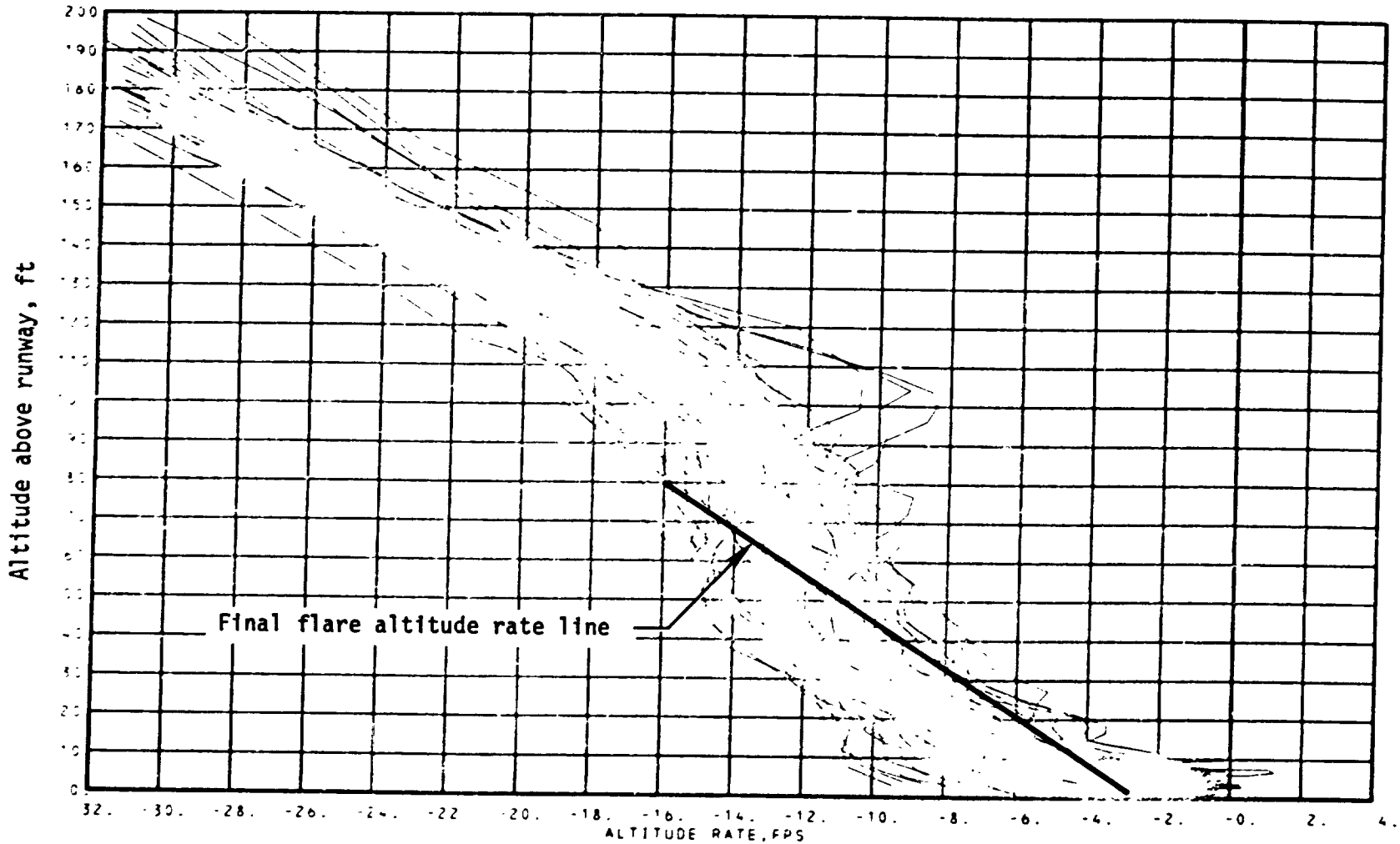

(d) Final flare altitude and altitude rate.

Figure 10.- Continued.

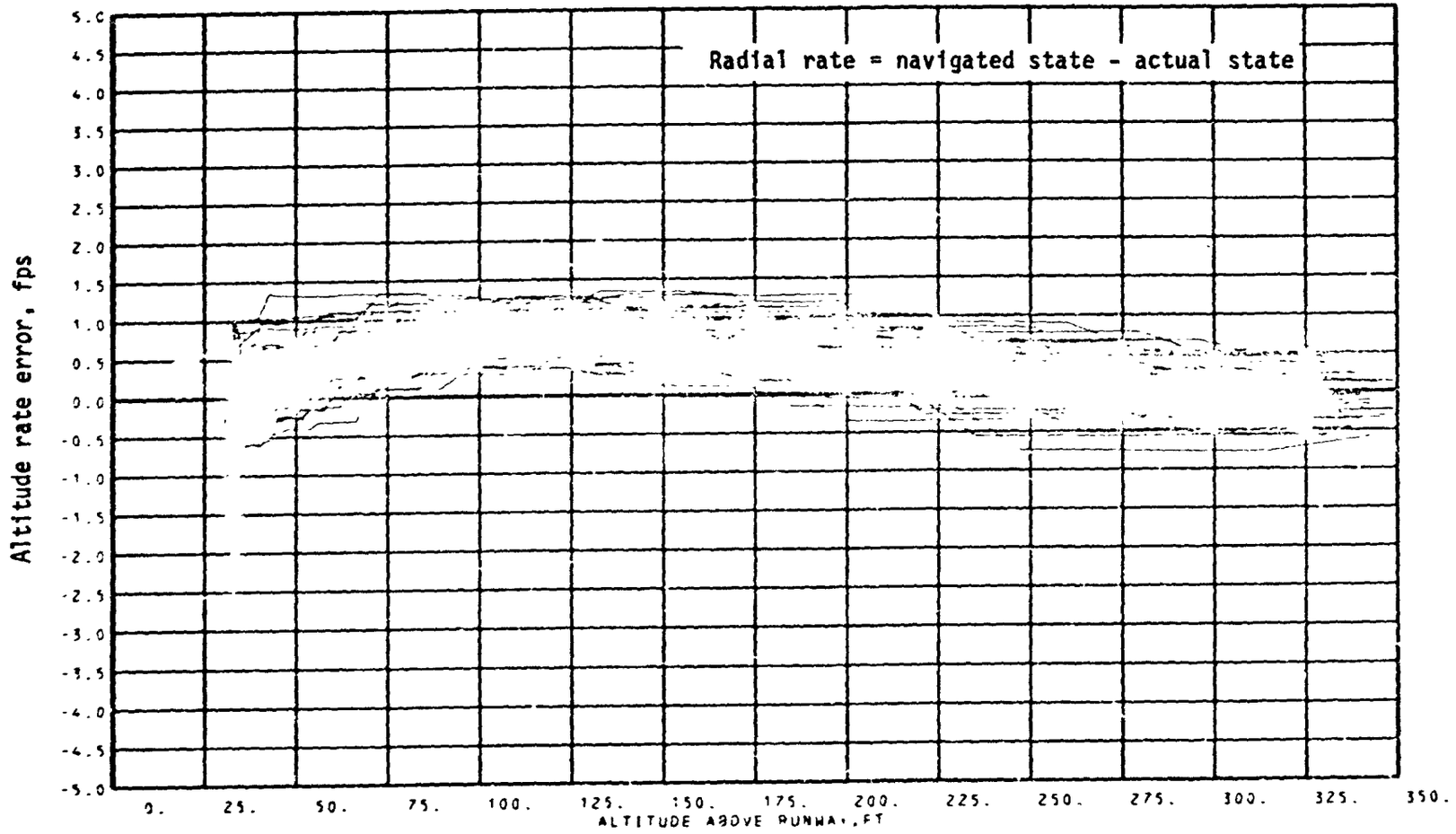

(e) Altitude rate errors.

Figure 10.- Continued.

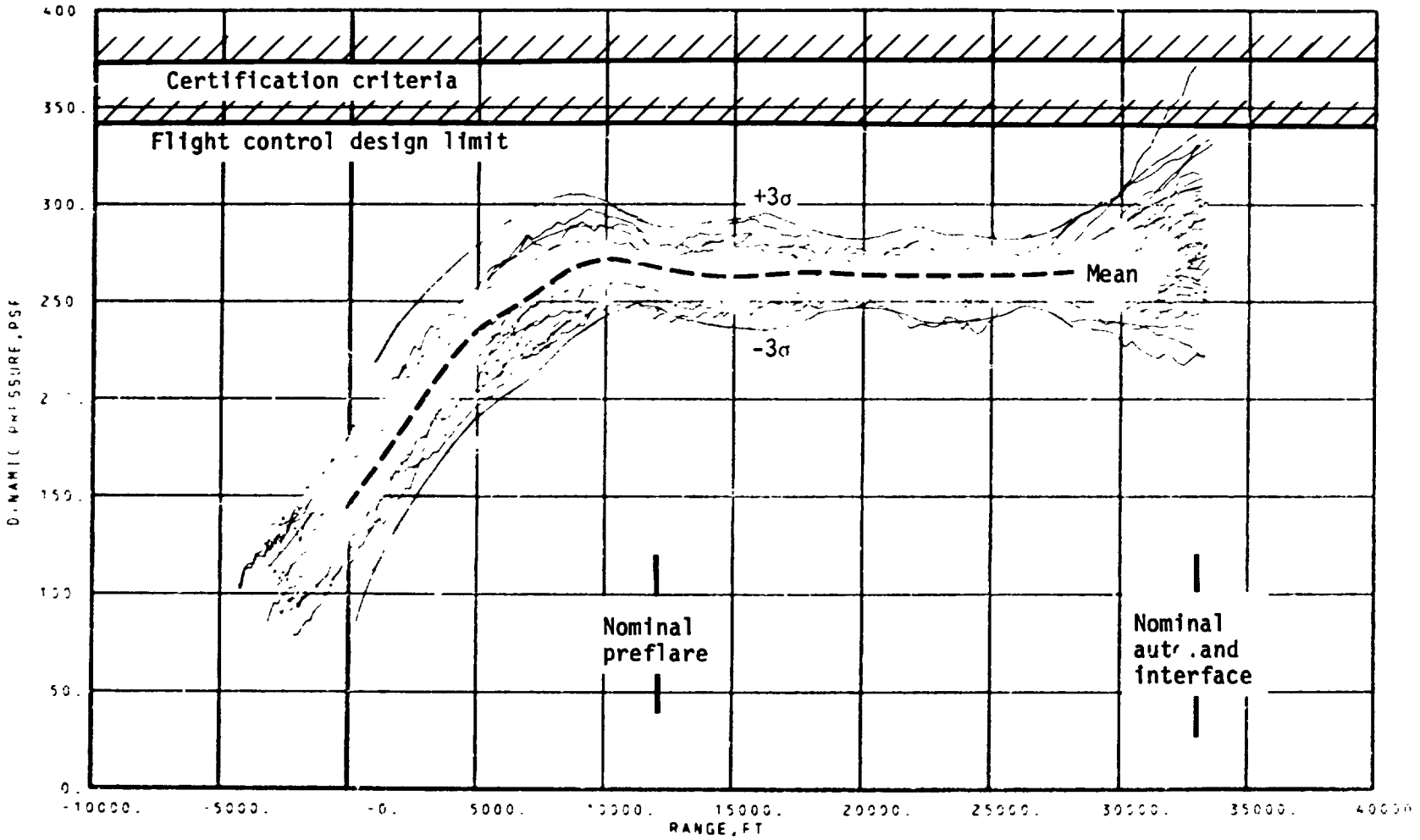

(f) Dynamic pressure versus range.

Figure 10.- Continued.

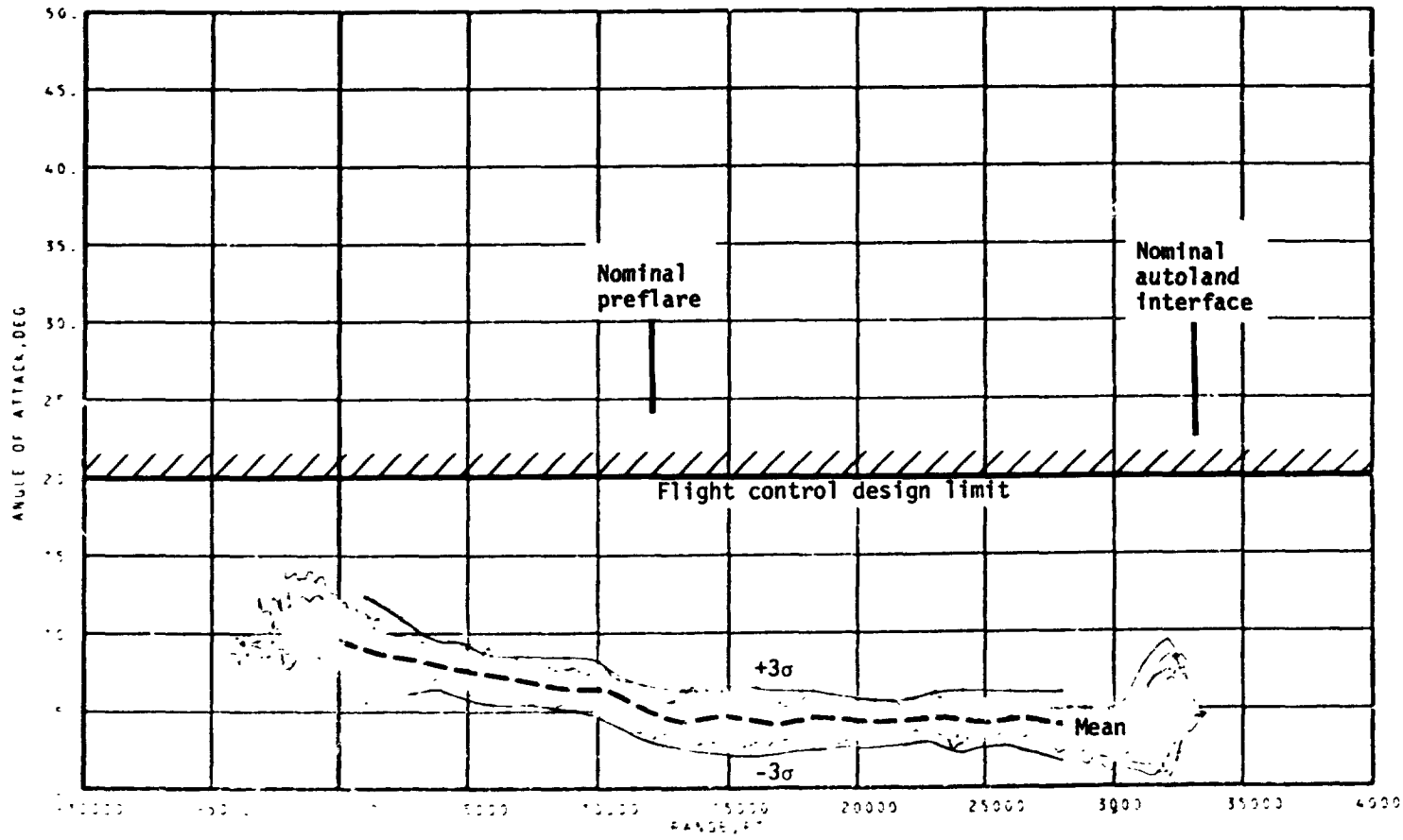

(g) Angle of attack.

Figure 10.- Continued.

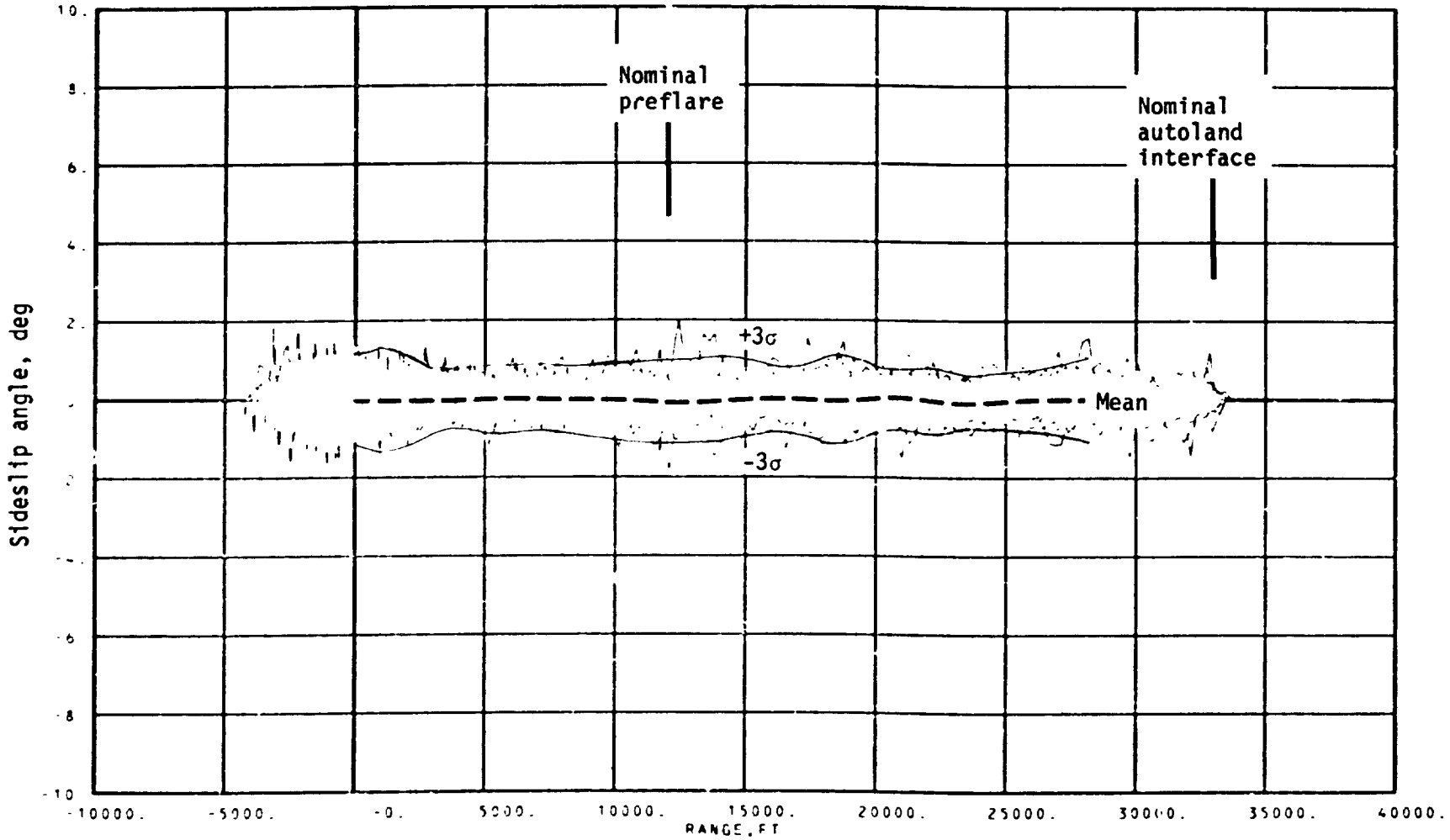

(h) Side slip angle.

Figure 10.- Continued.

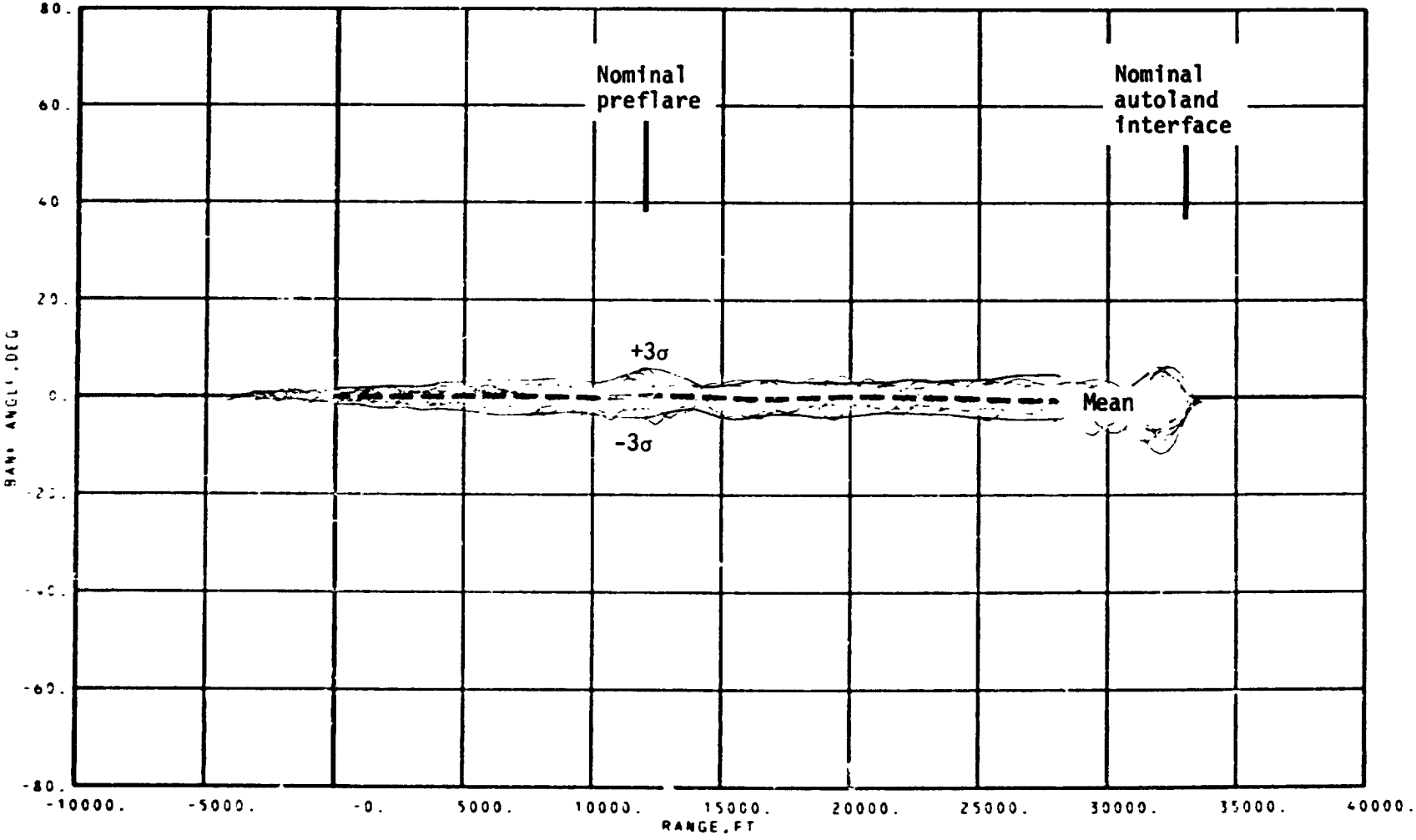

(f) Bank angle.

Figure 10.- Continued.

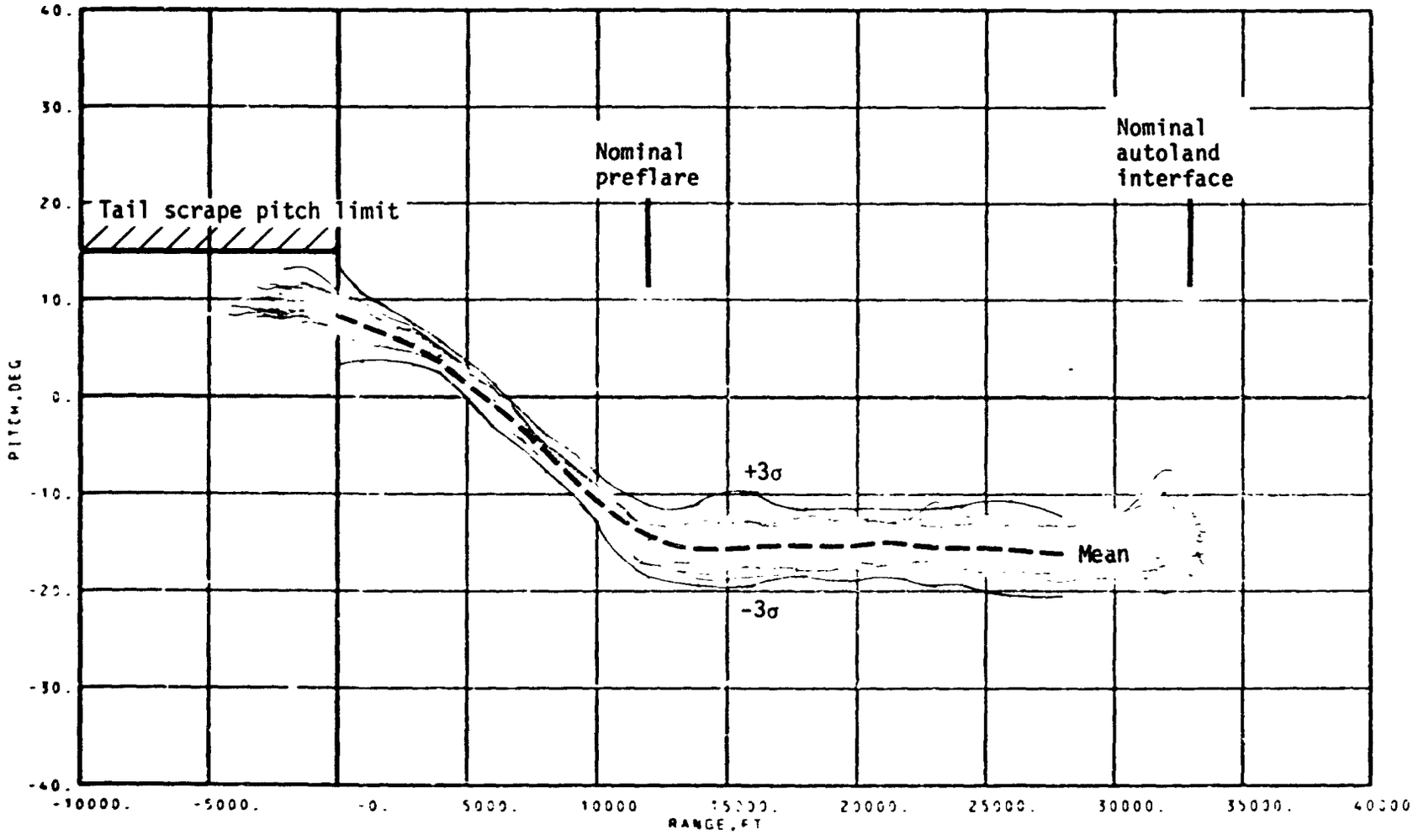

(j) Pitch.

Figure 10.- Continued.

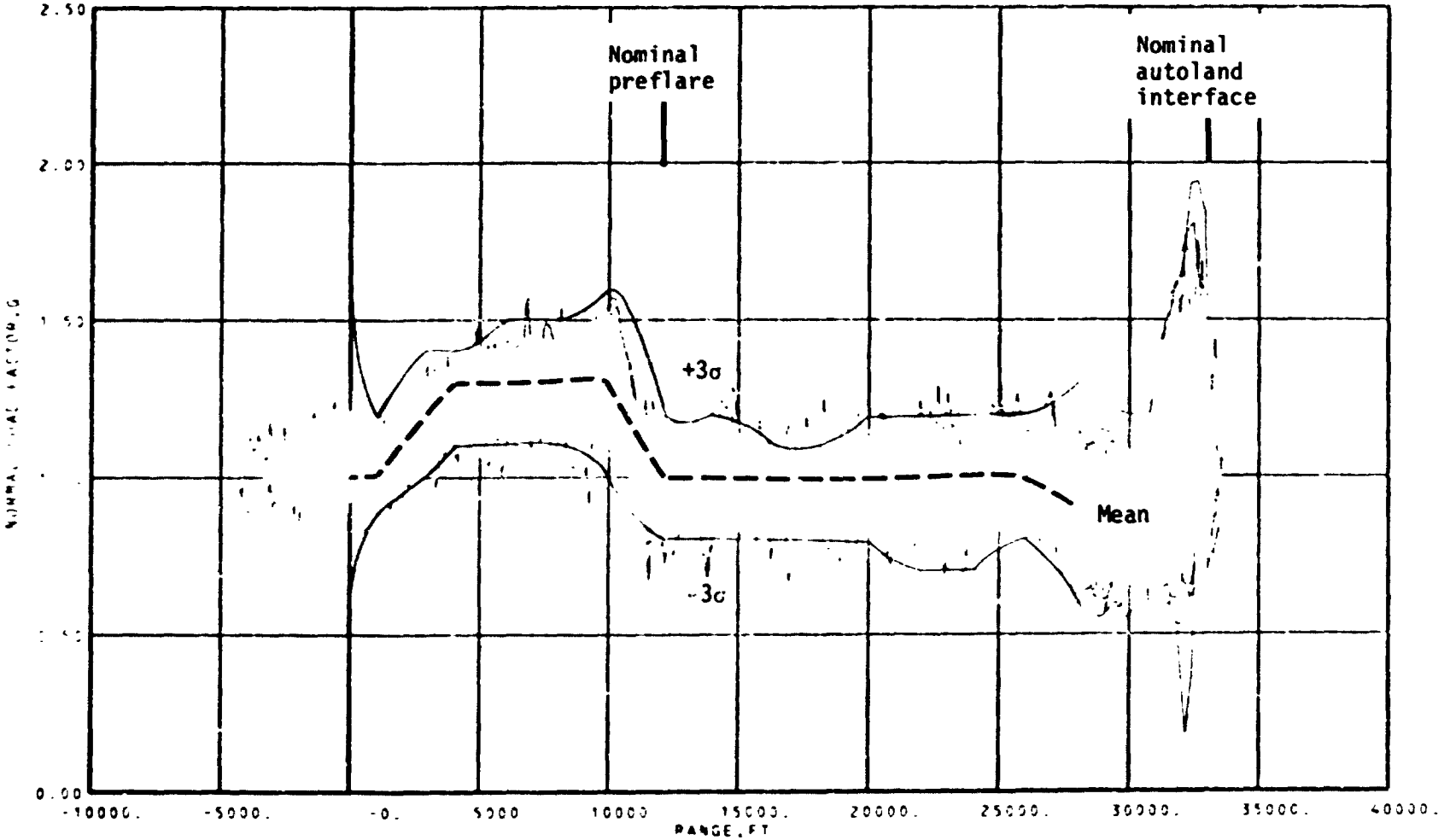

(k) Normal load factor.

Figure 10.- Continued.

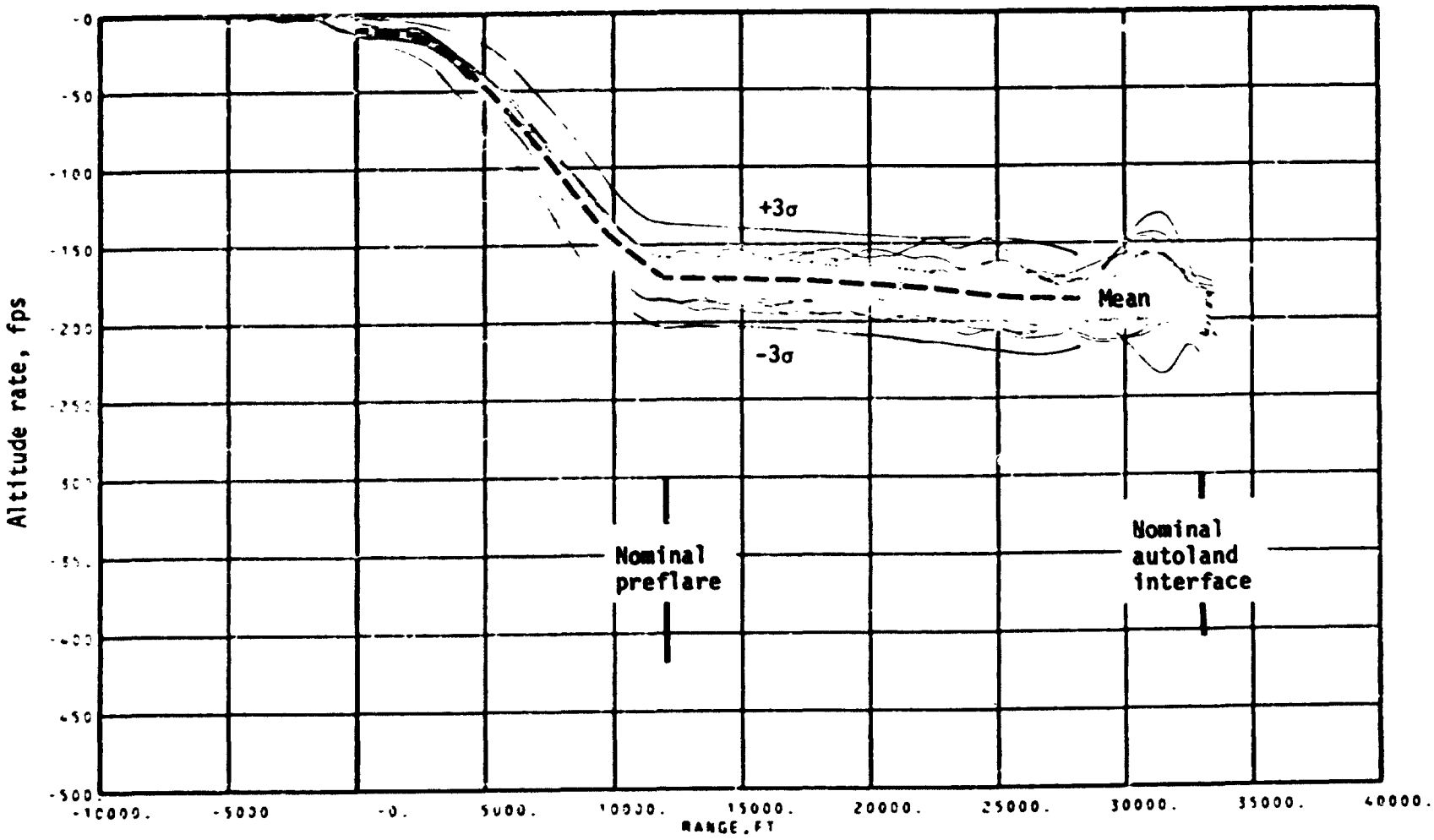

(1) Altitude rate.

Figure 10.- Continued.

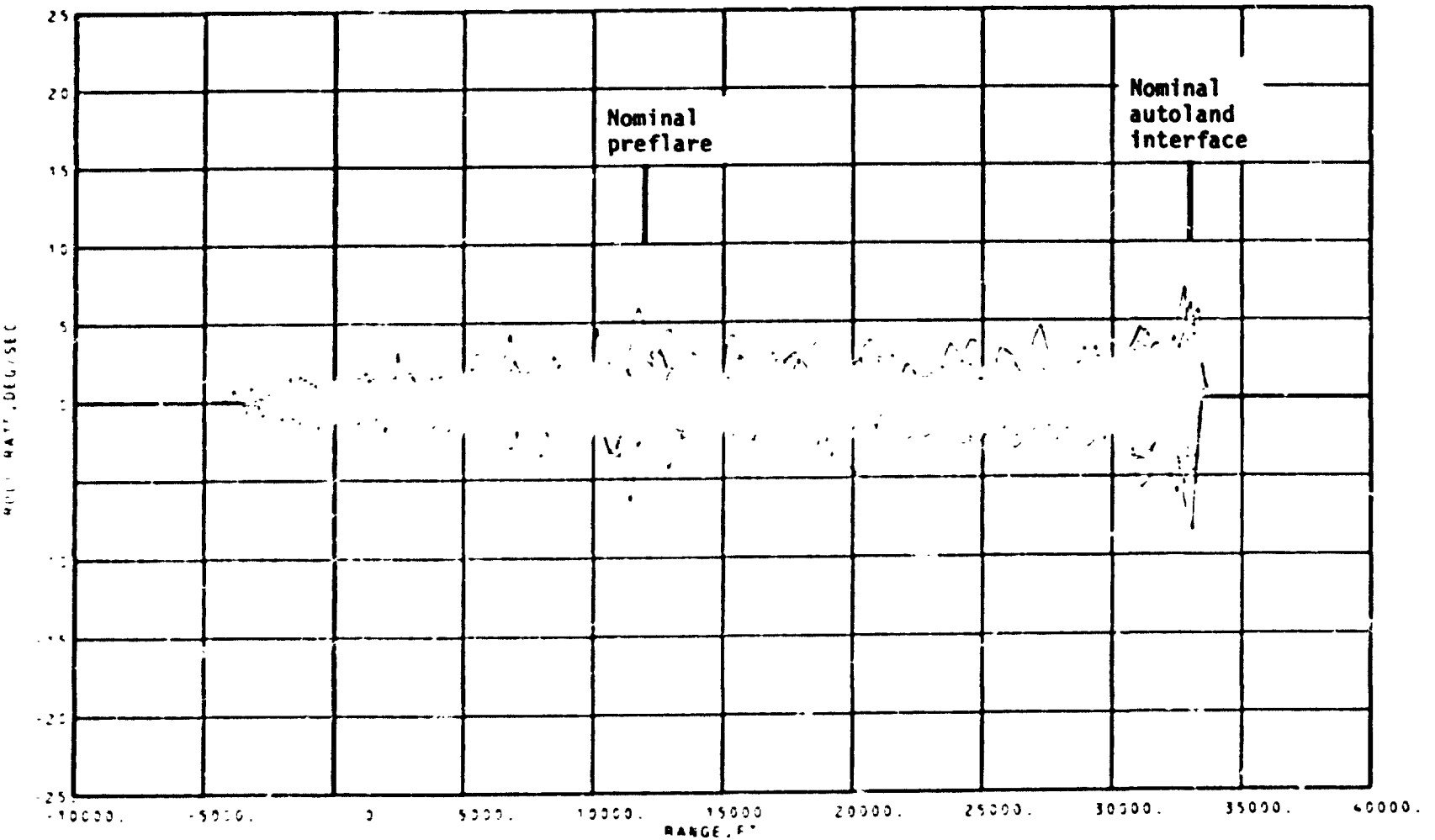

(m) Roll rate.

Figure 10.- Continued.

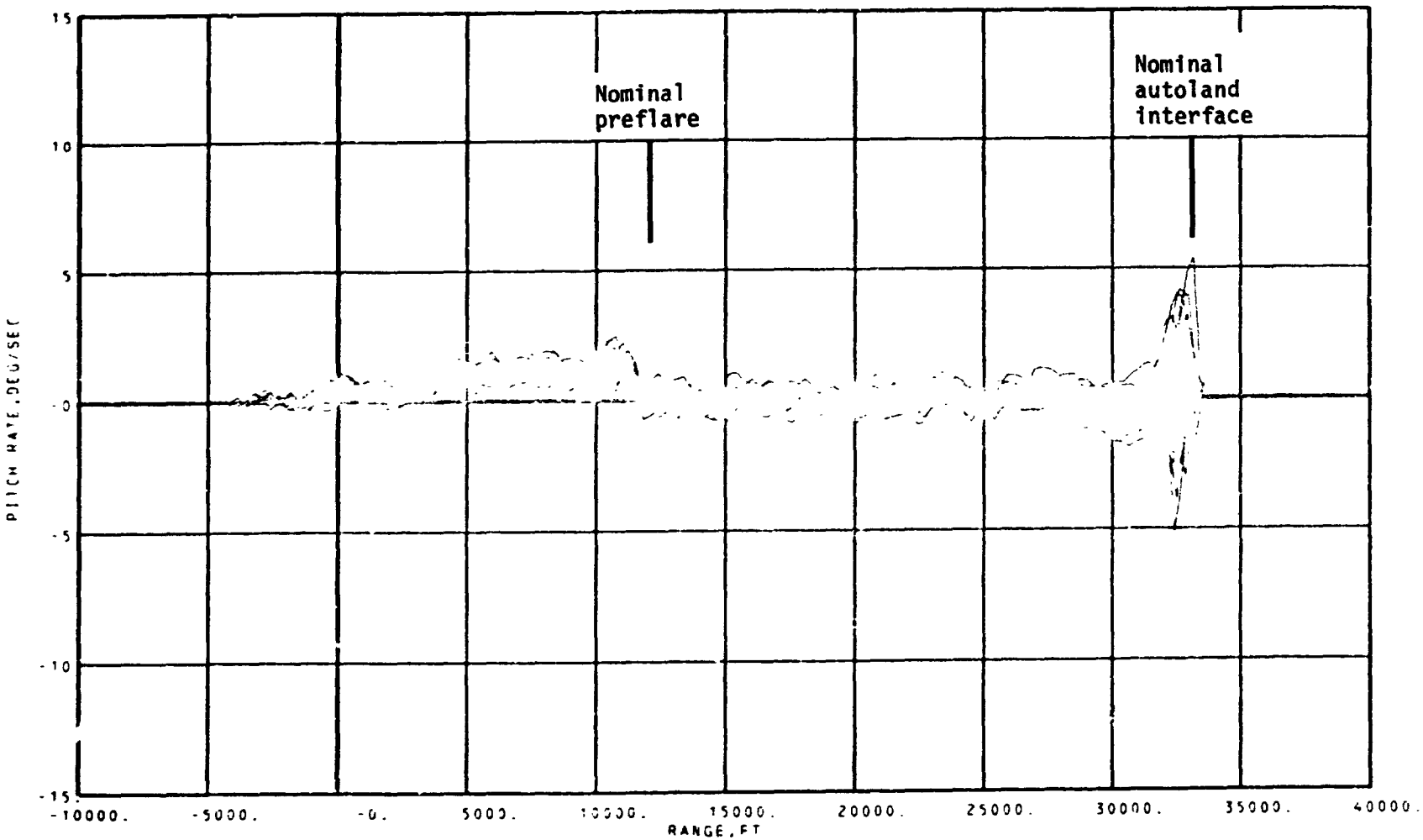

(n) Pitch rate.

Figure 10.- Continued.

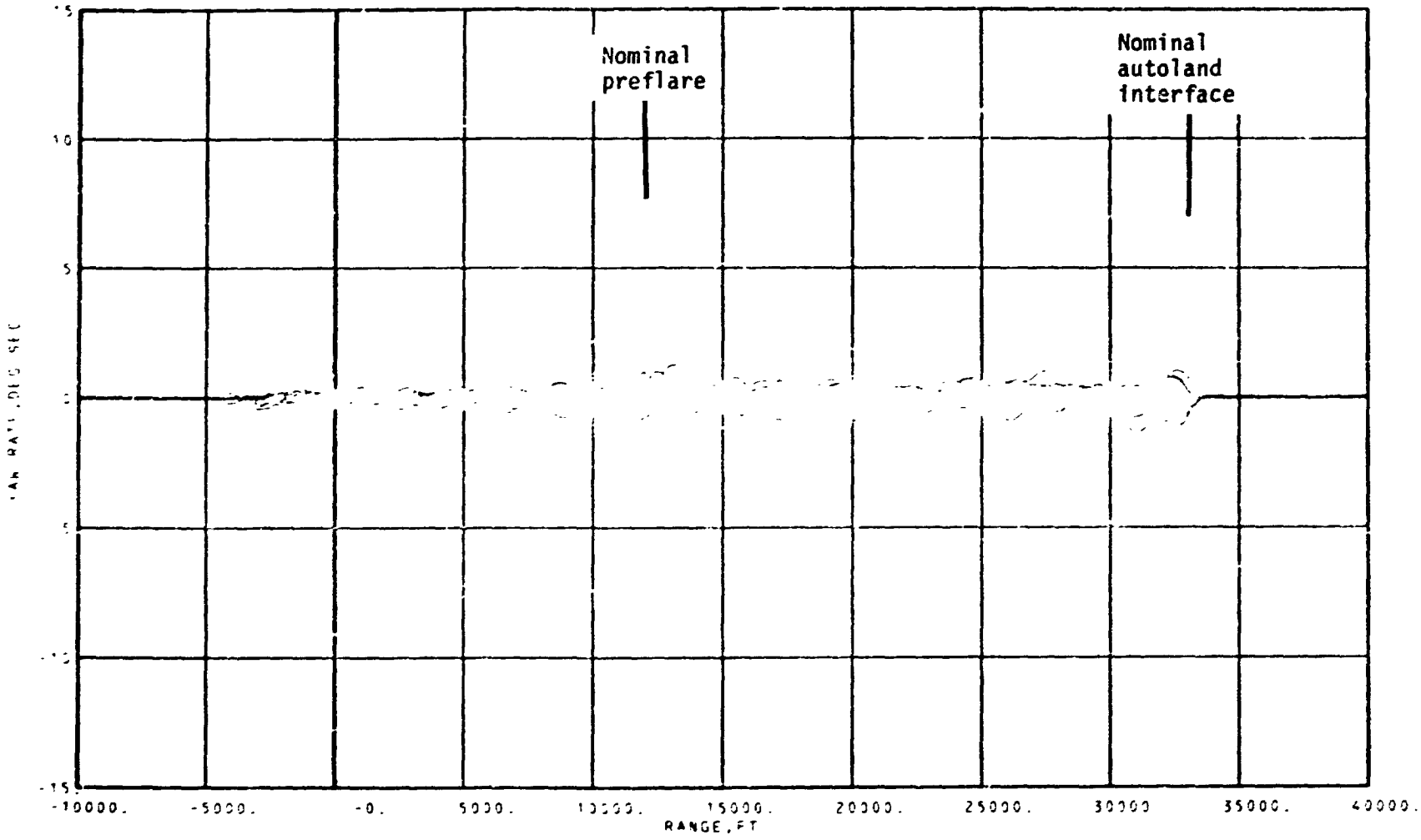

(o) Yaw rate.

Figure 10.- Continued.

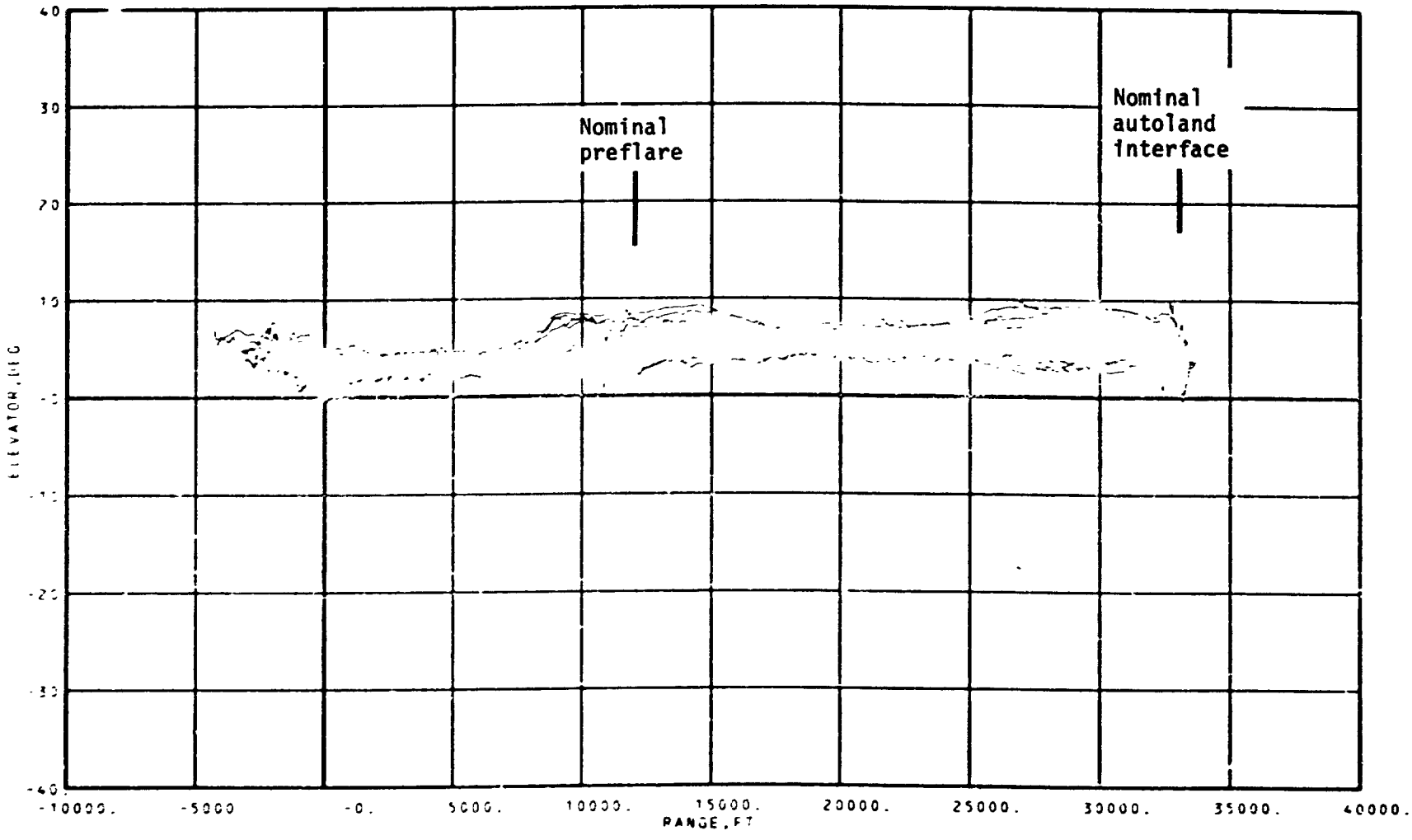

(p) Elevator deflections.

Figure 10.- Continued.

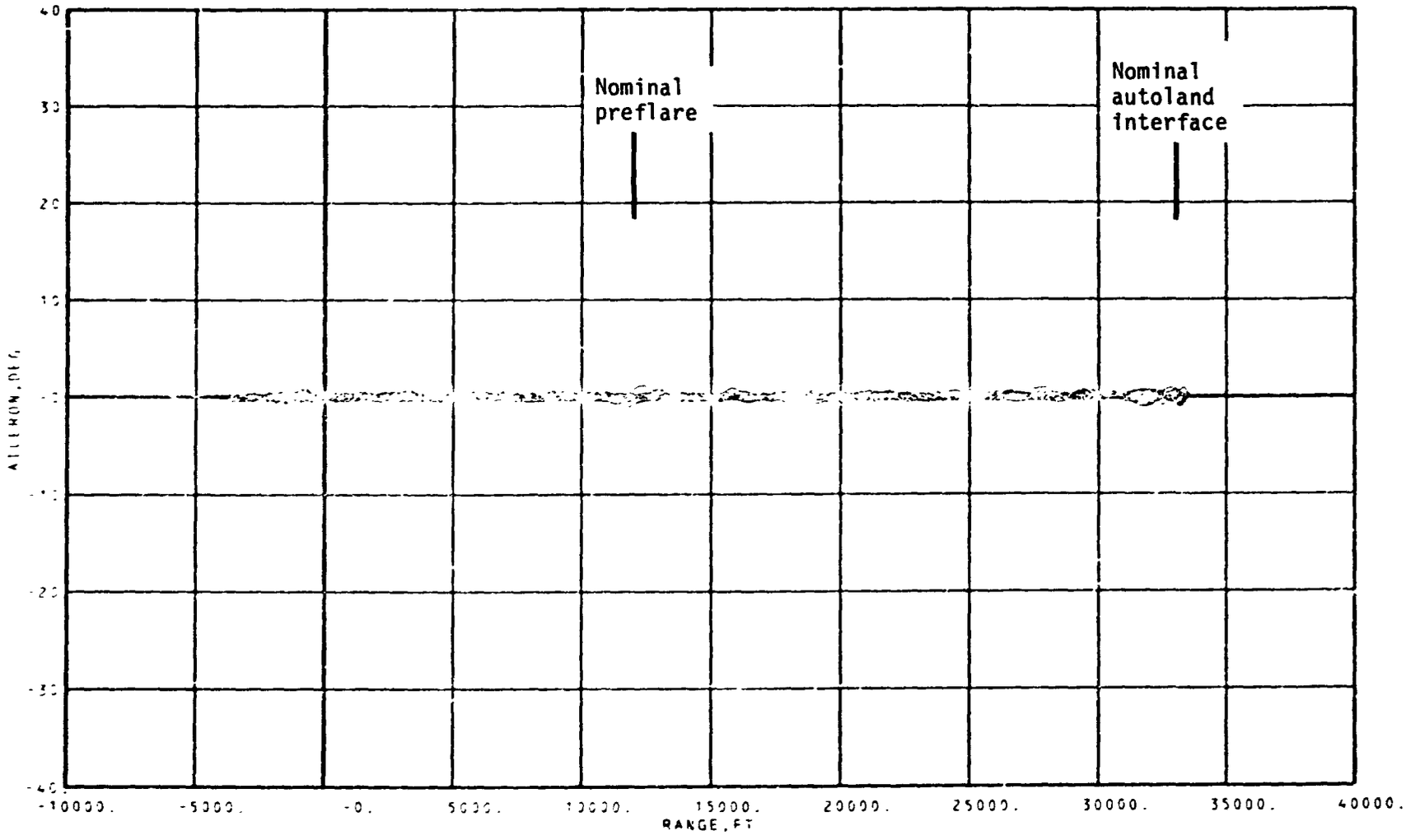

(q) Aileron.

Figure 10.- Continued.

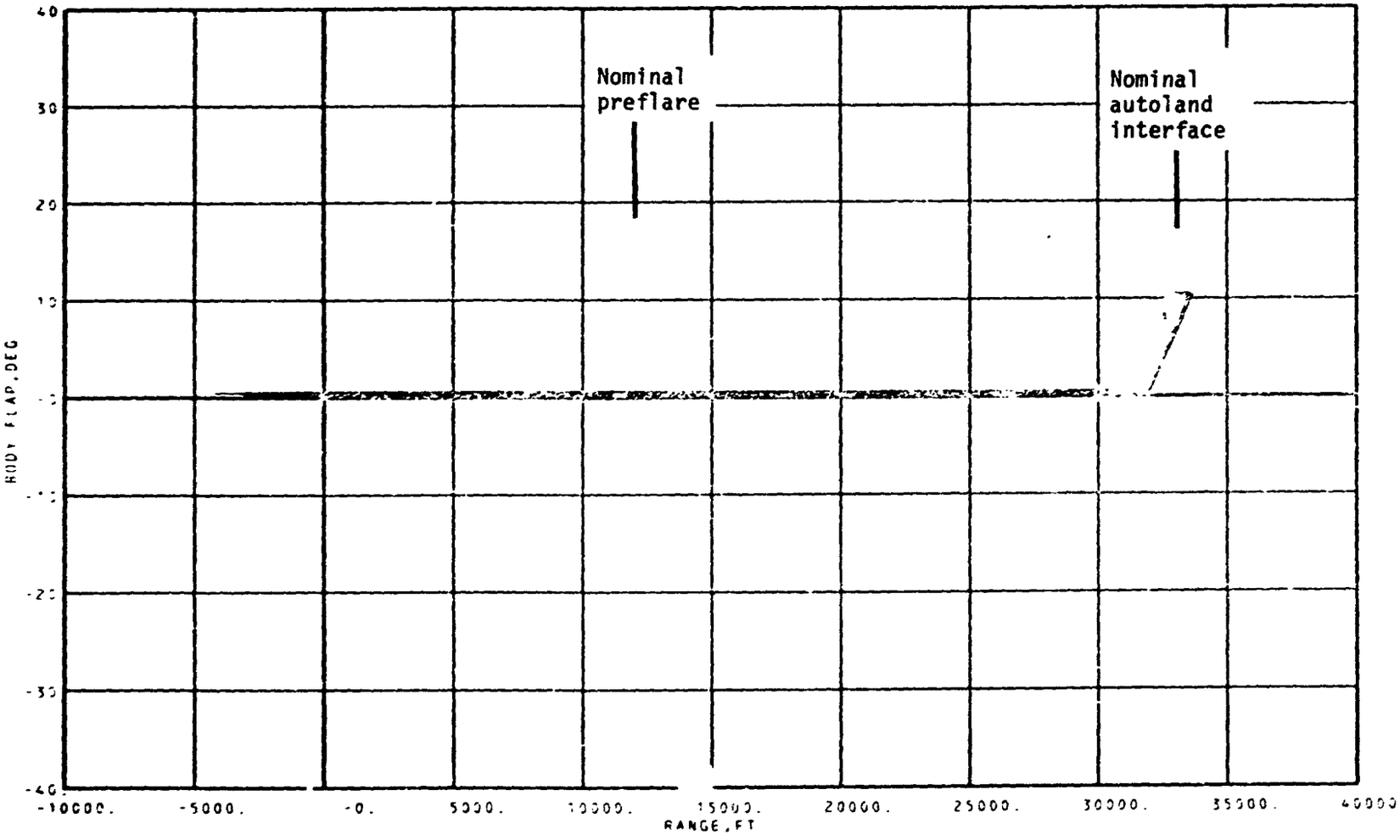

(r) Body flap deflections.

Figure 10.- Continued.

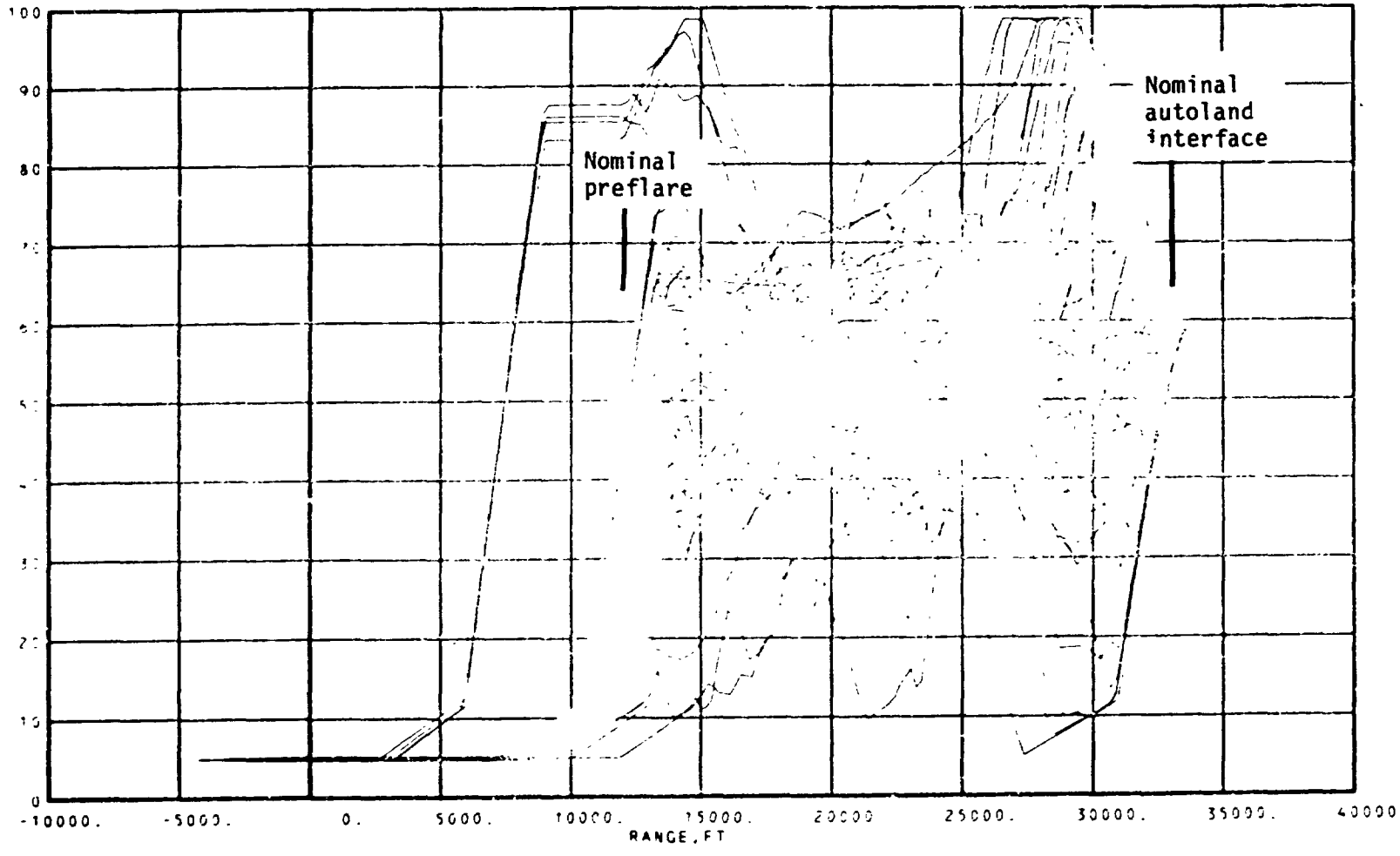

(s) Speedbrake deflections.

Figure 10.- Continued.

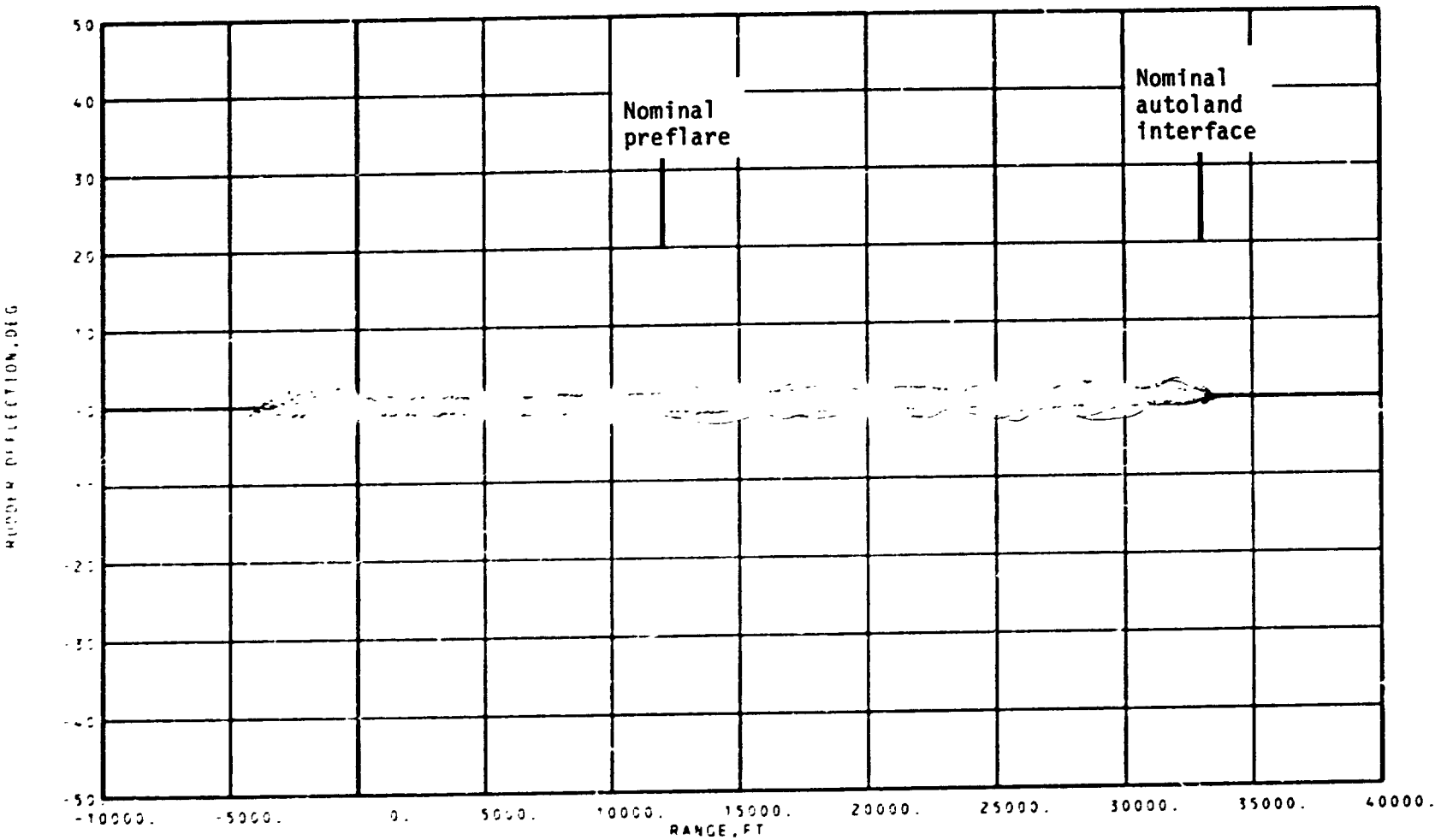

(t) Rudder deflections.

Figure 10.- Continued.

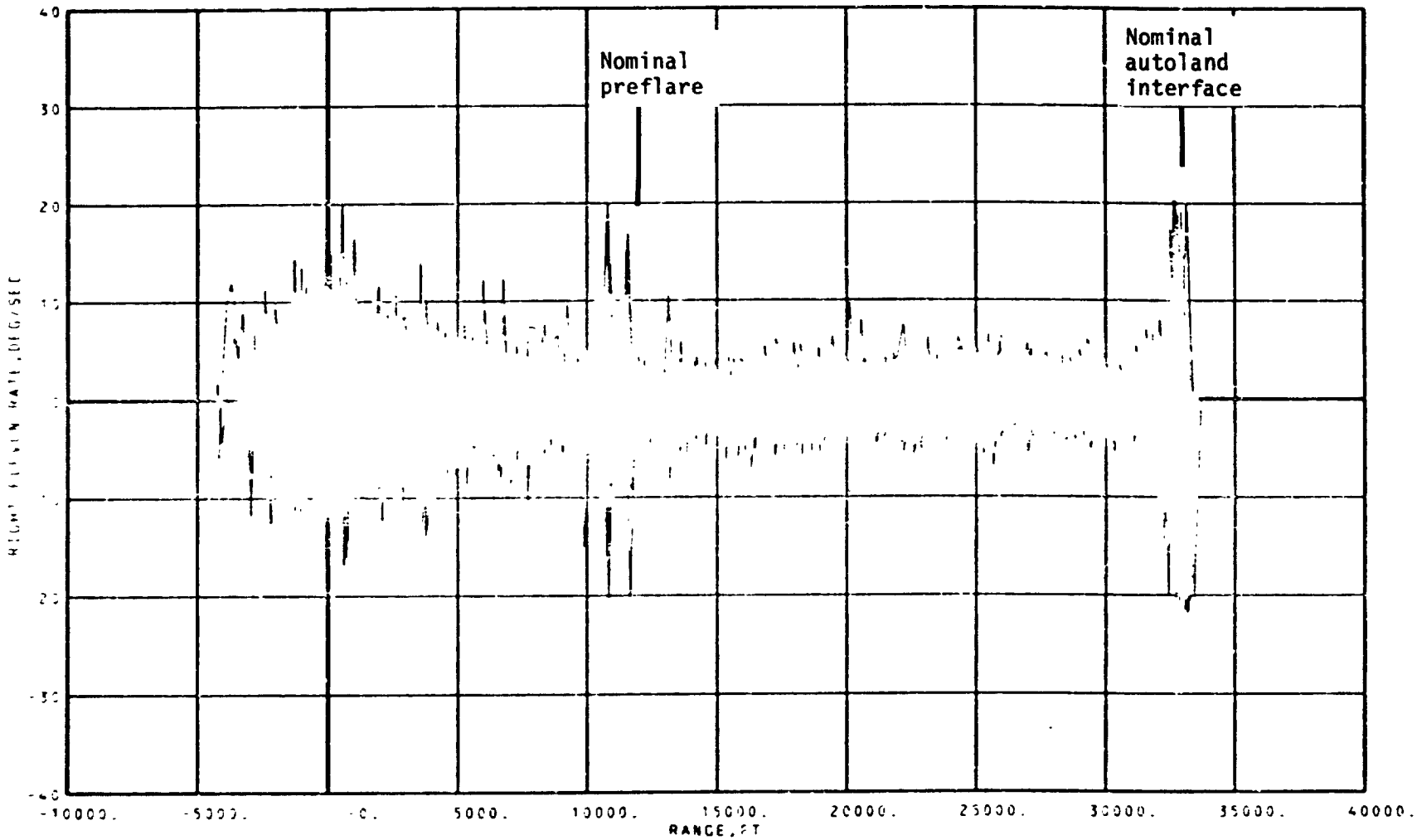

(u) Right elevon rate

Figure 10.- Continued.

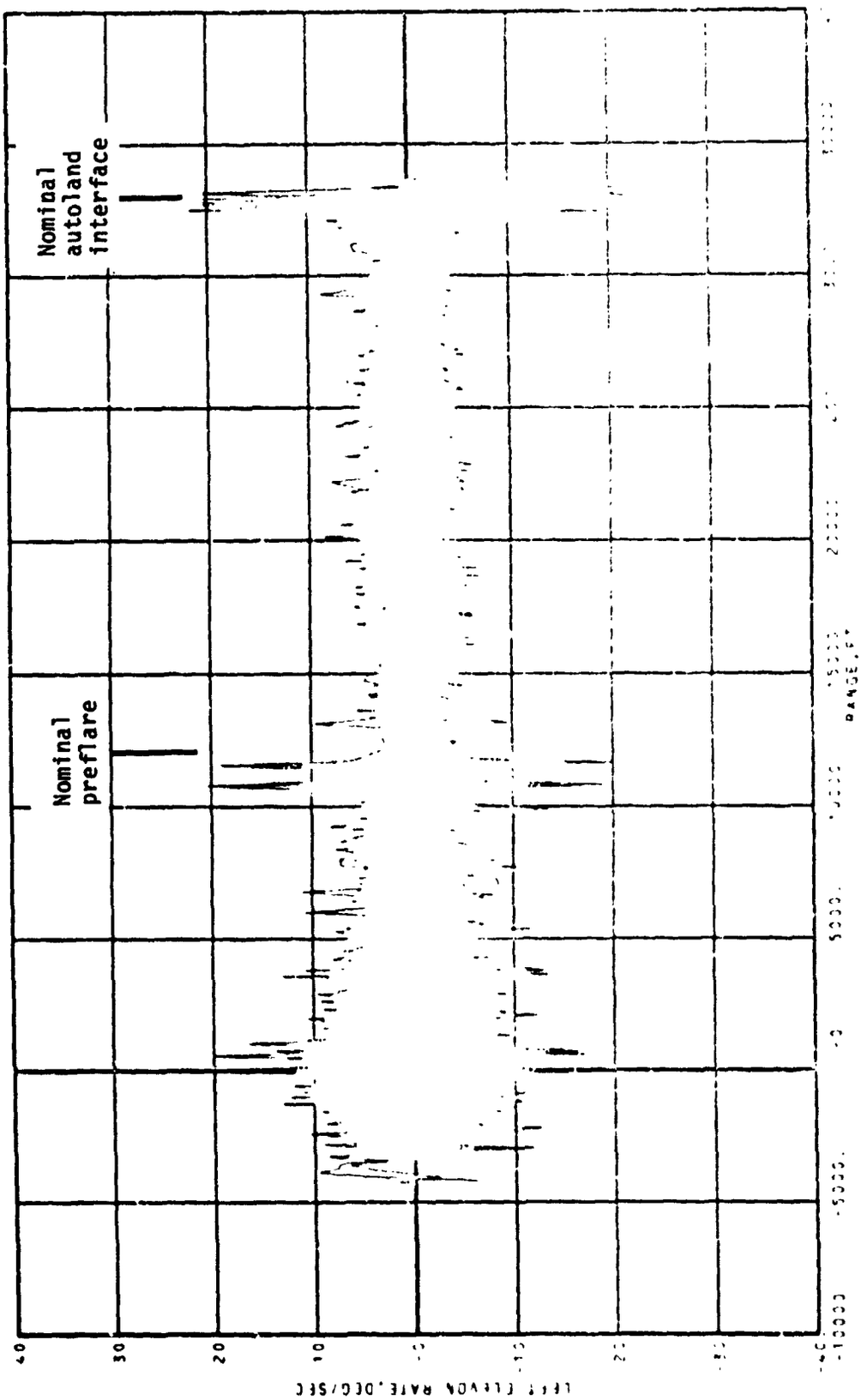

(v) Left elevon rate.

Figure 10.- Continued.

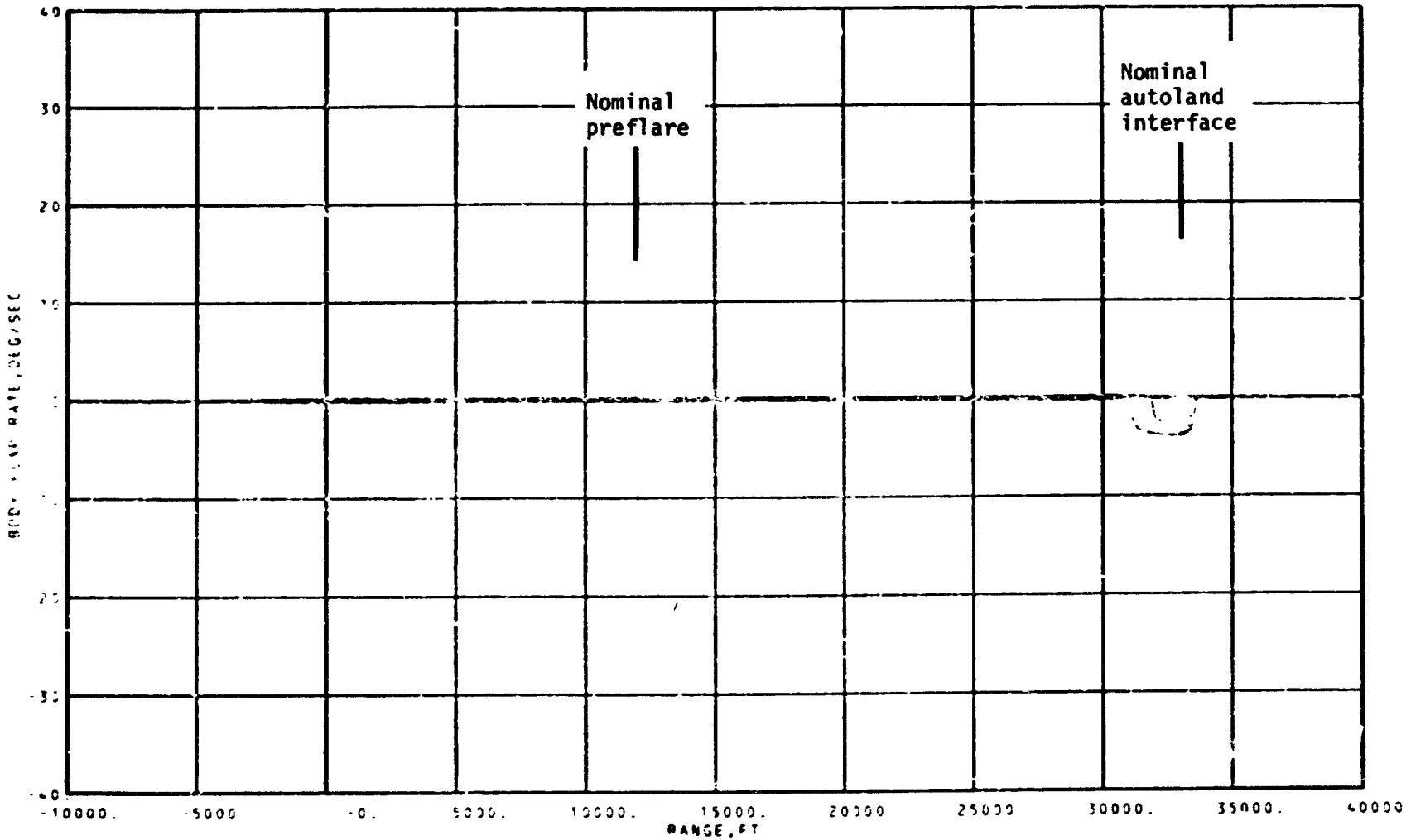

(w) Body flap rate.

Figure 10.- Continued.

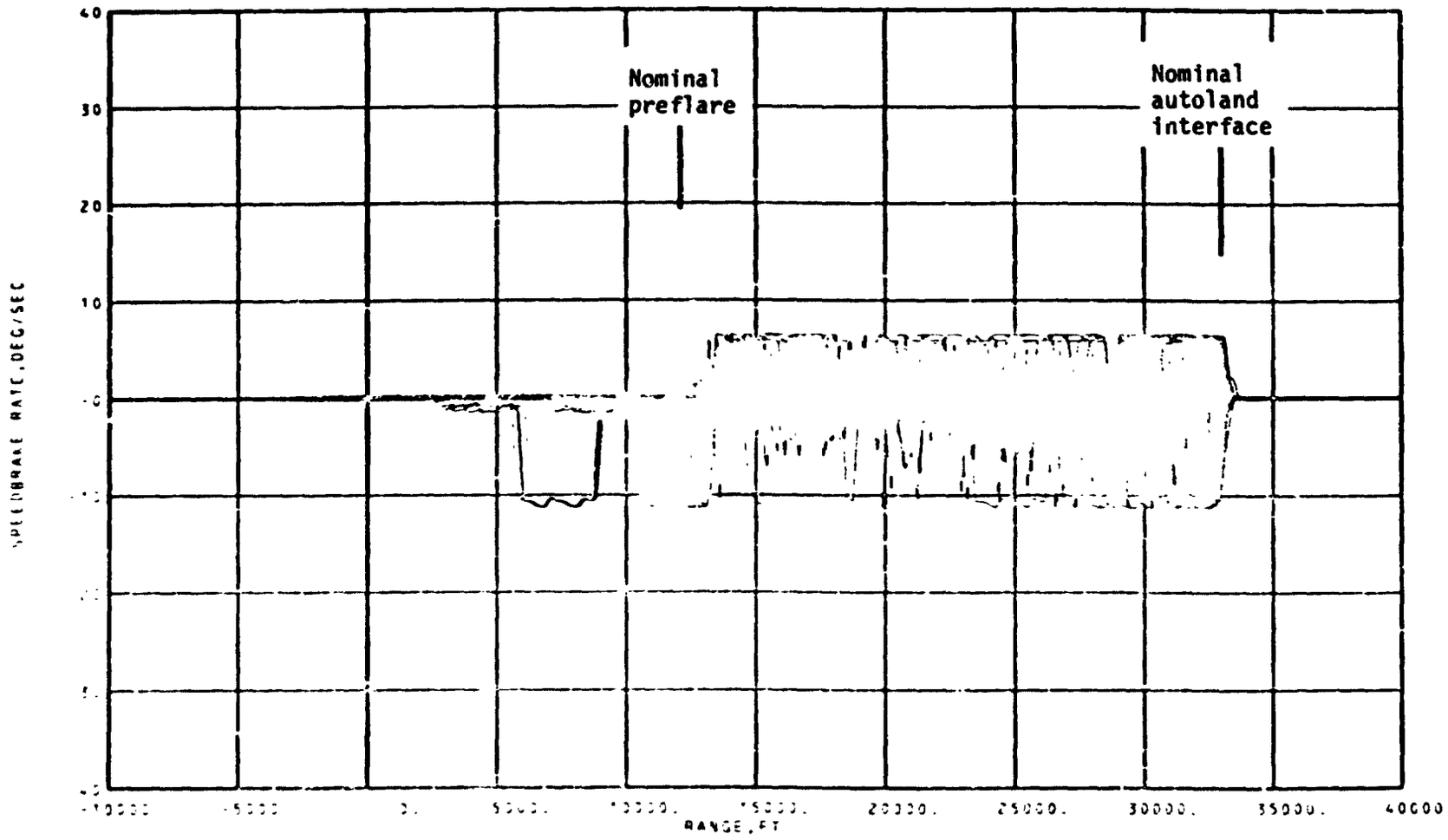

(x) Speedbrake rate.

Figure 10.- Continued.

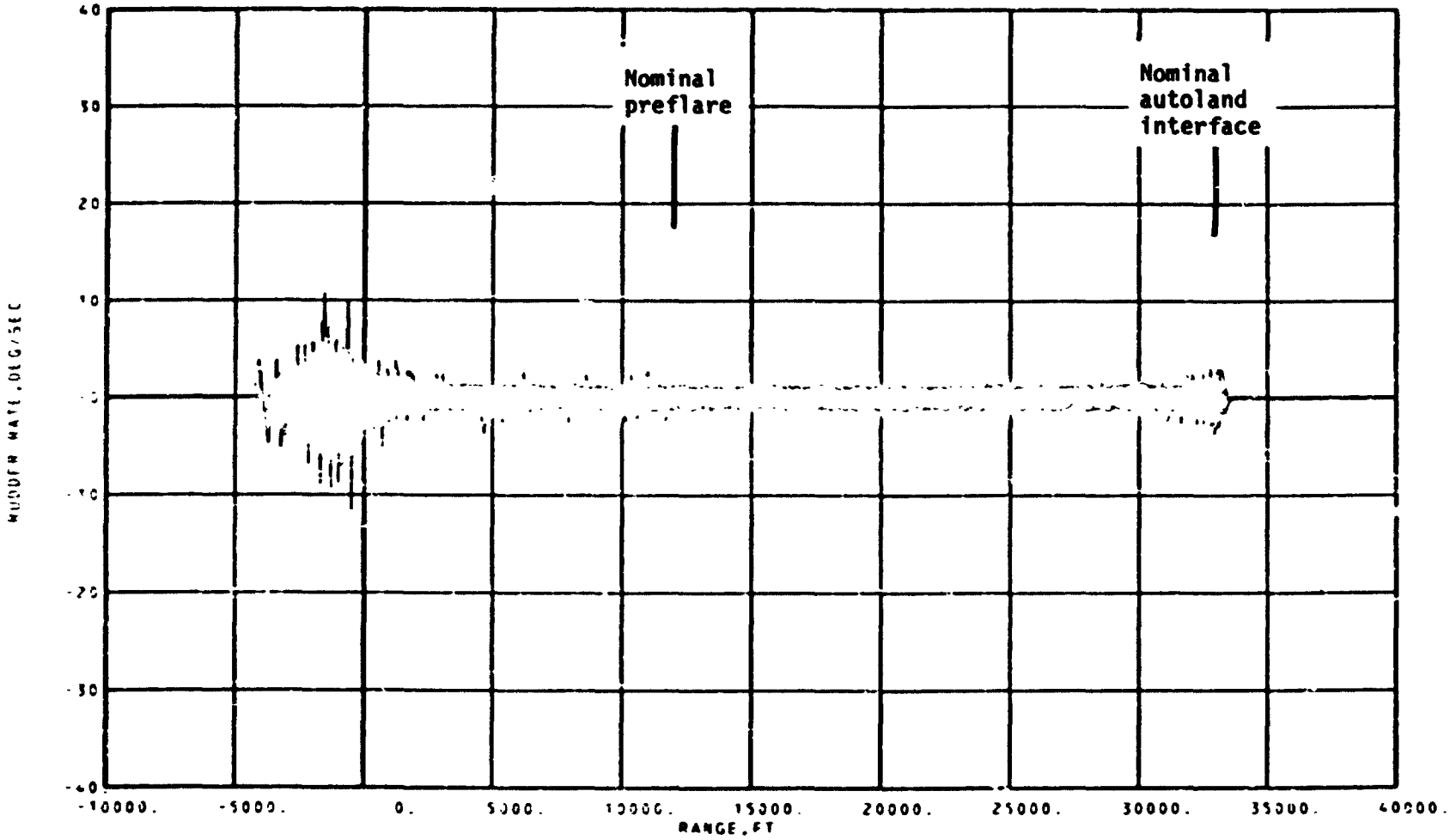

(y) Rudder rate.

Figure 10.- Continued.

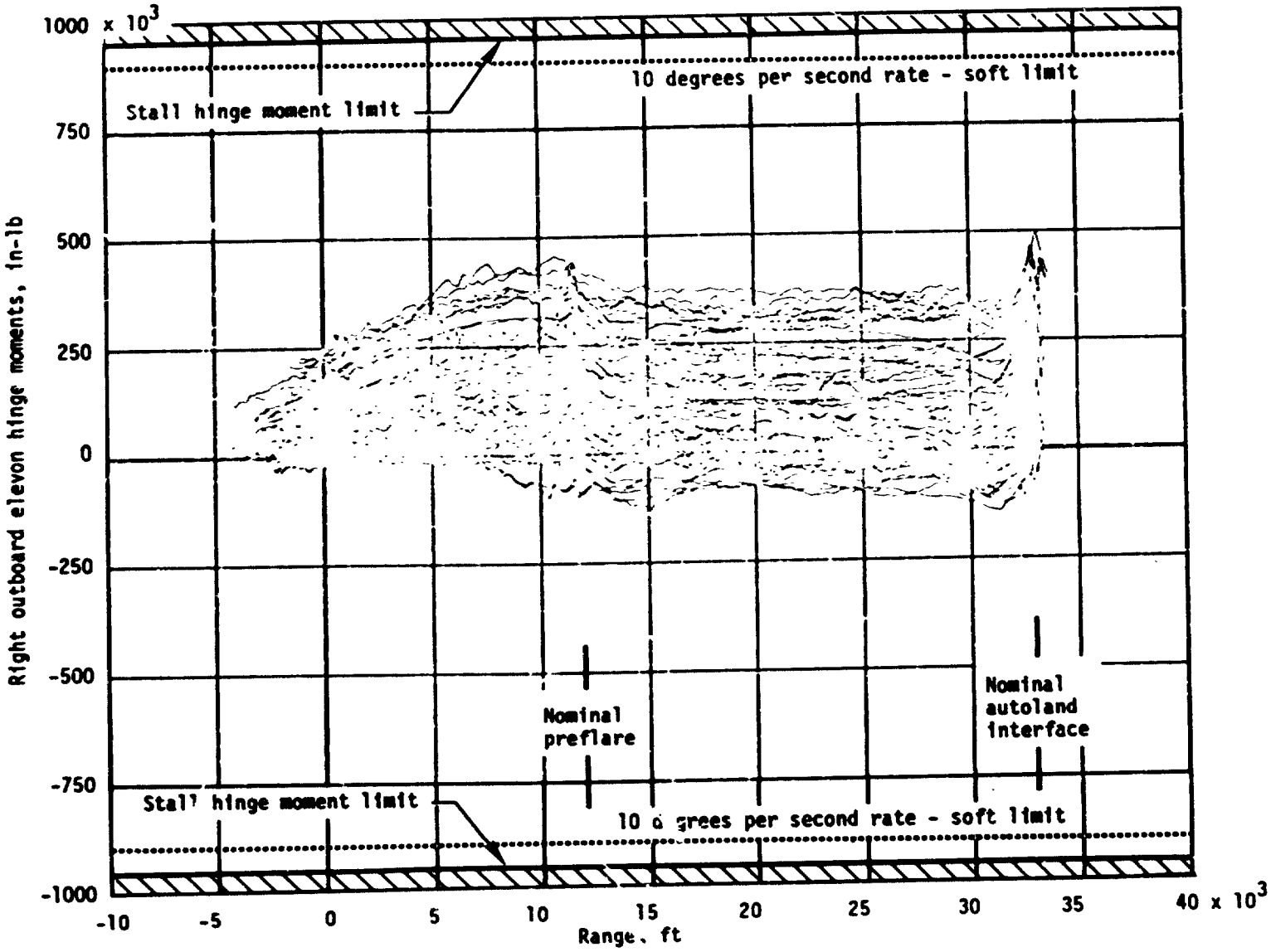

(z) Right inboard elevon hinge moments.

Figure 10.- Continued.

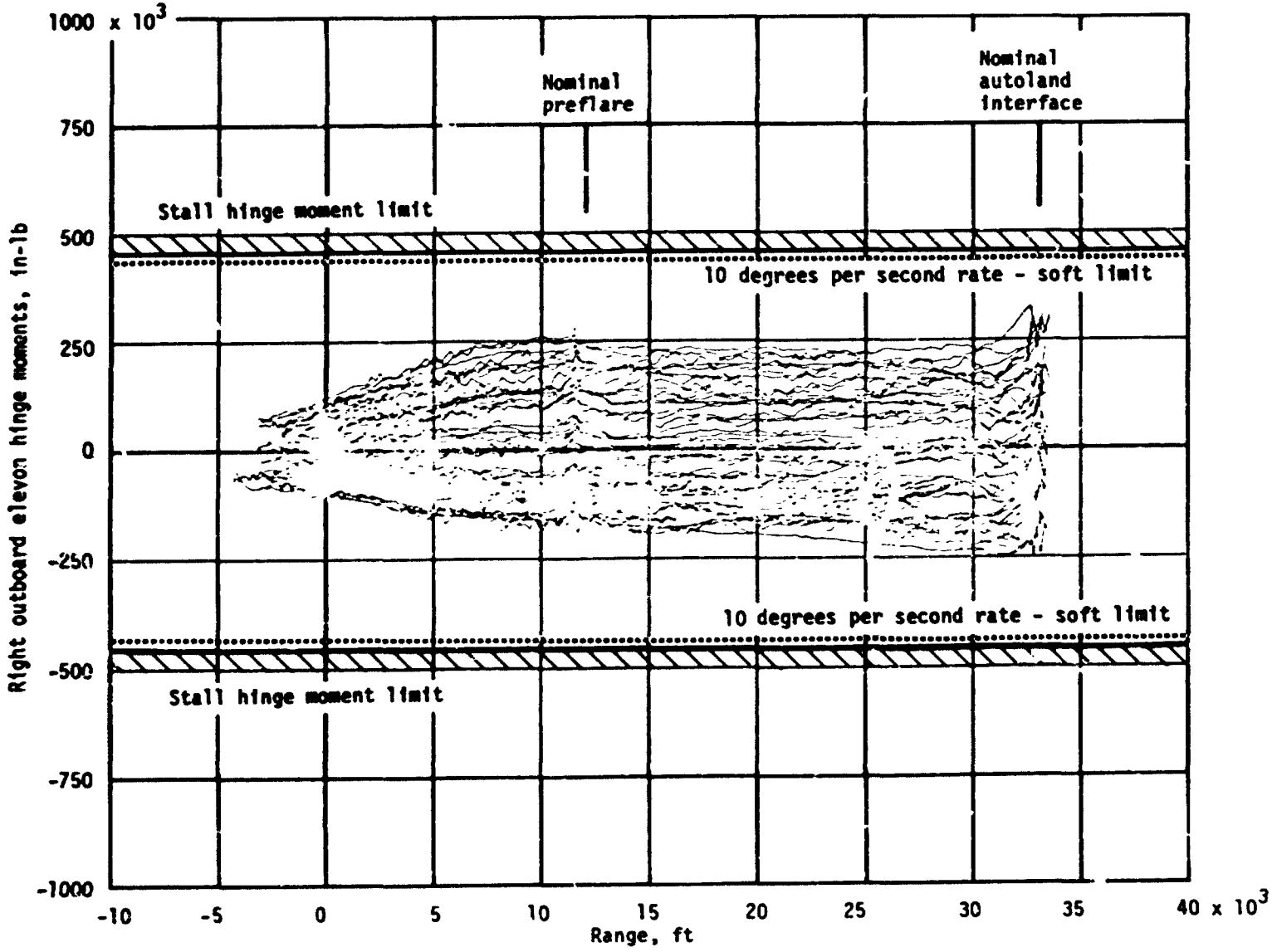

(aa) Right outboard elevon hinge moments.

Figure 10.- Continued.

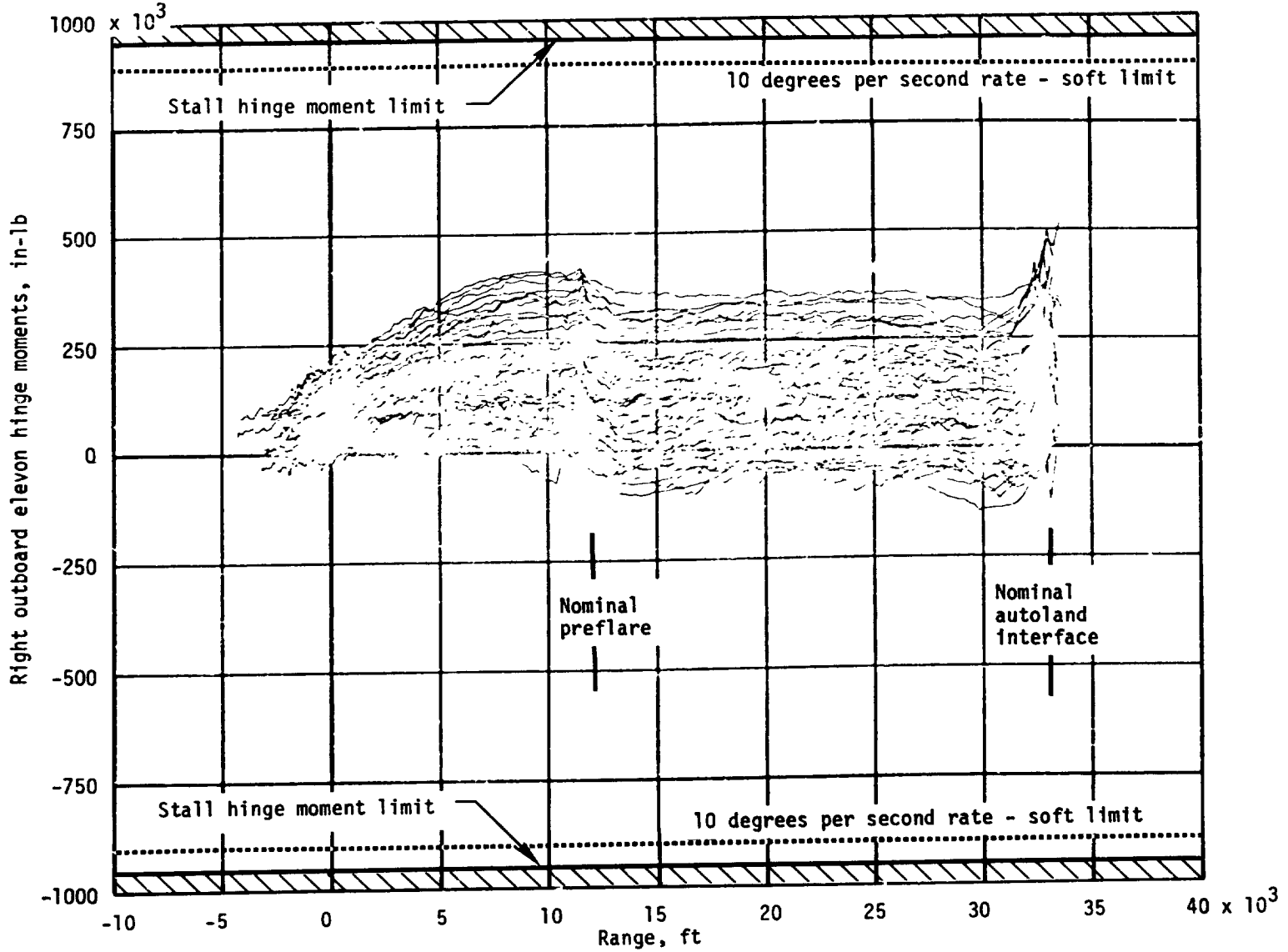

(bb) Left inboard elevon hinge moments.

Figure 10.- Continued.

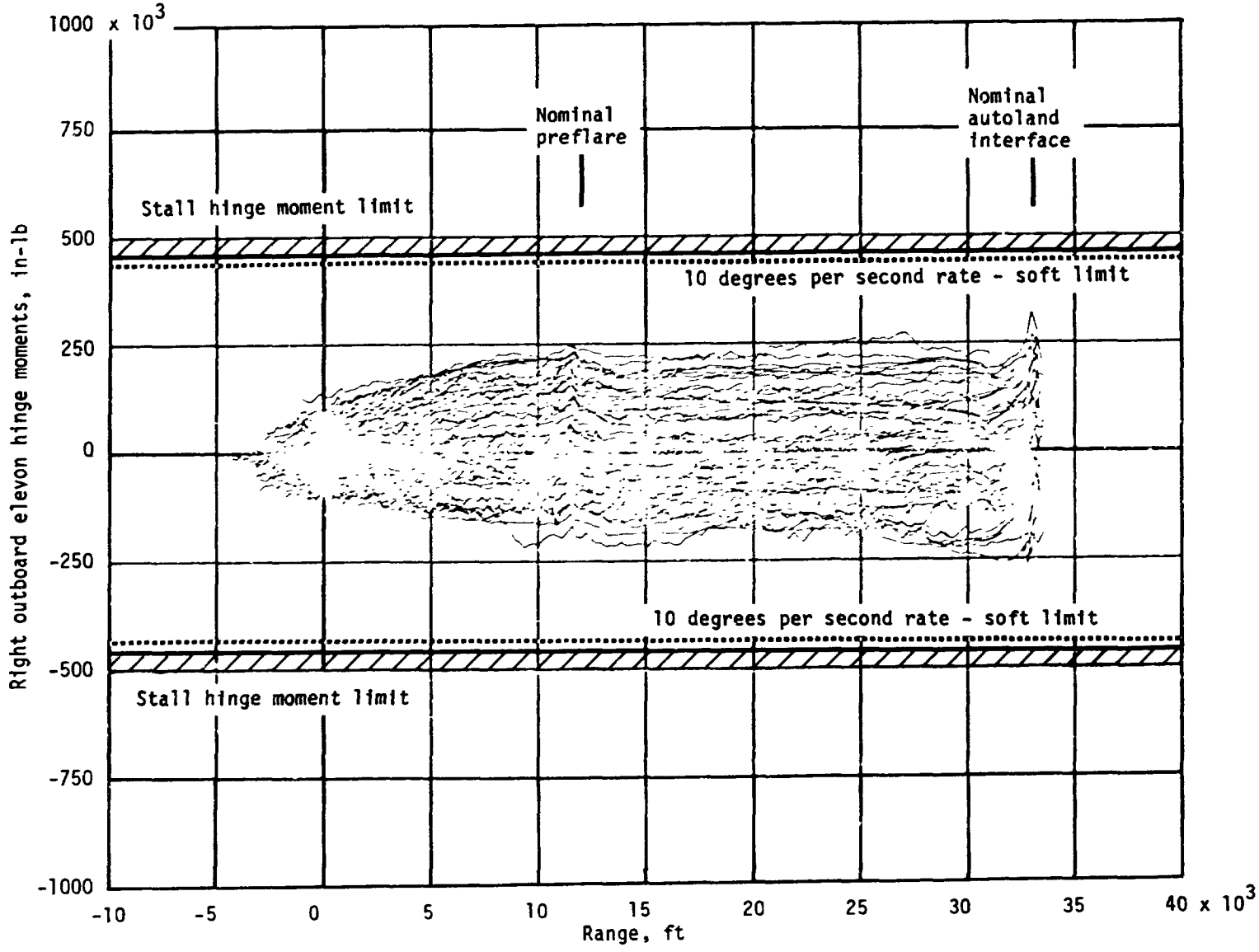

(cc) Left outboard elevon hinge moments.

Figure 10.- Continued.

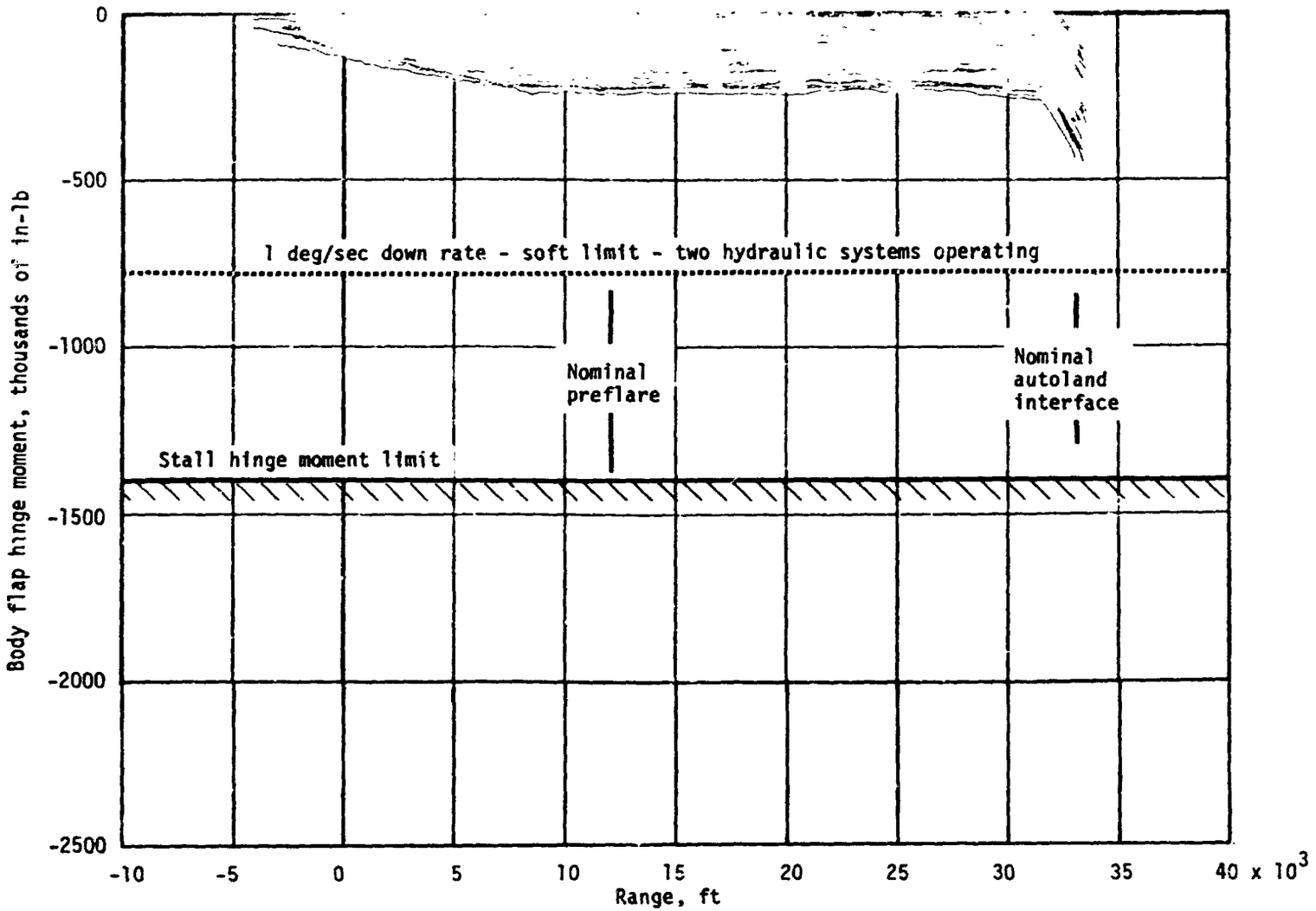

(dd) Body flap hinge moments.

Figure 10.- Continued.

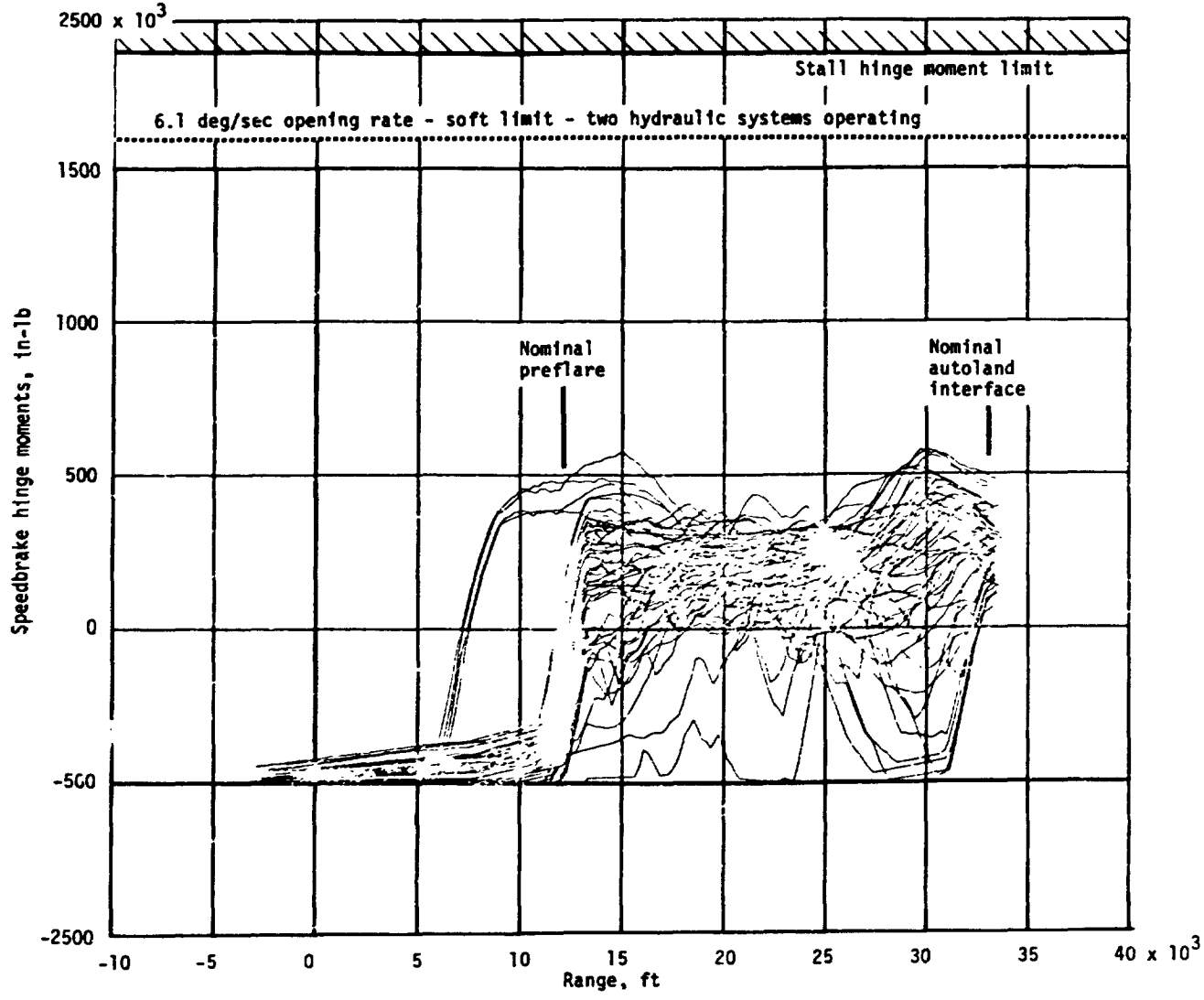

(ee) Speedbrake hinge moments.

Figure 10.- Continued.

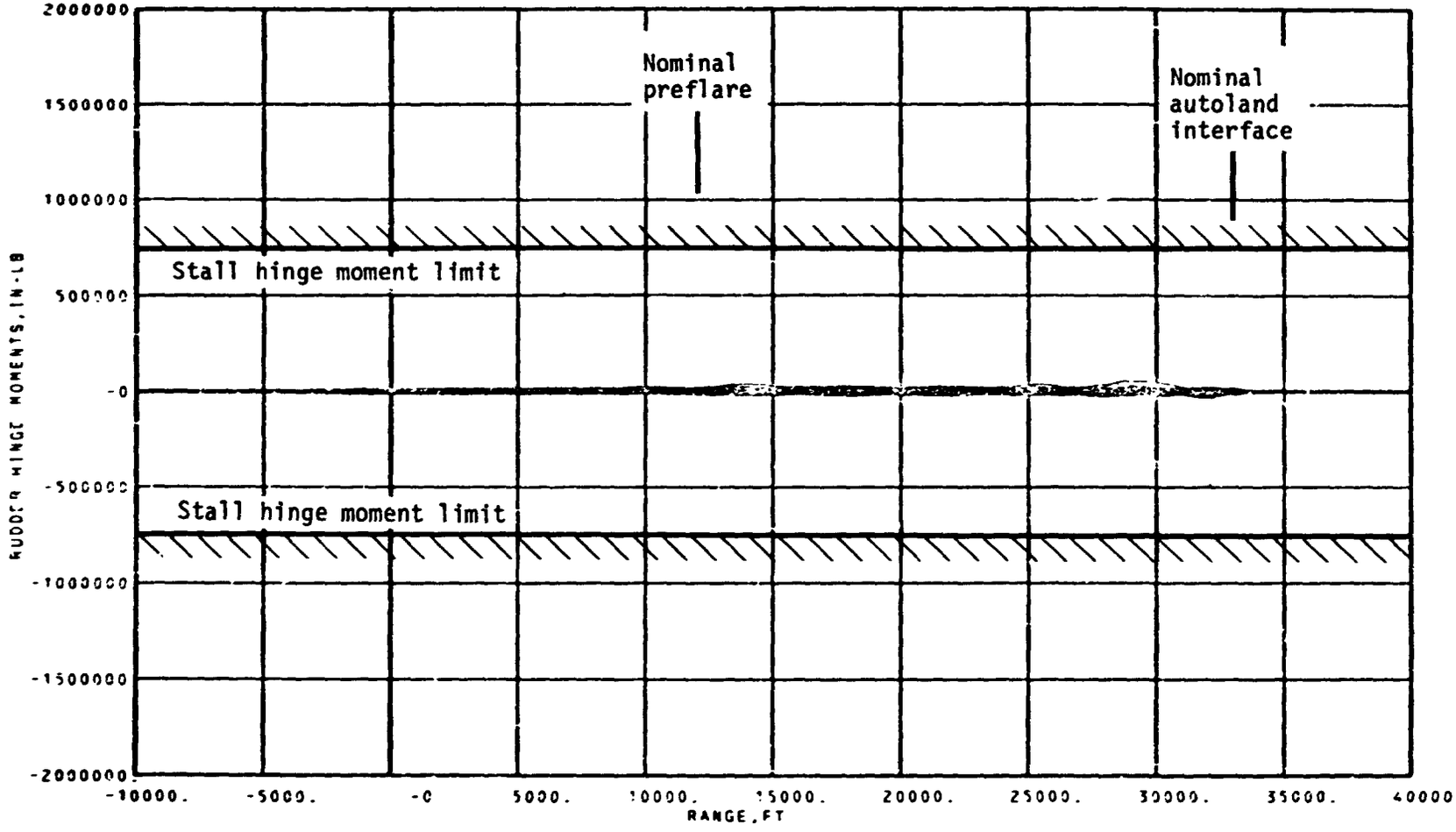

(ff) Rudder hinge moments.

Figure 10.- Concluded.

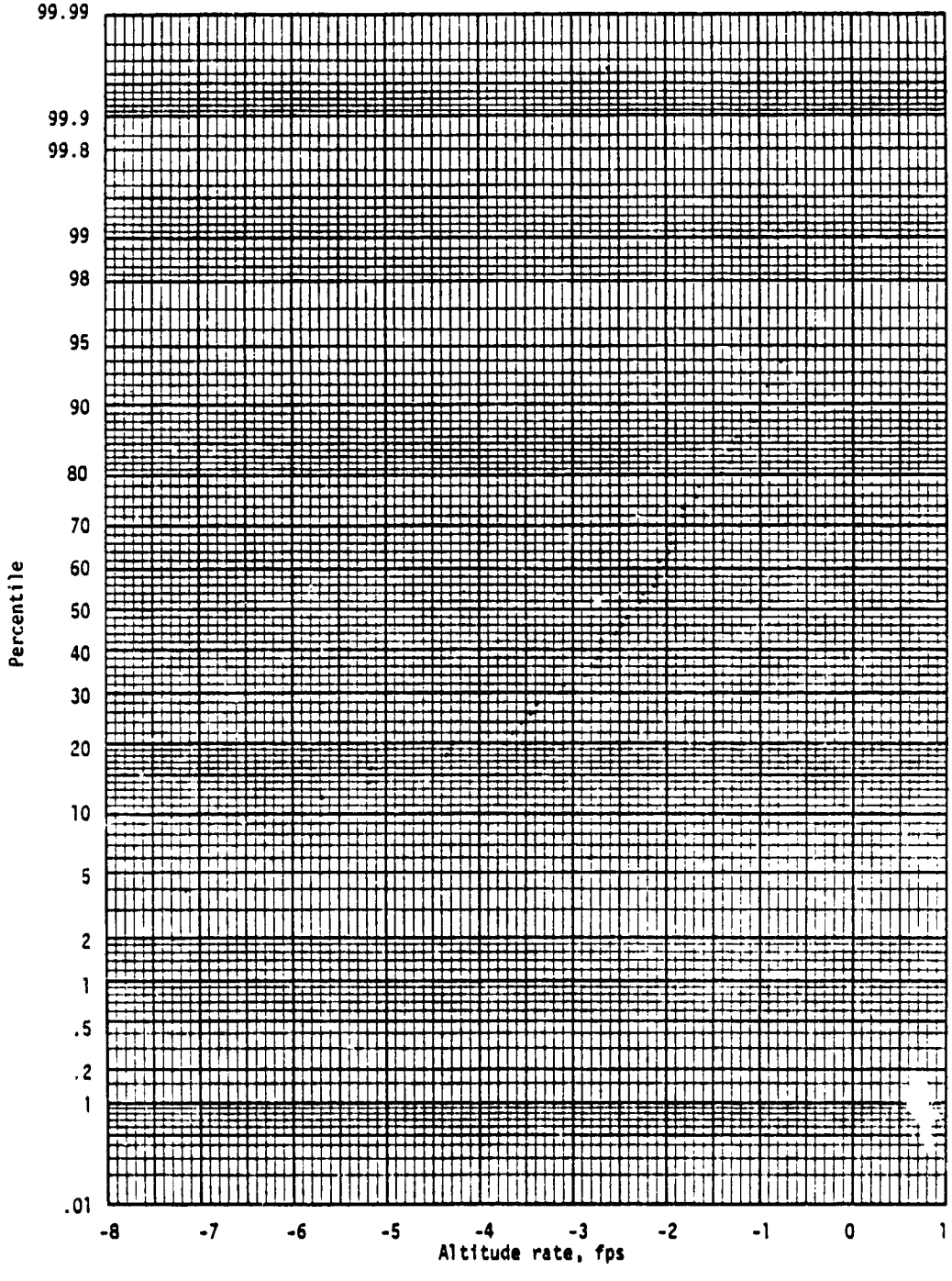

(a) Altitude rate.

Figure 11.- Landing statistics.

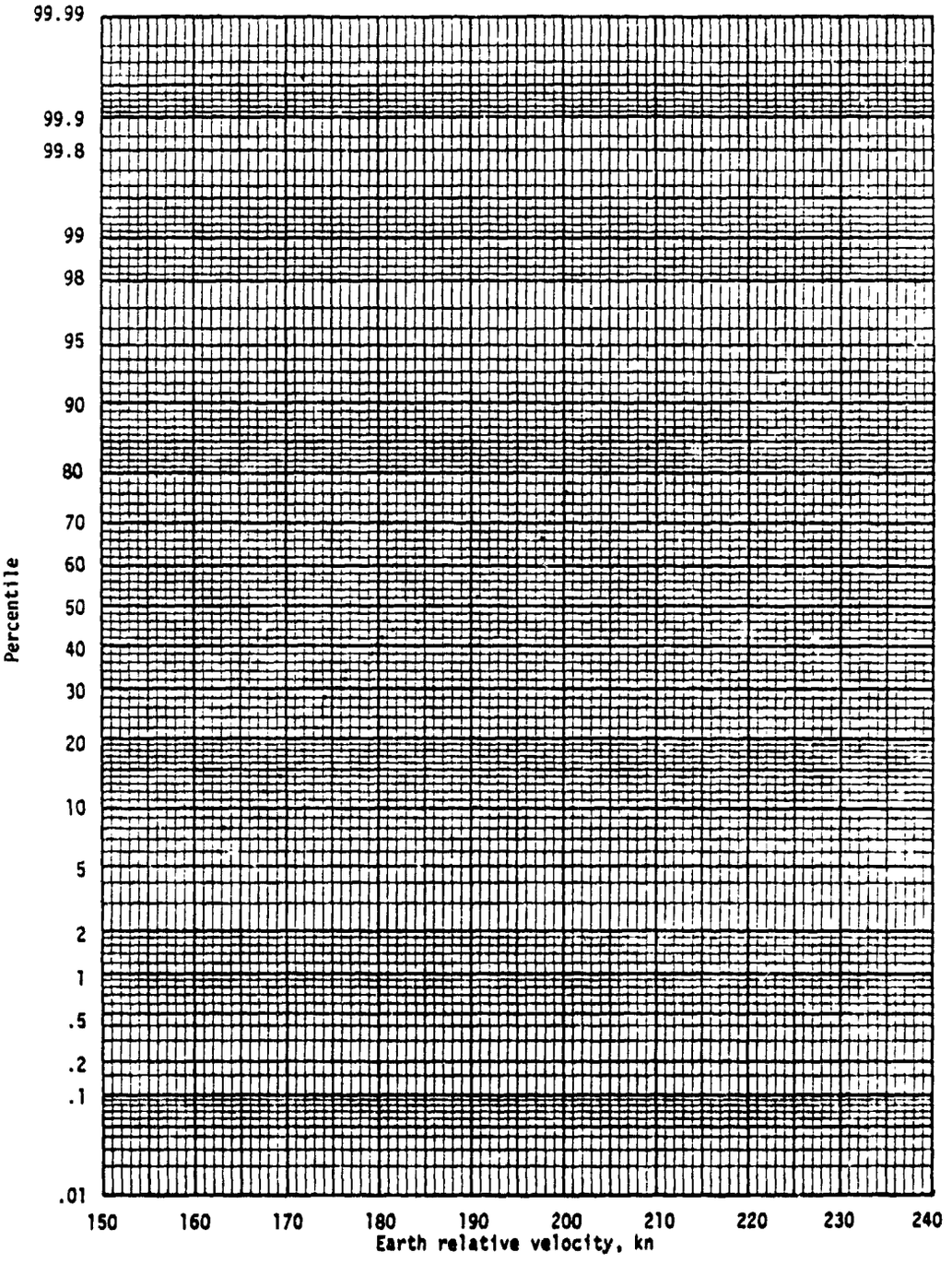

(b) Earth relative velocity.

Figure 11.- Continued.

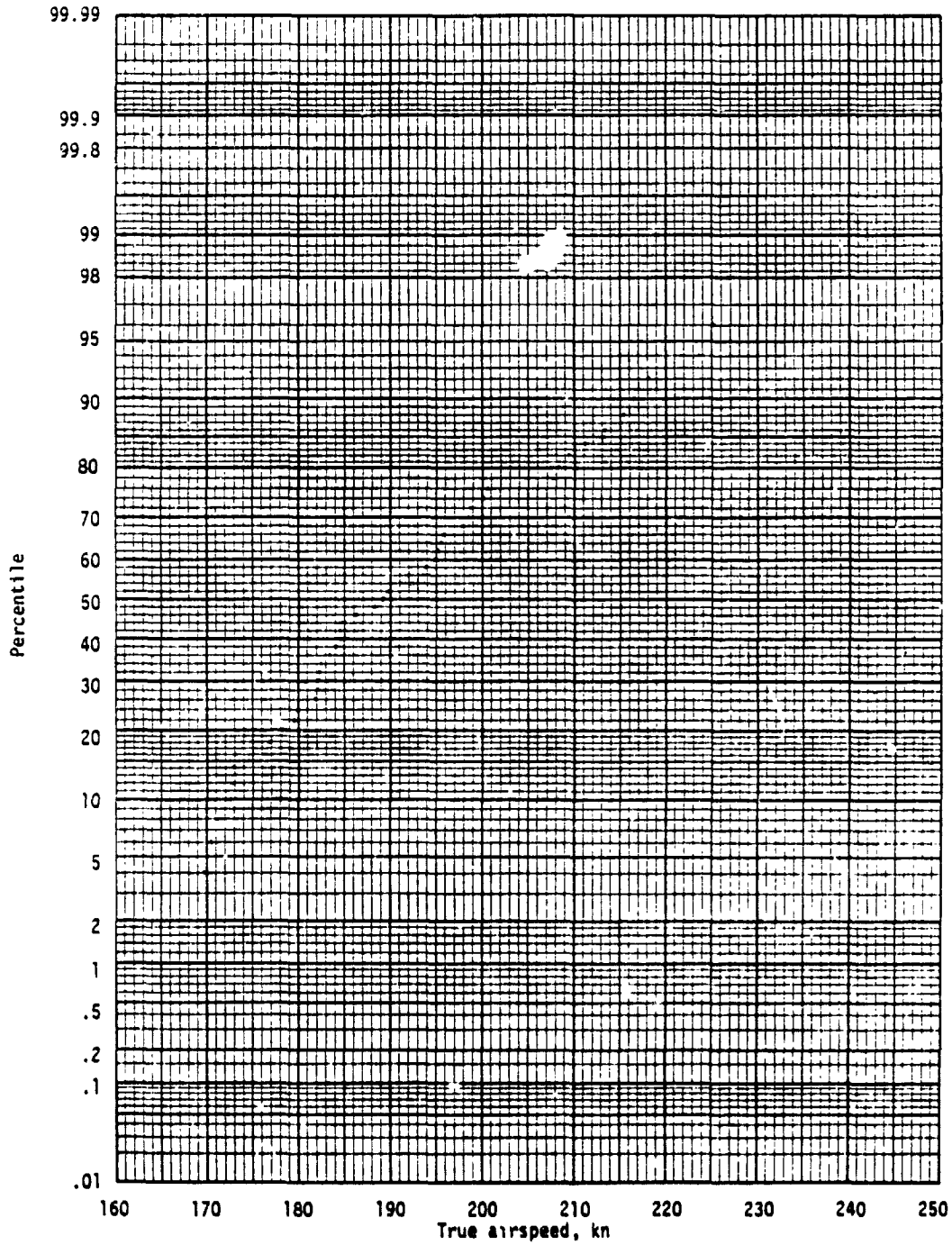

(c) True airspeed.

Figure 11.- Continued.

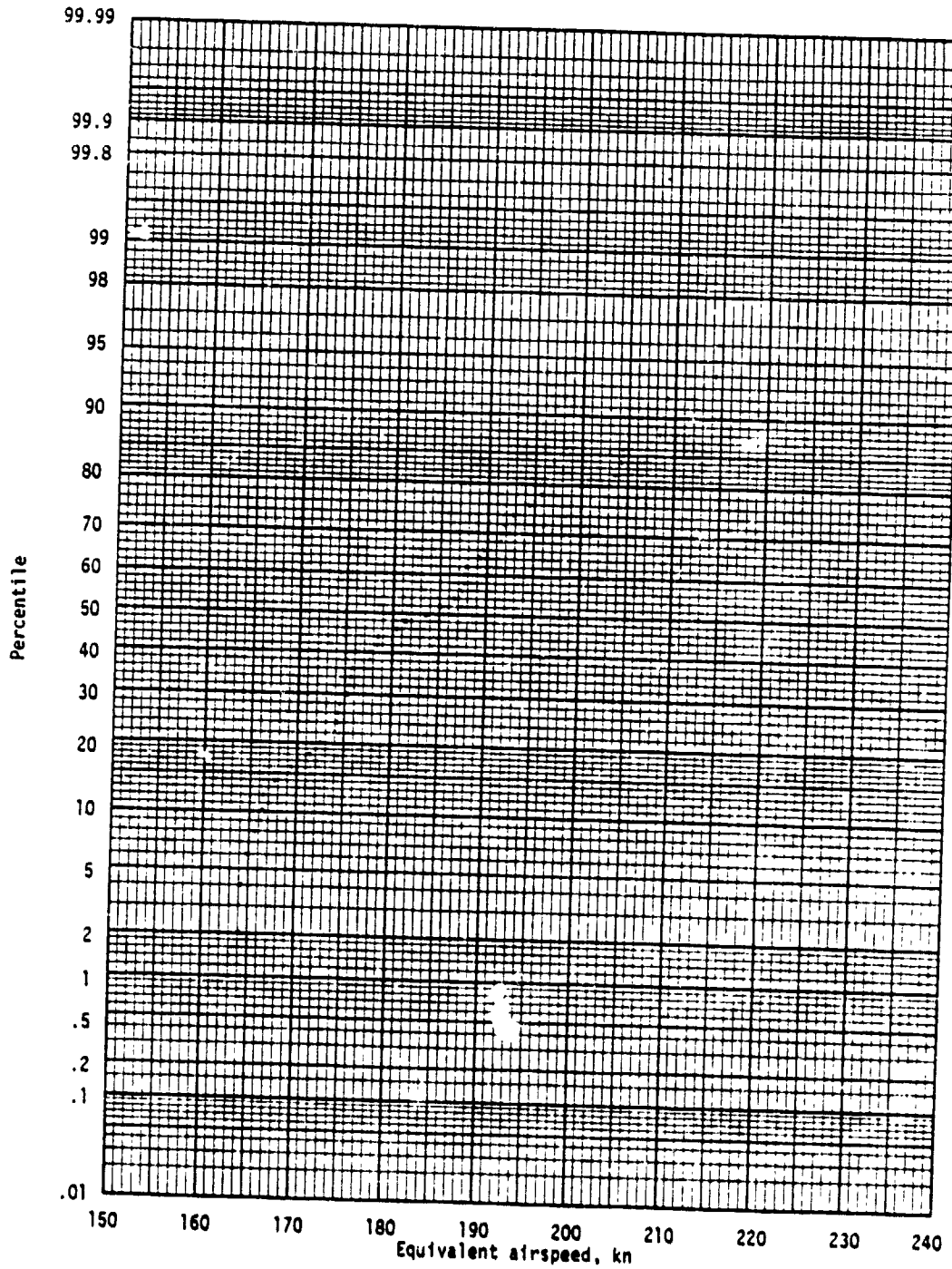

(d) Equivalent airspeed.

Figure 11.- Continued.

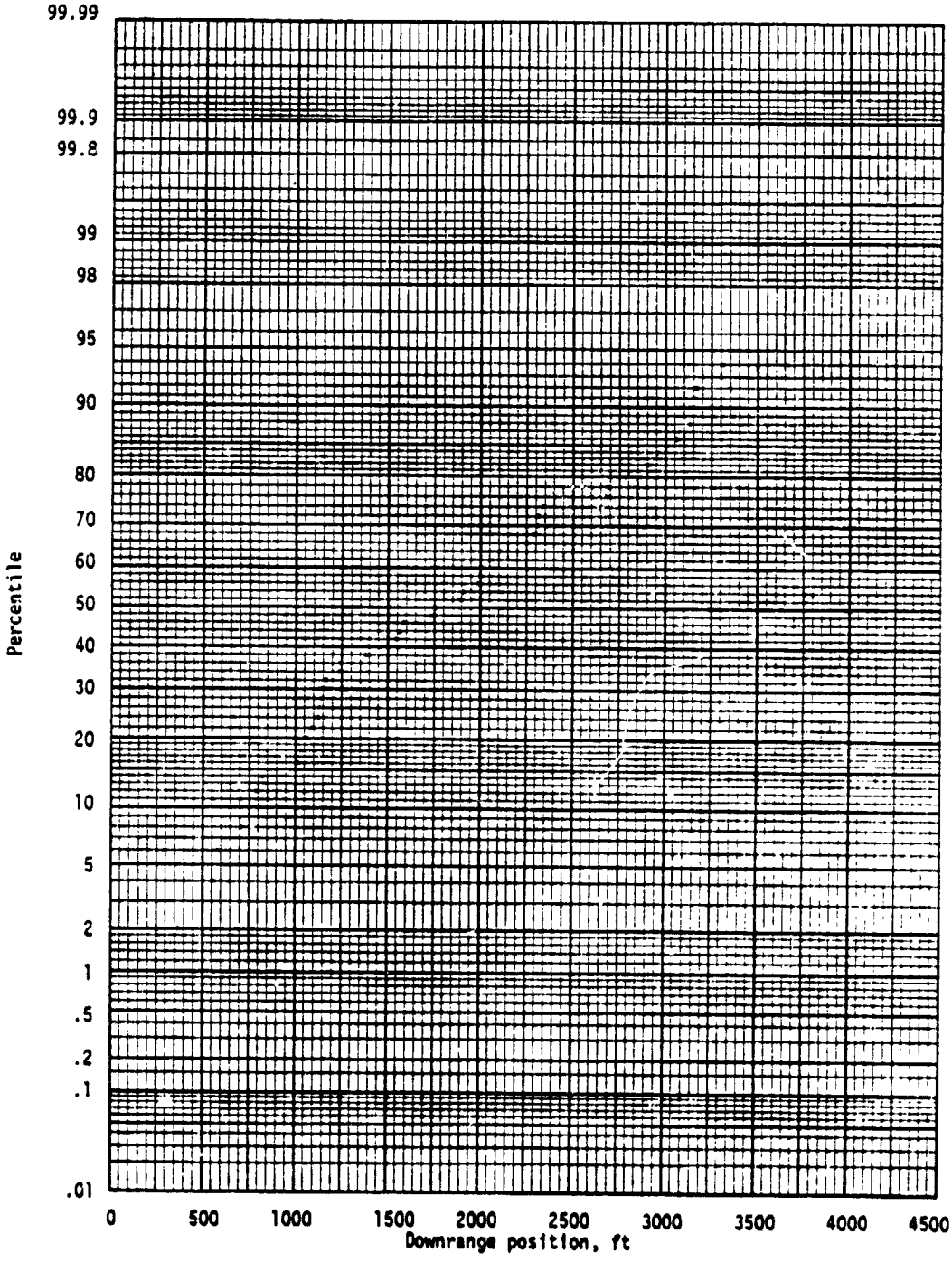

(e) Downrange position.

Figure 11.- Continued.

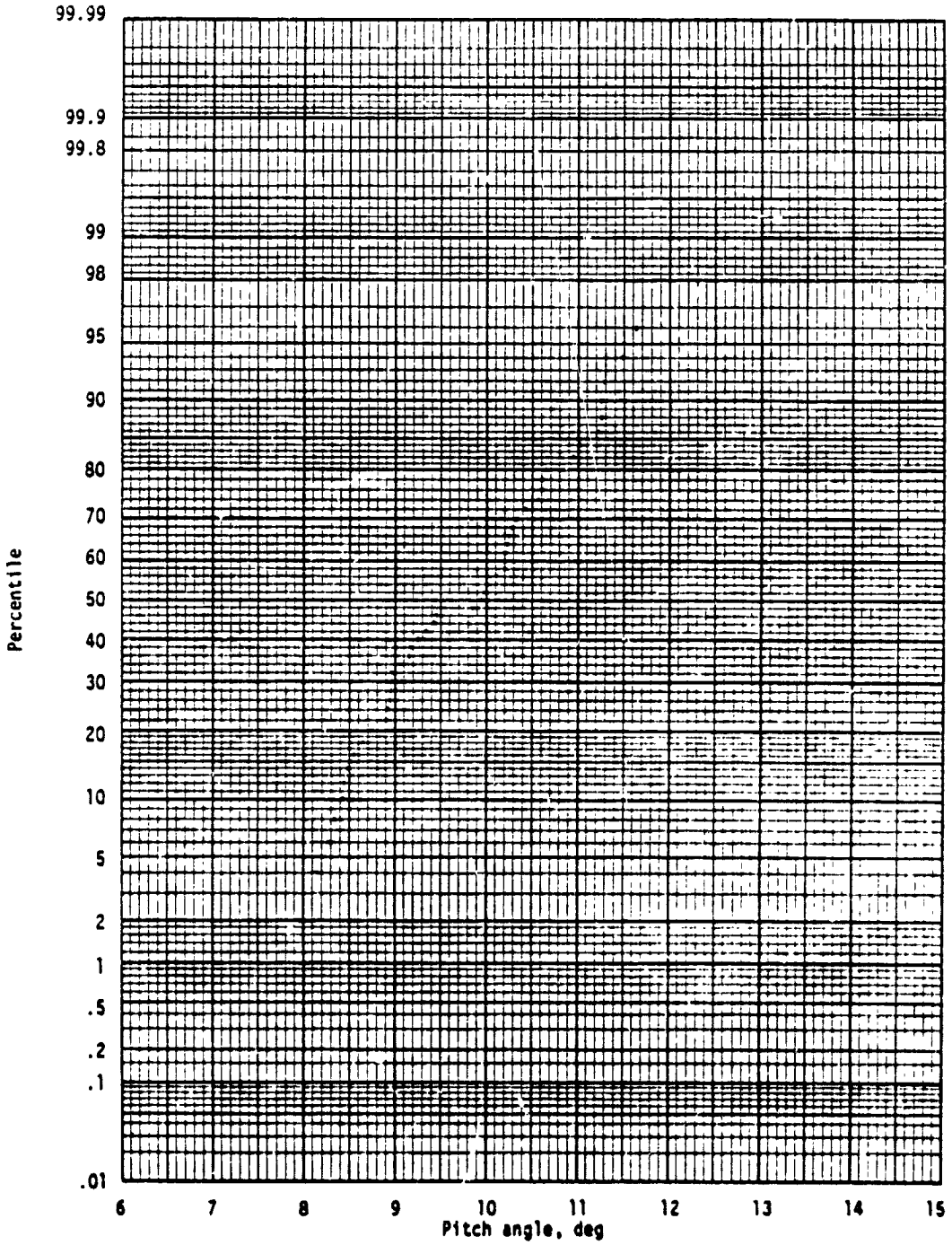

(f) Pitch angle.

Figure 11.- Continued.

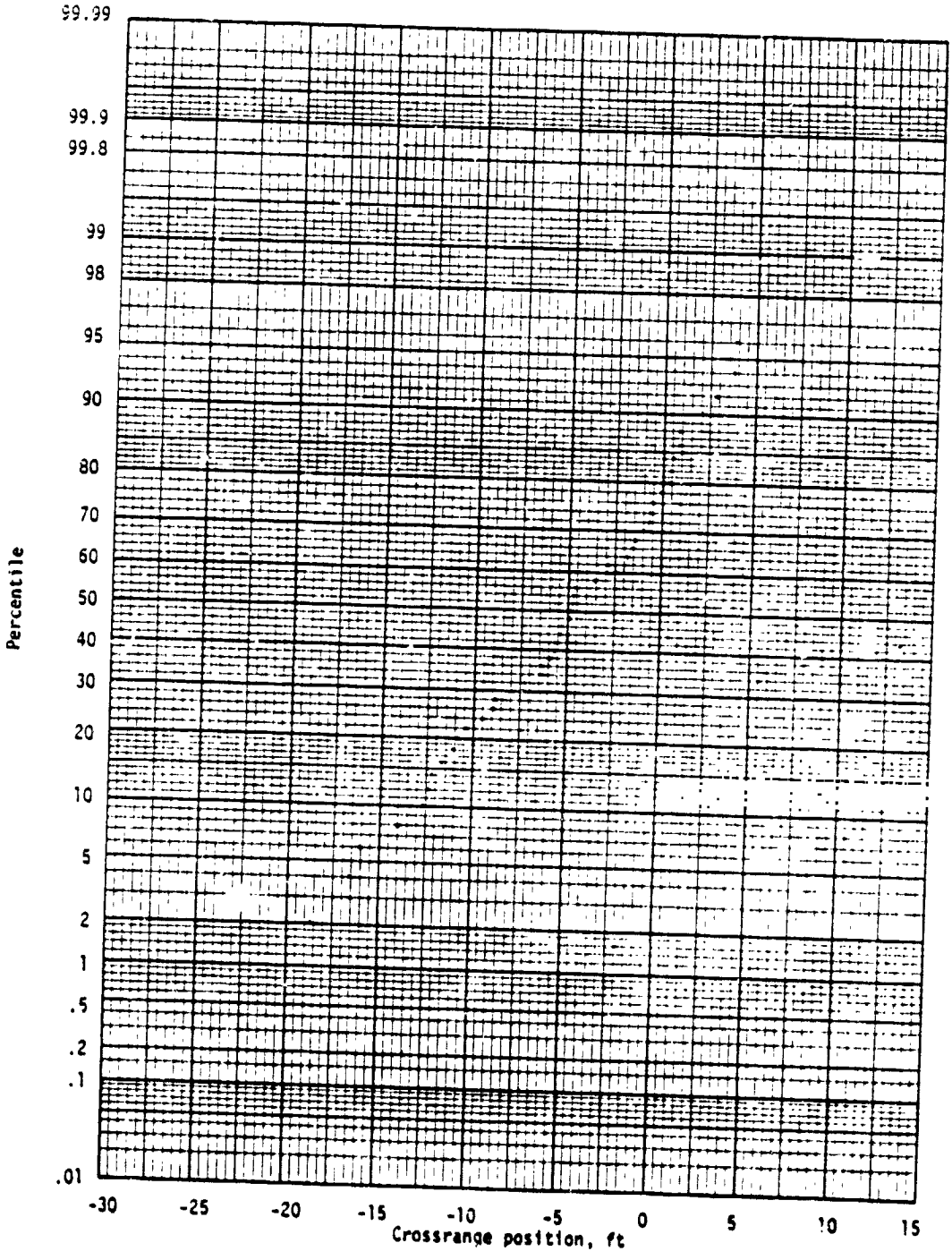

(g) Crossrange position.

Figure 11.- Continued.

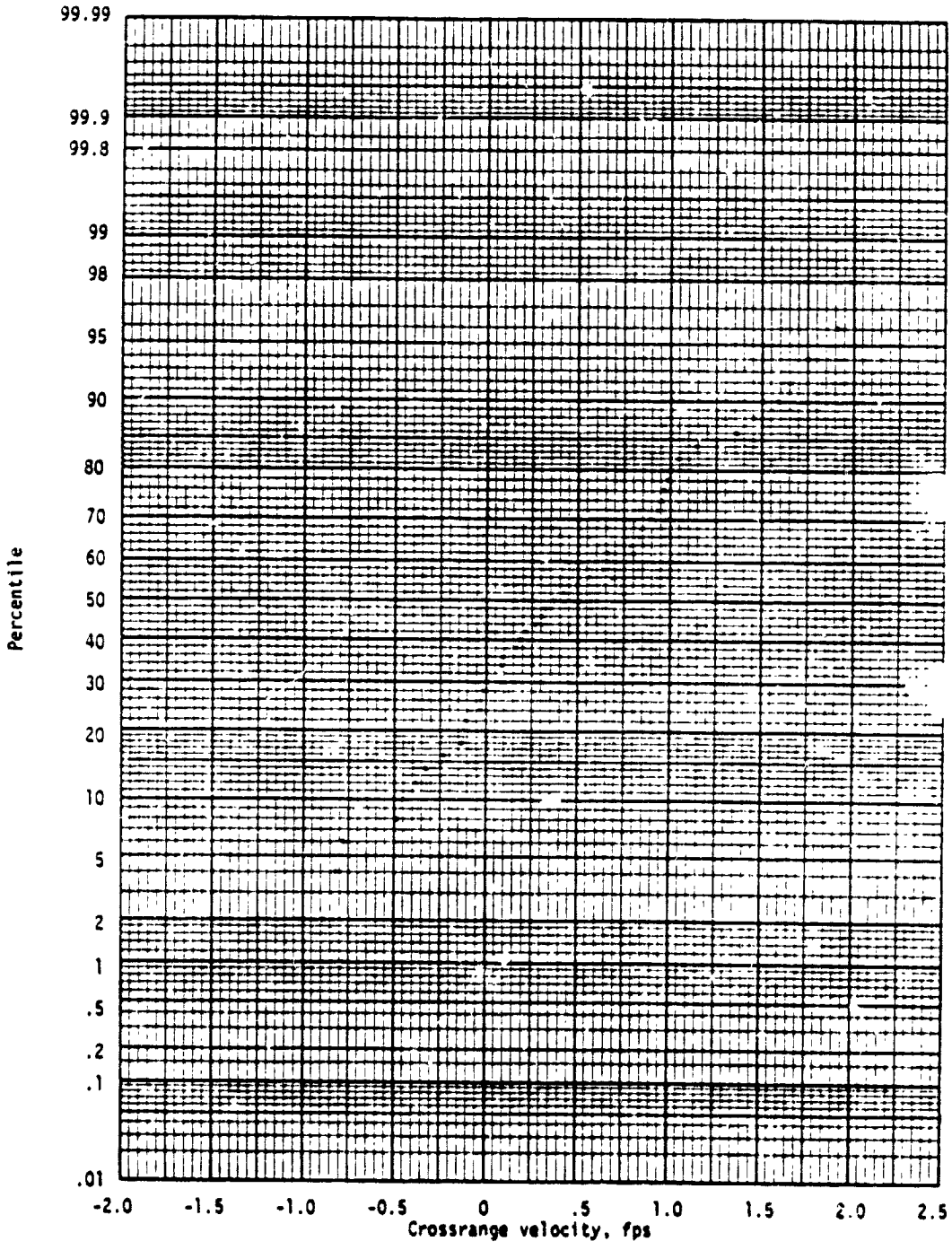

(h) Crossrange velocity.

Figure 11.- Concluded.

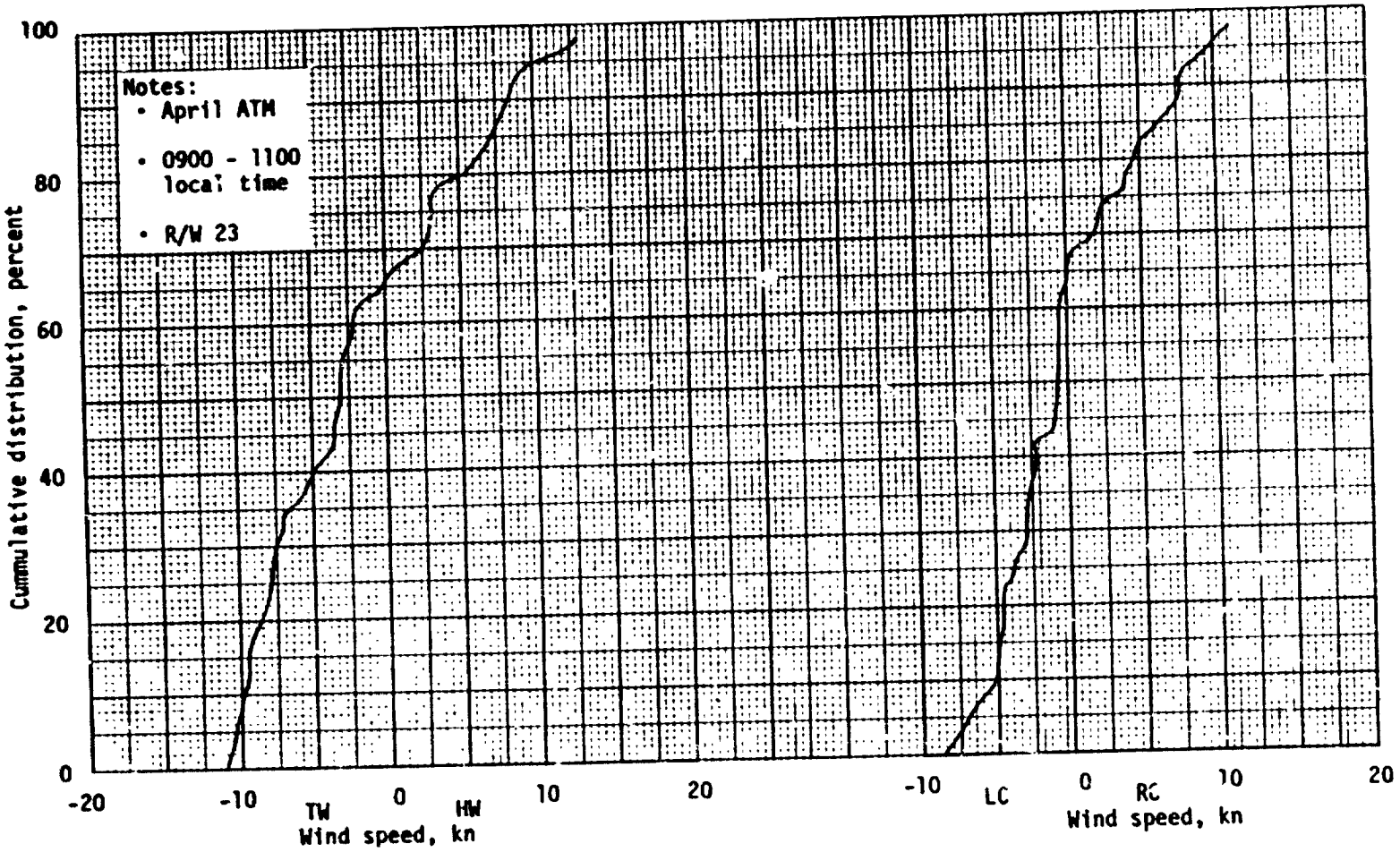

(a) Head and tail wind magnitude.

(b) Crosswind magnitude.

Figure 12.- EAFB surface wind statistics.

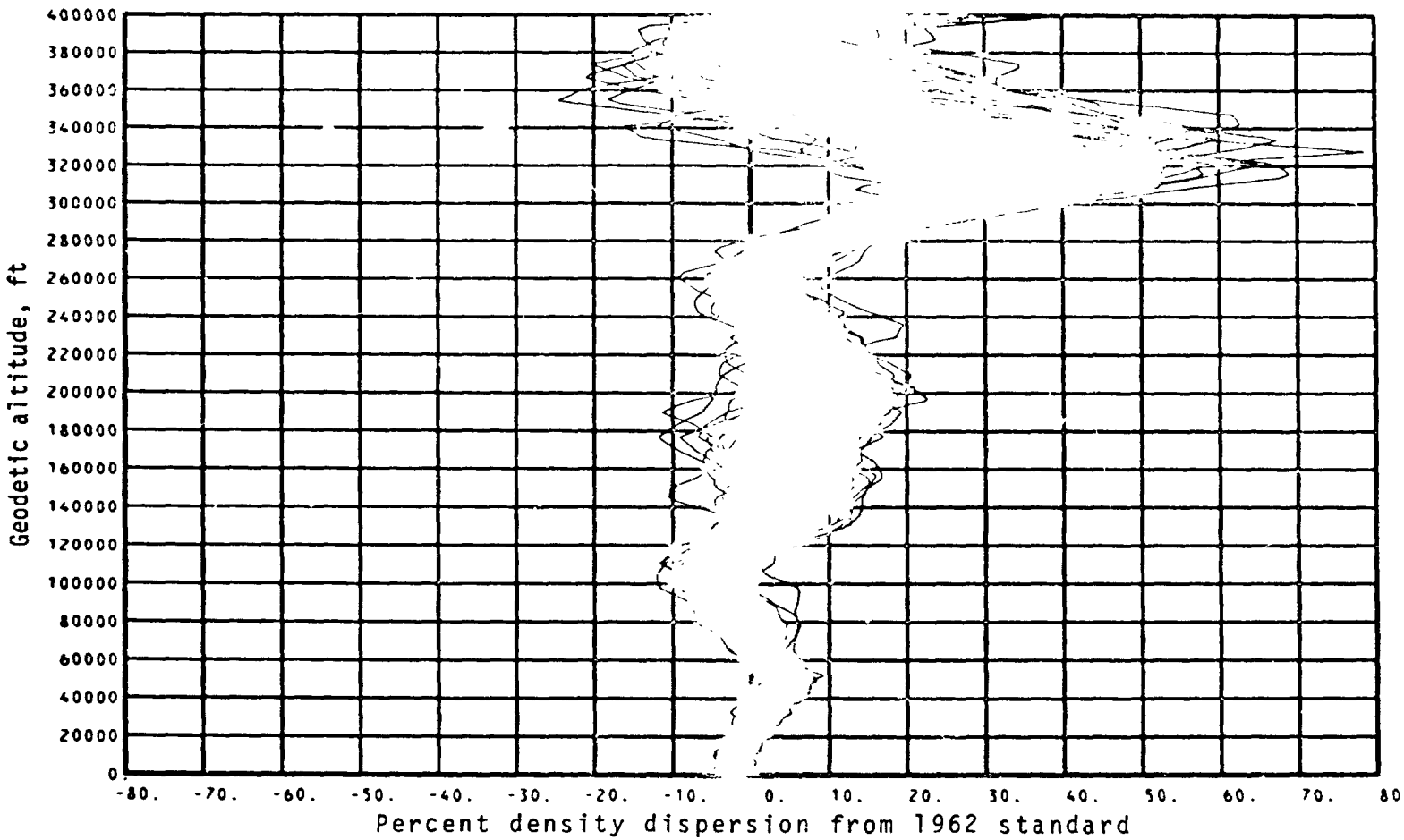

(a) Density.

Figure 13.- Atmospheric dispersions - April - abort once around.

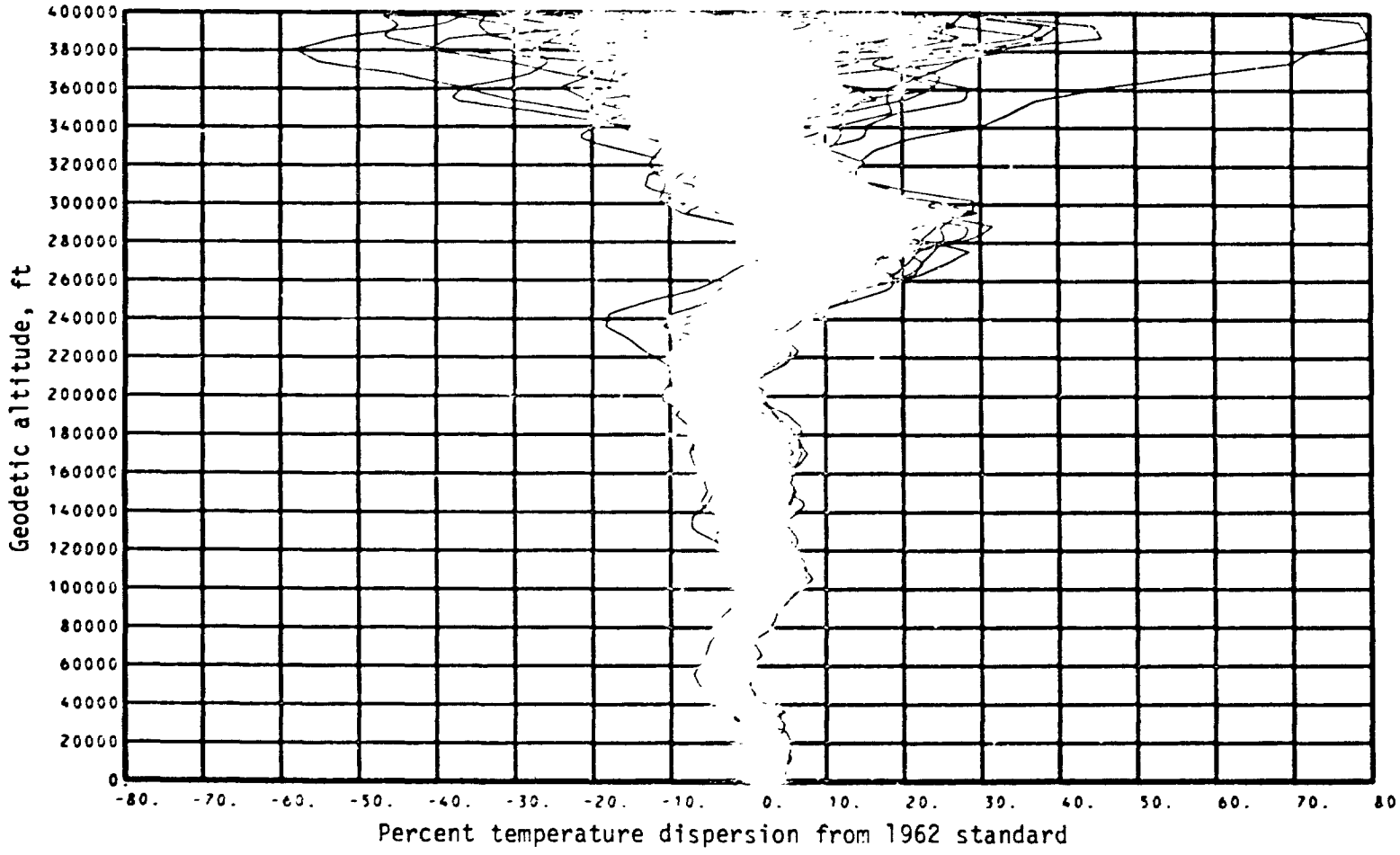

(b) Temperature.

Figure 13.- Continued.

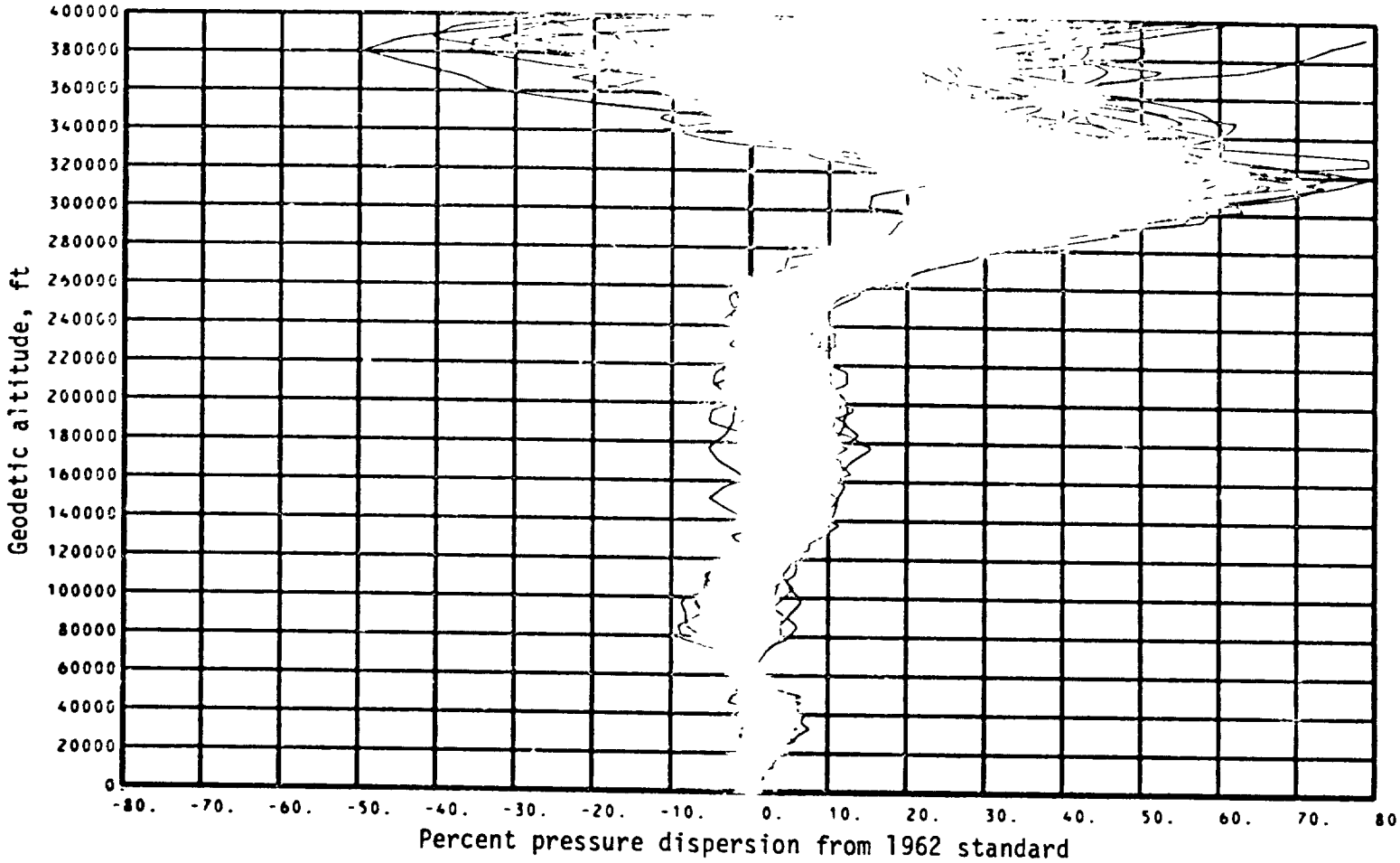

(c) Pressure.

Figure 13.- Continued.

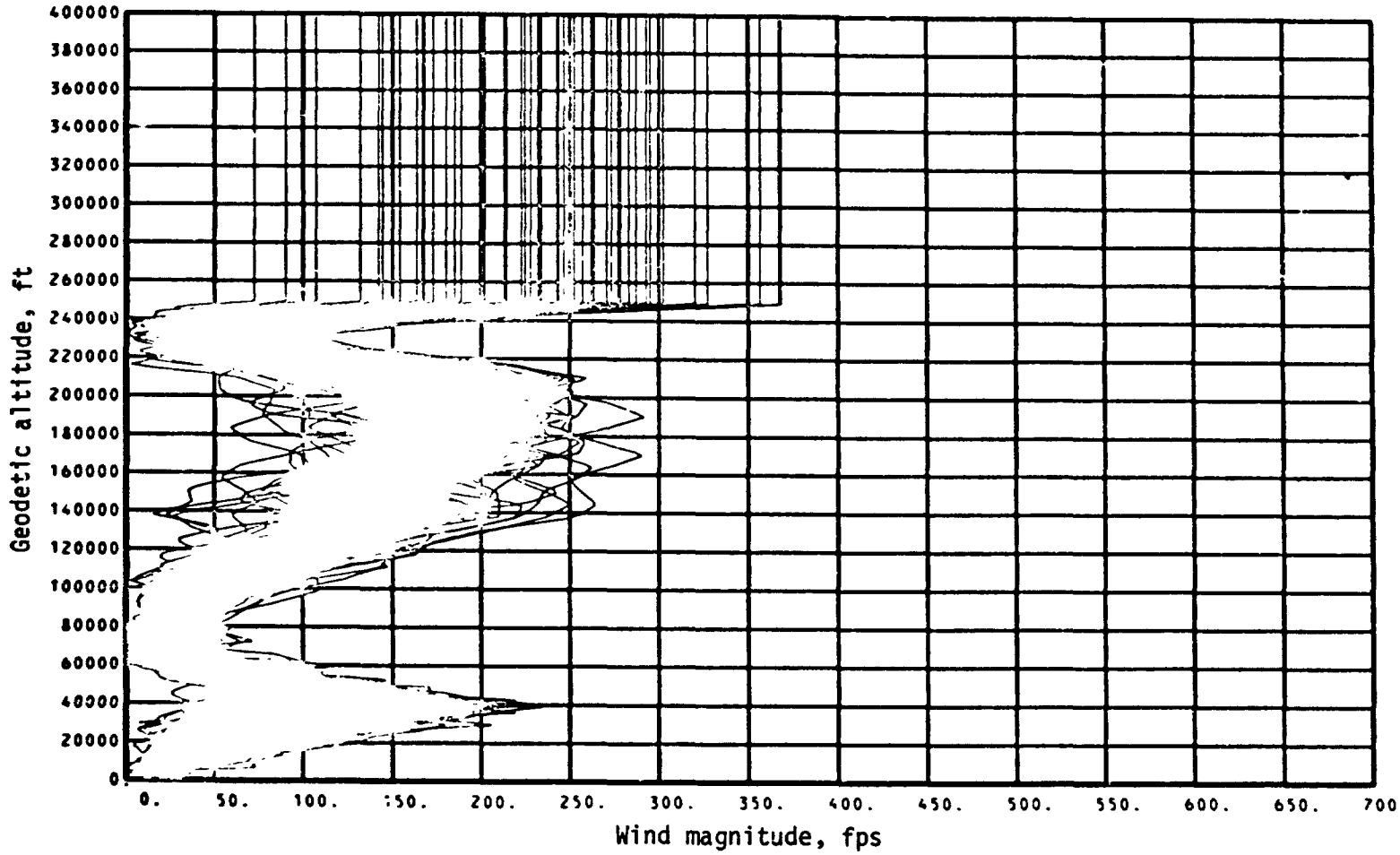

(d) Wind magnitude.

Figure 13.- Continued.

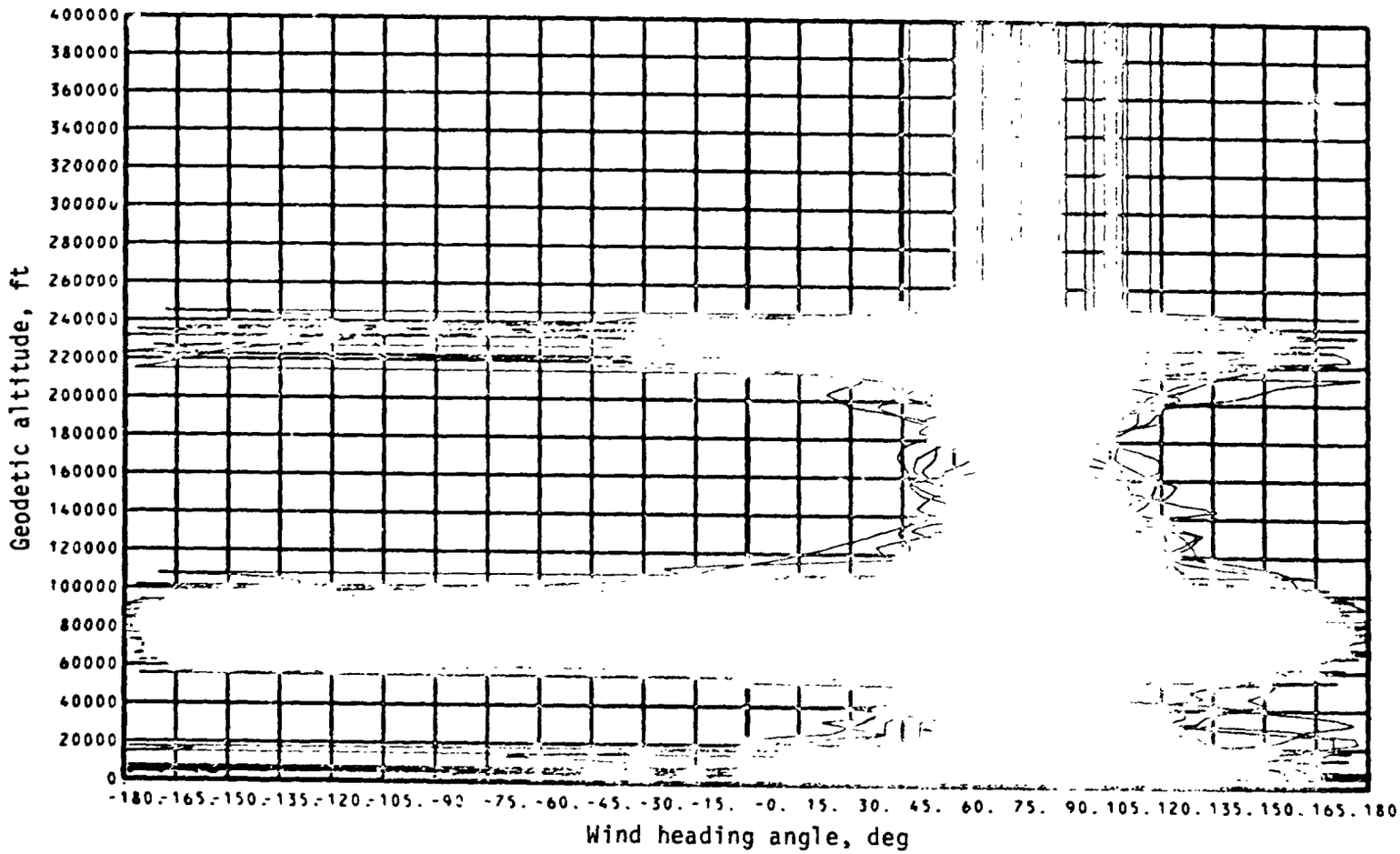

(e) Wind heading.

Figure 13.- Concluded.

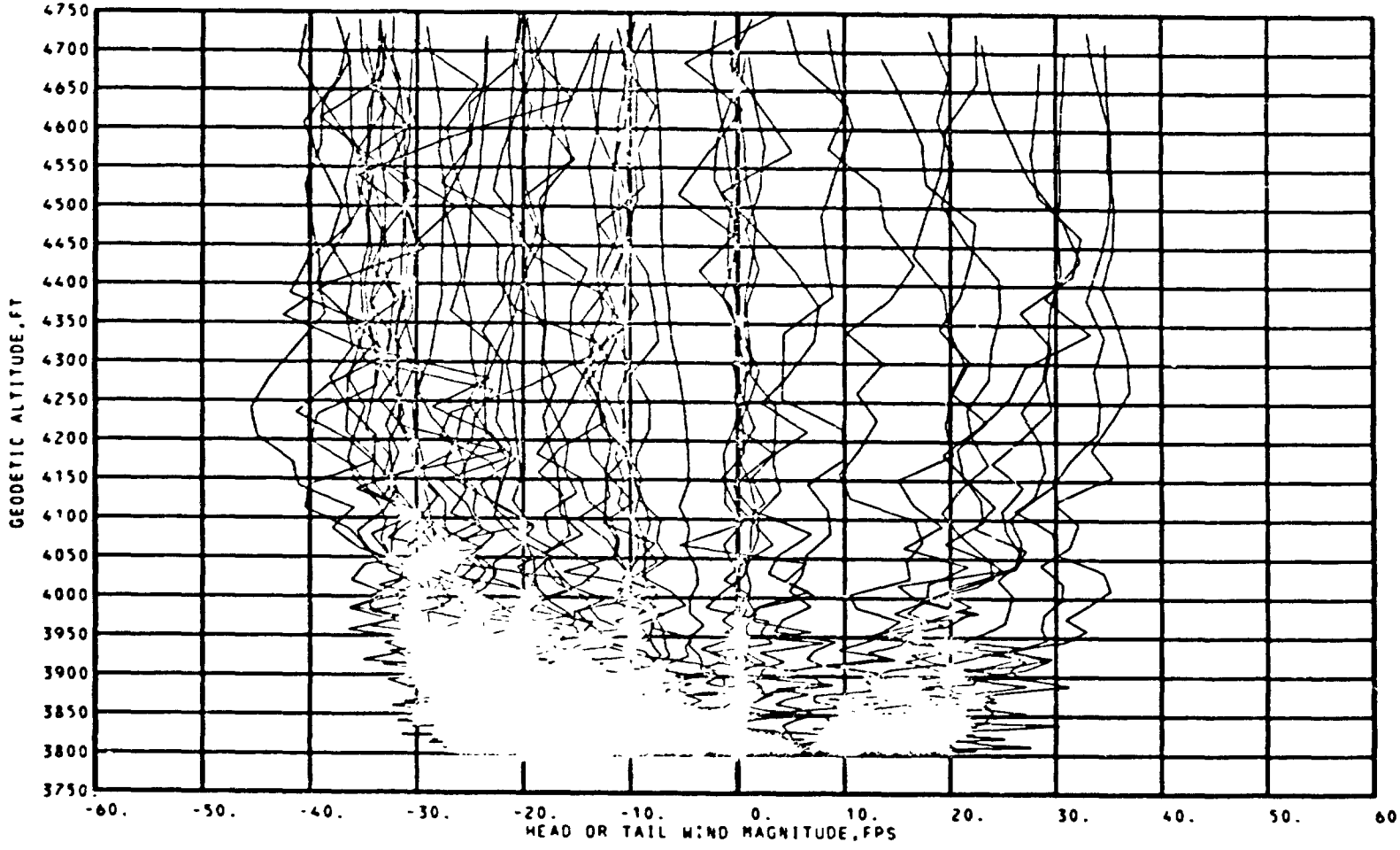

(a) Head or tail wind magnitudes.

Figure 14.- Surface winds - abort once around.

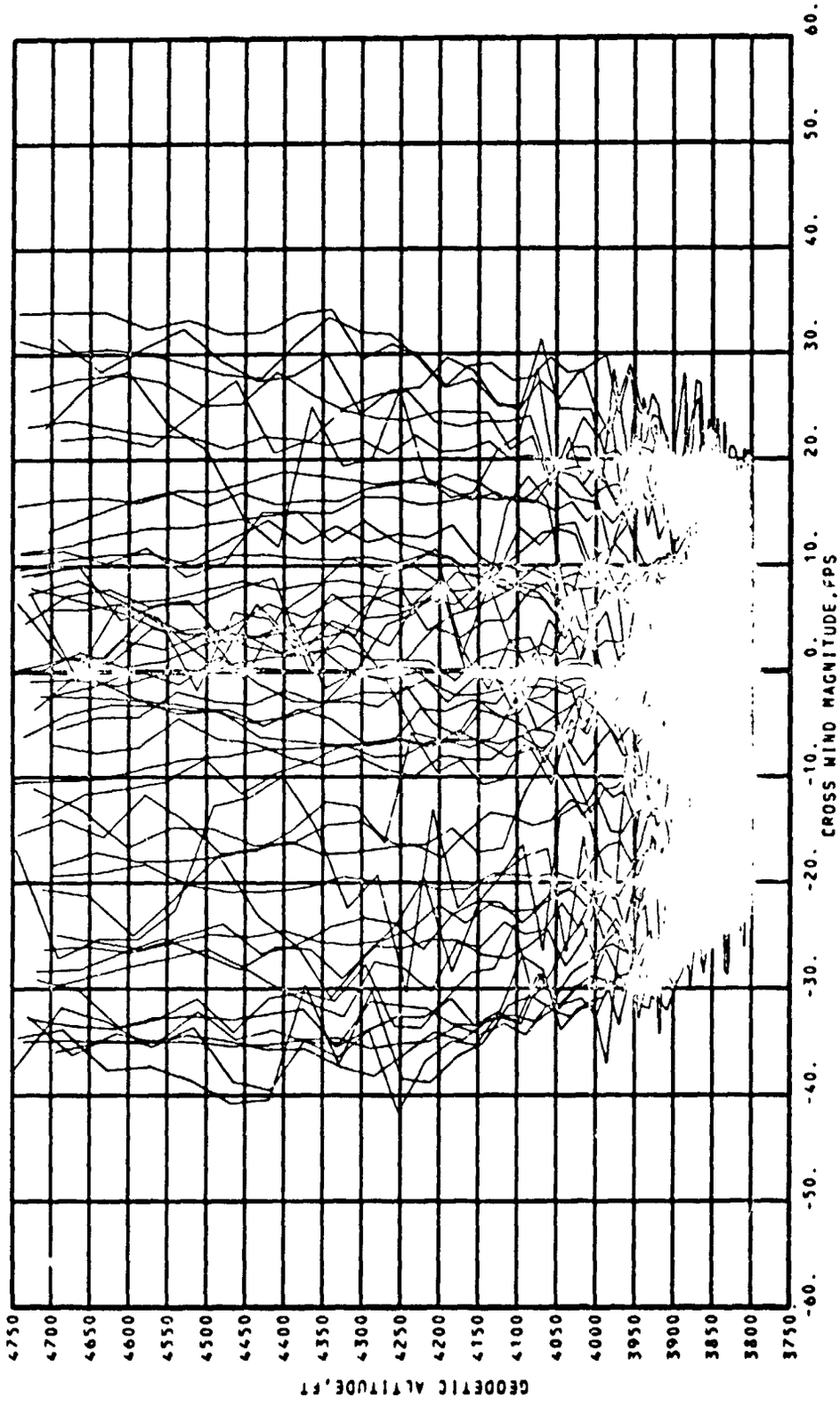

(b) Cross wind magnitudes.

Figure 14.- Concluded.

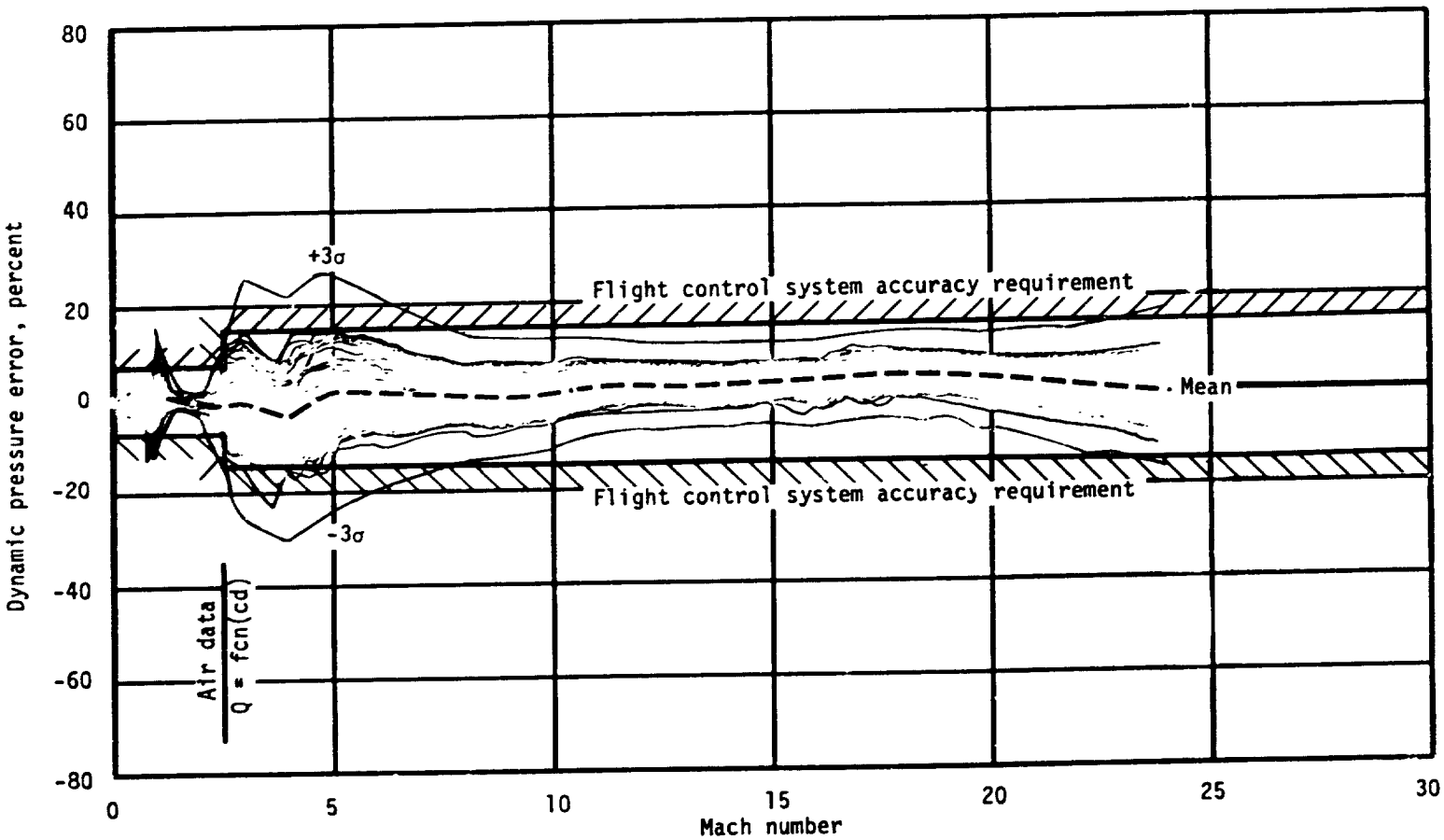

(a) Percent dynamic pressure error.

Figure 15.- Nav derived and/or air data derived parameter performance-abort once around.

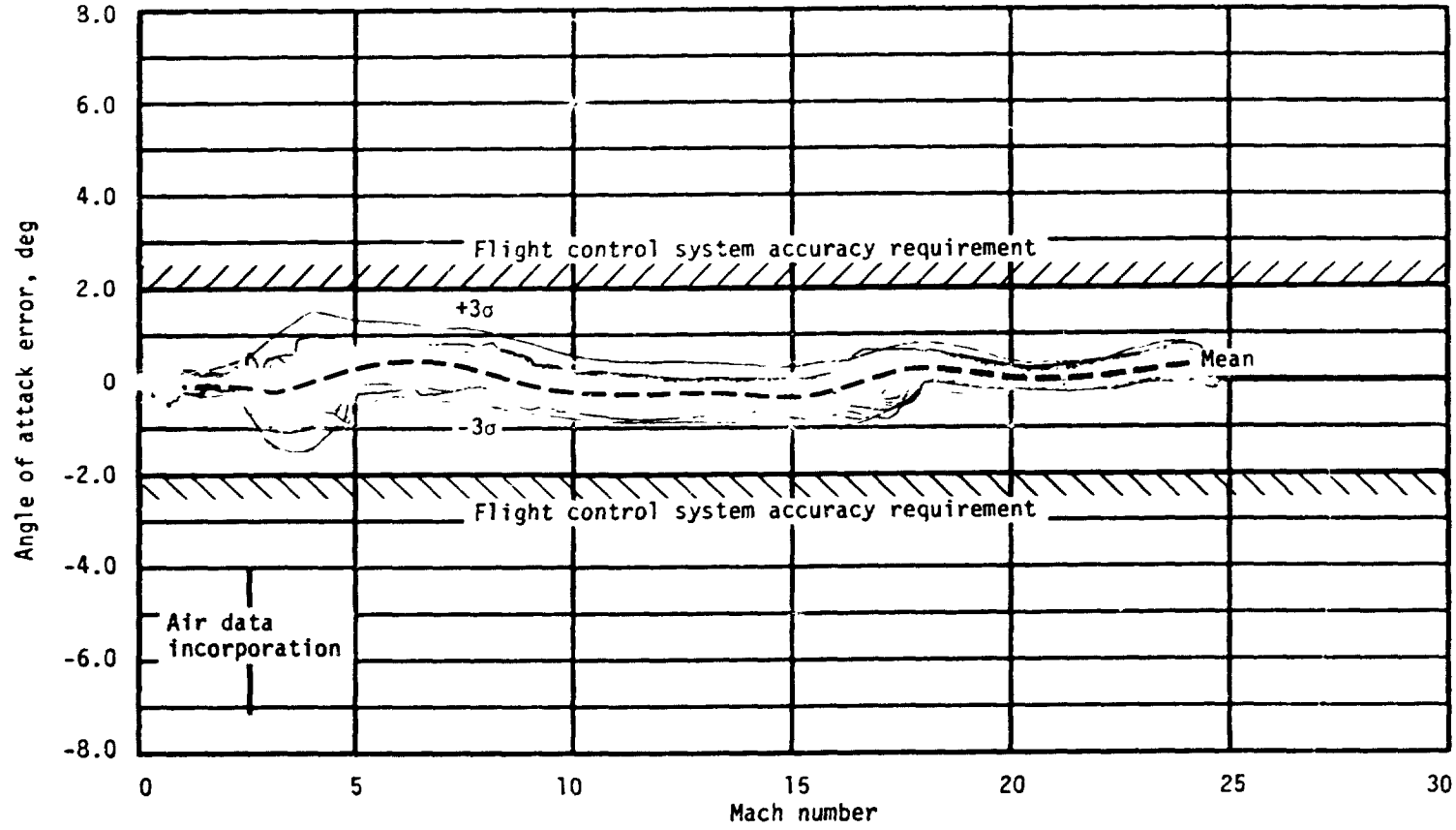

(b) Angle of attack error.

Figure 15.- Continued.

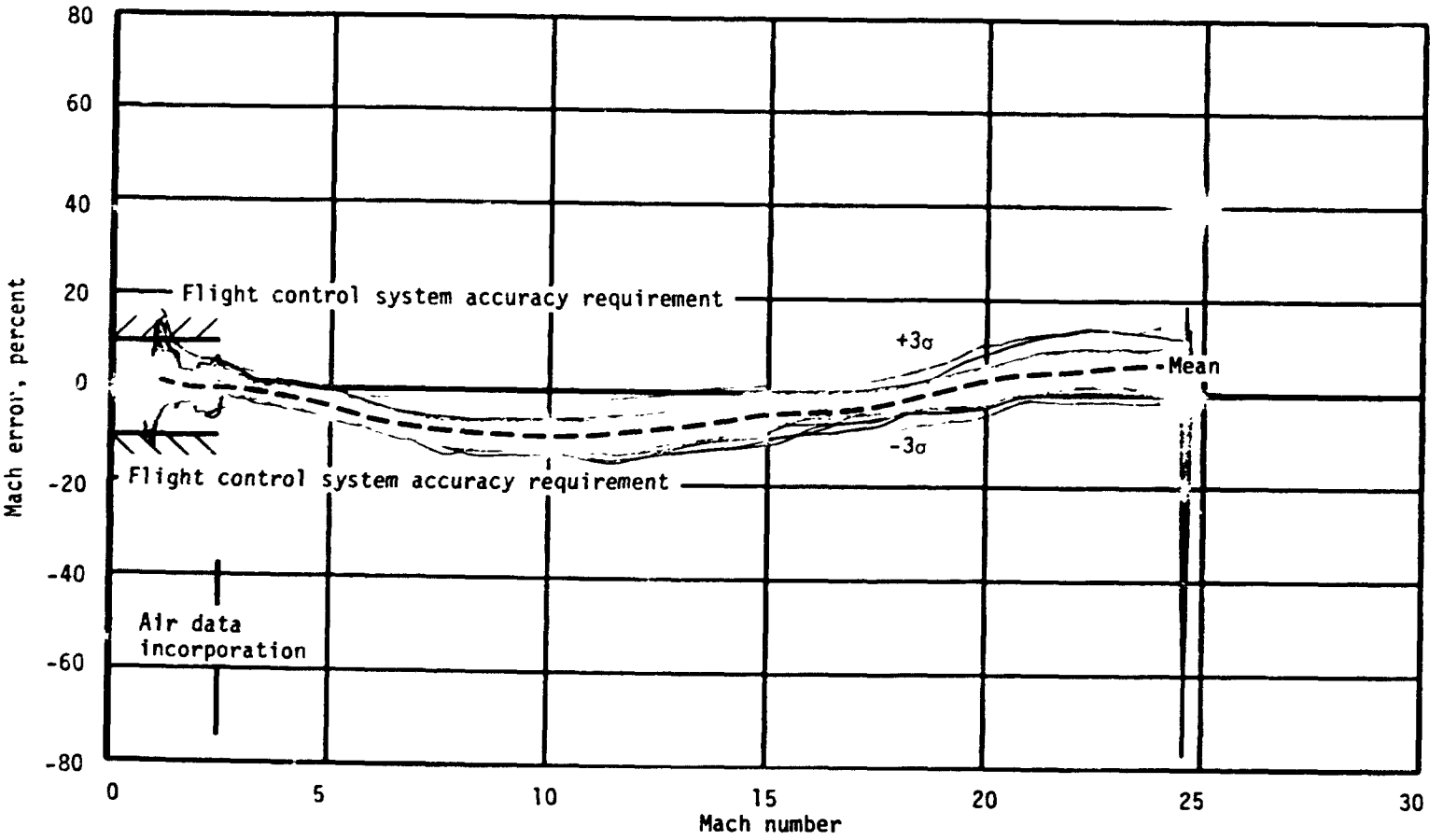

(c) Percent mach number error.

Figure 15.- Continued.

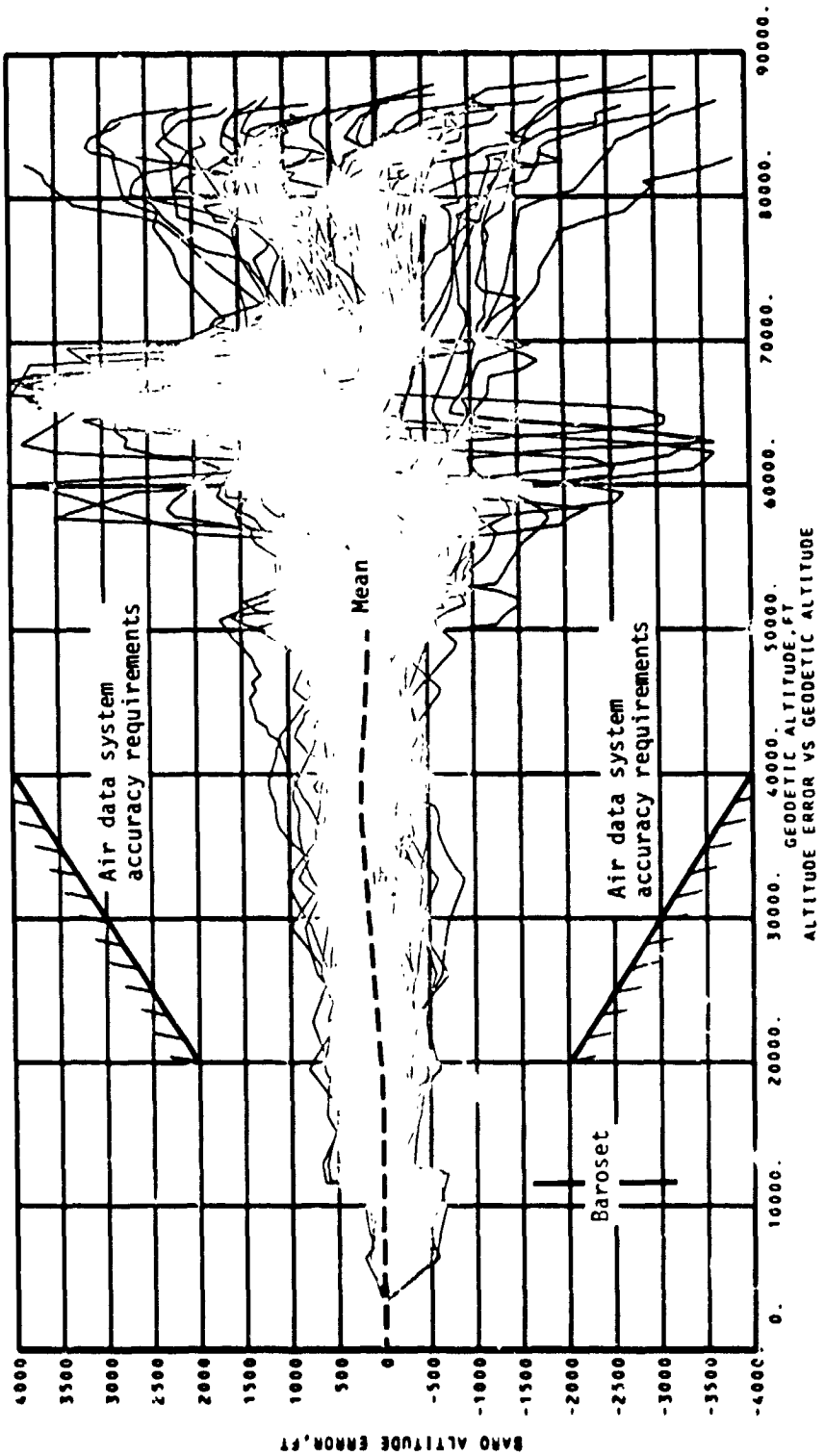

(d) Baro altitude error.

Figure 15.- Concluded.

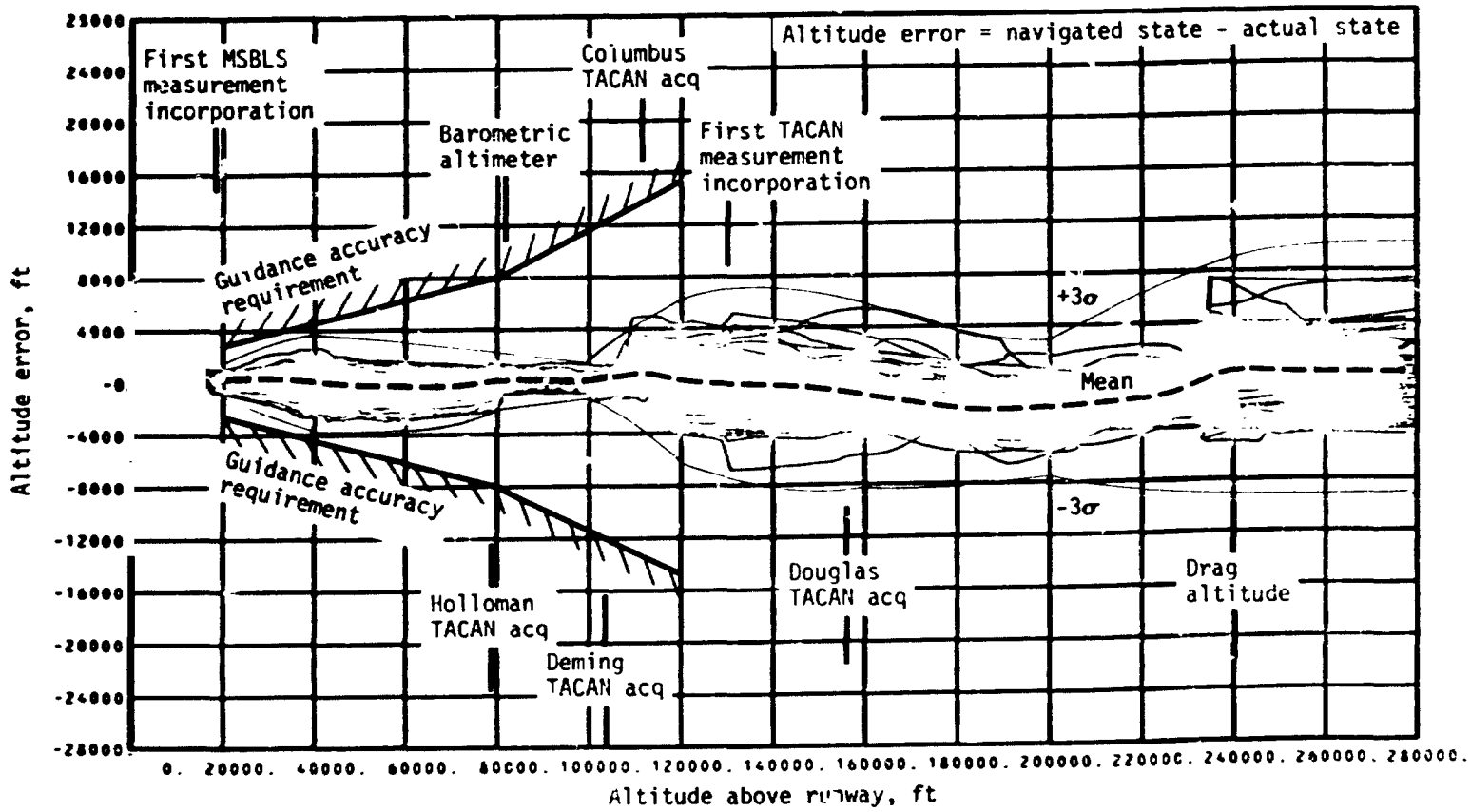

(a) Altitude error.

Figure 16.- Navigated state vector performance - steep abort once around.

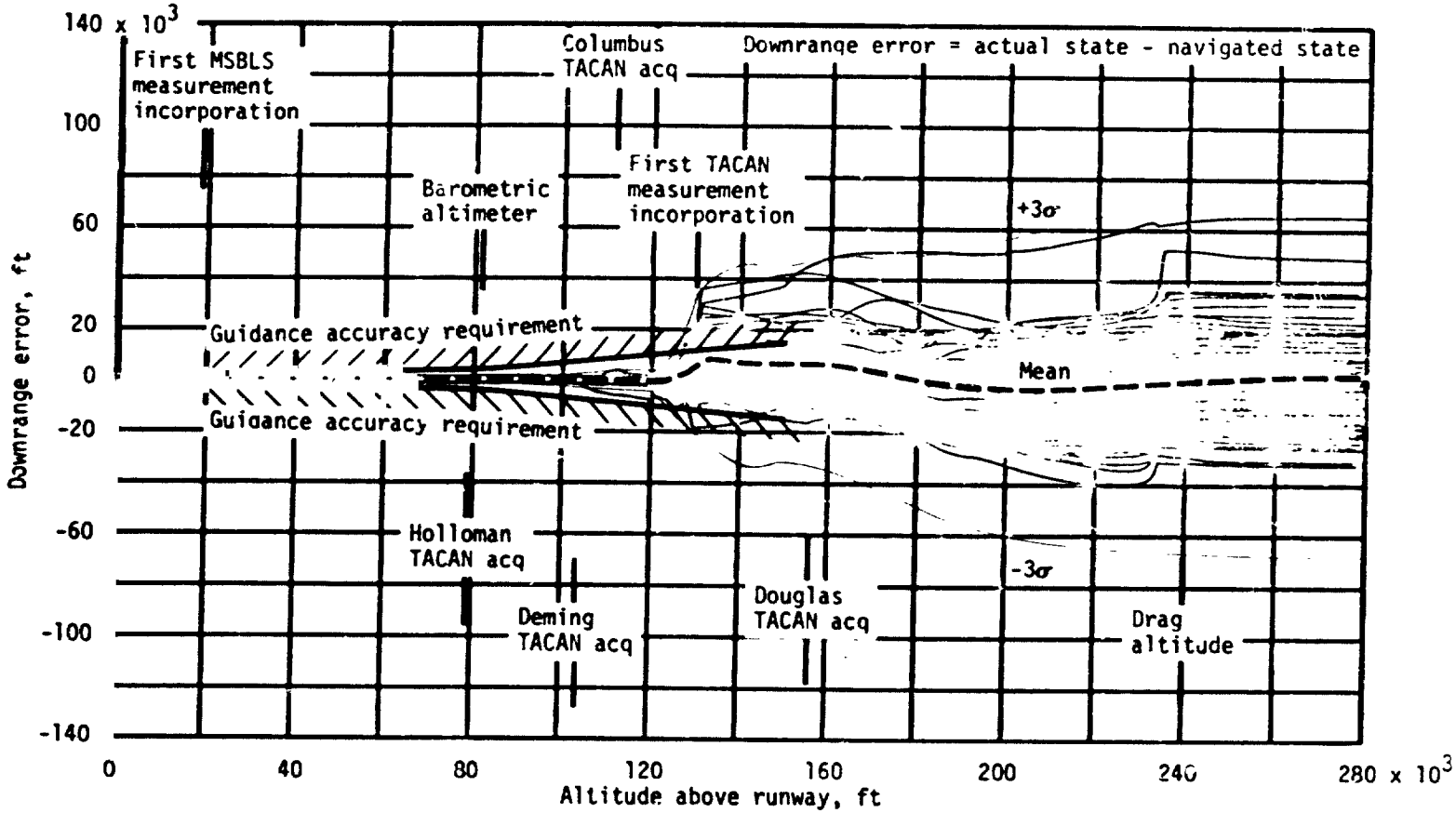

(b) Downrange error.

Figure 16.- Continued.

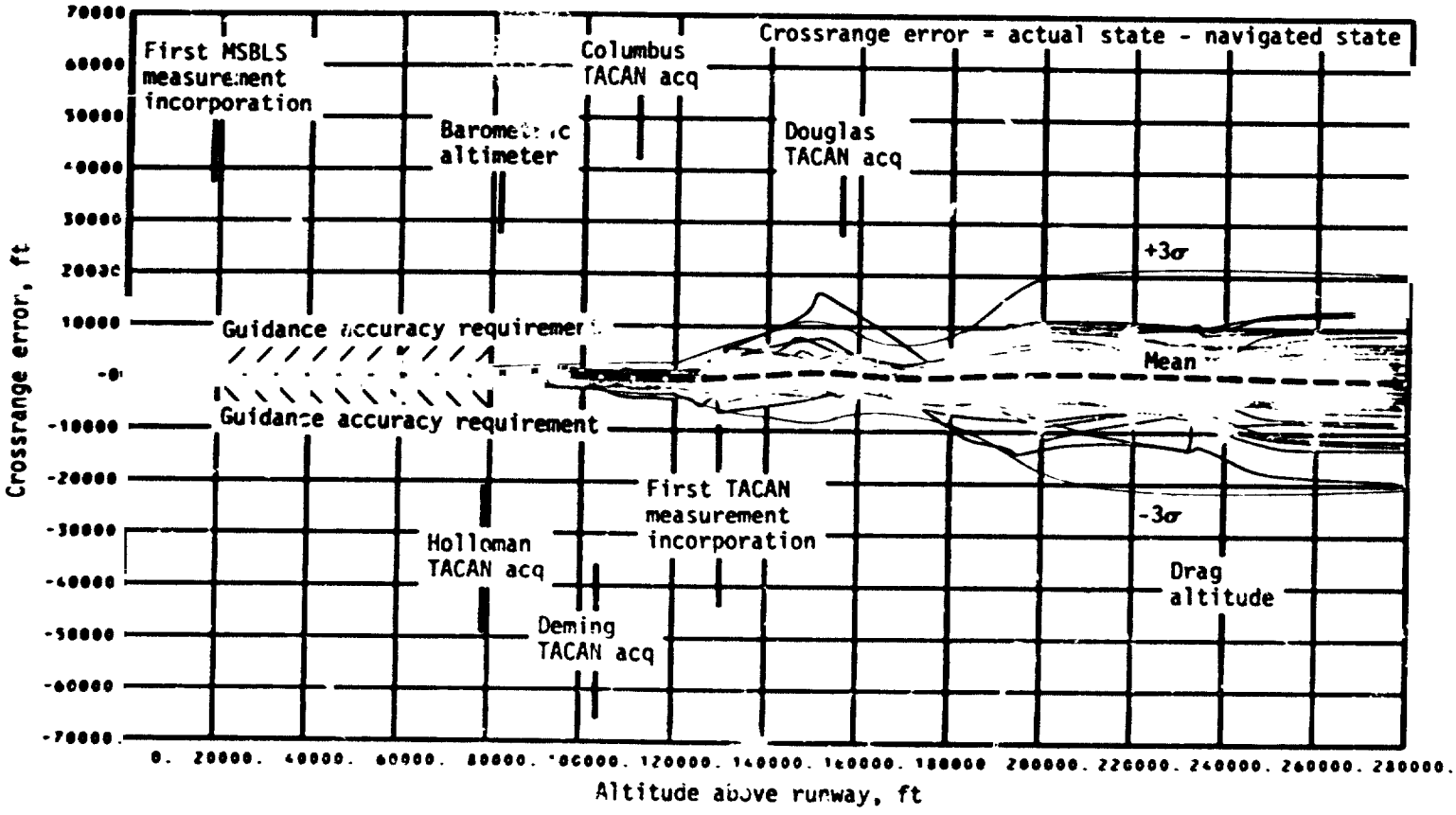

(c) Crossrange error.

Figure 16.- Continued.

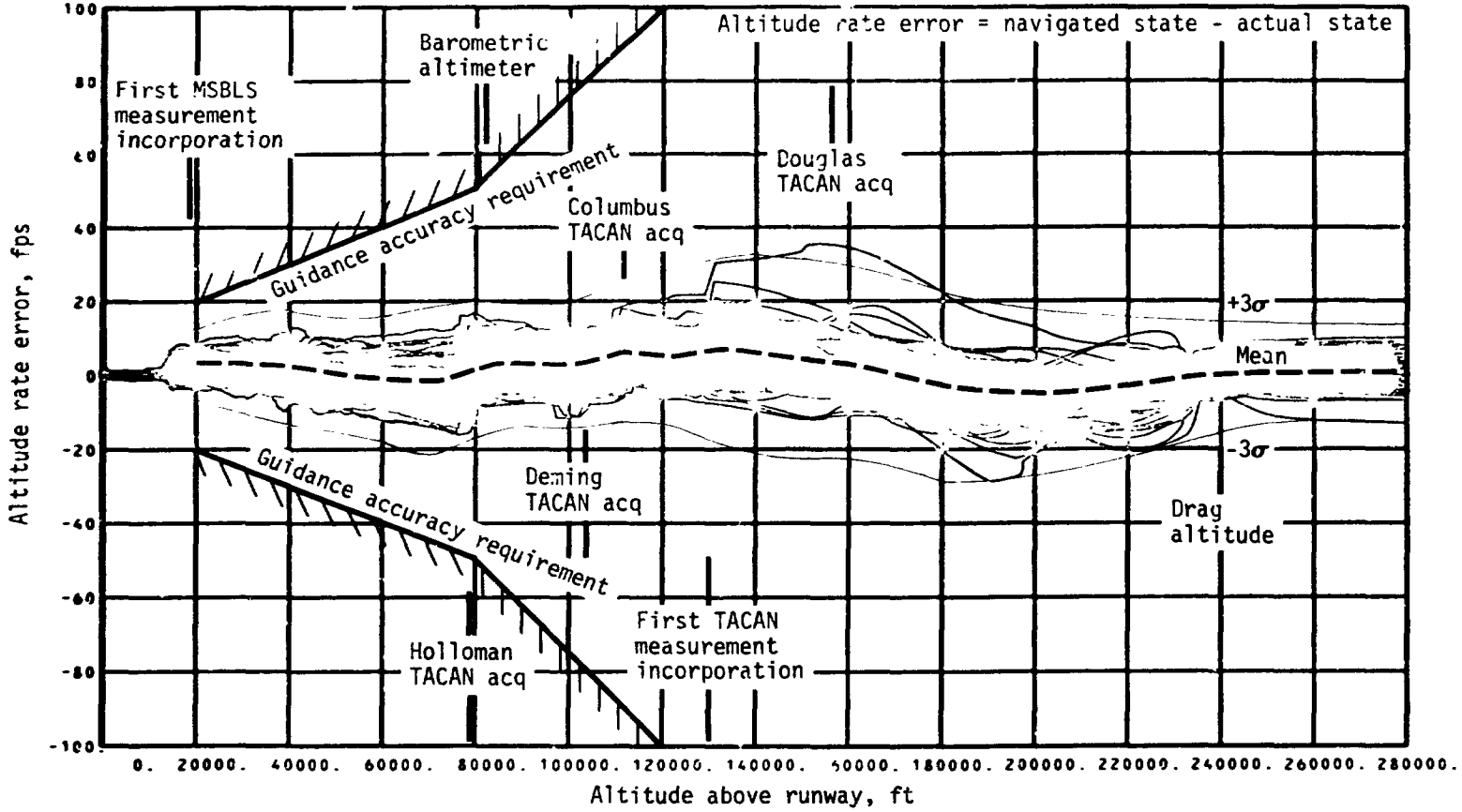

(d) Altitude rate error.

Figure 16.- Continued.

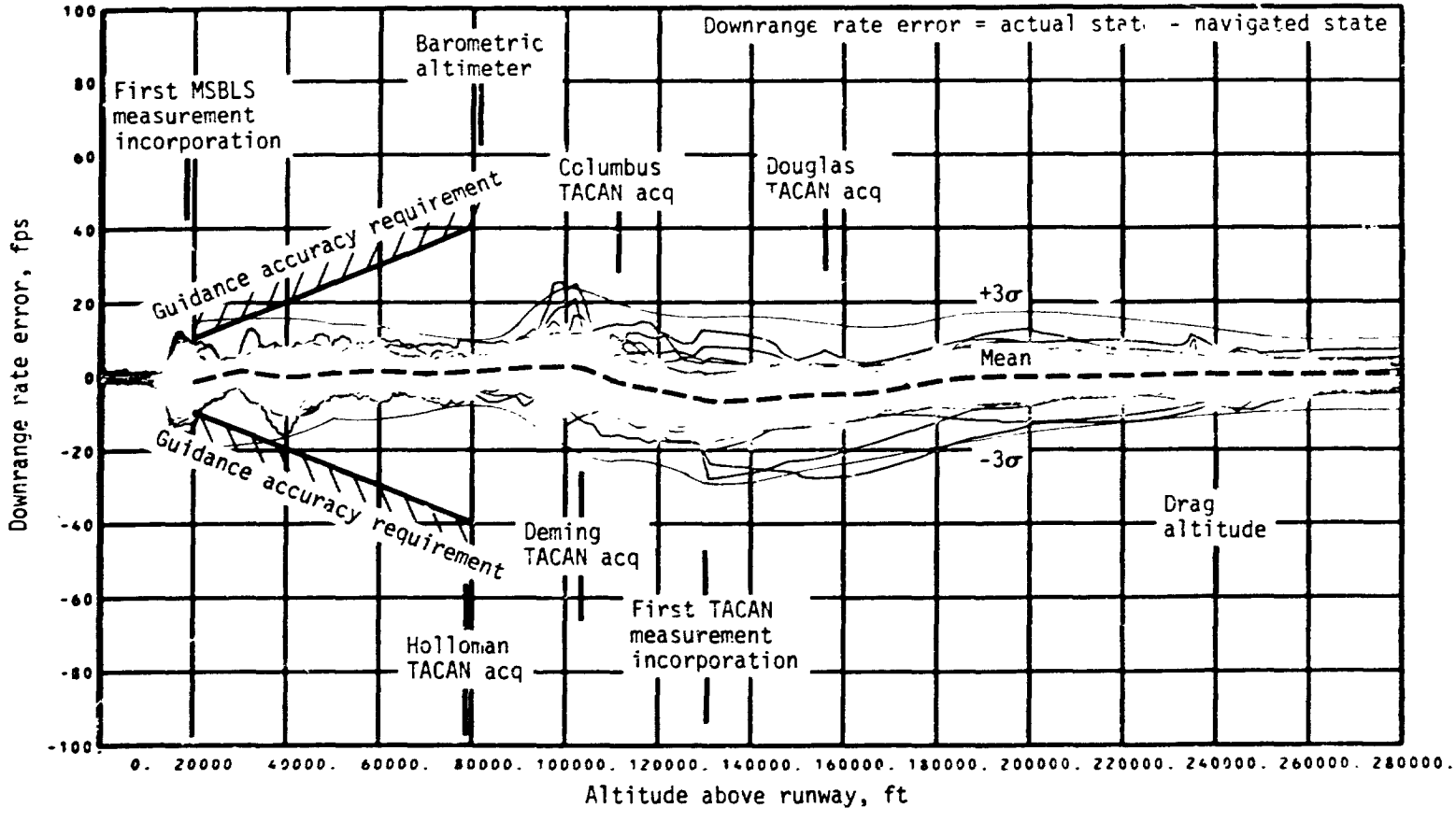

(e) Downrange rate error.

Figure 16.- Continued.

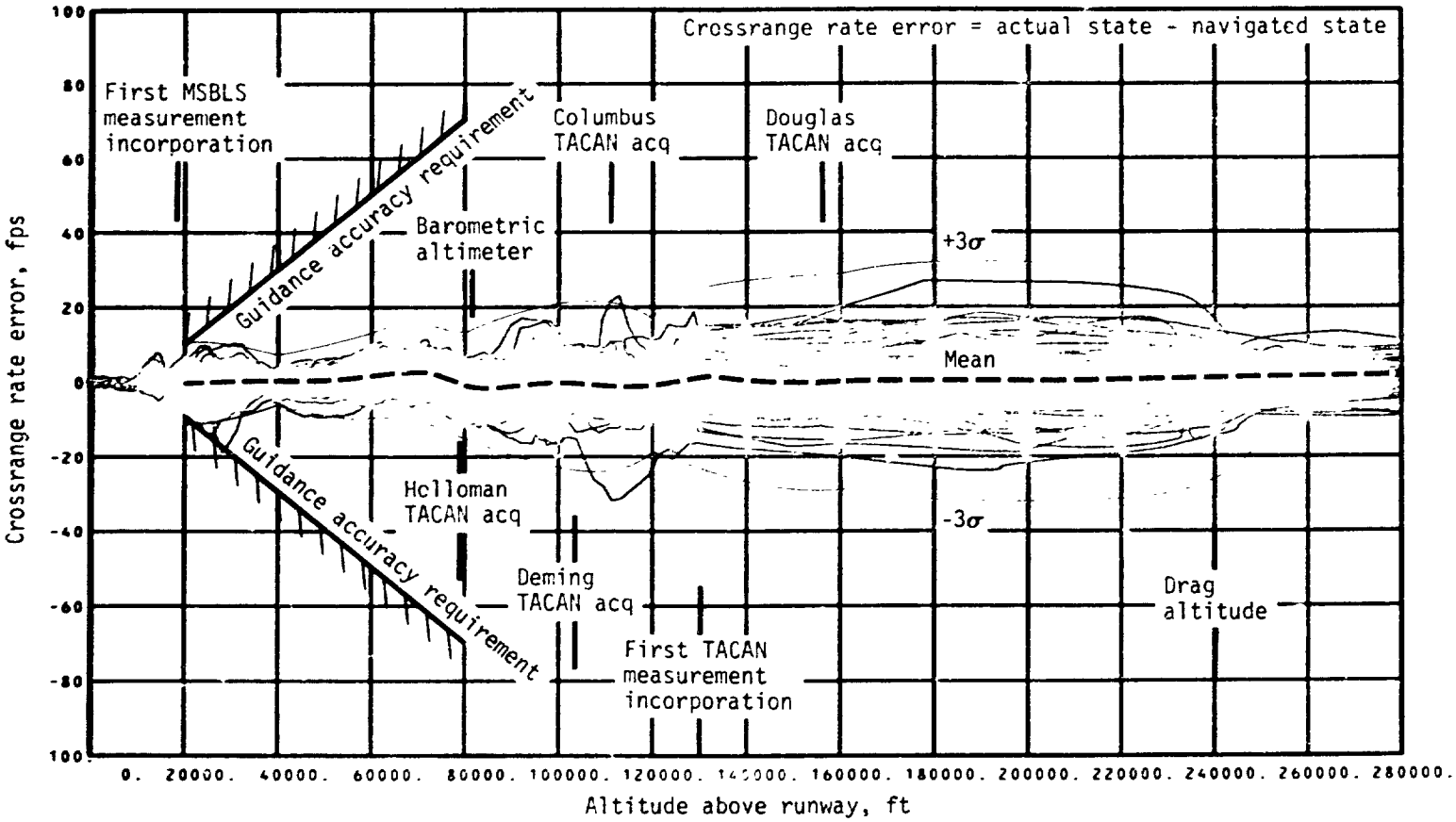

(f) Crossrange rate error.

Figure 16.- Continued.

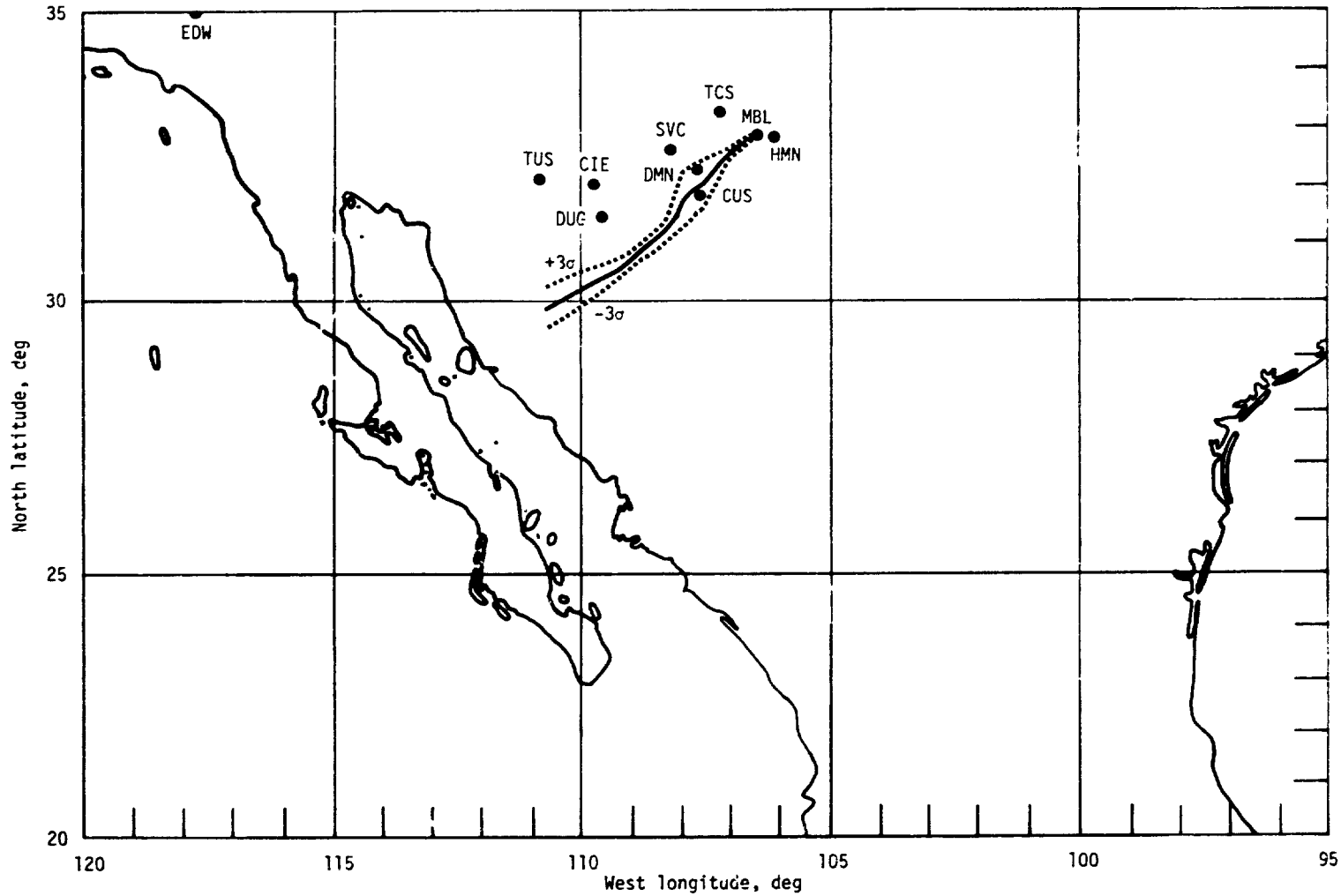

(g) TACAN station locations and groundtrack.

Figure 16.- Concluded.

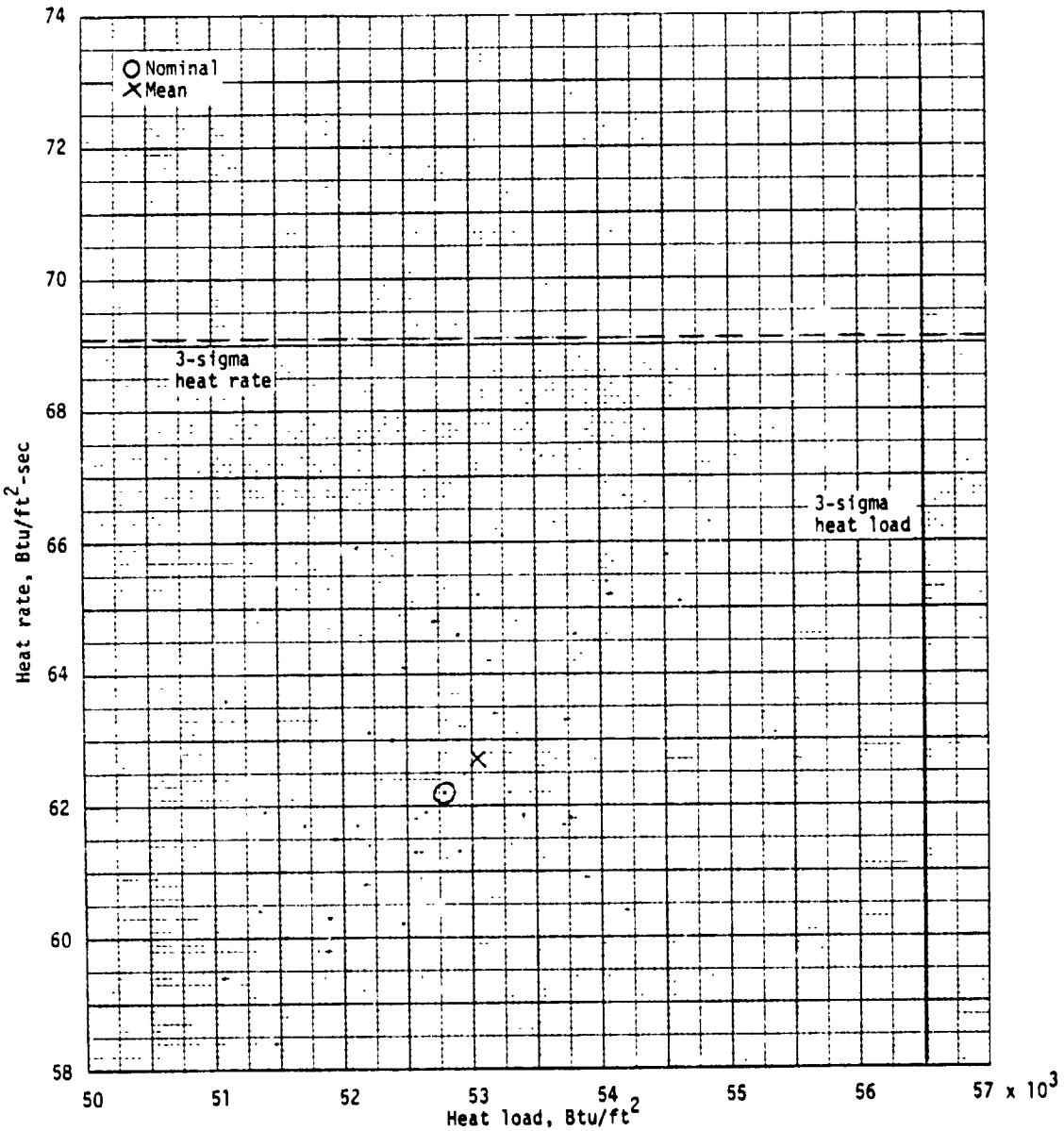

Figure 17.- Heat rate - heat load scatter plot - steep abort once around.

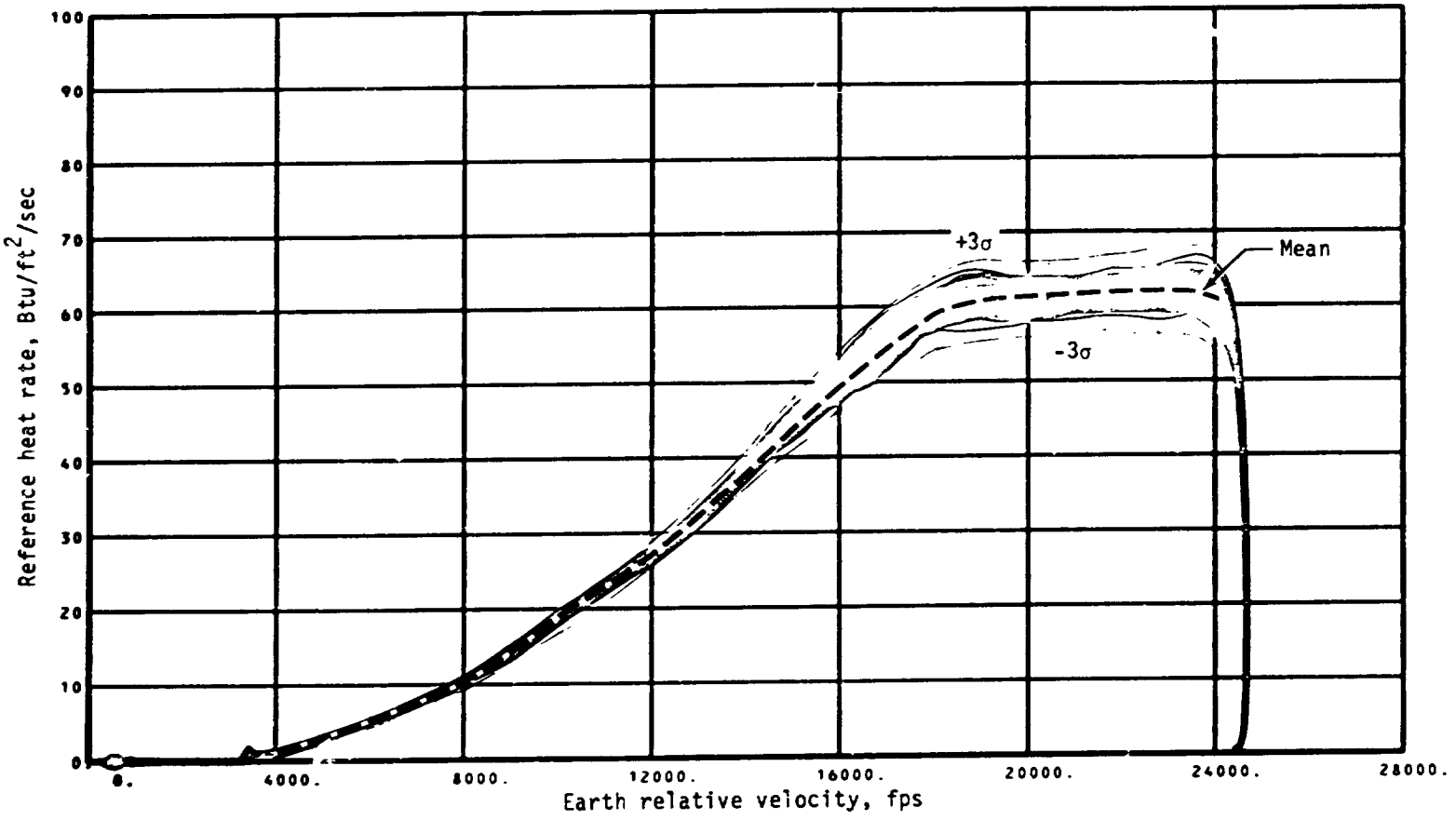

(a) Heat rate.

Figure 18.- TPS performance - steep abort once around.

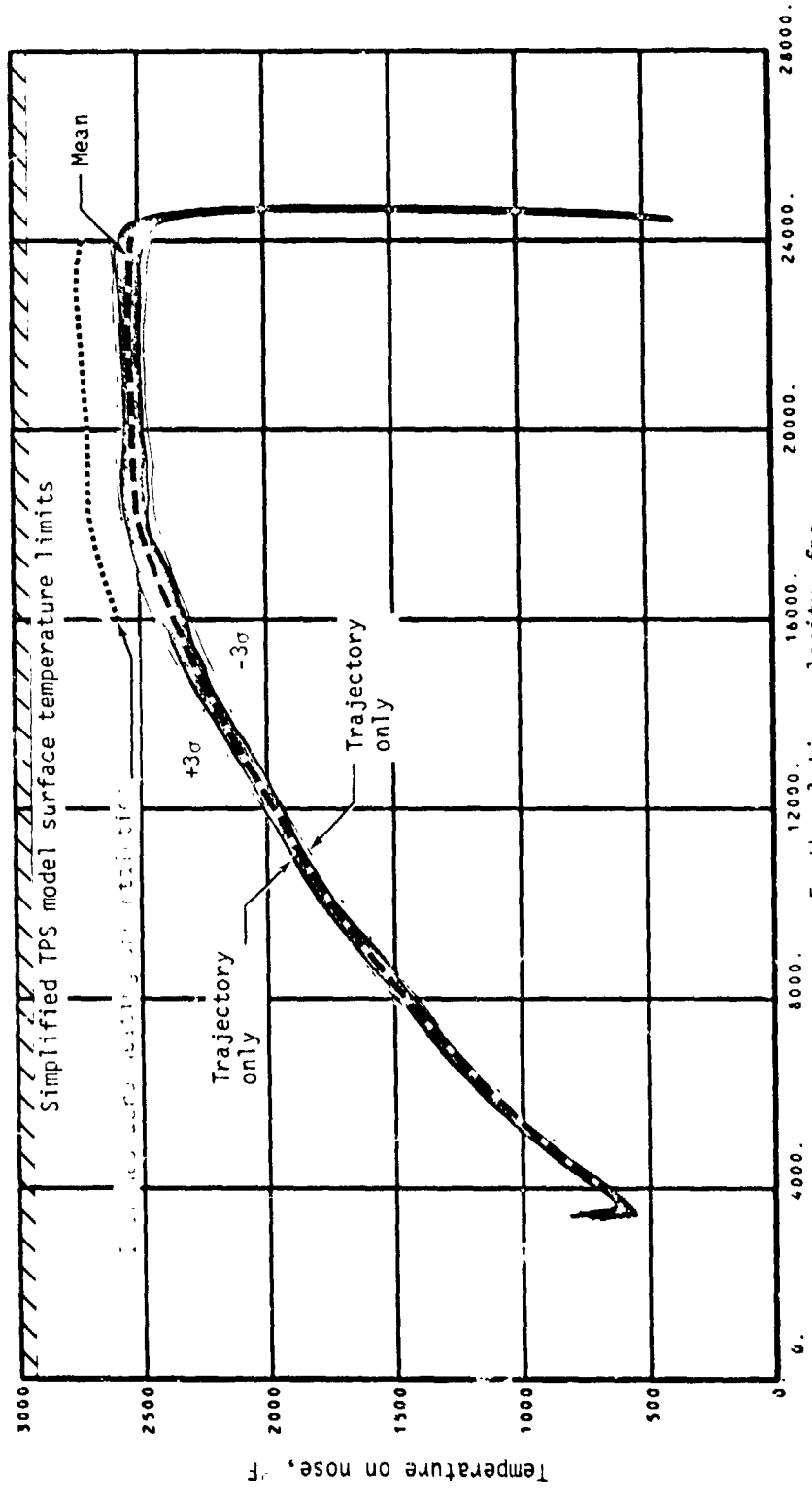

(b) Nose surface temperature.

Figure 18.- Continued.

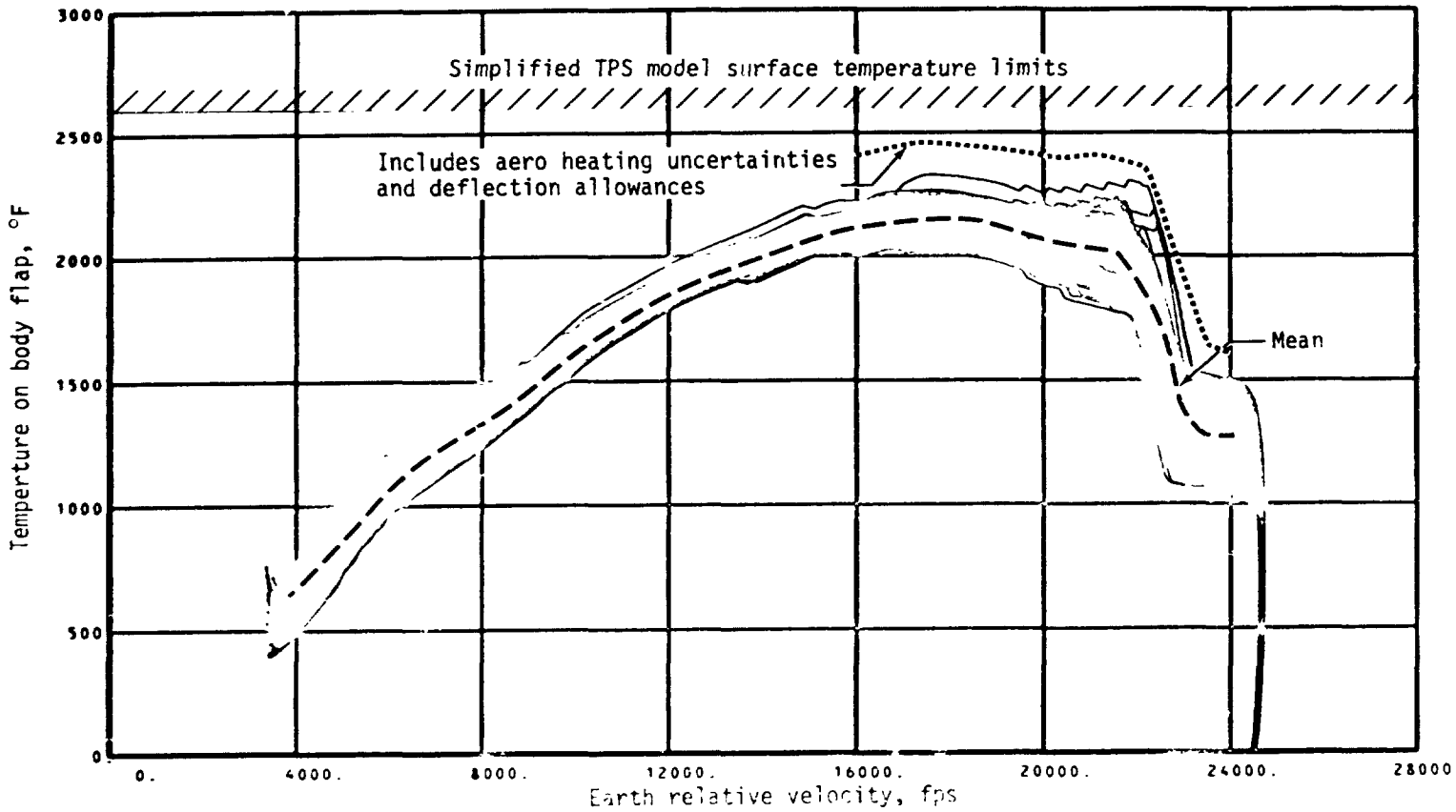

(c) Body flap surface temperature.

Figure 16.- Continued.

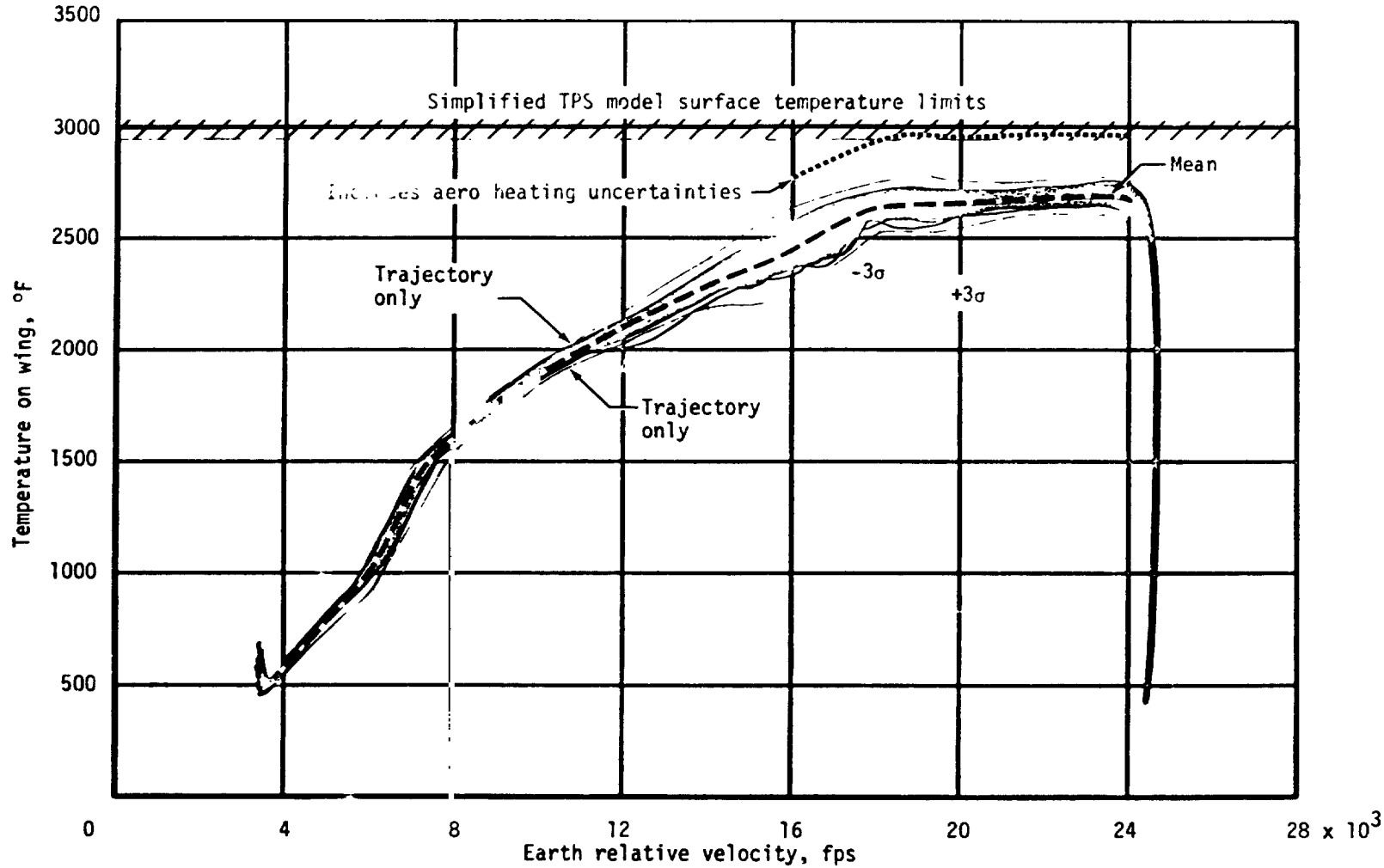

(d) Wing surface temperature.

Figure 18.- Continued.

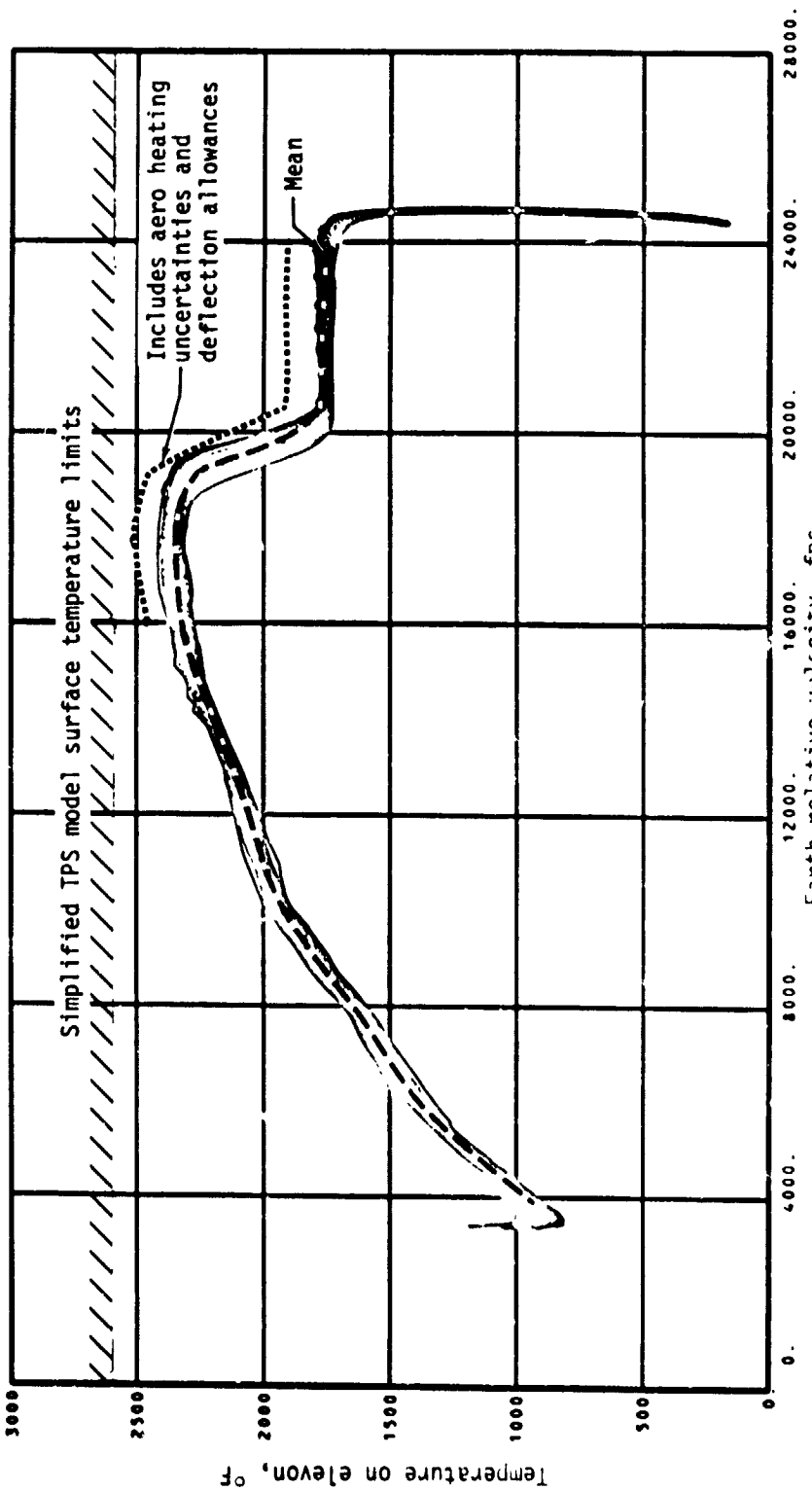

(e) Elevon surface temperature.

Figure 18.- Continued.

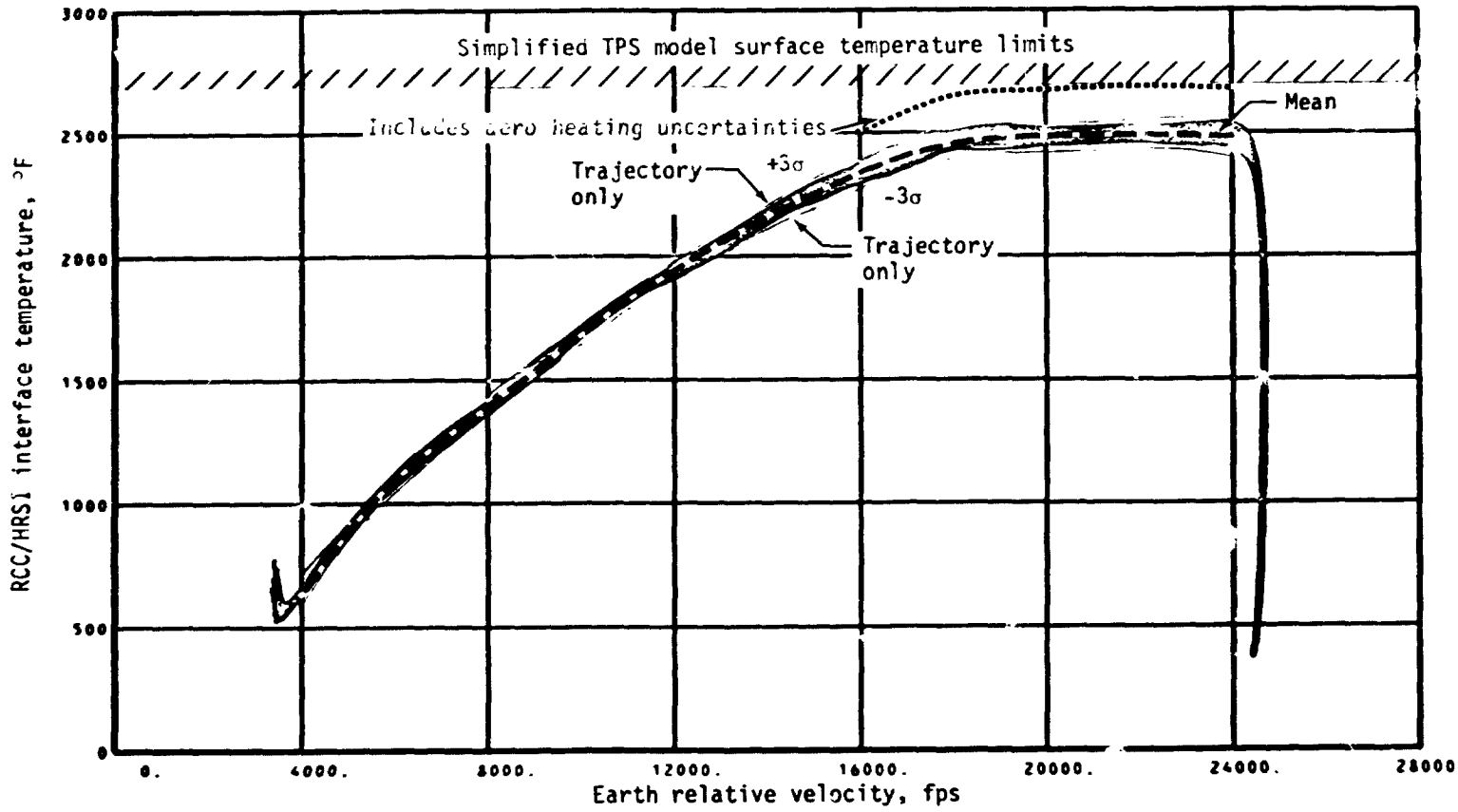

(f) RCC/HRSI interface (CP6) surface temperature.

Figure 18.- Concluded.

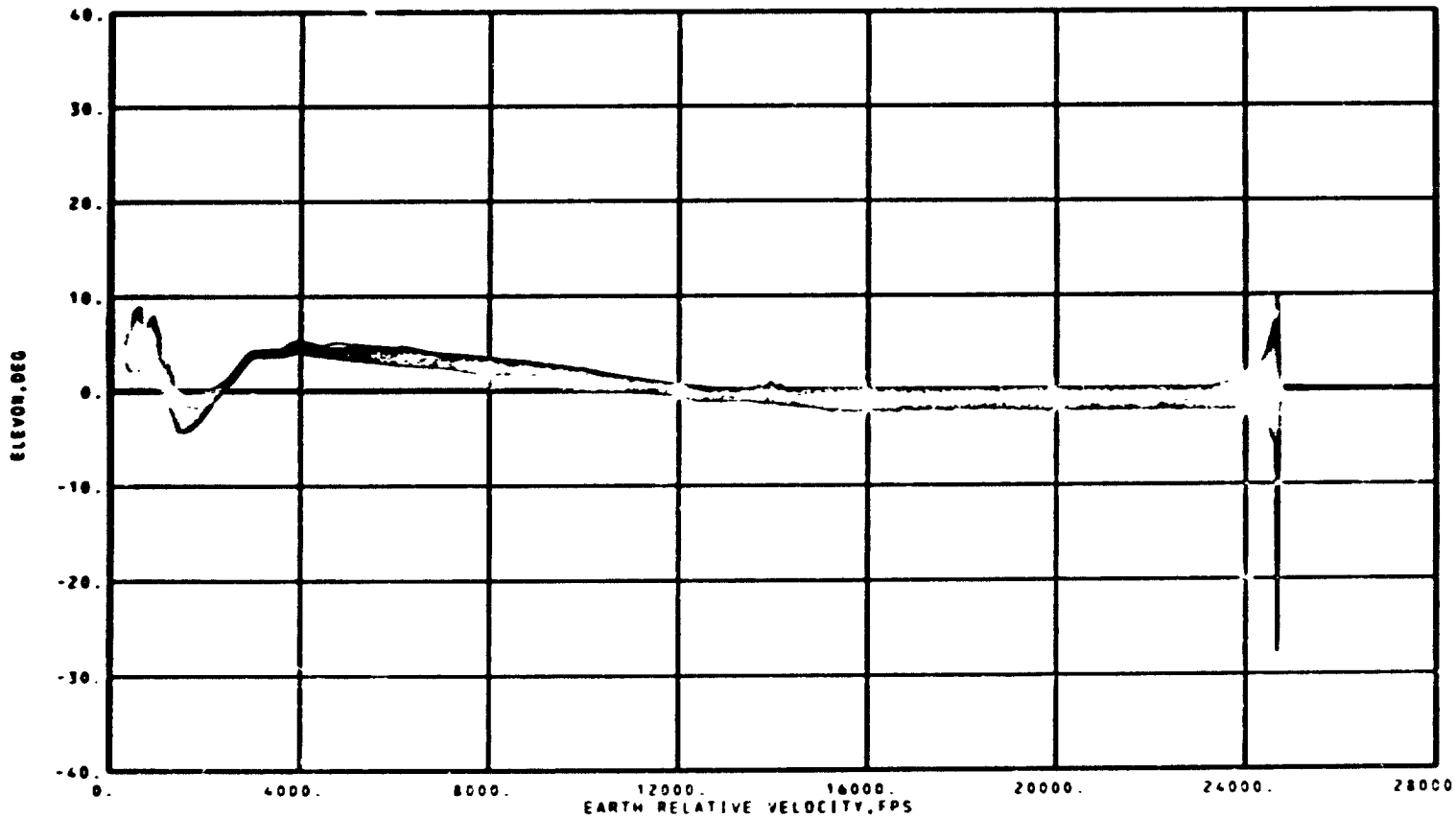

(a) Elevon deflection.

Figure 19.- Control surface deflections and hinge moments - steep abort once around.

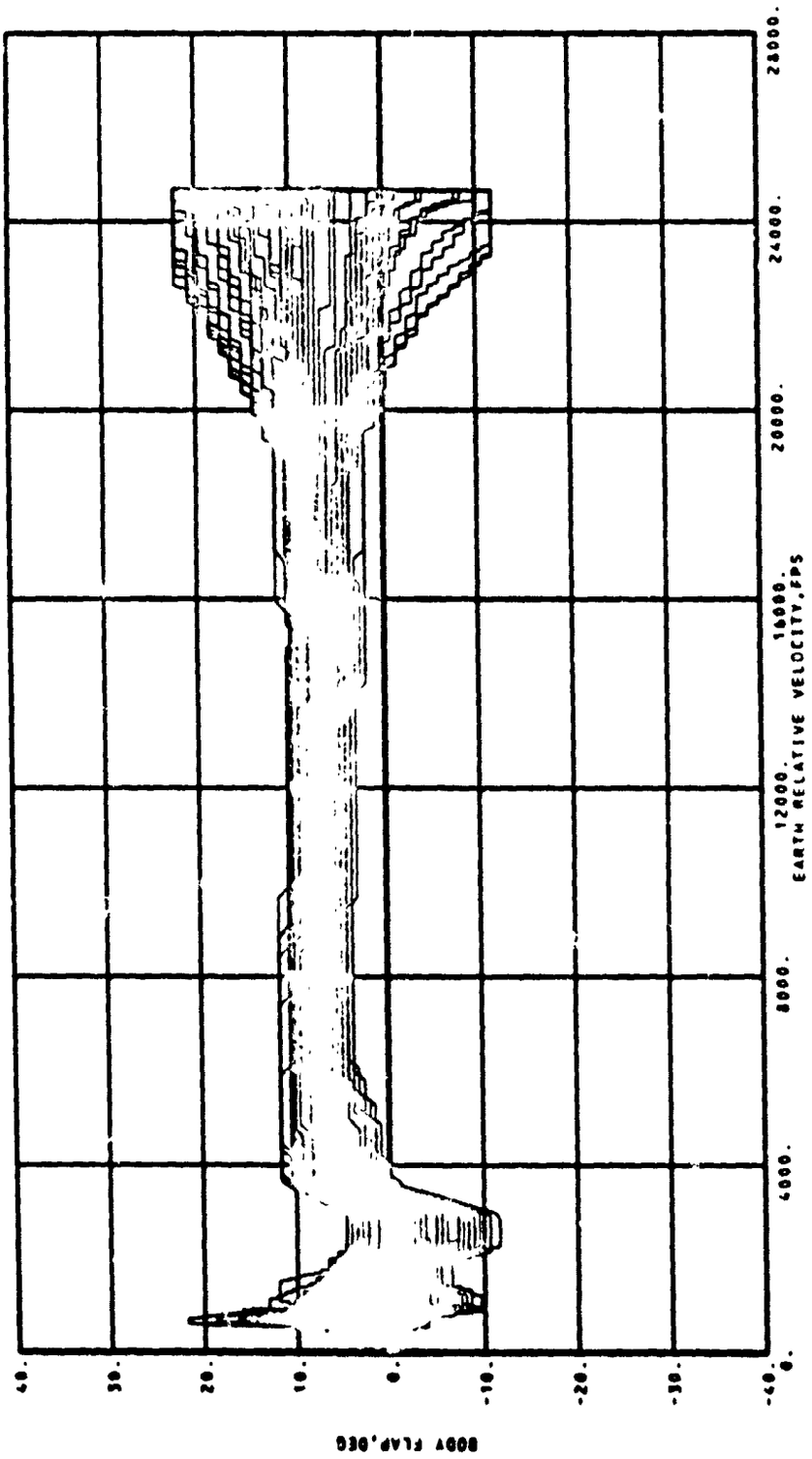

(b) Body flap deflection.

Figure 19.- Continued.

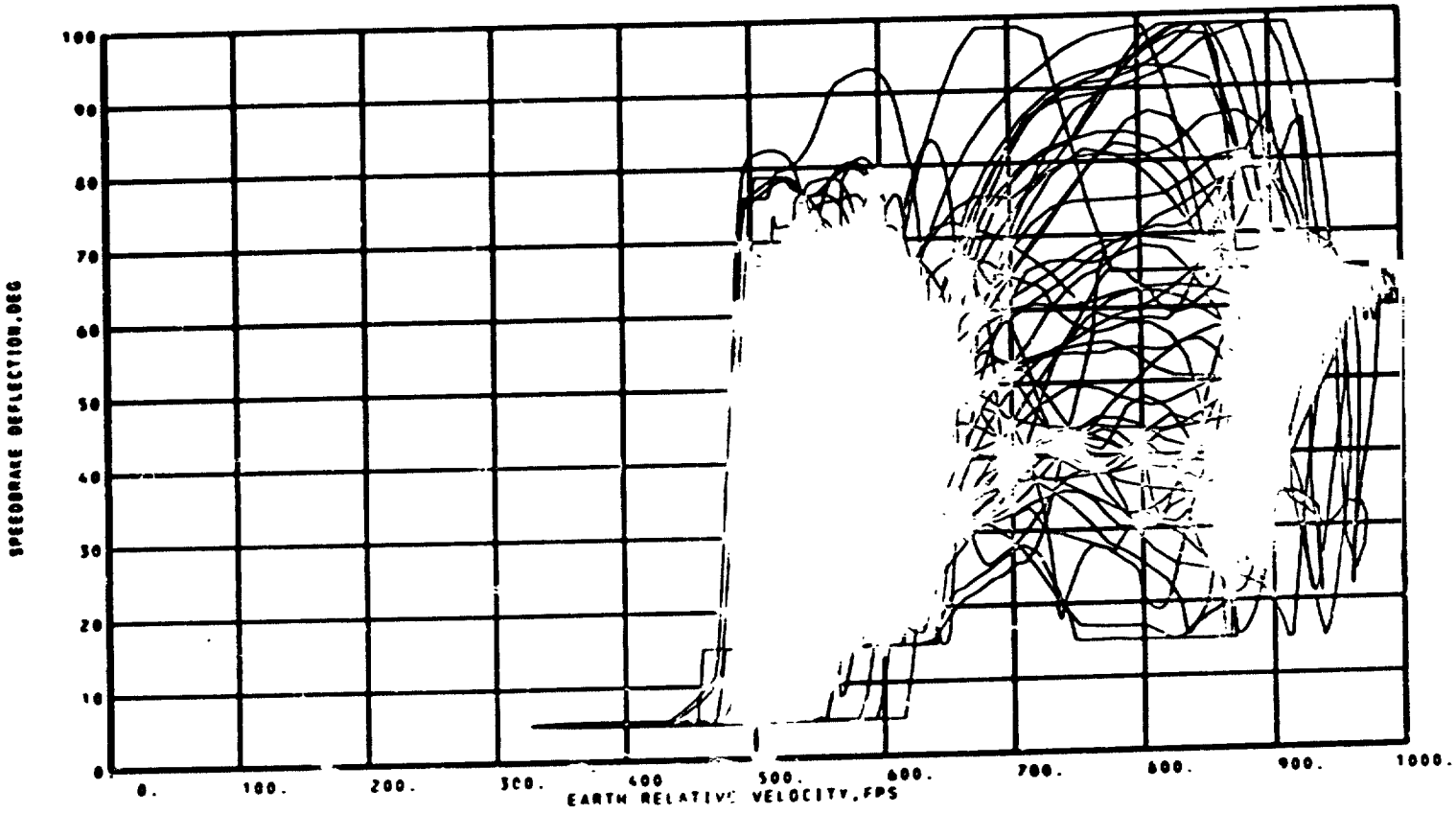

(c) Speedbrake deflection.

Figure 19.- Continued.

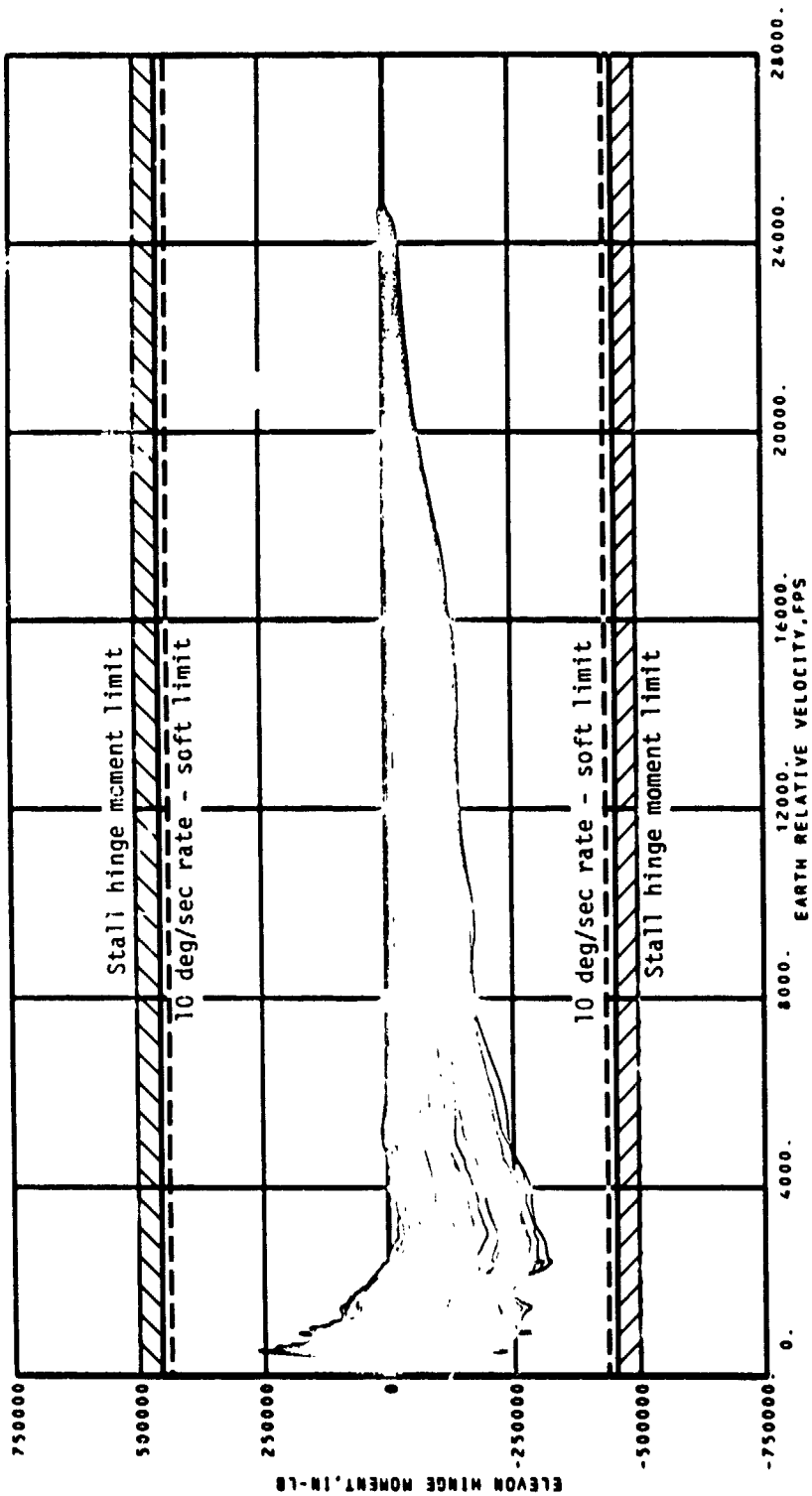

(d) Outboard elevon hinge moment.

Figure 19.- Continued.

C-3

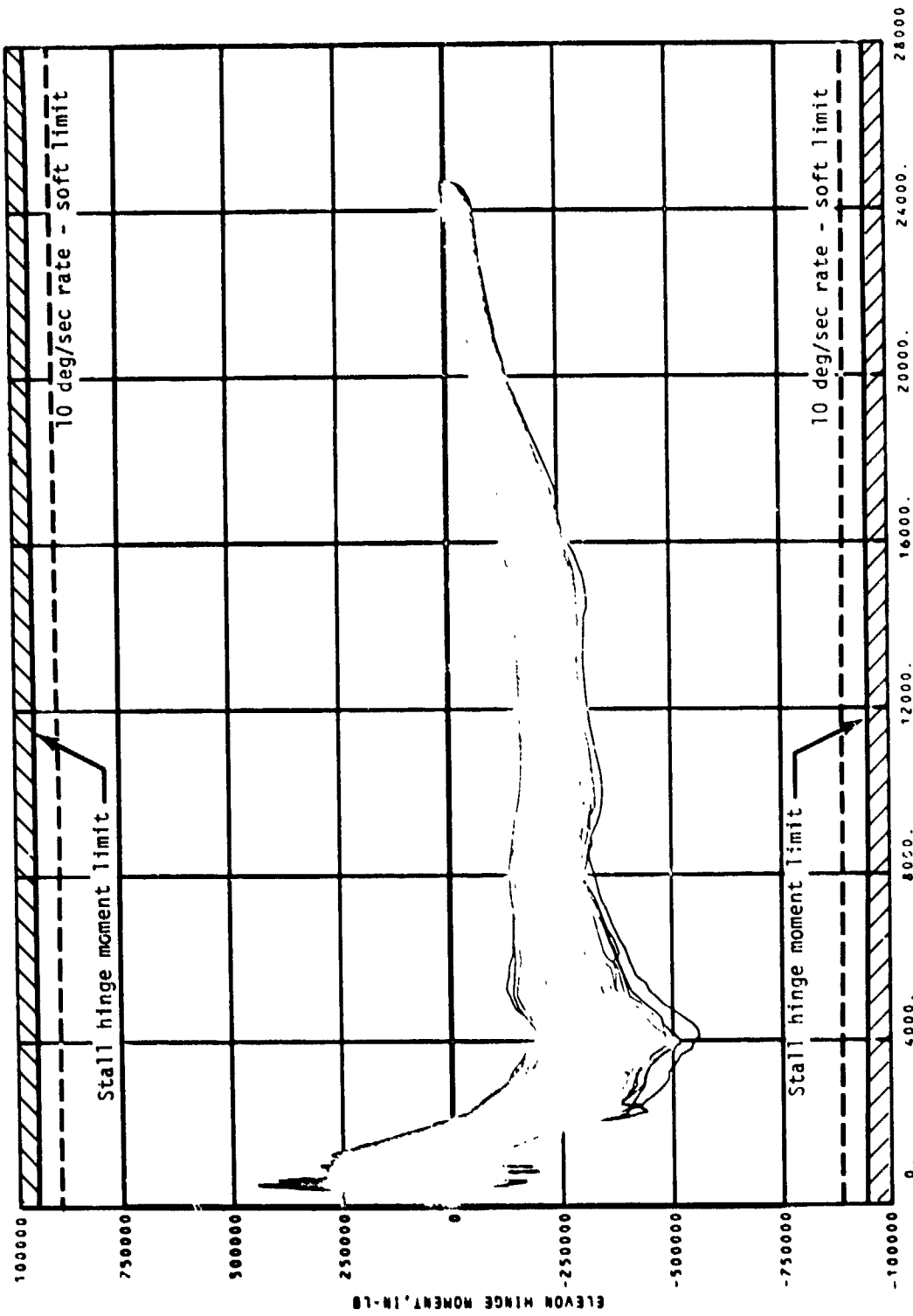

(e) Inboard elevon hinge moment.

Figure 19.- Continued.

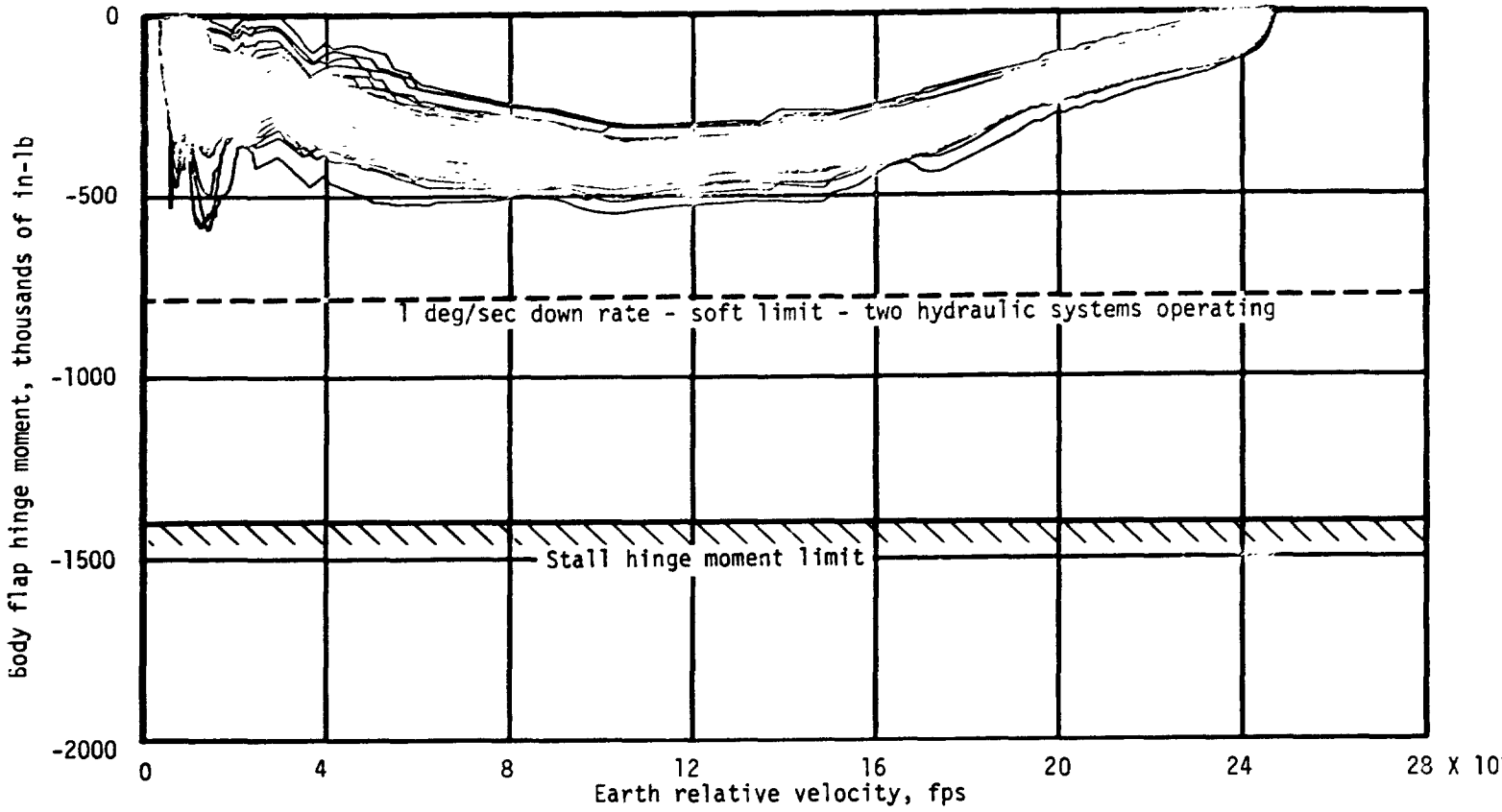

(f) Body flap hinge moment.

Figure 19.- Continued.

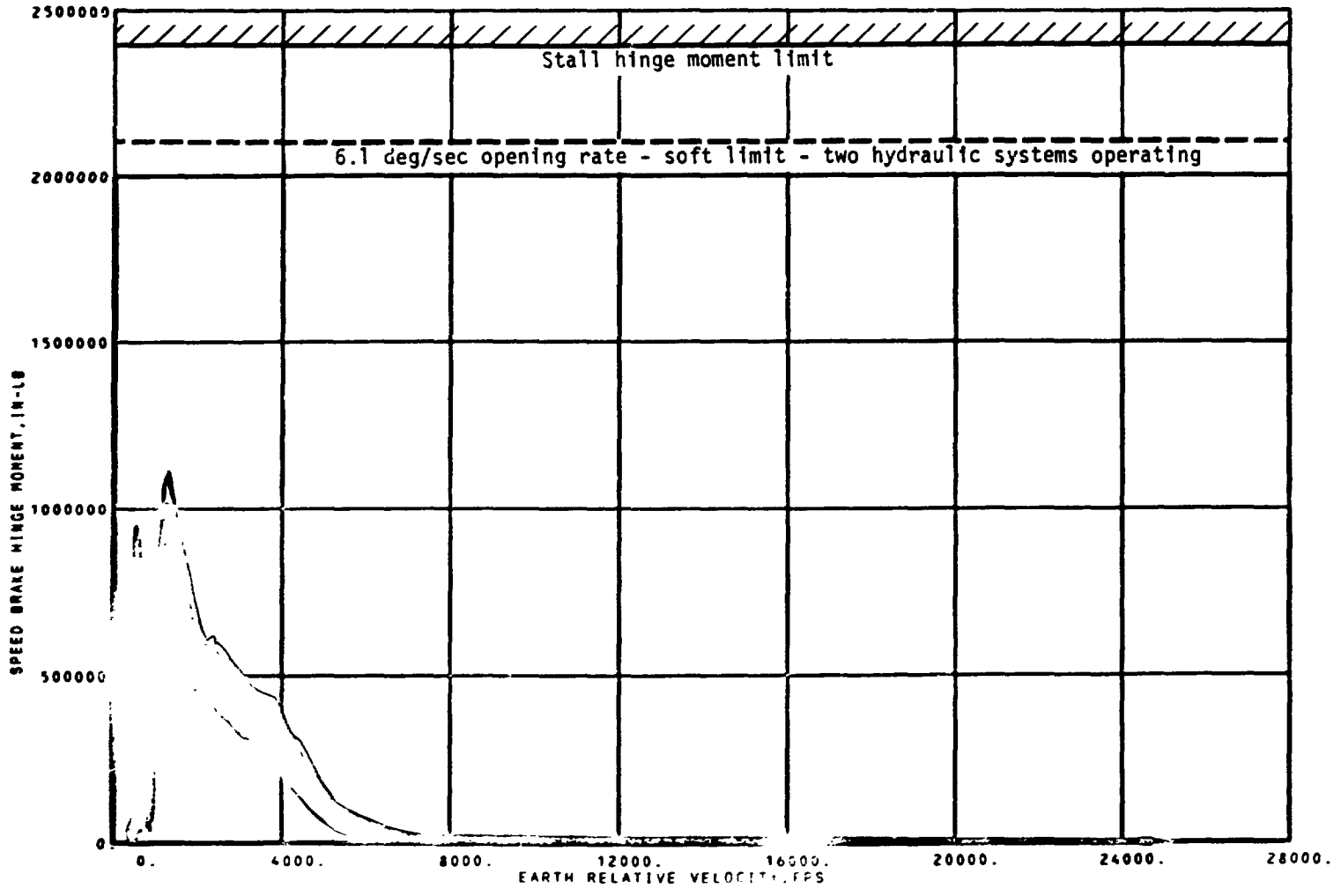

(g) Speedbrake hinge moment.

Figure 19.- Concluded.

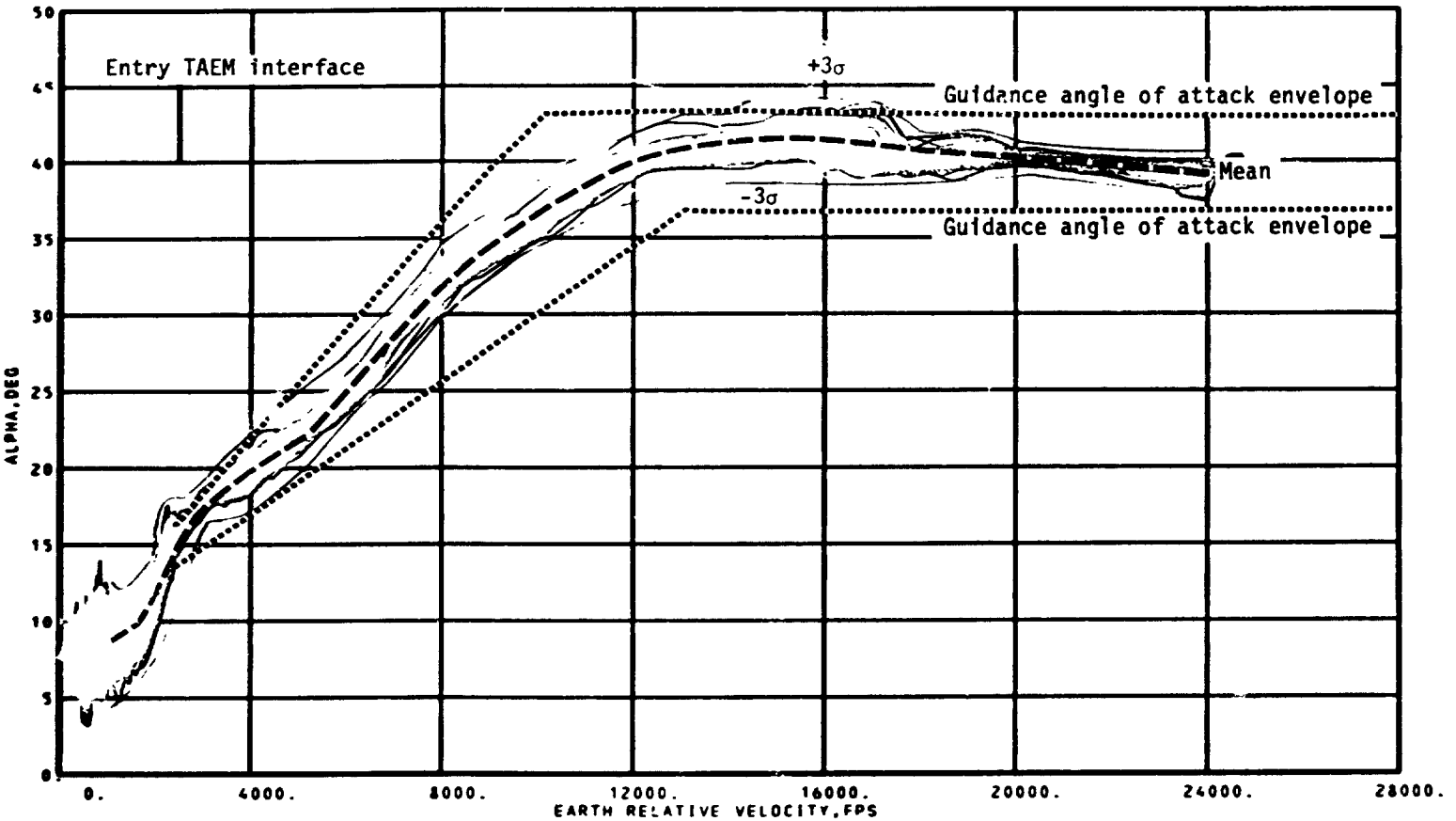

(a) Angle of attack.

Figure 20.- Entry guidance performance parameters - steep abort once around.

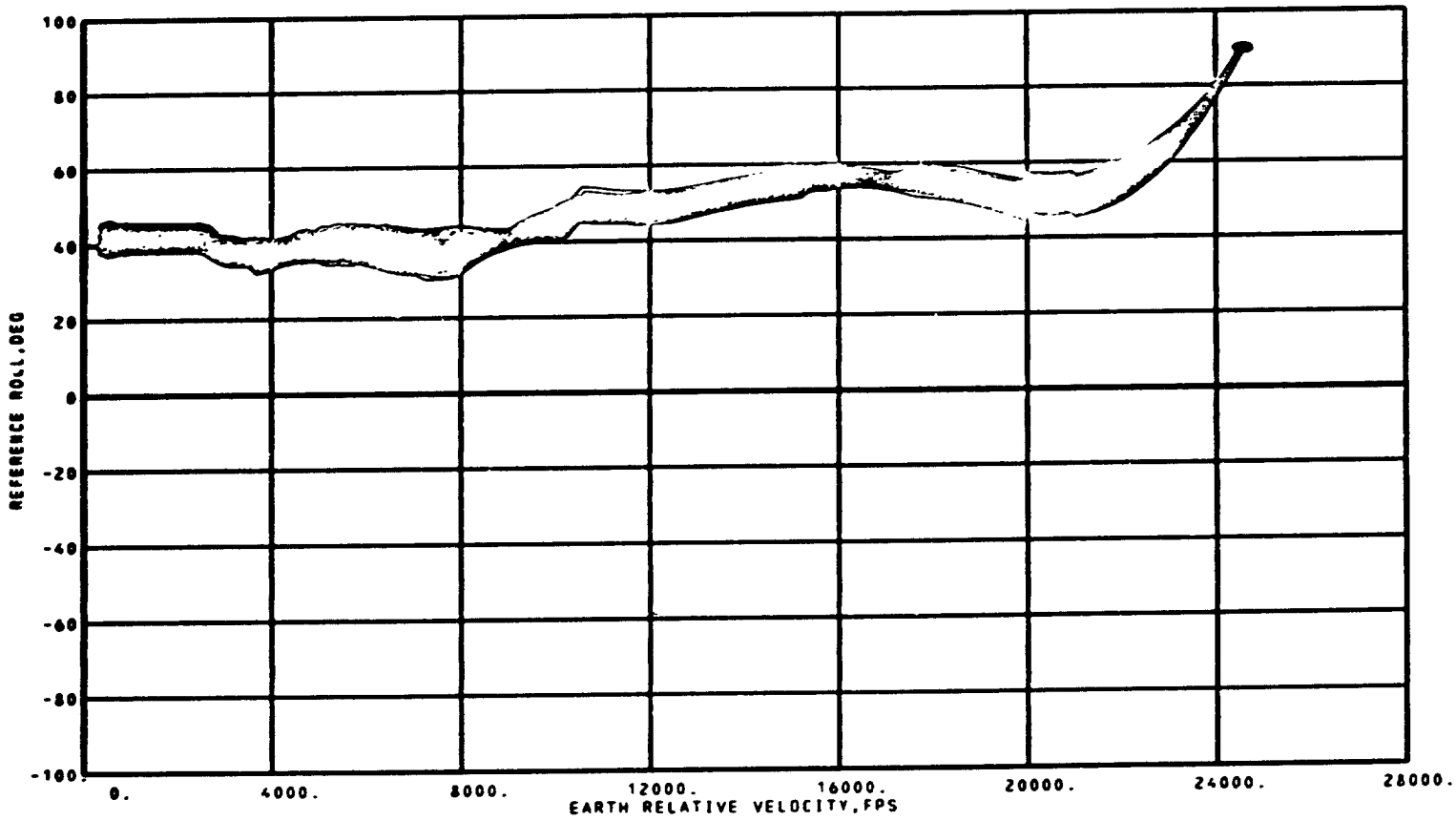

(b) Reference bank angle.

Figure 20.- Continued.

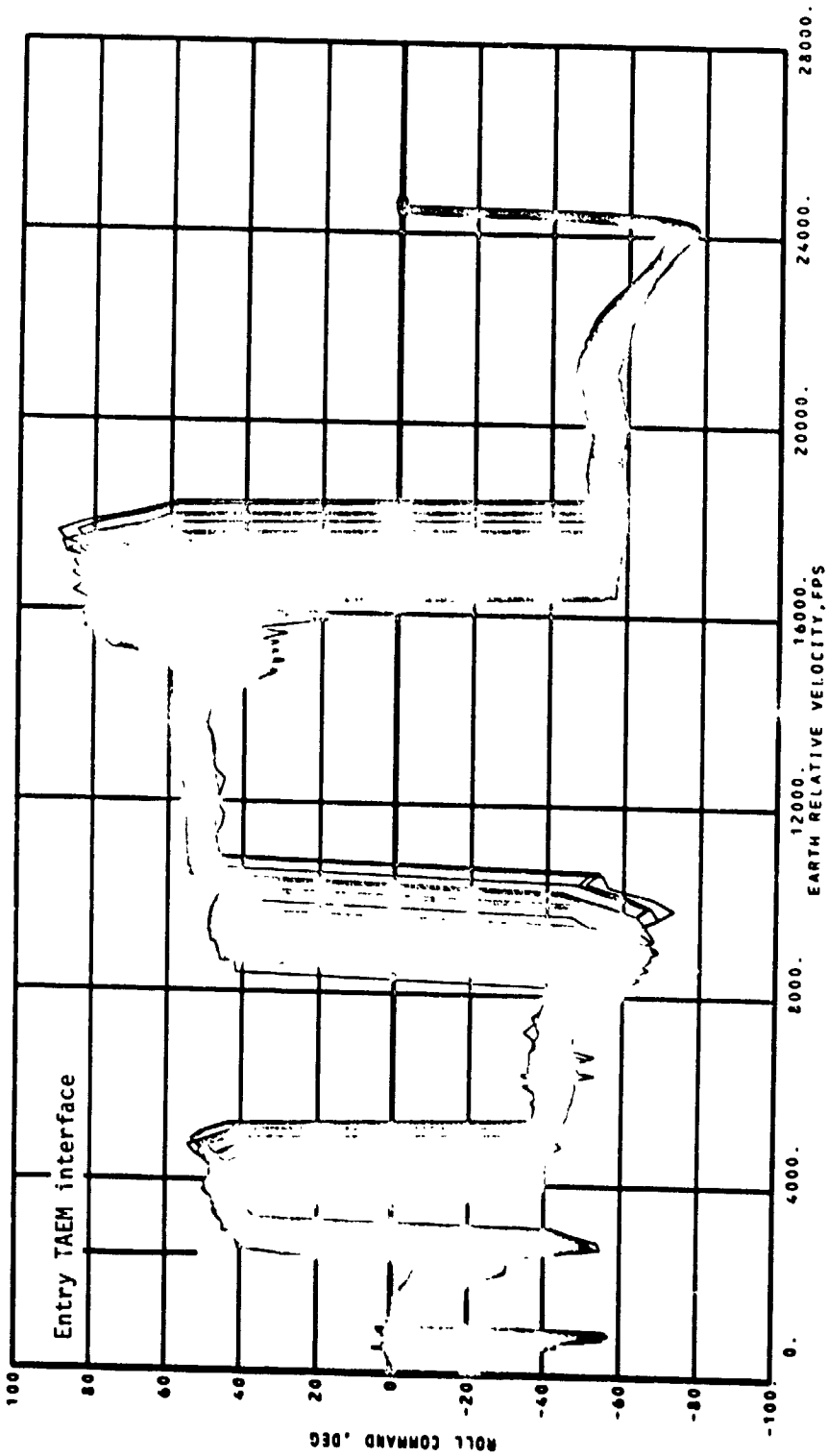

(c) Bank command.

Figure 20.- Continued.

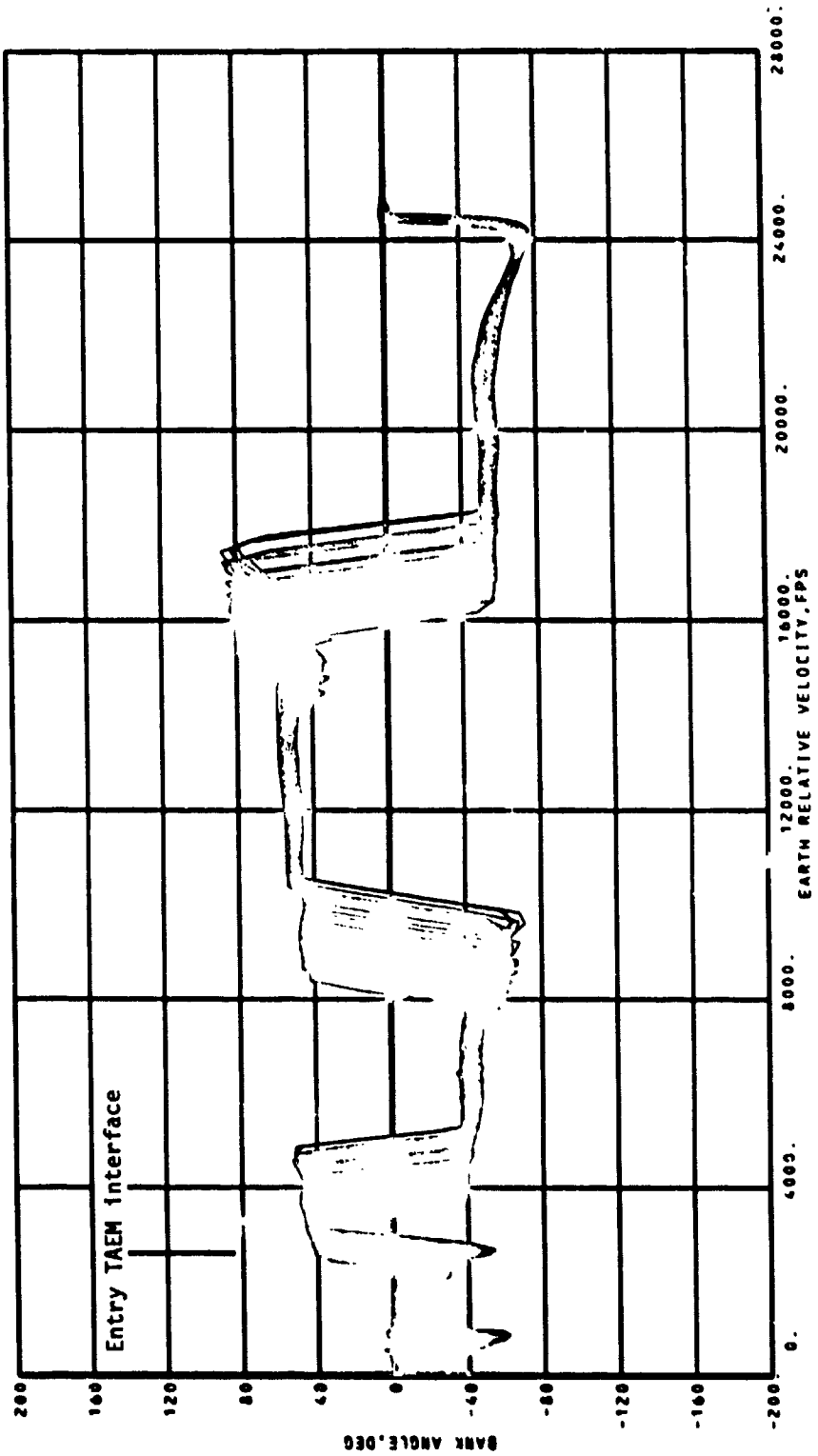

(d) Bank angle.

Figure 20.- Continued.

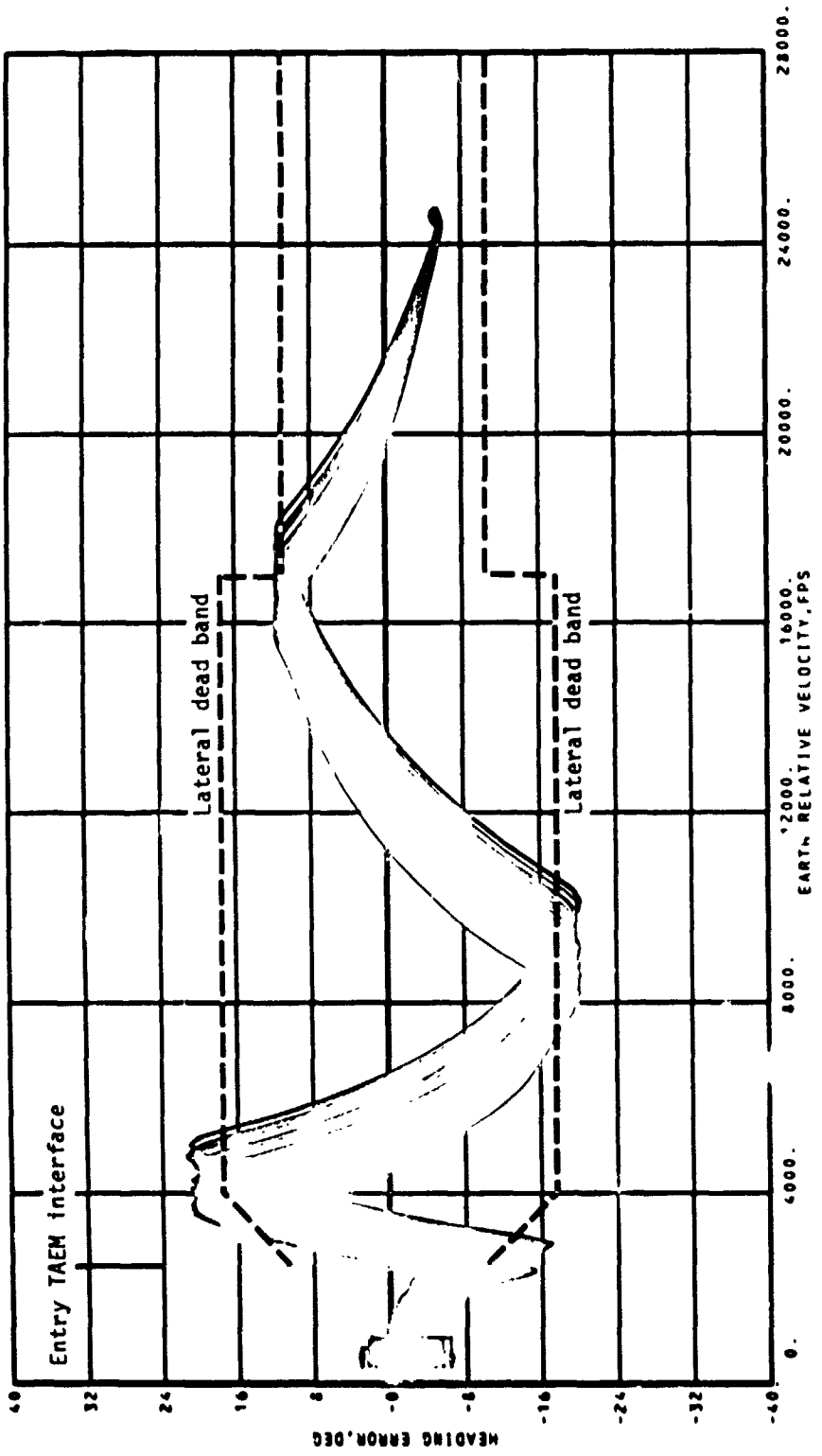

(e) Navigated heading error.

Figure 20.- Continued.

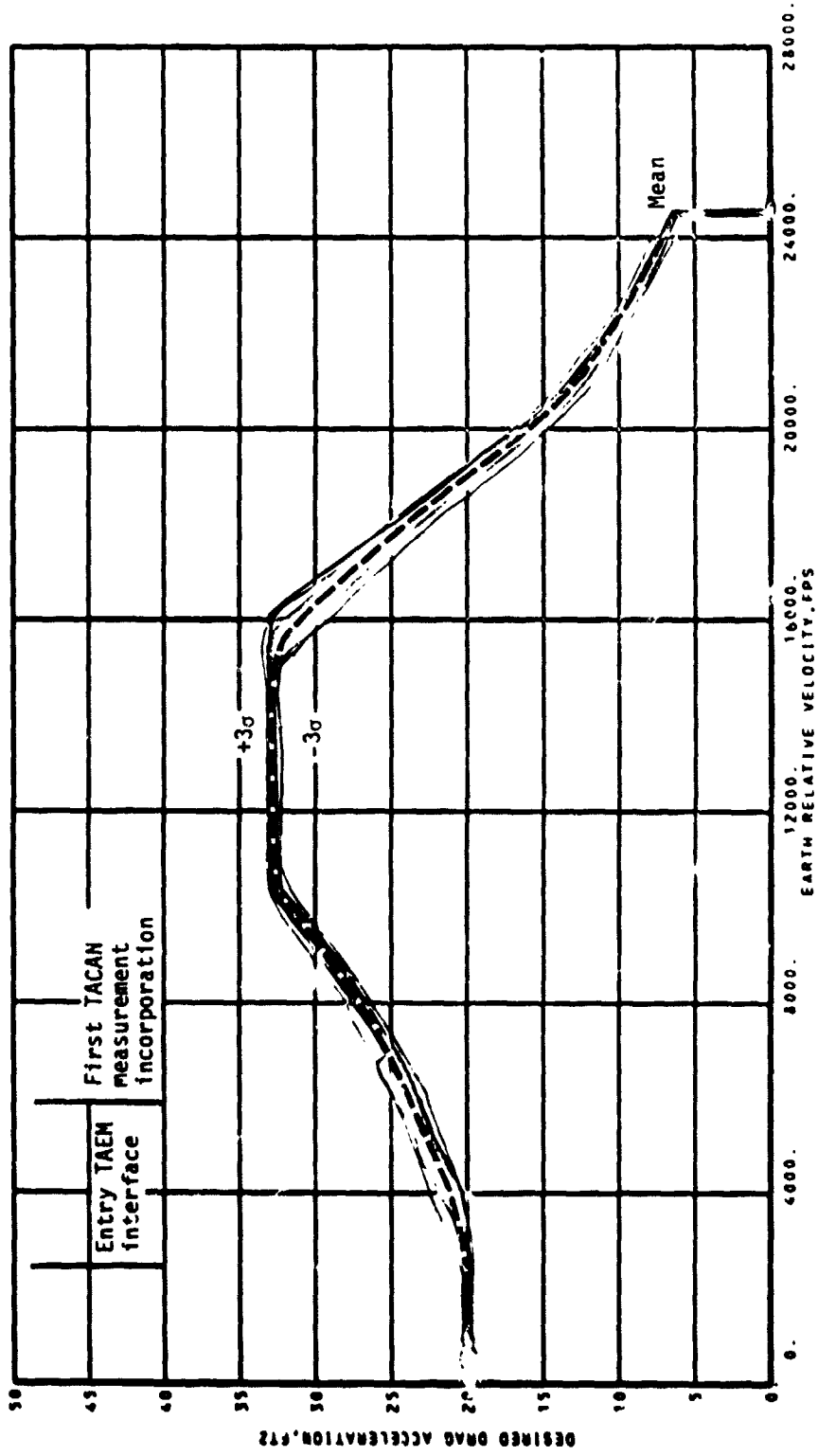

(f) Desired drag acceleration.

Figure 20.- Continued.

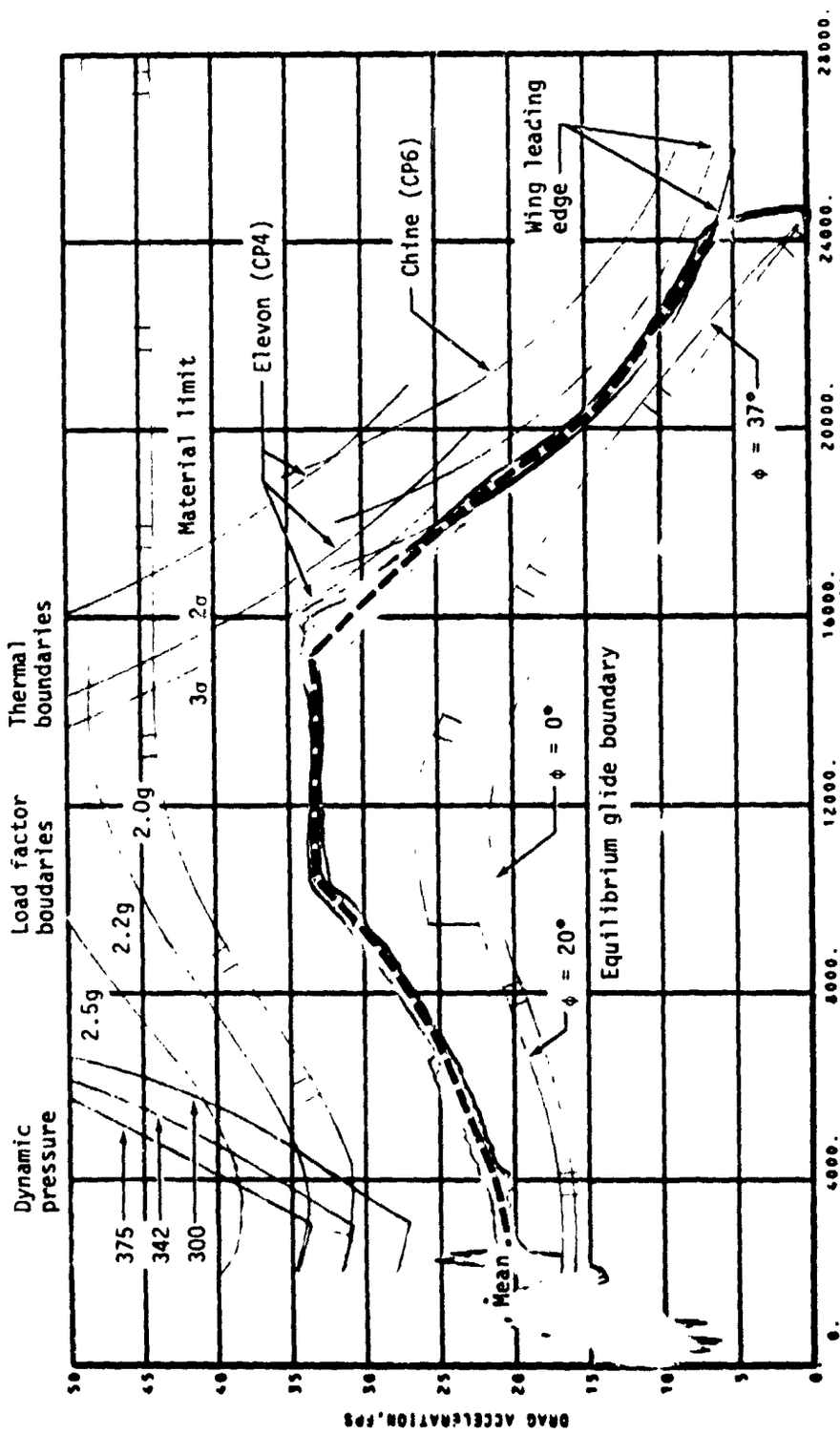

(g) Drag acceleration.

Figure 20.- Continued.

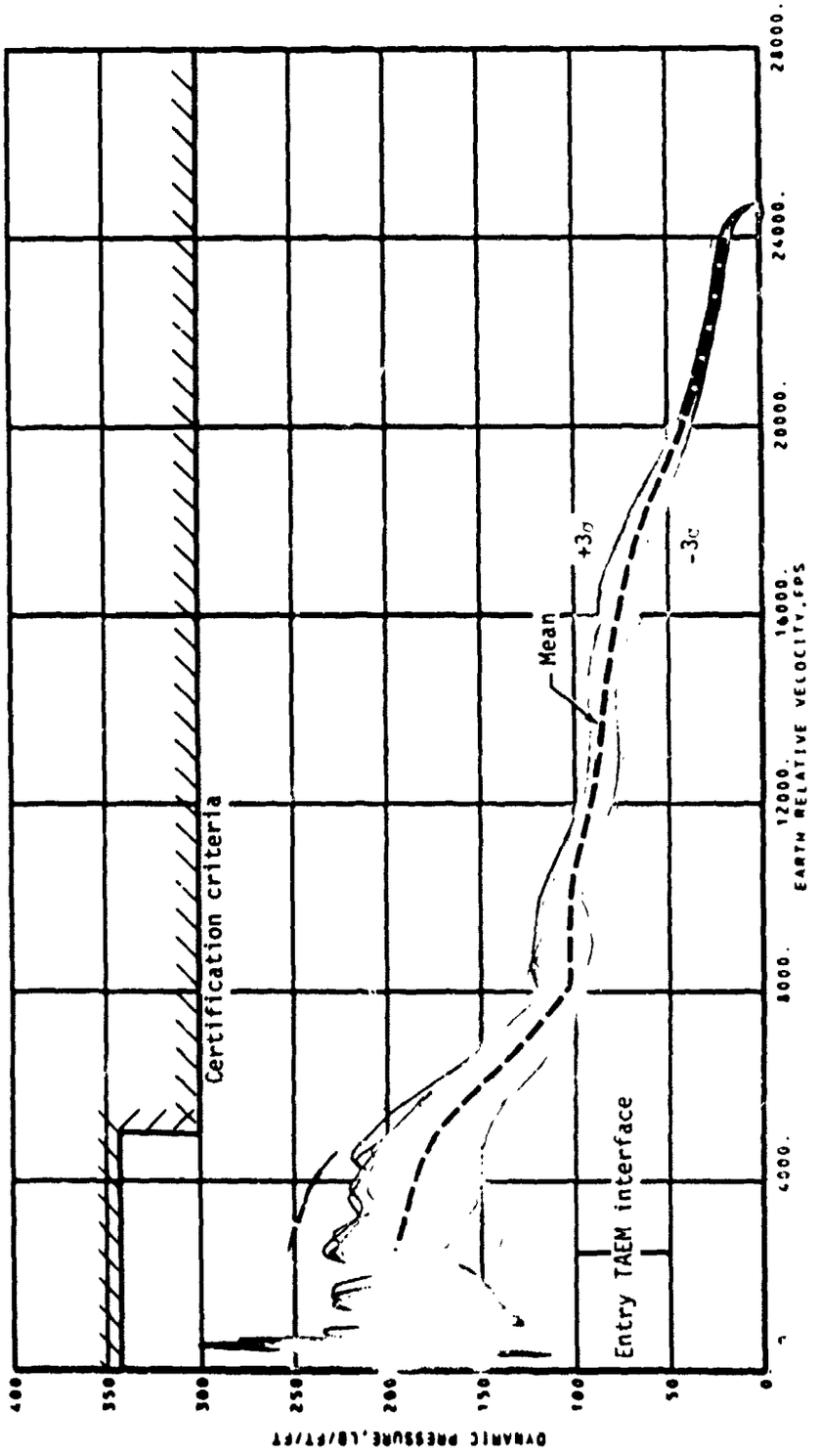

(h) Dynamic pressure.

Figure 20.- Continued.

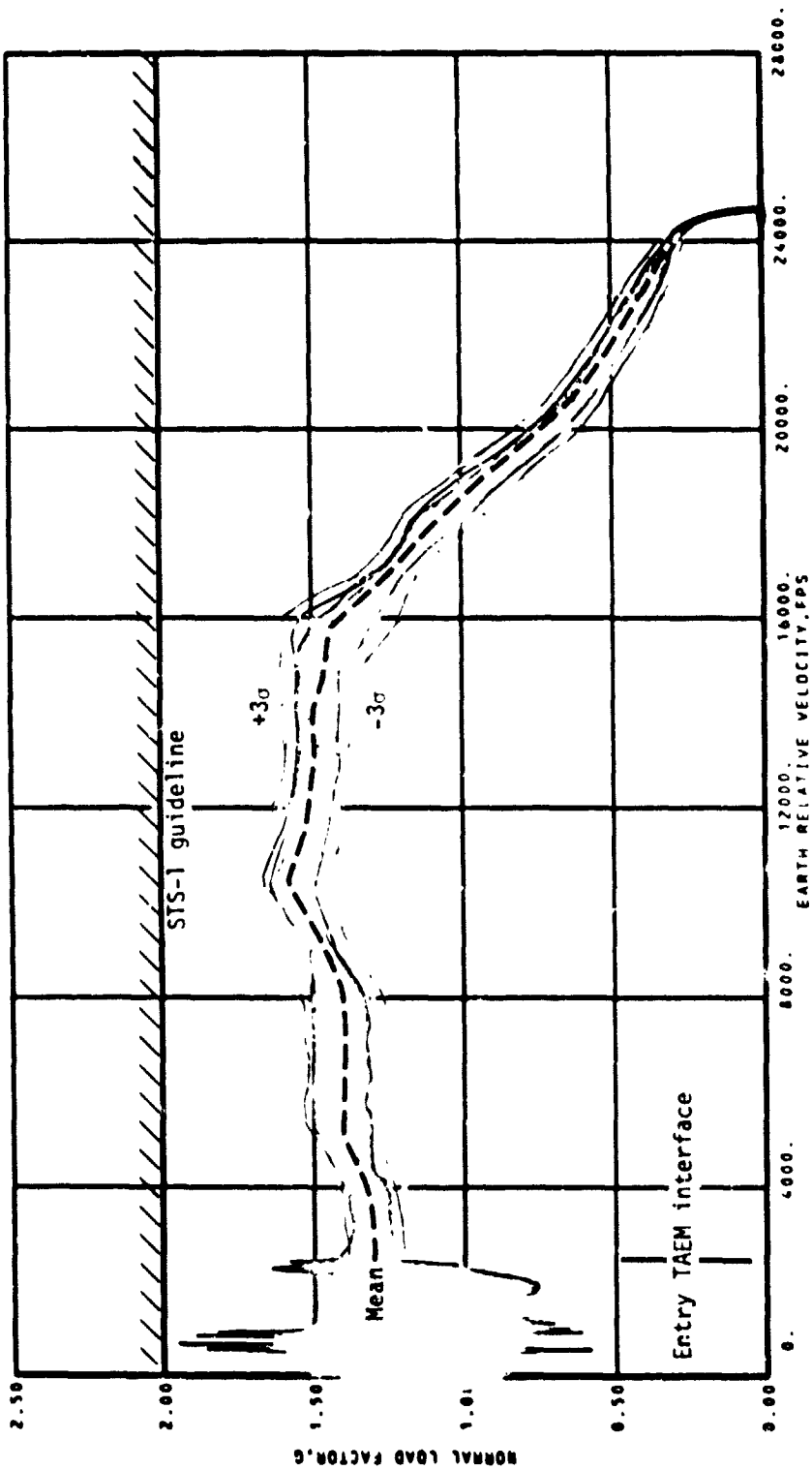

(i) Normal load factor.

Figure 20.- Continued.

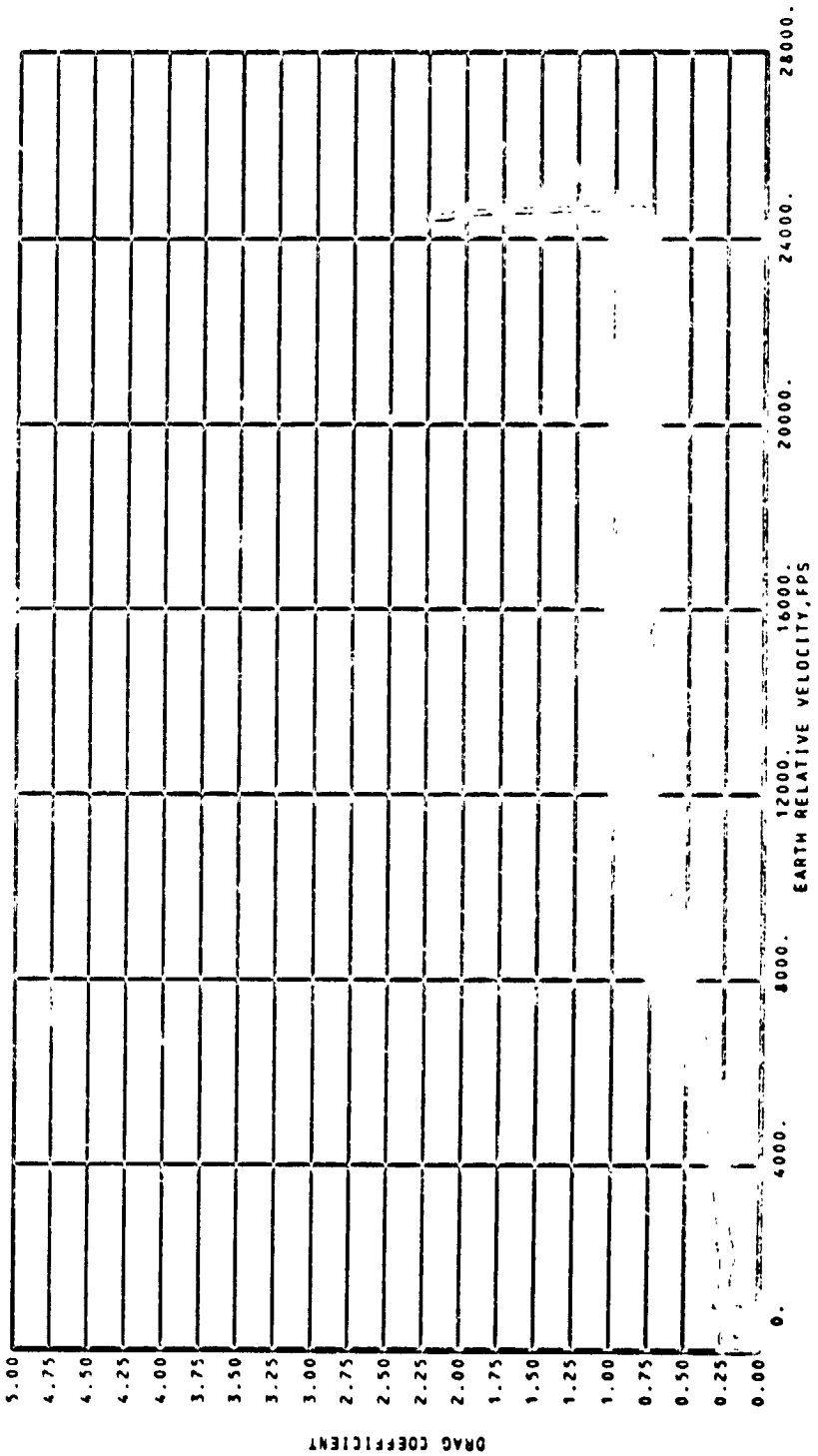

(j) Drag coefficient.

Figure 20.- Continued.

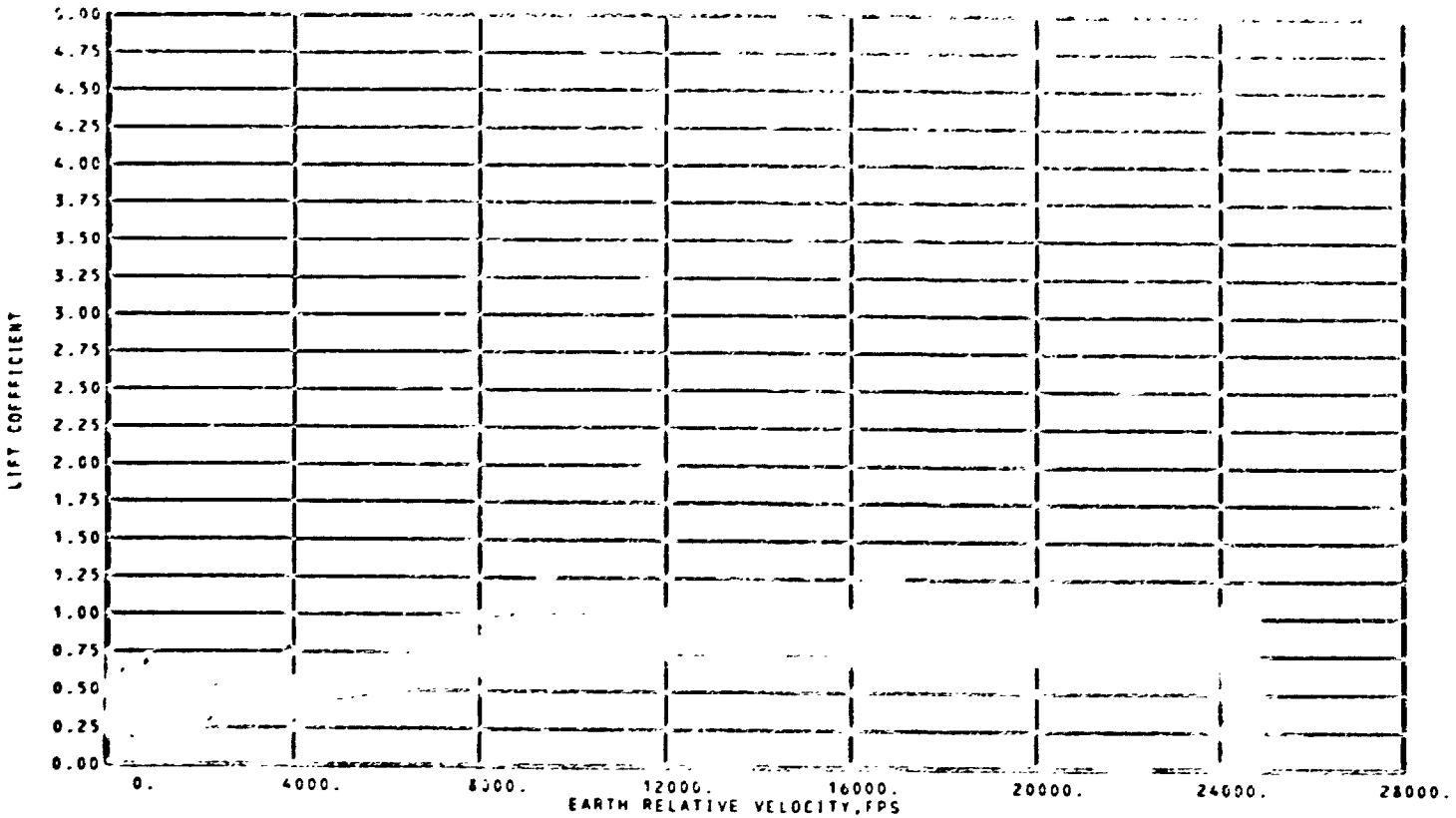

(k) Lift coefficient.

Figure 20.- Continued.

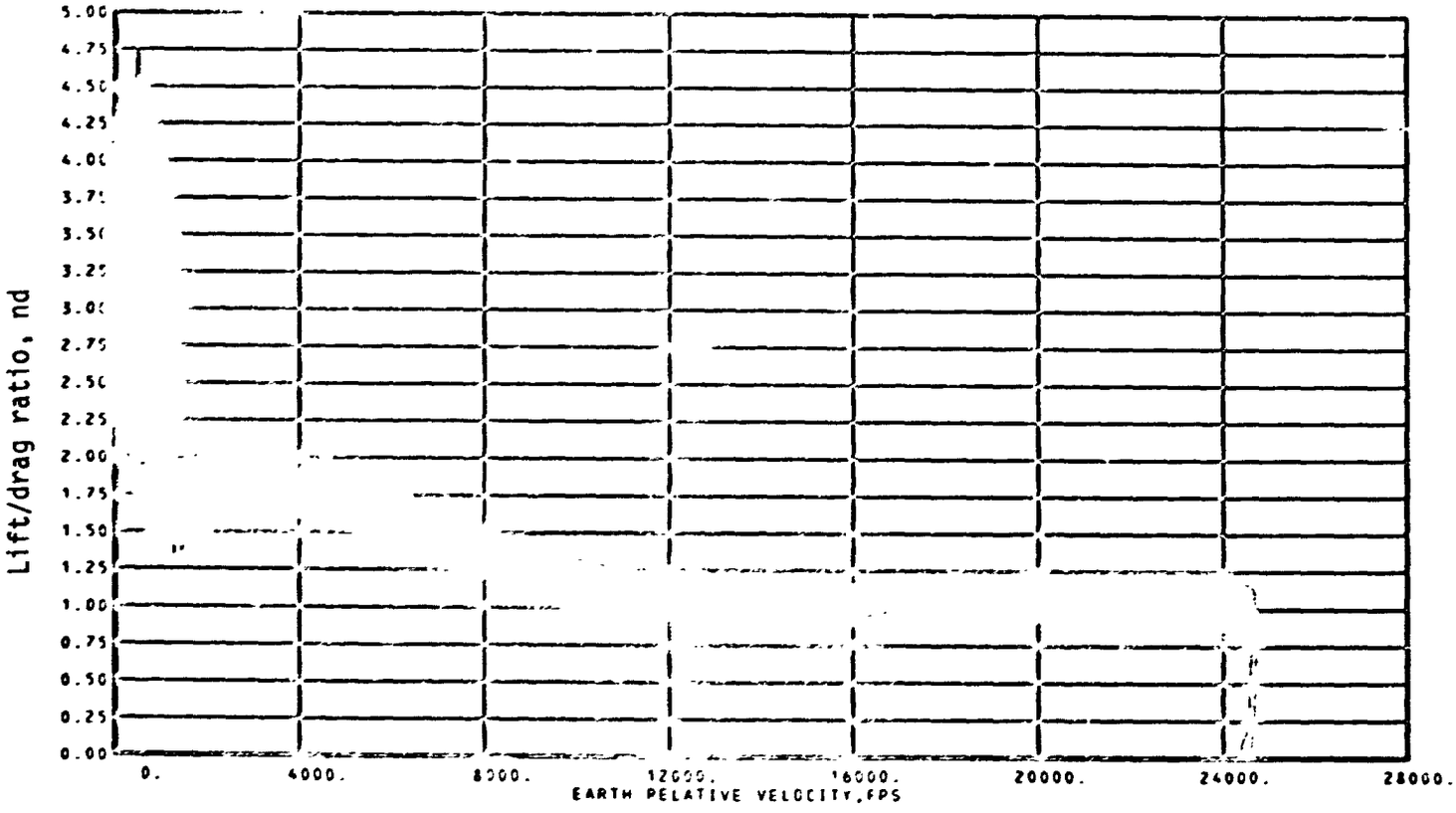

(1) Lift to drag ratio.

Figure 20.- Continued.

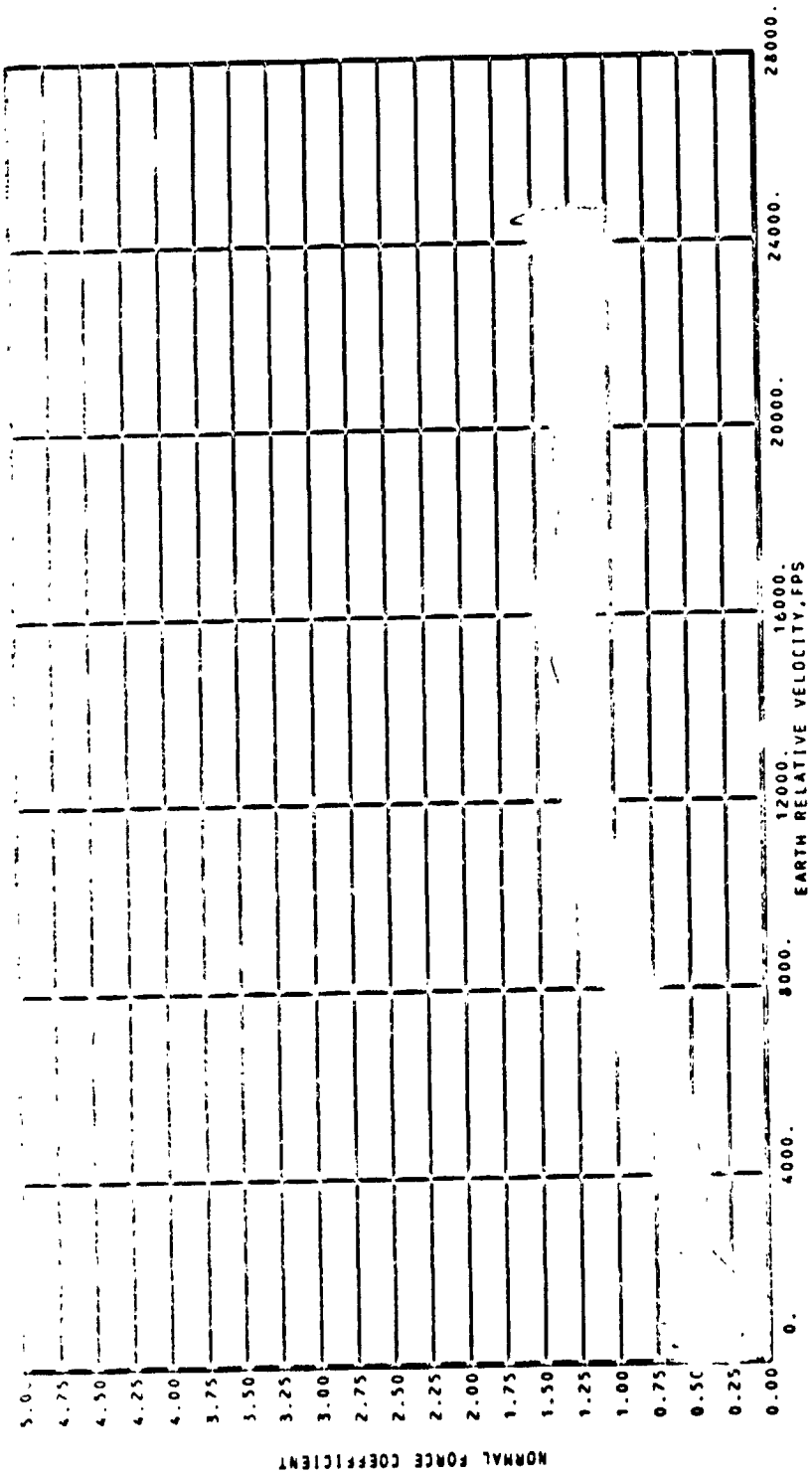

(m) Normal force coefficient.

Figure 20.- Continued.

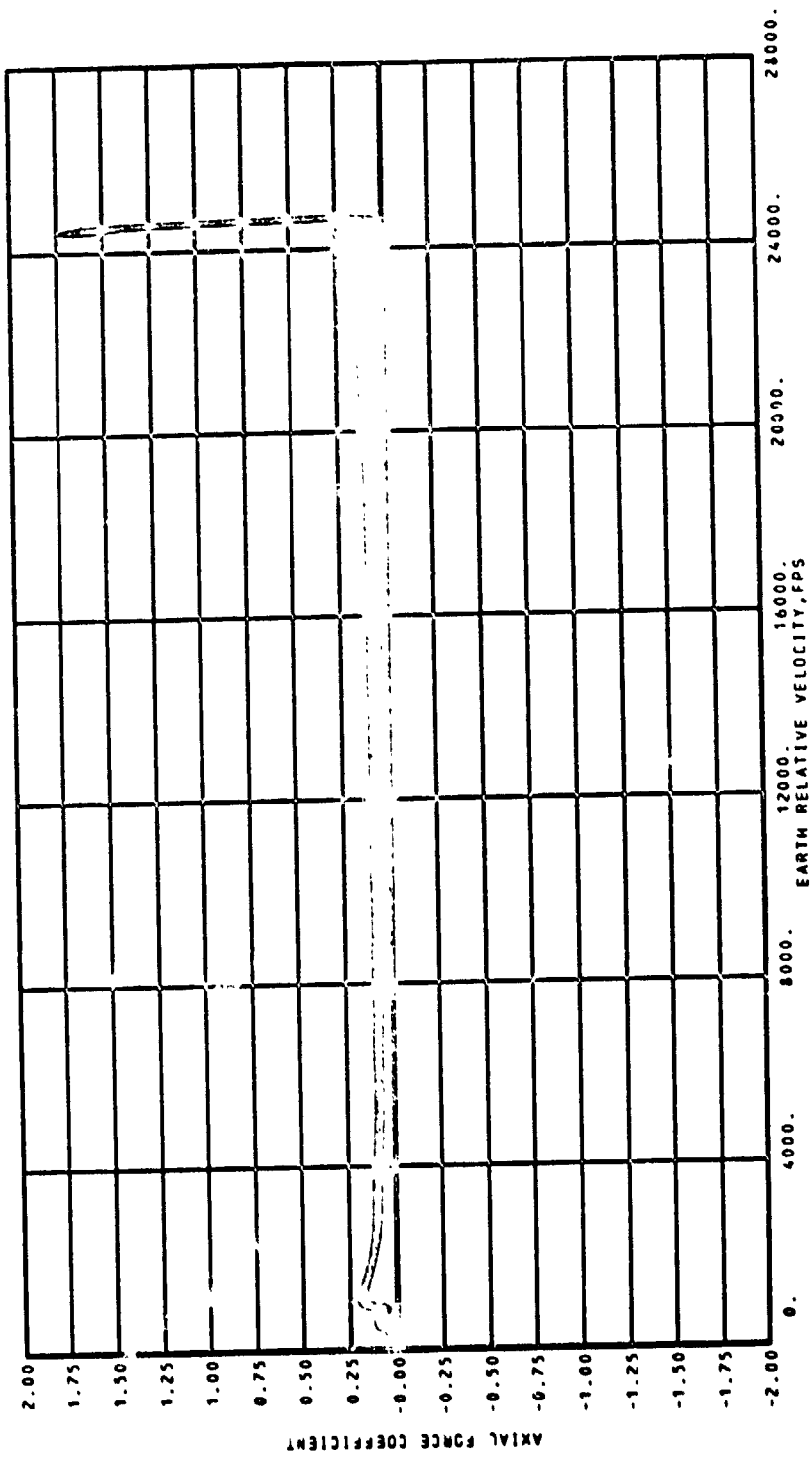

(n) Axial force coefficient.

Figure 20.- Continued.

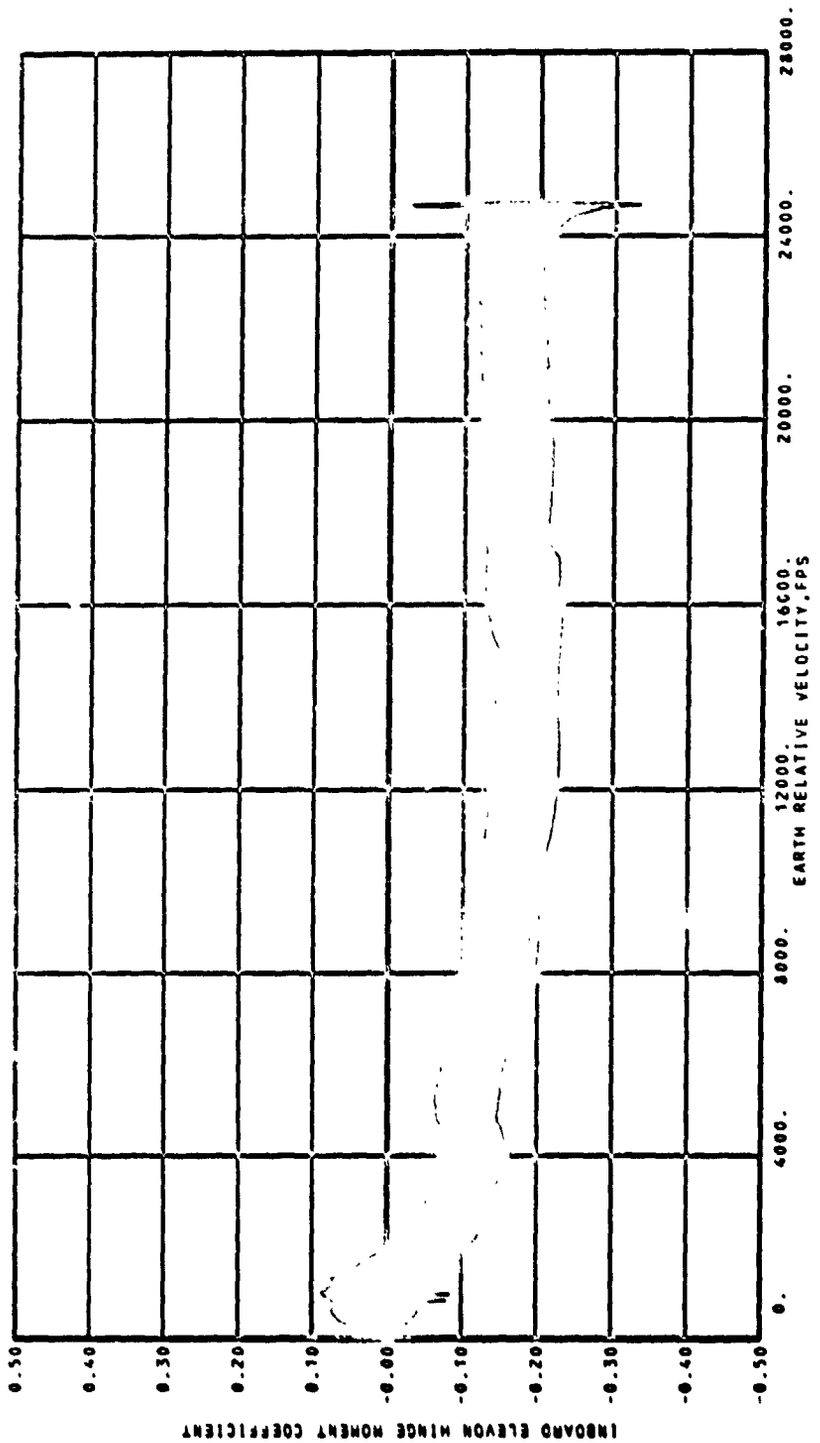

(o) Inboard elevon hinge moment coefficient.

Figure 20.- Continued.

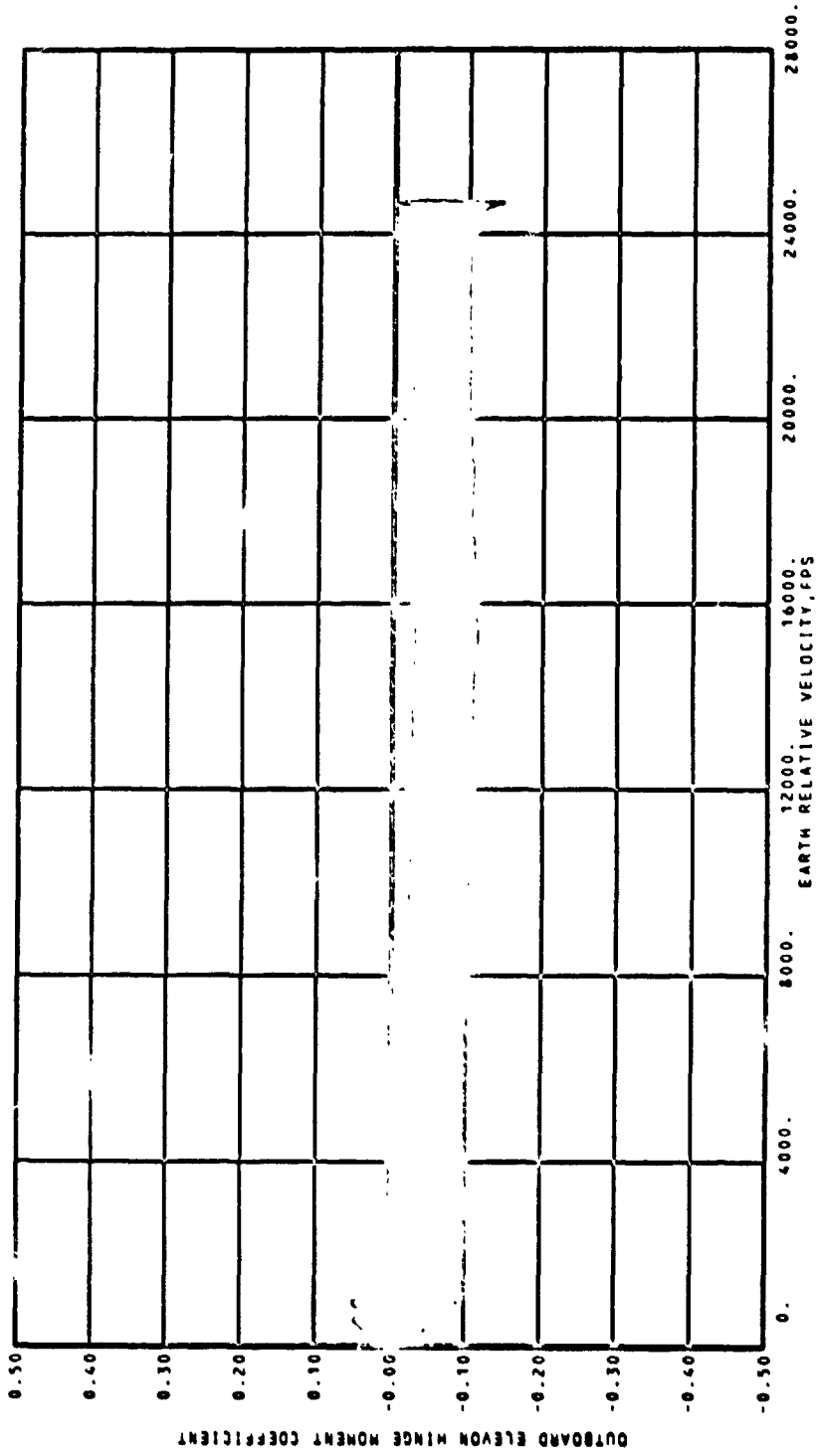

(p) Outboard elevon hinge moment coefficient.

Figure 20.- Continued.

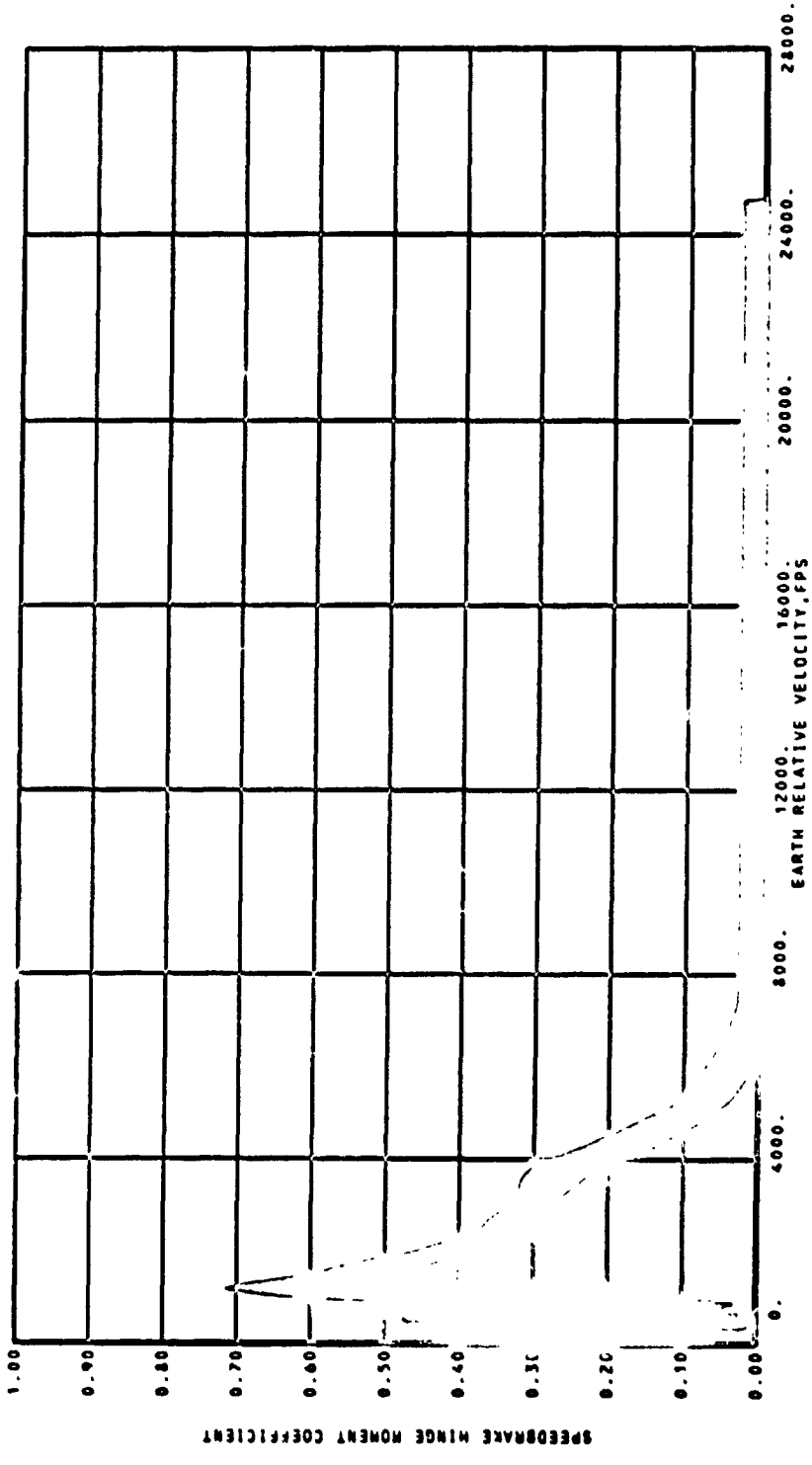

(q) Speedbrake hinge moment coefficient.

Figure 20.- Continued.

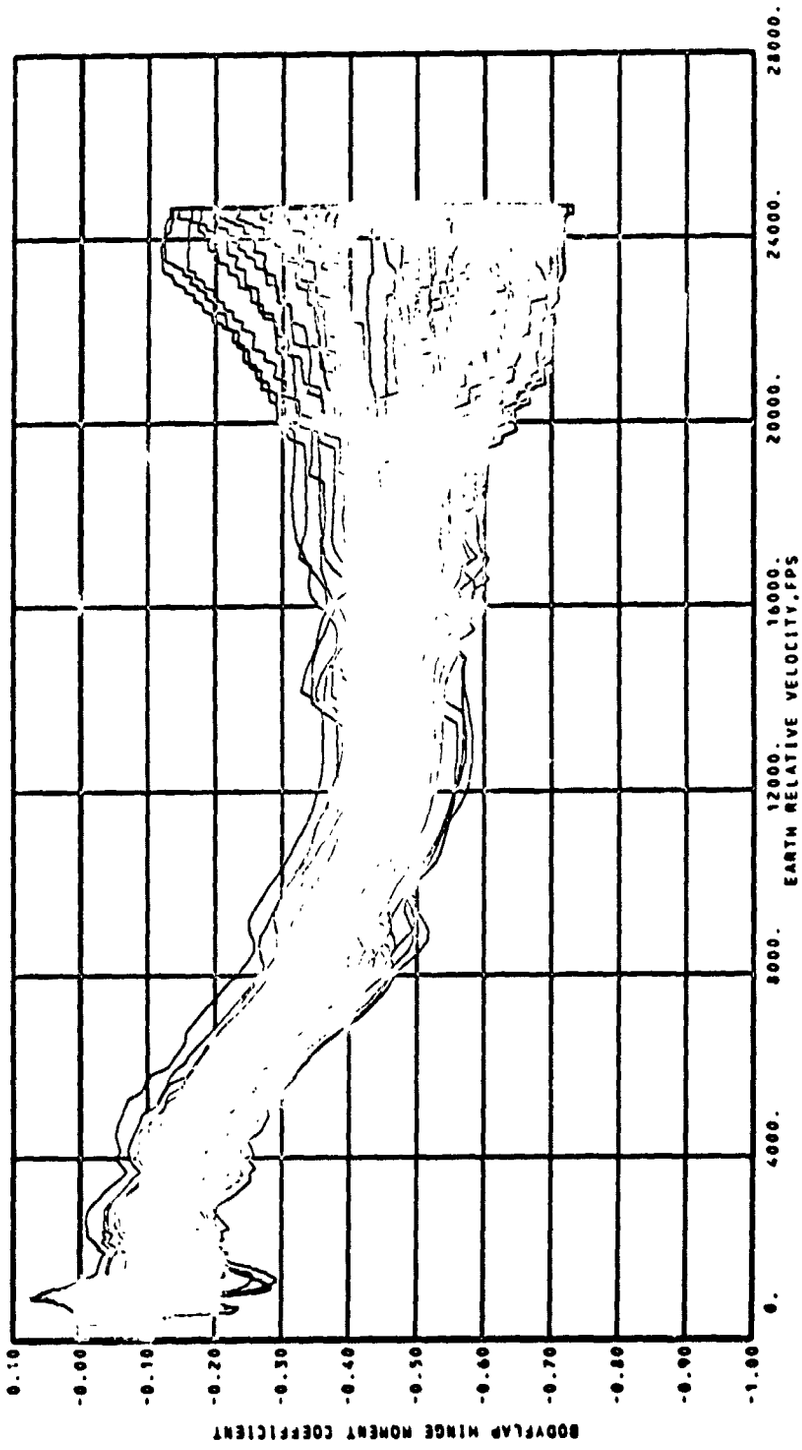

(r) Body flap hinge moment coefficient.

Figure 20.- Continued.

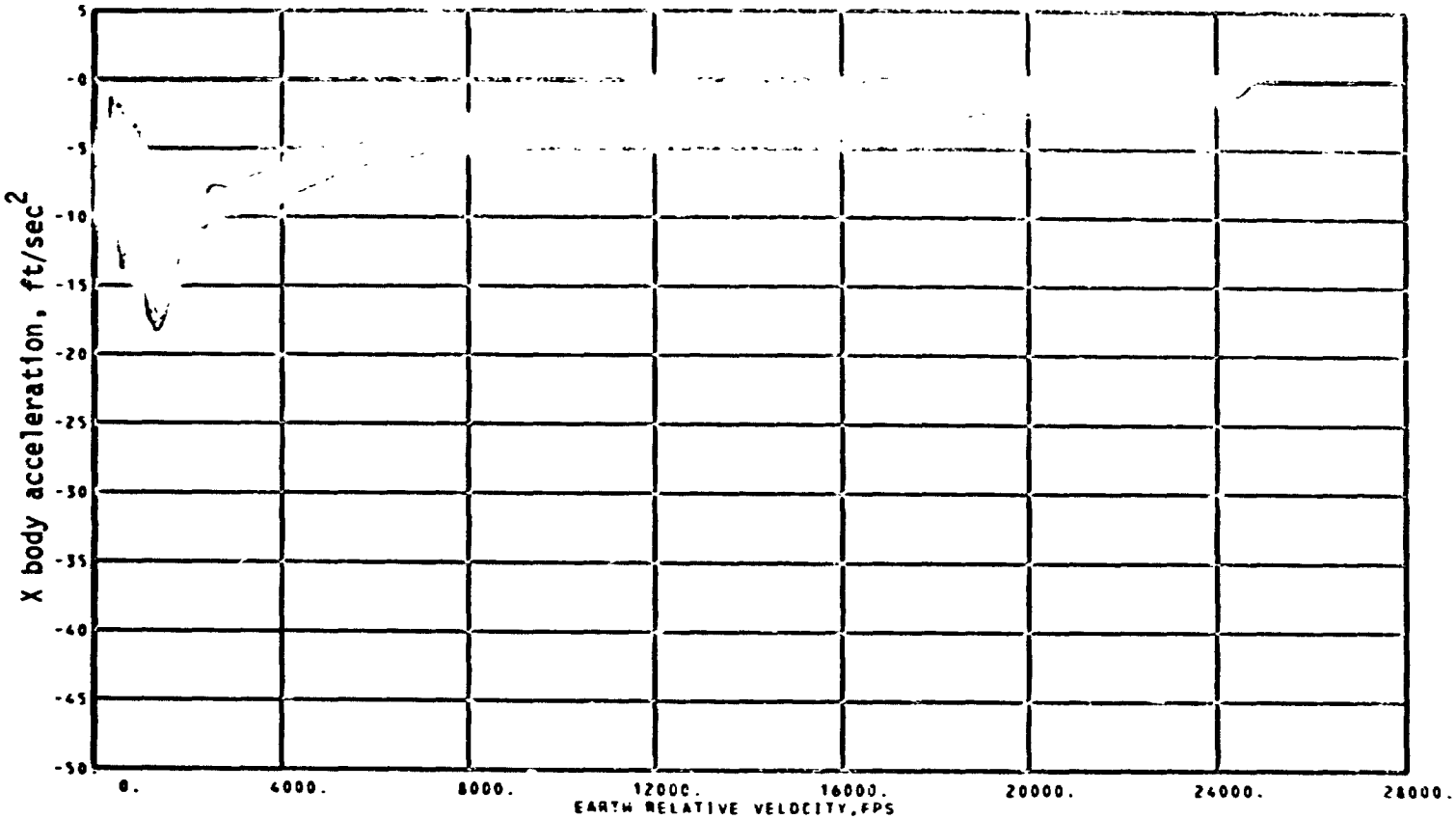

(s) X body acceleration.

Figure 20.- Continued.

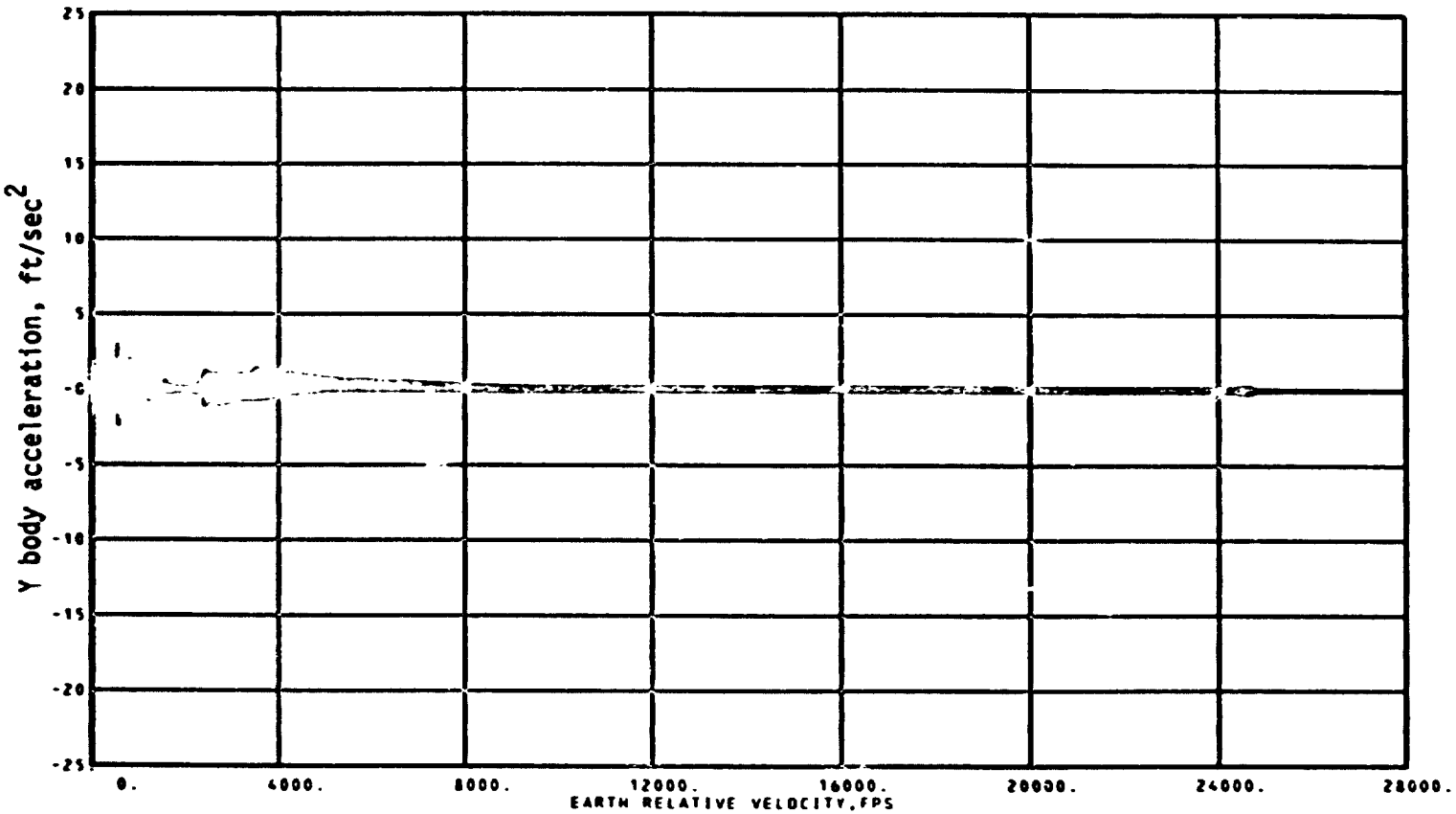

(t) Y body acceleration.

Figure 20.- Continued.

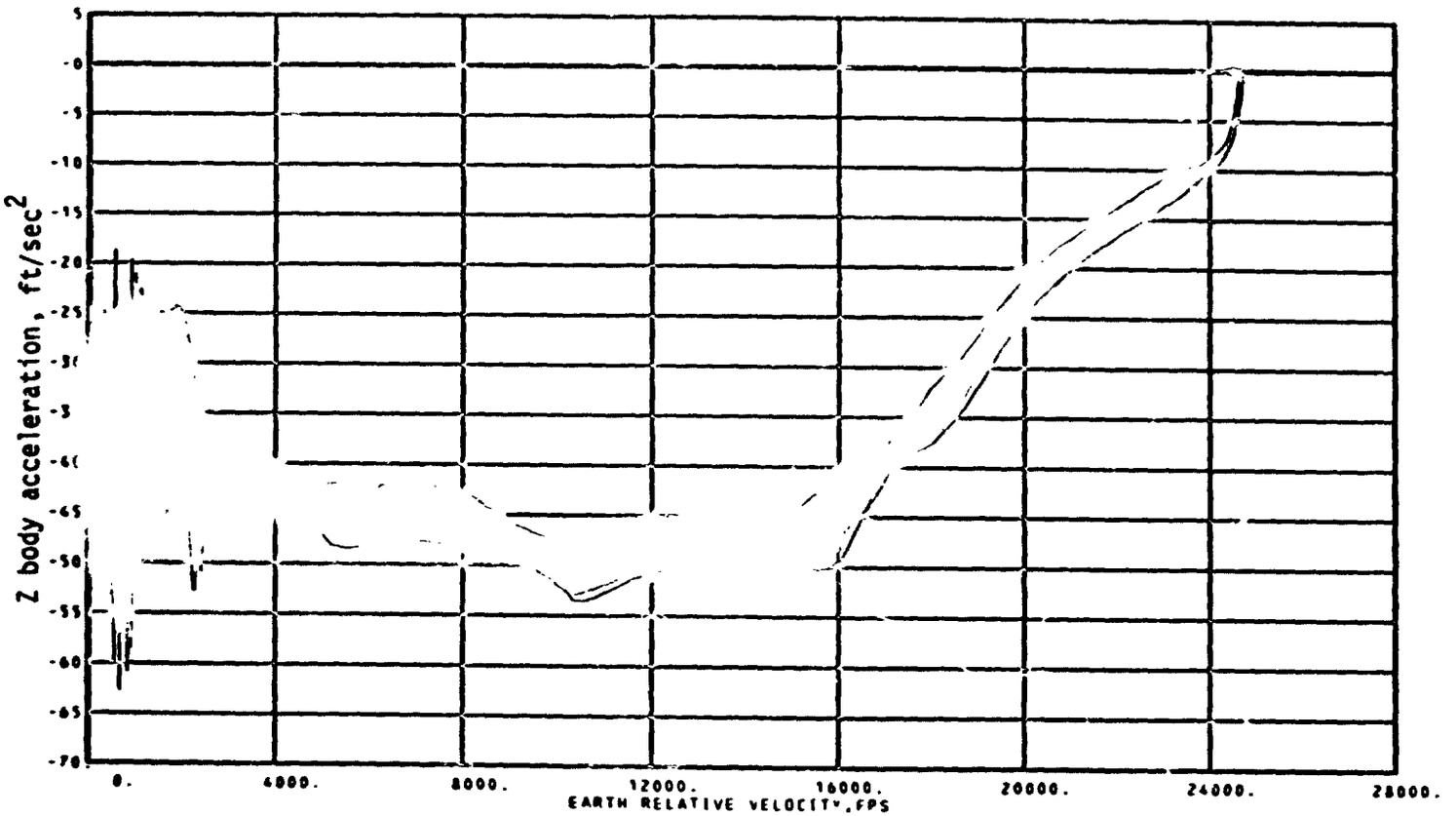

(u) Z body acceleration.

Figure 20.- Concluded.

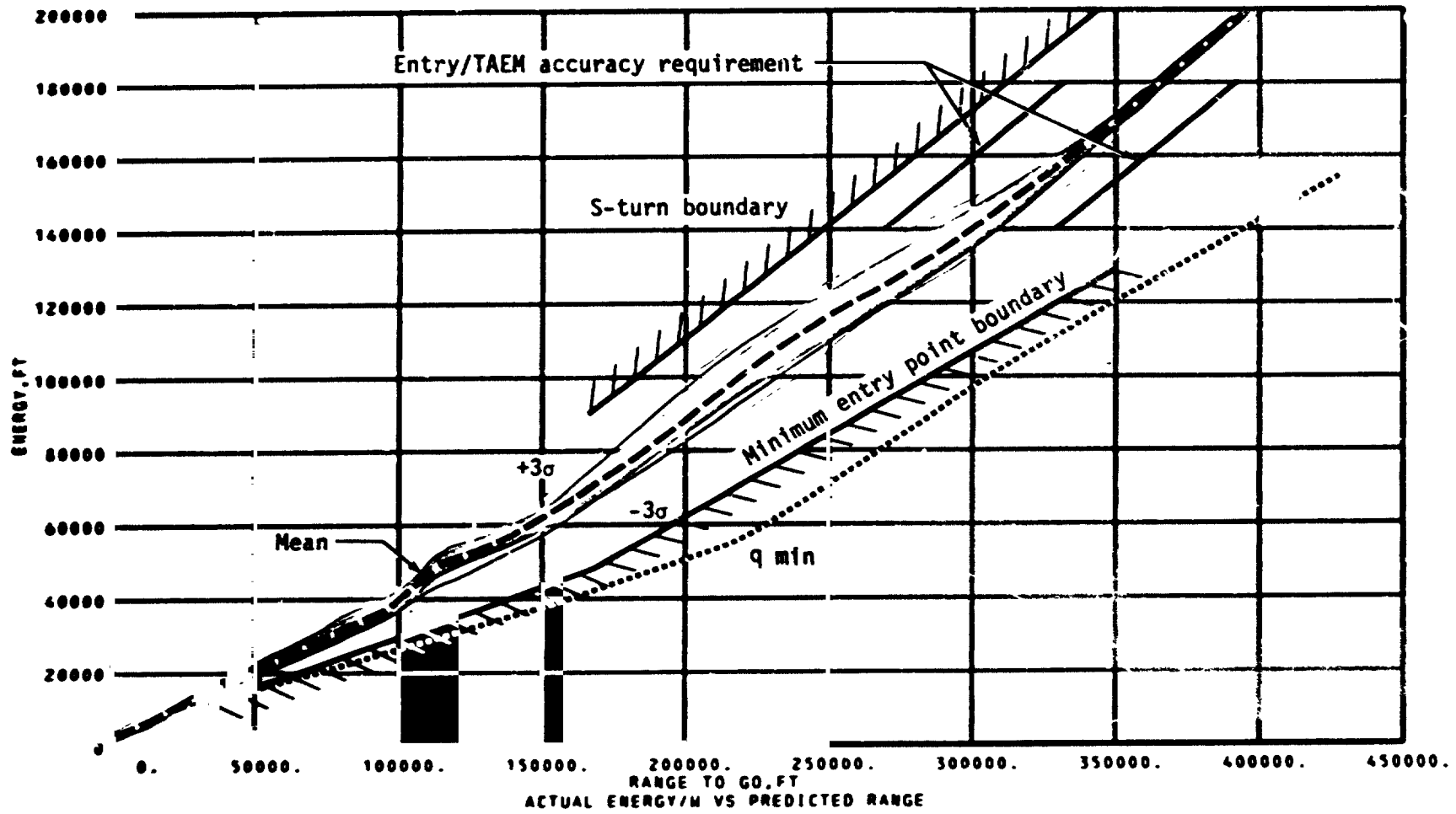

(a) Energy/weight.

Figure 21.- TAEM guidance performance parameter - steep abort once around.

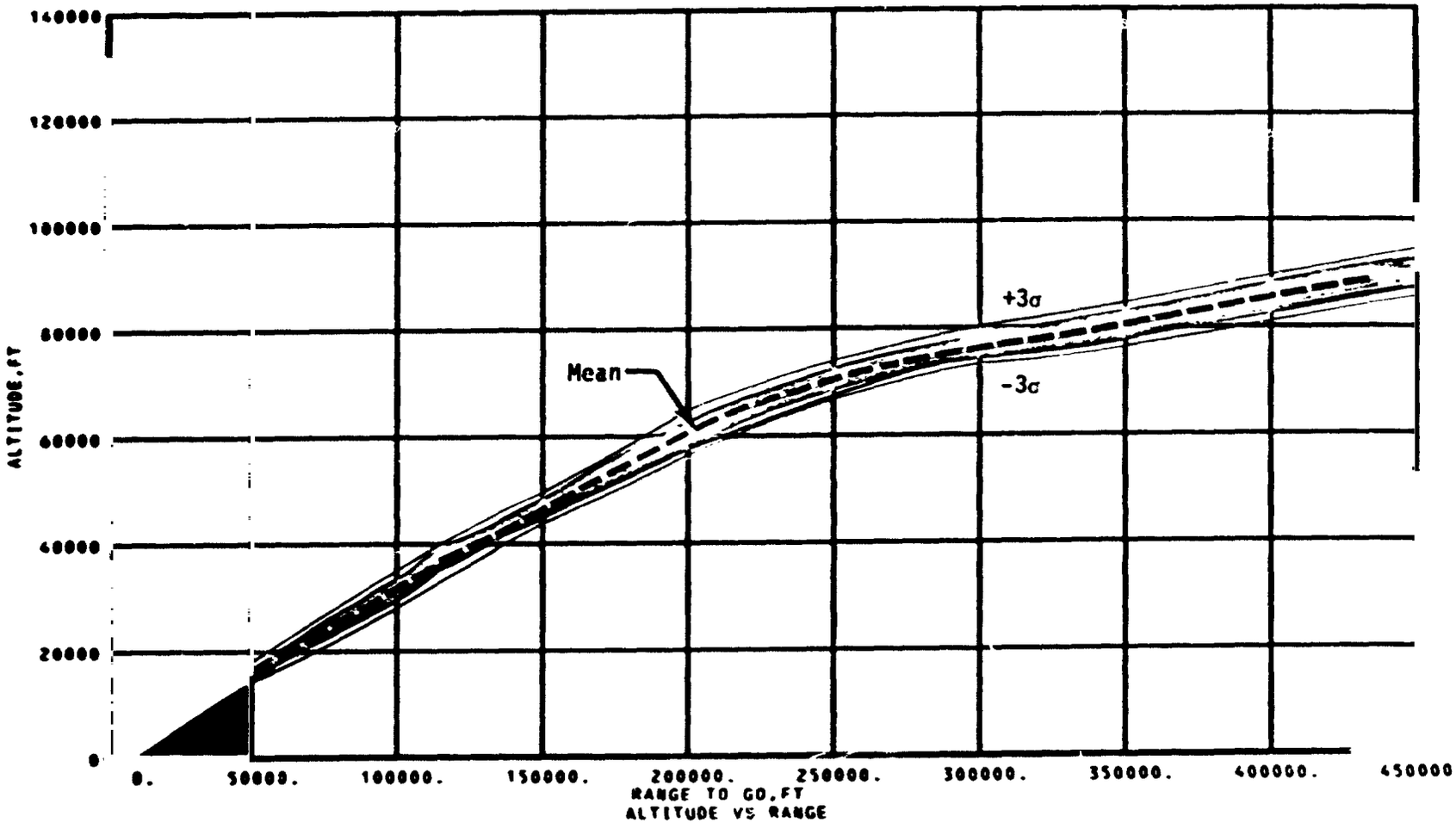

(b) Altitude.

Figure 21.- Continued.

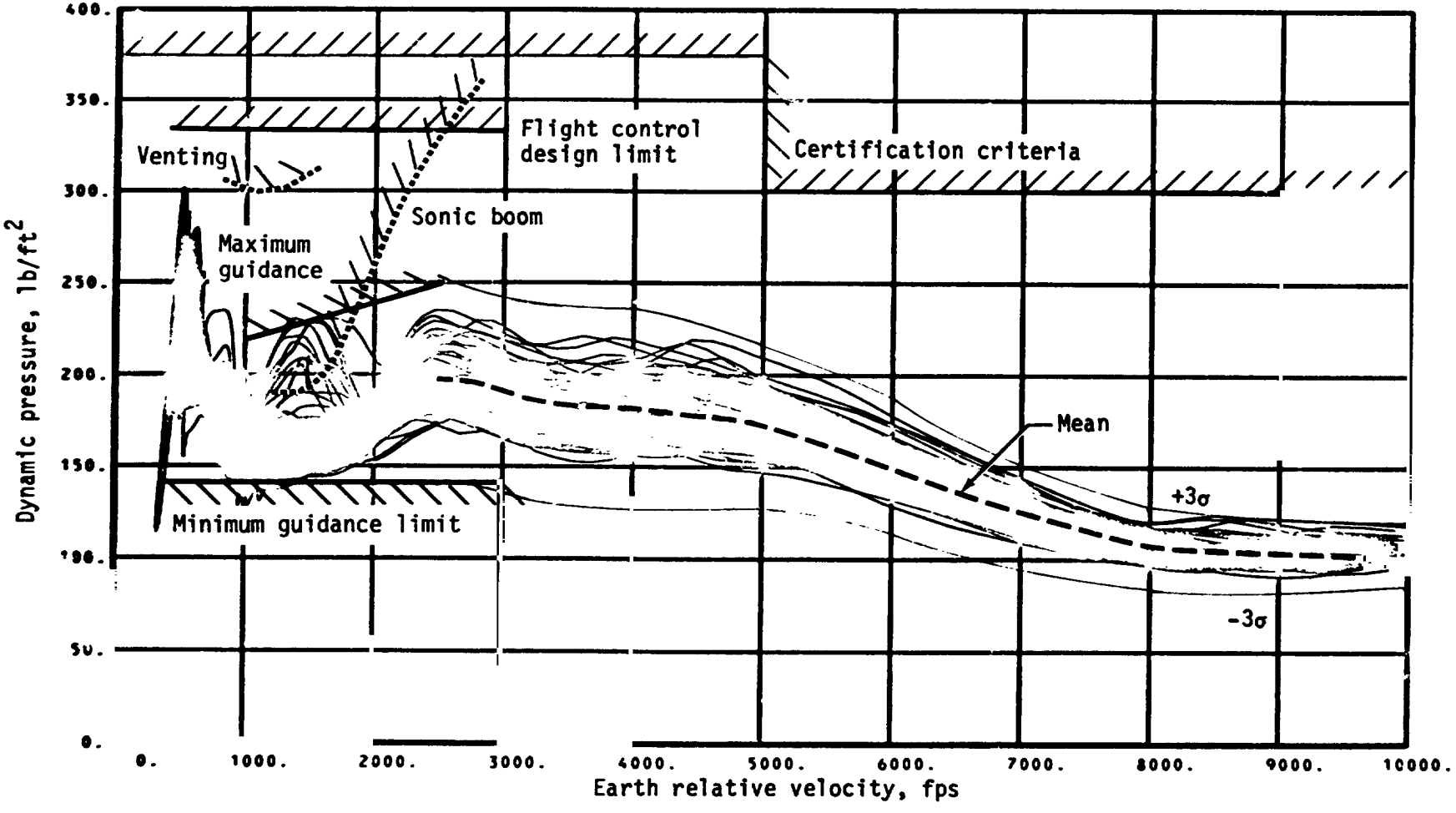

(c) Dynamic pressure.

Figure 21.- Continued.

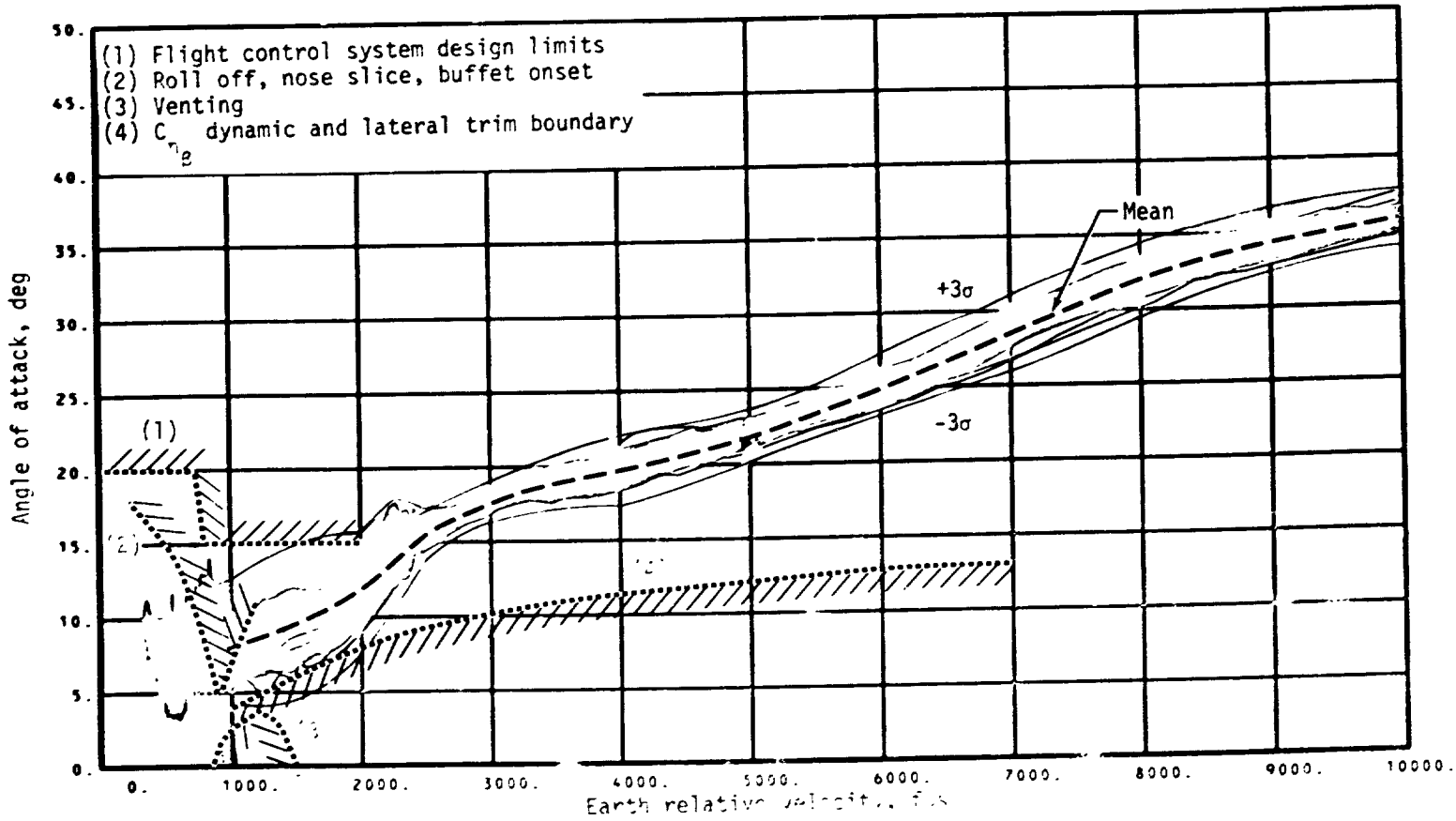

(b) Angle of attack.

Figure 21.- Continued.

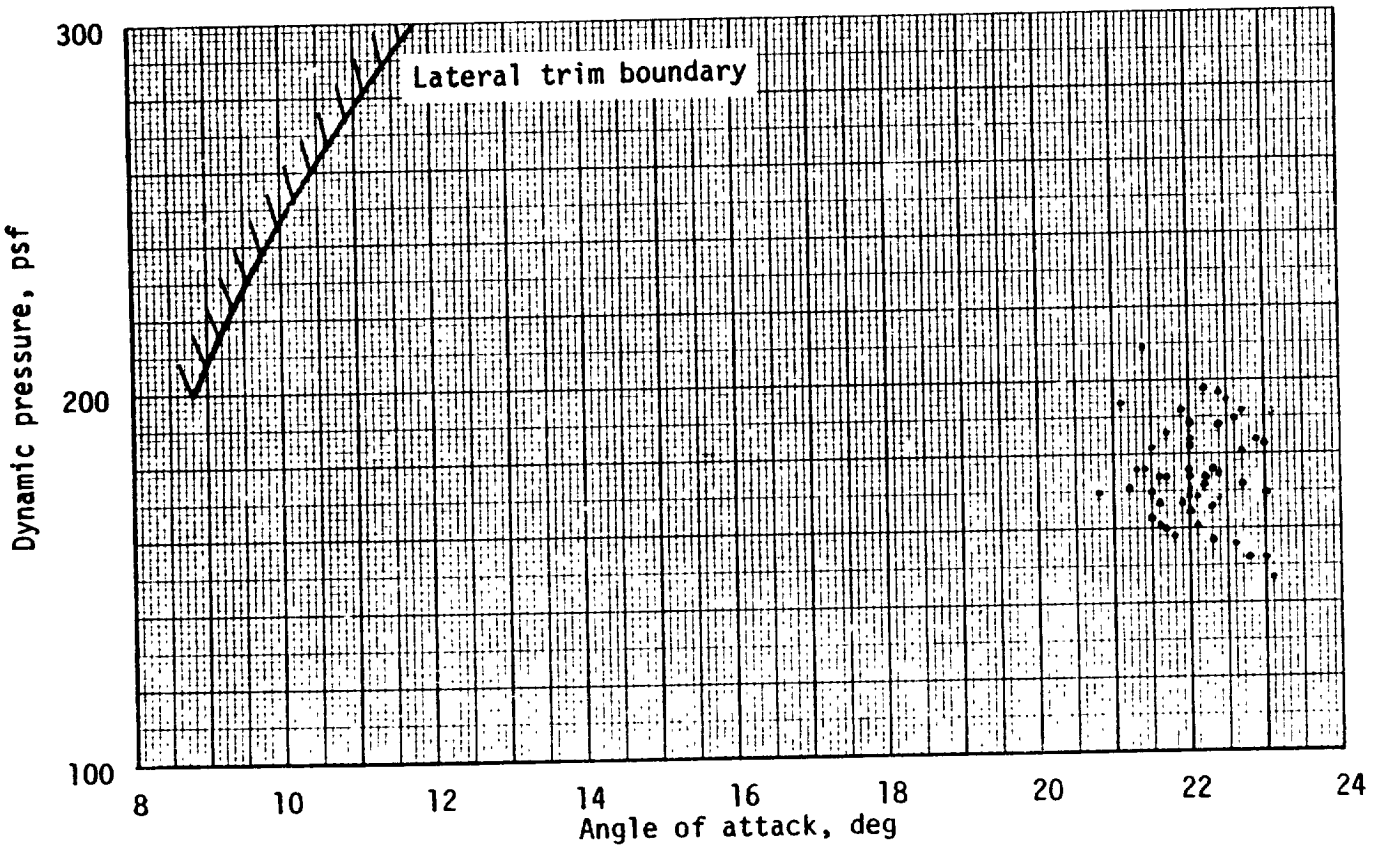

(e) Dynamic pressure - angle of attack scatter plot - Mach = 5.

Figure 21.- Continued.

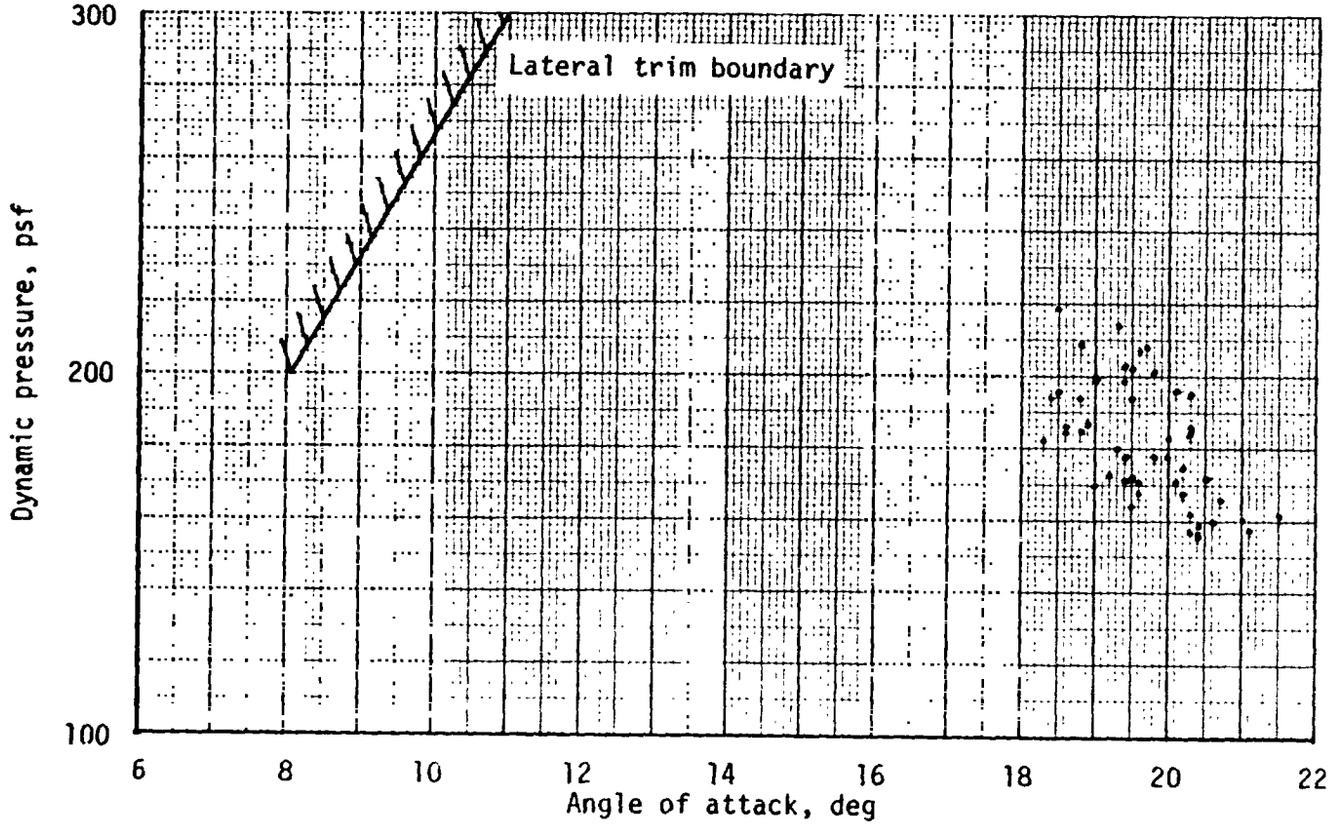

(f) Dynamic pressure - angle of attack scatter plot - Mach = 4.

Figure 21.- Continued.

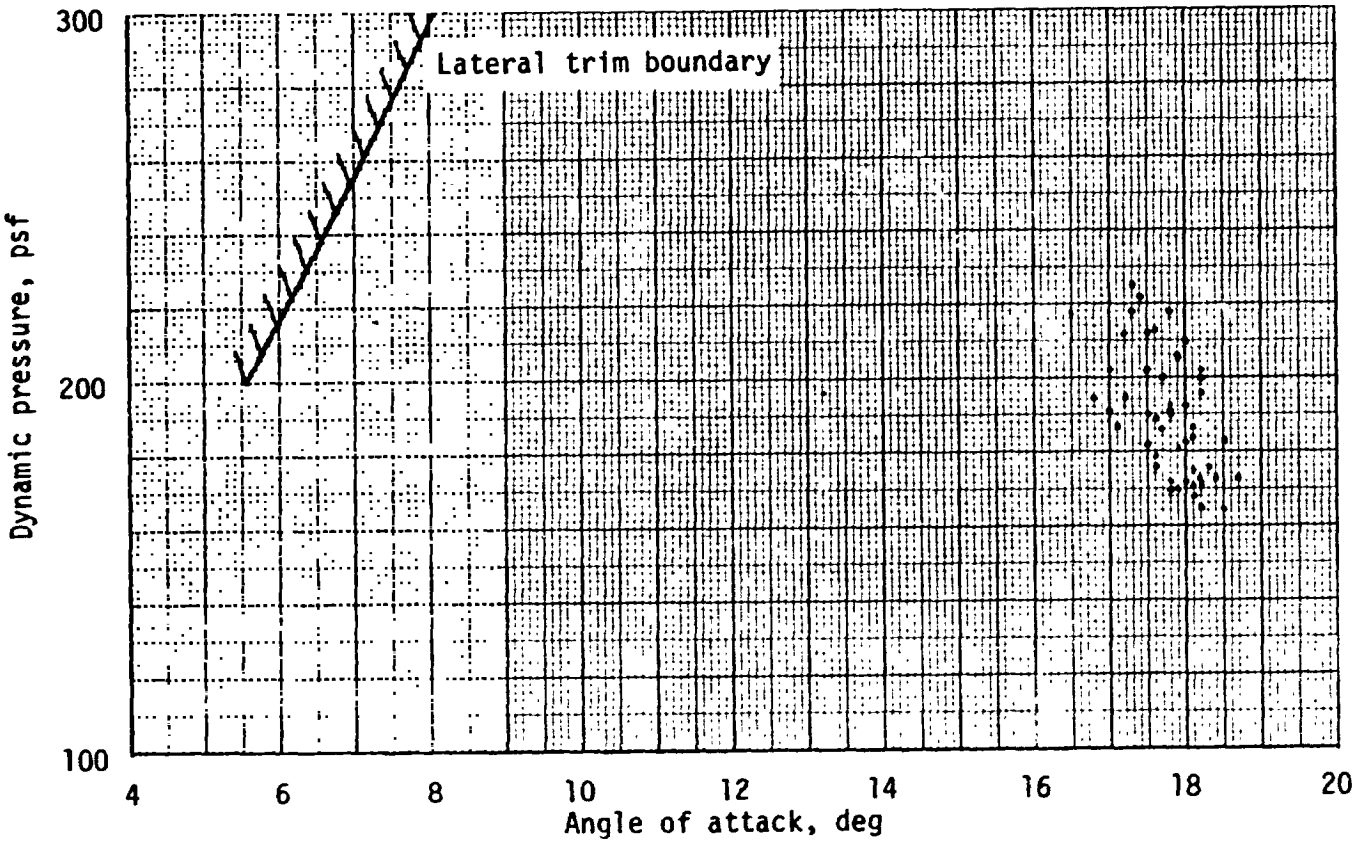

(g) Dynamic pressure - angle of attack scatter plot - Mach = 3.

Figure 21.- Continued.

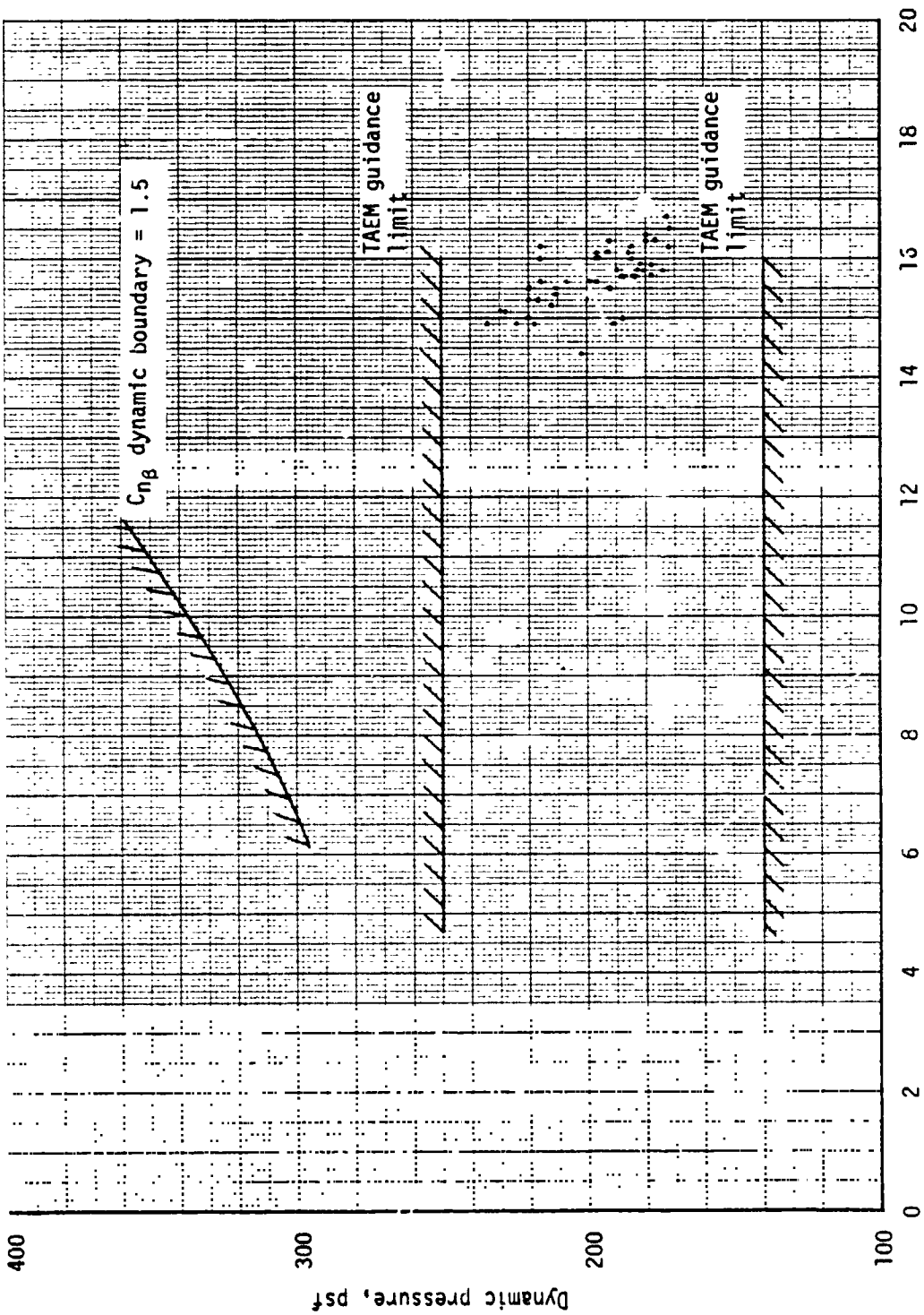

(h) Dynamic pressure - angle of attack scatter plot - Mach = 2.5.

Figure 21.- Continued.

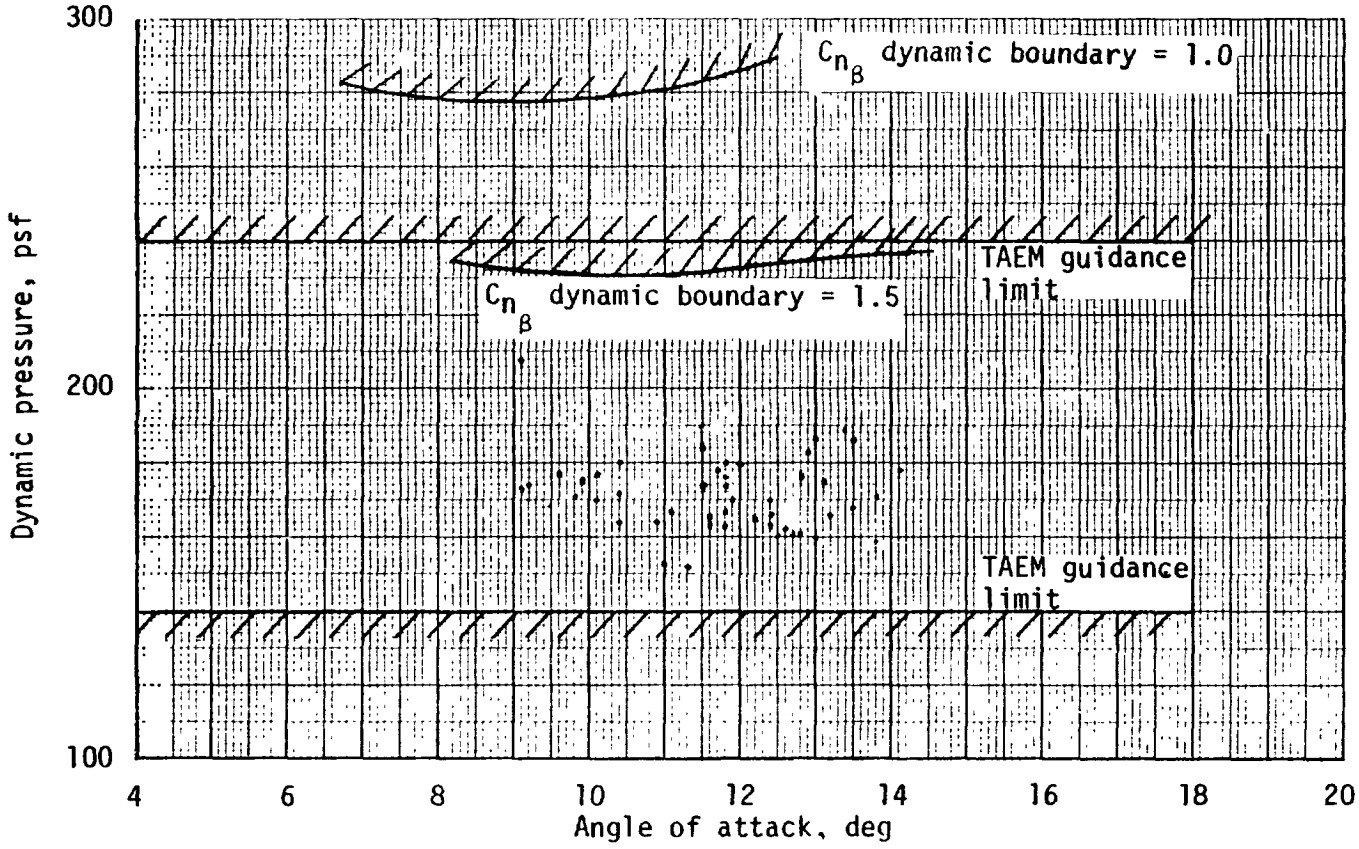

(i) Dynamic pressure - angle of attack scatter plot - Mach = 2.

Figure 21.- Continued.

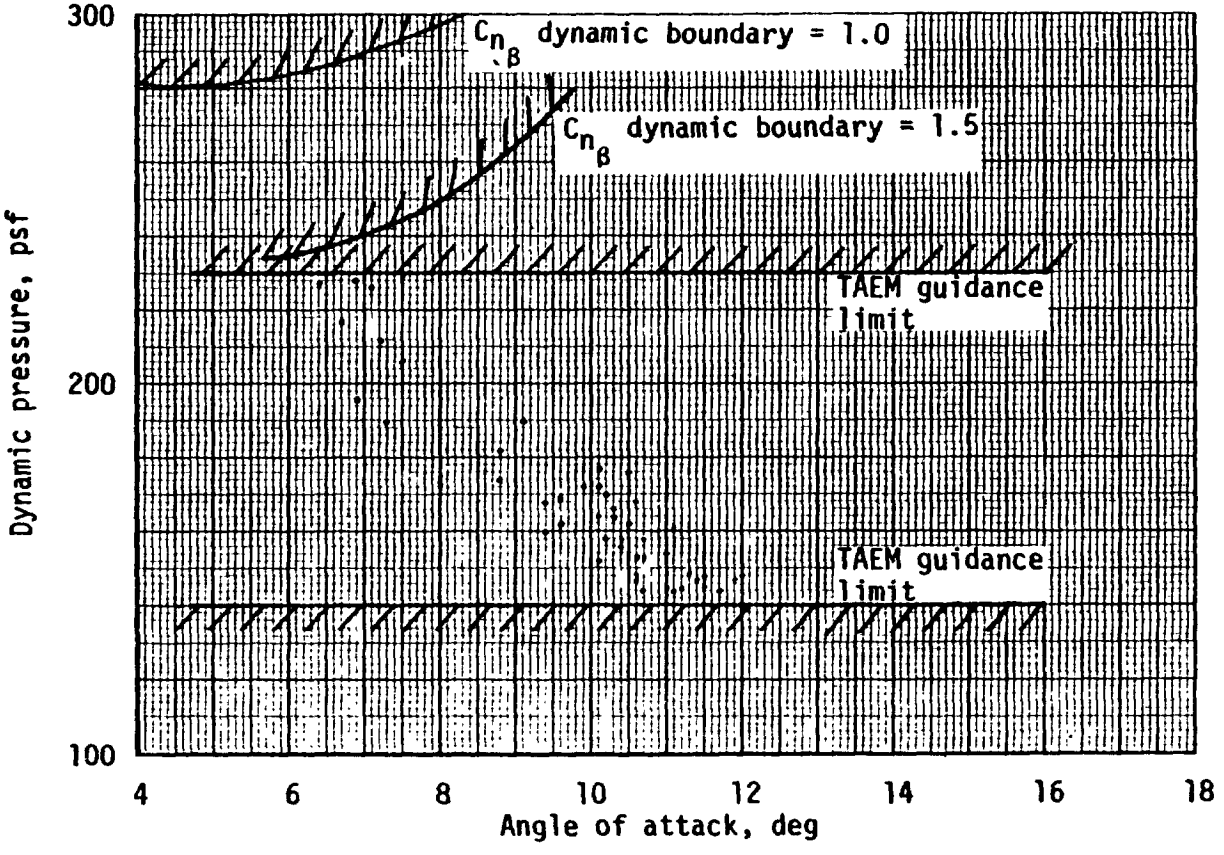

(j) Dynamic pressure - angle of attack scatter plot - Mach = 1.5.

Figure 21.- Continued.

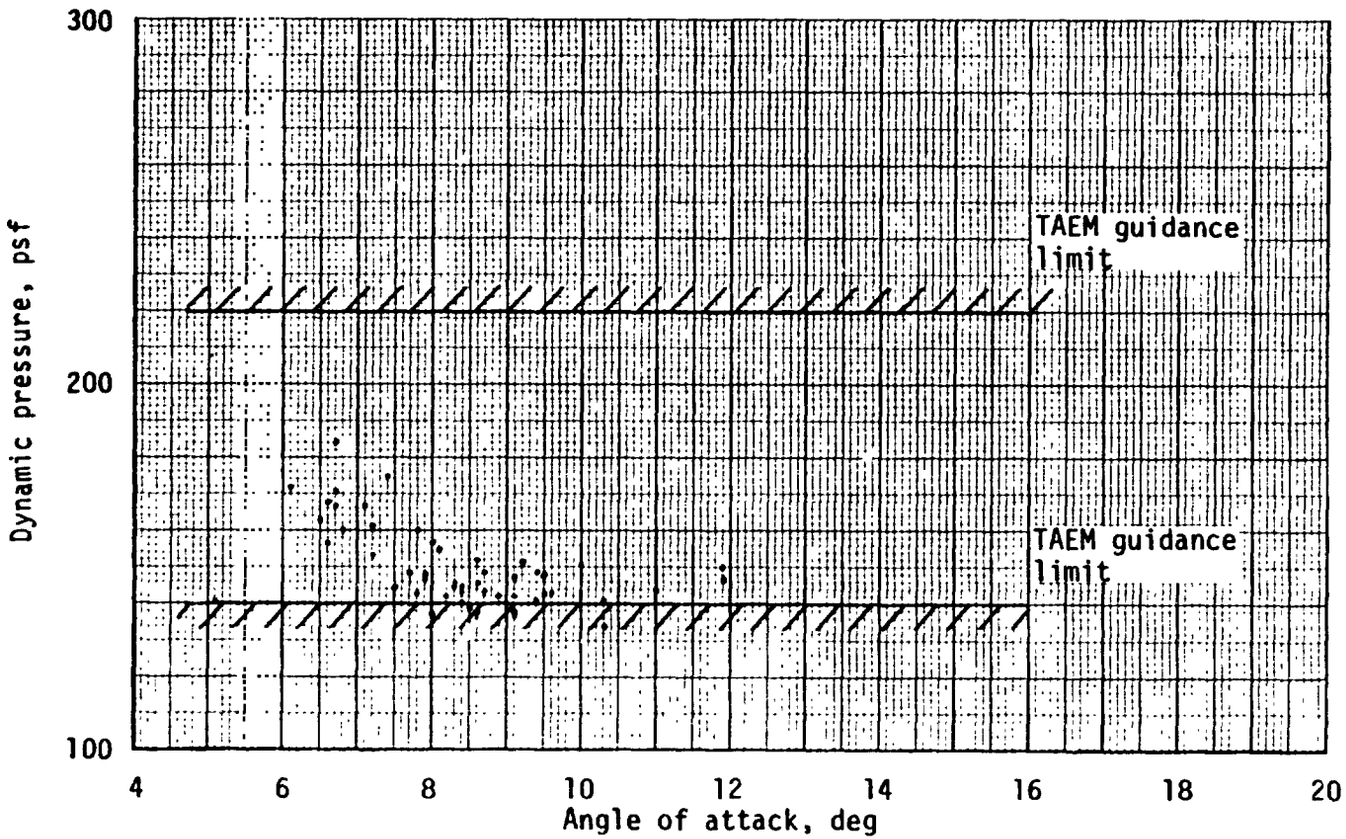

(k) Dynamic pressure - angle of attack scatter plot - Mach = 1.

Figure 21.- Continued.

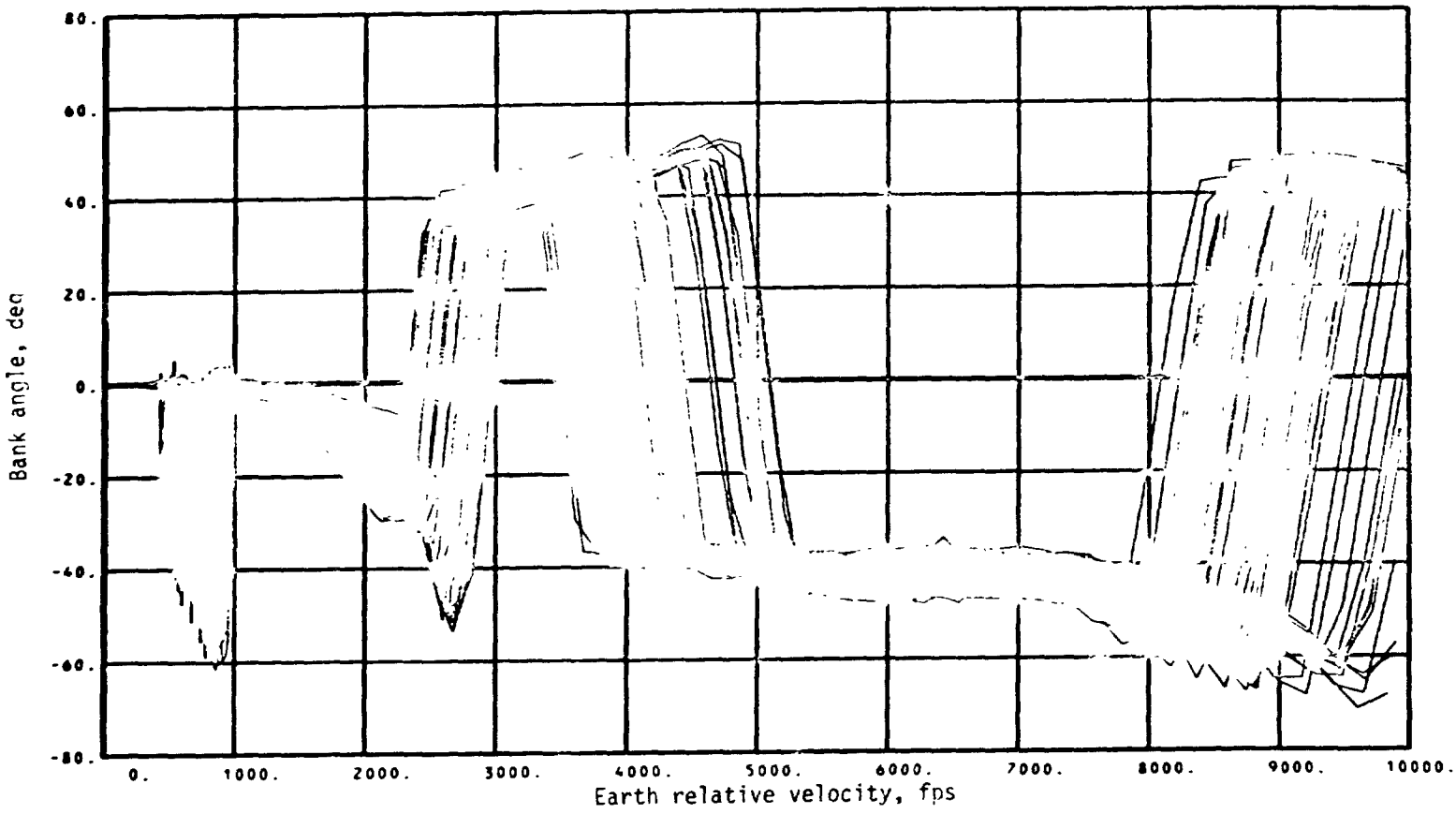

(1) Bank angle.

Figure 21.- Continued.

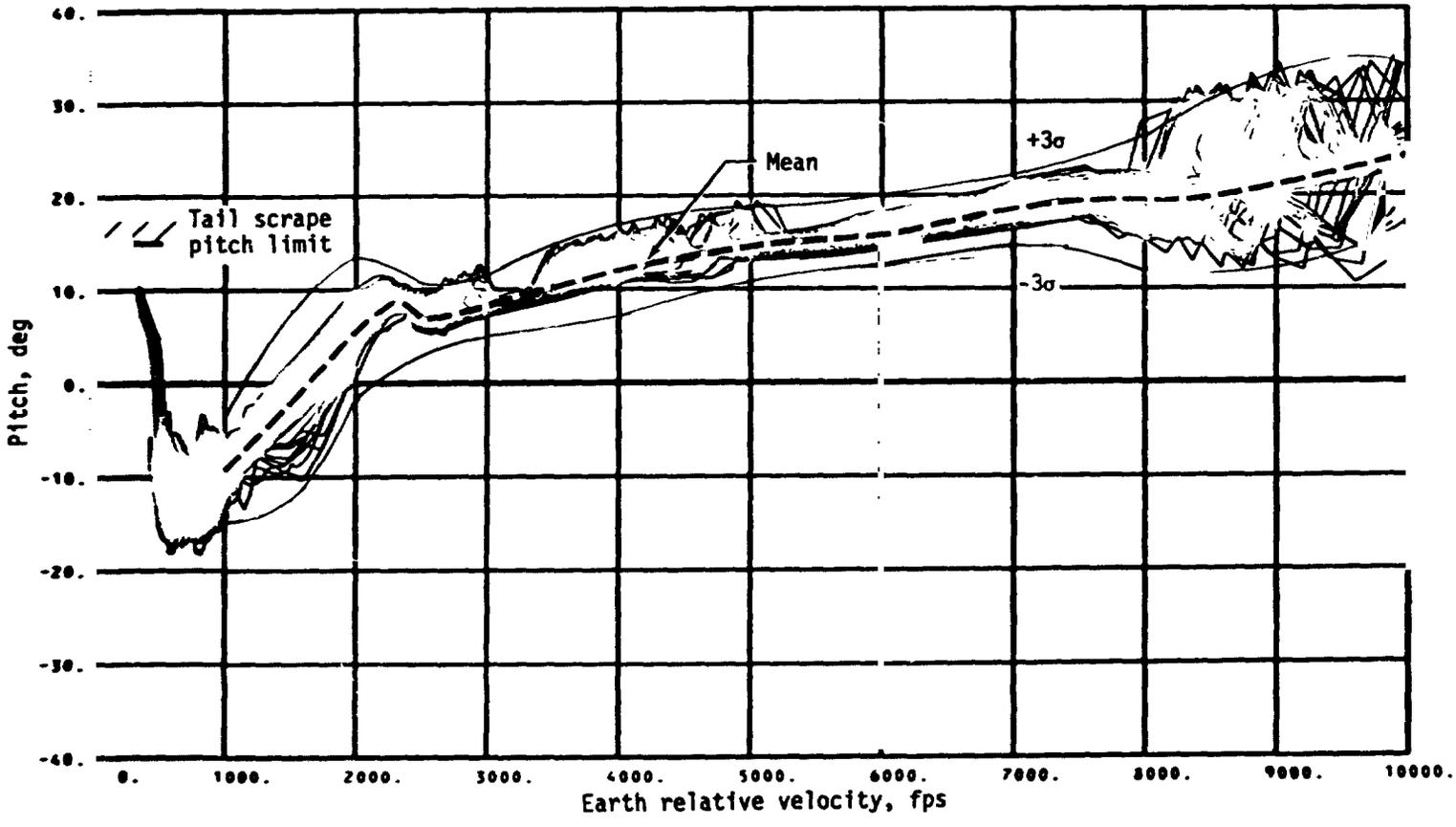

(m) Pitch angle.

Figure 21.- Continued.

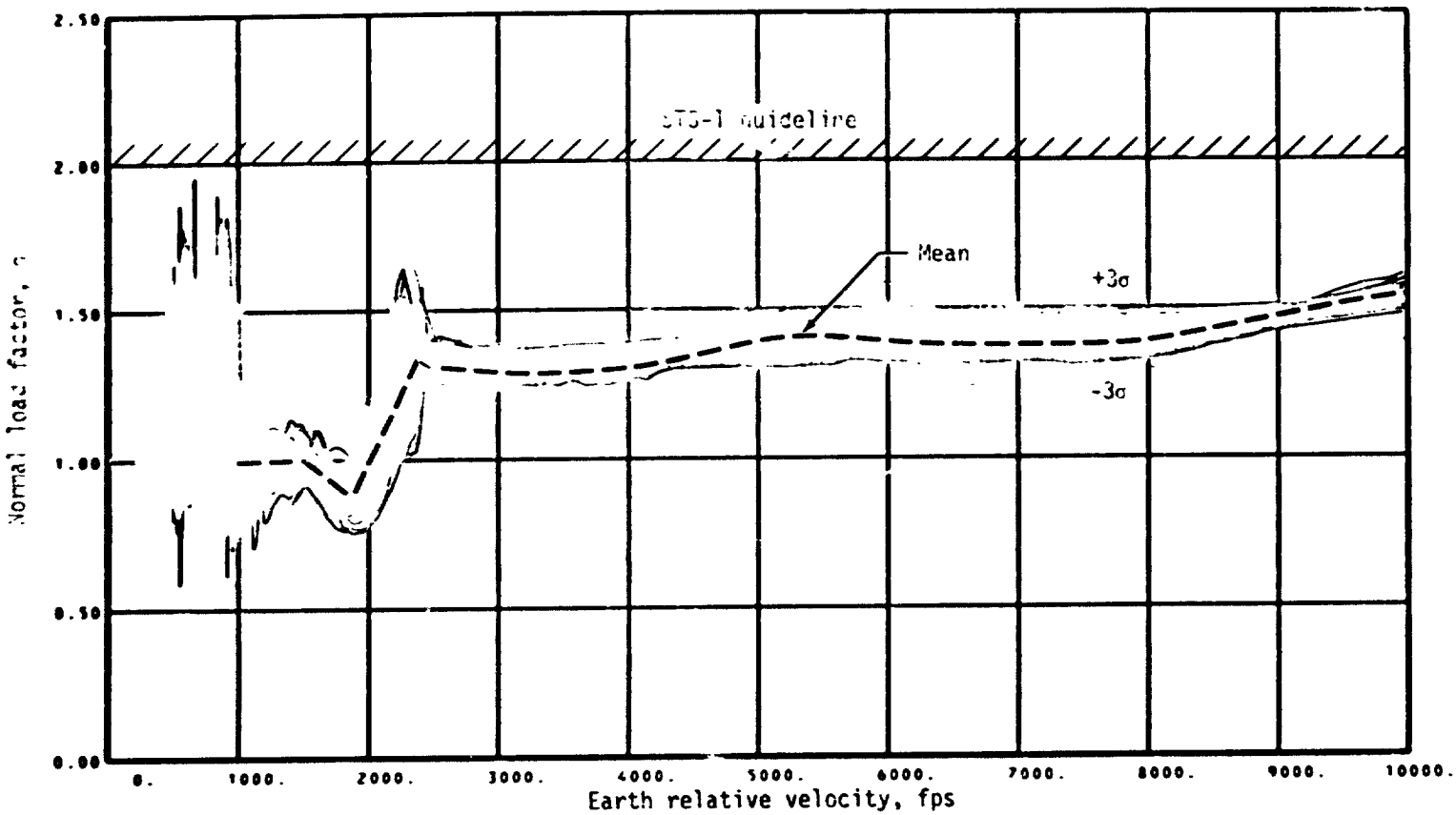

(n) Normal load factor.

Figure 21.- Continued.

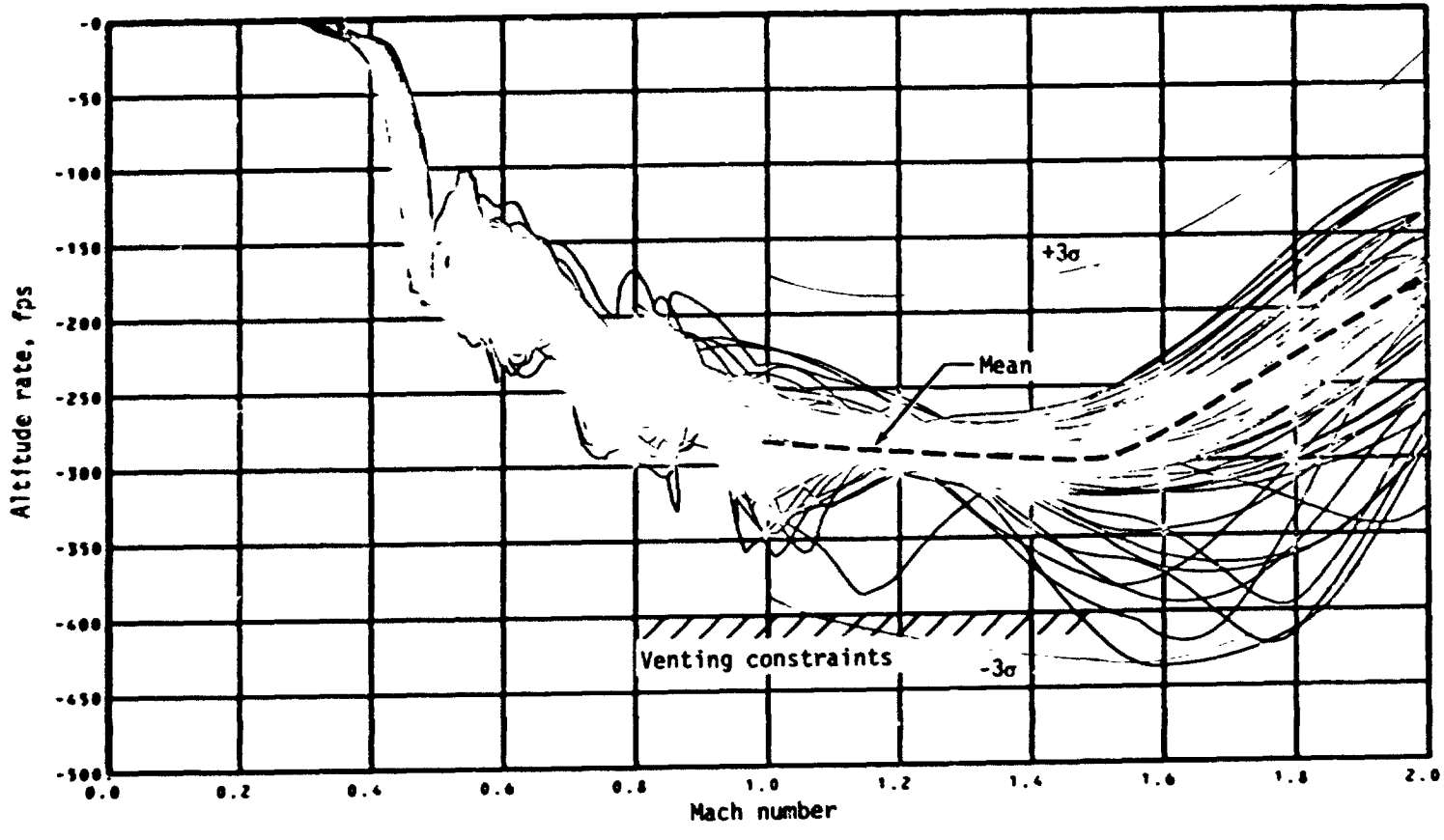

(o) Altitude rate.

Figure 21.- Concluded.

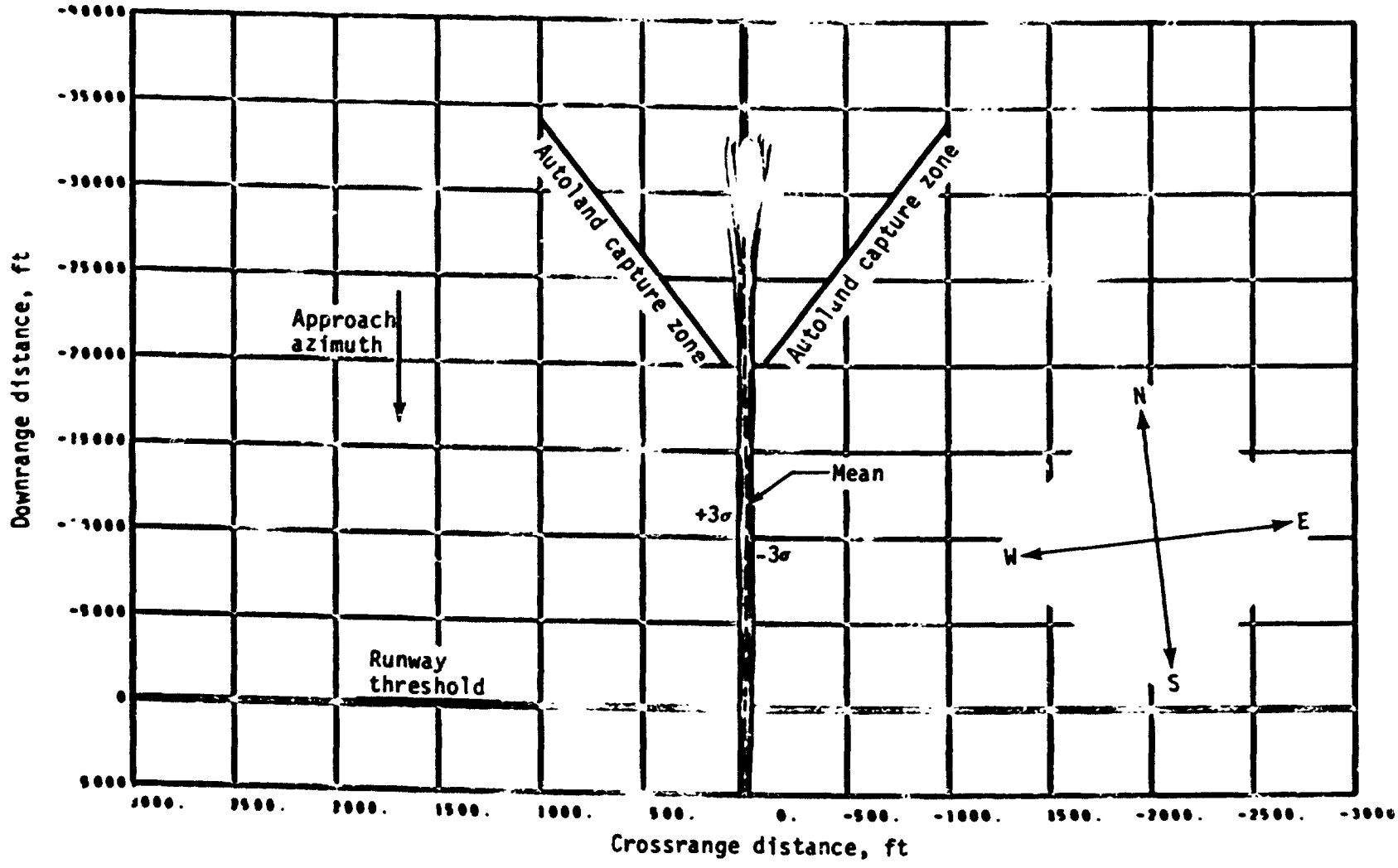

(a) Groundtrack.

Figure 22.- Autoland guidance performance parameters - abort once around.

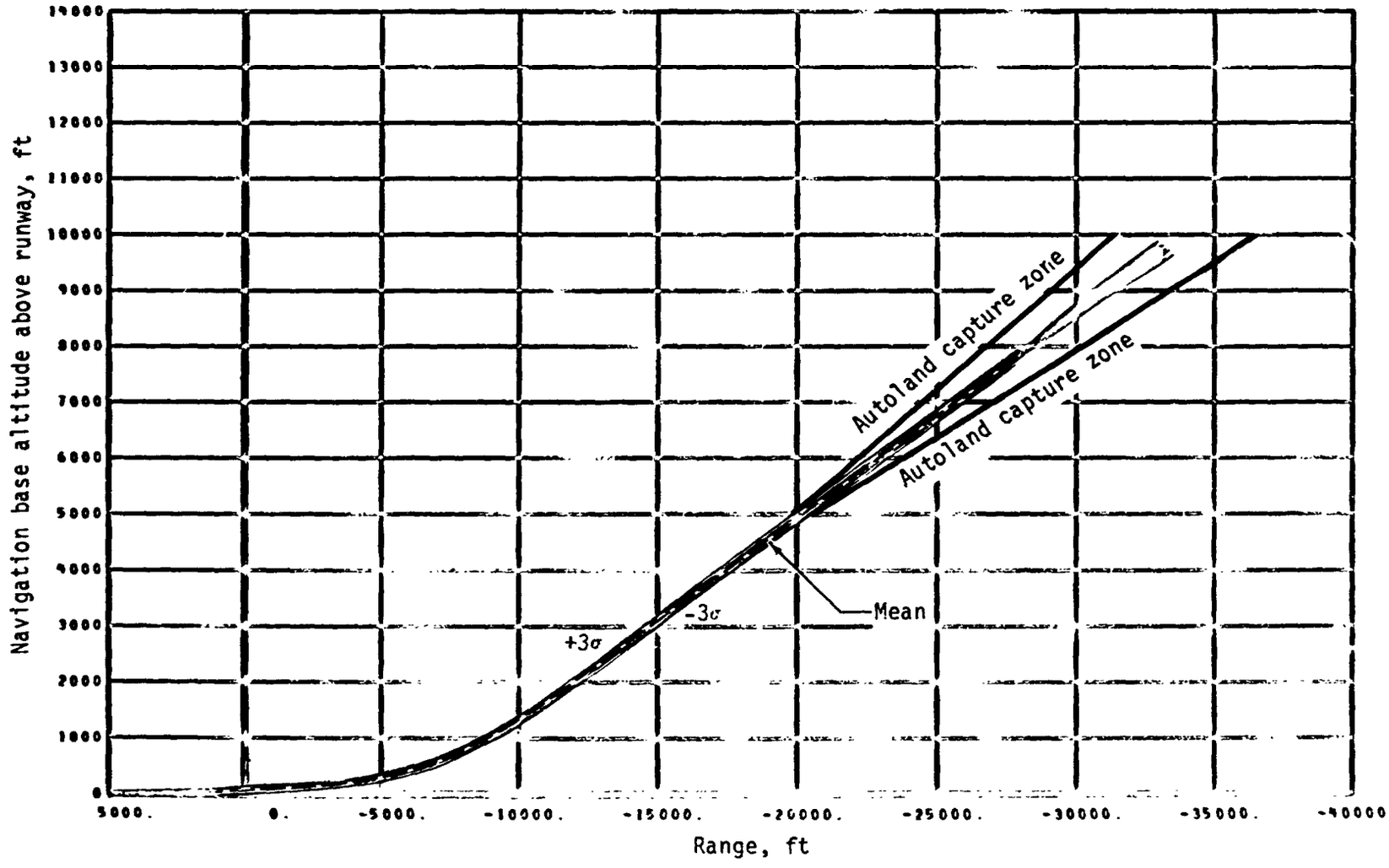

(b) Navigation base altitude (10 000 feet to landing).

Figure 22.- Continued.

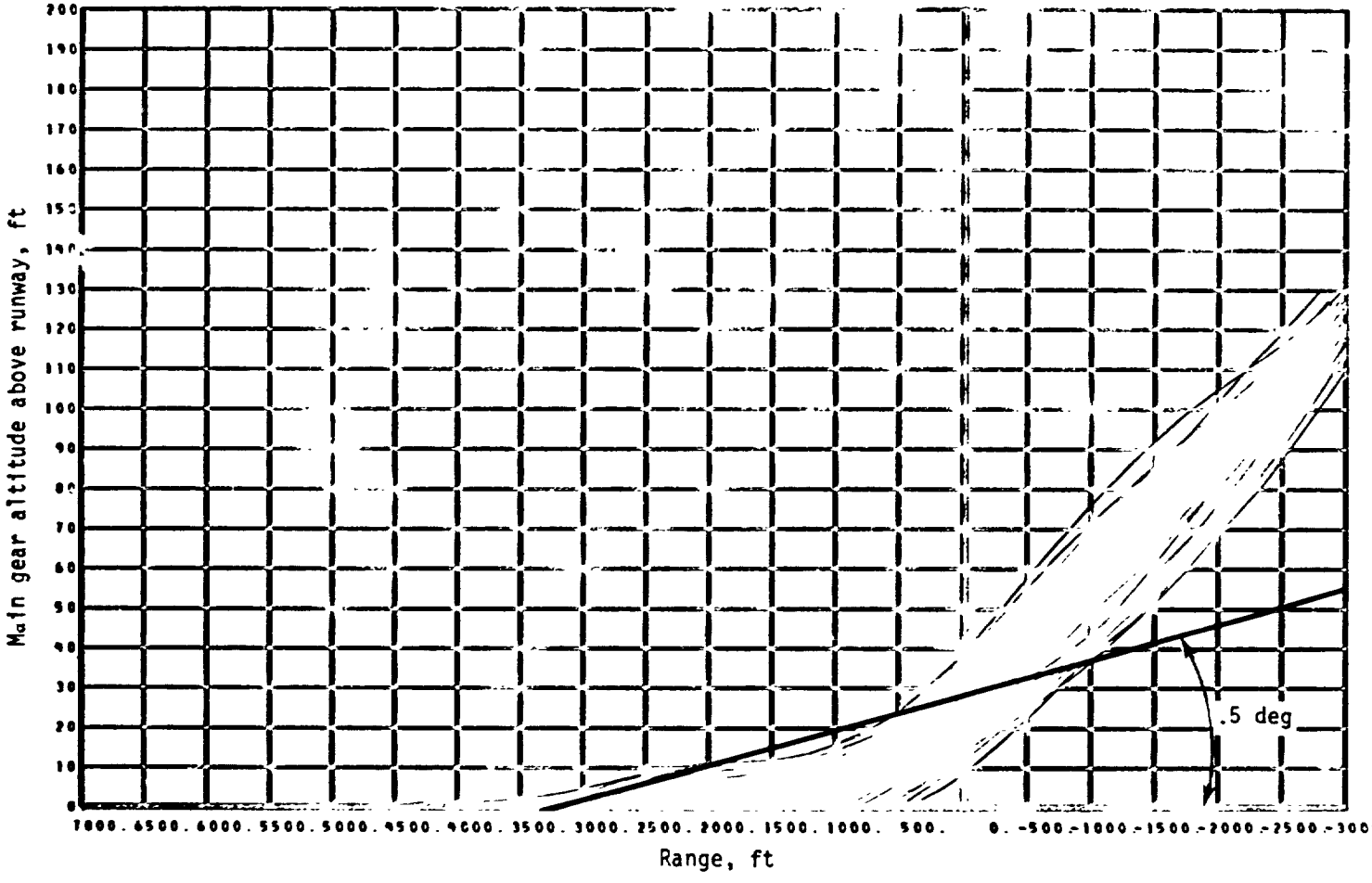

(c) Main gear altitude (200 feet to landing).

Figure 22.- Continued.

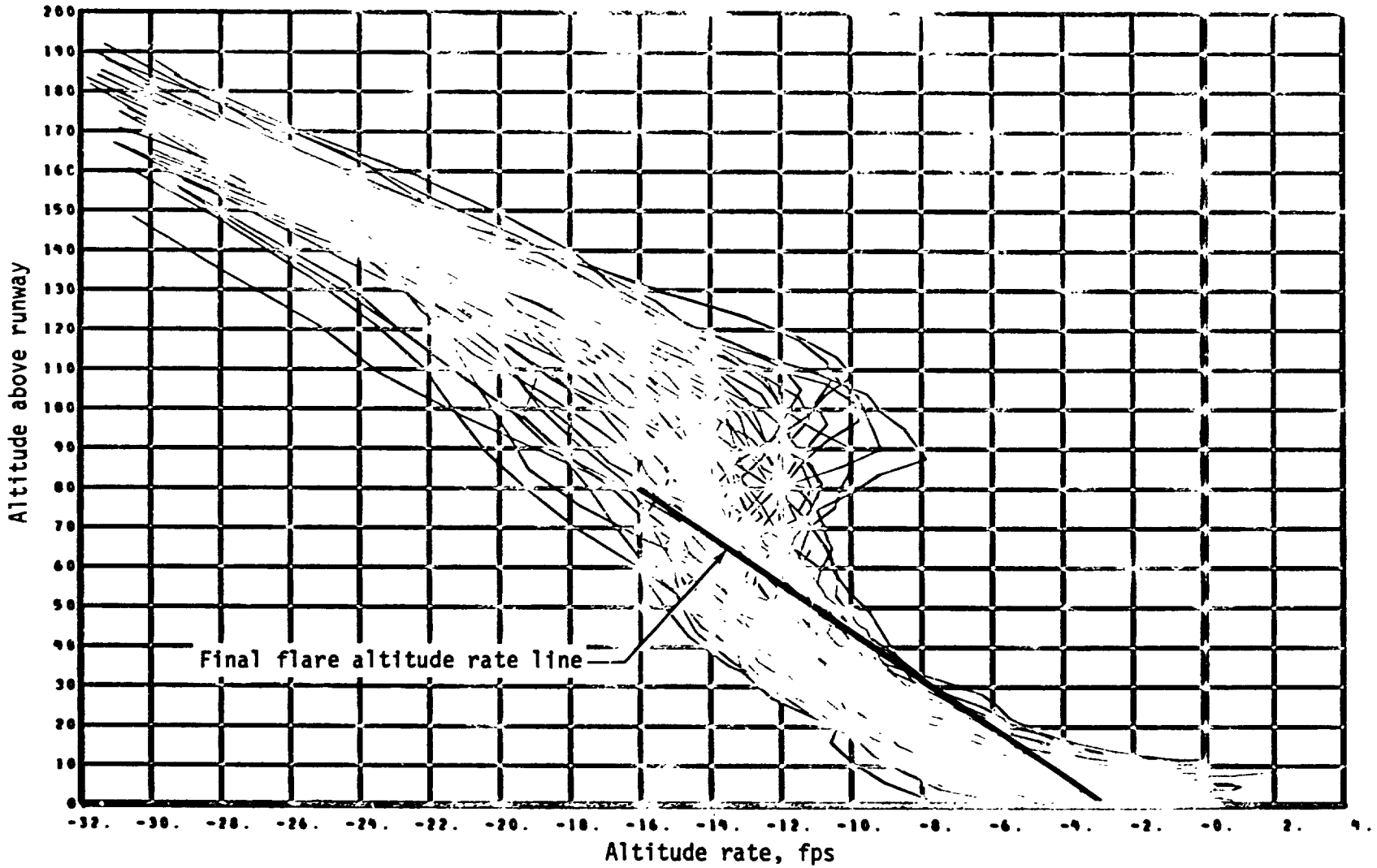

(d) Final flare altitude and altitude rate.

Figure 22.- Continued.

(e) Altitude rate errors.

Figure 22.- Continued.

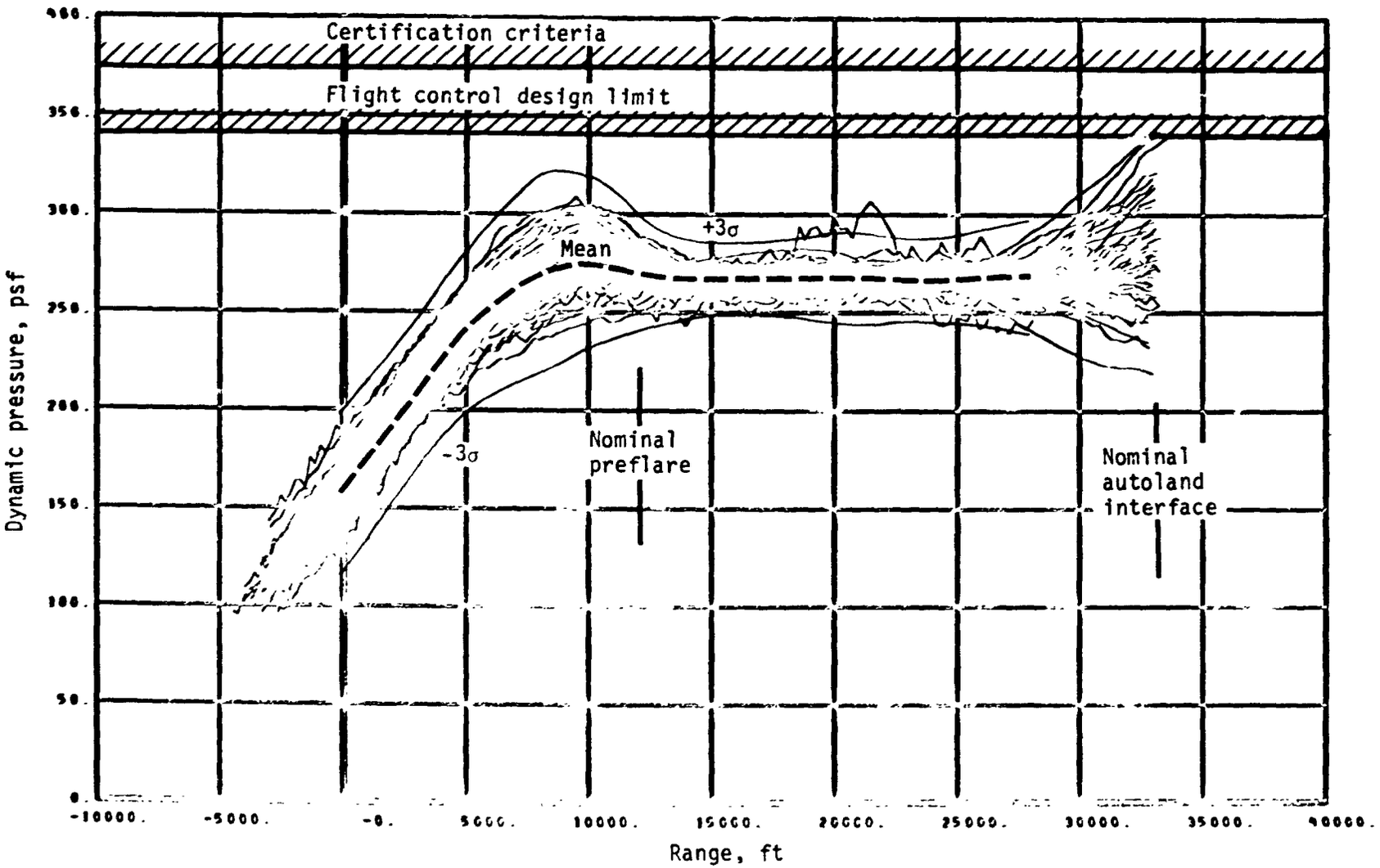

(f) Dynamic pressure.

Figure 22.- Continued.

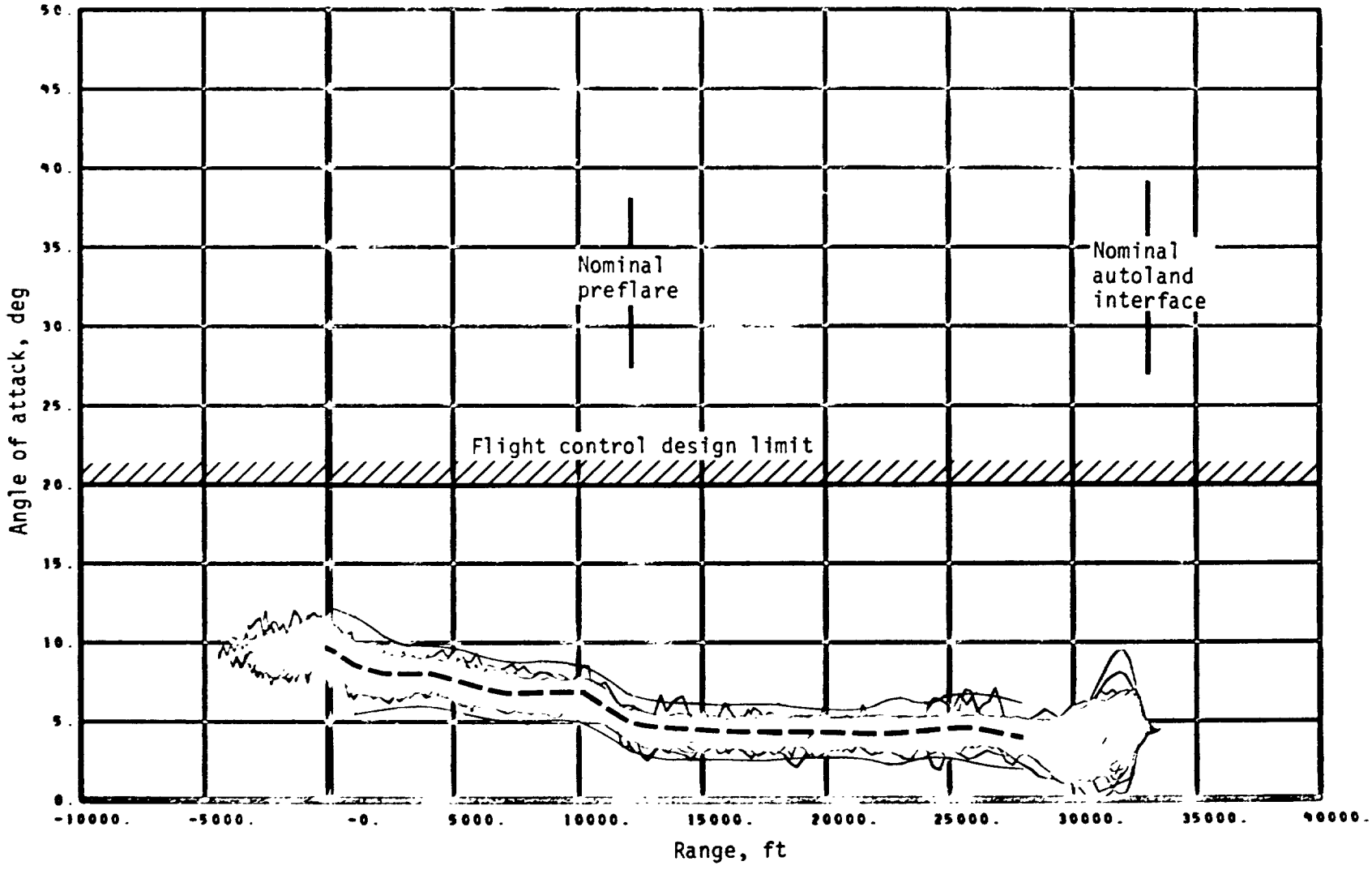

(g) Angle of attack.

Figure 22.- Continued.

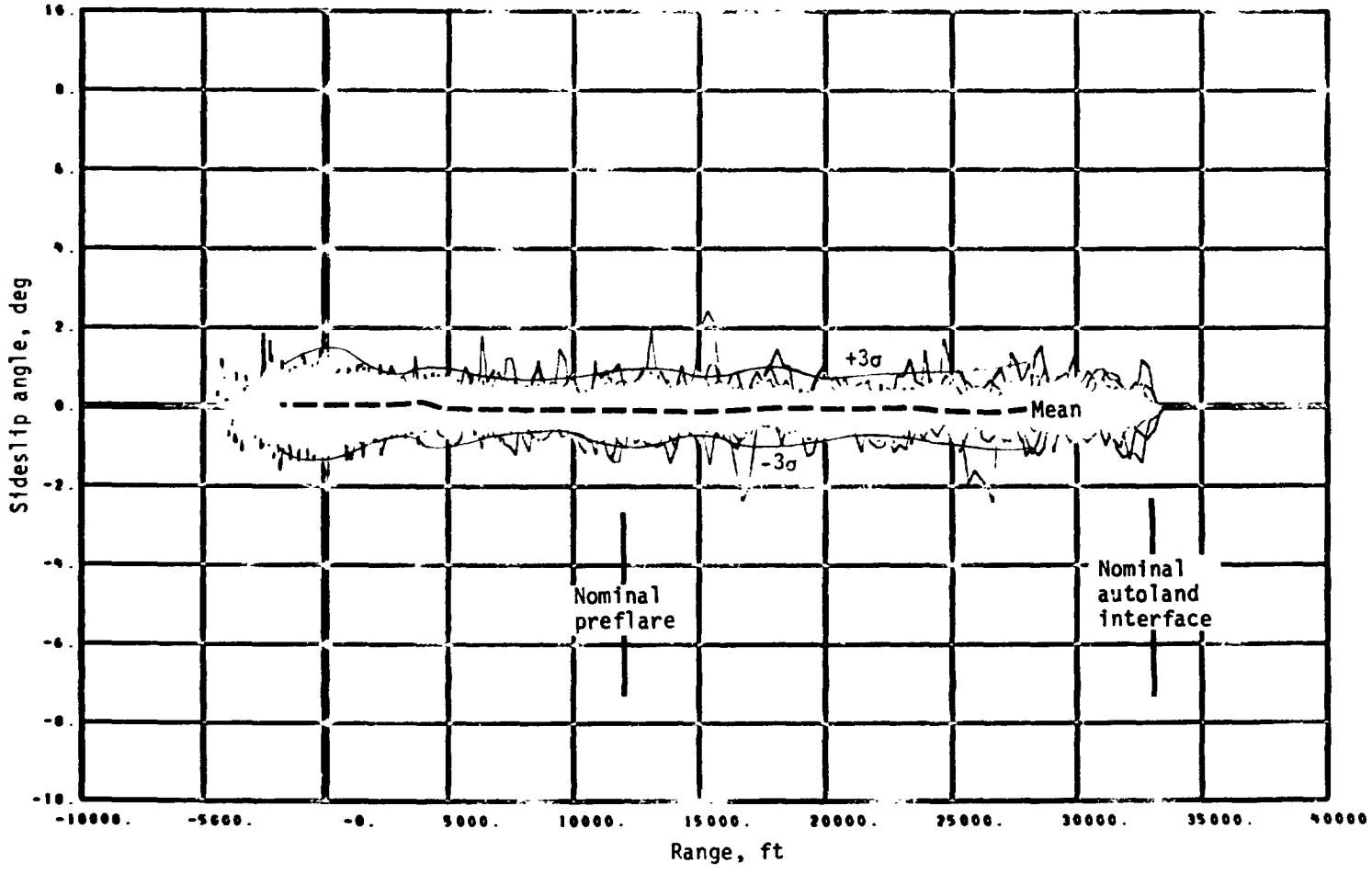

(h) Sideslip angle.

Figure 22.- Continued.

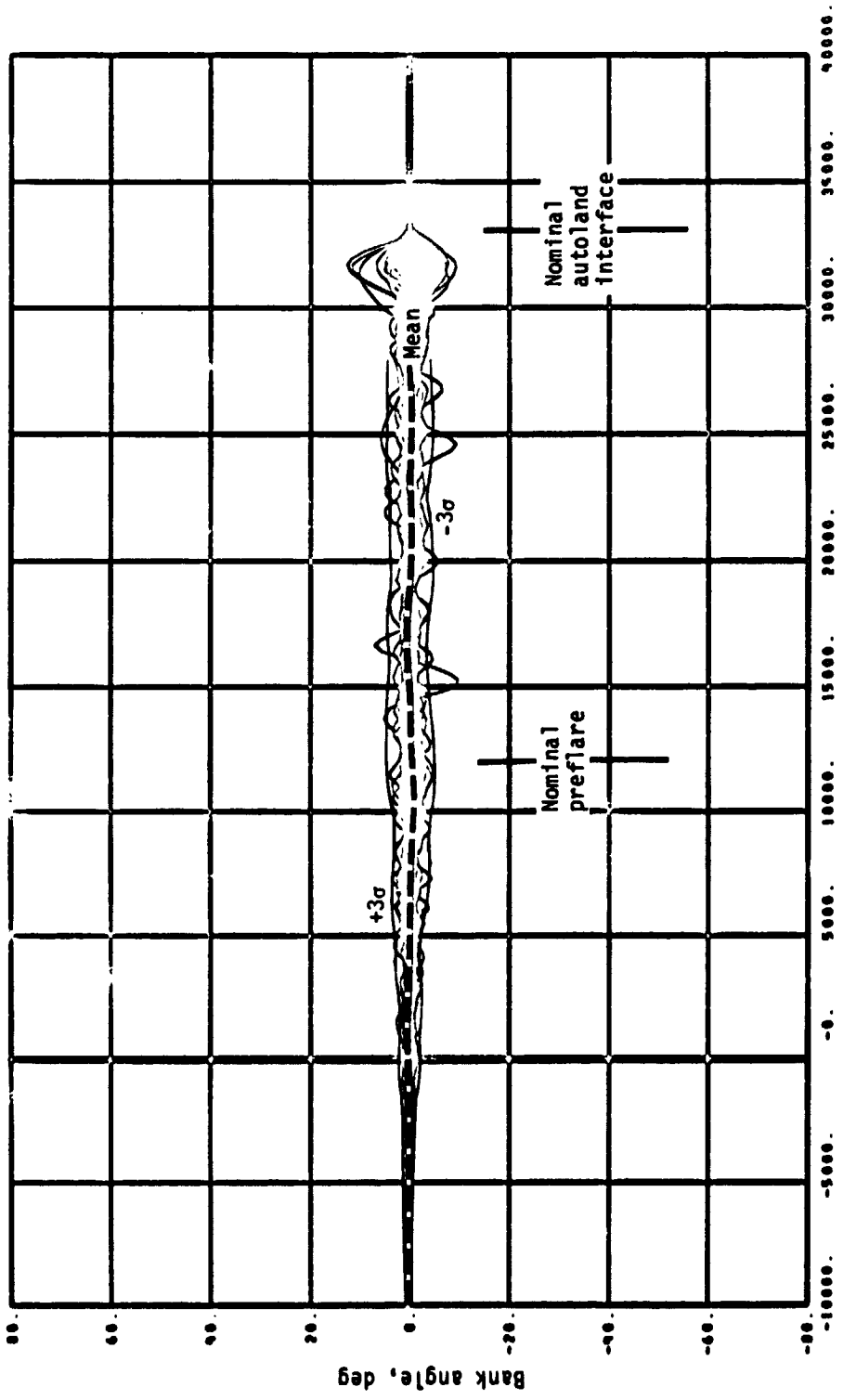

(l) Bank angle.

Figure 22.- Continued.

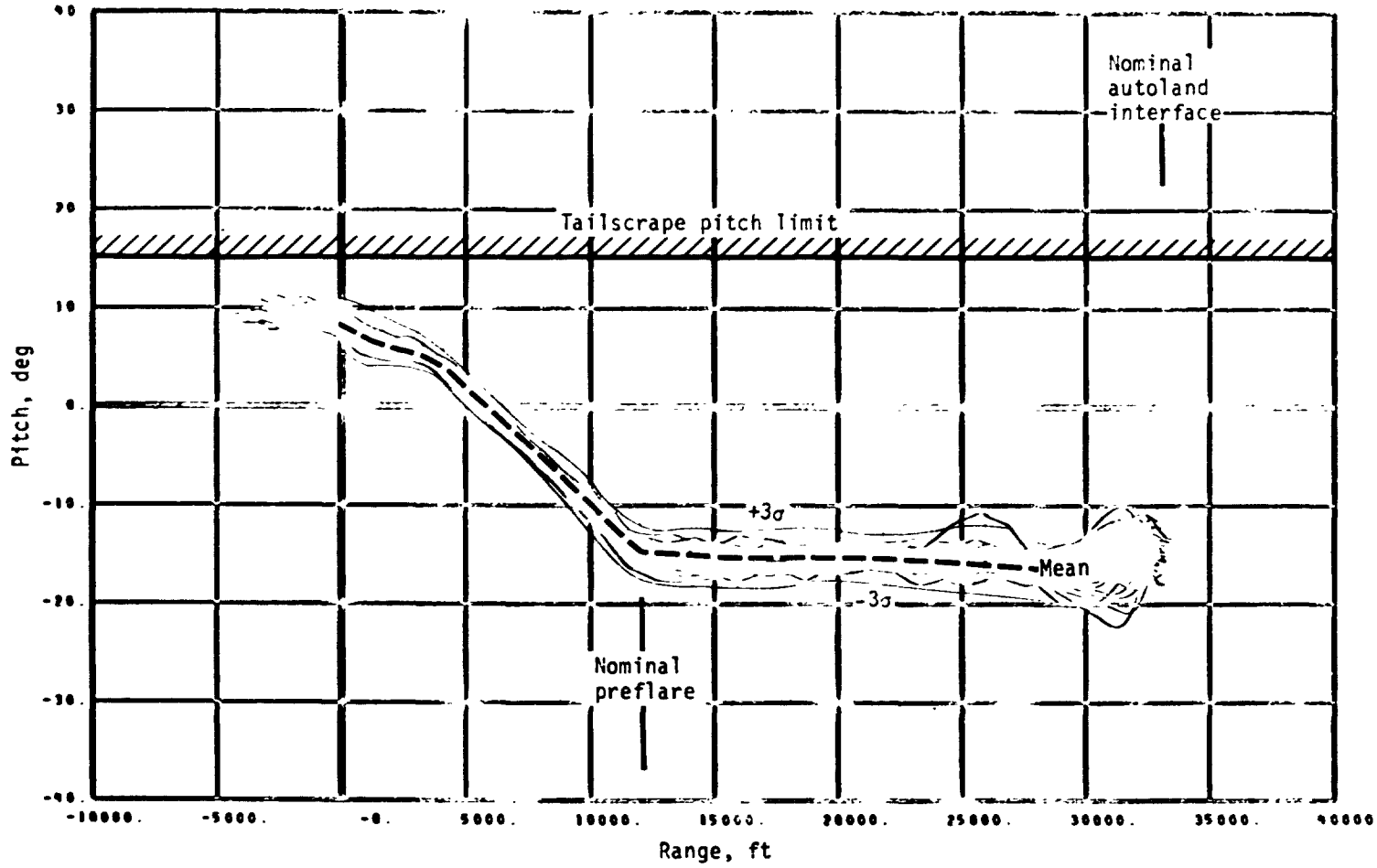

(j) Pitch angle.

Figure 22.- Continued.

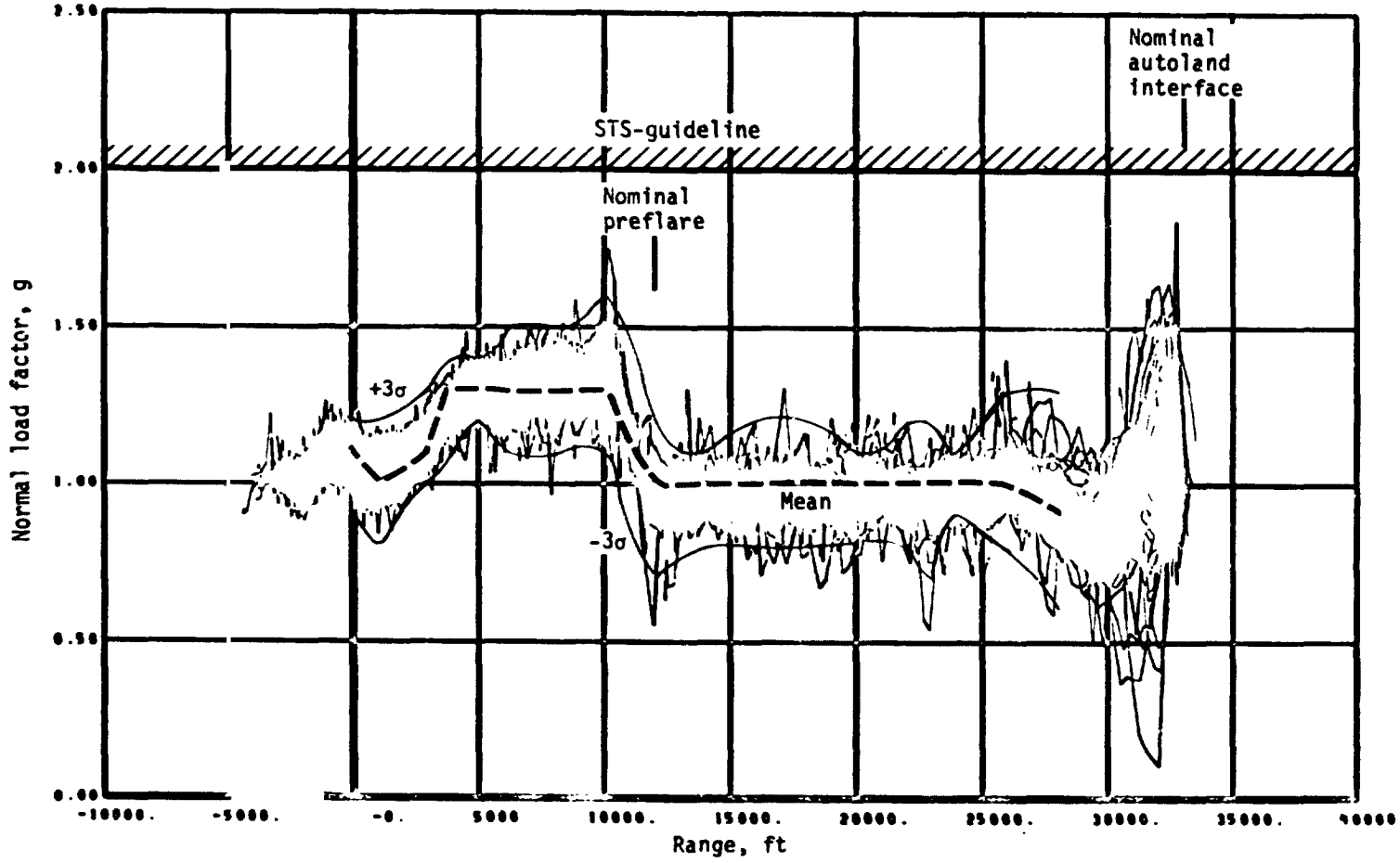

(k) Normal load factor.

Figure 22.- Continued.

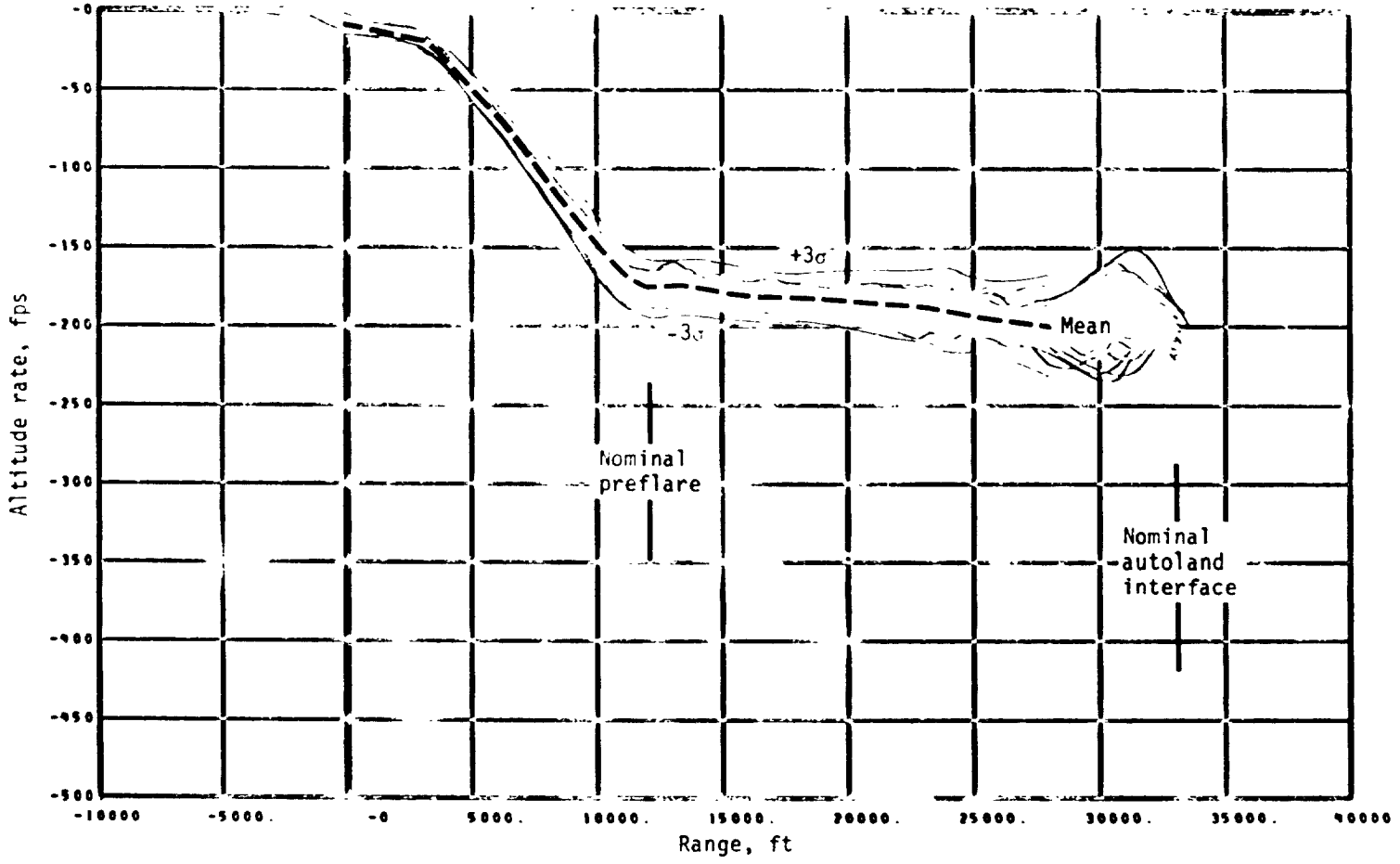

(1) Altitude rate.

Figure 22.- Continued.

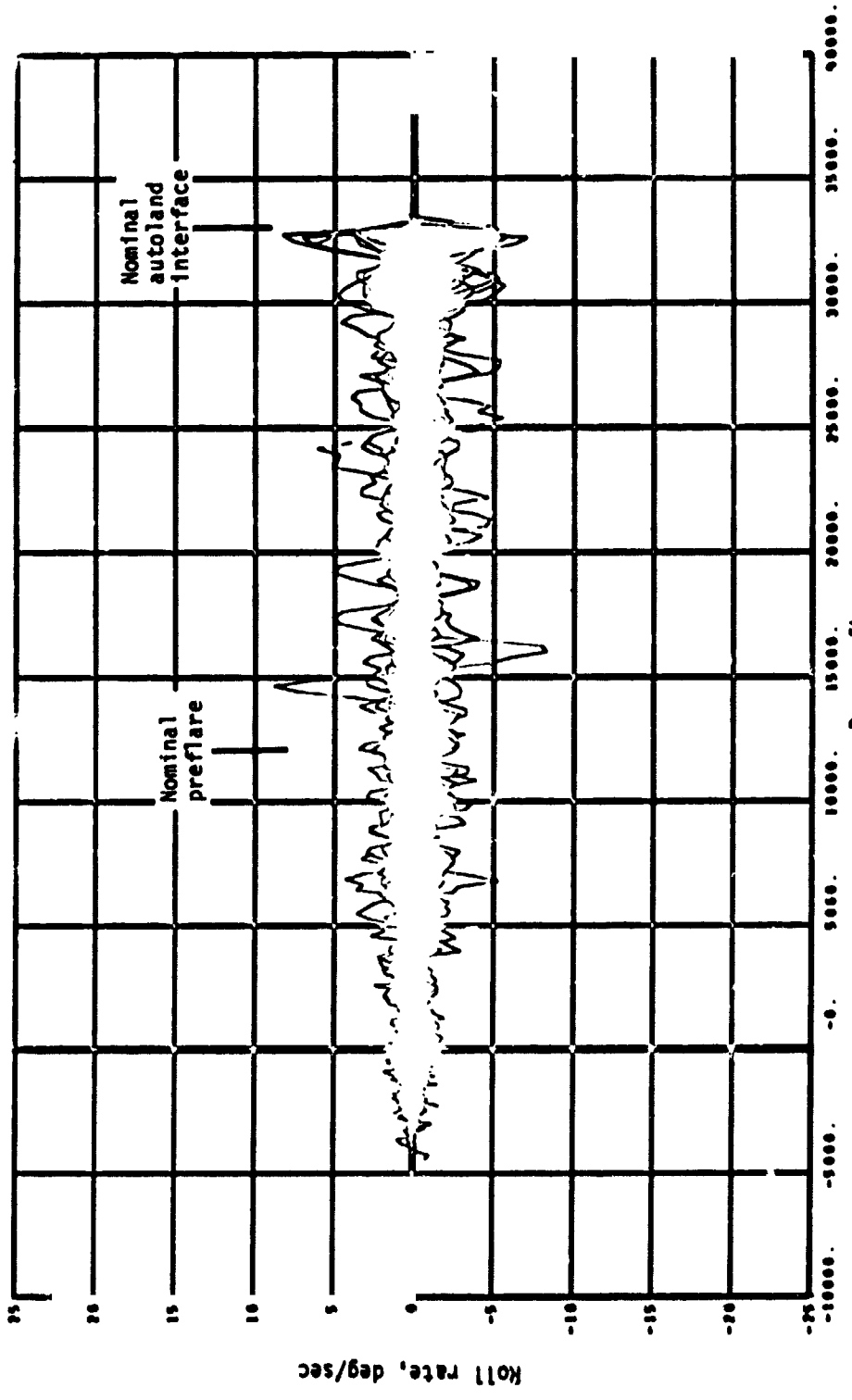

(m) Roll rate.

Figure 22.- Continued.

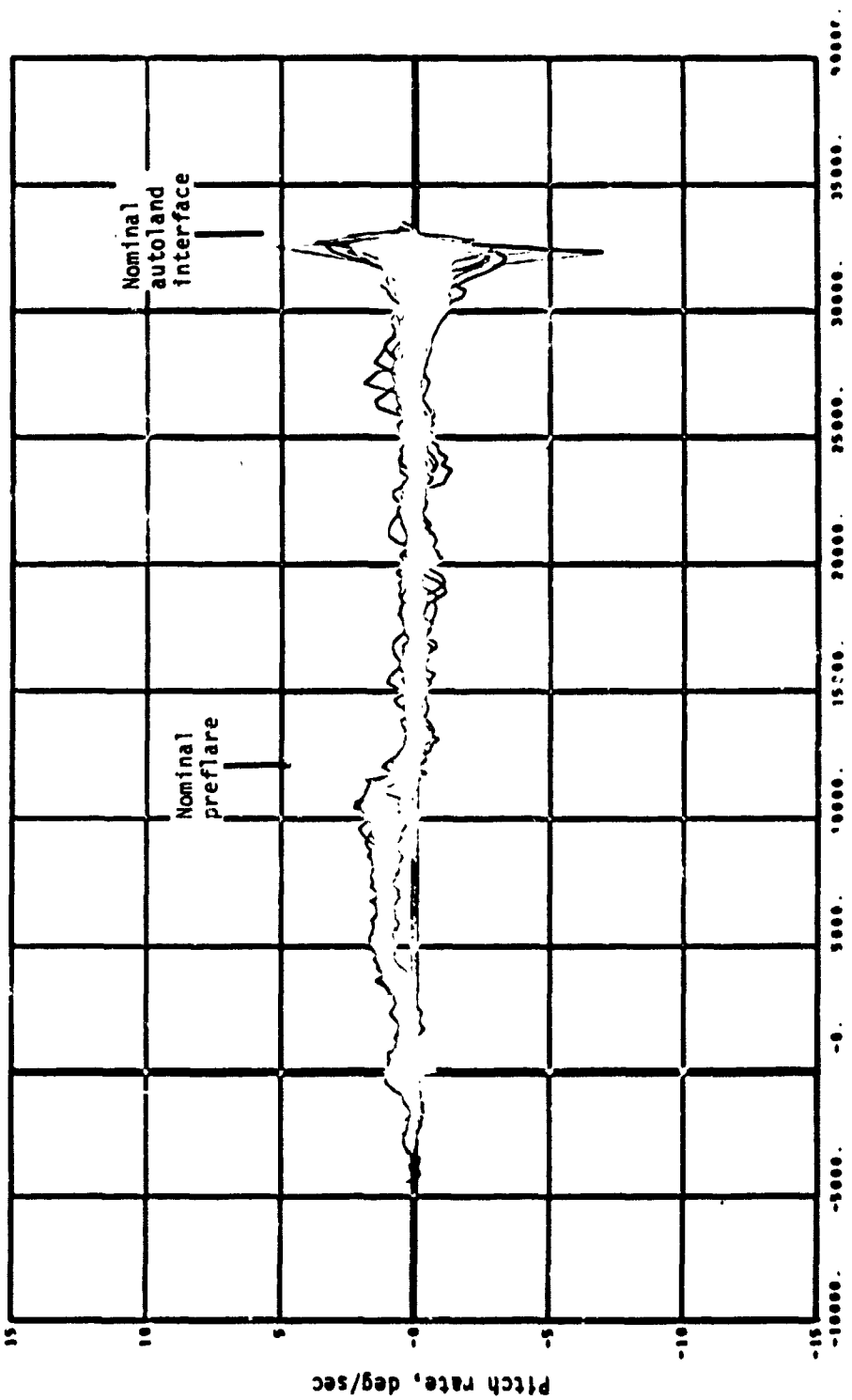

(n) Pitch rate.

Figure 22.- Continued.

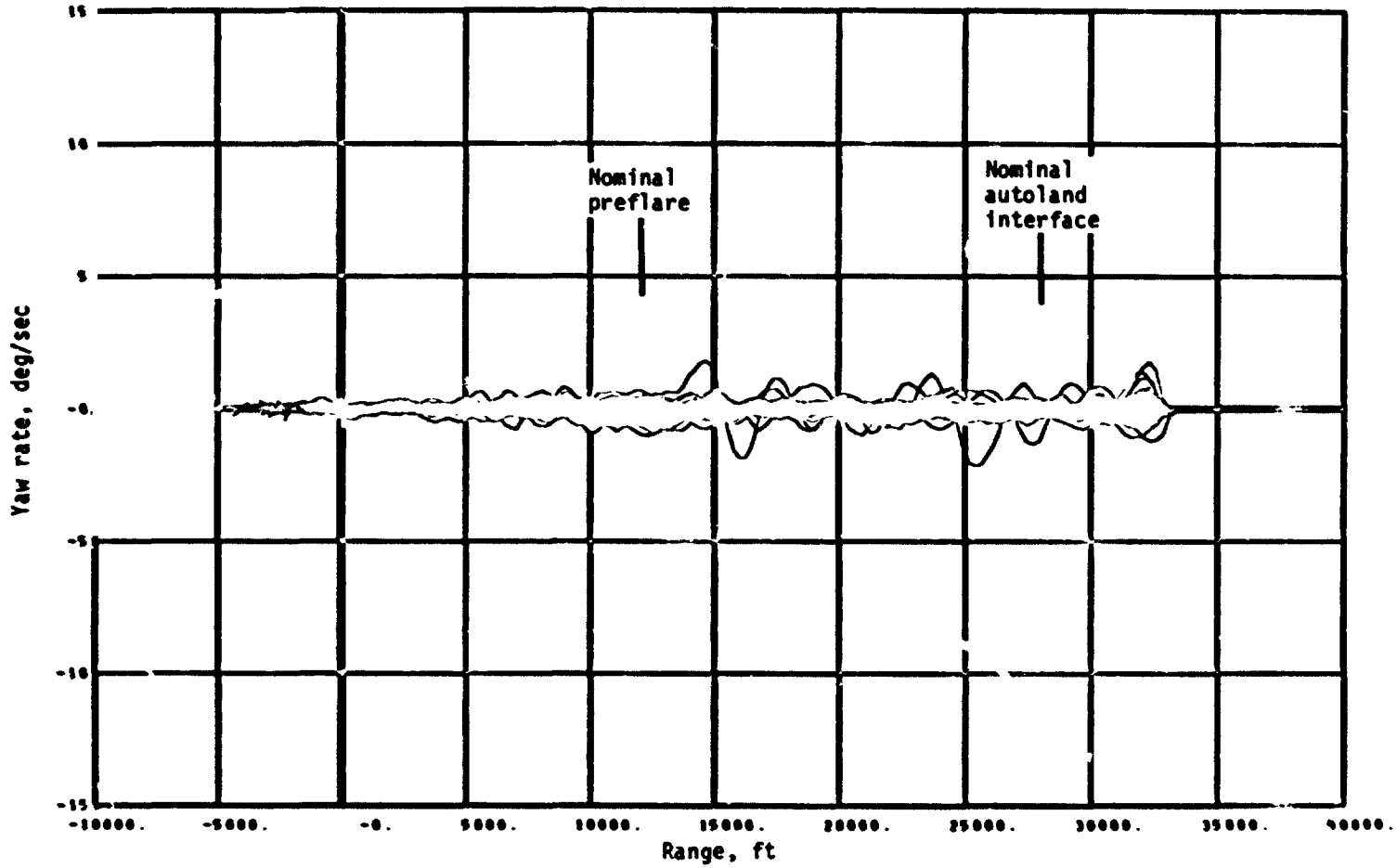

(o) Yaw rate.

Figure 22.- Continued.

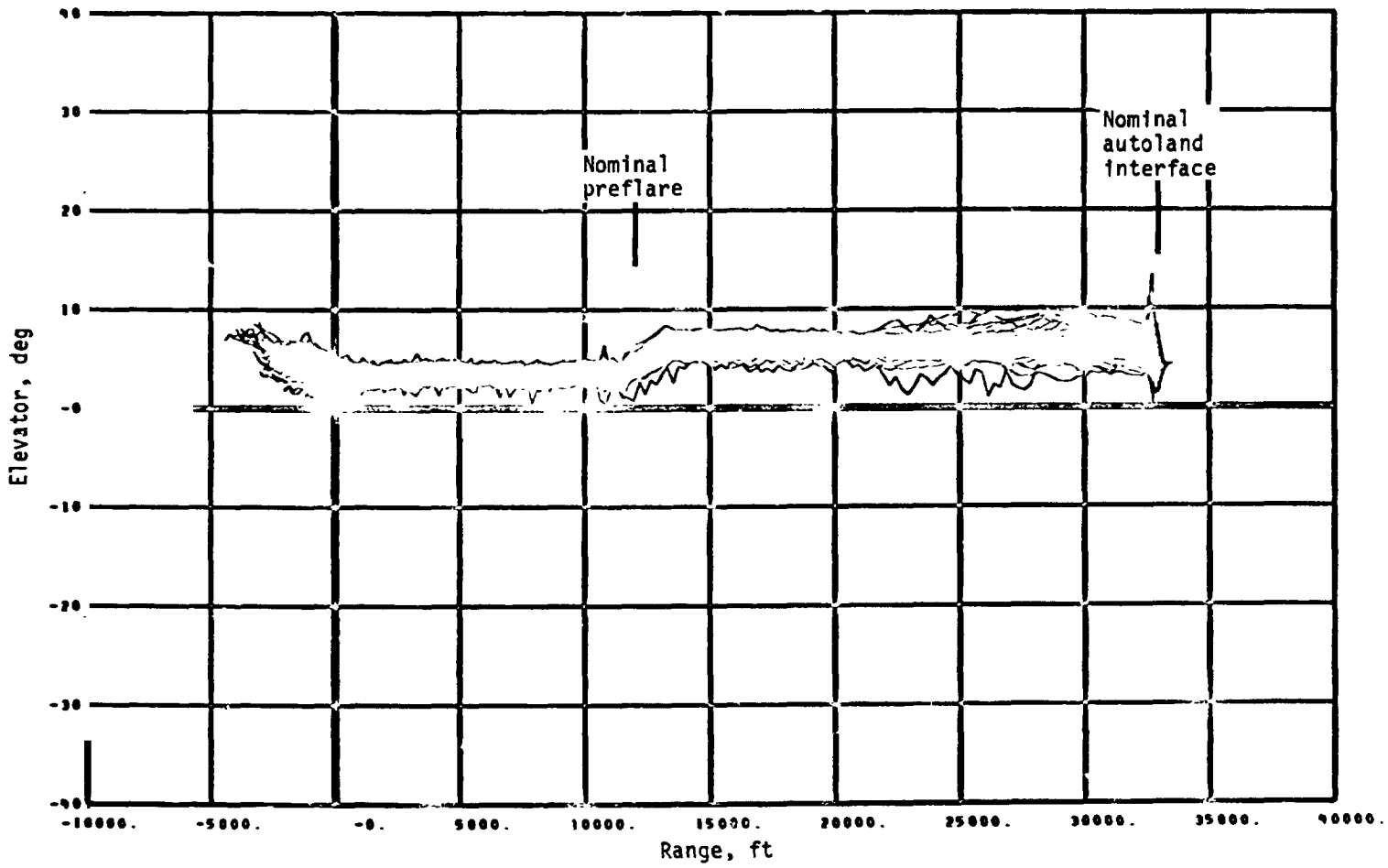

(p) Elevator deflection.

Figure 22.- Continued.

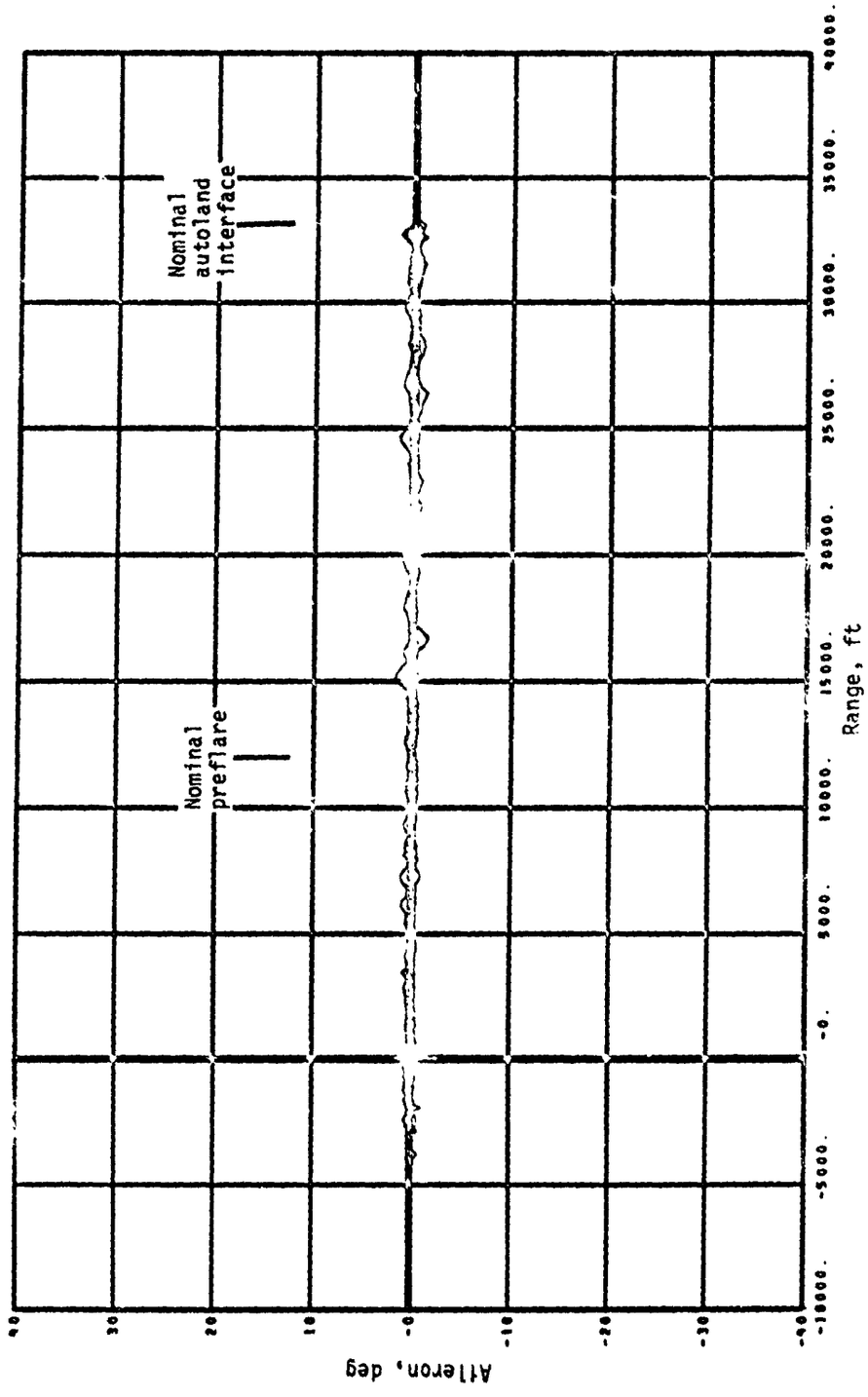

(q) Aileron.

Figure 22.- Continued.

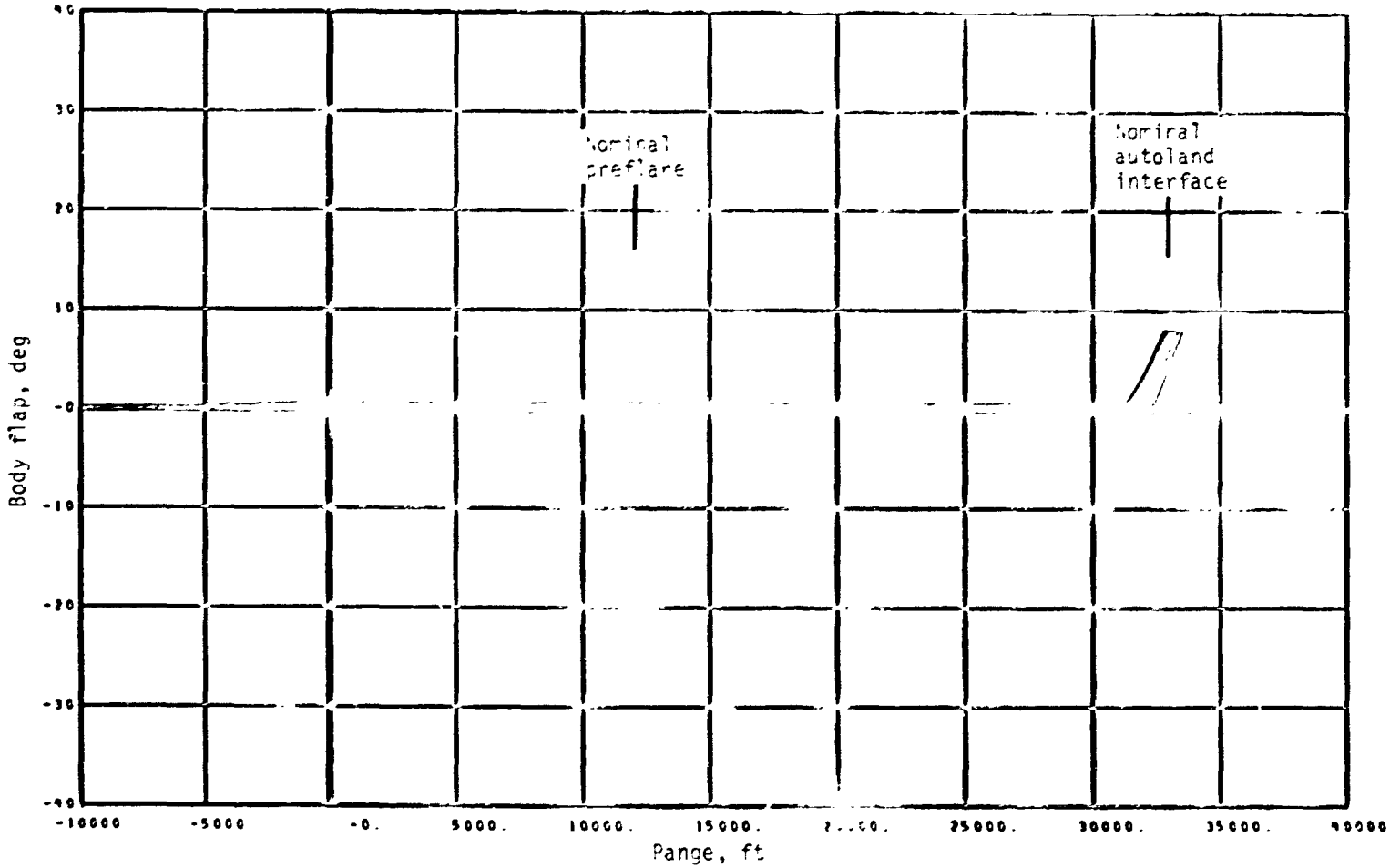

(r) Body flap deflection.

Figure 22.- Continued

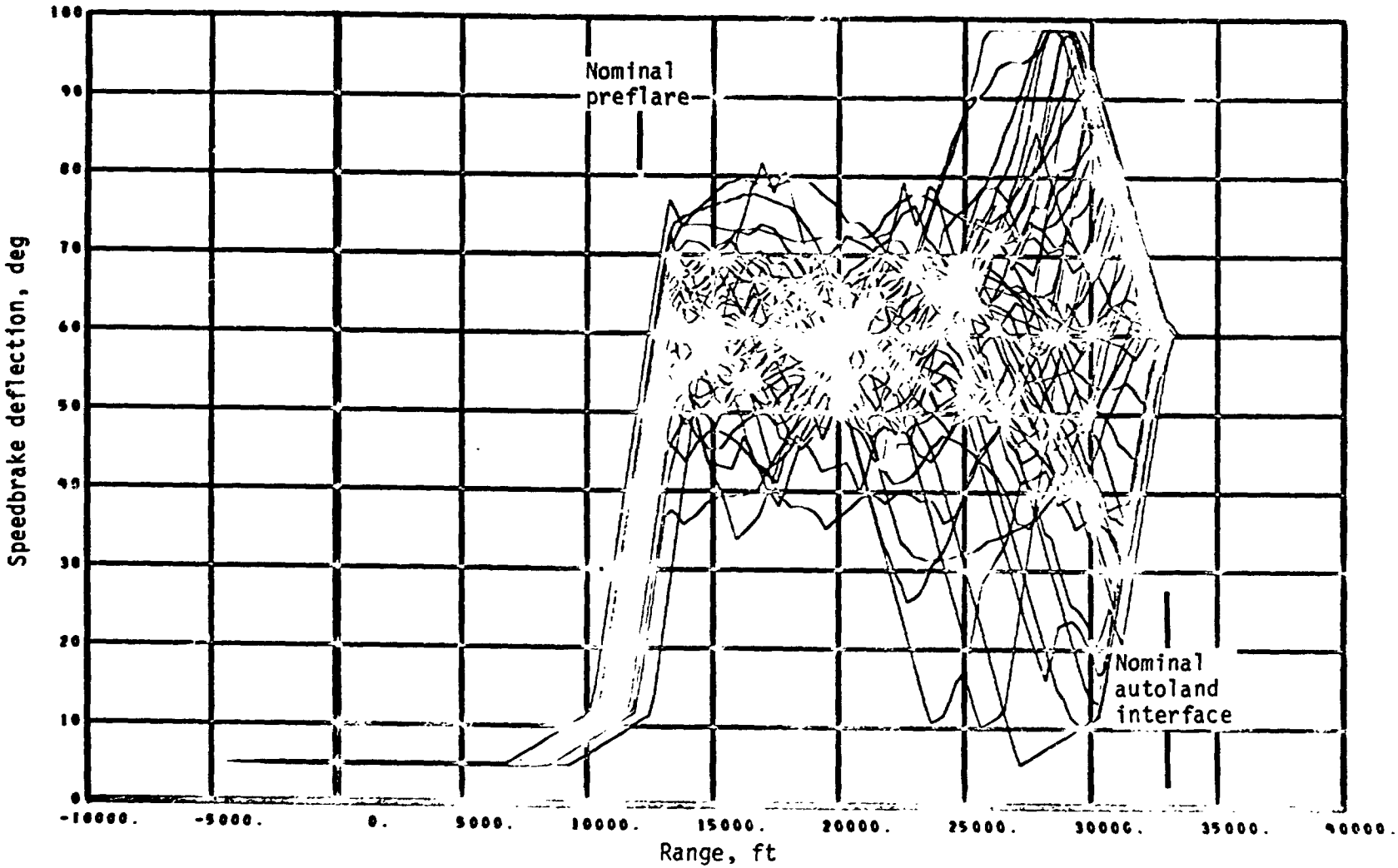

(s) Speedbrake deflection.

Figure 22.- Continued.

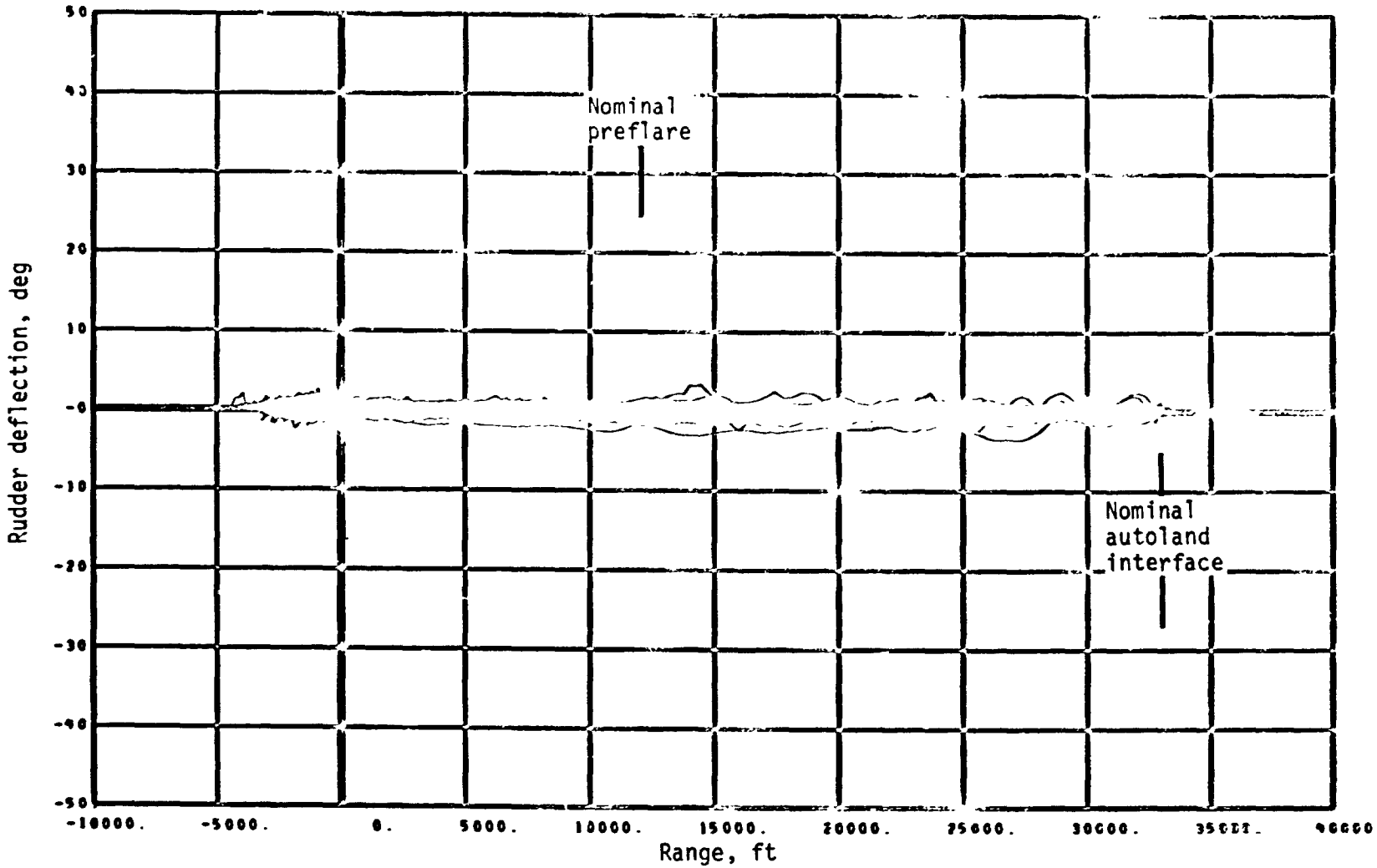

(t) Rudder deflection.

Figure 22.- Continued.

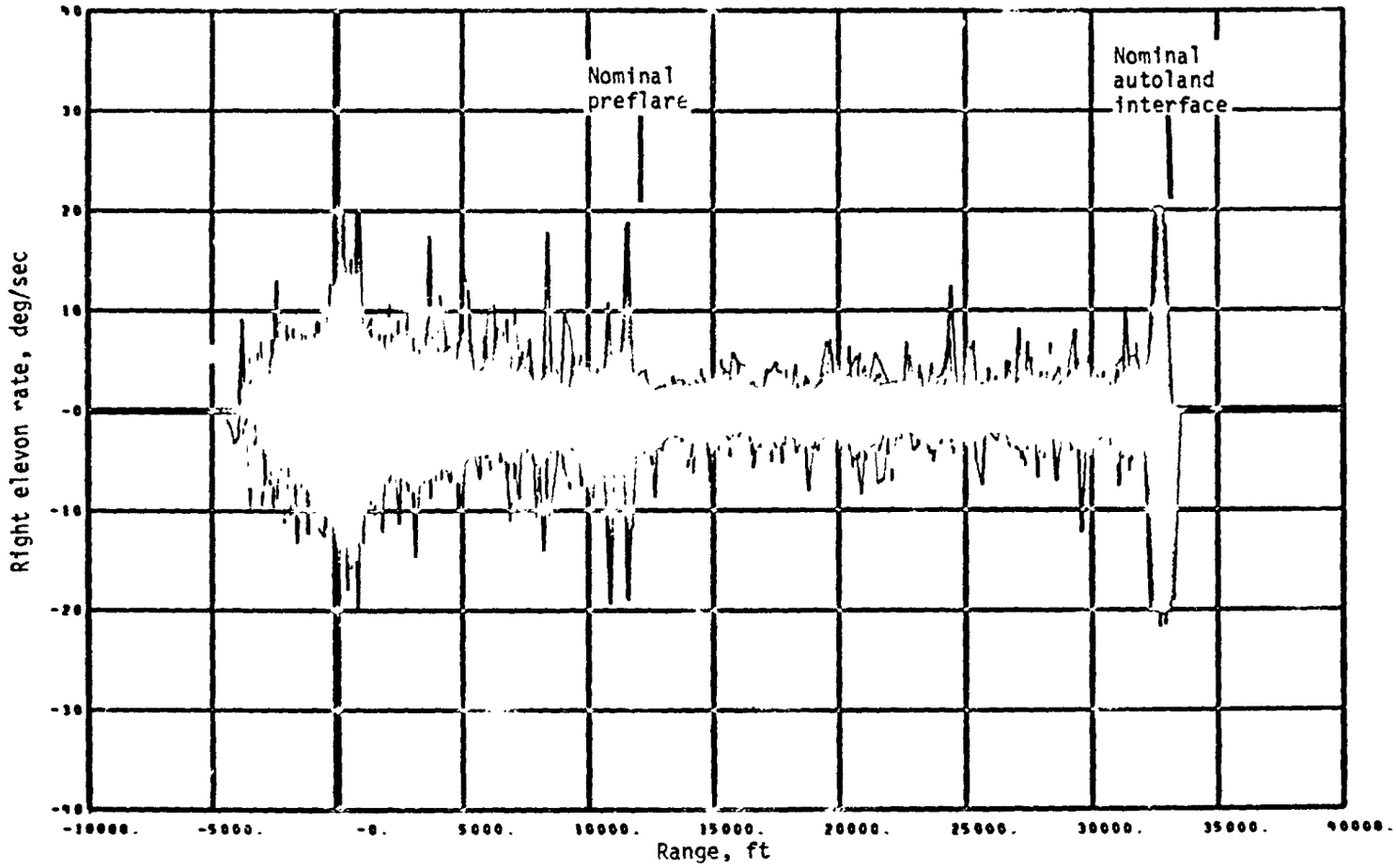

(u) Right elevon rate.

Figure 22.- Continued.

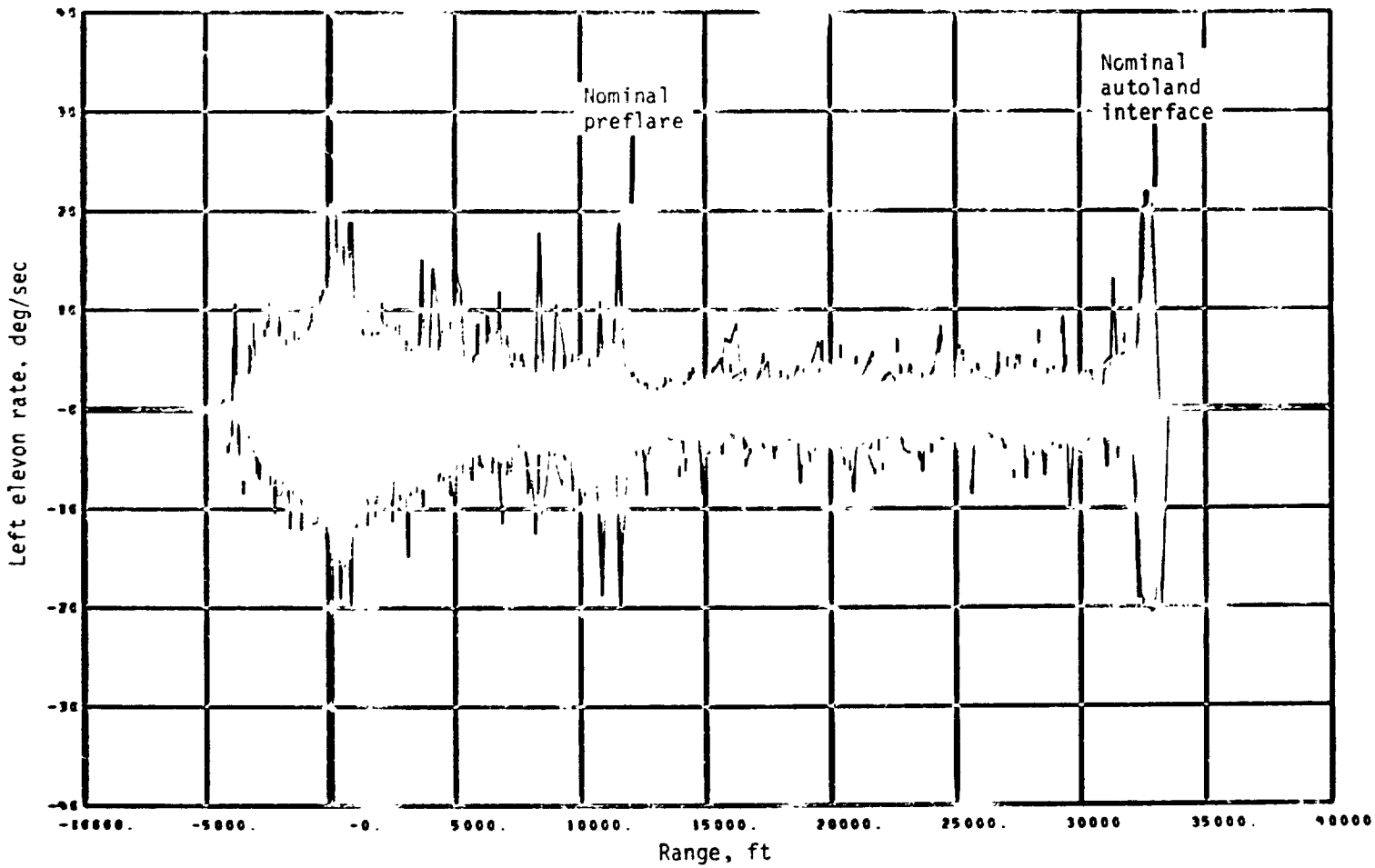

(v) Left elevon rate.

Figure 22.- Continued.

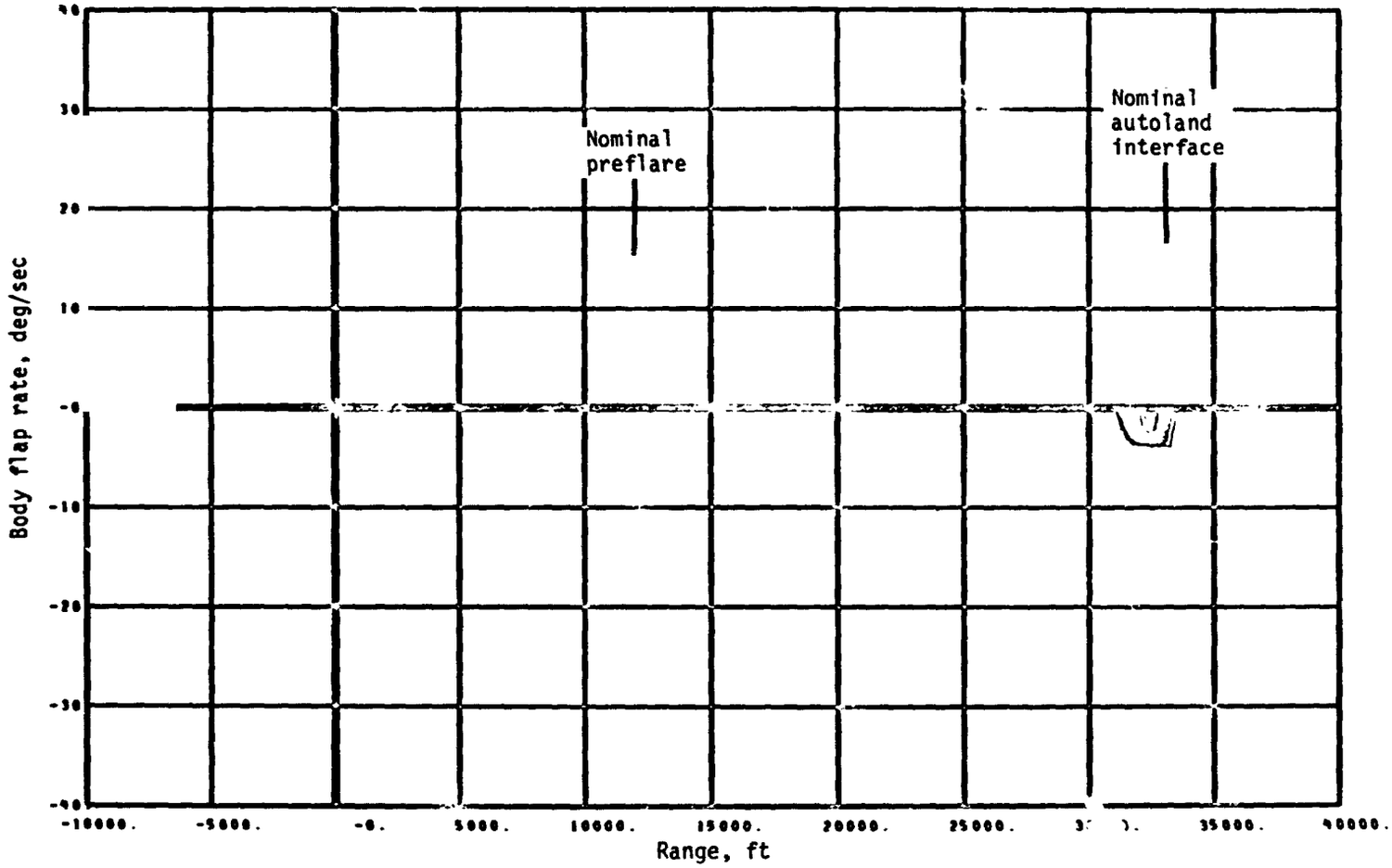

(w) Body flap rate.

Figure 22.- Continued.

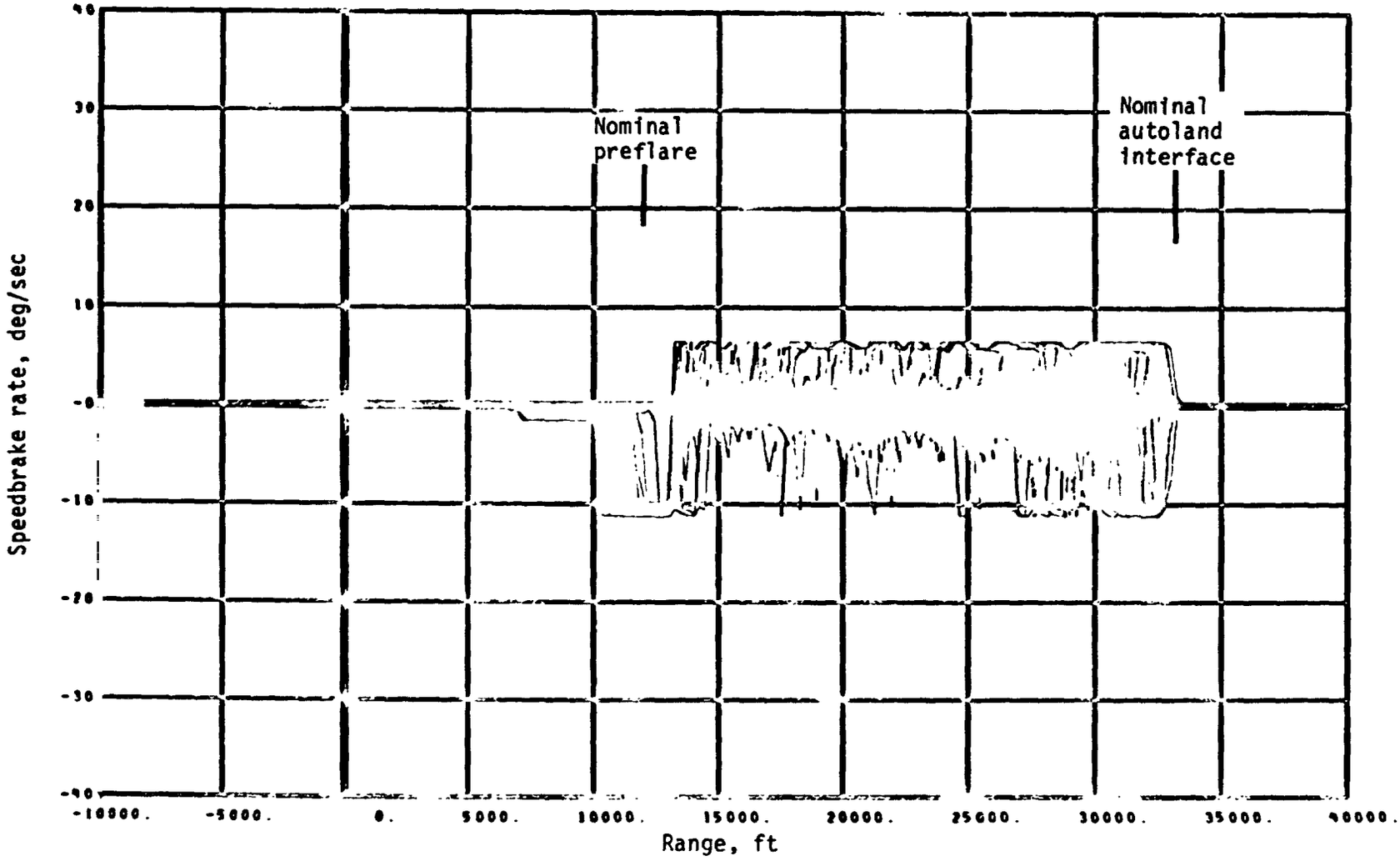

(x) Speedbrake rate.

Figure 22.- Continued.

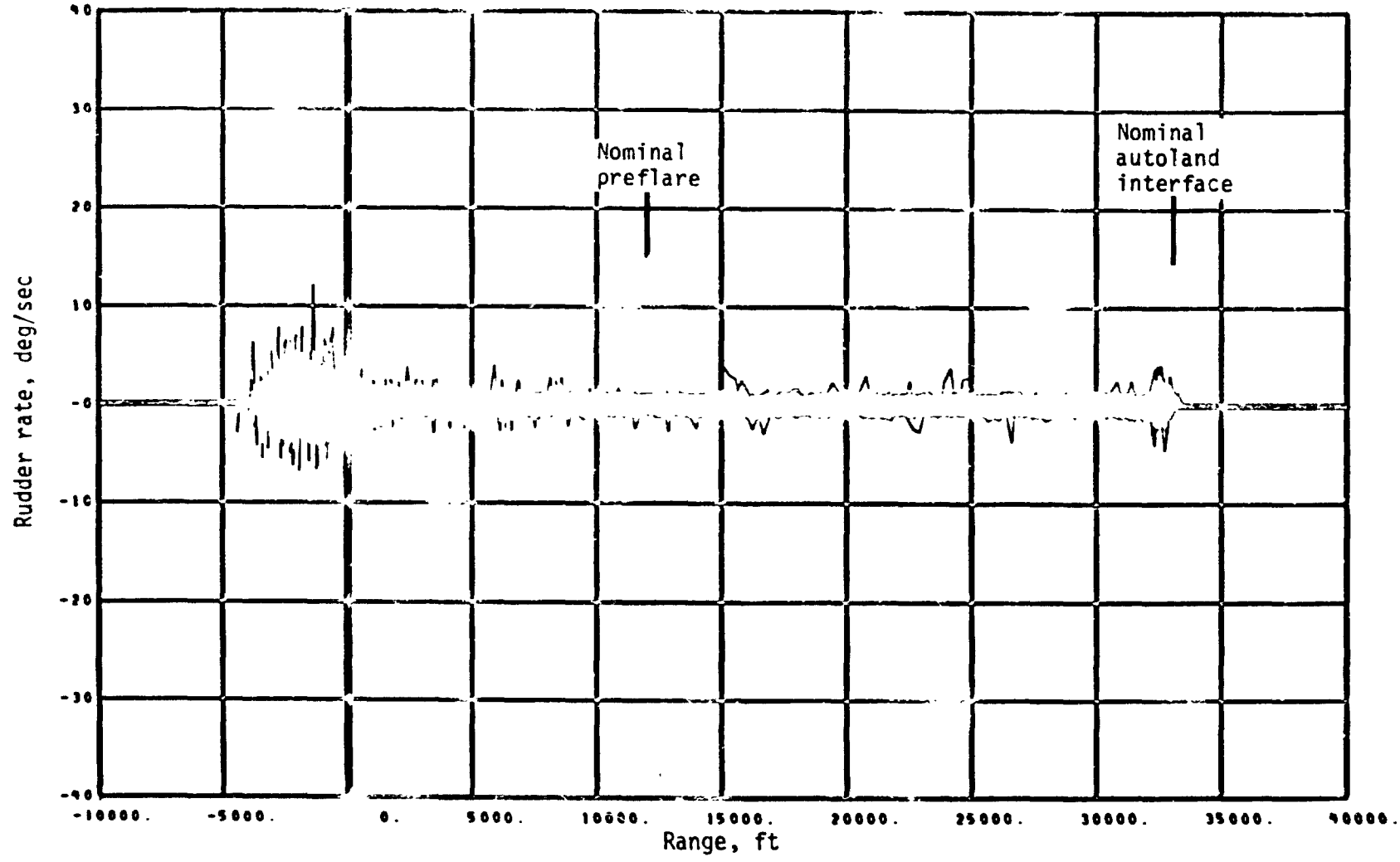

(y) Rudder rate.

Figure 22.- Continued.

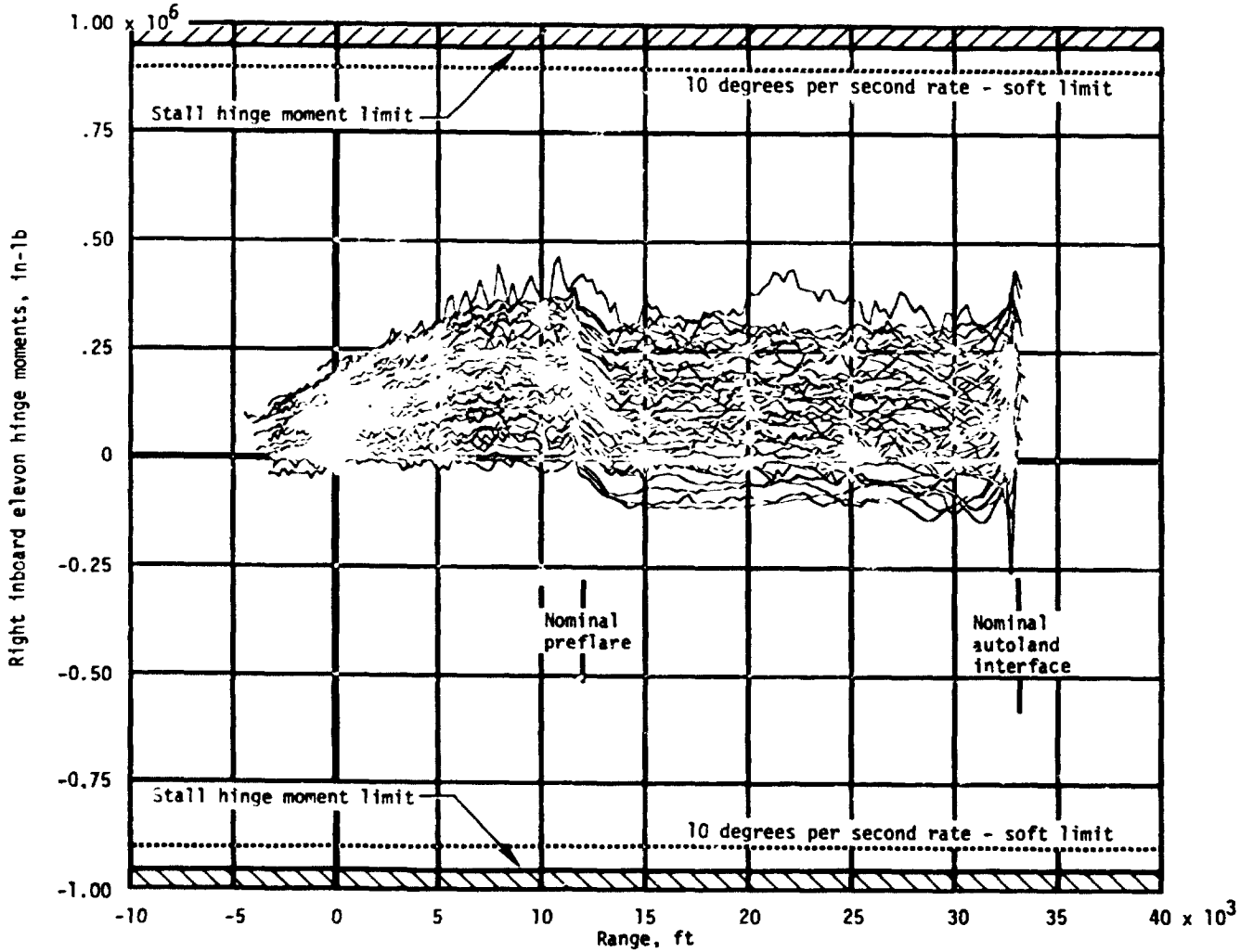

(z) Right inboard elevon hinge moments.

Figure 22.- Continued.

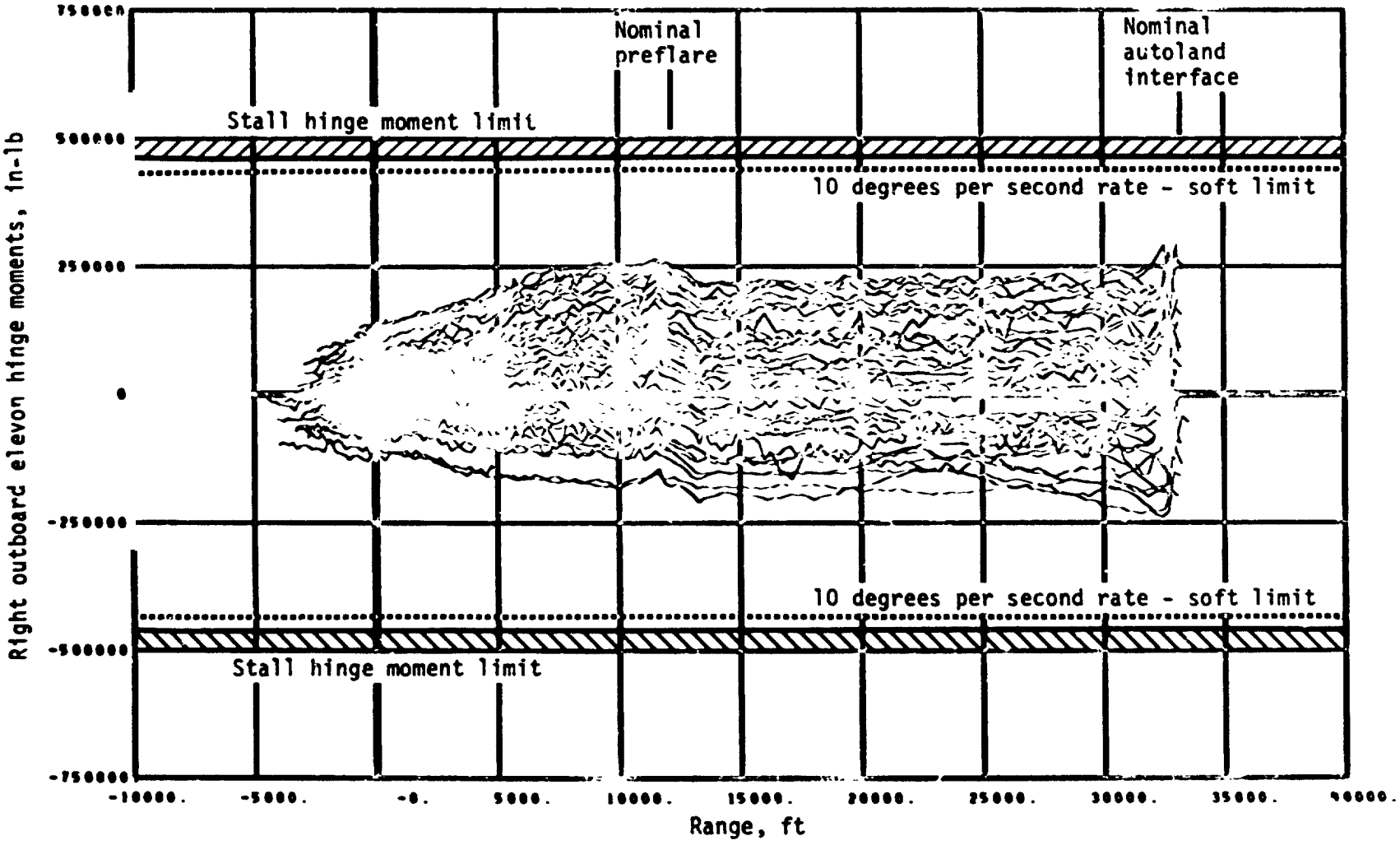

(aa) Right outboard elevon hinge moments.

Figure 22.- Continued

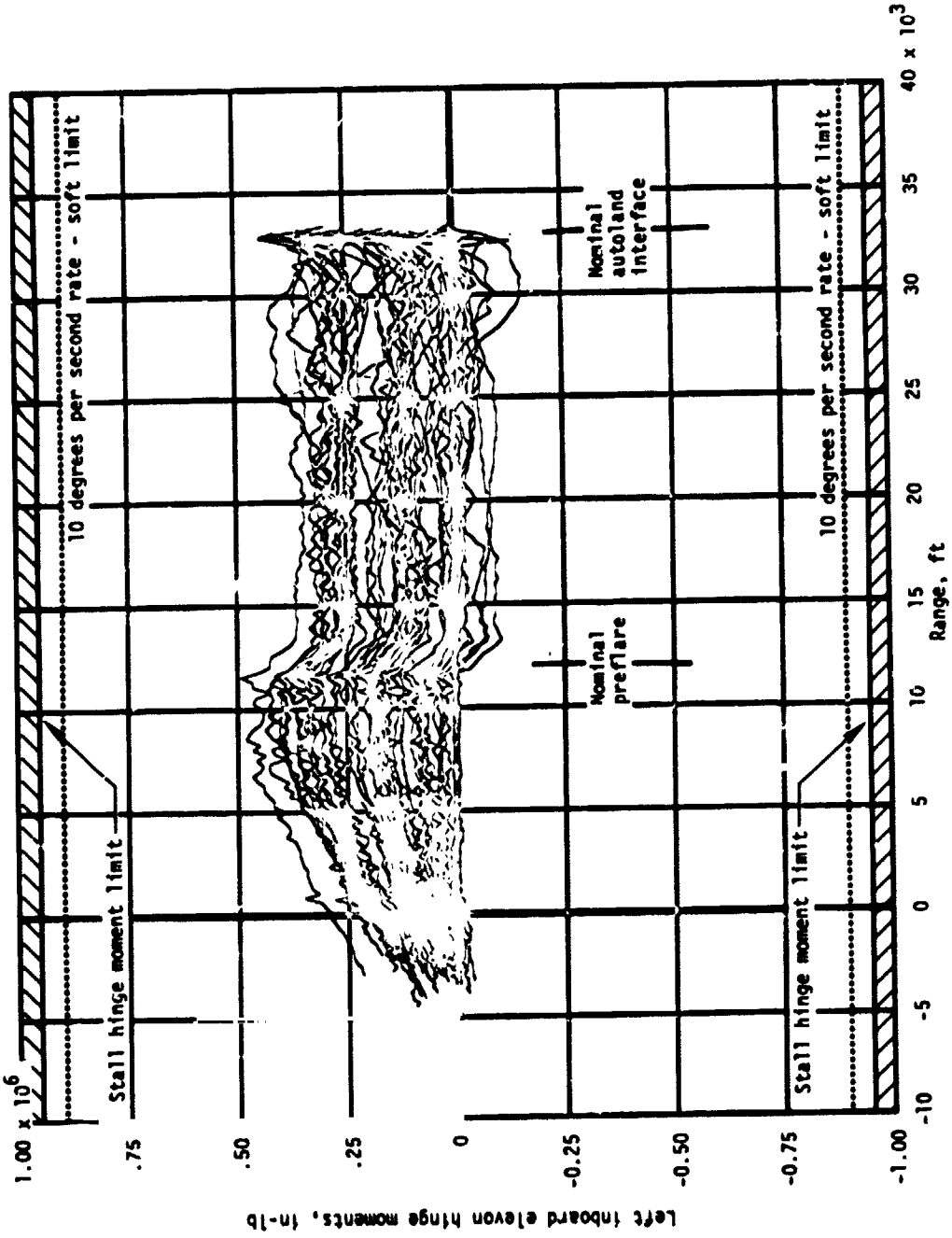

(bb) Left inboard elevon hinge moments

Figure 22.- Continued.

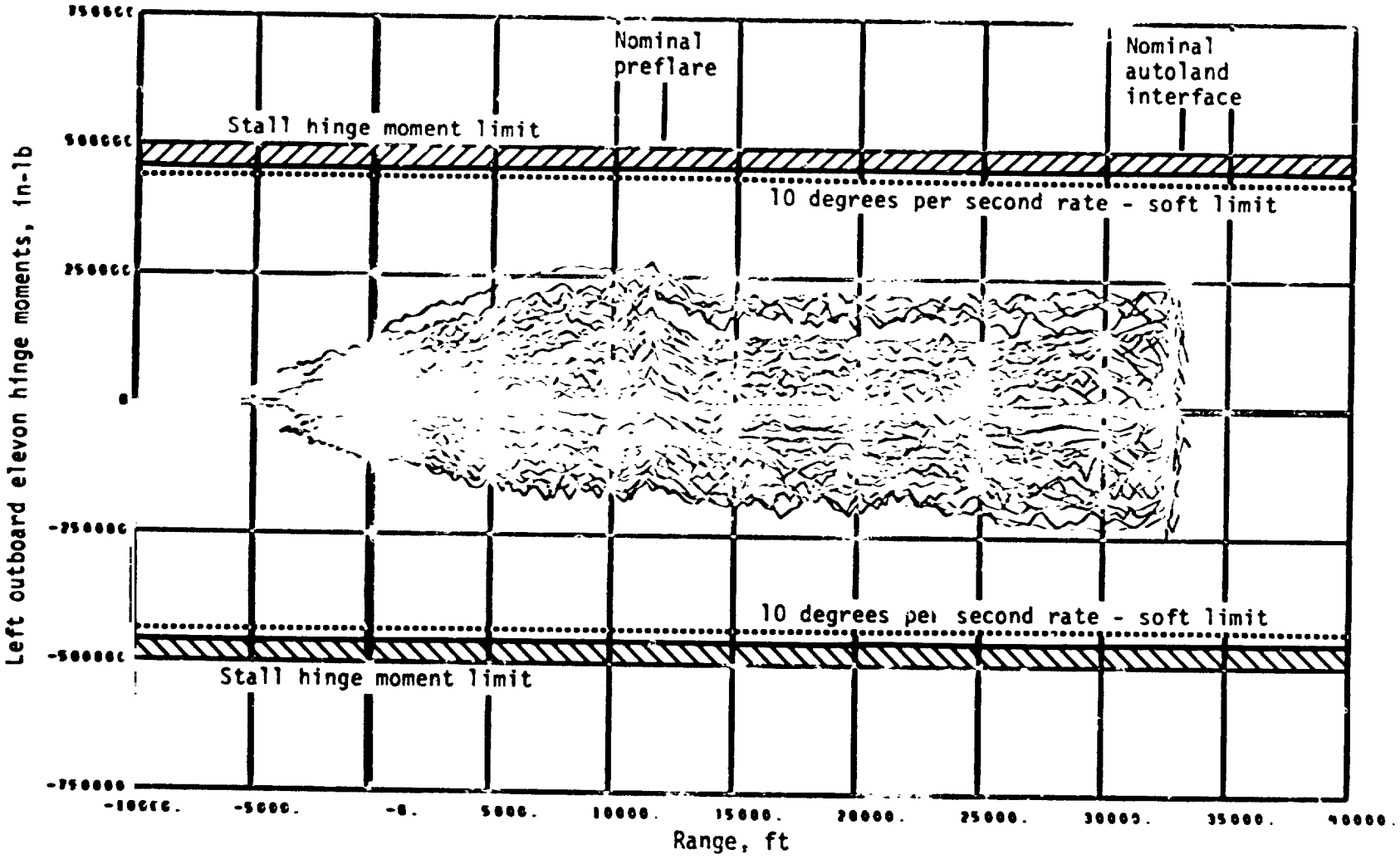

(cc) Left outboard elevon hinge moments.

Figure 22.- Continued.

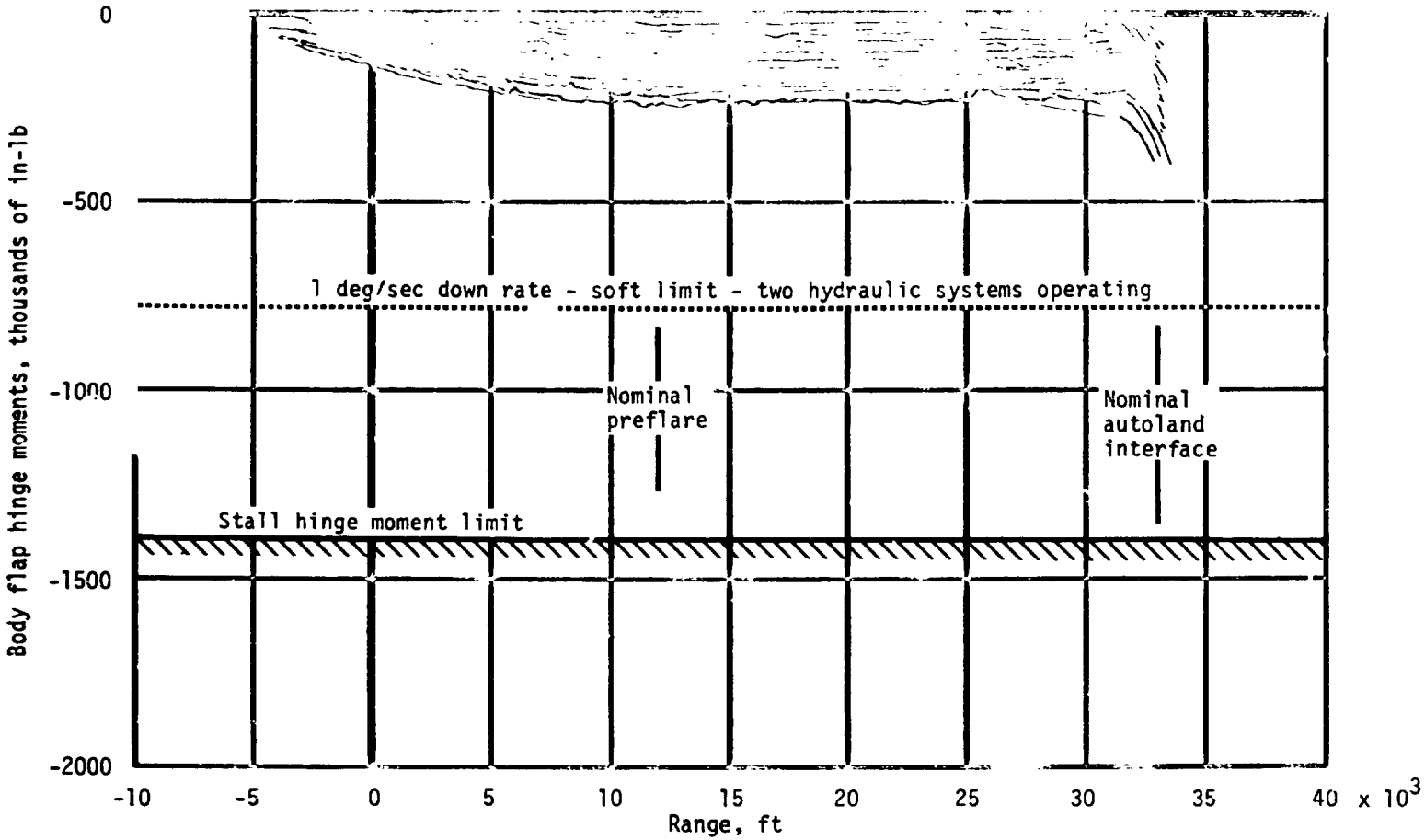

(dd) Body flap hinge moments.

Figure 22.- Continued.

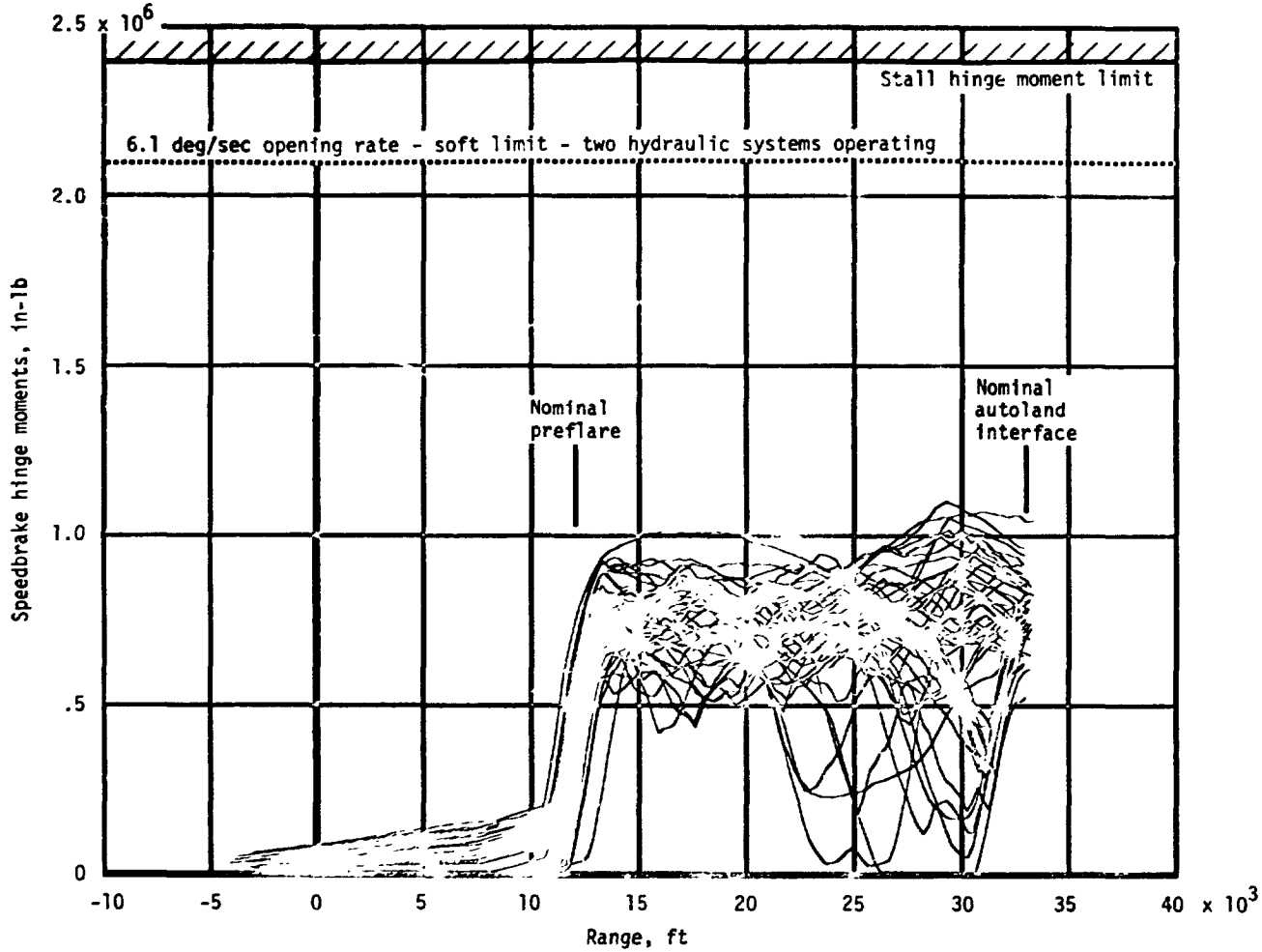

(ee) Speedbrake hinge moments.

Figure 22.- Continued.

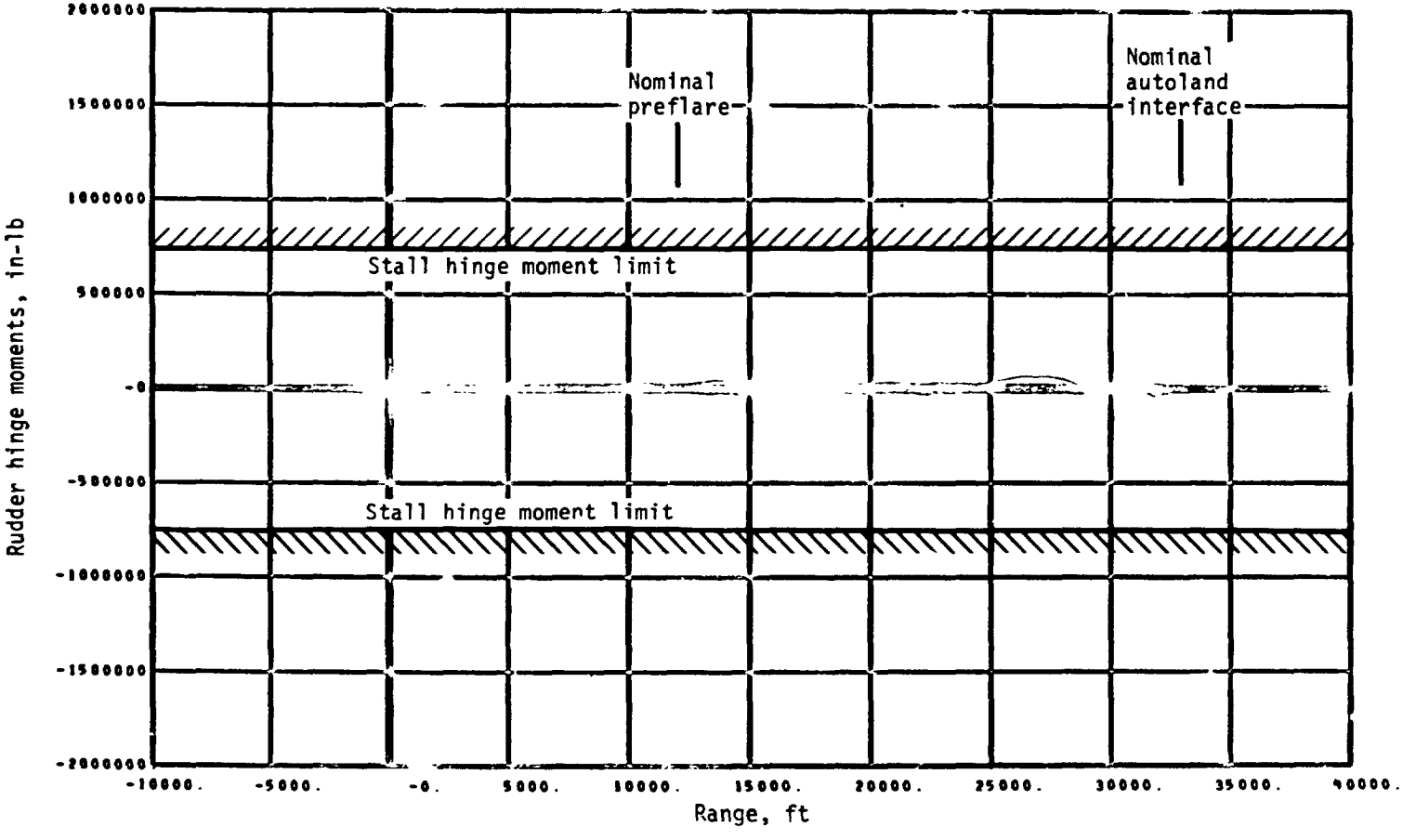

(ff) Rudder hinge moments.

Figure 22.- Concluded.

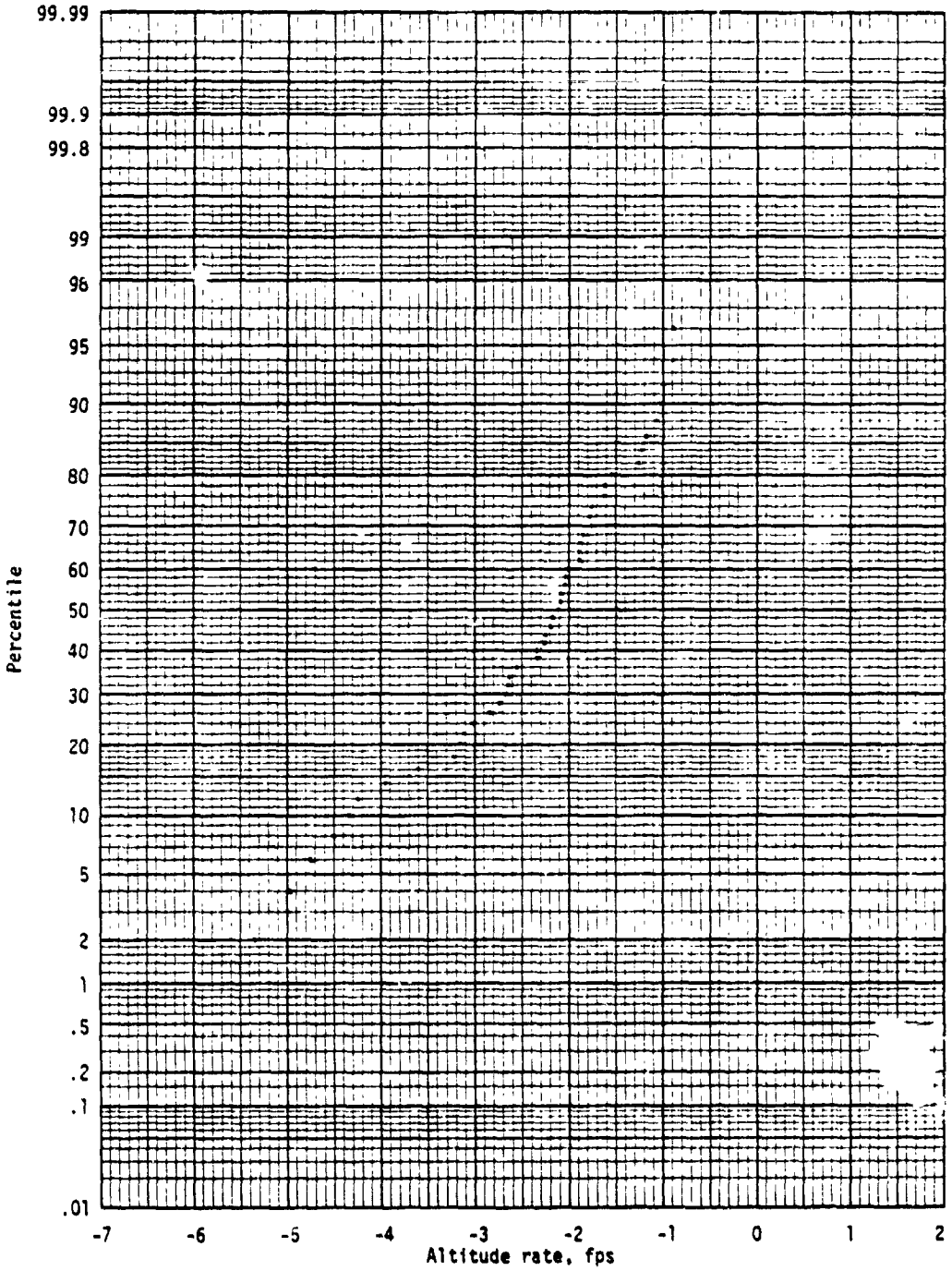

(a) Altitude rate.

Figure 23.- Landing statistics.

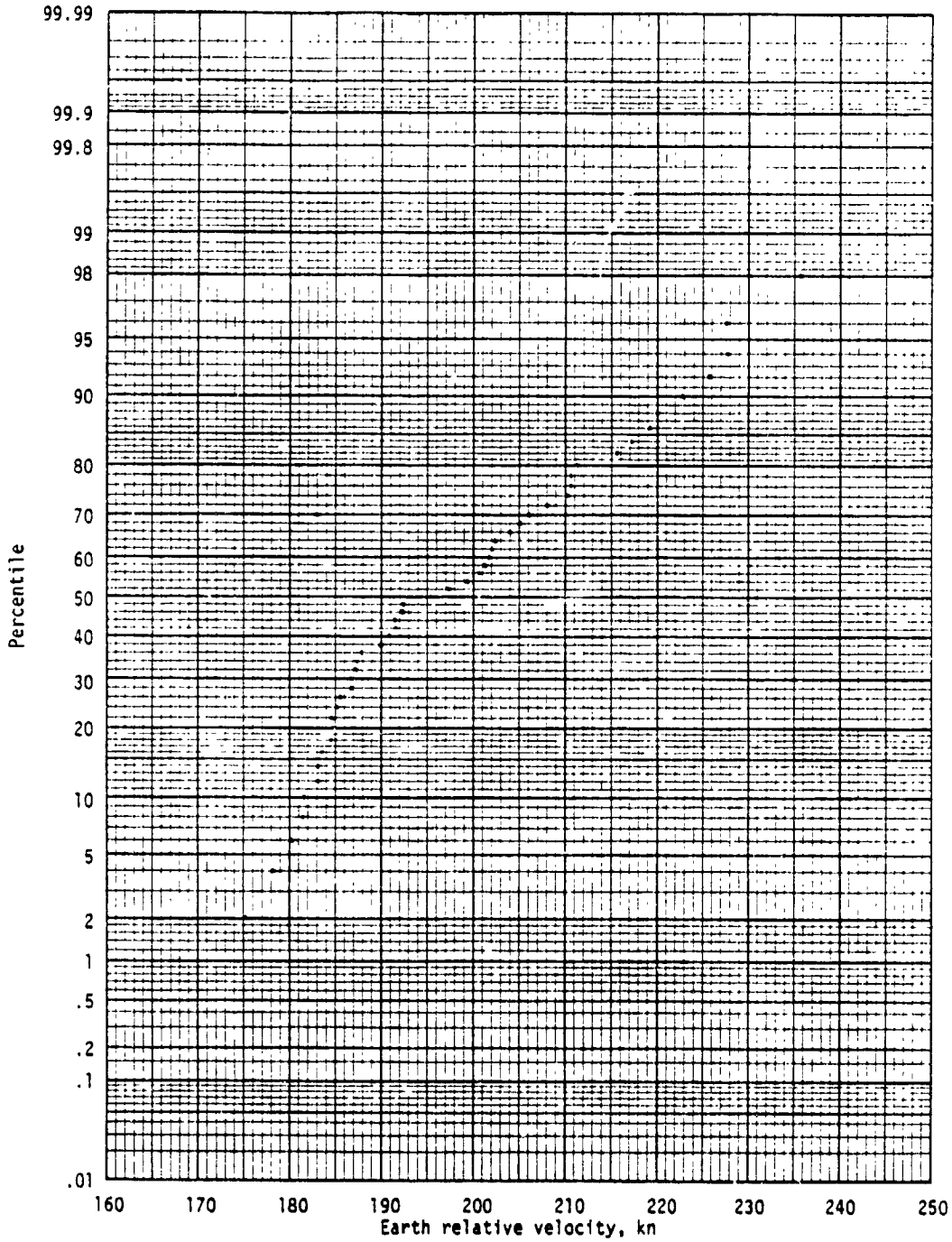

(b) Earth relative velocity.

Figure 23.- Continued.

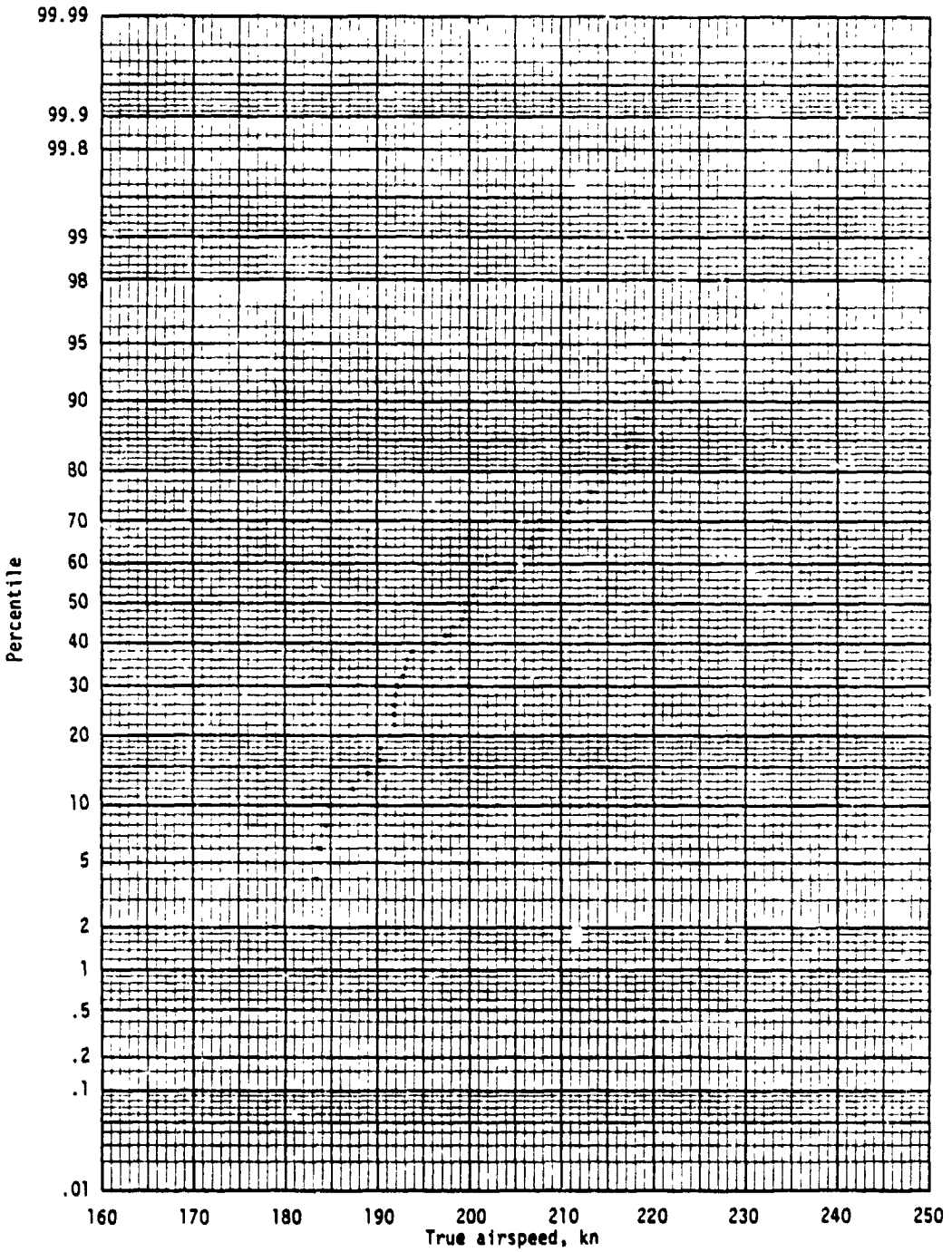

(c) True airspeed.

Figure 23.- Continued.

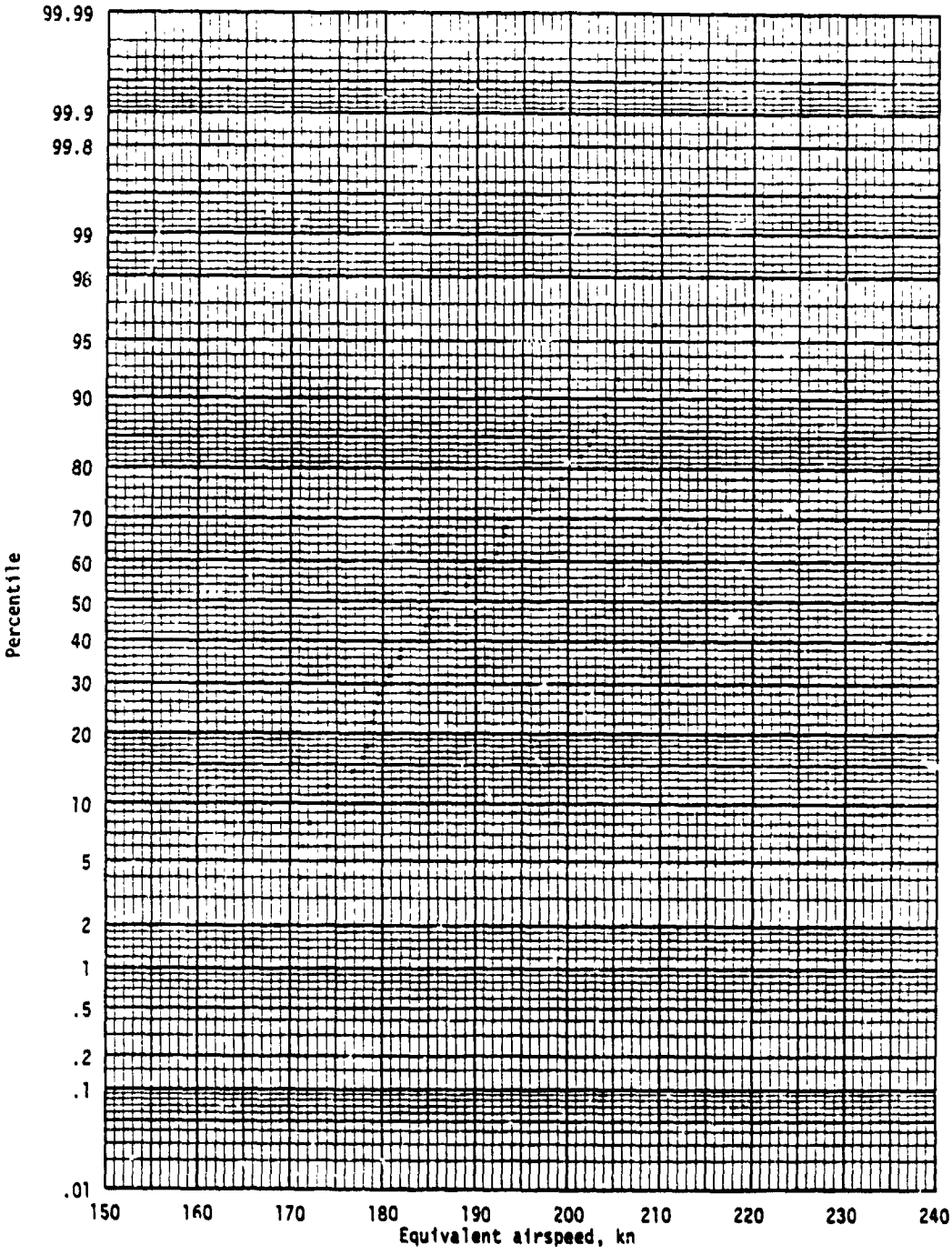

(d) Equivalent airspeed.

Figure 23.- Continued.

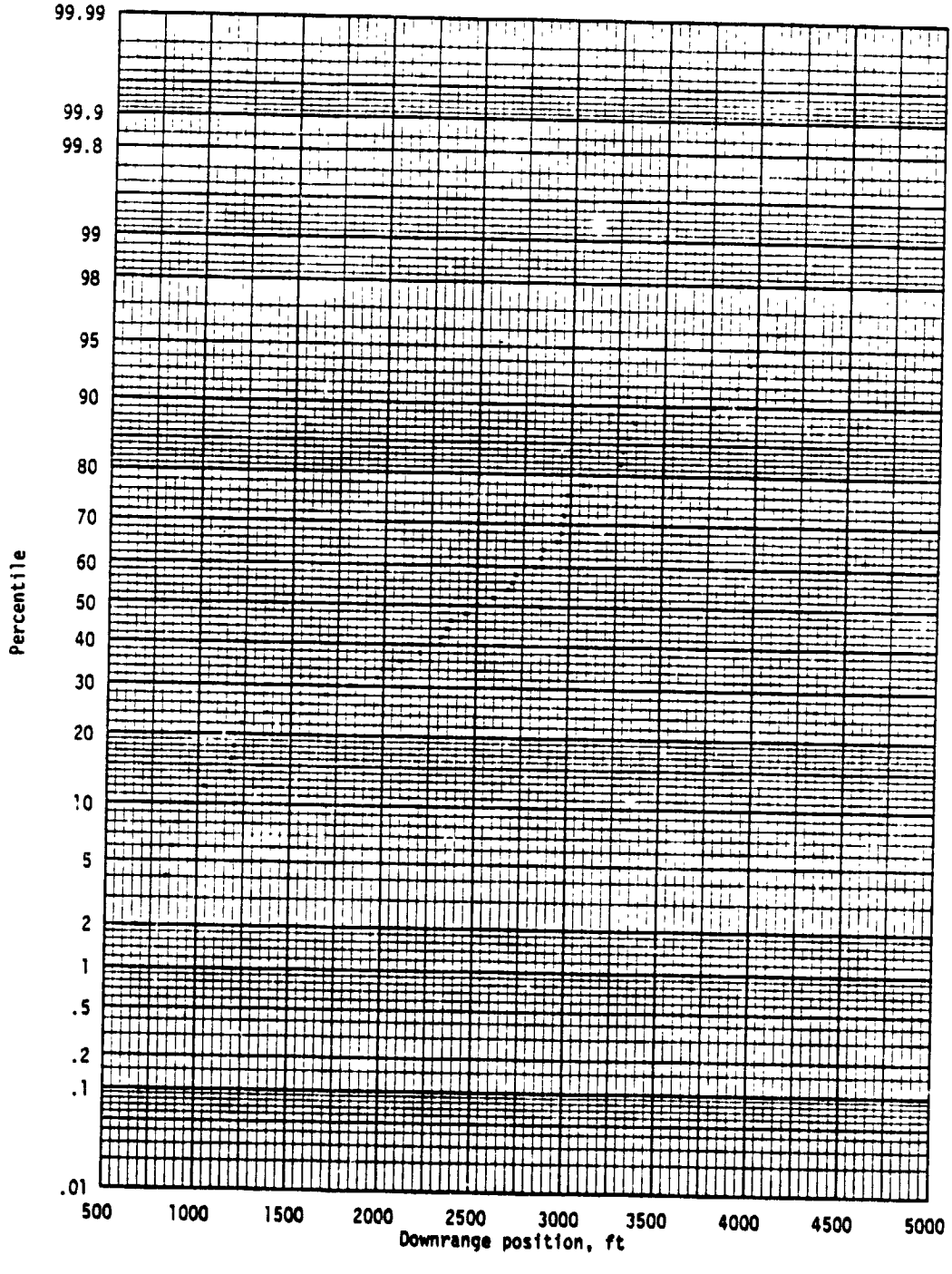

(e) Downrange position.

Figure 23.- Continued.

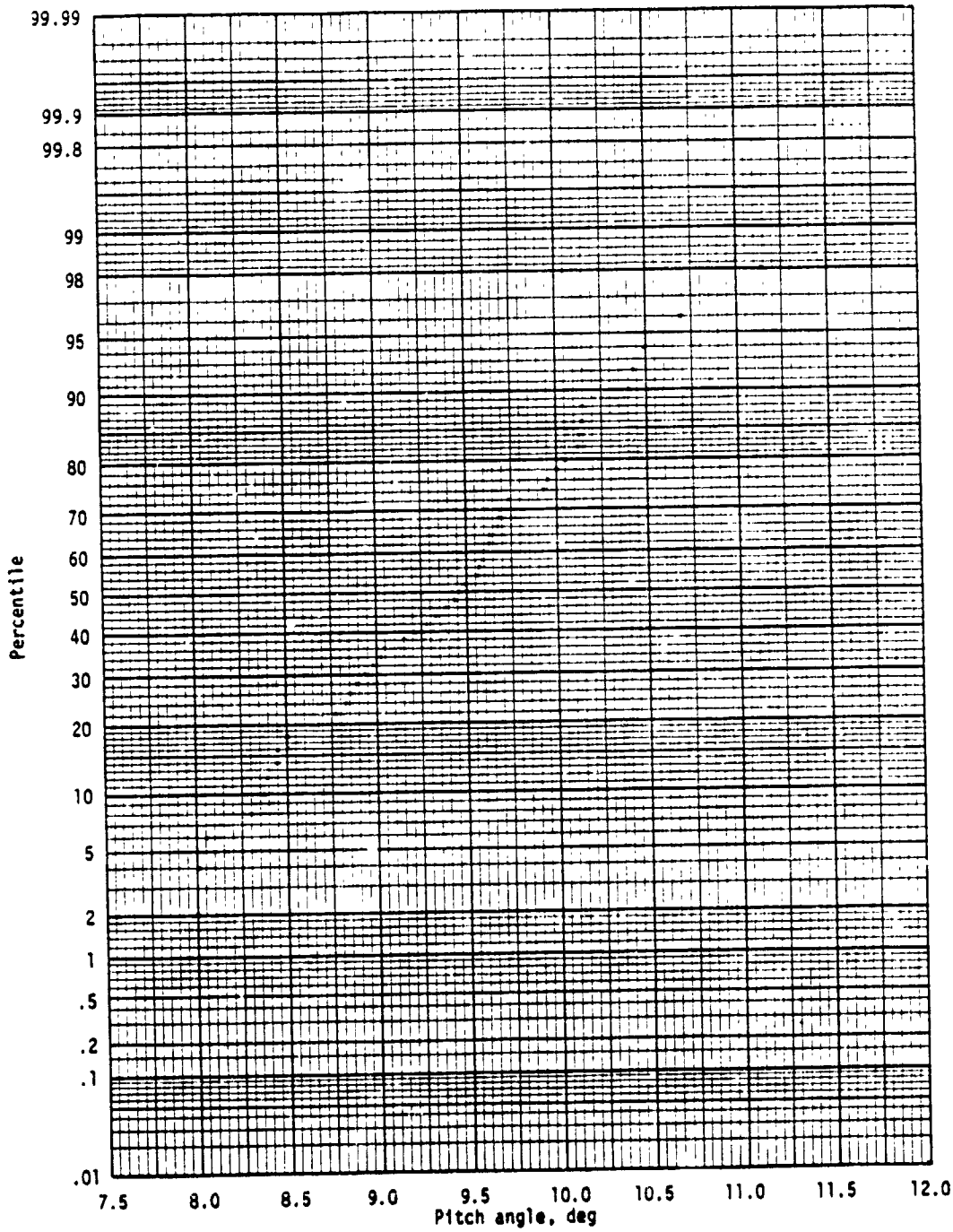

(f) Pitch.

Figure 23.- Continued.

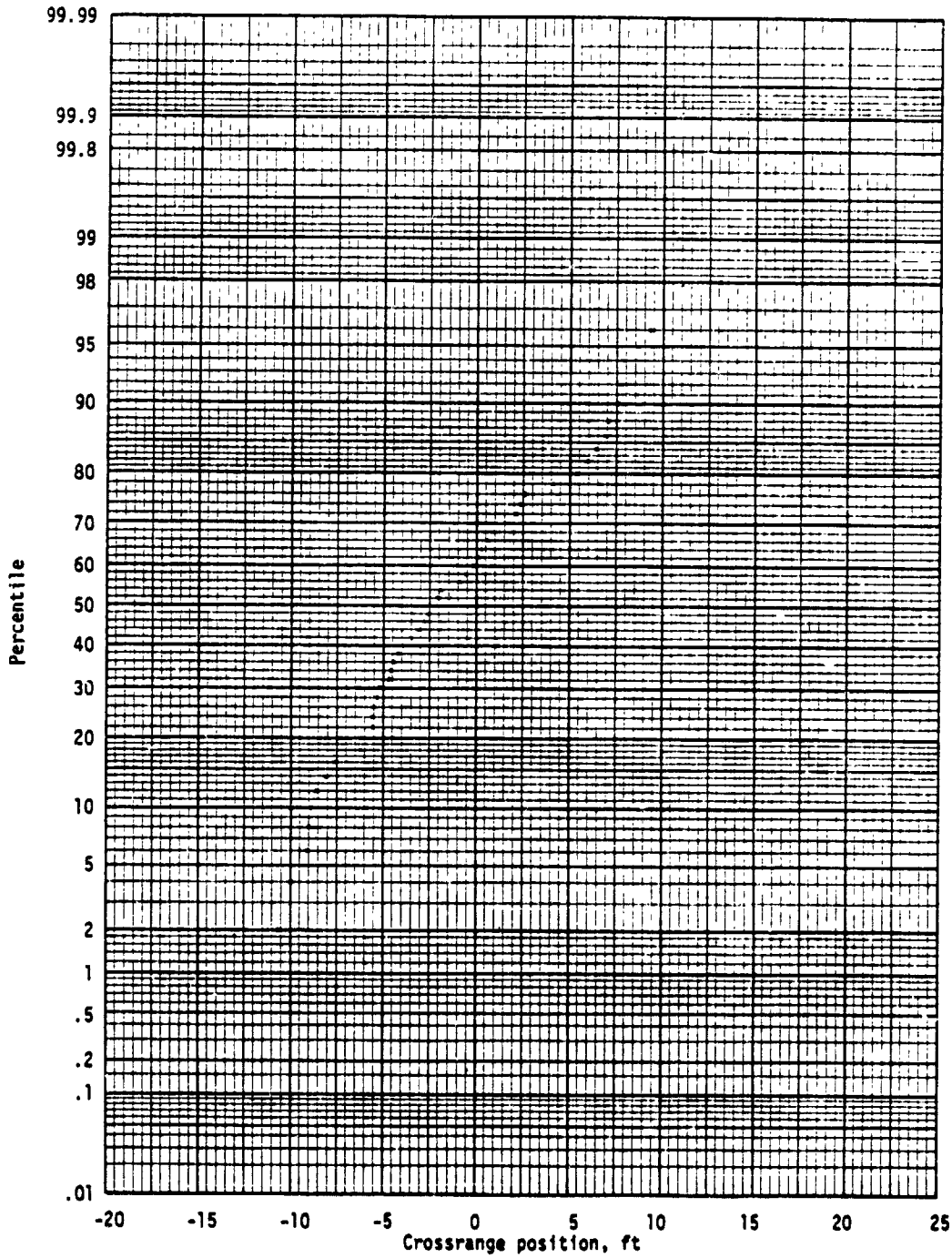

(g) Crossrange position.

Figure 23.- Continued.

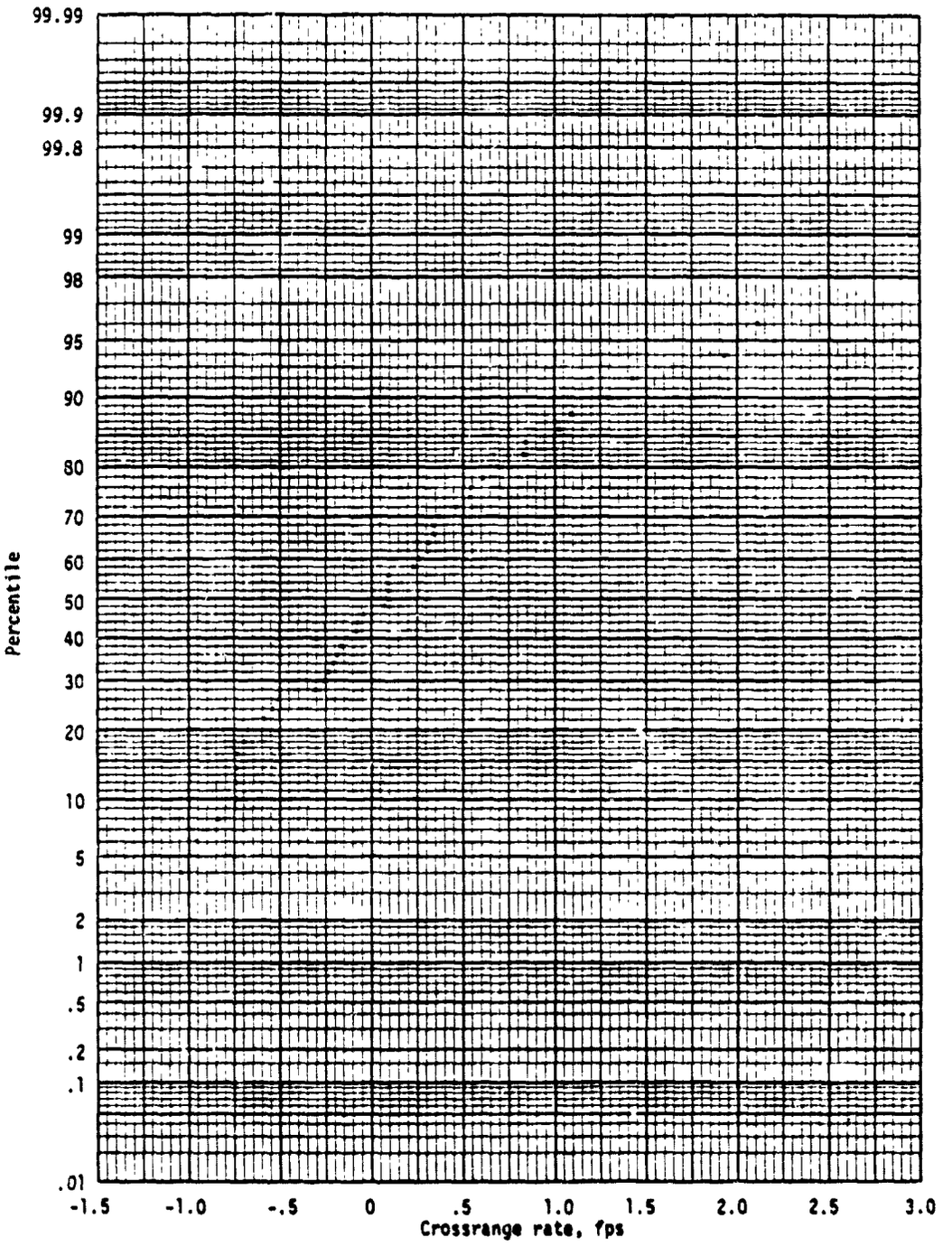

(h) Crossrange velocity.

Figure 23.- Concluded.

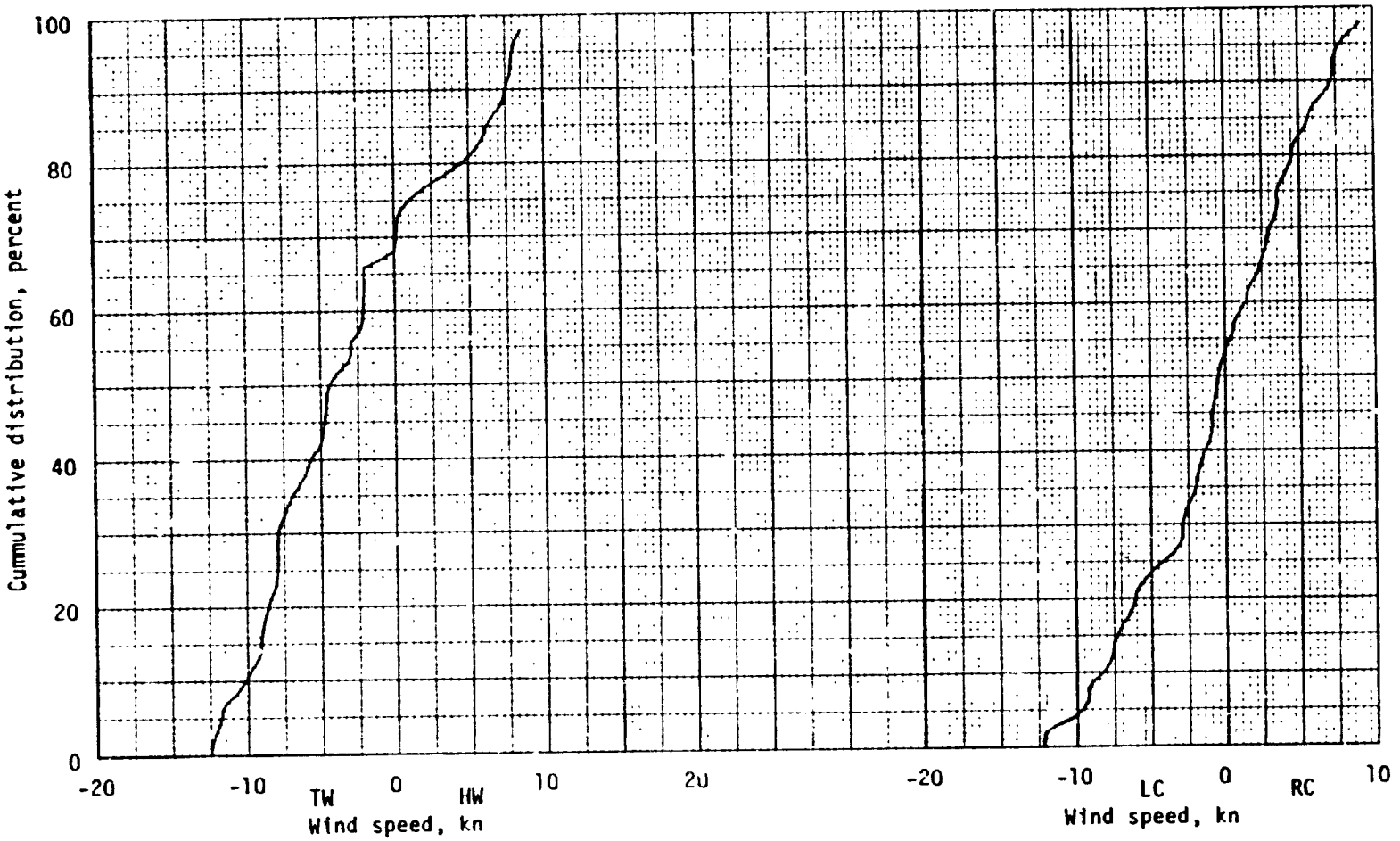

(a) Head or tail wind magnitude.

(b) Cross wind magnitude.

Figure 24.- Northrup strip surface wind statistics.

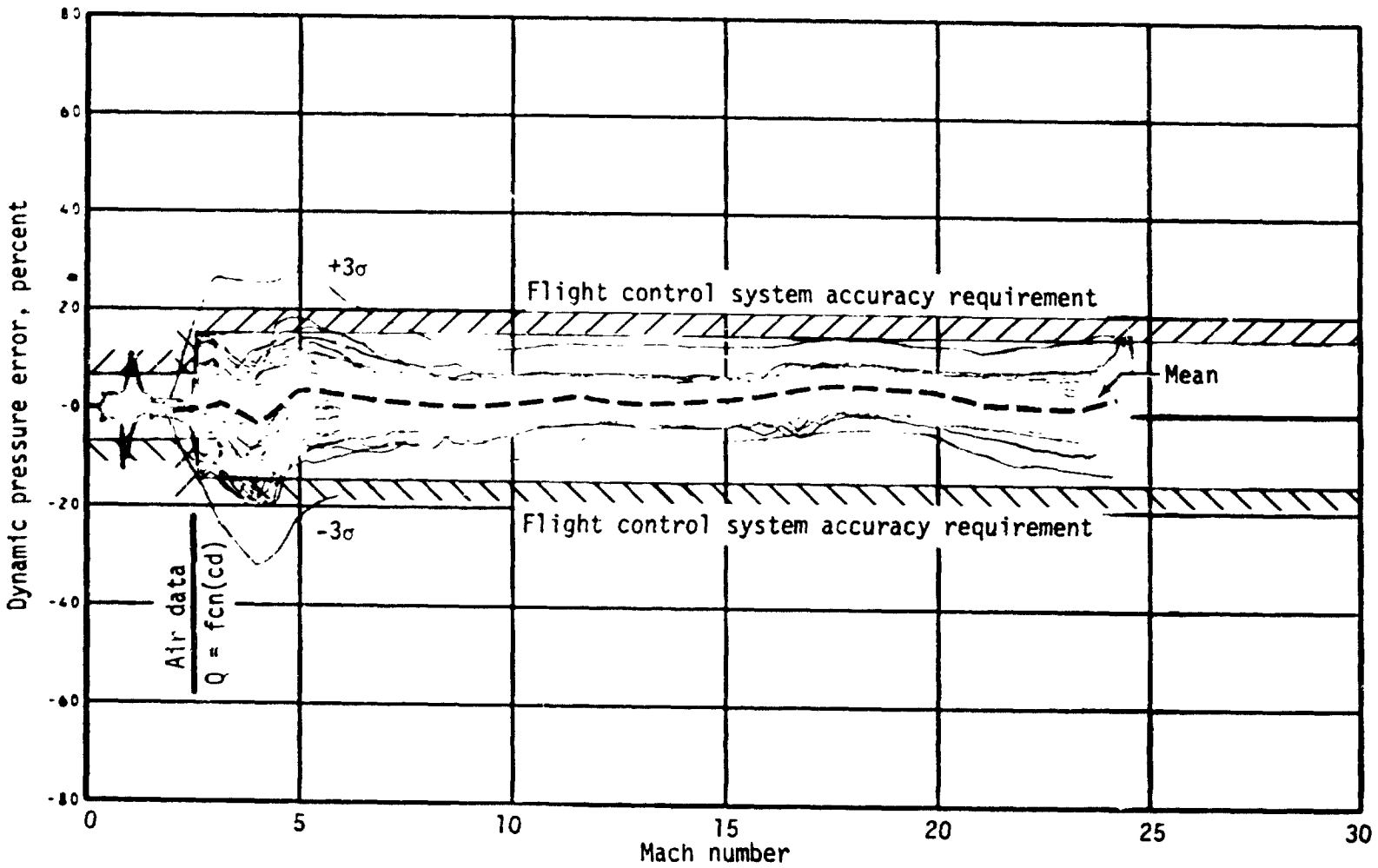

(a) Percent dynamic pressure error.

Figure 25.- Navigation derived and/or data derived parameter performance - shallow abort once around.

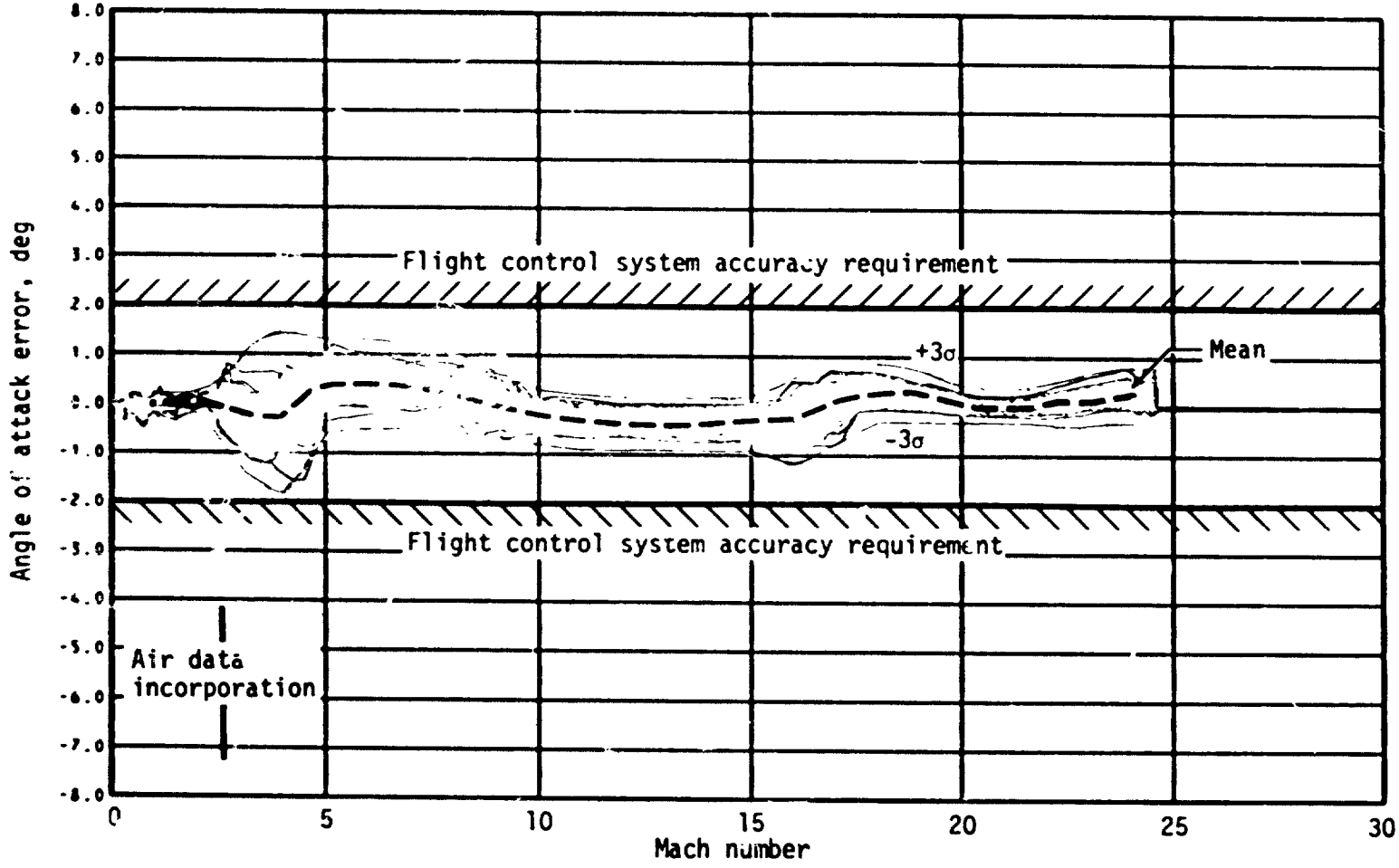

(b) Angle of attack error.

Figure 25.- Continued.

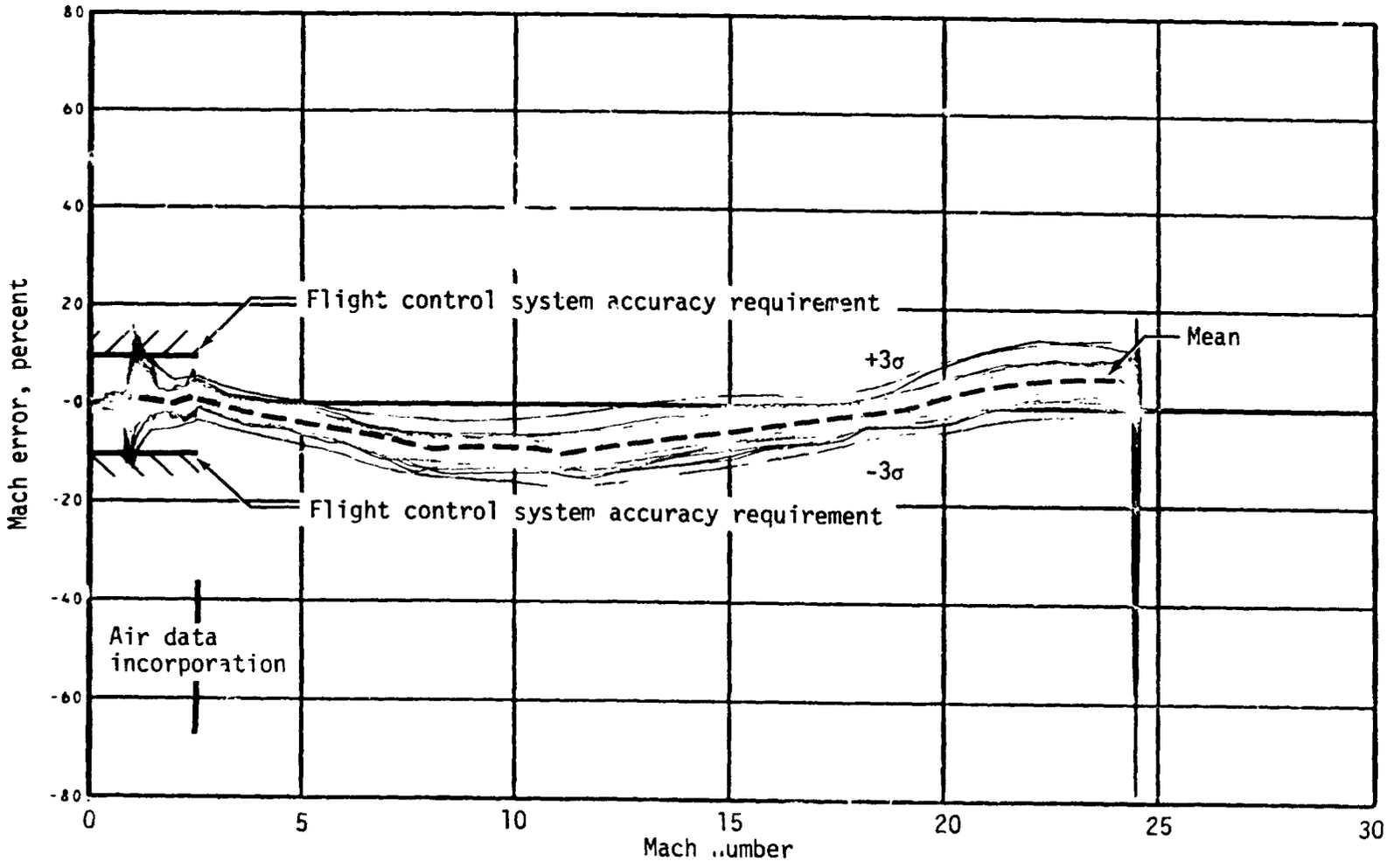

(c) Percent mach number error.

Figure 25.- Continued.

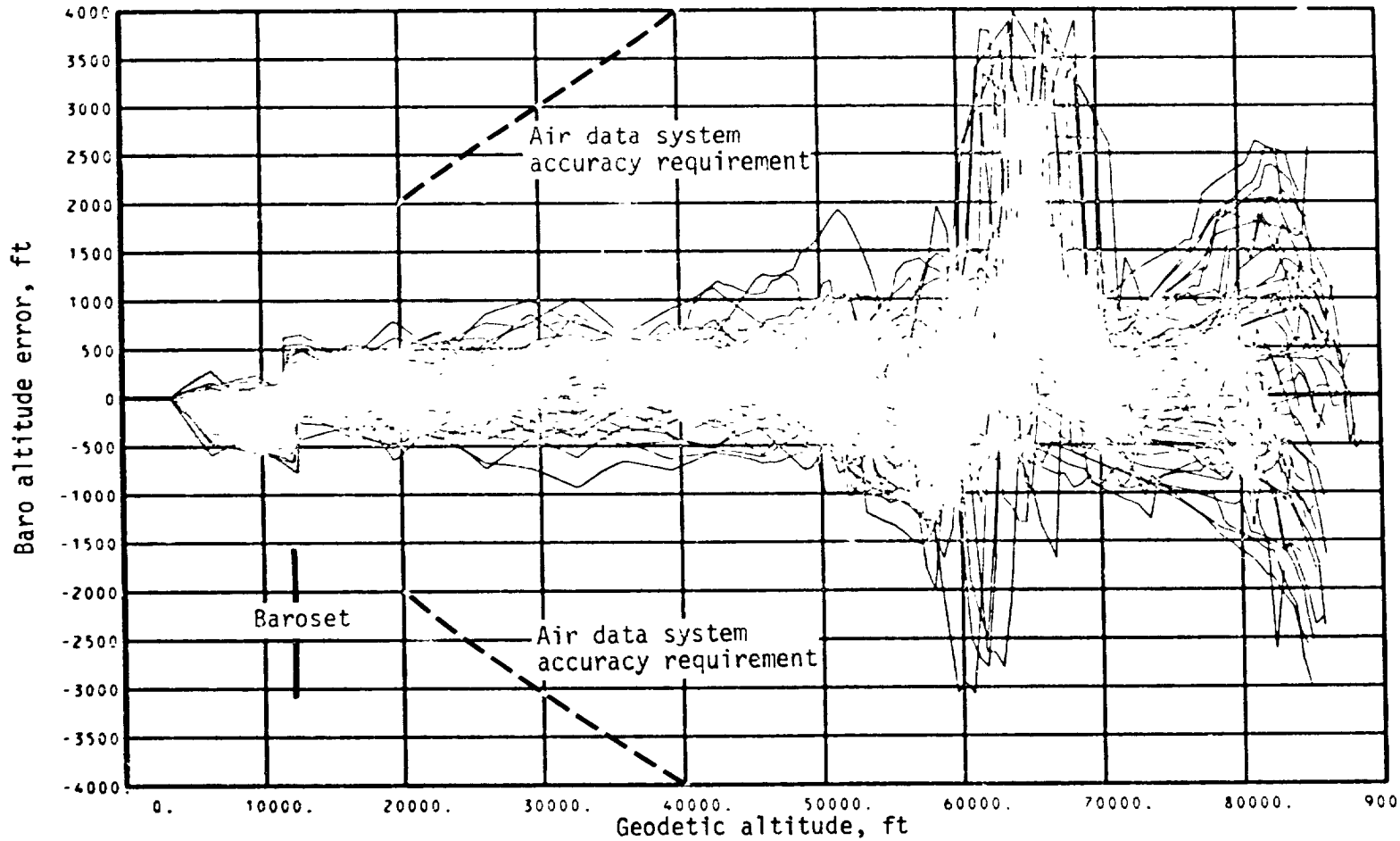

(d) Baro altitude error.

Figure 25.- Concluded.

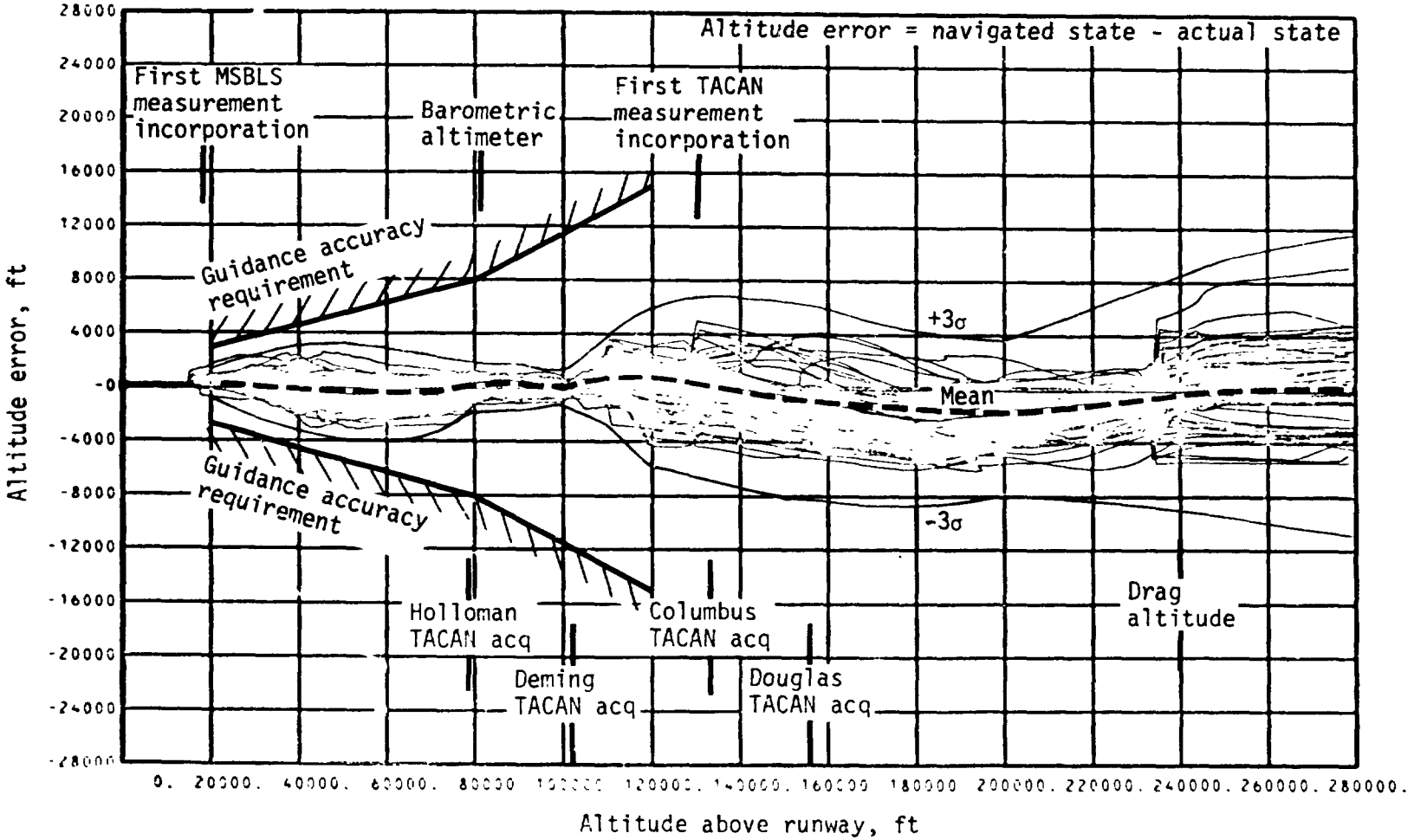

(a) Altitude error.

Figure 26.- Navigated state vector performance - shallow abort once around.

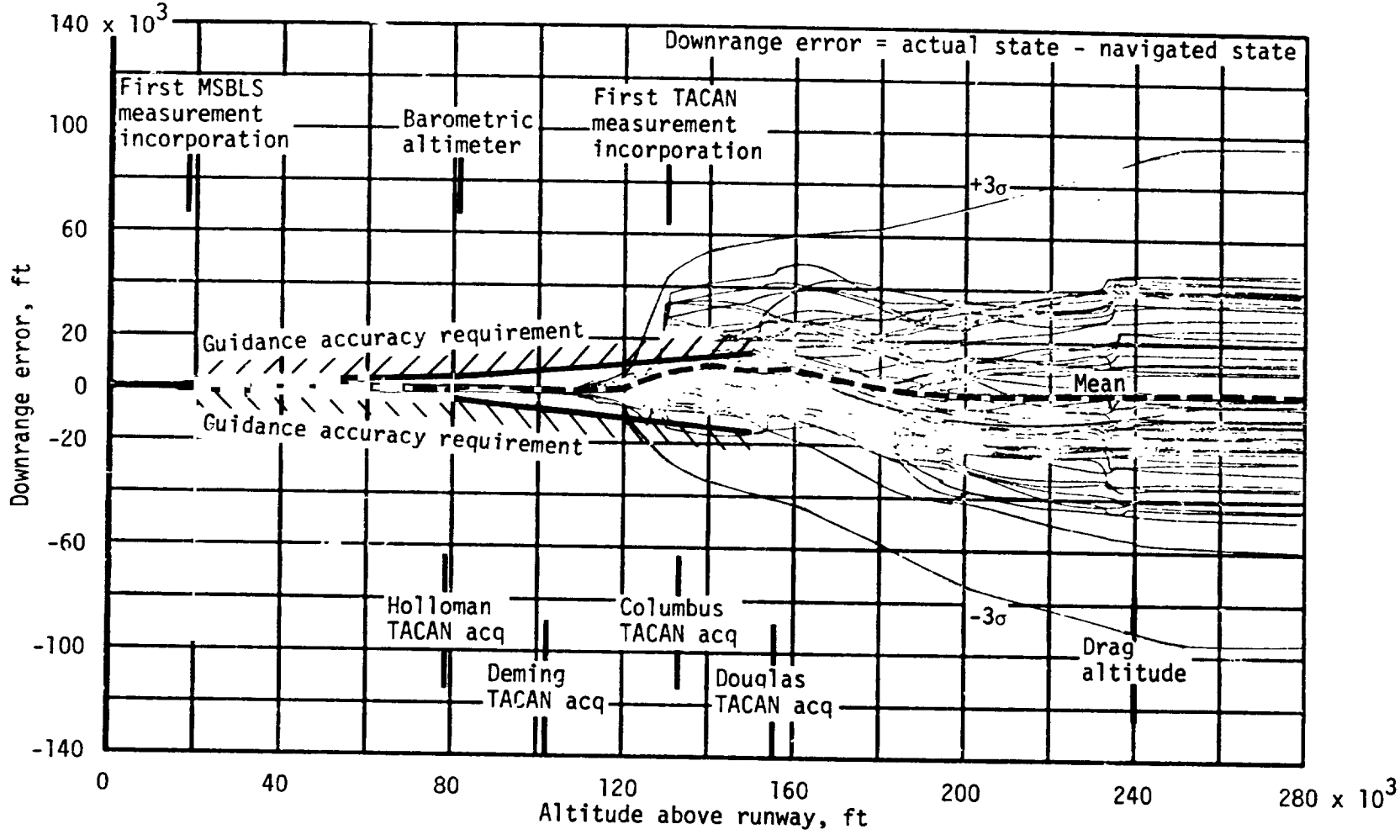

(b) Downrange error.

Figure 26.- Continued.

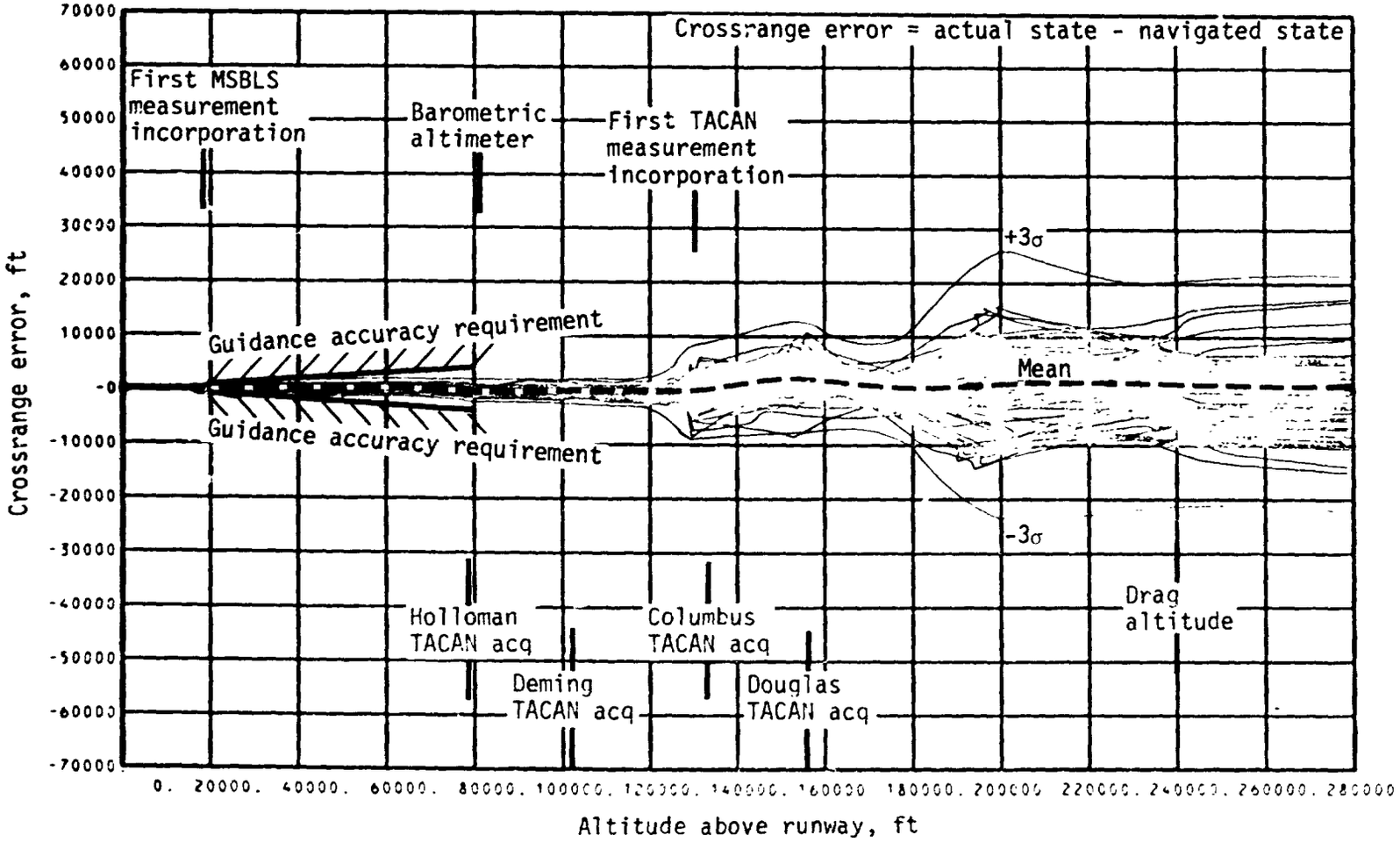

(c) Crossrange error.

Figure 26.- Continued.

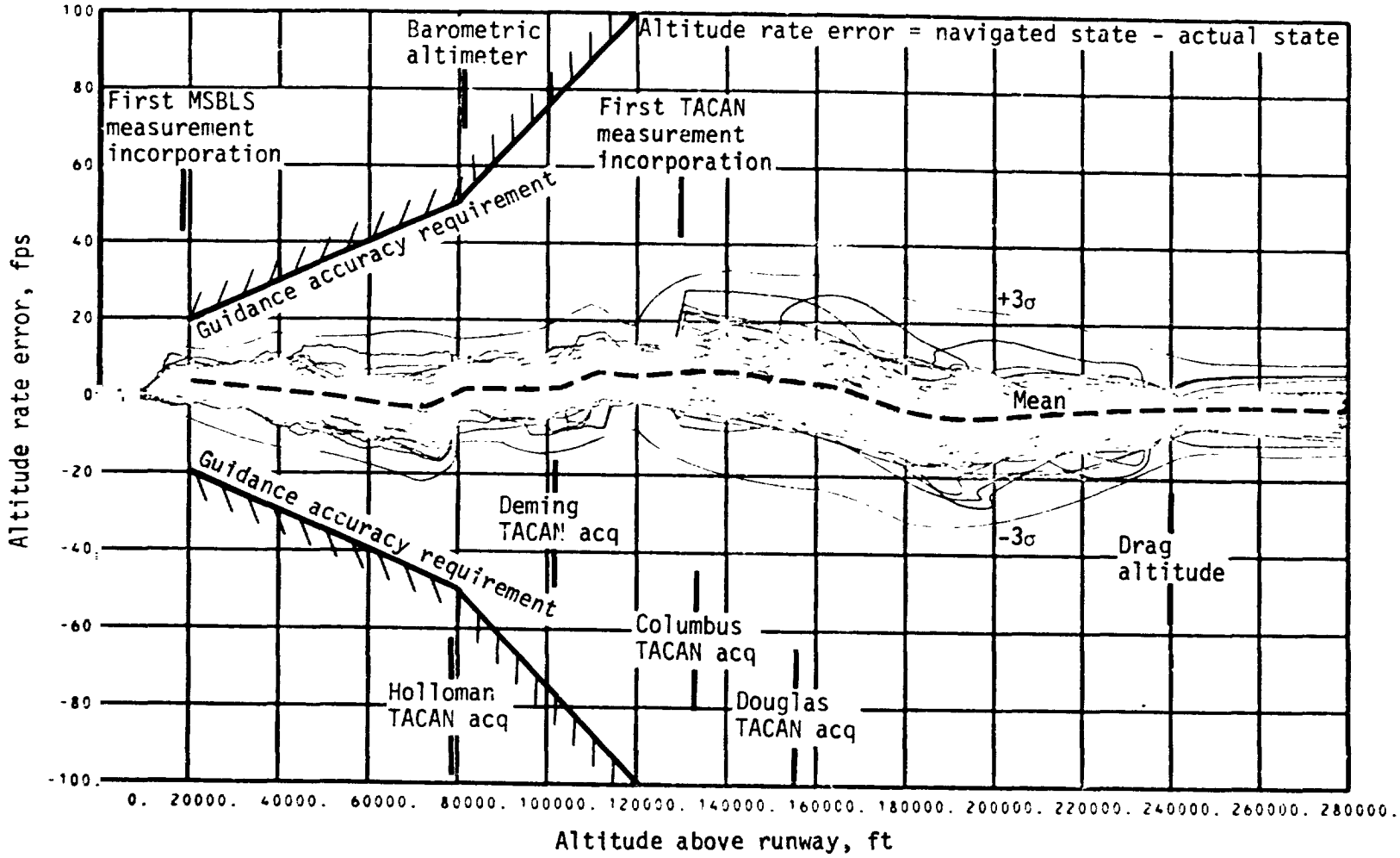

(d) Altitude rate error.

Figure 26.- Continued.

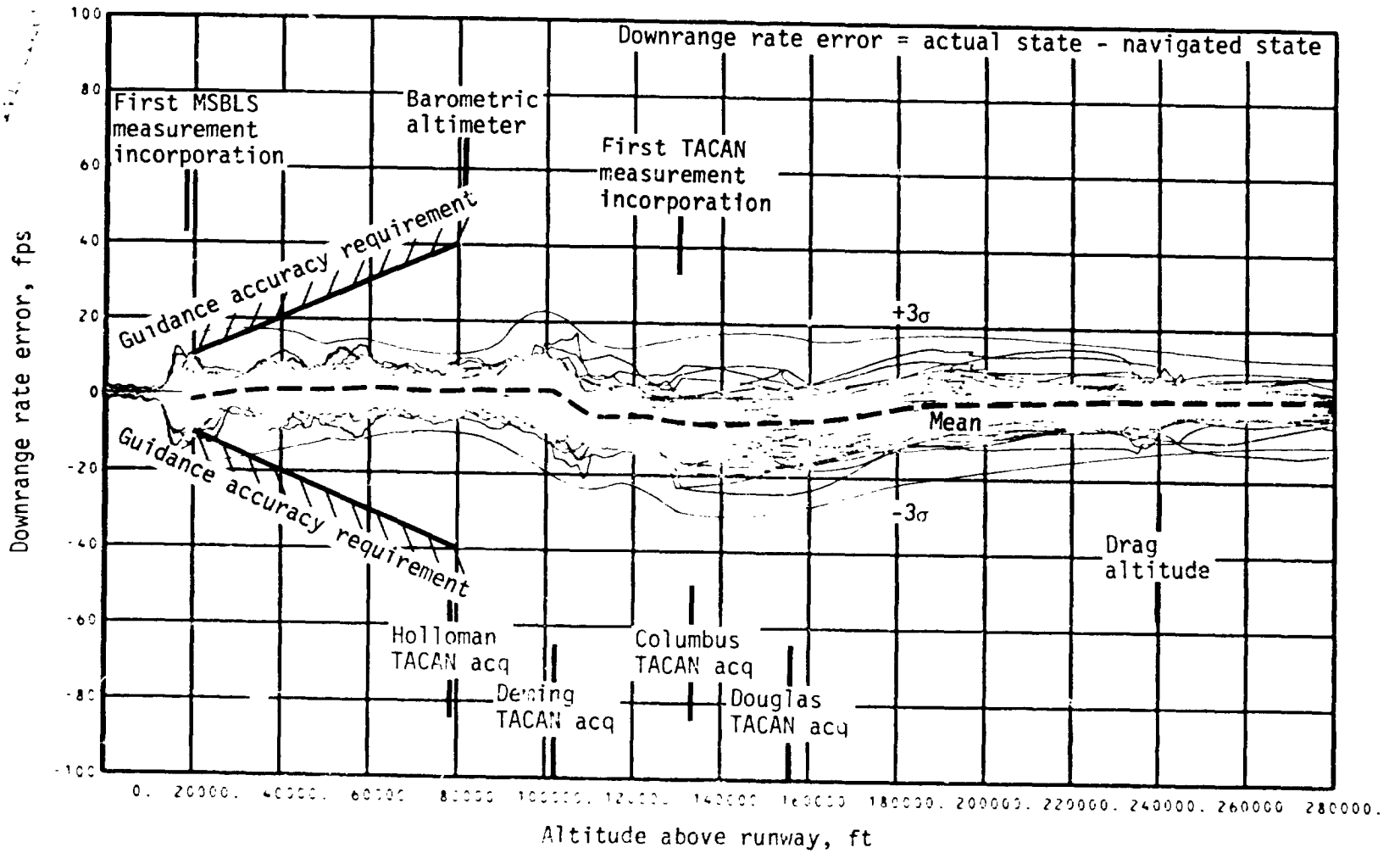

(e) Downrange rate error.

Figure 26.- Continued.

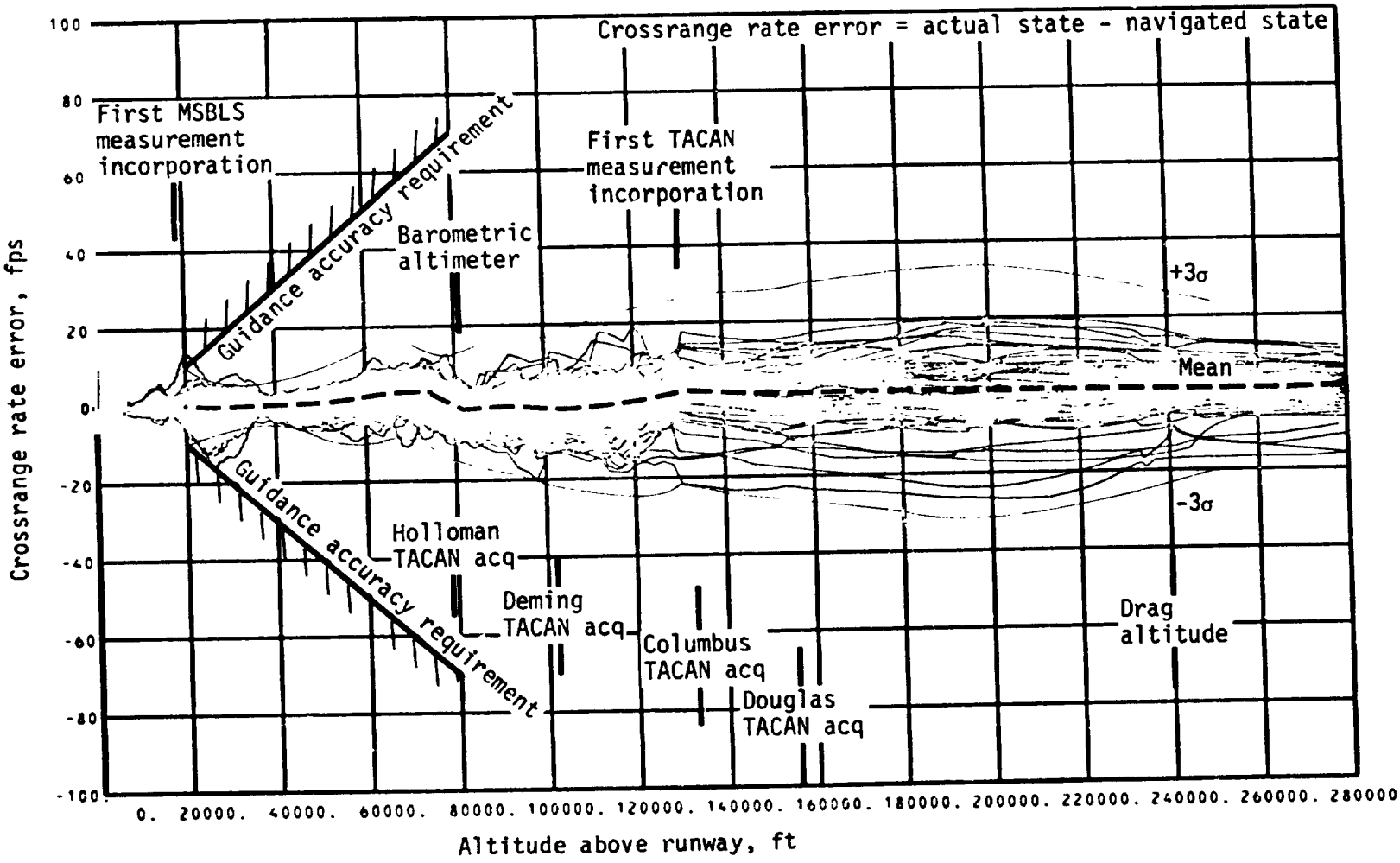

(f) Crossrange rate error.

Figure 26.- Continued.

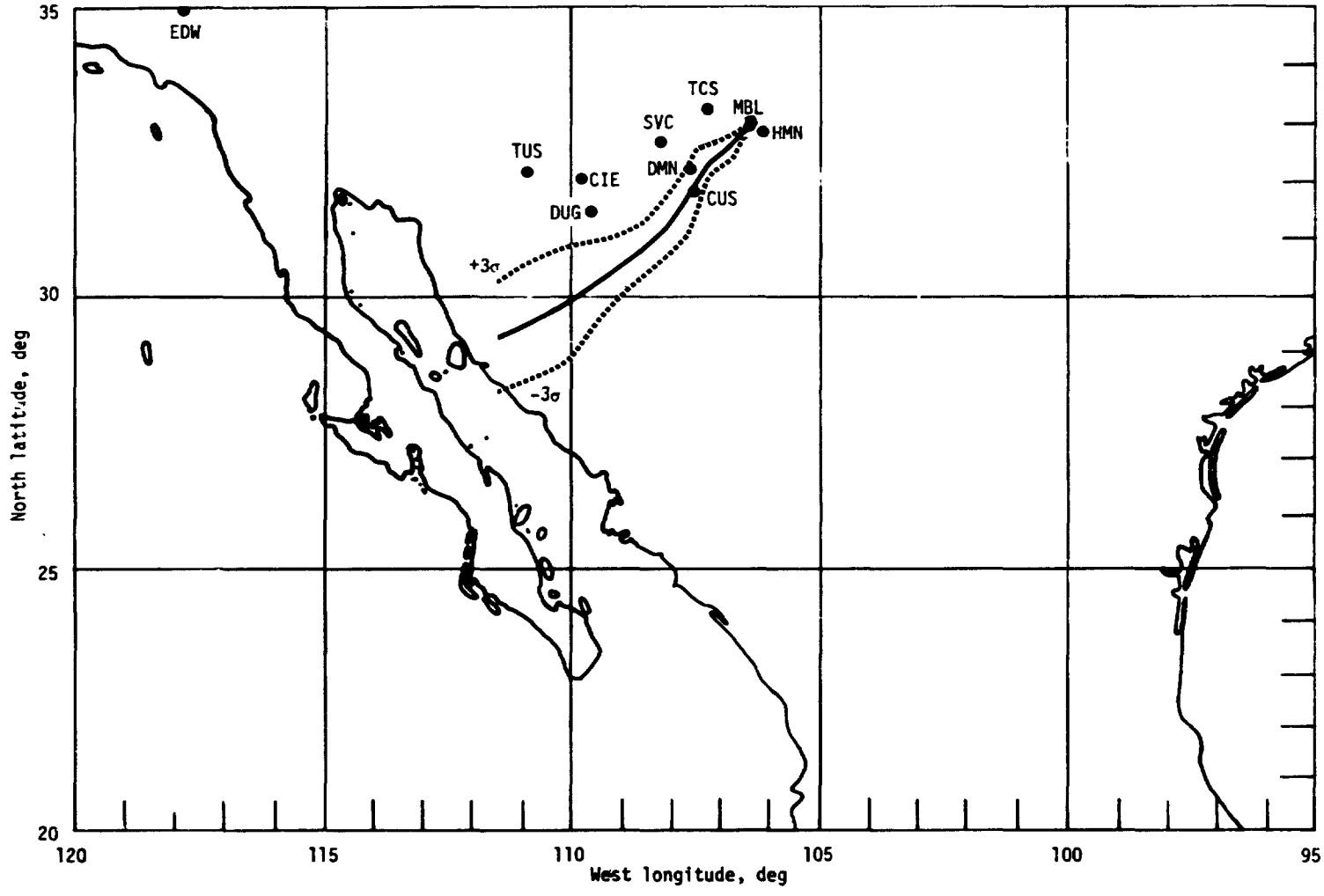

(g) TACAN station locations and groundtrack.

Figure 26.- Concluded.

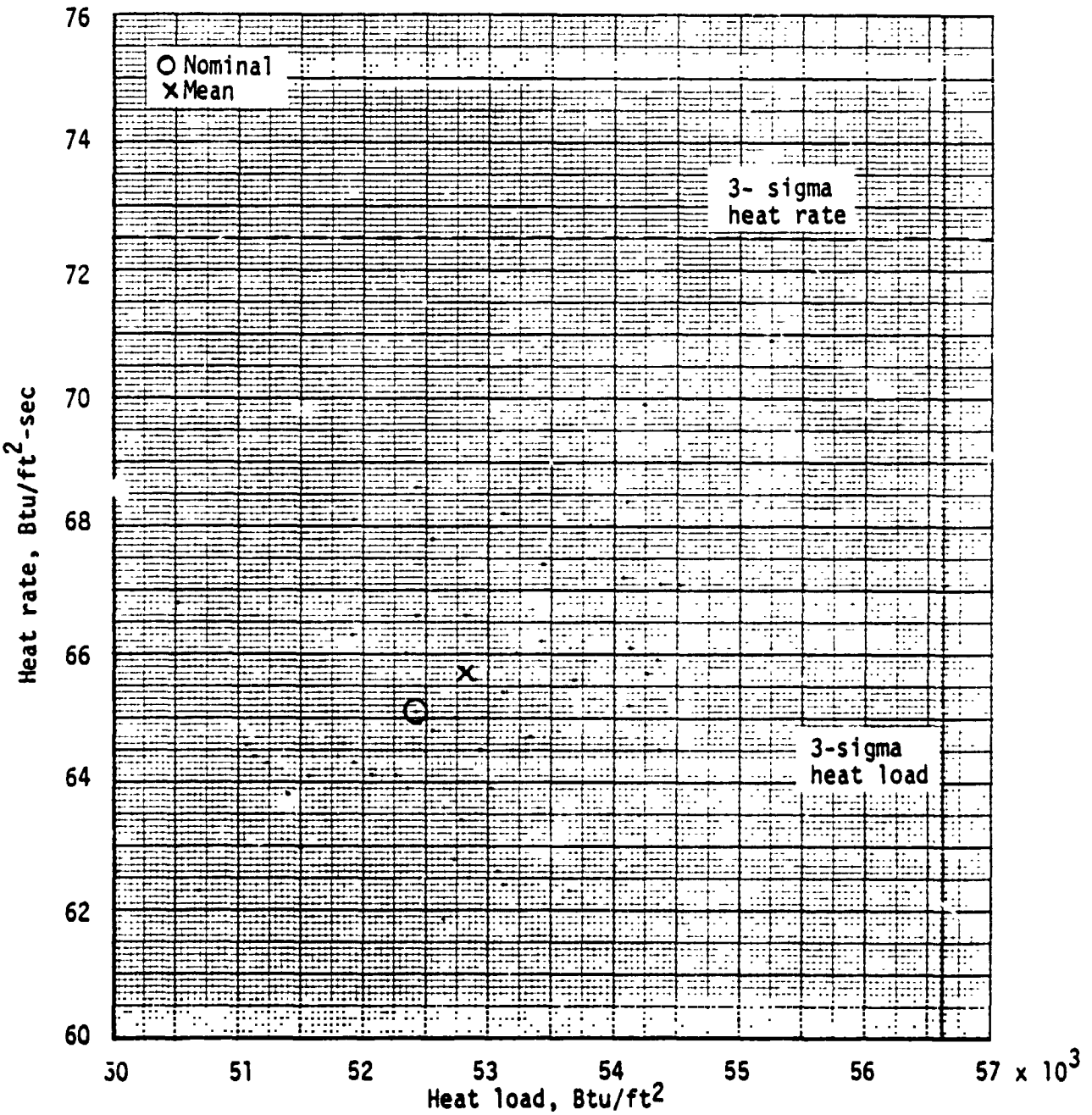

Figure 27.- Heat rate - heat load scatter plot - shallow abort once around.

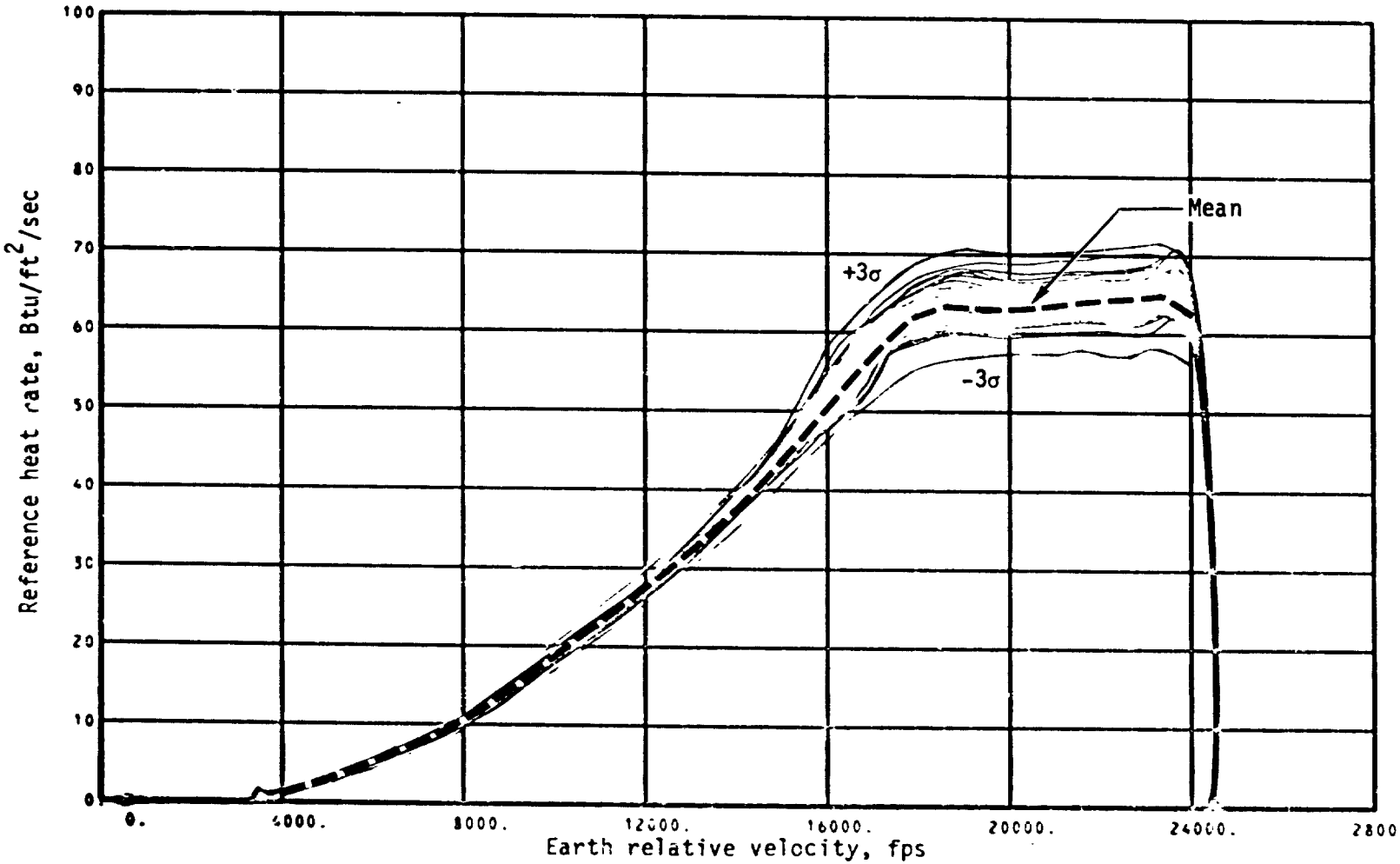

(a) Heat rate.

Figure 28.- TPS performance - shallow abort once around.

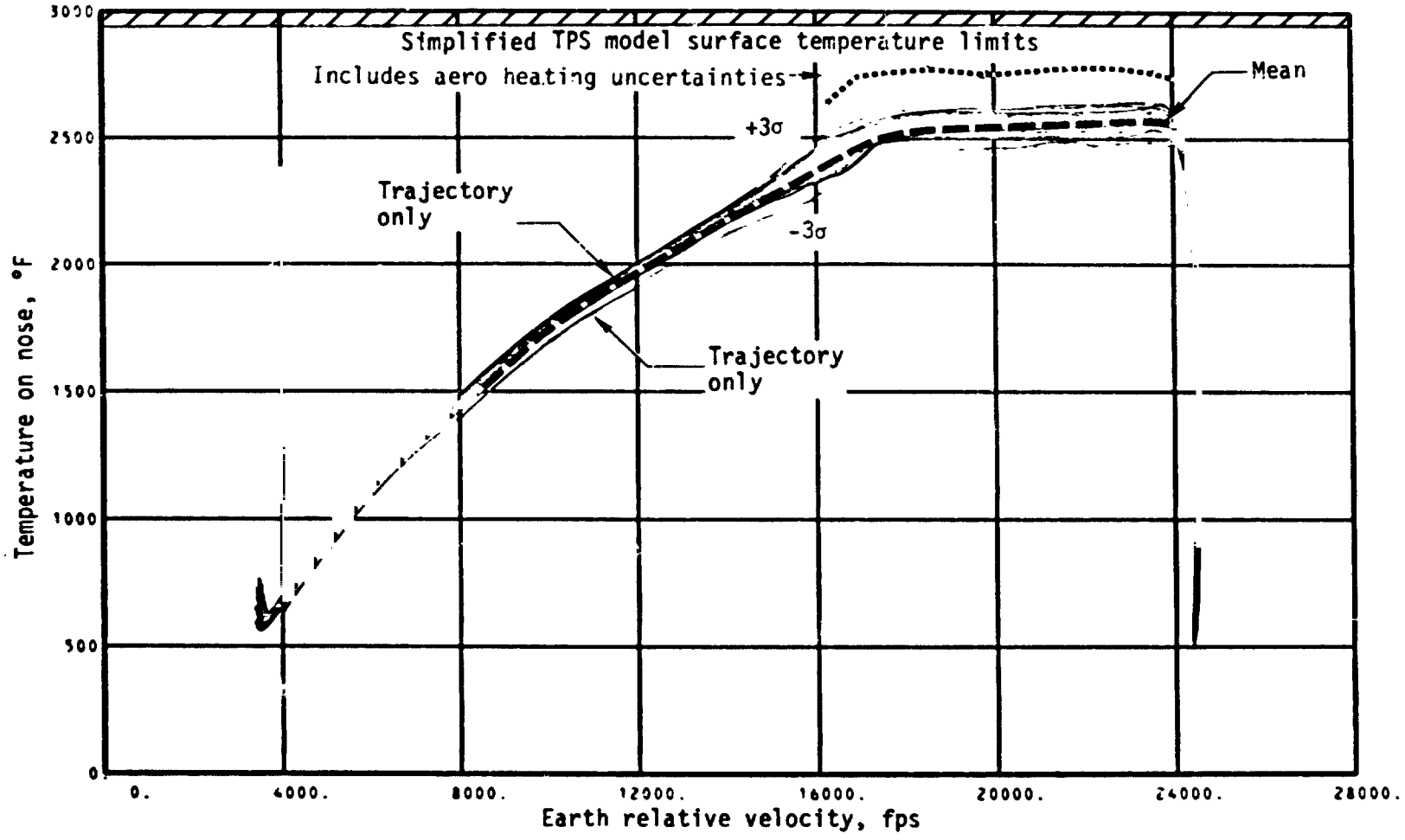

(b) Nose surface temperature.

Figure 28.- Continued.

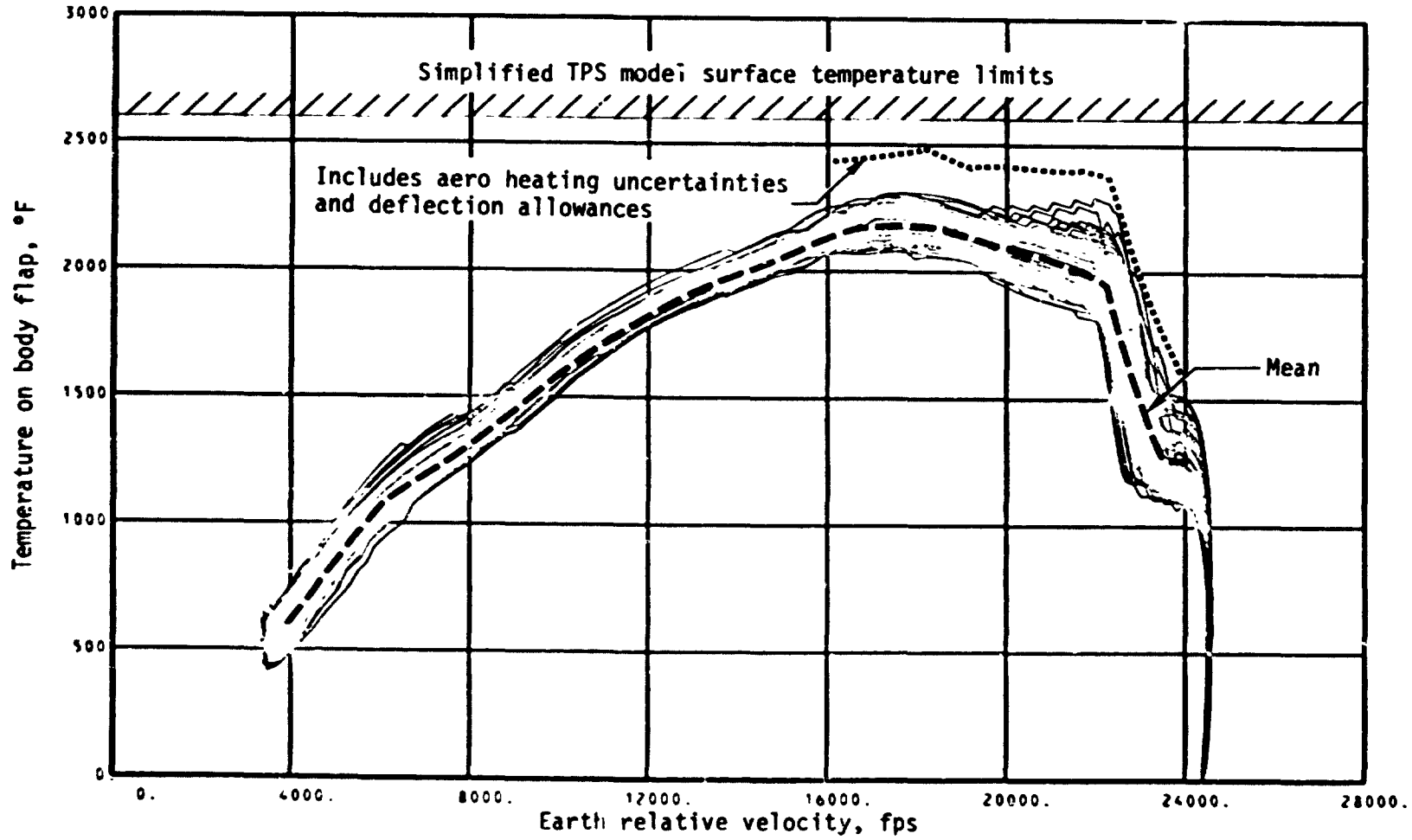

(c) Body flap surface temperature.

Figure 28.- Continued.

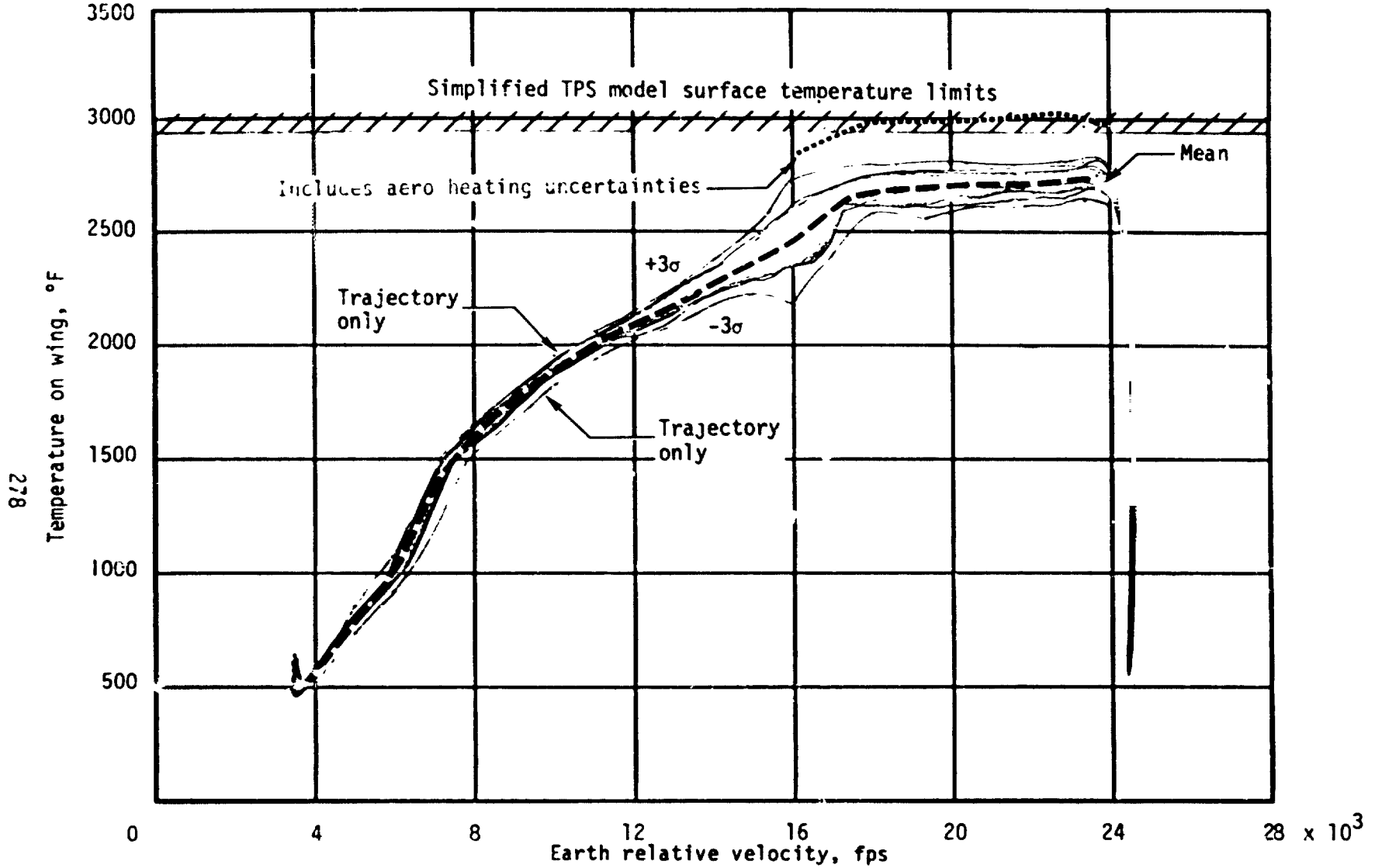

(d) Wing surface temperature.

Figure 28.- Continued.

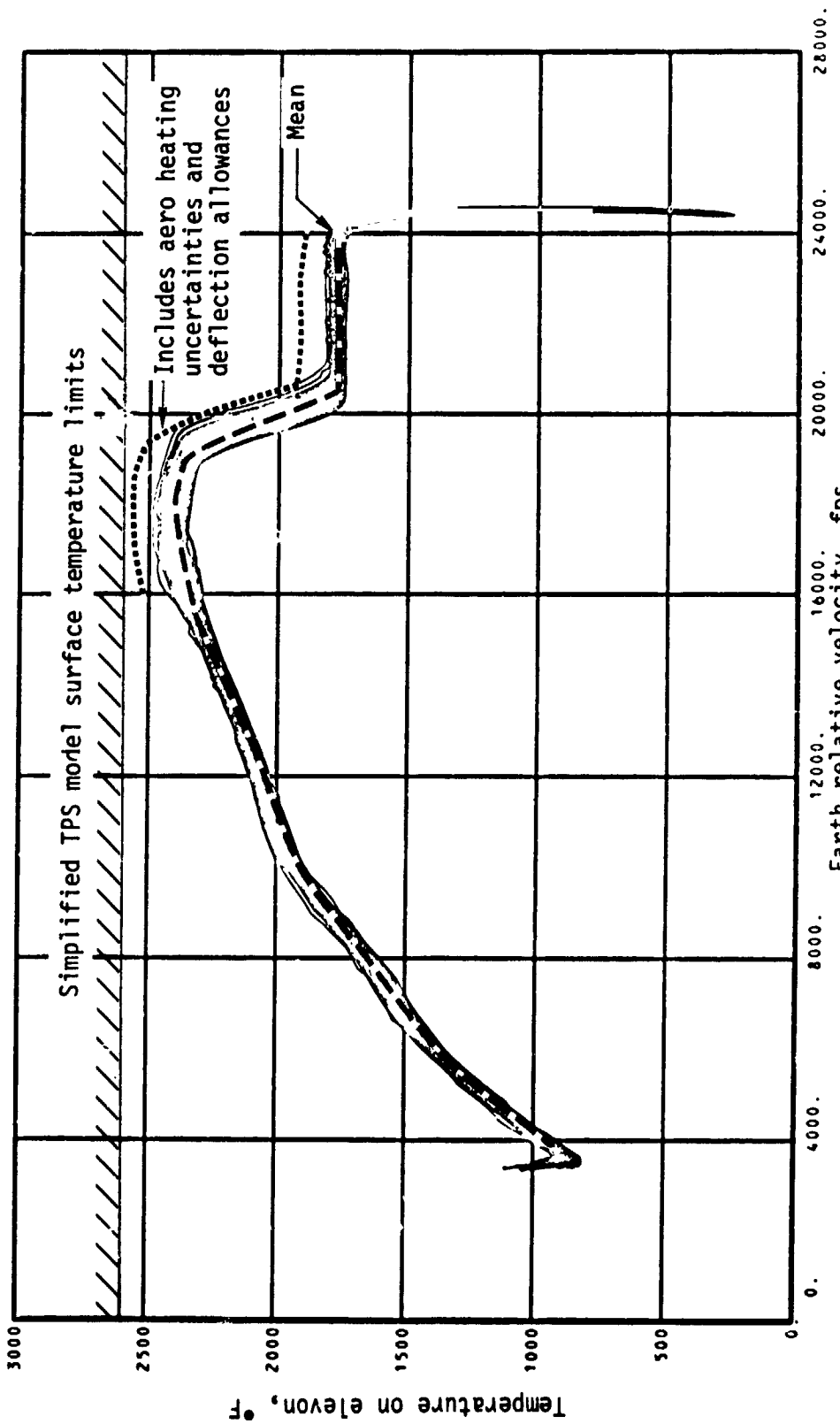

(e) Elevon surface temperature.

Figure 28.- Continued.

C-4

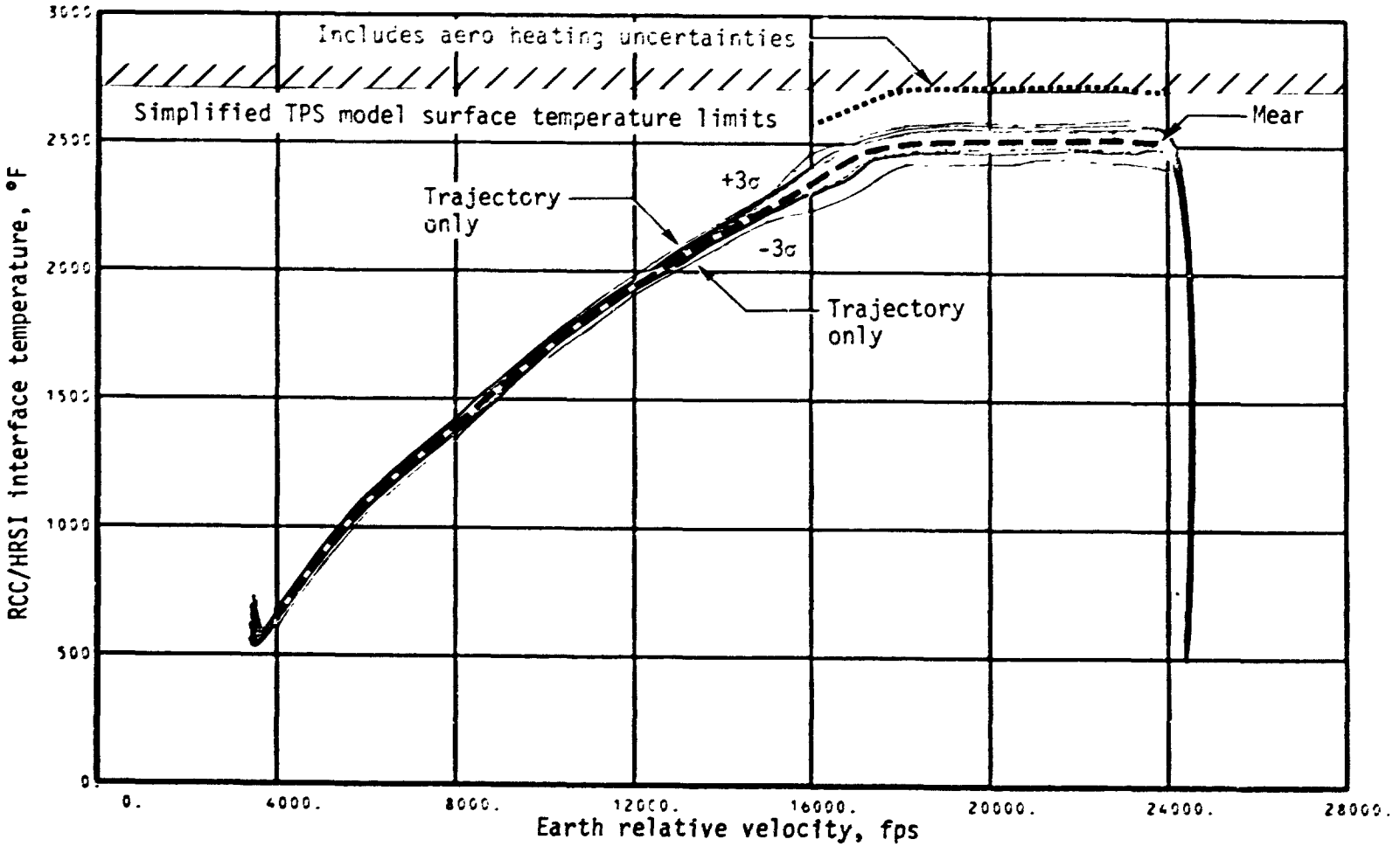

(f) RCC/HRSI interface (CP5) surface temperature.

Figure 28.- Concluded.

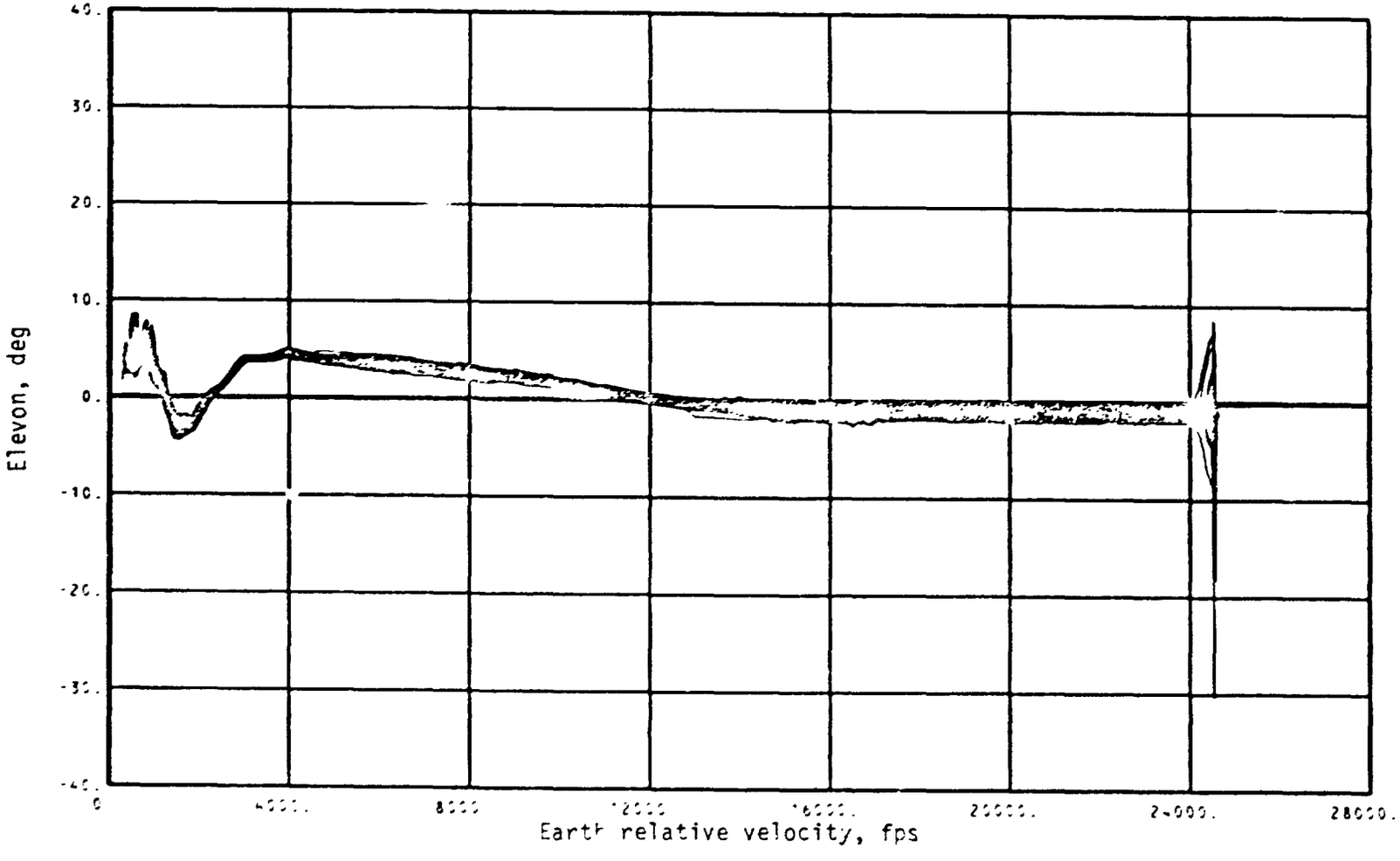

(a) Elevon deflection.

Figure 29.- Control surface deflections and hinge moments - shallow abort once around.

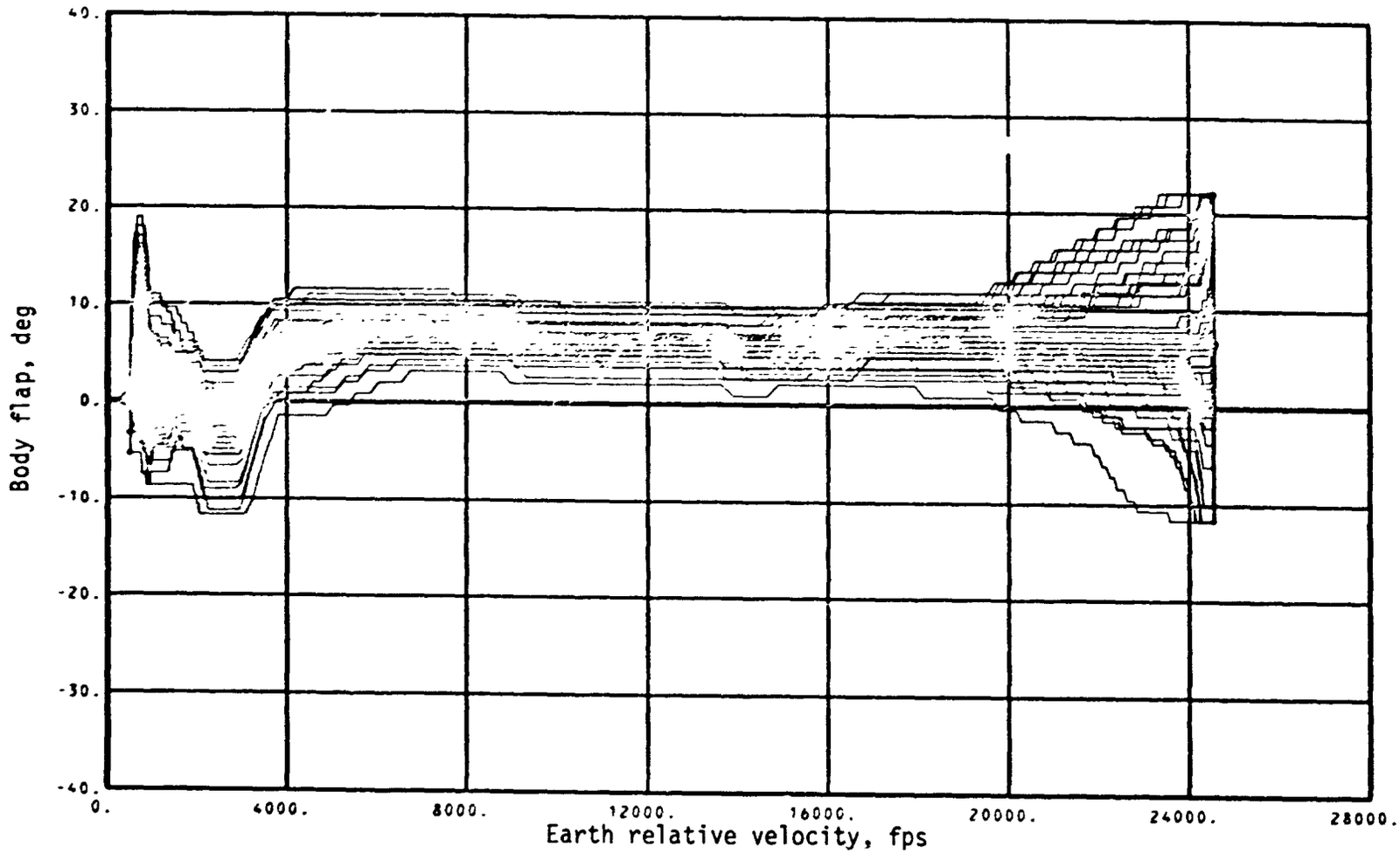

(b) Body flap deflection.

Figure 29.- Continued.

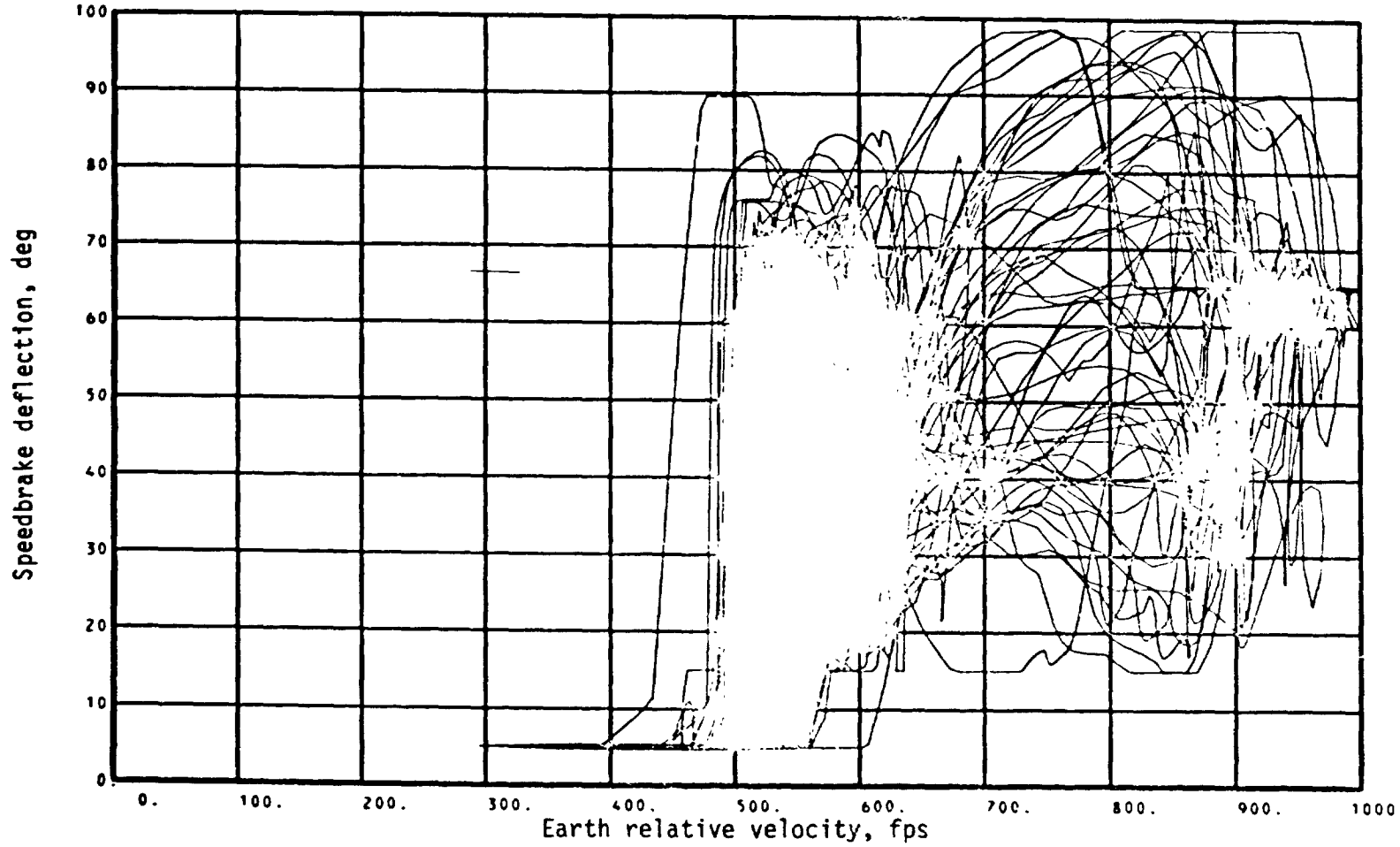

(c) Speedbrake deflection.

Figure 29.- Continued.

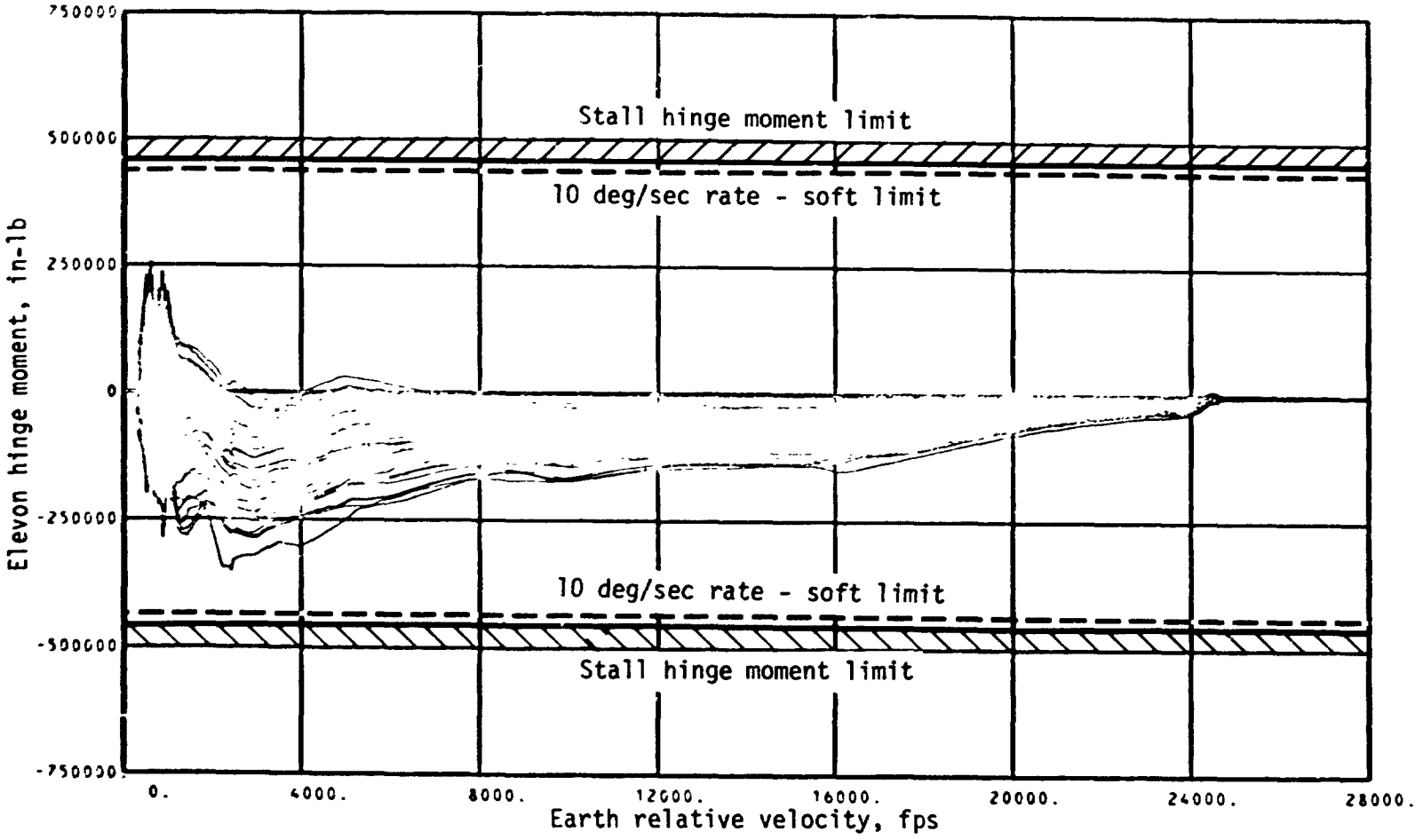

(d) Outboard elevon hinge moment.

Figure 29.- Continued.

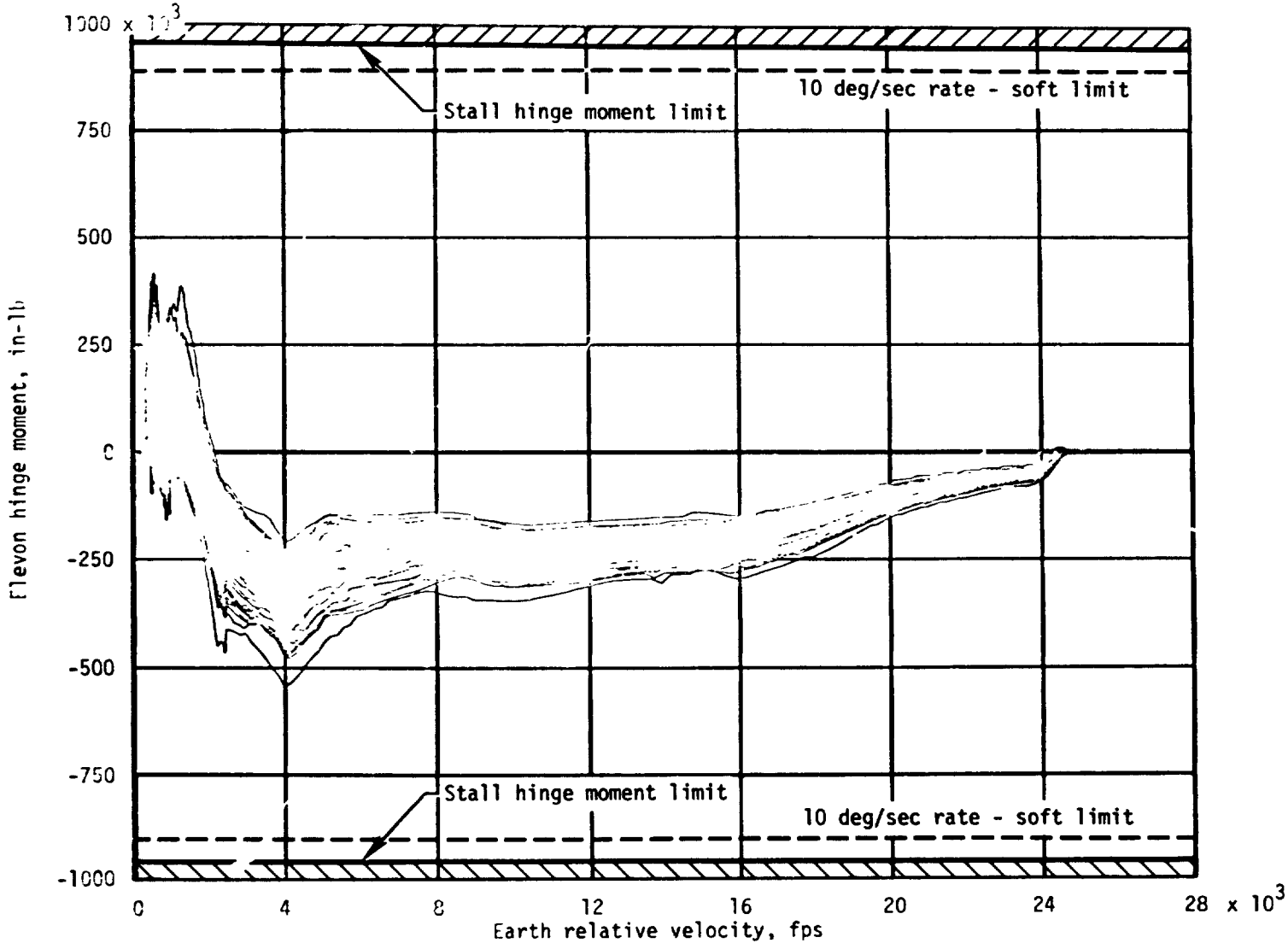

(e) Inboard elevon hinge moment.

Figure 29.- Continued.

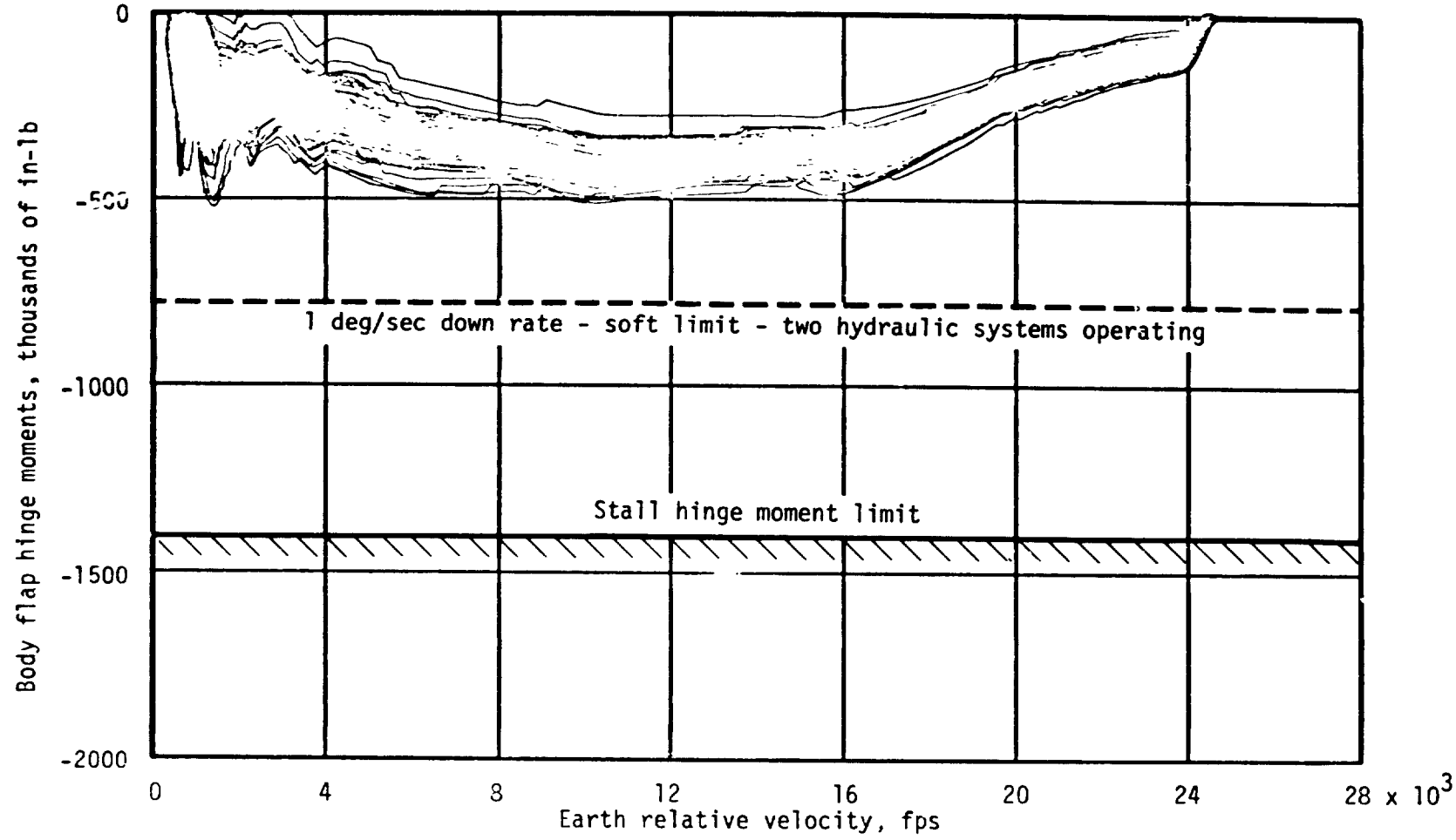

(f) Body flap hinge moment.

Figure 29.- Continued.

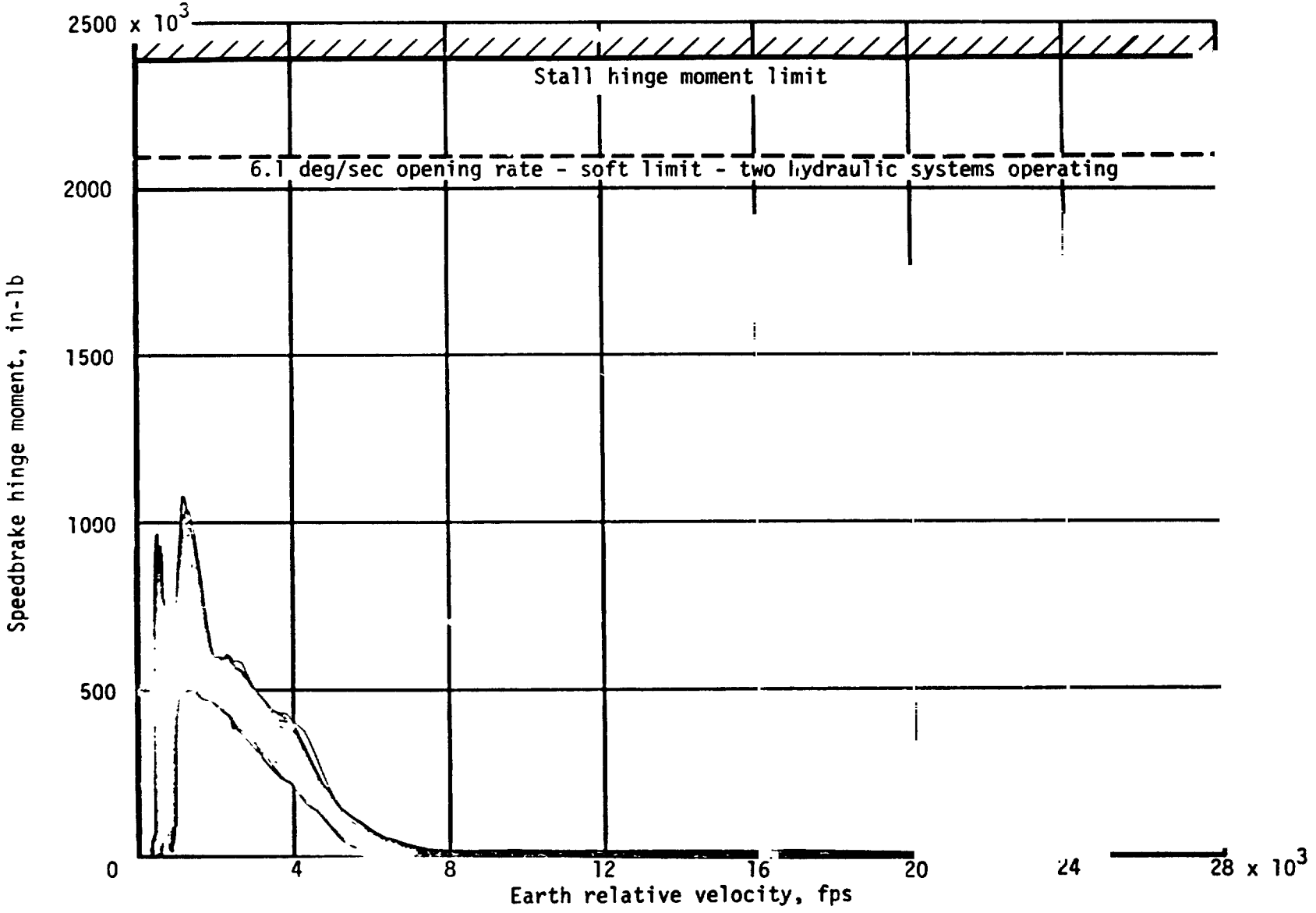

(g) Speedbrake hinge moment.

Figure 29.- Concluded.

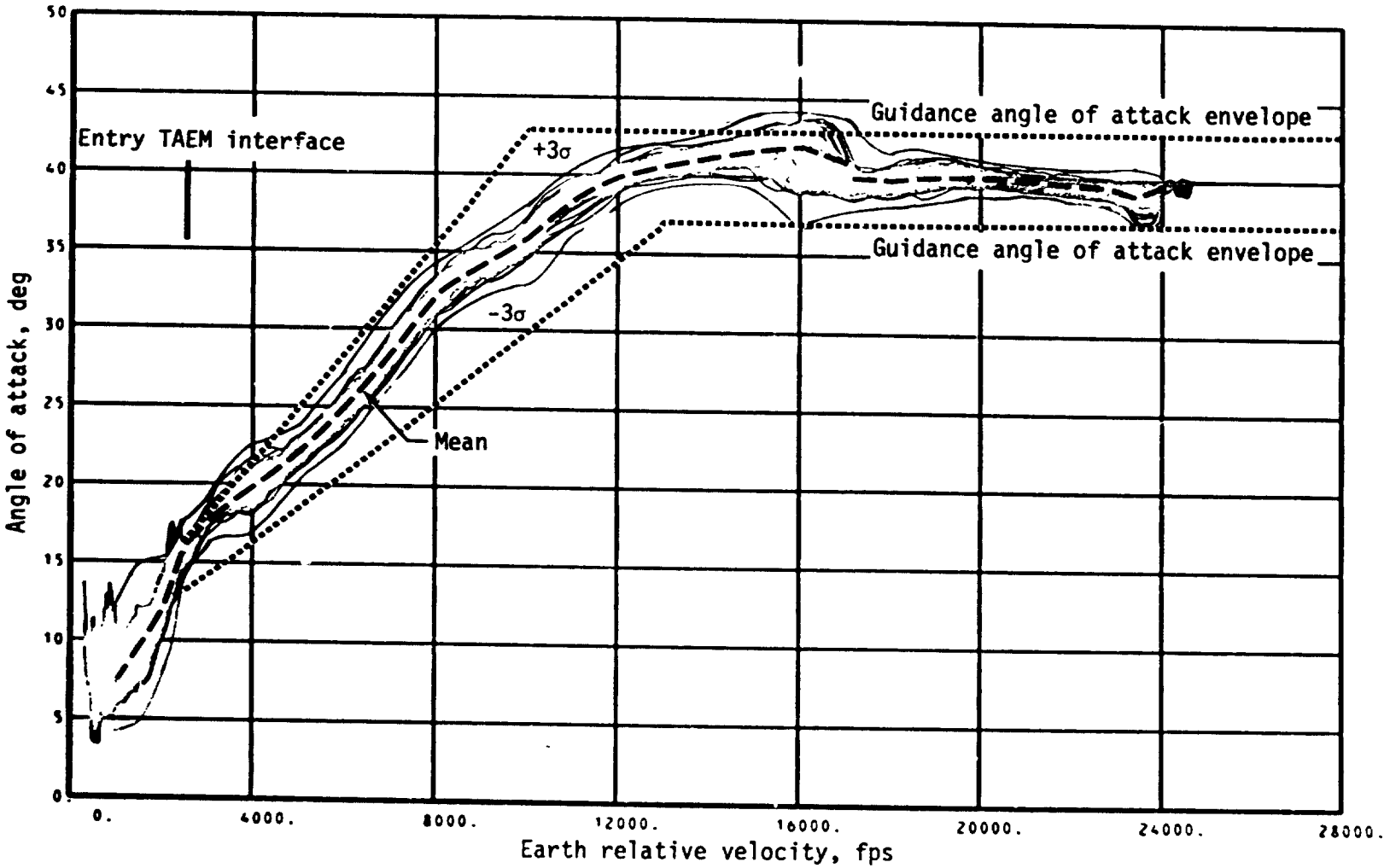

(a) Angle of attack.

Figure 30.- Entry guidance performance parameters - shallow abort once around.

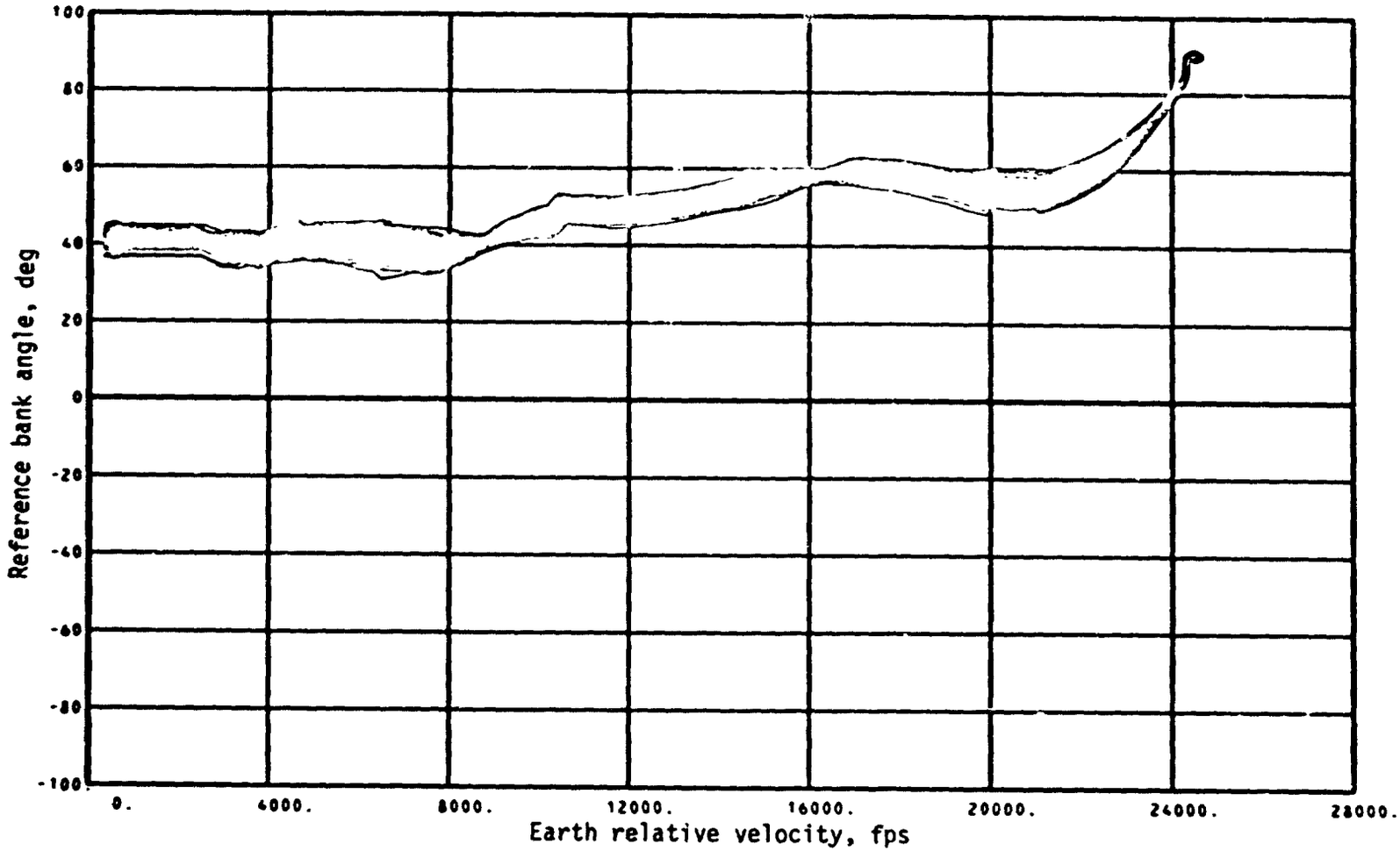

(b) Reference bank angle.

Figure 30.- Continued.

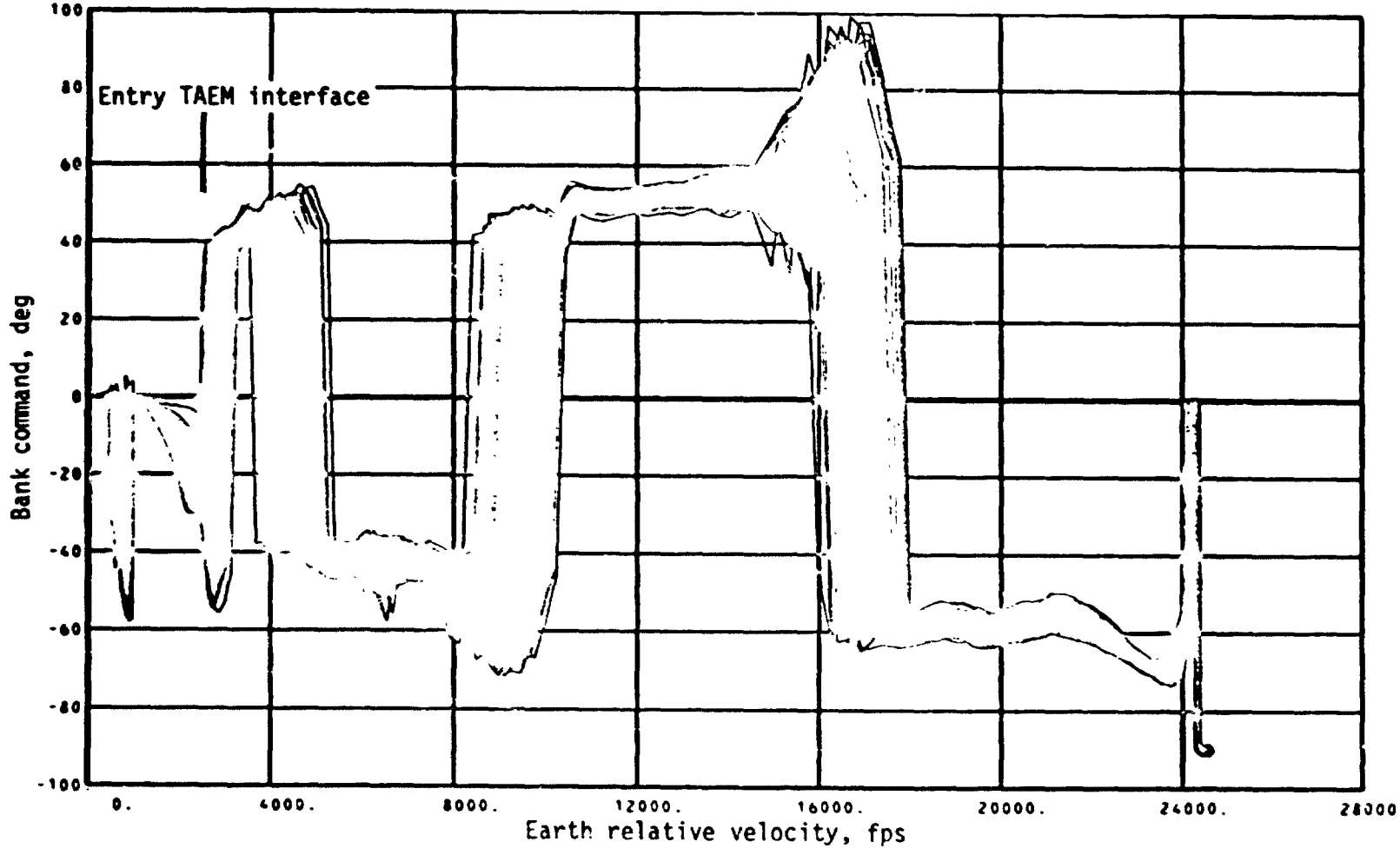

(c) Bank command.

Figure 30.- Continued.

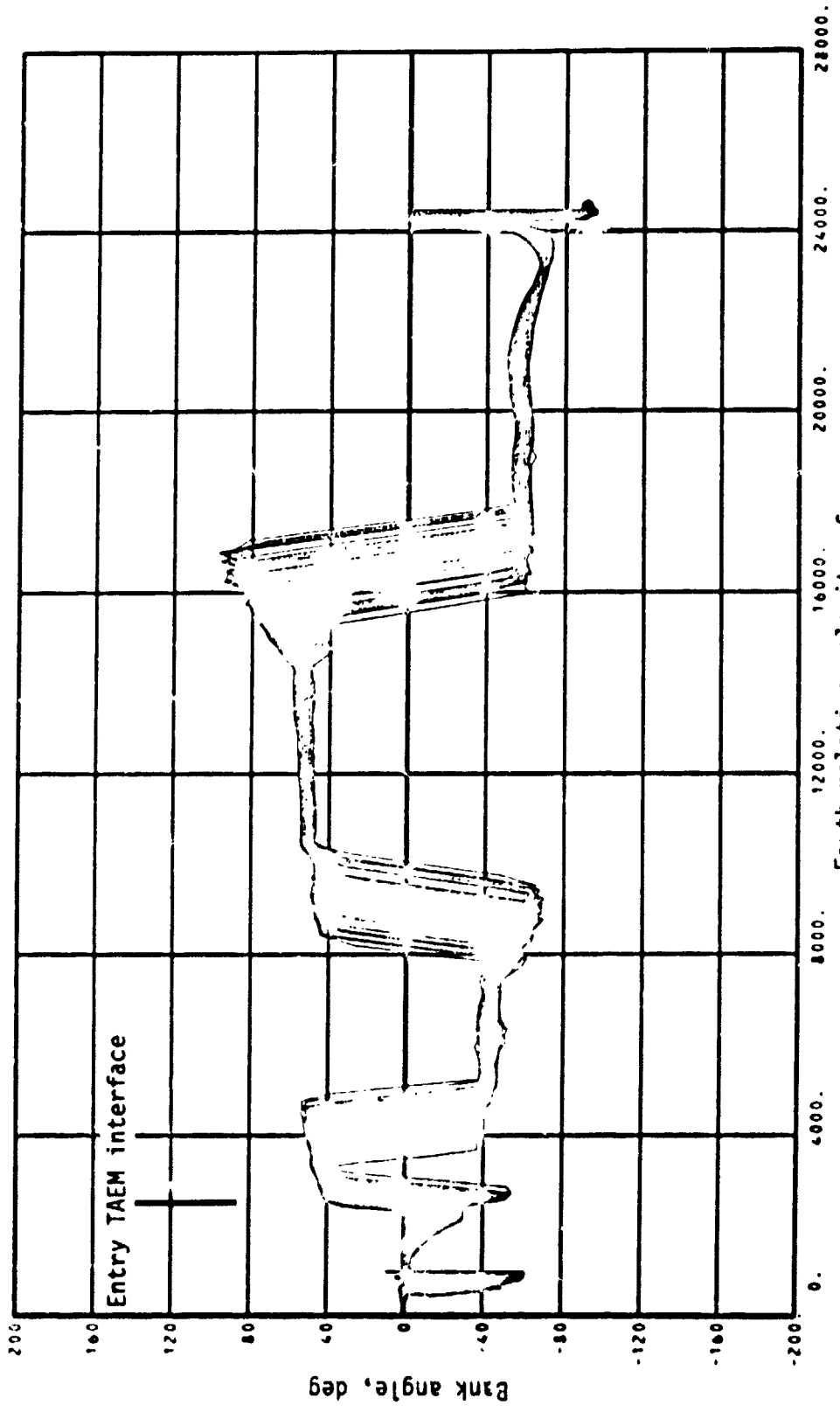

(d) Bank angle.

Figure 30.- Continued.

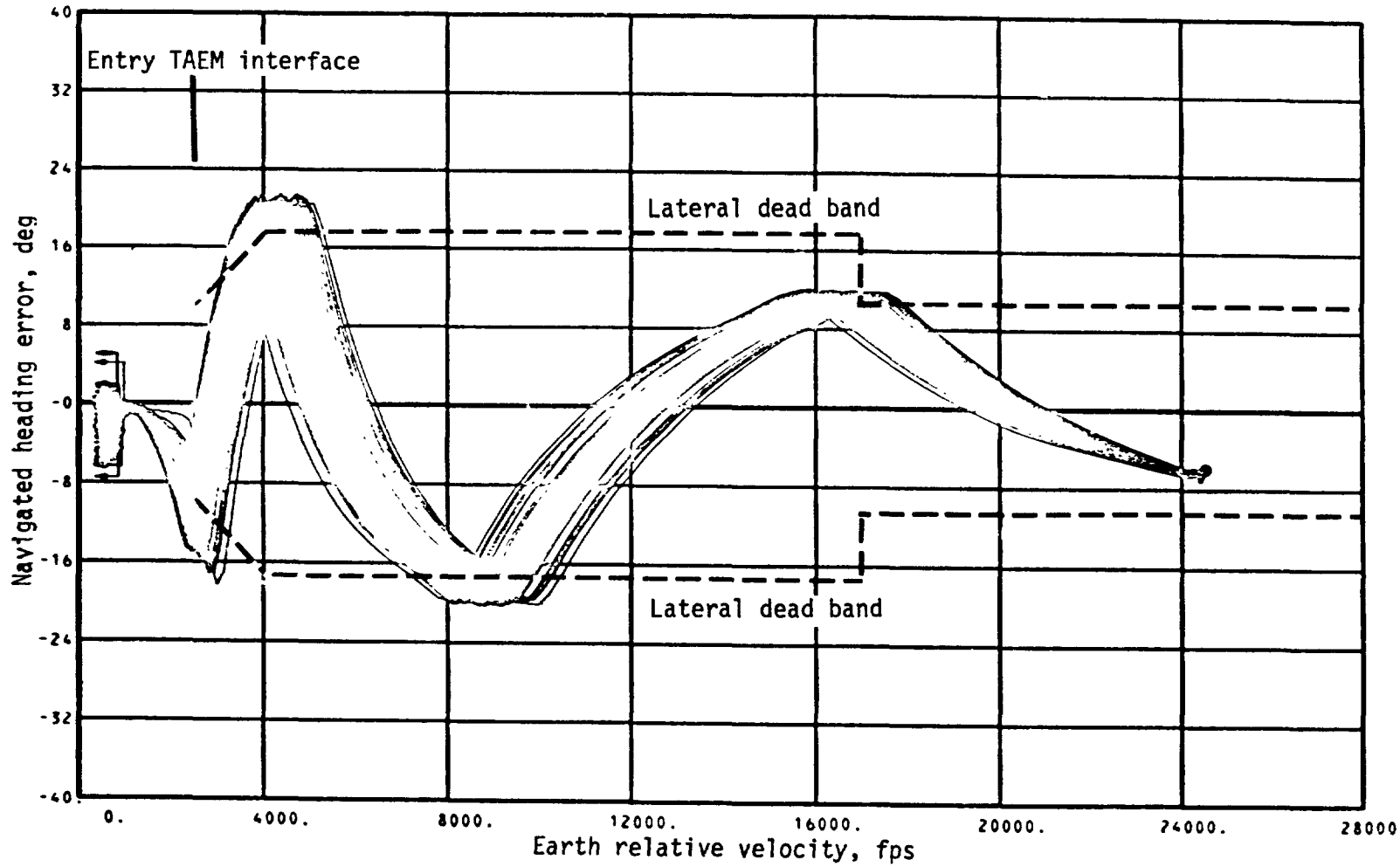

(e) Navigated heading error.

Figure 30.- Continued.

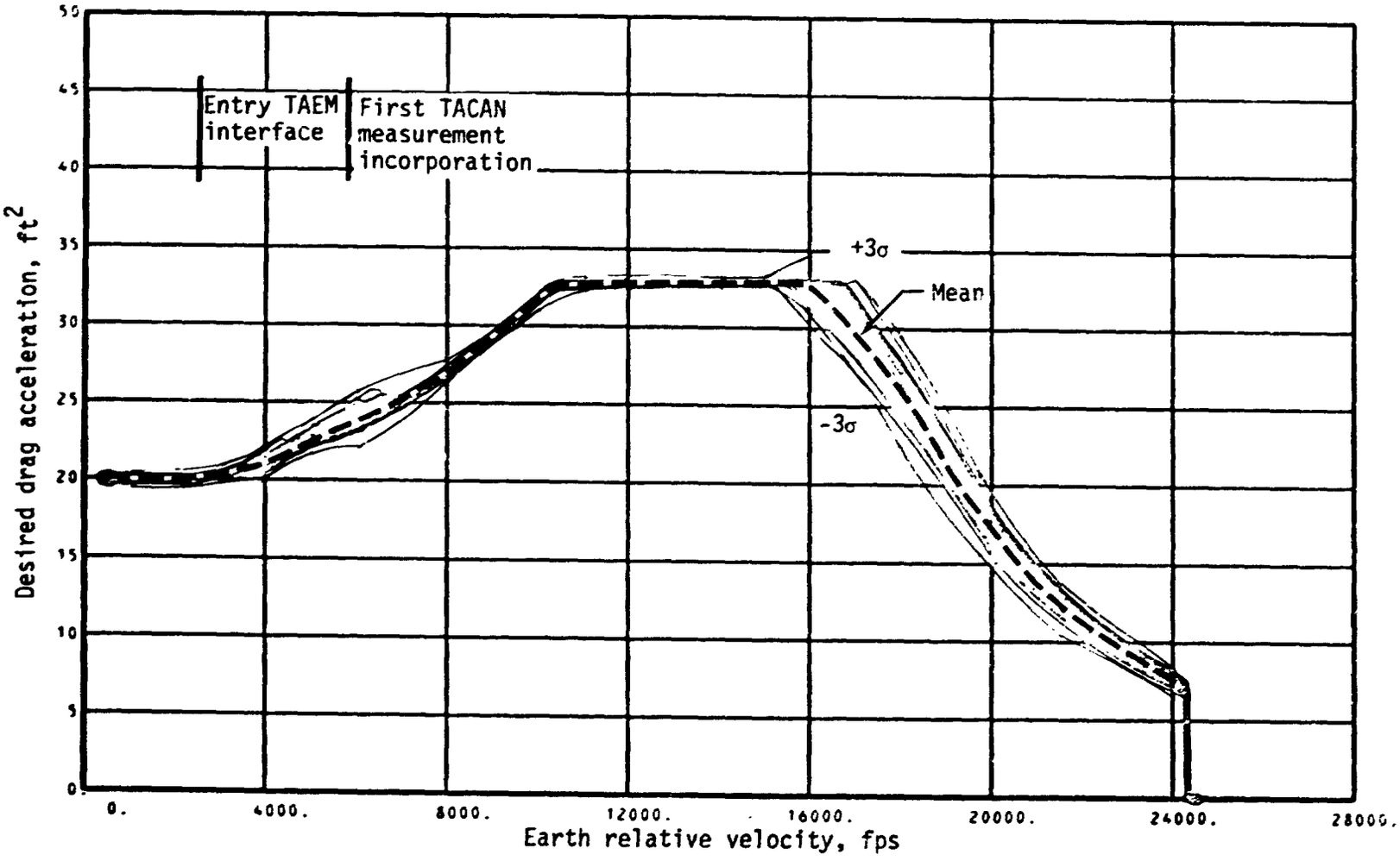

(f) Desired drag acceleration.

Figure 30.- Continued.

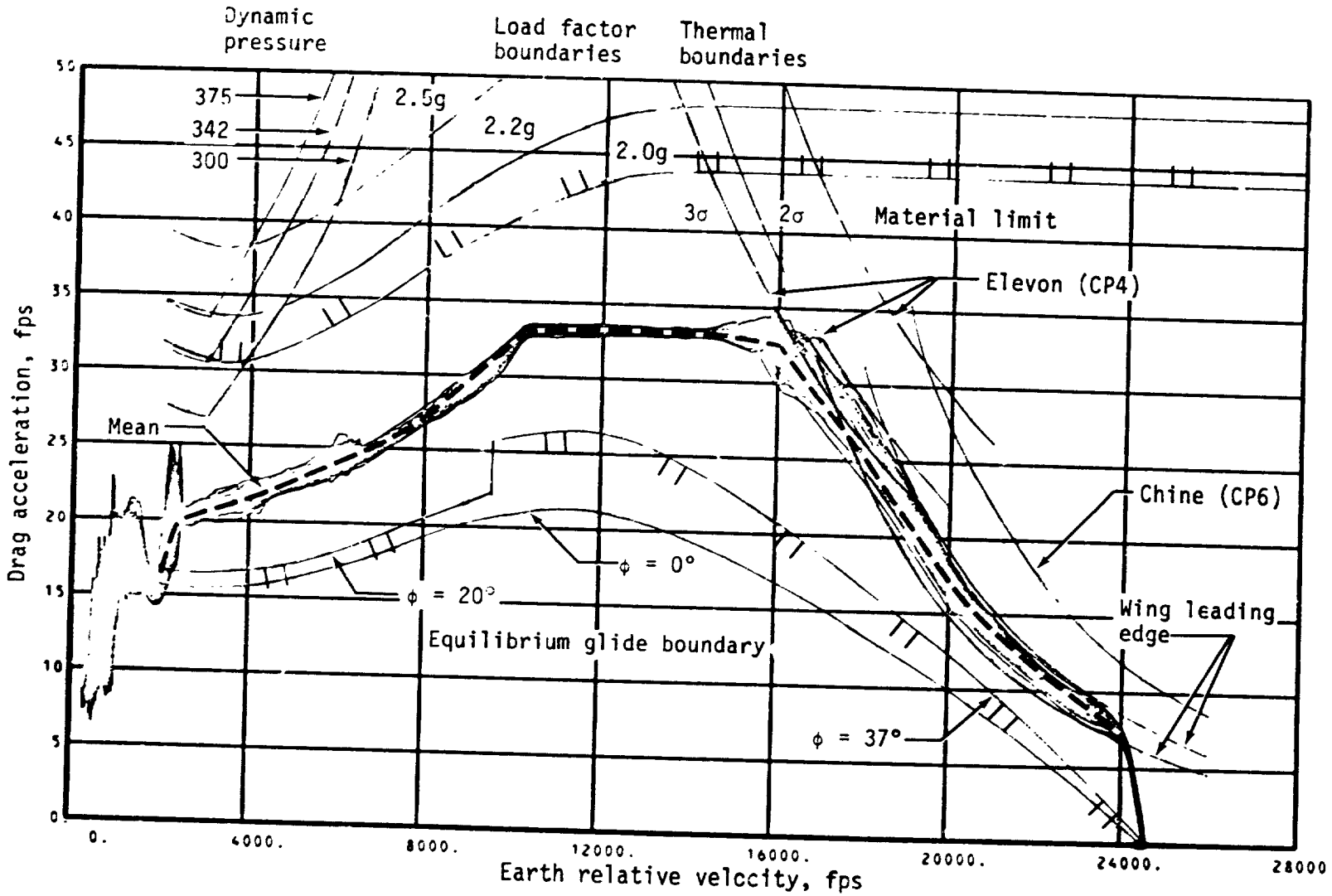

(g) Drag acceleration.

Figure 30.- Continued.

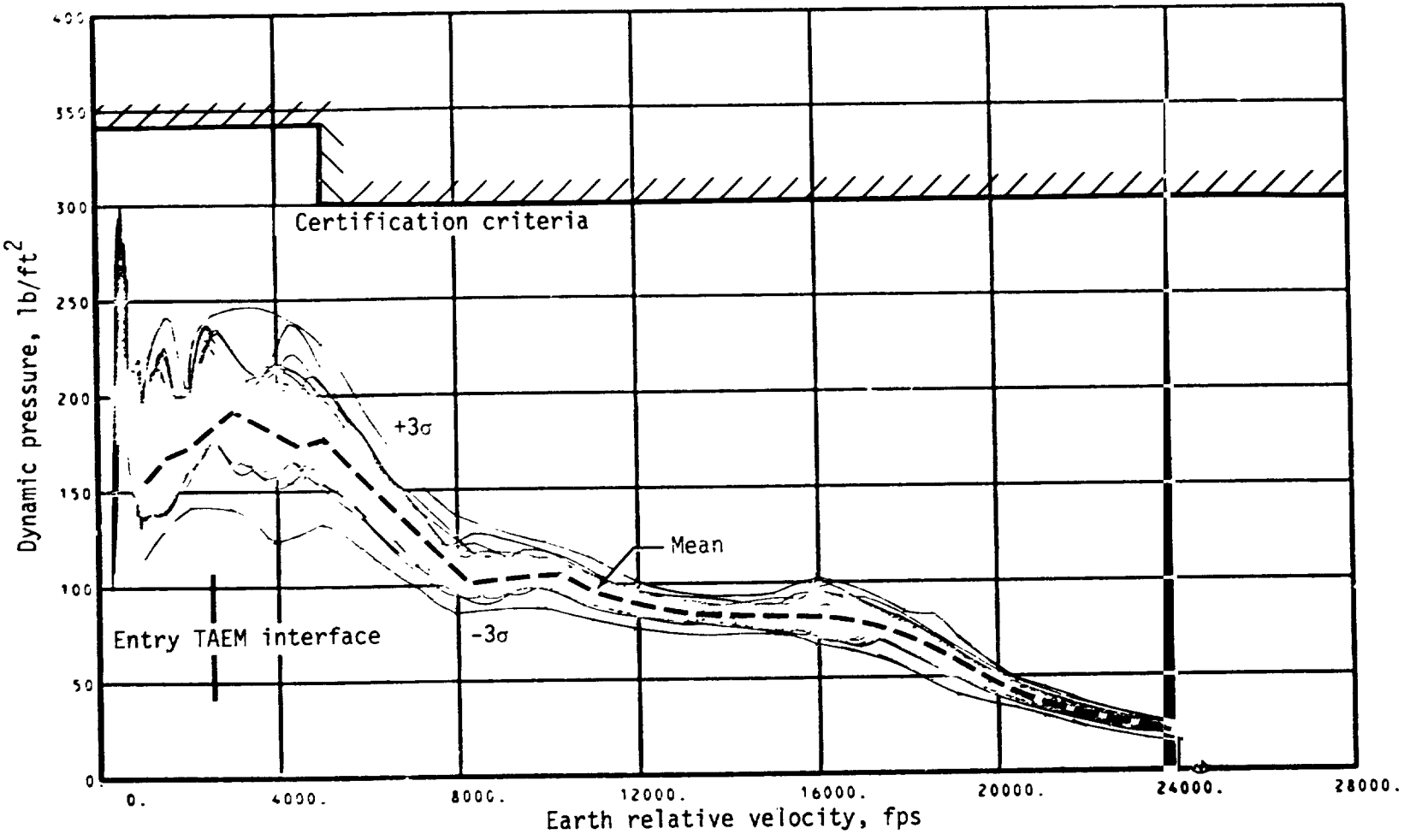

(h) Dynamic pressure.

Figure 30.- Continued.

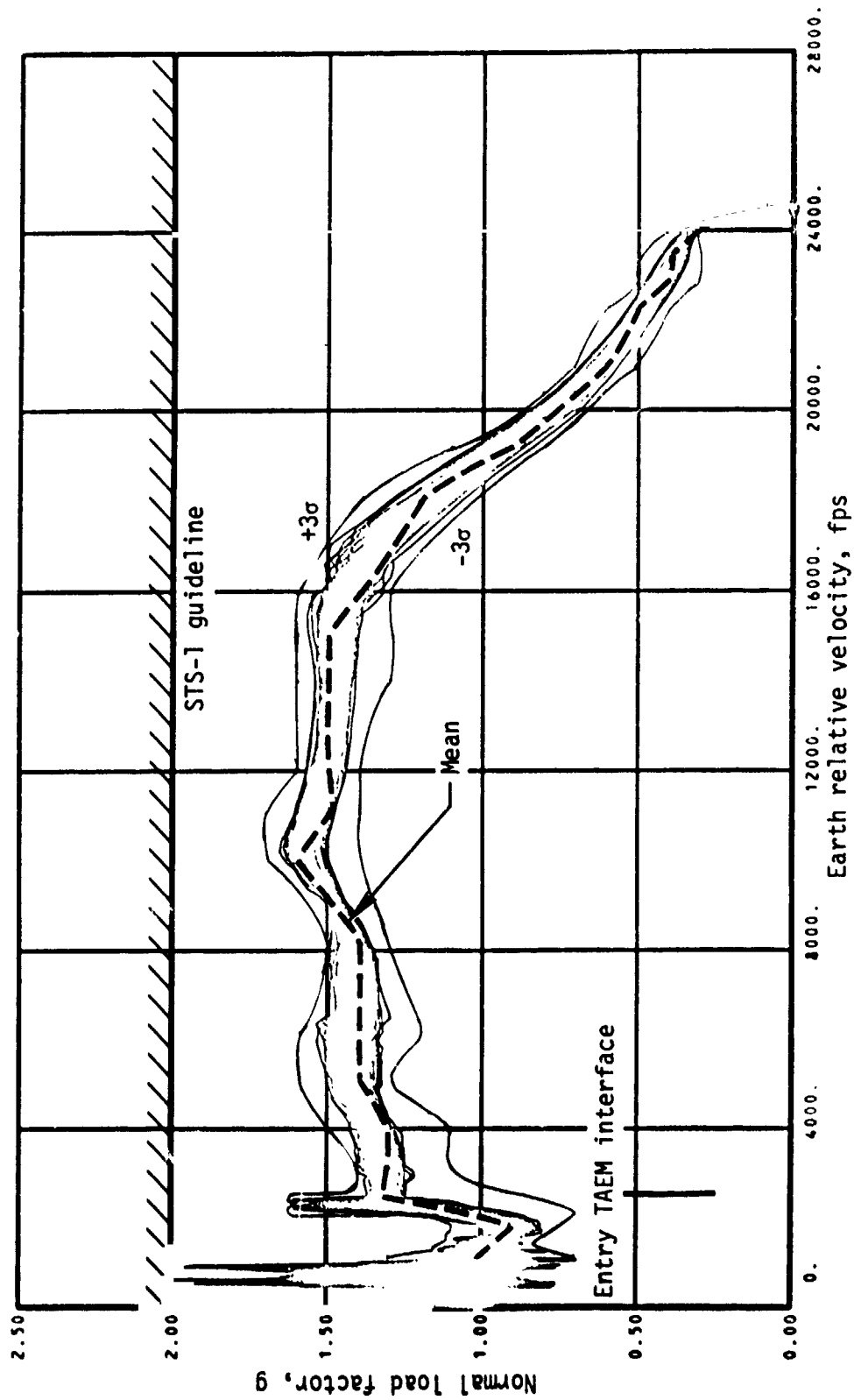

(i) Normal load factor.

Figure 30.- Continued.

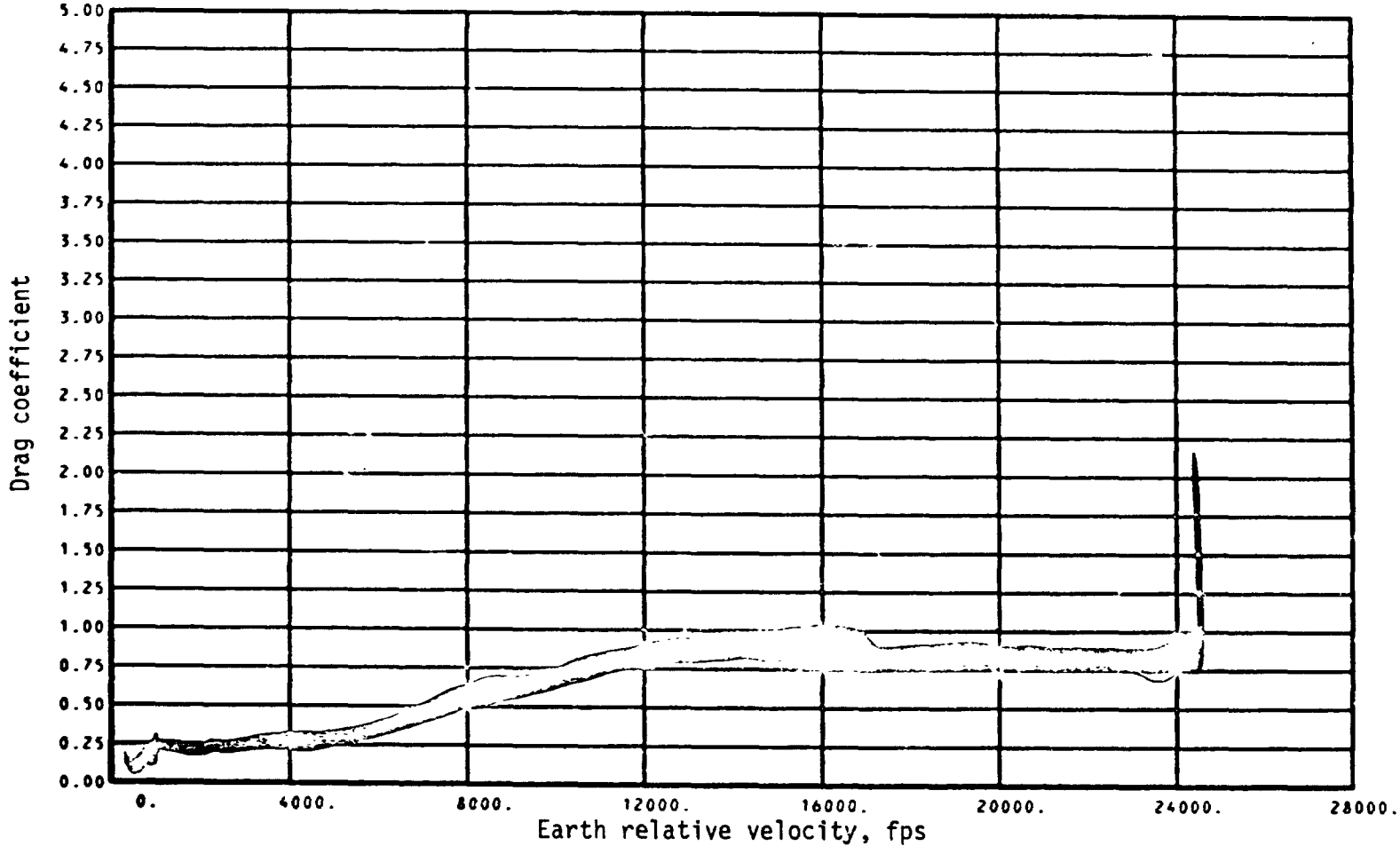

(j) Drag coefficient.

Figure 30.- Continued.

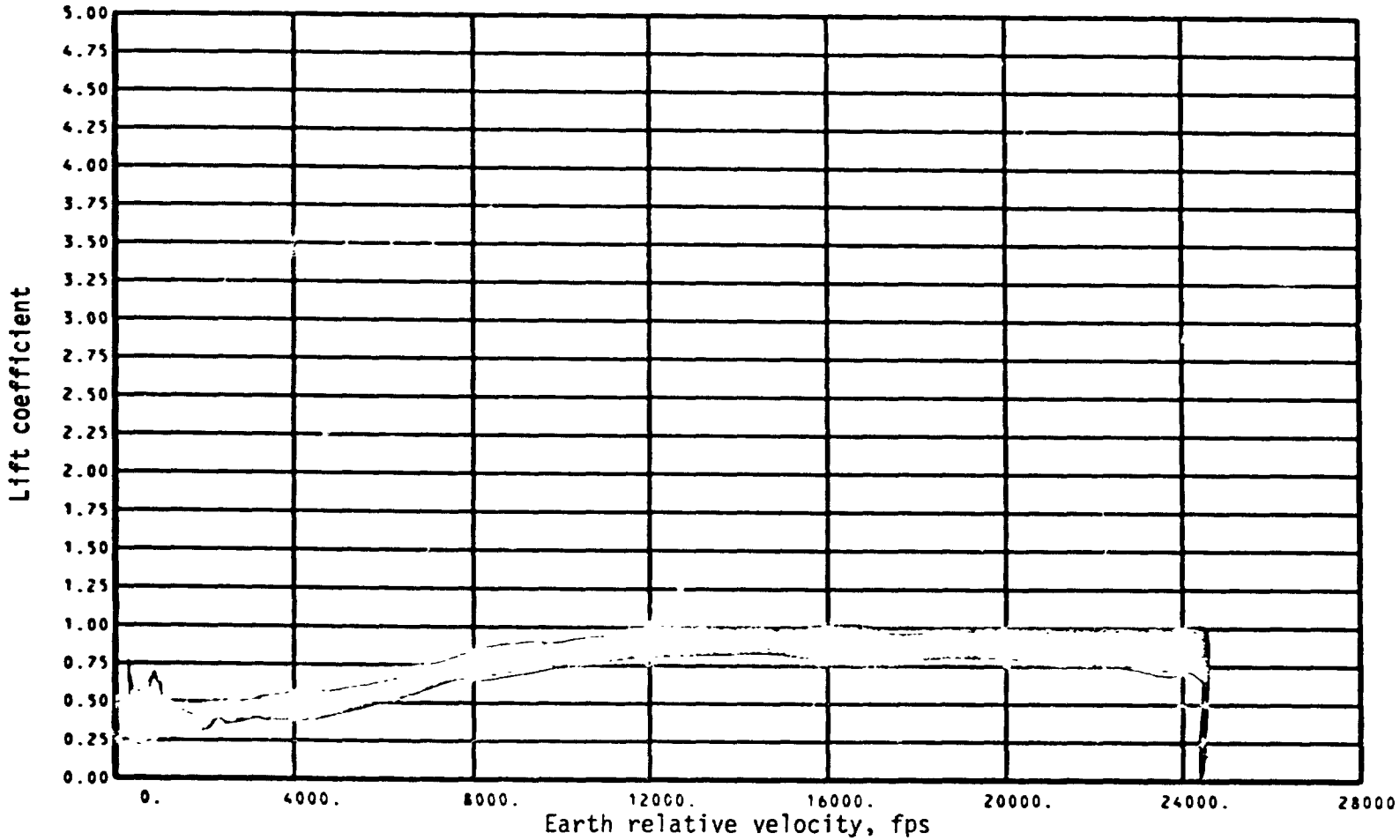

(k) Lift coefficient.

Figure 30.- Continued.

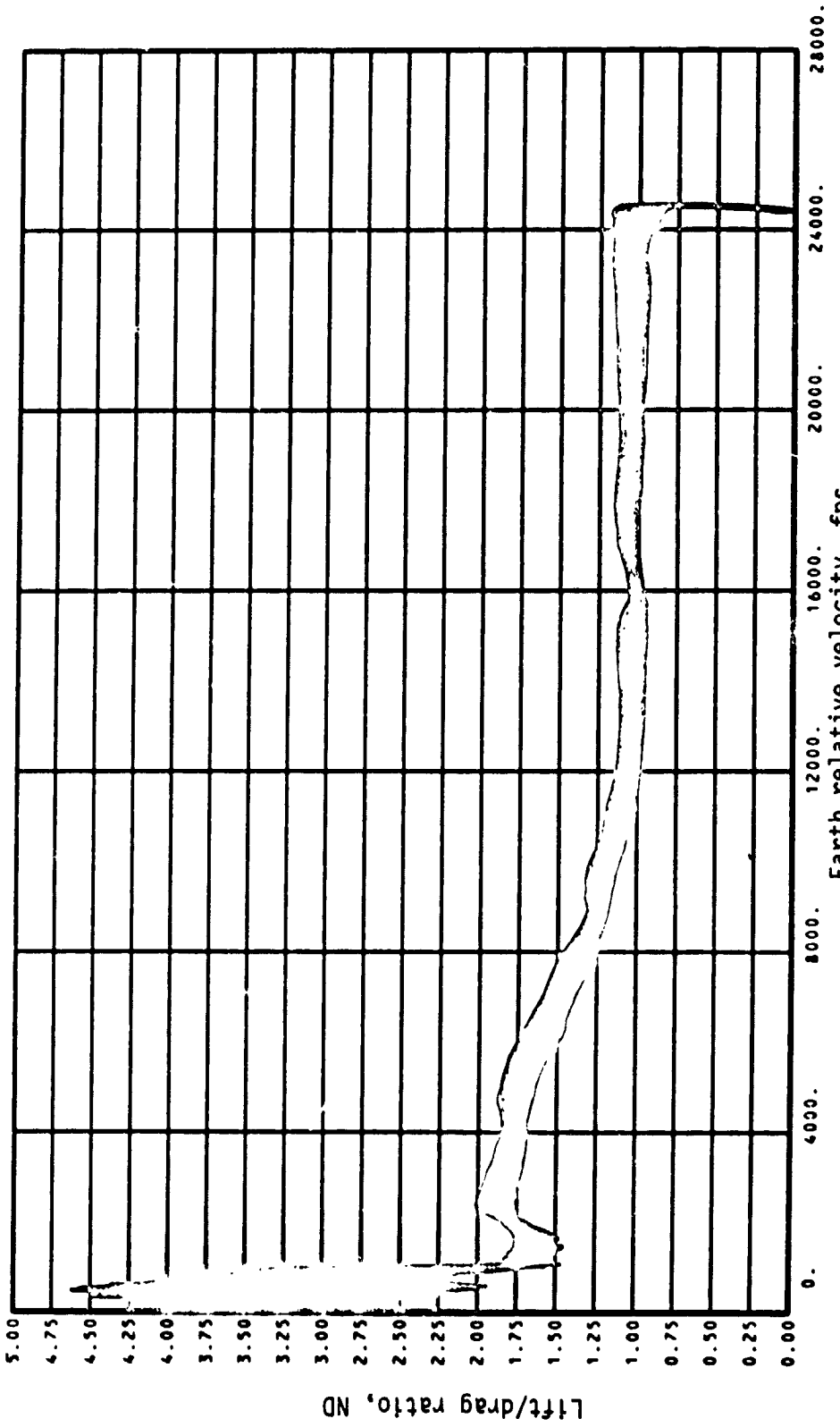

(1) Lift to drag ratio.

Figure 30.- Continued.

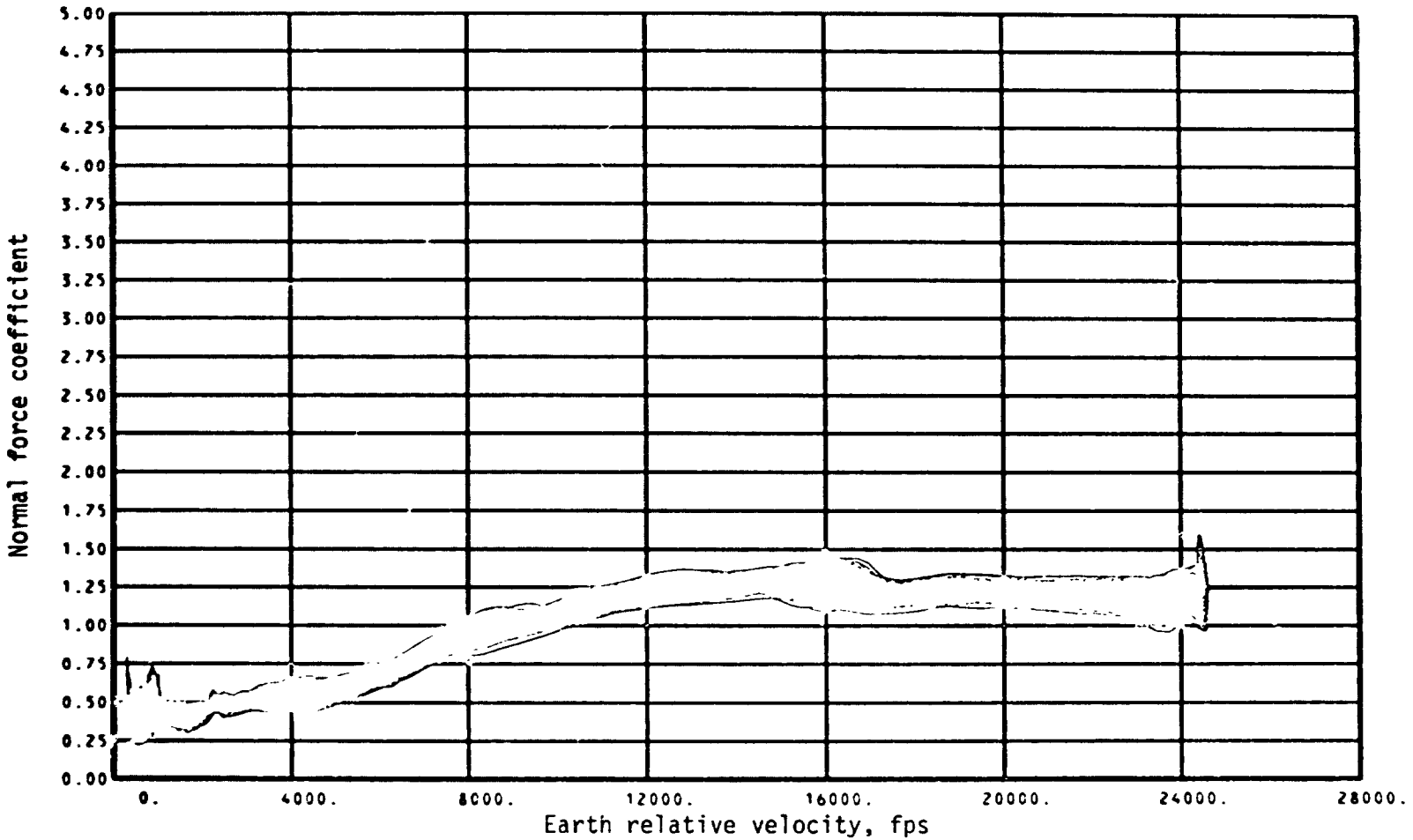

(m) Normal force coefficient.

Figure 30.- Continued.

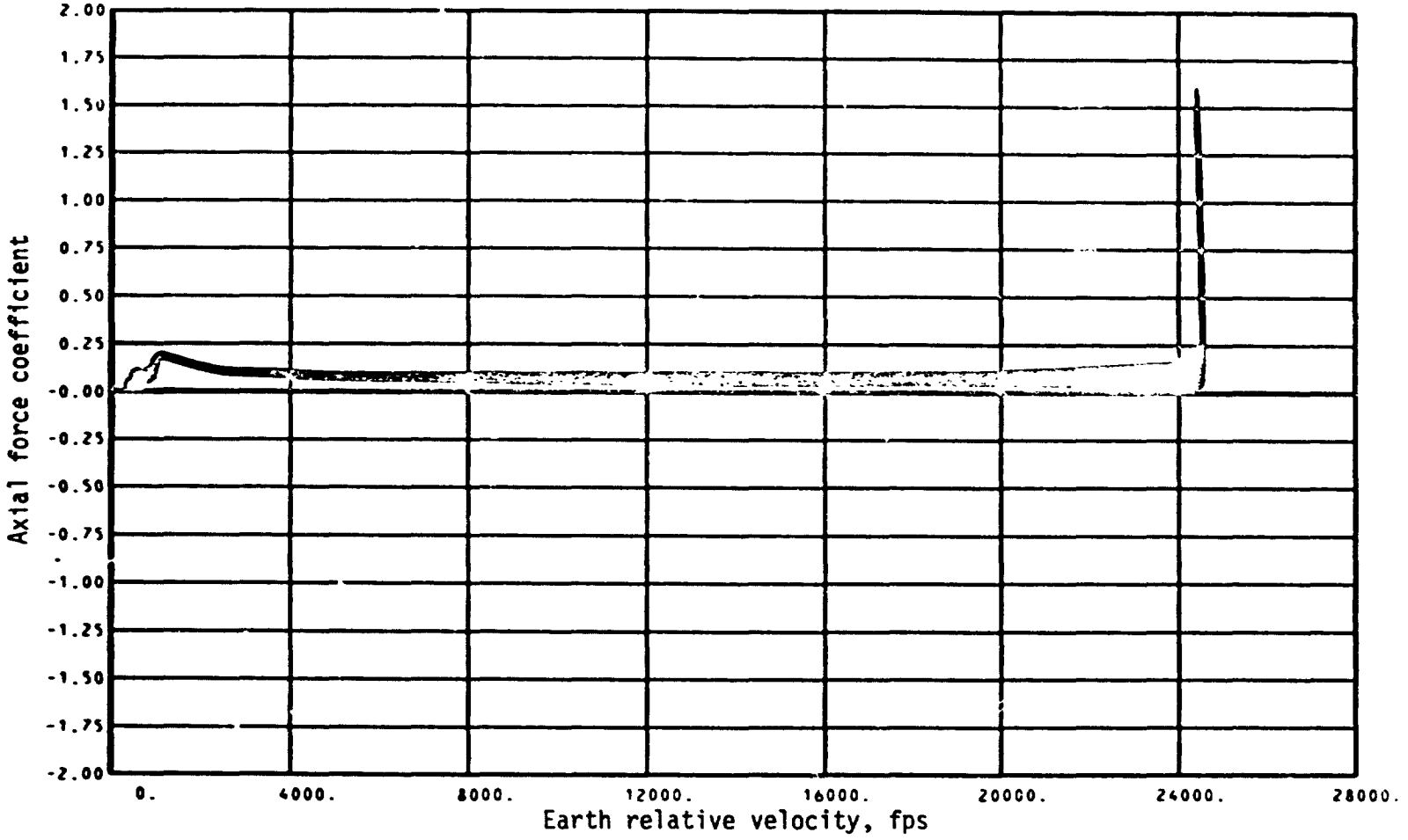

(n) Axial force coefficient.

Figure 30.- Continued.

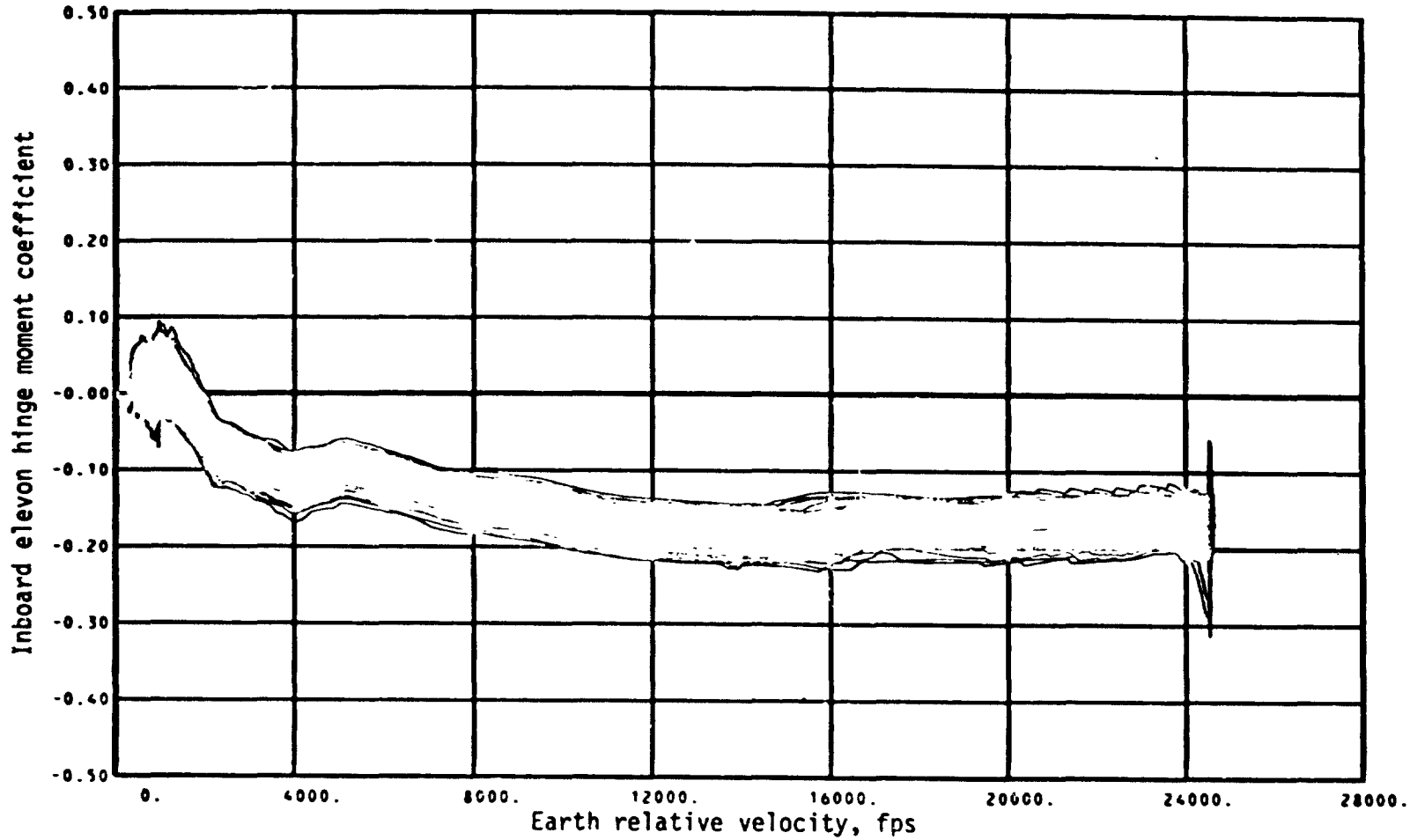

(o) Inboard elevon hinge moment coefficient.

Figure 30.- Continued.

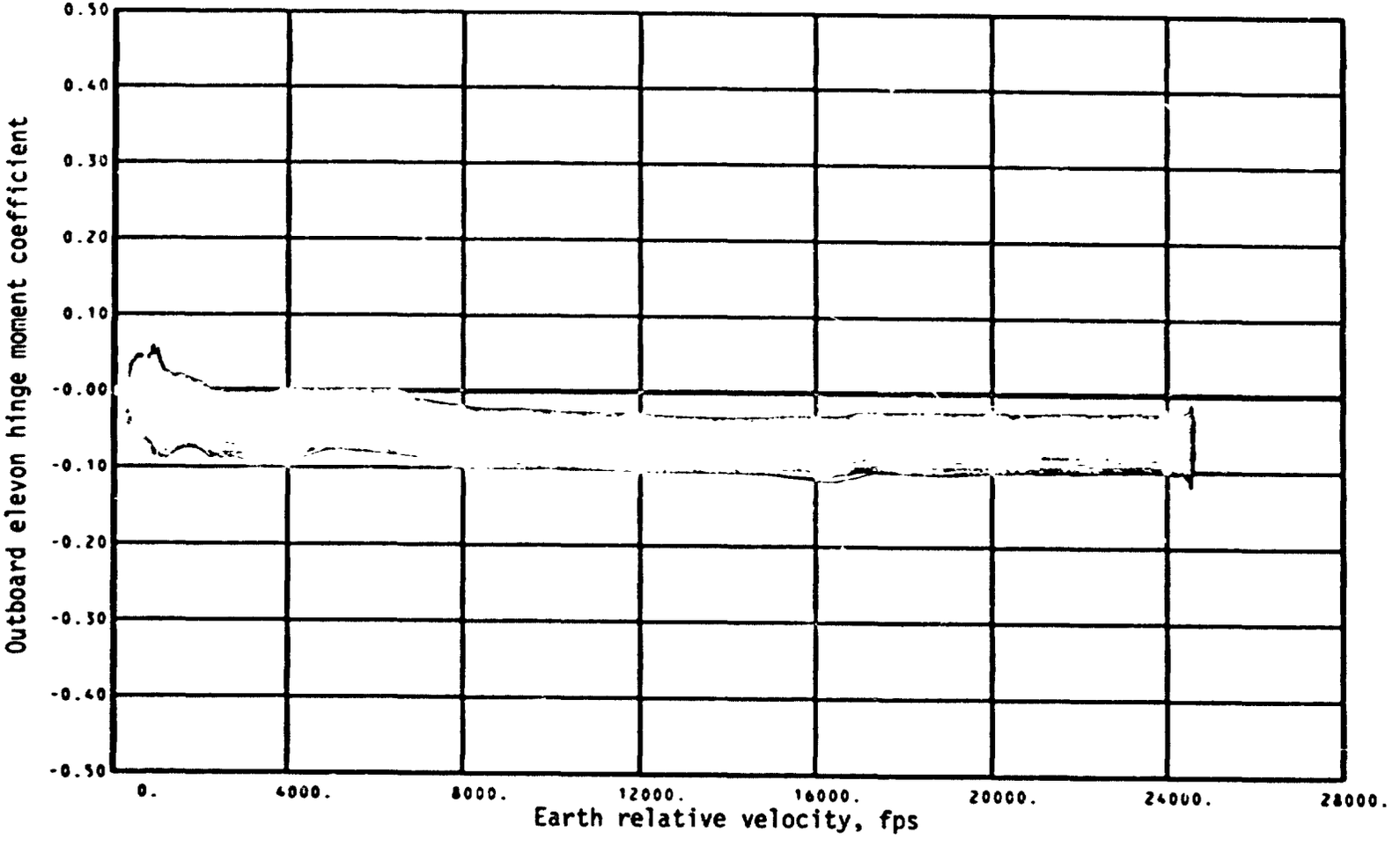

(p) Outboard elevon hinge moment coefficient.

Figure 30.- Continued.

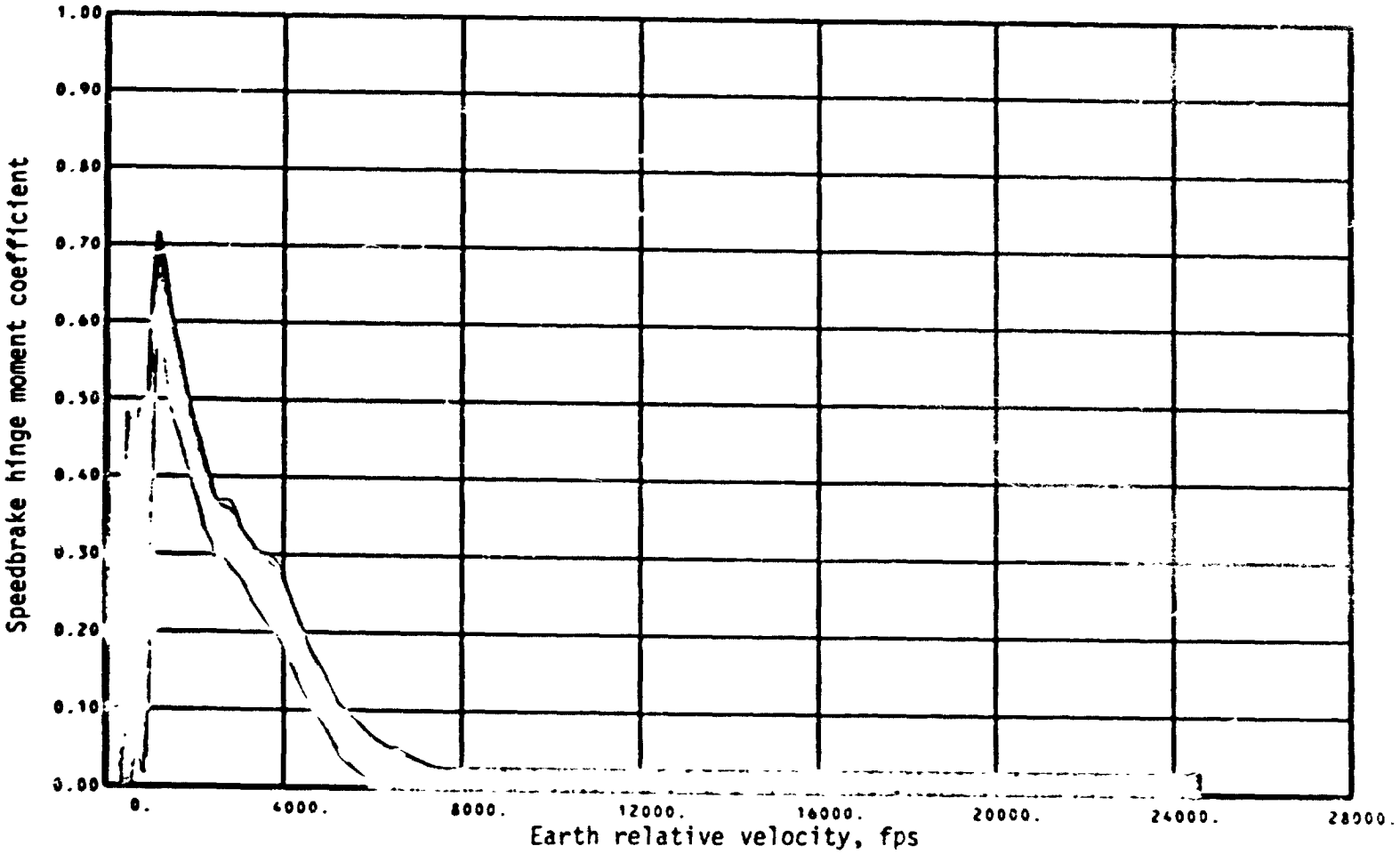

(ς) Speedbrake hinge moment coefficient.

Figure 30.- Continued.

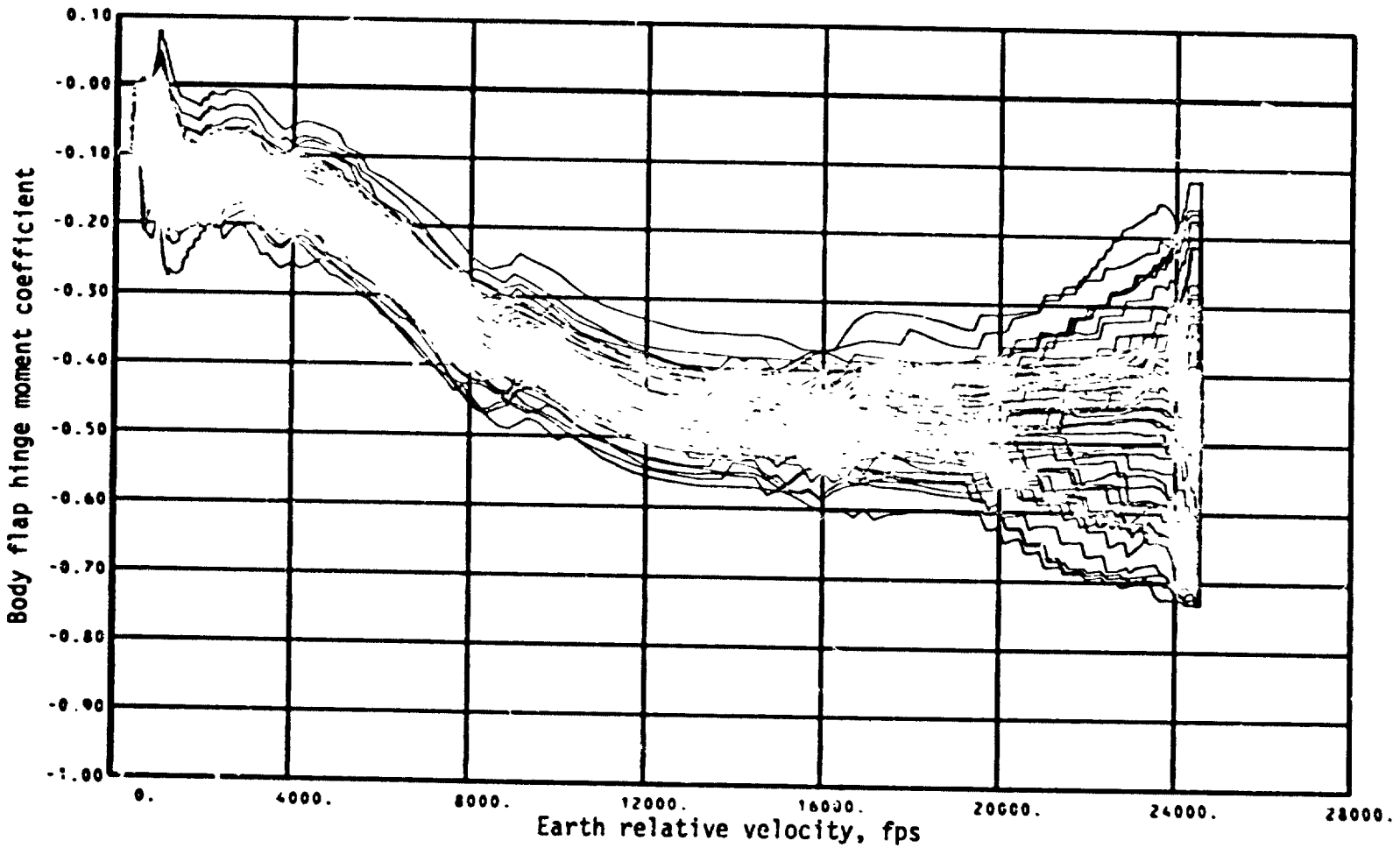

(r) Body flap hinge moment coefficient.

Figure 30.- Continued.

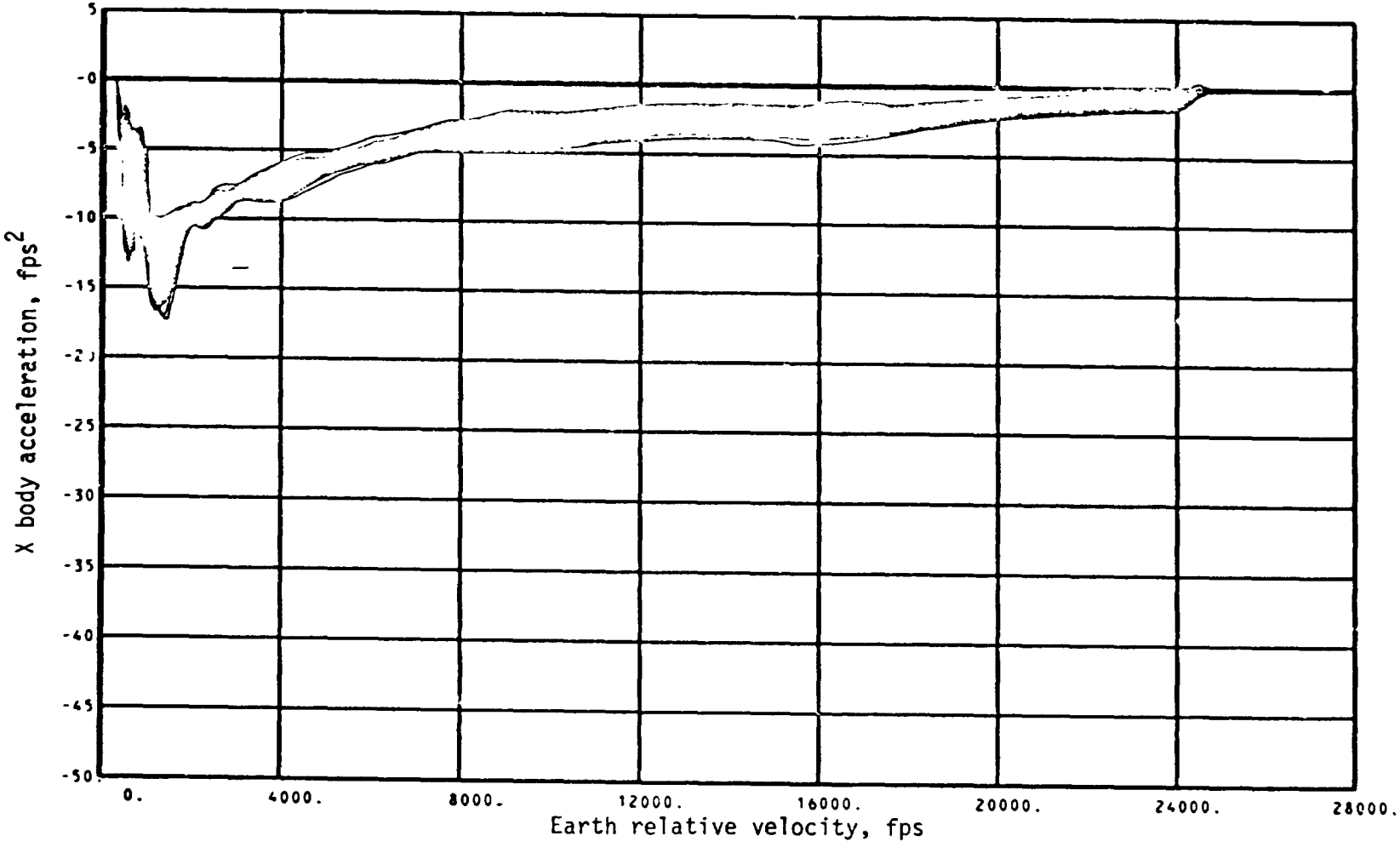

(s) X body acceleration.

Figure 30.- Continued.

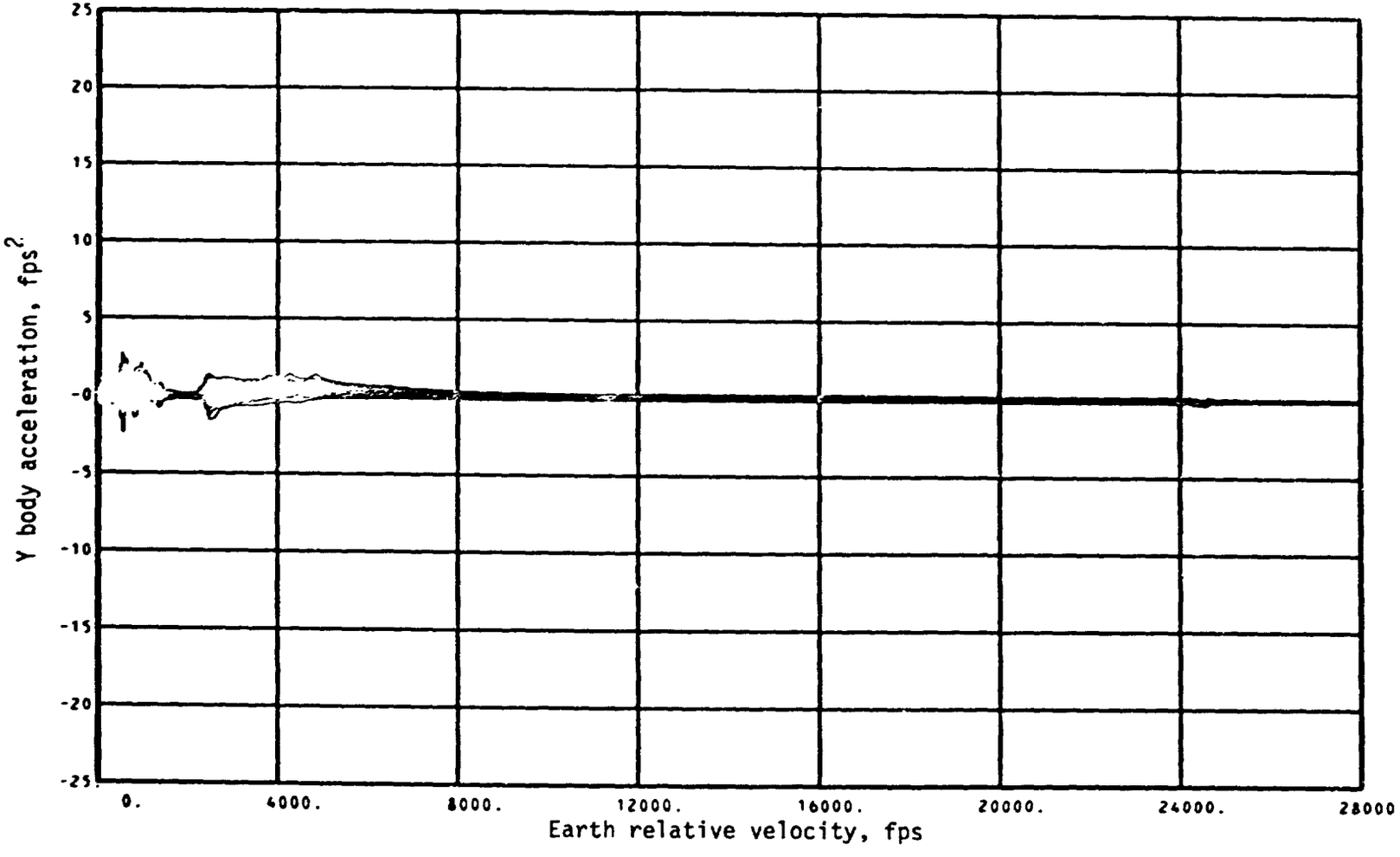

(t) Y body acceleration.

Figure 30.- Continued.

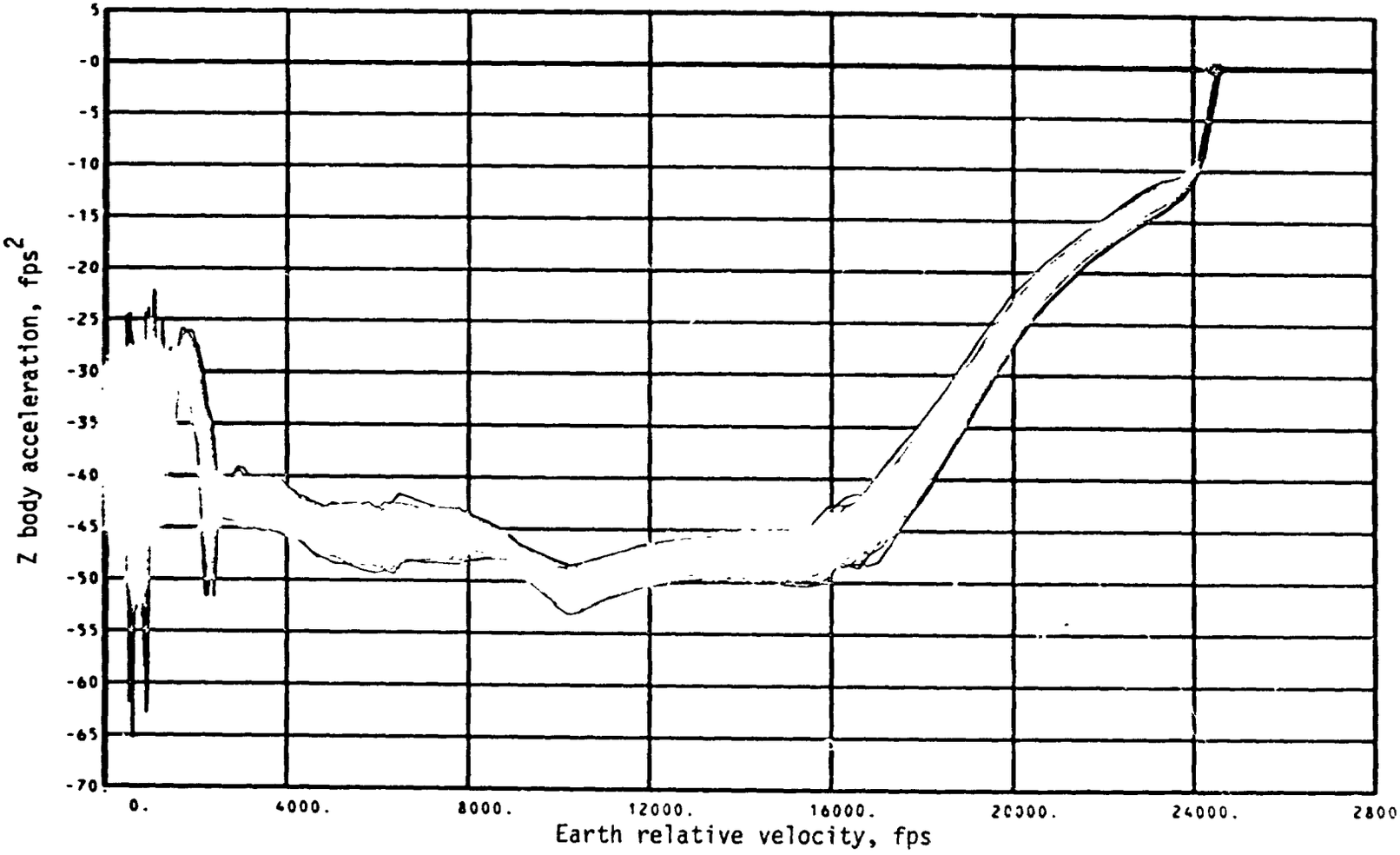

(u) Z body acceleration.

Figure 30.- Concluded.

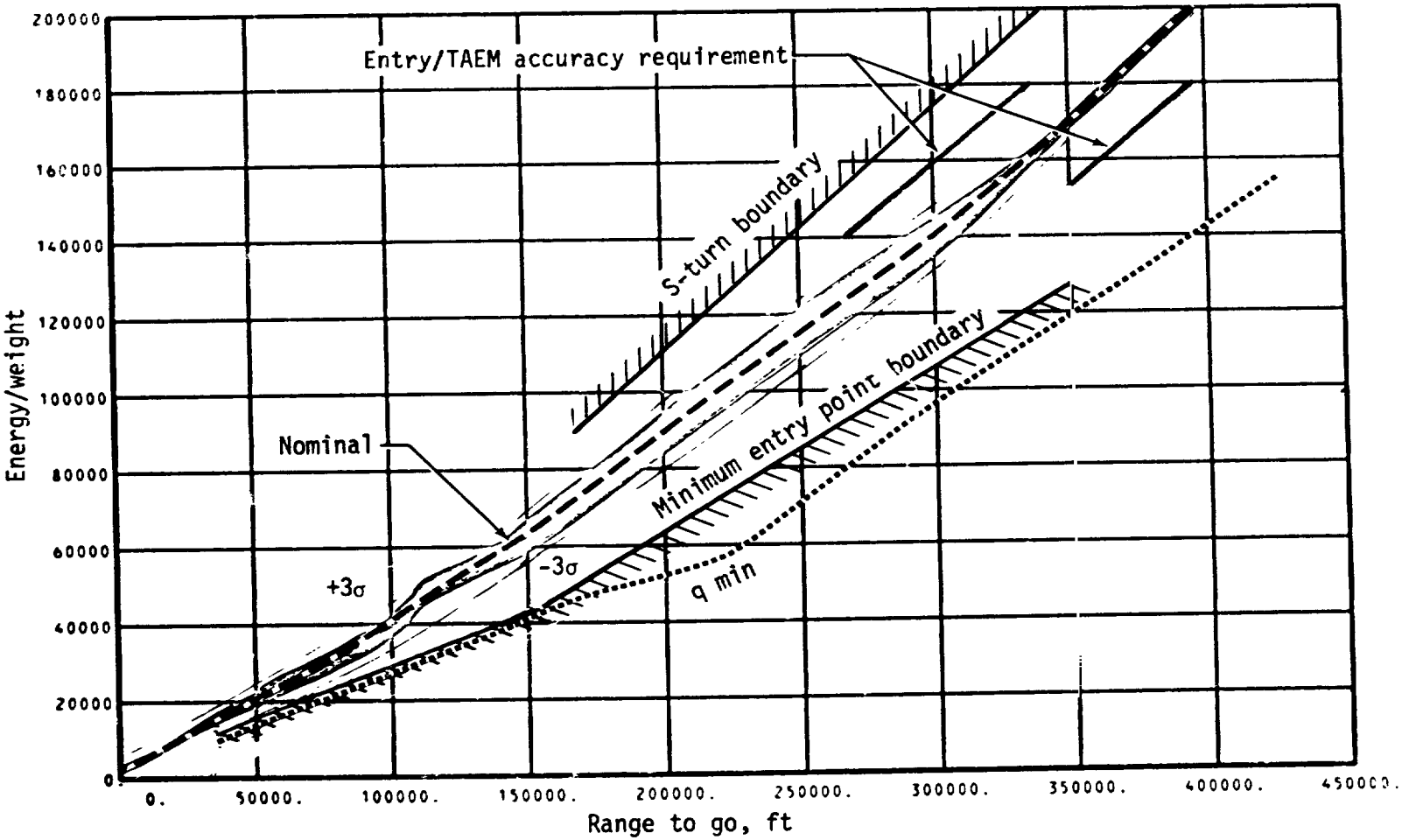

(a) Energy/weight.

Figure 31.- TAEM guidance performance parameter - shallow abort once around.

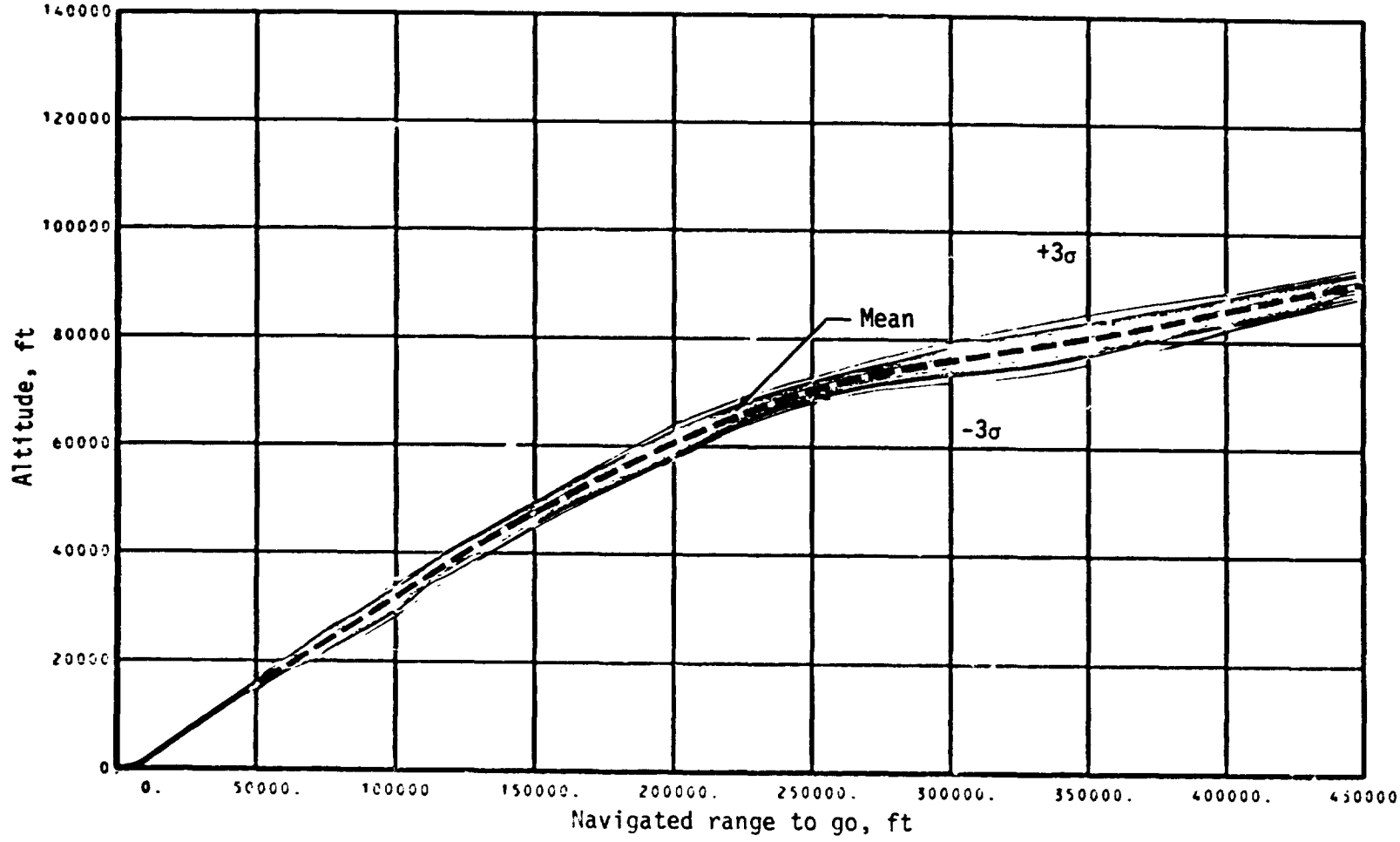

(b) Altitude.

Figure 31.- Continued.

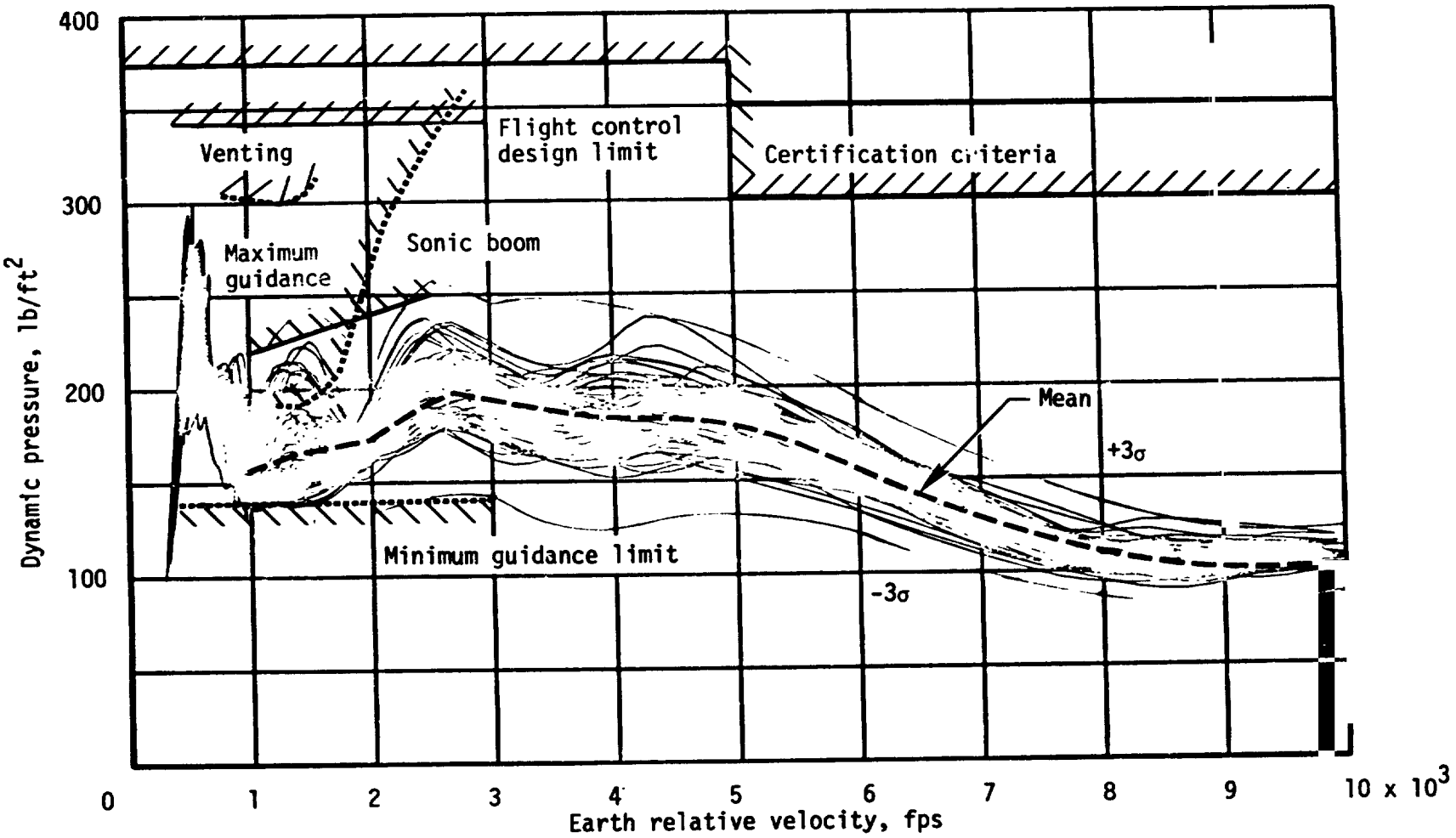

(c) Dynamic pressure.

Figure 31.- Continued.

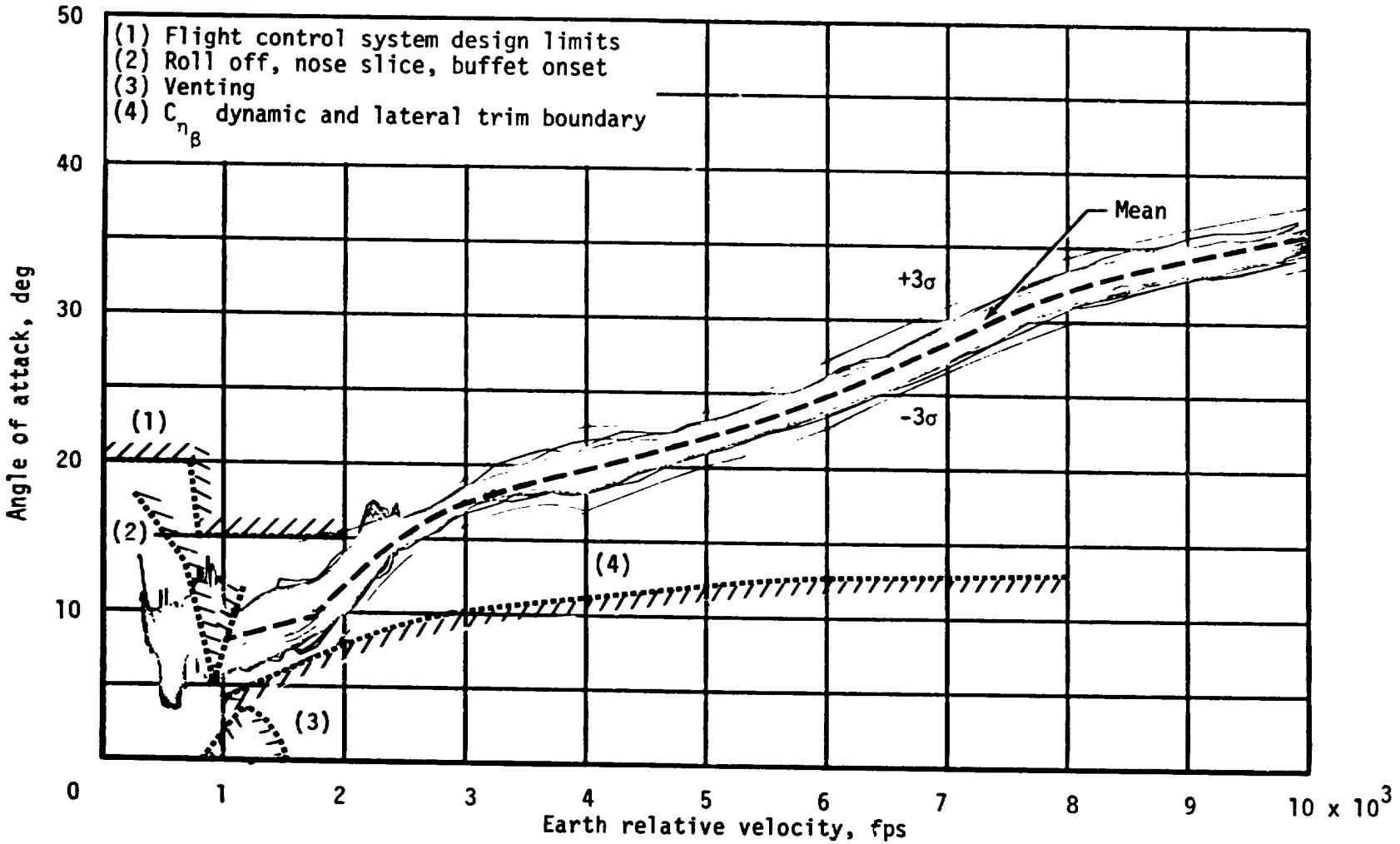

(d) Angle of attack.

Figure 31.- Continued.

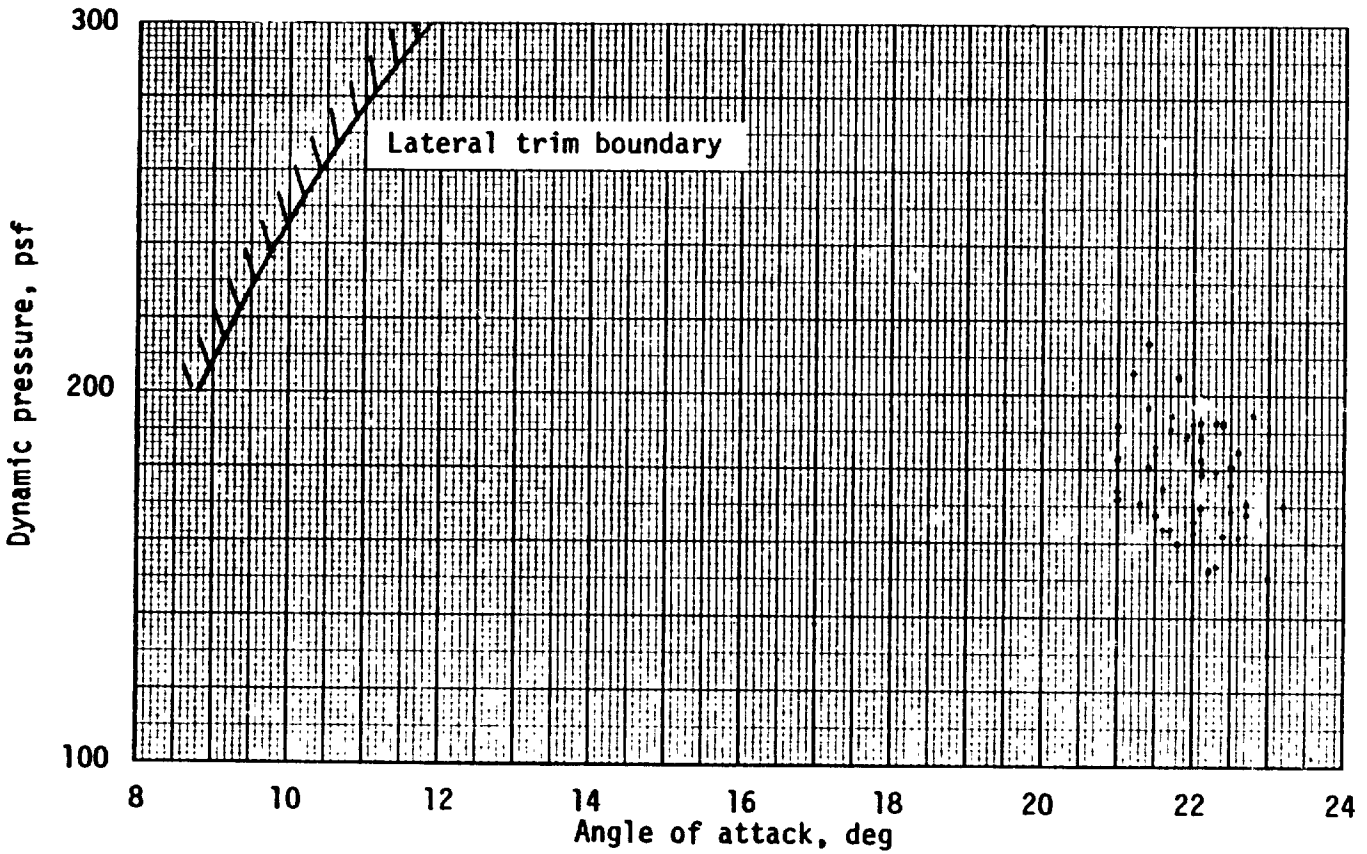

(e) Dynamic pressure - angle of attack scatter plot - Mach = 5.0

Figure 31.- Continued.

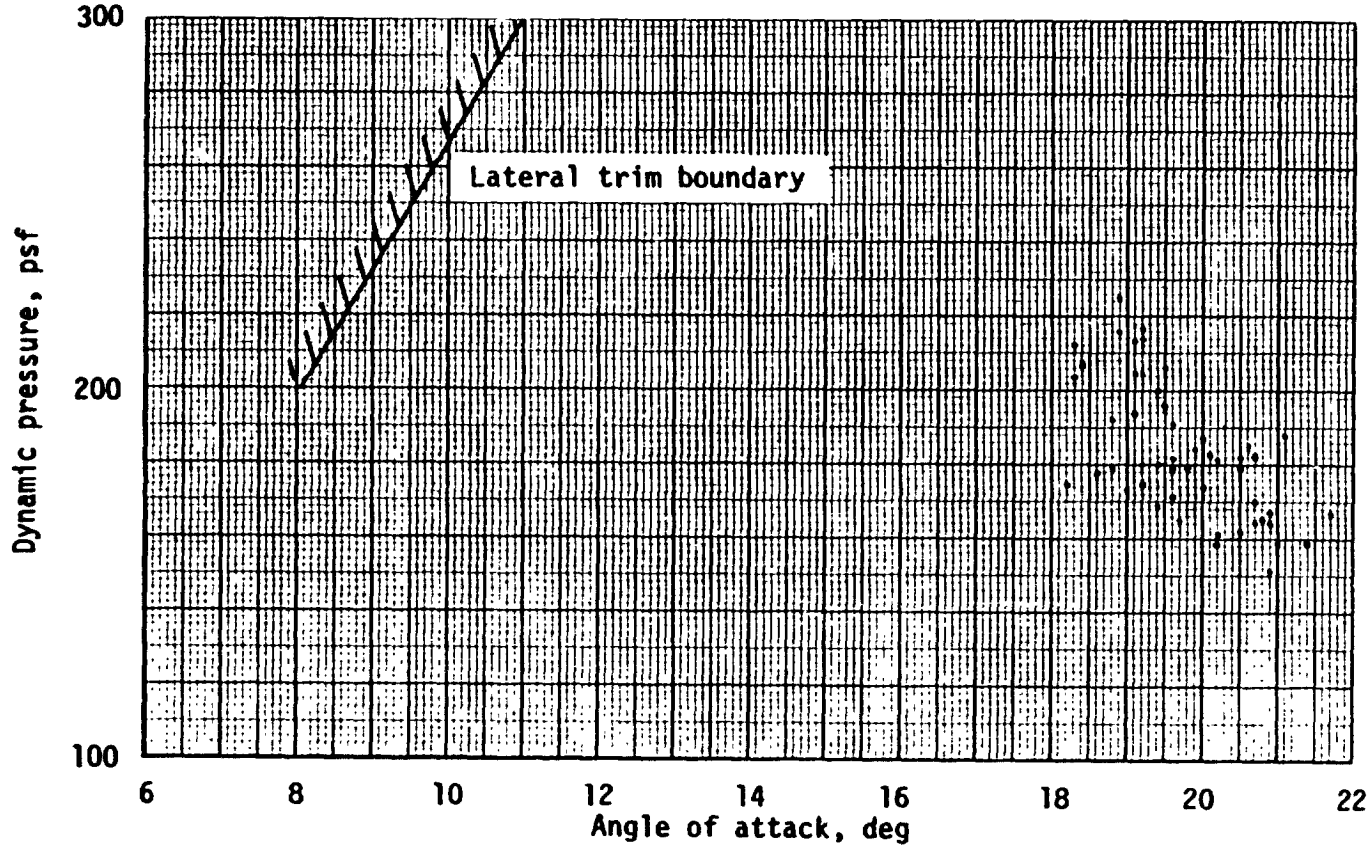

(f) Dynamic pressure - angle of attack scatter plot - Mach = 4.0

Figure 31.- Continued.

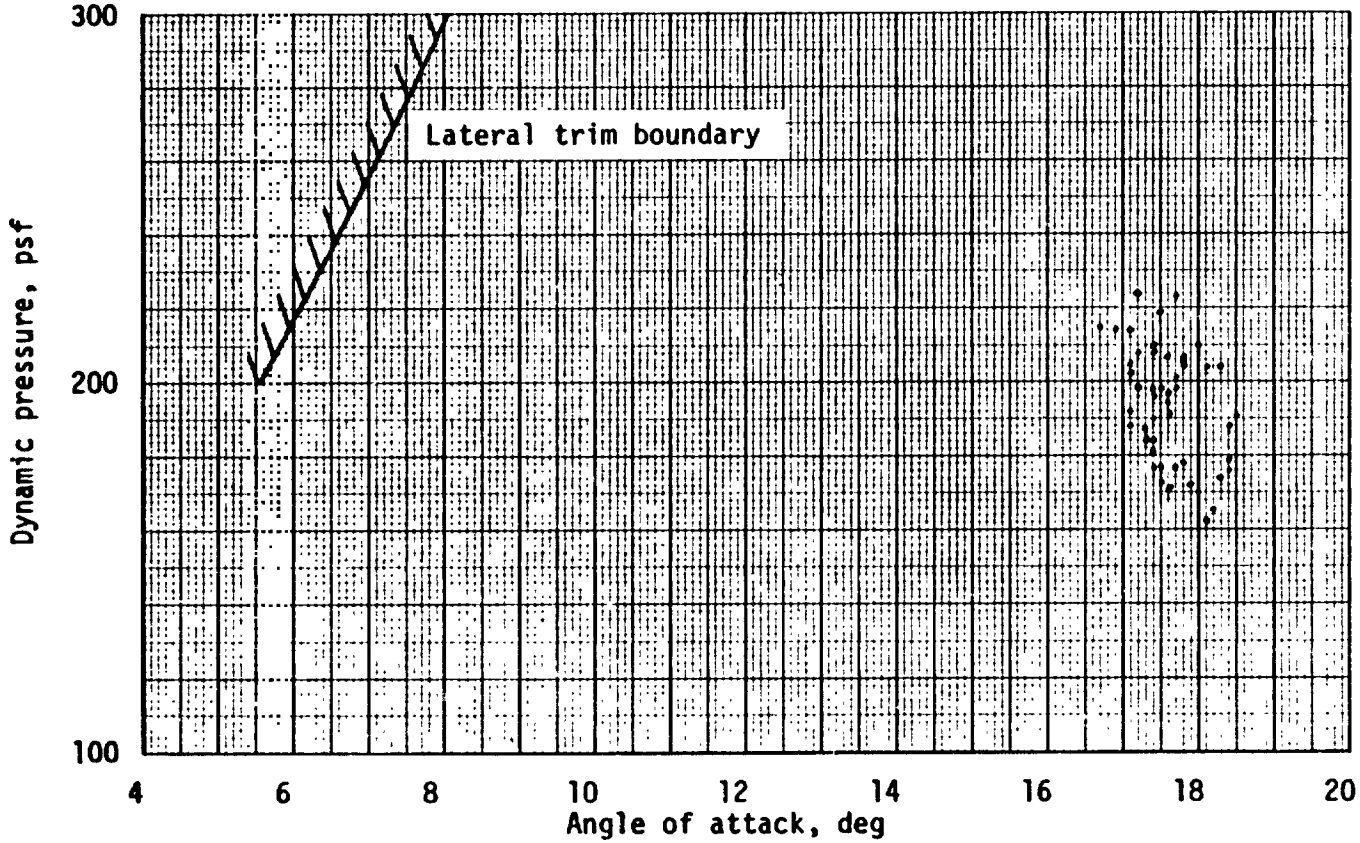

(g) Dynamic pressure - angle of attack scatter plot - Mach 3.0

Figure 31.- Continued.

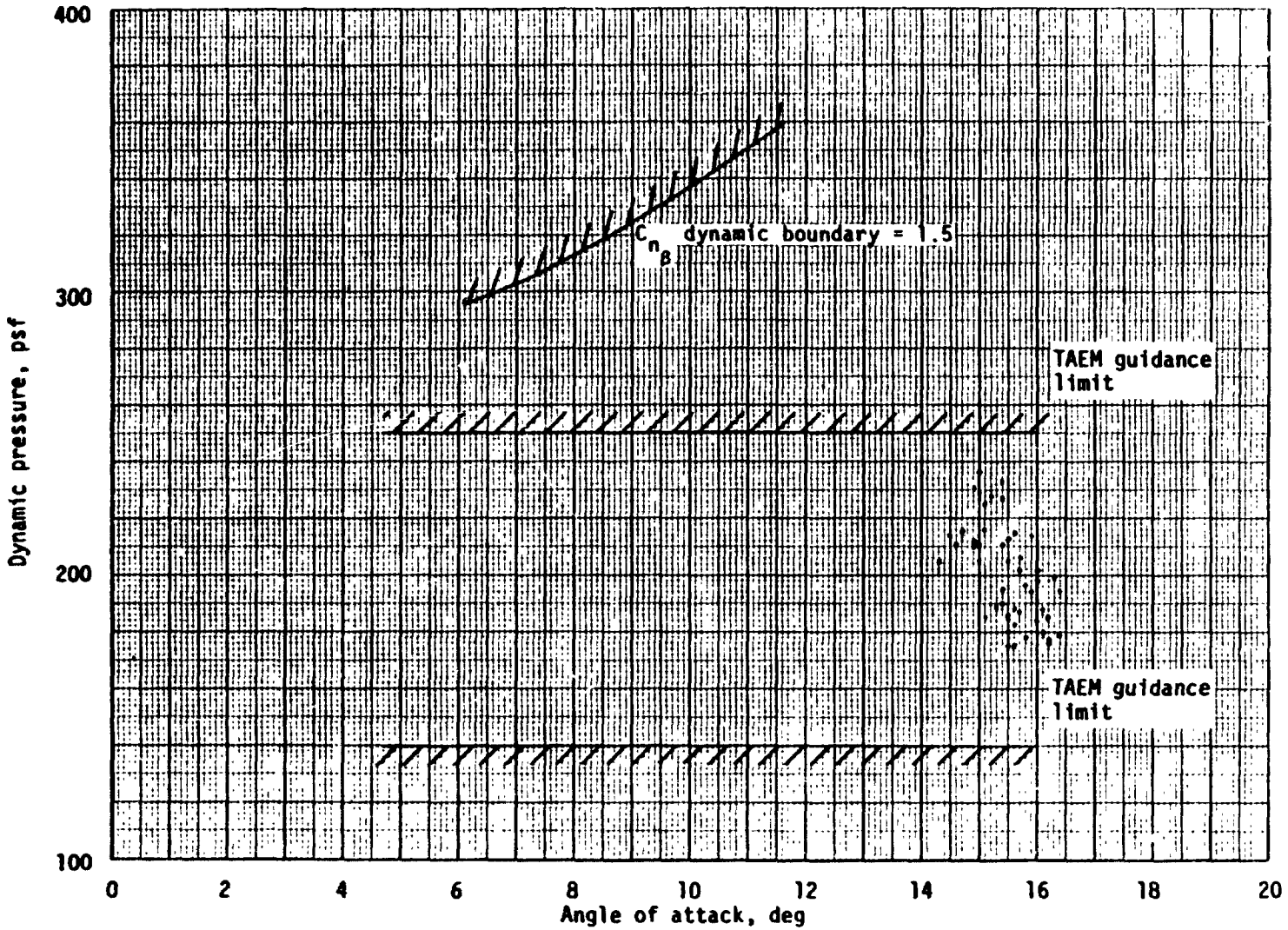

(h) Dynamic pressure - angle of attack scatter plot - Mach = 2.5.

Figure 31.- Continued.

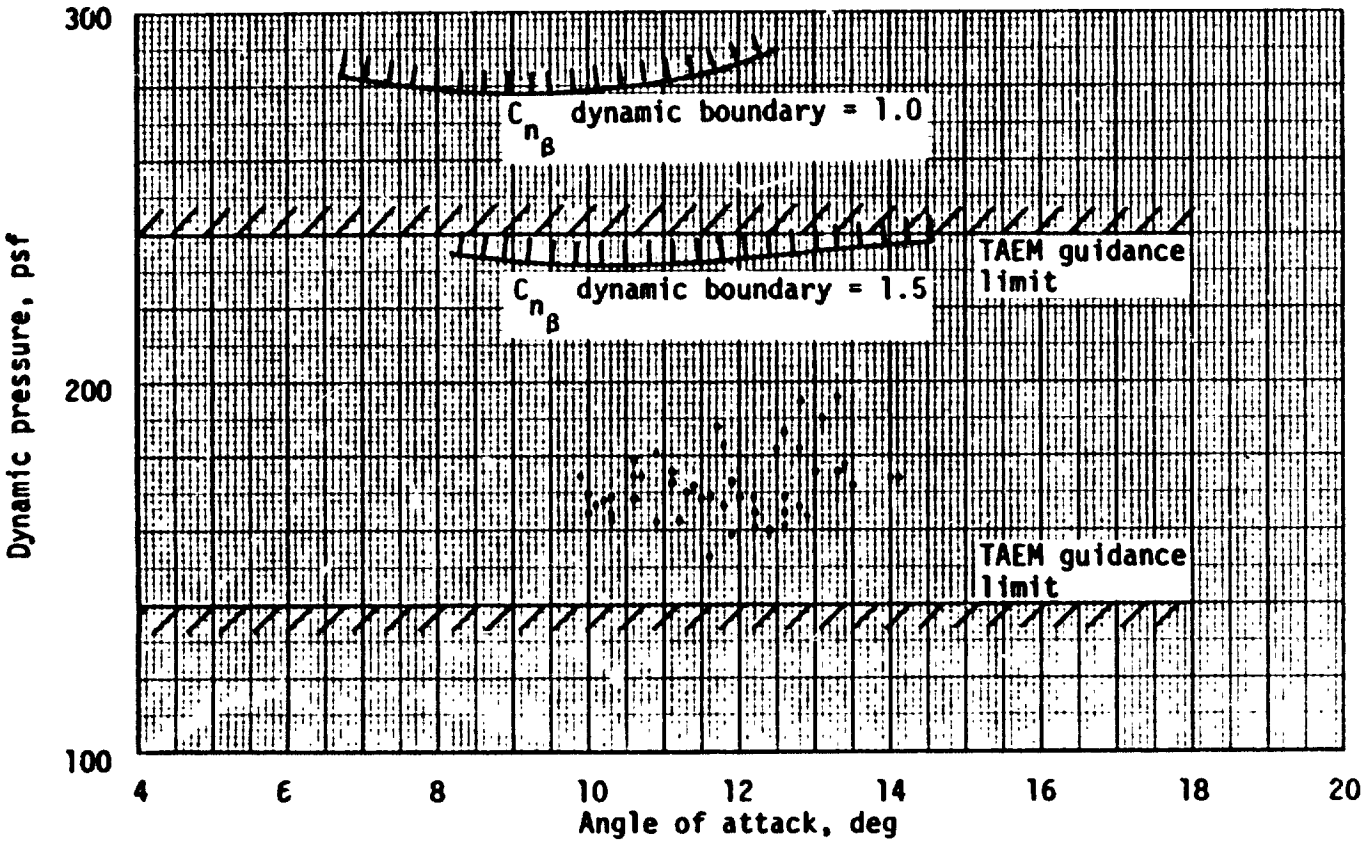

(i) Dynamic pressure - angle of attack scatter plot - Mach = 2.0

Figure 31.- Continued.

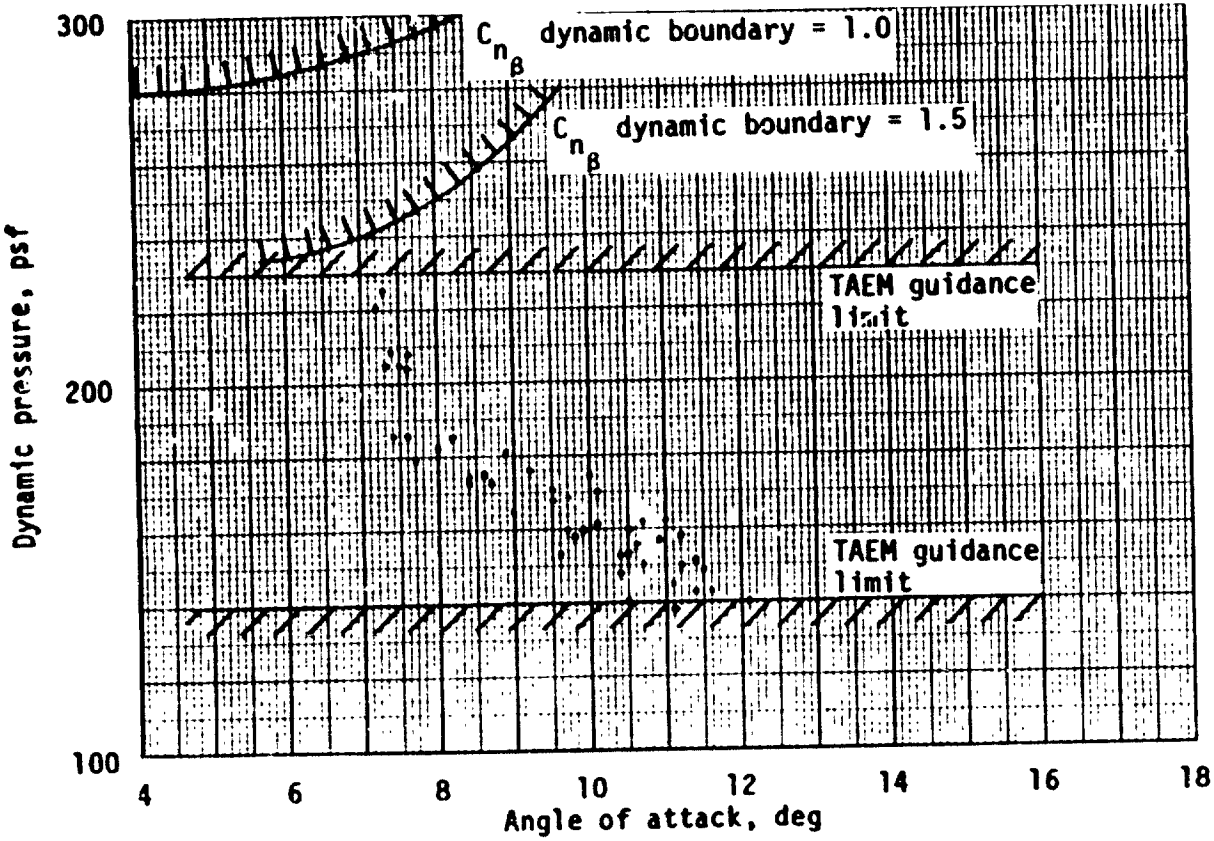

(j) Dynamic pressure - angle of attack scatter plot - Mach 1.5

Figure 31.- Continued.

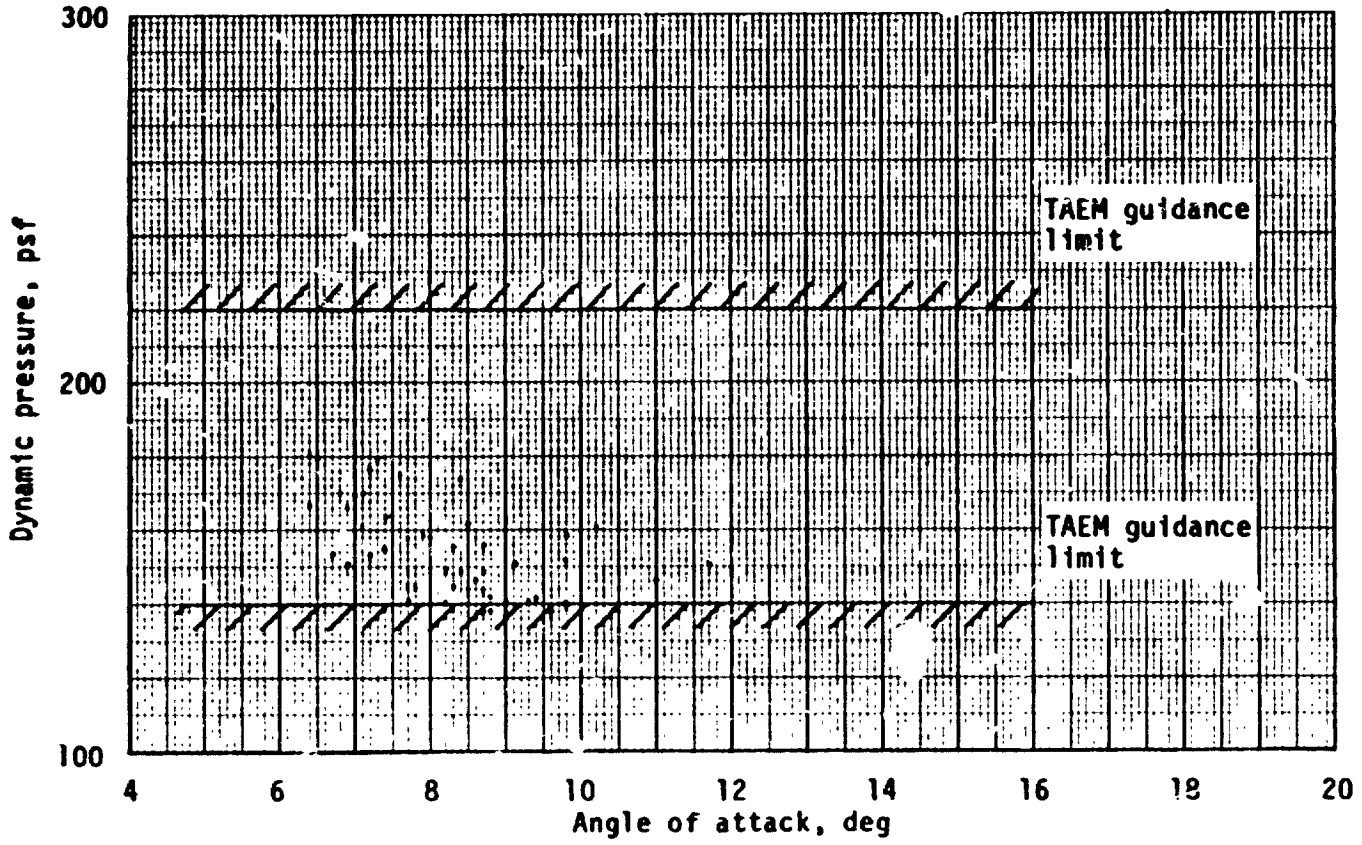

(k) Dynamic pressure - angle of attack scatter plot - Mach = 1.0

Figure 31.- Continued.

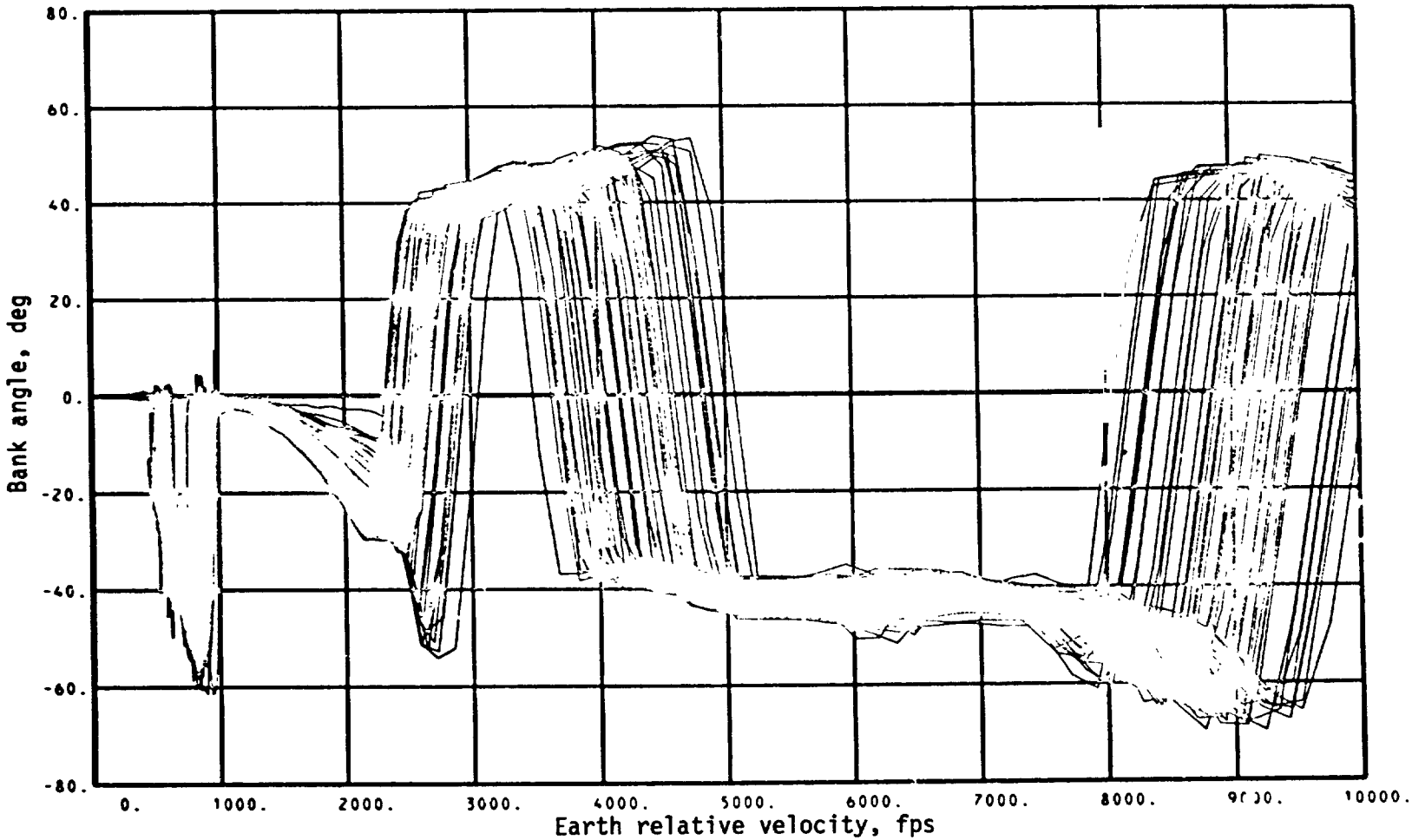

(1) Bank angle.

Figure 31.- Continued.

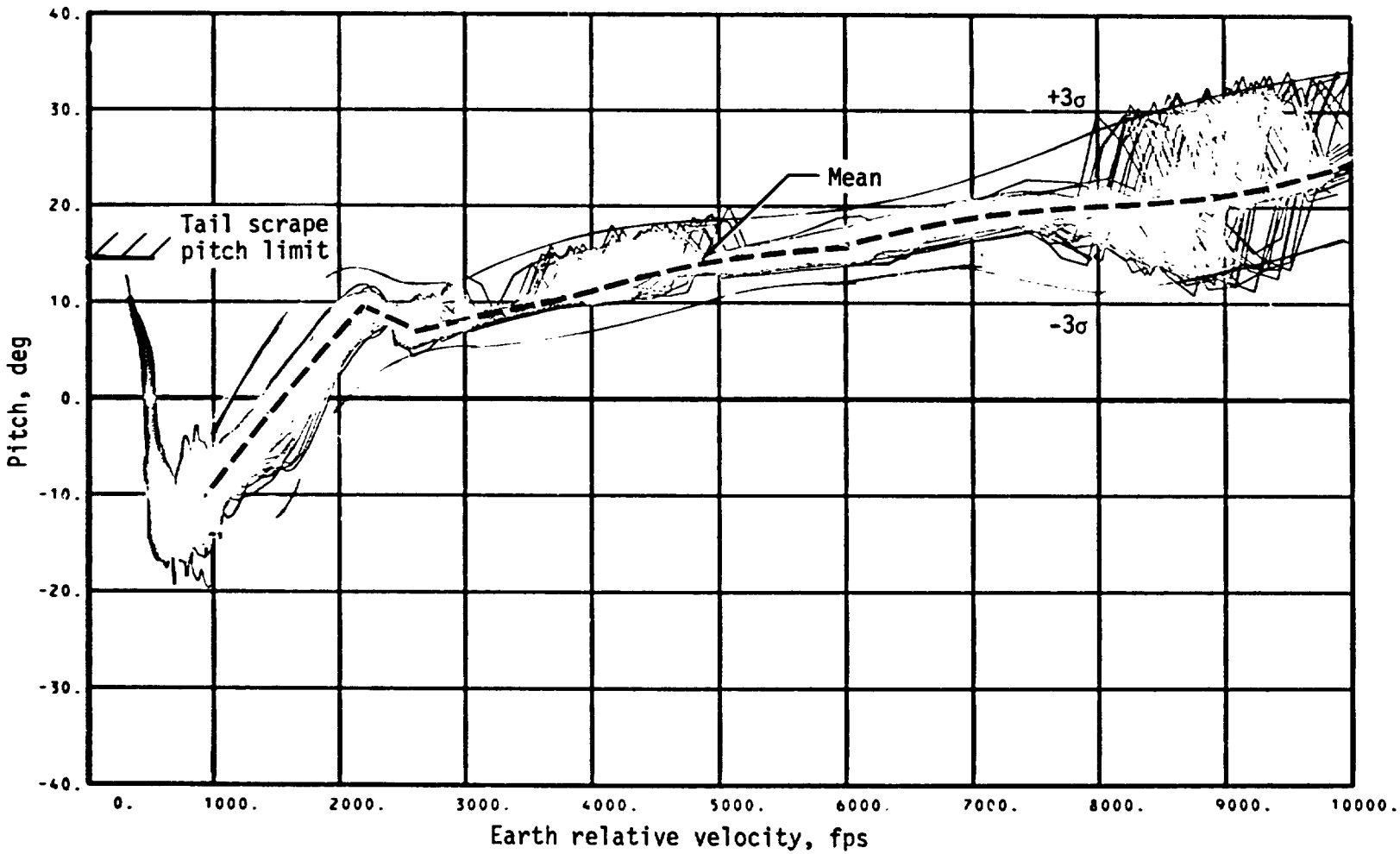

(m) Pitch angle.

Figure 31.- Continued.

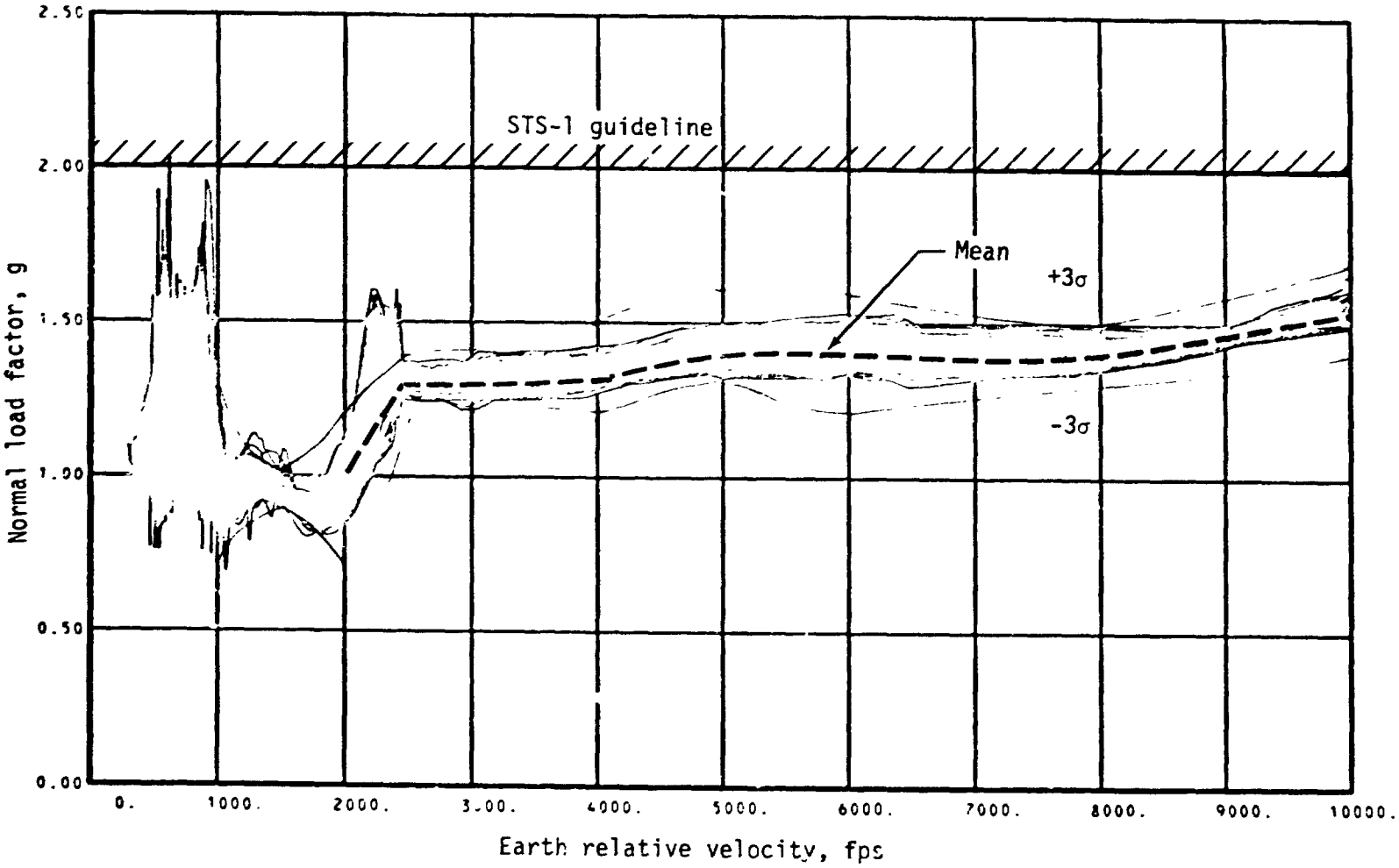

(n) Normal load factor.

Figure 31.- Continued.

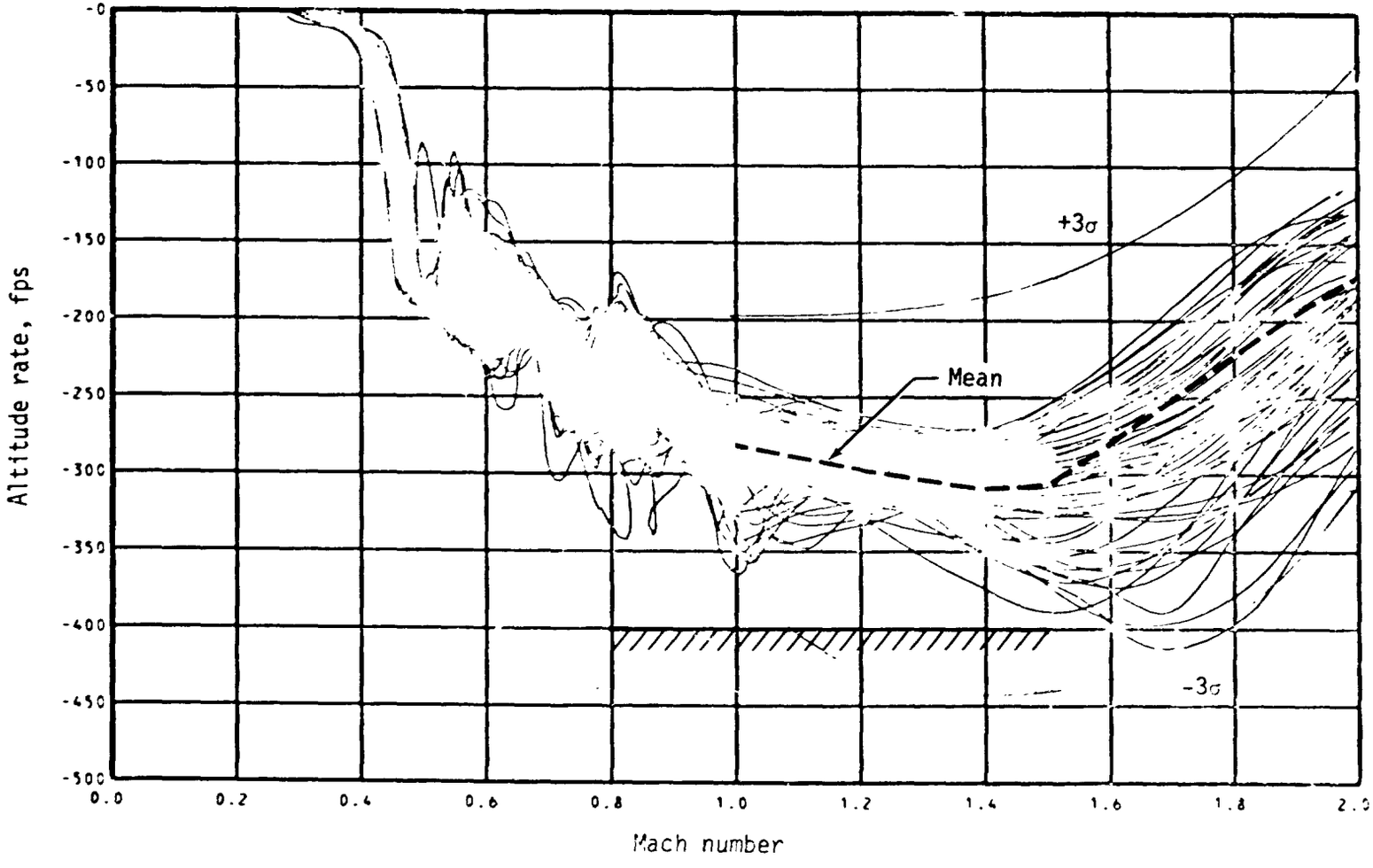

(o) Altitude rate.

Figure 31.- Concluded.